

**DEVELOPMENT AND MECHANISTIC ANALYSIS OF *N*-HETEROCYCLIC
CARBENE-CATALYZED REACTIONS**

by

Matthew T. Berry

B.Sc., San Jose State University, 2011

A THESIS SUBMITTED IN PARTIAL FULFILLMENT OF
THE REQUIREMENTS FOR THE DEGREE OF

DOCTOR OF PHILOSOPHY

in

THE FACULTY OF GRADUATE AND POSTDOCTORAL STUDIES
(Chemistry)

THE UNIVERSITY OF BRITISH COLUMBIA
(Vancouver)

July 2018

© Matthew T. Berry, 2018

The following individuals certify that they have read, and recommend to the Faculty of Graduate and Postdoctoral Studies for acceptance, the dissertation entitled:

DEVELOPMENT AND MECHANISTIC ANALYSIS OF N-HETEROCYCLIC CARBENE-
CATALYZED REACTIONS

submitted by Matthew Berry in partial fulfillment of the requirements for

the degree of Doctor of Philosophy

in Chemistry

Examining Committee:

Jason Hein

Supervisor

Glenn Sammis

Supervisory Committee Member

Pierre Kennepohl

Supervisory Committee Member

Gregory Dake

University Examiner

Dan Bizzotto

University Examiner

Additional Supervisory Committee Members:

Michael Fryzuk

Supervisory Committee Member

Supervisory Committee Member

Abstract

A new class of *N*-heterocyclic carbene (NHC) organocatalysts were developed based on the 1,2,3-triazolium core architecture. These catalysts were found to facilitate the oxidative esterification of aromatic aldehydes, and a small substrate scope was examined. Using reaction progress monitoring by HPLC, a detailed kinetic analysis was performed. Mechanistic studies showed the reaction to be positive order in both aldehyde and base, and zero order in oxidant and methanol. A key carbene-aldehyde adduct was isolated and characterized by X-ray crystallography, and it was shown to exhibit catalytic activity.

The NHC-catalyzed oxidative acylation of electron-poor nucleophiles was also developed, using a 1,2,4-triazolium salt precatalyst. A brief substrate scope was examined, and a kinetic analysis was performed using ^1H NMR reaction monitoring. The mechanistic analysis revealed that the reaction is positive order in aldehyde and base, and zero order in catalyst, oxidant, and sulfonamide nucleophile. In addition, the origin of catalyst deactivation was investigated in the NHC-catalyzed oxidative amidation of aldehydes with amines. Two carbene-amine adducts were discovered, and they were characterized by 1-D and 2-D NMR techniques. A minor carbene-carbene condensation product was also discovered, and characterized by X-ray crystallography.

Finally, a new method of synthesizing dihydropyrimidone precursors for isothiurea organocatalysts was developed, and a brief substrate scope was examined. Experimental and computational results showed that the cyclization reaction proceeds through an α,β -unsaturated mixed imide intermediate, rather than by direct conjugate addition to the α,β -unsaturated amide starting material. These computational results also revealed a 7.6 kcal/mol difference between

the imide cyclization pathway and the direct acrylamide cyclization pathway. Using HPLC reaction monitoring methods, a preliminary mechanistic analysis was performed. These preliminary results showed that electron-withdrawing substituents on the benzothiazole ring slow down the reaction, while electron-donating substituents do not enhance the reaction rate.

Lay Summary

Understanding the intricacies of catalytic reactions and how they work is crucial to the development of new catalytic processes. By understanding exactly how catalysts work and why they succeed, new and better catalysts can be developed, and new catalytic reactions can be discovered. By understanding how catalysts fail and are inhibited, we can tweak catalyst structure or change reaction conditions that allow for the desired reaction to take place. In this work, a new type of catalyst was developed and its reaction was studied in detail. Using a slightly different catalyst, a similar reaction was studied in detail, and a major pathway of catalyst deactivation was identified. Comparing these two different yet similar catalysts, their mechanisms of action are very similar, and we can make a generalization about these types of catalysts as a whole.

Preface

The research presented in chapters two, three, and four of this thesis was conducted in the laboratory of Dr. Jason Hein. Dr. Hein provided guidance, experimental suggestions, and suggested edits of the current manuscript. I was responsible for all experiments and synthesized compounds in this thesis, unless otherwise specified. All data analysis was performed by me, with assistance from Dr. Hein when needed.

A version of Chapter 2 has been previously published: Berry, M. T.; Castrejon, D.; Hein, J. E. *Org. Lett.* **2014**, *16* (14), 3676–3679. I wrote the manuscript, and Dr. Hein and I edited the manuscript. My undergraduate student, Disnay Castrejon, performed some of the intermediate tracking experiments in Chapter 2. The entirety of the work was performed at The University of California, Merced, before the lab relocated to UBC.

A version of Chapter 3 has been prepared for publication. Disnay Castrejon assisted in setting up reactions in Sections 3.2 and 3.3, and I was responsible for isolating and purifying compounds in those sections. The work described in Sections 3.2 and 3.3 was performed at The University of California, Merced. The mechanistic and catalyst deactivation studies described in Sections 3.4 and 3.5 were performed at UBC.

Chapter 4 has not been published. The work was conducted in collaboration with Dr. Daniel Romo and Dr. Paul Ha-Yeon Cheong at Baylor University and Oregon State University, respectively. Dr. Romo provided us with authentic samples of HBTM, and Dr. Cheong performed the computations described in Section 4.4.

Table of Contents

Abstract.....	iii
Lay Summary	v
Preface.....	vi
Table of Contents	vii
List of Tables	xii
List of Figures.....	xiii
List of Schemes	xix
List of Abbreviations	xxv
Acknowledgements	xxxi
Dedication	xxxiii
Chapter 1: Introduction	1
1.1 <i>N</i> -heterocyclic carbenes	2
1.1.1 Properties of NHCs	4
1.1.1.1 Factors affecting the stability of NHCs	4
1.1.1.2 Acidity of NHC precursor salts.....	7
1.1.1.3 Nucleophilicity.....	9
1.1.2 Synthesis of NHC precursors.....	11
1.1.3 NHC Reactivity.....	16
1.1.3.1 Mechanism of action - the benzoin condensation as a model.....	16
1.1.3.2 The Breslow intermediate	22
1.1.4 Reactions catalyzed by NHCs.....	26
	vii

1.1.4.1	The asymmetric benzoin and cross-acyloin condensations	27
1.1.4.2	The Stetter reaction	32
1.1.4.3	A ³ -d ³ umpolung: extended Breslow intermediates	34
1.1.4.4	Acyl azolium catalysis	41
1.2	Kinetic analysis by reaction monitoring	48
1.2.1	Michaelis-Menten kinetics	48
1.2.2	Reaction progress kinetic analysis	50
1.2.3	Reaction monitoring techniques	54
1.2.3.1	Fourier transform infrared spectroscopy (FTIR)	54
1.2.3.2	High performance liquid chromatography (HPLC)	56
1.2.3.3	Nuclear magnetic resonance (NMR) spectroscopy	60
Chapter 2: Mesoionic 1,2,3-Triazolyl <i>N</i>-Heterocyclic Carbene Organocatalysts		62
2.1	Introduction	62
2.1.1	Mesoionic <i>N</i> -heterocyclic carbenes	62
2.2	Design and synthesis of 1,2,3-triazolium salt precatalysts	64
2.2.1	Scope of synthesized triazoles and triazolium salts	66
2.3	Initial reaction trials	70
2.4	Methylation and acidity measurements	73
2.4.1	Methylation studies	76
2.4.2	Acidity measurements by ¹ H NMR	83
2.4.3	Catalytic activity	85
2.4.4	Correlations between nucleophilicity, acidity, and reactivity	87

2.5	Application of 1,2,3-triazolium precatalysts to the oxidative esterification of aldehydes – scope and limitations.....	91
2.6	Mechanistic analysis and identification of resting state	96
2.6.1	Reaction order with respect to aldehyde	98
2.6.2	Reaction order with respect to methanol	100
2.6.3	Reaction order with respect to base	102
2.6.4	Reaction order with respect to oxidant	104
2.6.5	Revised mechanism	106
2.7	Identification and isolation of a catalytically active intermediate	107
2.8	Conclusions.....	113
2.9	Experimental	114
2.9.1	General considerations.....	114
2.9.2	Synthesis of 1,2,3-triazoles	114
2.9.3	Synthesis of 1,2,3-triazolium salts	119
2.9.4	General procedure for methylation experiments.....	124
2.9.5	General procedure for NMR exchange experiments	125
2.9.6	General procedure for reaction monitoring experiments	125
2.9.7	General procedure for the oxidative esterification of aldehydes	126
Chapter 3: <i>N</i>-Heterocyclic Carbene-Catalyzed Oxidative <i>N</i>-Acylation of Electron-Poor <i>N</i>-Nucleophiles.....		128
3.1	Introduction.....	128
3.1.1	Current methods of NHC-catalyzed oxidative amidation.....	128

3.2	Discovery of NHC-catalyzed oxidative coupling of 4-chlorobenzaldehyde with 1,1,3,3-tetramethylguanidine.....	132
3.3	Extension to sulfonamides and other electron-poor nucleophiles	140
3.4	Mechanistic investigations.....	147
3.4.1	Same “excess” experiments to probe catalyst deactivation	154
3.4.2	Different “excess” experiments to determine order in each reaction component...	159
3.5	Catalyst deactivation pathways.....	171
3.5.1	<i>In situ</i> identification of a carbene-amine adduct.....	174
3.5.2	Isolation and characterization of a carbene-carbene adduct	184
3.6	Conclusions.....	186
3.7	Experimental	187
3.7.1	General considerations.....	187
3.7.2	Synthesis of <i>N</i> -(bis(dimethylamino)methylene)-4-chlorobenzamide (3.9)	187
3.7.3	General procedure for oxidative <i>N</i> -acylation of sulfonamides	188
3.7.4	General procedure for the oxidative coupling of aldehydes to electron-poor nucleophiles	190

Chapter 4: Development of a New Synthetic Method for Isothiourea Organocatalyst

Precursors.....	193
4.1 Introduction.....	193
4.1.1 Overview of isothiourea Lewis base catalysts.....	193
4.1.2 Synthesis of HBTM	199
4.2 Initial synthetic attempts to access key dihydropyrimidinone intermediate.....	201
4.3 Lewis acid and NaI-catalyzed cyclization of acrylamide to DHP	202

4.4	Computational results	210
4.5	Extension of cyclization chemistry to other substrates and limitations	212
4.6	Preliminary mechanistic studies	214
4.7	Conclusion	221
4.8	Experimental	221
4.8.1	General considerations	221
4.8.2	Synthesis of <i>N</i> -(benzo[<i>d</i>]thiazol-2-yl)acrylamide (4.23)	222
4.8.3	Synthesis of <i>N</i> -(benzo[<i>d</i>]thiazol-2-yl)-3-chloropropanamide (4.25)	223
4.8.4	General procedure for synthesis of acetamides	223
4.8.5	General procedure for cyclization of acetamides to dihydropyrimidinones	226
Chapter 5: Conclusions and Future Work		231
5.1	Conclusions and future work – 1,2,3-triazolylidene organocatalysts	231
5.2	Conclusions and future work – NHC-catalyzed oxidative acylation	233
5.3	Conclusions and future work – dihydropyrimidone synthesis	236
5.4	NHC/ITU dual catalysis	236
References		239
Appendices		248
Appendix A NMR Spectra from Chapter 2		248
Appendix B NMR spectra from Chapter 3		282
Appendix C NMR from Chapter 4		295
Appendix D X-ray Crystallography Data		316
D.1	X-ray data for compound 2.53	316
D.2	X-ray data for compound 3.39	318

List of Tables

Table 1.1: Example set of experiments for RPKA.	53
Table 2.1: Scope of 1,2,3-triazolium salt precursors.	67
Table 2.2: Scope of synthesized 1,2,3-triazolium salts.....	69
Table 2.3: Substrate scope of 1,2,3-triazolylidene-catalyzed oxidative esterification of aldehydes.	95
Table 3.1: Substrate scope for the NHC-catalyzed oxidative acylation of primary sulfonamides.	144
Table 3.2: Substrate scope of NHC-catalyzed oxidative acylation of aldehydes with electron-poor nucleophiles.	146
Table 4.1: Systematic variation of amide, acid chloride, and NaI addition.....	208
Table D.1: Crystal data and structure refinement for 2.48	316
Table D.2: Crystal data and structure refinement for compound 3.39.....	319

List of Figures

Figure 1.1: Stabilization of N-heterocyclic carbenes by lone pair donation into the adjacent empty p orbital.	3
Figure 1.2: Grubb's 2 nd -generation olefin metathesis catalyst, which incorporates an N-heterocyclic carbene as a ligand. ²	3
Figure 1.3: Thiamine, a biologically relevant N-heterocyclic carbene.....	4
Figure 1.4: Stable carbenes isolated by Arduengo and Enders.....	6
Figure 1.5: pK _a values in H ₂ O of select NHC precursors.	9
Figure 1.6: Nucleophilicity parameters for N-heterocyclic carbenes determined by Mayr et. al. ^{17,18}	11
Figure 1.7: Classes of N-heterocyclic carbenes.....	12
Figure 2.1: Classical, remote, and mesoionic N-heterocyclic carbenes.	63
Figure 2.2: 1,2,3-triazolium salts used in methylation and acidity studies. Counterion for all salts is NTf ₂ ⁻	75
Figure 2.3: Reaction progress curves for the methylation of 1,2,3-triazoliums 2.23a-d.	78
Figure 2.4: Reaction progress curves for the methylation of triazoliums 2.23g-j.	79
Figure 2.5: Progress curves of deuterium incorporation into triazolium salts 2.23a-j.....	84
Figure 2.6: Product formation curves of 2.38 with varying 1,2,3-triazolium precatalysts.	87
Figure 2.7: Triazoliums 2.23a-j ranked in order of increasing nucleophilicity, acidity, and reactivity. Relative nucleophilicities for triazoliums 2.23e and 2.23f were not able to be determined due to decomposition in the presence of base.....	90

Figure 2.8: Product formation curves for the oxidative esterification of cinnamaldehyde with methanol. Each curve represents a different reaction solvent.....	92
Figure 2.9: Product formation curves for the oxidative esterification of cinnamaldehyde with methanol. Each curve represents a different base.	93
Figure 2.10: Product formation curves for the oxidative esterification of cinnamaldehyde (2.34) with methanol. Each curve represents a different initial concentration of cinnamaldehyde.	98
Figure 2.11: Product formation curves for the oxidative esterification of cinnamaldehyde (2.34) with methanol. Each curve represents a different initial concentration of methanol.....	100
Figure 2.12: Product formation curves for the oxidative esterification of cinnamaldehyde (2.34) with methanol. Each curve represents a different initial concentration of 1,1,3,3-tetramethylguanidine (TMG).	102
Figure 2.13: Product formation curves for the oxidative esterification of cinnamaldehyde (2.34) with methanol. Each curve represents a different initial concentration of oxidant 2.39.	104
Figure 2.14: a) Conditions used to synthesize carbene-aldehyde adduct 2.53. b) X-ray crystal structure of 2.53, showing hydrogen bonding between the hydroxyl group and the NTf ₂ counterion.	109
Figure 3.1: Structures of the non-nucleophilic bases TMG, DBU, and DBN.	132
Figure 3.2: a) Aldehyde consumption curves for each precatalyst. b) Product formation curves for each precatalyst.	137
Figure 3.3: a) Product formation curves generated by HPLC with different bases. b) Product formation curves generated by HPLC with different solvents.....	142
Figure 3.4: Top: model reaction used for studying the NHC-catalyzed oxidative amidation of aldehydes with sulfonamides. Bottom: stacked ¹ H NMR spectra of the reaction mixture. Each	

spectrum represents ten minutes of reaction time. The aromatic region ($\delta = 7-8$ ppm) is shown to emphasize peak overlap as the reaction proceeds. 148

Figure 3.5: Top: magnification of the aromatic region used for integration to generate overall product curves. Because of overlap after 60 minutes, the integration limits for H_a are set only for the first 60 minutes. Bottom: the individual integration curves for H_a and H_b spliced together. 150

Figure 3.6: Reaction progress curves showing all species present in the reaction. 151

Figure 3.7: Reaction progress curves showing benzoic anhydride formation when benzoic acid is used as nucleophile. 153

Figure 3.8: Product formation curve of 3.24d generated by 1H NMR, emphasizing both reaction regimes. 154

Figure 3.9: Reaction progress curves of aldehyde consumption, run at the same $[e]=0$ 157

Figure 3.10: Benzaldehyde consumption curves from Figure 3.9, mathematically manipulated in the time domain so that the start of Regime II in the 50 mM reaction (red curve) overlays at a point on the 70 mM reaction (blue curve). The point where the two curves overlay is at approximately 35 mM. 158

Figure 3.11: Product formation curves with differing initial concentrations of benzaldehyde (3.27). $[3.28]_0 = 70$ mM, $[3.7]_0 = 70$ mM, $[3.15]_0 = 5$ mM, $[DBU]_0 = 9$ mM. 161

Figure 3.12: Product formation curves with different initial concentrations of p-toluenesulfonamide (3.28). $[3.27]_0 = 70$ mM, $[3.7]_0 = 70$ mM, $[3.15]_0 = 5$ mM, $[DBU]_0 = 9$ mM. 162

Figure 3.13: Product formation curves with differing initial concentrations of oxidant (3.7). $[3.27]_0 = 70$ mM, $[3.28]_0 = 70$ mM, $[3.15]_0 = 5$ mM, $[DBU]_0 = 9$ mM. 163

Figure 3.14: Product formation curves with different initial concentrations of triazolium precatalyst (3.15). [3.27] ₀ = 70 mM, [3.28] ₀ = 70 mM, [3.7] ₀ = 70 mM. DBU was omitted for this set of experiments.	164
Figure 3.15: Product formation curves of 3.24d with different initial concentrations of DBU. [3.27] ₀ = 70 mM, [3.28] ₀ = 70 mM, [3.7] ₀ = 70 mM, [3.15] ₀ = 5 mM.	166
Figure 3.16: Product formation of 3.24d during Regime II only when the initial concentration of DBU is varied. [3.27] ₀ = 70 mM, [3.28] ₀ = 70 mM, [3.7] ₀ = 70 mM, [3.15] ₀ = 5 mM.	167
Figure 3.17: a) Reaction progress curves generated by ReactIR of 3.27 and 3.24d when one equivalent of DBU is used. [3.27] ₀ = 70 mM, [3.28] ₀ = 70 mM, [3.7] ₀ = 70 mM, [3.15] ₀ = 5 mM, [DBU] ₀ = 70 mM. b) First order rate plot of ln[3.27] as a function of time.	168
Figure 3.18: Reaction progress curves generated in the oxidative amidation of 4-chlorobenzaldehyde with benzylamine.	172
Figure 3.19: a) ¹ H NMR spectra of reaction mixture after 30 minutes. b) Reaction progress curves of key ¹ H NMR resonances.	176
Figure 3.20: ¹ H and ¹³ C NMR assignments for key resonances in 3.36 and 3.38, obtained from HSQC (Figure 3.21) and HMBC (Figure 3.22). The black arrows show observed HMBC correlations.	177
Figure 3.21: HSQC spectra of reaction mixture after 30 minutes containing 1 equiv each of 3.15, benzylamine, and TMG in CDCl ₃ . Blue boxes show HSQC correlations for 3.36, green boxes show HSQC correlations for 3.38.	178
Figure 3.22: HMBC spectra of reaction mixture after 30 minutes containing 1 equiv each of 3.15, benzylamine, and TMG in CDCl ₃ . Blue boxes show HMBC correlations for 3.36, green boxes show HMBC correlations for 3.38.	179

Figure 3.23: Selective 1D-TOCSY spectra showing three unique spin systems in the reaction mixture.	181
Figure 3.24: 1D-selective TOCSY spectra integrals as a function of time. The doublet at 6.05 ppm is selectively pulsed.	182
Figure 3.25: ¹ H NMR spectrum of reaction mixture containing 3.29 and 3.30. Key resonances are labeled.	183
Figure 3.26: X-ray crystal structure of 3.39.	185
Figure 4.1: Proposed transition state and mode of chiral recognition for chiral ITU catalysts. .	196
Figure 4.2: HPLC traces of the crossover experiment taken at different intervals.	205
Figure 4.3: Reaction progress profiles of 4.18, 4.23, and 4.20 in a reaction using Romo's conditions.	206
Figure 4.4: Reaction progress profiles generated by HPLC showing rapid generation and consumption of imide 4.29.	210
Figure 4.5: Reaction coordinate diagram showing energy barrier differences between direct acrylamide cyclization (red) and imide cyclization (blue). Level of theory: SCS-MP2/def2- ∞ //B3LYP/6-31G*	211
Figure 4.6: Substrate scope. Isolated yields determined after purification by column chromatography.	213
Figure 4.7: Amide starting materials used in competition experiments.	214
Figure 4.8: Reaction progress curves for the competition reaction between 4.28 and 4.32d.	216
Figure 4.9: Comparison of product formation curves for 4.33d and 4.20 in both competition and standalone reactions.	218

Figure 4.10: Comparison of product formation curves for 4.20 and 4.33d in standalone reactions only.	218
Figure 4.11: Reaction progress curves in the competition reaction between 4.28 and 4.32f.	220
Figure 5.1: Proposed electron-rich 1,2,3-triazolium precatalyst and its associated Breslow intermediate that can potentially participate in classical NHC reactions.	232
Figure 5.2: Pharmaceuticals containing the N-acylsulfonamide functionality.	235

List of Schemes

Scheme 1.1: a) Wanzlick's observation of carbene dimer 1.7. b) Lemal's experiment probing the Wanzlick equilibrium. c) Denk's confirmation of the Wanzlick equilibrium.	5
Scheme 1.2: Synthesis of thiazolium carbene precursors.	12
Scheme 1.3: Synthetic methods for imidazolium and imidazolinium carbene precursors.	14
Scheme 1.4: Synthetic methods for 1,2,4-triazolium carbene precursors.	15
Scheme 1.5: The benzoin condensation.	17
Scheme 1.6: López-Calahorra's proposed benzoin condensation mechanism.	19
Scheme 1.7: Rehbein's proposed SET mechanism of the benzoin condensation.	20
Scheme 1.8: Radical [1,3]-rearrangements of Breslow intermediates.	21
Scheme 1.9: Generation, resonance forms, and tautomers of the Breslow intermediate.	22
Scheme 1.10: Synthesis of keto-Breslow intermediates by a) Metzger and b) Berkessel.	23
Scheme 1.11: Formation of spirocyclic dioxolane resting state by Berkessel.	23
Scheme 1.12: Trapping of Breslow intermediates via a thermal Claisen rearrangement.	24
Scheme 1.13: Aza-Breslow analogues prepared and characterized by Rovis's group.	25
Scheme 1.14: Catalytic intermediates prepared and characterized by Berkessel et. al.	26
Scheme 1.15: Possible NHC reaction pathways from the Breslow intermediate.	27
Scheme 1.16: a.) The first report of an asymmetric benzoin condensation. b.) Connon and Zeitler's enantioselective benzoin condensation.	28
Scheme 1.17: Possible products in the cross-benzoin condensation.	29
Scheme 1.18: Divergent selectivities between thiazolium and 1,2,4-triazolium salt NHC catalyst precursors in the cross-acyloin condensation. ⁵⁶	31

Scheme 1.19: Enhanced chemoselectivity in the cross-benzoin reaction reported by Gravel's group.	32
Scheme 1.20: Mechanism of the Stetter reaction.....	33
Scheme 1.21: Prototypical mechanism for reactions involving an extended Breslow intermediate.	35
Scheme 1.22: Synthesis of γ -butyrolactones by NHC homoenolate catalysis. a) Bode's first report of NHC homoenolate activity. ⁶³ b) Glorius's simultaneous report of NHC homoenolate activity ⁶⁴ . c) Schiedt's improvement of γ -butyrolactone enantioselectivity by NHC/Lewis acid cooperative catalysis. ⁶⁵	36
Scheme 1.23: Synthesis of spirocyclic γ -butyrolactones by NHC-catalyzed homoenolate addition to isatins.	37
Scheme 1.24: Synthesis and proposed mechanism of trans-cyclopentenones by NHC-catalyzed homoenolate addition to chalcones.	38
Scheme 1.25: a) Bode's synthesis of γ -lactams via homoenolate addition to N-sulfonylimines. b) Bode's use of cyclic ketimines as superior electrophiles.....	39
Scheme 1.26: Choice of base determines product formation in homoenolate NHC catalysis.	40
Scheme 1.27: Different methods of accessing acyl azolium intermediates.....	41
Scheme 1.28: Examples of NHC-catalyzed reactions that proceed through an acyl azolium intermediate.....	42
Scheme 1.29: NHC-catalyzed generation of acyl azoliums via internal redox reaction.	43
Scheme 1.30: Organic oxidants used in NHC catalysis.....	44
Scheme 1.31: Studer's biomimetic oxidation with TEMPO.	45

Scheme 1.32: a) NHC-catalyzed oxidative azidation. b) NHC-catalyzed oxidative thioesterification. c) NHC-catalyzed kinetic resolution of chiral alcohols.	46
Scheme 1.33: a) Studer's chemoselective oxidative esterification in the presence of amines. b) Binding energy calculations performed between carbene and MeOH/MeNH ₂	47
Scheme 1.34: Strategies for NHC-catalyzed oxidative amidation.	48
Scheme 1.35: Simple enzymatic mechanism.	48
Scheme 1.36: Mechanism for a simple catalytic reaction involving two substrates (A, B), one intermediate (Int), and one product (C).	51
Scheme 1.37: Cu(I) deactivation via BCA quench solution.	58
Scheme 2.1: Examples of mesoionic 1,2,3-triazolylienes found in the literature.	64
Scheme 2.2: Synthetic methods towards 1,2,3-triazoles.	65
Scheme 2.3: a) Common 1,2,4-triazolium NHC precatalysts found in the literature. b) Proposed 1,2,3-triazolium analogues of common 1,2,4-triazolium NHC precatalysts. c) Synthetic strategy towards 1,2,3-triazolium NHC precatalysts.	66
Scheme 2.4: Spontaneous cyclization of 1,2,3-triazole oils.	68
Scheme 2.5: Synthesis of 1,2,4-trisubstituted 1,2,3-triazolium regioisomer 2.27.	70
Scheme 2.6: Reaction trials with 1,2,3-triazolium NHC precatalysts: a) benzoin condensation; b) Morita-Baylis-Hillman/Stetter reaction; c) homoenolate lactonization. Each reaction trial did not show evidence of expected product formation.	71
Scheme 2.7: a) Successful reaction trial with 1,2,3-triazolium precatalyst 2.23c. The observed product of the reaction is the oxidative esterification product, rather than the redox esterification product. b) Improved conversion observed in the oxidative esterification reaction after addition of chemical oxidant 2.39. c) Unsuccessful reaction trial with 1,2,3-triazolium precatalyst 2.27.	72

Scheme 2.8: a) Highly efficient oxidative esterification of cinnamaldehyde by 1,2,4-triazolium precatalyst 2.16 reported by Bode. ⁹⁶ b) Relatively poor performance in the oxidative esterification of cinnamaldehyde by 1,2,3-triazolium precatalyst 2.23c.	74
Scheme 2.9: a) Studies to probe the nucleophilicity of carbenes 2.23a-j' by monitoring the rate of methyl incorporation at C5. b) Studies to probe the relative acidities of 2.23a-j by monitoring the rate of deuterium incorporation at C5 by ¹ H NMR.....	75
Scheme 2.10: a) Possible N-methylation of triazolium salts 2.23a-j by methyl iodide. c) Methylation control experiment, showing that triazolium salt 2.23a shows no evidence of chemical transformation in the presence of methyl iodide.	76
Scheme 2.11: Synthesis of C-5-methylated bicyclic 1,2,3-triazolium salts by Tseng et. al. ⁹⁷	77
Scheme 2.12: a) Decomposition of 1,2,3-triazolium salts described by Bouffard et. al. ⁹⁰ b) Possible decomposition pathway for triazolium salts 2.23g-j.	81
Scheme 2.13: Nucleophilic aromatic substitution reaction of triazoliums 2.23e and 2.23f.	82
Scheme 2.14: Base-mediated isomerization of tetrahedral intermediate 2.48 to Breslow intermediate 2.49.....	94
Scheme 2.15: Proposed catalytic cycle for the oxidative esterification of aldehydes by 1,2,3-triazolylidene organocatalysts.....	97
Scheme 2.16: Proposed catalytic cycle for the oxidative esterification of aldehydes by 1,2,3-triazolylidene organocatalysts, with fast and slow steps highlighted.	106
Scheme 2.17: Possible tautomeric forms of carbene-aldehyde adduct observed by HPLC/MS.	108
Scheme 2.18: Experiments demonstrating the catalytic activity of 2.53.	110
Scheme 2.19: Possible oxidation pathways to acyl azolium intermediate 2.50.....	111

Scheme 2.20: a) Scheidt's proposed mechanism of hydride transfer in the NHC-catalyzed hydroacylation of activated ketones. ⁹⁸ b) Experiment to probe the hydride transfer pathway for 1,2,3-triazolylidene catalysts.	111
Scheme 2.21: Attempts to oxidize 2.53 by quinone oxidants 2.39 and DDQ.	112
Scheme 3.1: Synthetic methods for amides.	129
Scheme 3.2: Select examples of metal-mediated oxidative amidations of aldehydes.	130
Scheme 3.3: Strategies for indirect oxidative amidation by NHC catalysis.	131
Scheme 3.4: Observation of aldehyde-guanidine adduct.....	133
Scheme 3.5: Control experiments to rule out non-NHC-catalyzed pathways to form N-acylguanidine 3.9.	133
Scheme 3.6: Possible transamidation pathway to form 3.7.	134
Scheme 3.7: Synthesis of 3.9 using stoichiometric TMG.....	135
Scheme 3.8: Experiments probing the formation and stability of N-acyl guanidine 3.9.....	138
Scheme 3.9: Resonance structures of the conjugate acid of 1,1,3,3-tetramethylguanidine (TMG).	140
Scheme 3.10: Observation of N-acyl benzenesulfonamide by HPLC/MS.	140
Scheme 3.11: Overall scheme for the reaction studied by reaction progress analysis methodology.	154
Scheme 3.12: a) Generation of active carbene catalyst by DBU. b) Inhibition of catalyst by product.	159
Scheme 3.13: Proposed acid/base equilibrium between triazolium 3.15 and carbene 3.15'. pK _a values for 3.15 ¹⁹ and HBF ₄ ¹¹⁹ were determined experimentally.	165
Scheme 3.14: Dominant acid/base equilibria present during a) Regime I and b) Regime II.	169

Scheme 3.15: a) Proposed catalytic cycle; b) catalyst initiation pathway; c) catalyst deactivation pathway.	170
Scheme 3.16: Possible carbene deactivation pathways in the direct oxidative amidation of aldehydes with benzylamine.	173
Scheme 3.17: Observed proton exchange between 3.15 and benzylamine 3.33.	175
Scheme 3.18: Proposed mechanism for the formation of 3.36 and 3.38.	184
Scheme 3.19: Proposed mechanism for the formation of 3.39.	186
Scheme 4.1: Amidine and isothiourea organocatalysts.	194
Scheme 4.2: General mechanism for HBTM-catalyzed acyl transfer reactions.	195
Scheme 4.3: Select examples of enantioselective isothiourea catalysis.	198
Scheme 4.4: Birman's synthesis of HBTM.	199
Scheme 4.5: Romo's synthesis of racemic HBTM.	200
Scheme 4.6: Proposed mechanism of NaI conjugate addition to form 4.20.	201
Scheme 4.7: Synthetic strategy towards DHP 4.20.	201
Scheme 4.8: Synthetic attempts towards DHP 4.20 from chloroamide 4.25.	202
Scheme 4.9: Synthetic attempts towards DHP 4.20 from acrylamide 4.23.	203
Scheme 4.10: Unsuccessful attempts at cyclization via Lewis acid activation.	203
Scheme 4.11: Experiment to probe the role of acryloyl chloride.	204
Scheme 4.12: Proposed mechanism for the formation of DHP 4.20 from amide 4.28.	209
Scheme 4.13: a) Proposed decomposition of 4.20 under HPLC conditions. b) Decomposition of 4.36 to betaine 4.37 observed by Greco and Warchol. ¹³⁹	214
Scheme 5.1: Generalized mechanism for oxidative NHC organocatalysis.	234
Scheme 5.2: Possible mode of dual catalysis with both NHCs and ITUs.	238

List of Abbreviations

©	copyright
1D	1-dimensional
2D	2-dimensional
Å	Angstrom, 10^{-10} meters
Ac	acetyl
aq	aqueous
Ar	aryl
ATR	attenuated total reflectance
BCA	bicinchoninic acid
Bn	benzyl
BTM	benzotetramisole
Bu	butyl
Bz	benzoyl
cat	catalyst or catalytic
CF ₃ -PIP	(<i>R</i>)-2-phenyl-6-trifluoromethyl-dihydroimidazo[1,2- <i>a</i>]pyridine
Cl-PIQ	(<i>R</i>)-7-chloro-2-phenyl-1,2-dihydroimidazo[1,2- <i>a</i>]quinoline
cm	centimeters
CuAAC	copper-catalyzed azide-alkyne cycloaddition
Cyp	cyclopentyl
d	doublet (NMR spectroscopy)
DBU	1,8-diazabicycloundec-7-ene
DCM	dichloromethane

DDQ	2,3-dichloro-5,6-dicyano-1,4-benzoquinone
de	diastereomeric excess
DHP	dihydropyrimidone
DIPEA	<i>N,N</i> -diisopropylethylamine
DMAP	4-dimethylaminopyridine
DMF	<i>N,N</i> -dimethylformamide
dr	diastereomeric ratio
[e]	excess (RPKA)
E	electrophile
ee	enantiomeric excess
EI	electron ionization
equiv.	equivalents
ELSD	evaporative light scattering detector
ESI-MS	electrospray ionization - mass spectrometry
Et	ethyl
EtOAc	ethyl acetate
EtOH	ethanol
Fc	ferrocenyl
FID	flame ionization detector
FTIR	fourier transform infrared spectroscopy
g	gram
GC	gas chromatography
h	hour

HBTM	homobenzotetramisole
HFIP	hexafluoroisopropanol
HMBC	heteronuclear multiple bond coherence
HOAt	1-hydroxy-7-azabenzotriazole
HPLC	high performance liquid chromatography
HSQC	heteronuclear single quantum coherence
Hz	hertz
IMes	1,3-dimesitylimidazol-2-ylidene
iPr	isopropyl
IR	infrared
ITU	isothiourea
J	coupling constant (NMR spectroscopy)
k	rate constant
kcal	kilocalorie
KOtBu	potassium <i>tert</i> -butoxide
L	liter
L.A.	Lewis acid
LC	liquid chromatography
LiNTf ₂	lithium bis(trifluoromethane)sulfonamide
m	multiplet (NMR spectroscopy)
M	concentration (moles/liter)
<i>m</i>	meta
M	metal

Me	methyl
MeCN	acetonitrile
MEK	methyl ethyl ketone
MeOH	methanol
mg	milligram
MHz	megahertz
MIC	mesoionic carbene
min	minute
mL	milliliter
mM	concentration (millimoles/liter)
mol	mole
MS	mass spectrometry
MTBE	methyl- <i>tert</i> -butyl ether
n/a	not available
n/d	not determined
Na ₂ CO ₃	sodium carbonate
NaBAR ^F ₄	sodium tetrakis[3,5-bis(trifluoromethyl)phenyl]borate
NaHCO ₃	sodium bicarbonate
NEt ₃	Triethylamine
NHC	<i>N</i> -heterocyclic carbene
NMR	nuclear magnetic resonance
NOE	nuclear Overhauser effect
Nuc	nucleophile

NR	no reaction
<i>o</i>	ortho
OAc	acetate
OMe	methoxy
OTf	triflate, trifluoromethanesulfonate
<i>p</i>	para
PEEK	polyether ether ketone
pet ether	petroleum ether
PG	protecting group
Ph	phenyl
PhMe	toluene
PPh ₃	triphenylphosphine
PTFE	polytetrafluoroethylene
q	quartet (NMR spectroscopy)
R	organic group
R ²	coefficient of determination (statistics)
RPKA	reaction progress kinetic analysis
RRF	relative response factors
rt	room temperature
s	second, selectivity, or singlet (NMR spectroscopy)
SET	single electron transfer
t	triplet (NMR spectroscopy)
TBTA	tris(<i>tert</i> -butyltriazolyl)amine

tBu	<i>tert</i> -butyl
tBuOH	<i>tert</i> -butyl alcohol
TEA	triethylamine
Tf ₂ O	trifluoromethanesulfonic anhydride
TFA	trifluoroacetic acid
THF	tetrahydrofuran
TLC	thin layer chromatography
TMG	1,1,3,3-tetramethylguanidine
TMS	trimethylsilyl
TOCSY	total correlation spectroscopy (NMR spectroscopy)
TTTA	tris((1- <i>tert</i> -butyl-1 <i>H</i> -1,2,3-triazolyl)methyl)amine
UV	ultraviolet
°	degrees
α	alpha
β	beta
δ	chemical shift in ppm
ΔG [‡]	Gibbs' free energy of activation
γ	gamma
λ	(wavelength)
μ	mu, micro (10 ⁻⁶)
μL	microliter
ρ	rho
σ	sigma

Acknowledgements

First and foremost, I would like to thank both The University of British Columbia and The University of California, Merced, for supporting this work, and for providing teaching assistantships, research fellowships, and travel grants. I especially thank the Department of Chemistry at UBC for allowing me to transfer into their graduate program.

I would also like to thank my committee members at both universities: Dr. Matt Meyer, Dr. Ryan Baxter, Dr. Meng-lin Tsao, Dr. Javier Read de Alaniz, Dr. Glenn Sammis, Dr. Michael Fryzuk, and Dr. Pierre Kennepohl. Their advice, guidance, and perspectives are all greatly appreciated.

This thesis would not have been possible without the institutional support I received from both UBC and UC Merced. I would like to thank NMR gurus Dave Russell, Paul Xia, and Maria Ezhova for training me on the spectrometers, and for useful NMR insights. I would like to thank Dr. Brian Patrick at UBC and Dr. Curtis Moore at The University of California, San Diego for their assistance in the determination of the X-ray crystal structures presented in this dissertation. I would like to thank my collaborator Dr. Daniel Romo at Baylor University for providing the starting point for the work presented in Chapter 4, as well as authentic samples. I would also like to thank the Paul Ha-Yeon Cheong group at Oregon State University for the computational work they did that is presented in Chapter 4.

I am deeply indebted to my family and friends for their love and support throughout my time in graduate school. I wish to thank my mother, Pamela Berry, and my uncle, Richard Warner, for their unconditional love, support, and understanding (even if they don't fully understand the chemistry). I wish to thank Taven Barton, Amanda Chrestensen, Angel Goss, Richard Hargrove, Karina Nielsen, Jennifer Page, Luke Reed, and Amanda Vargas for all of their

support. By encouraging me when I needed it the most, letting me vent my frustrations, going to concerts with me on Valentine's Day, bro-ing out about Star Wars, sending silly cat pictures, or simply taking coffee breaks with me, they have all been instrumental in keeping my sanity during the preparation of this dissertation, especially during the final stretch. I give all of you my sincerest thanks.

I would like to thank all current and former members of the Hein lab for helping me brainstorm ideas, providing a fun environment to do chemistry in, and for all of the shenanigans, both in and out of the lab. In particular, I want to thank Diana Yu, Ivy Price, Céline Rougeot, Aagam Patel, Blessing Cao, and Henry Situ. I especially want to thank my undergraduate students Disnay Castrejon and Jacob Lewis, for allowing me to mentor them during their undergraduate studies.

Last, and certainly not least, I am deeply indebted to my advisor, Dr. Jason Hein, for taking me on as his first graduate student. Thank you for supporting me through thick and thin, when others wouldn't; thank you for your guidance, and for suggesting experiments to run when I was out of ideas; thank you for guiding me towards becoming an independent researcher in my own right, and for providing me the skills and tools to do so; thank you for letting me follow you to UBC with Diana and Céline; thank you for letting me name the lab's first HPLC. Finally, thank you for helping to get me over the finish line. Without your support and guidance, this thesis would not have been possible.

This thesis is dedicated to my mother, Pamela Berry, for her unconditional love and support, for igniting the scientific spark in me at a young age, and for introducing me to my first HPLC.

“If I have seen further it is by standing on ye shoulders of giants.”

Sir Isaac Newton - 1676

Chapter 1: Introduction

For research groups that focus on reaction development and methodology, reaction optimization is a crucial step in the development and reporting of any new chemical transformation. Through systematic variation of a number of variables such as catalyst, solvent, concentration, temperature, and time, optimization tables can be generated to identify the best conditions for a given reaction. This “top-down” approach to method optimization is widely used by most research groups, as it allows for rapid screening of optimal conditions for a reaction that most likely already works well. However, the only metrics used to determine the effectiveness of a certain reaction condition or variable are product conversion, selectivity, and percent yield, which are usually determined when the reaction is considered finished. For some chemical transformations, these metrics can change over the course of a reaction – a desired product is susceptible to hydrolysis, a catalytic reaction is reversible, or a product slowly racemizes after it is formed. By using only the endpoint of a reaction to determine its success or efficiency, valuable information about these metrics over the course of the reaction is lost.

The converse of the “top-down” approach is the “bottom-up” approach to reaction optimization – by using analytical tools to track the progress of a reaction as it proceeds, knowledge such as the presence of different reaction regimes, catalytic speciation, catalyst deactivation, and the existence of transient intermediates can be gained. With this knowledge, informed decisions about optimization parameters can be made and correlated to catalytic efficiency. For example, the product formation curve of a reaction can tell the researcher that irreversible catalyst death is occurring, the researcher can formulate a hypothesis for why it is

occurring, and they can screen a set of additives that may prevent catalyst death. Analytical spectroscopic techniques such as ReactIR or NMR allow for the acquisition of reaction trends with high rates of data sampling under synthetically relevant conditions, while highly sensitive separation techniques like HPLC/MS or GC/MS can aid in the identification of unknown catalytic intermediates, off-cycle species, or previously unknown reaction byproducts. Using this “bottom-up” approach, different reaction variables or conditions can be correlated to catalytic efficiency during different regimes of a reaction.

This dissertation focuses on two main themes: the development of *N*-heterocyclic carbene-catalyzed reactions, and the use of analytical methods for the monitoring of reaction progress to study their mechanism. As such, this chapter is split up in to two main sections: *N*-heterocyclic carbene organocatalysis and reaction progress kinetic analysis methodology.

1.1 *N*-heterocyclic carbenes

Carbenes are a class of compounds that share a key feature: the presence of a neutral divalent carbon atom, represented by the formula :CR_2 . The simultaneous presence of a lone pair and a vacant p orbital gives the carbene ambiphilic properties; the empty p orbital acts as an electron acceptor, while the filled sp^2 hybrid orbital acts as an electron donor. Prior to 1960, carbenes had been considered as unstable, electrophilic reactive intermediates, and their existence could only be inferred by indirect methods. It was during the 1960s that Wanzlick¹ postulated that both the stability and polarity of a carbene could be modified by incorporation of electron-donor groups adjacent to the carbene center. When such electron-donor groups are alkyl and aryl amino groups, the carbene is considered an *N*-heterocyclic carbene (NHC). The effect of

the nitrogen atom adjacent to the carbene center is illustrated in Figure 1.1: the nitrogen atom helps to stabilize the carbene by donation of its lone pair into the empty out-of-plane p-orbital.

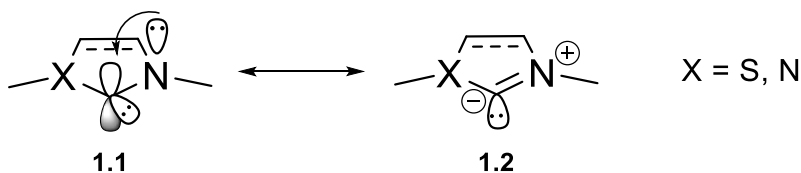


Figure 1.1: Stabilization of *N*-heterocyclic carbenes by lone pair donation into the adjacent empty p orbital.

N-heterocyclic carbenes have seen widespread use in the field of organometallic chemistry, due to their use as stabilizing ligands for organometallic complexes. A wide array of NHC-metal complexes with various transition metals have been synthesized and characterized, including Grubbs' second generation catalyst for olefin metathesis² (Figure 1.2). NHC-metal complexes are robust and resistant to oxidation, making them desirable catalysts in a practical sense. In addition, the nature of the NHC affects both the sterics and the electronics of the transition metal catalyst. By tuning the electronic and steric properties of the NHC ligand, a wide variety of catalysts can be made that span a range of reactivities and selectivities. Organometallic NHC complexes are crucial to understanding the physical properties of the free carbenes as well; studying how an NHC bonds to a metal center can give insight into the nucleophilic properties of a potential organocatalyst.

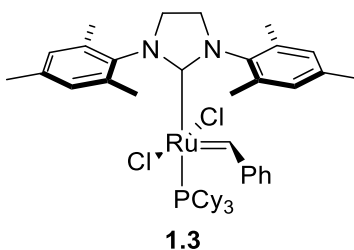


Figure 1.2: Grubbs' 2nd-generation olefin metathesis catalyst, which incorporates an *N*-heterocyclic carbene as a ligand.²

N-heterocyclic carbenes also have foundations in biology and nature. Thiamine, colloquially known as Vitamin B1, is an essential nutrient, and it acts as a cofactor for a number of enzymes, including transketolase and pyruvate decarboxylase.³ In 1951, the active form of thiamine was proposed to be a nucleophilic carbene by Mizuhara et. al⁴ (Figure 1.3), and in 1958 Breslow proposed the structure of a key reactive intermediate involved in thiamine-dependent biochemical processes, based on a model system.⁵ These early works laid the foundation for the development of *N*-heterocyclic carbene organocatalysis as a major field of study, and as a result, a multitude of catalysts and chemical transformations have been developed, which will be detailed later in this chapter.

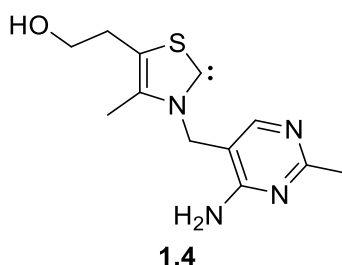


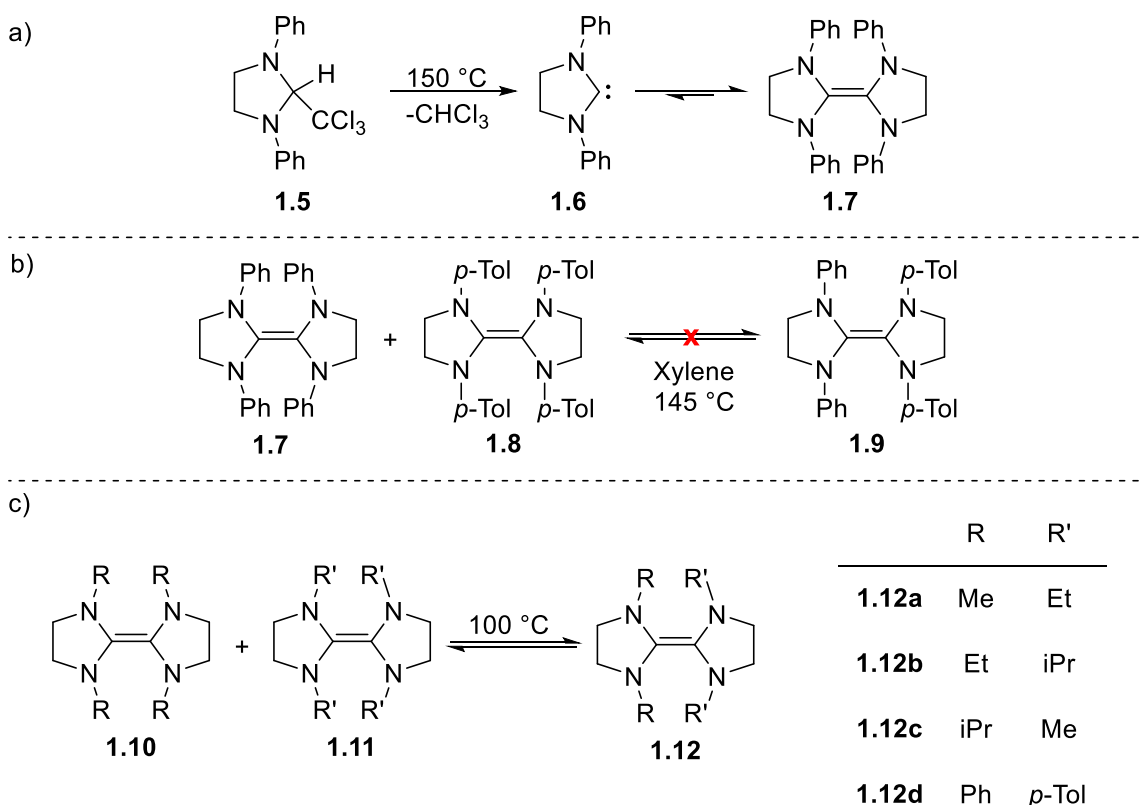
Figure 1.3: Thiamine, a biologically relevant *N*-heterocyclic carbene.

1.1.1 Properties of NHCs

1.1.1.1 Factors affecting the stability of NHCs

In the early 1960s, Wanzlick¹ postulated that carbenes could be stabilized by the incorporation of heteroatoms adjacent to the carbene, stabilizing the carbene by donation of lone pairs into the carbene's empty out-of-plane p-orbital. Wanzlick's initial attempts at isolation of a free carbene were unsuccessful, instead isolating dimer **1.7**, postulating that the free carbene **1.6** existed in an equilibrium with dimer **1.7** that favors the dimer (Scheme 1.1a). This conjecture was challenged by Lemal et al. in 1964, who did not observe mixed dimer **1.9** when a mixture of

dimers **1.7** and **1.8** was heated in xylene⁶ (Scheme 1.1b). If a carbene-dimer equilibrium was present, then mixed dimer **1.9** would be formed *in situ* by condensation of the two respective free carbenes. Lemal's experiment was revisited in 1999 by Denk et al.,⁷ who did in fact observe a variety of mixed carbene dimers (Scheme 1.1c), supporting Wanzlick's original postulation. While Denk et al. observed statistical mixtures of *N*-alkyl-substituted dimers **1.12a-c**, they did not for *N*-aryl-substituted dimer **1.12d**, the same dimer that Lemal expected to observe. Denk suggested the low solubility of *N*-phenyl-substituted dimer **1.10** in benzene as a rationalization for this observation.



Scheme 1.1: a) Wanzlick's observation of carbene dimer **1.7**. b) Lemal's experiment probing the Wanzlick equilibrium. c) Denk's confirmation of the Wanzlick equilibrium.

It wasn't until 1991 that the first stable crystalline carbene was isolated and characterized by Arduengo et al.,⁸ and in the years since, a number of stable crystalline carbenes have been isolated and characterized (Figure 1.4). The first stable crystalline carbene isolated by Arduengo et al. (**1.13**) was a bis-adamantyl-substituted imidazolylidene, and its stability was initially primarily attributed to the large steric bulk of the *N*-adamantyl groups. They postulated that the steric bulk of the *N*-adamantyl groups contributed to the kinetic stability by preventing carbene-carbene dimerization. They also proposed that the π -backbone helped to stabilize the carbene, by electron donation into the carbene out-of-plane p-orbital. A year later, the same group reported the isolation and characterization of bis-methyl-substituted **1.14**, which has considerably less steric bulk than its bis-adamantyl analogue.⁹ The isolation of **1.14** suggested that the electronic structure of the imidazolylidene is sufficient to stabilize the carbene, and the steric bulk of the *N*-substituents play less of a role in carbene stability. A few years later, Arduengo et. al reported the isolation and characterization of bis-mesityl-substituted imidazolinylidene **1.15**,¹⁰ which lacks the unsaturated backbone of carbenes **1.13** and **1.14**. For this particular carbene, the stability is most likely attributed to the steric bulk of the *N*-mesityl groups, preventing dimerization of the kind previously observed by Wanzlick.

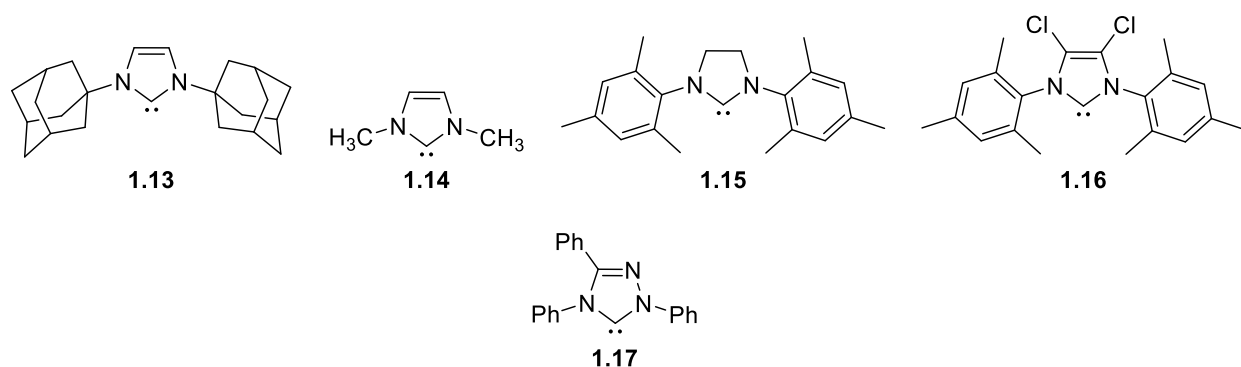


Figure 1.4: Stable carbenes isolated by Arduengo and Enders.

While carbenes **1.13-1.15** are considered stable, they are only relatively so – they decompose in the presence of air and moisture. The first air-stable carbene (**1.16**) was reported in 1997 by Arduengo et. al.¹¹ A unique feature of carbene **1.16** is the presence of two chlorine atoms on the imidazole backbone. They proposed that the chlorine atoms help to stabilize the carbene center by both π -donation (from the lone pairs of the Cl atoms) and σ -withdrawal by chlorine, which substantially reduces the basicity of the carbene lone pair. The isolation of stable carbenes is not restricted to imidazolylidenes (**1.13, 1.14, 1.16**) and imidazolinyliidenes (**1.15**), however. In 1995, Enders et. al reported the isolation and characterization of the first 1,2,4-triazolylidene **1.17**.¹² The C-N bond lengths between the carbenic carbon and the adjacent nitrogens exhibit more sp^2 character than sp^3 , suggesting that the sp^2 nitrogen on the backbone makes a significant contribution to the stability of this carbene. In general, the stability of an *N*-heterocyclic carbene is determined by both the electronic structure of the azole core, and by steric bulk of the *N*-substituents.

1.1.1.2 Acidity of NHC precursor salts

One of the key advantages of NHC organocatalysis is the ability to generate a reactive catalyst (a carbene) from a bench-stable precursor (an azolium salt) by deprotonation of the azolium salt. Naturally, a discussion of the physical properties of NHCs should involve a discussion of pK_a . Figure 1.5 shows pK_a values determined in water for some select NHC precursor salts. In general, imidazoliums and imidazoliniums are the least acidic ($pK_a \approx 20-24$), while 1,2,4-triazoliums and thiazoliums are more acidic ($pK_a \approx 16-19$).

For *N,N*-disubstituted imidazolium salts, substitution of one of the methyl groups for a longer chain has a negligible effect on the pK_a .¹³ *N,N*-dimethyl substituted imidazolium salt **1.18**

has a pK_a of 23.0, while *N*-octyl-*N*-methyl substituted imidazolium salt **1.22** has a pK_a of 23.4 – a seven carbon chain length difference results in only a 0.4 pK_a unit difference. There is a correlation between steric bulk of the *N*-substituent and pK_a for imidazolium salt NHC precursors – *N*-adamantyl-substituted imidazolium salt **1.27** ($pK_a = 25.4$) is much less acidic than *N*-mesityl substituted **1.24** ($pK_a = 20.8$) or *N*-2,6-diisopropylphenyl substituted **1.25** ($pK_a = 21.1$), a pK_a difference of approximately 4-5 pK_a units.¹⁴ While sterics not have a direct effect on the thermodynamic property of pK_a , sterics do affect the solvation and stabilization of the carbene conjugate base.

For thiazolium and 1,2,4-triazolium salts, the electronic structure of the *N*-substituent also plays a significant role.¹⁵ *N*-C₆F₅-substituted triazolium salt **1.31** is one pK_a unit more acidic than its *N*-phenyl-substituted analogue **1.32**, and *N*-cyanomethyl-substituted thiazolium **1.34** is more acidic than *N*-4-nitrobenzyl-substituted thiazolium **1.36** or thiamine hydrochloride (**1.35**). The inductive effects of these electron-withdrawing *N*-substituents directly influence the stability of the free carbene, and therefore the acidity of the carbene precursor salt. To put the acidity of these azolium salt carbene precursors into perspective, the most acidic precursor **1.31** ($pK_a = 16.5$) has a pK_a similar to diethyl malonate¹⁶ ($pK_a = 16.4$). The least acidic precursor, bis-adamantyl substituted **1.27** ($pK_a = 25.4$) has a pK_a similar to terminal alkynes¹⁷ ($pK_a \approx 25$).

	R	X	pK _a		R	pK _a		R	pK _a		Ar	pK _a
1.18	Me	NTf ₂	23.0	1.23	4-ClC ₆ H ₄	19.8	1.28	Mes	21.3	1.31	C ₆ F ₅	16.5
1.19	Et	Cl	23.0	1.24	Mes	20.8	1.29	2,6-(iPr) ₂ C ₆ H ₃	21.5	1.32	Ph	17.5
1.20	ⁿ Butyl	Cl	23.3	1.25	2,6-(iPr) ₂ C ₆ H ₃	21.1	1.30	4-OMeC ₆ H ₄	20.7	1.33	Mes	17.7
1.21	ⁿ hexyl	PF ₆	23.4	1.26	4-OMeC ₆ H ₄	20.7						
1.22	ⁿ octyl	Br	23.4	1.27	adamantyl	25.4						

1.34	1.35	1.37	1.38
pK _a = 16.9	pK _a = 18.0	pK _a = 18.5	pK _a = 17.4

1.36	1.39
pK _a = 17.8	pK _a = 16.8

Figure 1.5: pK_a values in H₂O of select NHC precursors.

1.1.1.3 Nucleophilicity

In the vast majority of *N*-heterocyclic carbene-catalyzed reactions, the first step in the catalytic cycle is nucleophilic addition of the carbene to an electrophile, usually an aldehyde. As *N*-heterocyclic carbenes are nucleophilic, correlating nucleophilicity with catalyst structure is important for both methodological development and catalyst design. Mayr et. al¹⁸ found that for

a nucleophilic species, its nucleophilicity and the rate of addition of the nucleophile to an electrophile is given by the equation:

$$\log k_{20\text{ }^{\circ}\text{C}} = s_N(N + E) \quad (1.1)$$

Where $k_{20\text{ }^{\circ}\text{C}}$ is the rate of addition of the nucleophile to an electrophile, N and s_N are solvent-dependent nucleophilicity and sensitivity parameters, respectively, and E is a solvent-independent electrophilicity parameter for the electrophile used to probe nucleophilicity. Using this method, they determined nucleophilicity parameters for a number of N -heterocyclic carbenes^{19,20} (Figure 1.6). They found that imidazolylidene **1.40** and imidazolidinylidene **1.15** were approximately 10^3 times more nucleophilic than triazolylidene **1.17**, which has a similar nucleophilicity to 1,8-diazabicycloundec-7-ene (DBU) and N,N -dimethylaminopyridine (DMAP). They also examined the effect of N -substituent on carbene nucleophilicity. N -2,6-(OMe)₂C₆H₃-substituted imidazolylidene (**1.41**) is more nucleophilic than other carbenes of its class, and N -*tert*-butyl-substituted imidazolylidene **1.42** shows lower nucleophilicity, but not as low as triazolylidene **1.17**. Notably, substitution of a mesityl for a methyl group does not result in a significant change in nucleophilicity (**1.40** vs **1.42**).

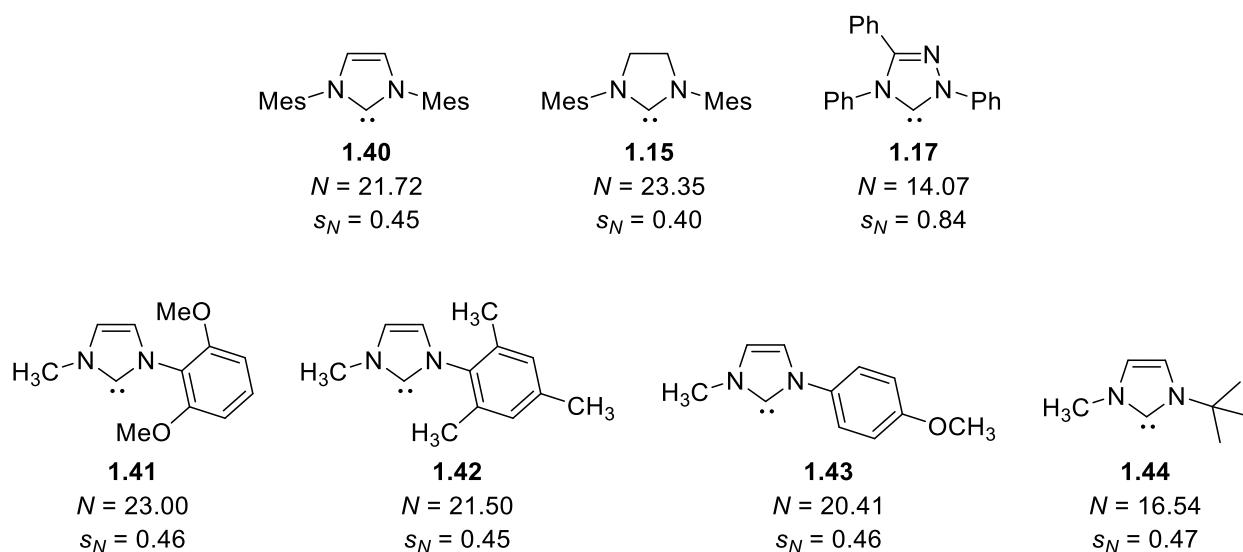


Figure 1.6: Nucleophilicity parameters for *N*-heterocyclic carbenes determined by Mayr et. al.^{19,20}

1.1.2 Synthesis of NHC precursors

The application of NHCs in organocatalysis has resulted in the development of a vast and structurally diverse library of useful carbenes to facilitate a wide variety of chemical transformations.²¹ Figure 1.7 shows the structures of the four main classes of *N*-heterocyclic carbenes used in organocatalysis. While the early years of NHC catalysis were dominated by thiazolylidenes (**1.45**) due to their structural similarities to thiamine, the field has evolved to include imidazolidinylidenes (**1.46**), imidazolylidenes (**1.47**), and triazolylidenes (**1.48**). Over the years, researchers have developed structurally diverse catalyst precursors that have varying *N*-substituents, as well as chiral and achiral backbones. Some of the methods towards these carbene precursors are detailed in this section.

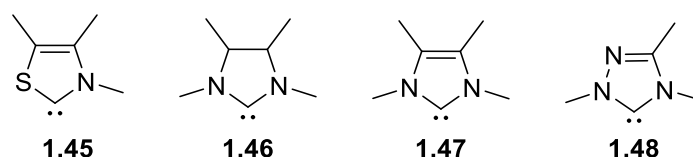
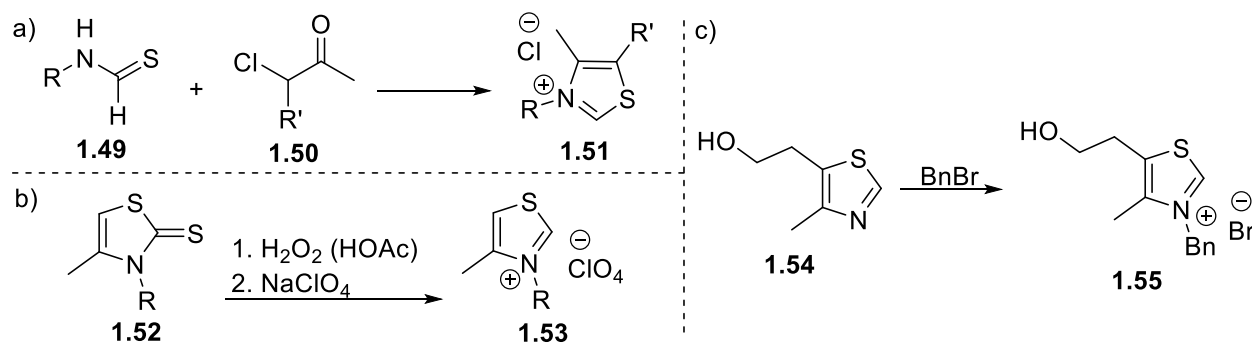


Figure 1.7: Classes of *N*-heterocyclic carbenes.

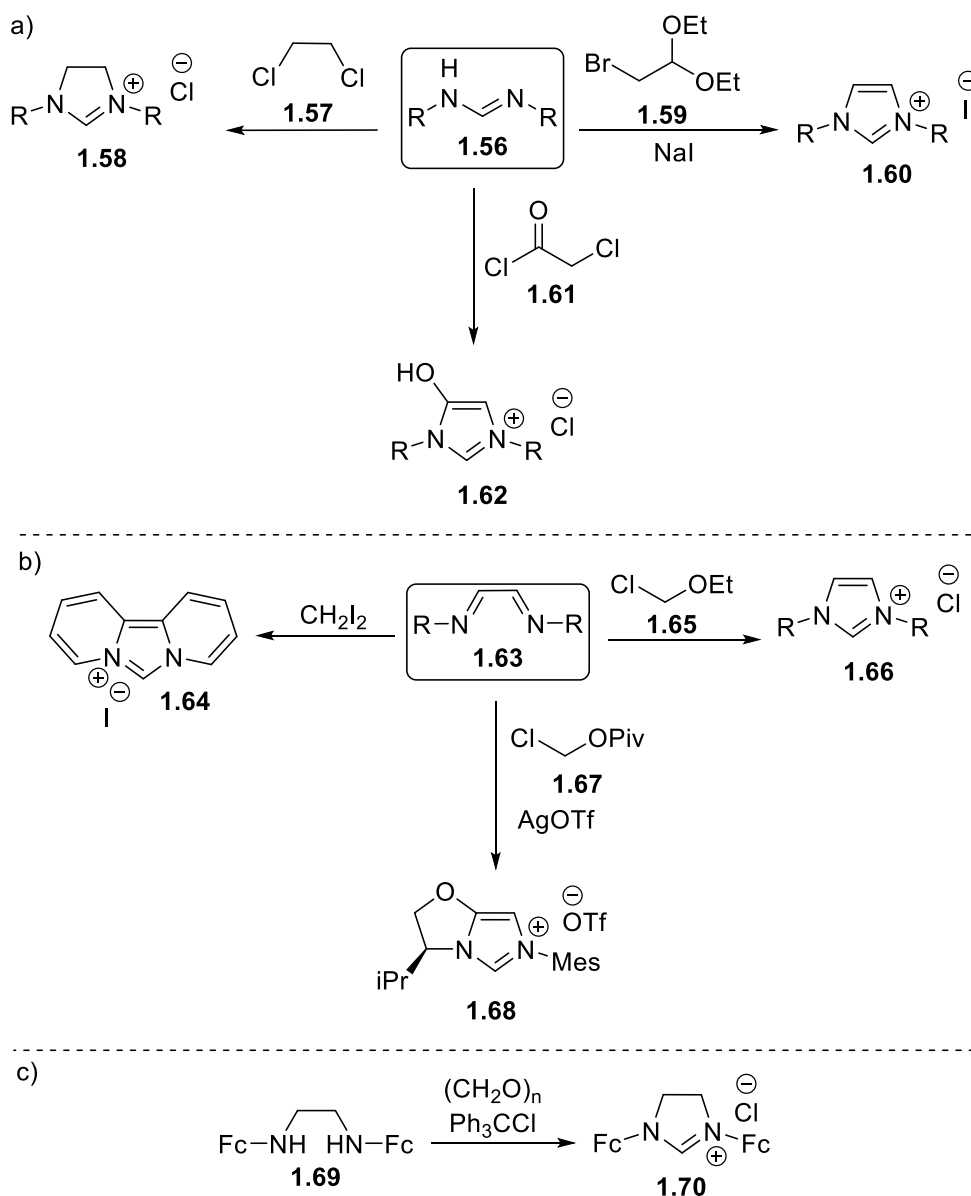
Scheme 1.2 details methods to synthesize thiazolium salt precursors for thiazolylidenes. Thiazolium salt precursors have been prepared by condensation of an α -chloro ketone with an *N*-substituted thioformamide²² (Scheme 1.2a), as well as by treatment of a thiazolin-2-thione with hydrogen peroxide and sodium perchlorate²³ (Scheme 1.2b). In addition, thiazolium salt precursors can be prepared by simple alkylation of the corresponding thiazole (Scheme 1.2c).



Scheme 1.2: Synthesis of thiazolium carbene precursors.

The syntheses of imidazolium and imidazolinium carbene precursors fall into two basic strategies: annulation of the two-carbon backbone onto an aminal (usually a formamidine), or annulation of a one-carbon component onto a diamine or diimine, introducing the precarbenic carbon at the final step. Variations of this strategy have been developed to increase the structural diversity of imidazolium and imidazolinium carbene precursors, such as cyclizations of formamidines with dichloroethane,²⁴ chloroacetyl chloride,²⁵ and bromoacetaldehyde diethylacetal²⁶ (Scheme 1.3a). The second strategy of one-carbon annulation with a diimine is

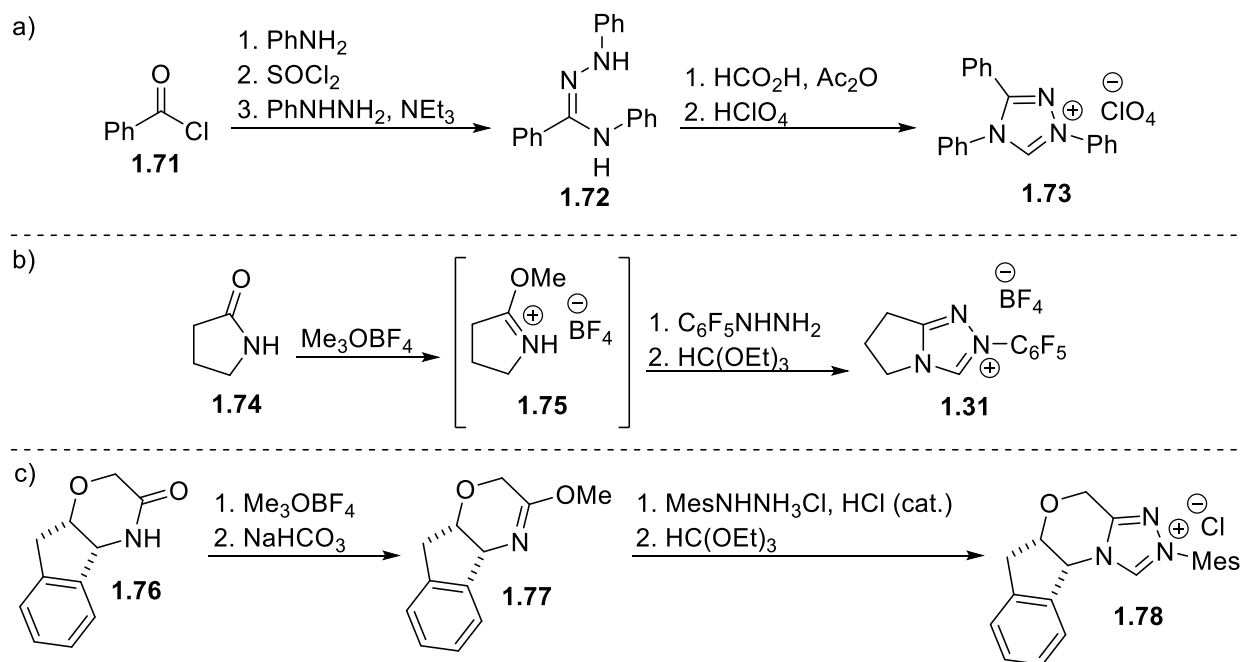
much more widely used, and a wide variety of imidazolium and imidazolinium salt precursors have been prepared using bis-electrophiles such as diiodomethane,²⁷ chloromethyl ethers,²⁸ and chloromethyl pivalates²⁹ (Scheme 1.3b). Imidazolinium salt precursors can also be prepared by condensation of formaldehyde with a diamine, followed by oxidation³⁰ (Scheme 1.3c). With both of these synthetic strategies, the choice of formamidine, diimine, or diamine starting material allows for variation of *N*-substituent, tuning the catalyst's steric and electronic properties. In addition, as with thiazolium precursors, imidazolium precursors can be synthesized by simple alkylation of the parent imidazole.³¹



Scheme 1.3: Synthetic methods for imidazolium and imidazolinium carbene precursors.

1,2,4-triazolium carbene precursors have become popular precatalysts in recent years due to their enhanced reactivities and selectivities, but unlike thiazolium and imidazolium salts, fewer synthetic methods have been developed for them. Enders et. al first introduced triazolium carbene precursors in 1995 using a five-step process starting from benzoyl chloride^{12,32} (Scheme 1.4a). The first chiral bicyclic triazolium carbene precursors for the asymmetric benzoin

condensation were developed by Knight and Leeper in 1998, starting from morpholine-3-ones.³³ In 2002, Enders and Kallfass extended this synthetic strategy to oxazolidinone starting materials, yielding a unique chiral catalyst with an oxazolidine backbone.³⁴ Rovis et. al further extended this synthetic strategy to aminoindanol-derived and 2-pyrrolidinone starting materials³⁵ (Scheme 1.4b). This method is reliable and tolerant to a wide variety of lactams, resulting in the development of a vast library of triazolium carbene precursors by various research groups.²¹ Problems with the stability of mesitylhydrazine led Bode's group to modify this synthesis by condensing mesitylhydrazine hydrochloride with the free-based 2-methoxytetrahydroindenoaxazine **1.77**³⁶ (Scheme 1.4c). With this modification, electron-rich *N*-aryl substituents can be installed into the catalyst in an easier fashion. This overall strategy of *O*-methylating a functionalized lactam followed by condensation with an aryl hydrazine is arguably the most popular synthetic method used when developing new NHC catalysts.

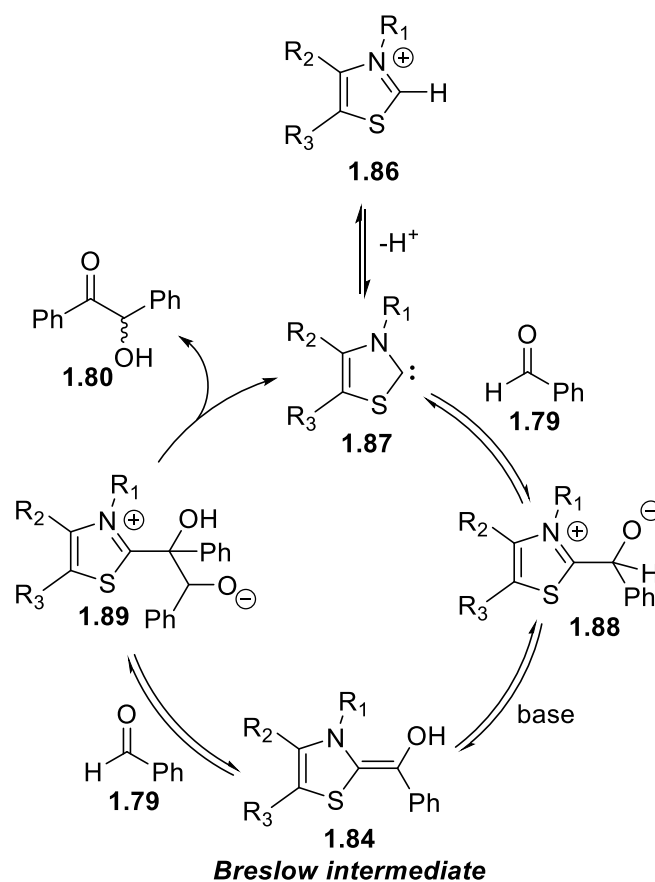
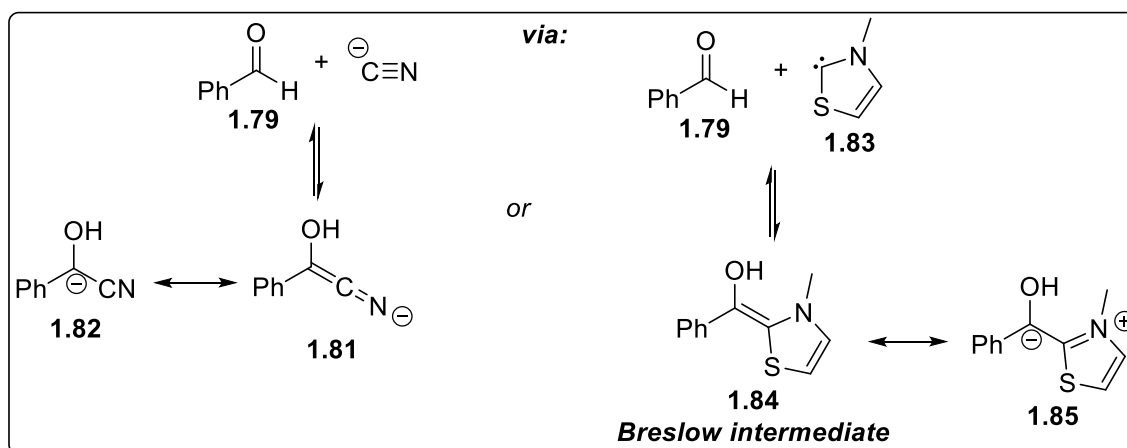
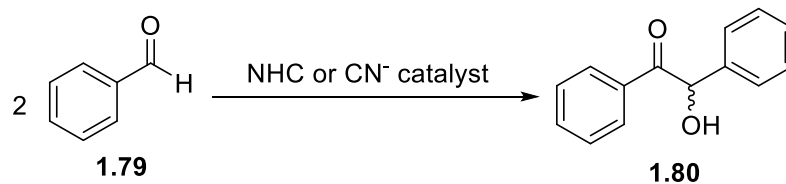


Scheme 1.4: Synthetic methods for 1,2,4-triazolium carbene precursors.

1.1.3 NHC Reactivity

1.1.3.1 Mechanism of action - the benzoin condensation as a model

N-heterocyclic carbene catalysis exemplifies the concept of umpolung: chemical modification of a functional group in order to reverse the polarity of that group³⁷ (e.g. electrophile to nucleophile). The cyanide ion-catalyzed benzoin condensation is the classical example of umpolung catalysis, where cyanide renders the electrophilic carbonyl of one molecule of benzaldehyde nucleophilic, allowing it to react with another molecule of benzaldehyde to form an α -hydroxy ketone^{38,39} (Scheme 1.5). In 1903, Lapworth proposed deprotonated cyanohydrin **1.82** to be the key intermediate in the cyanide-catalyzed benzoin condensation. In 1943, Ukai et. al discovered that the benzoin condensation could also be catalyzed by a thiazolium salt.⁴⁰ In 1958, Breslow proposed that the active catalyst was a free carbene, and that the key “active aldehyde” intermediate was enaminol **1.84**, commonly referred to as the Breslow intermediate.⁵ For both carbenes and cyanide, the proposed modes of action are identical: nucleophilic attack on to benzaldehyde renders the former aldehyde proton acidic, allowing for the formation of active intermediates **1.84** and **1.85**, where the former aldehyde carbon is nucleophilic. The nucleophilicity of the umpoled carbonyl can be explained by the resonance structures of **1.84** and **1.85**, where negative charge is localized on that carbon. In the same paper where he proposed the structure of the Breslow intermediate, Breslow proposed a mechanistic model for the thiazolium salt-catalyzed benzoin condensation, based on Lapworth’s proposed mechanism for the cyanide-catalyzed benzoin reaction (Scheme 1.5).

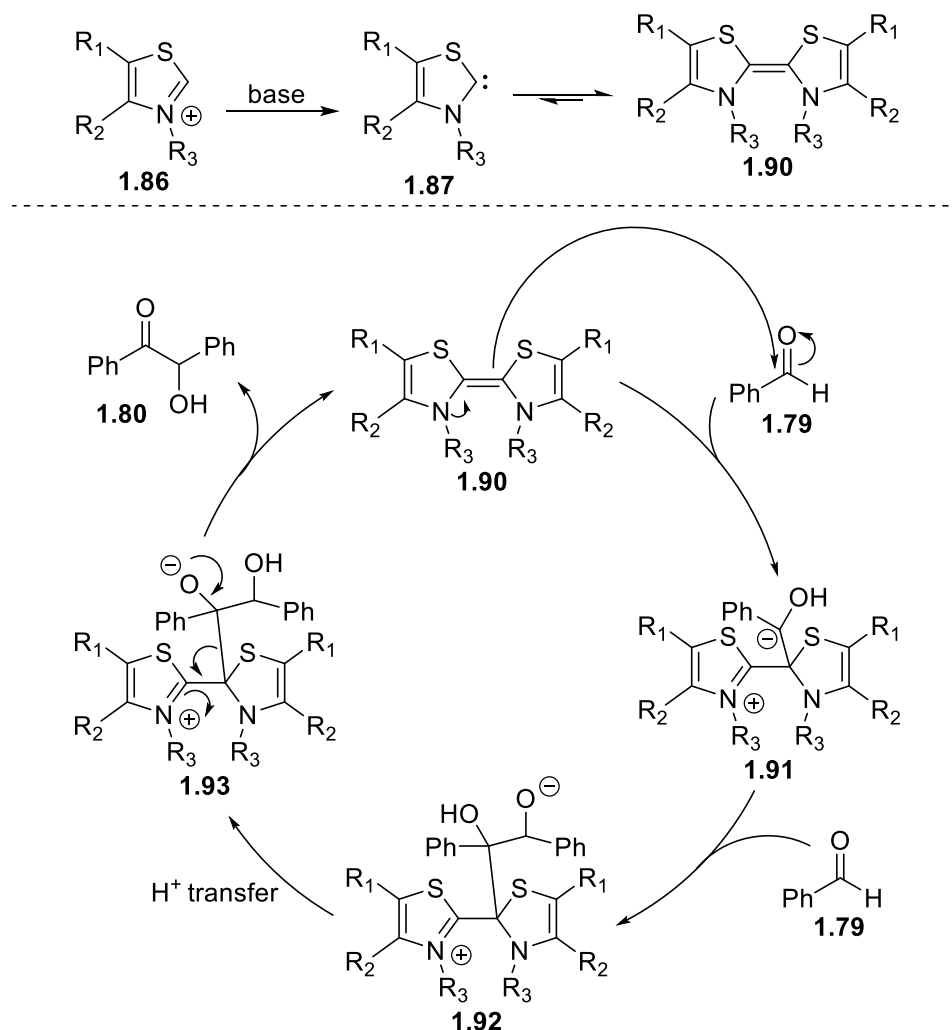


Scheme 1.5: The benzoin condensation.

In Breslow's proposed mechanism, the thiazolium salt **1.86** is deprotonated to form free carbene **1.87**, which then adds in a nucleophilic fashion to a molecule of aldehyde to form tetrahedral intermediate **1.88**. Via base-mediated proton transfer, intermediate **1.88** isomerizes to the key Breslow intermediate **1.84**. This nucleophilic enaminol then attacks another molecule of aldehyde to form intermediate **1.89**, which then collapses to yield benzoin and free catalyst back into the catalytic cycle.

While the catalytic cycle proposed in Scheme 1.5 has become the generally accepted mechanism of the thiazolium-catalyzed benzoin condensation, there has been some debate over the exact structures of the key active intermediates involved. In 1988, López-Calahorra et al.⁴¹ proposed that upon deprotonation of the thiazolium species, the carbene dimerizes to **1.52**, which they propose is the actual active catalyst (Scheme 1.6). If the active catalyst in the benzoin condensation is dimer **1.90**, then the "Breslow intermediate" would be of the form **1.91**, with a formal negative charge on the former carbonyl carbon. Dimers such as **1.90** have been found to be better catalysts than their related carbenes,⁴² which lends some credence to the proposed mechanism. For the mechanism proposed in Scheme 1.6 to be true, the reaction would need to demonstrate second-order behavior in thiazolium salt **1.86**. However, NMR mechanistic studies by Breslow⁴³ showed that the reaction was first order in thiazolium salt **1.86**, and they observed no trace of dimer **1.90** in solution. In addition, Pandit et al.⁴⁴ had previously determined the thiazolium ion-catalyzed benzoin condensation to be first order in thiazolium. In response to these studies, López-Calahorra et al.⁴⁵ performed a mechanistic analysis of their own, and their interpretation of the data led them to conclude that the reaction observes second-order behavior in both aldehyde and thiazolium salt **1.86**. In response to this, Breslow⁴⁶ published a paper with a re-interpretation of López-Calahorra's data, showing that the thiazolium-catalyzed benzoin

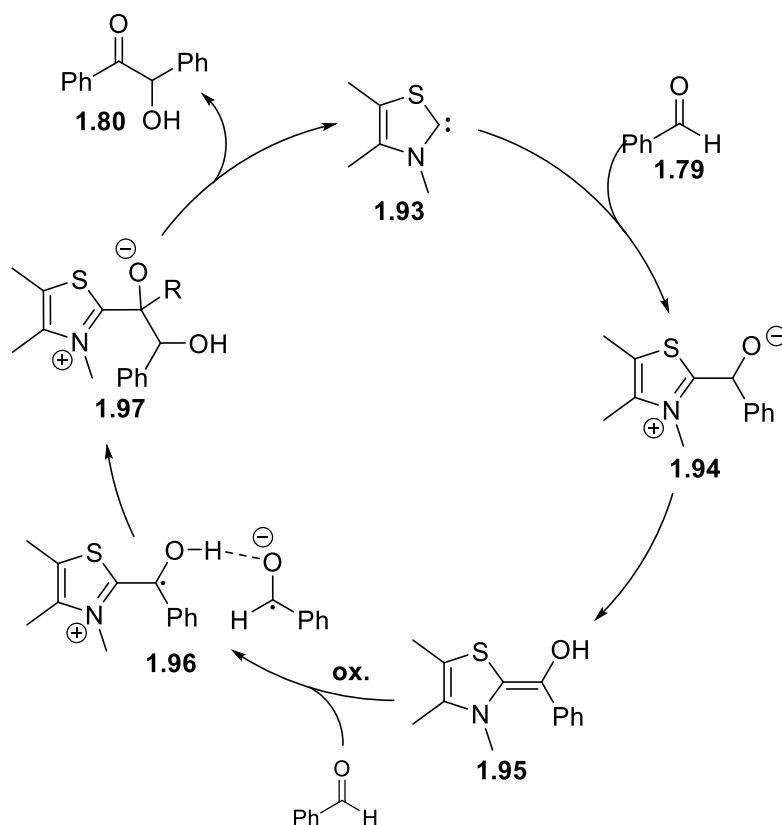
condensation is indeed first order in thiazolium ion, reaffirming Breslow's original proposed mechanism. Since then, the general consensus is that Breslow's mechanism is correct.



Scheme 1.6: López-Calahorra's proposed benzoin condensation mechanism.

In recent years, questions have arisen regarding whether the thiazolium-catalyzed benzoin condensation is a two-electron or single-electron transfer (SET) process. Rehbein et al.⁴⁷ proposed that a radical-pair intermediate **1.96** could be a possible intermediate in the benzoin condensation (Scheme 1.7). An electron paramagnetic resonance (EPR) spectrum of a standard benzoin condensation reaction showed that radical species were indeed present during the

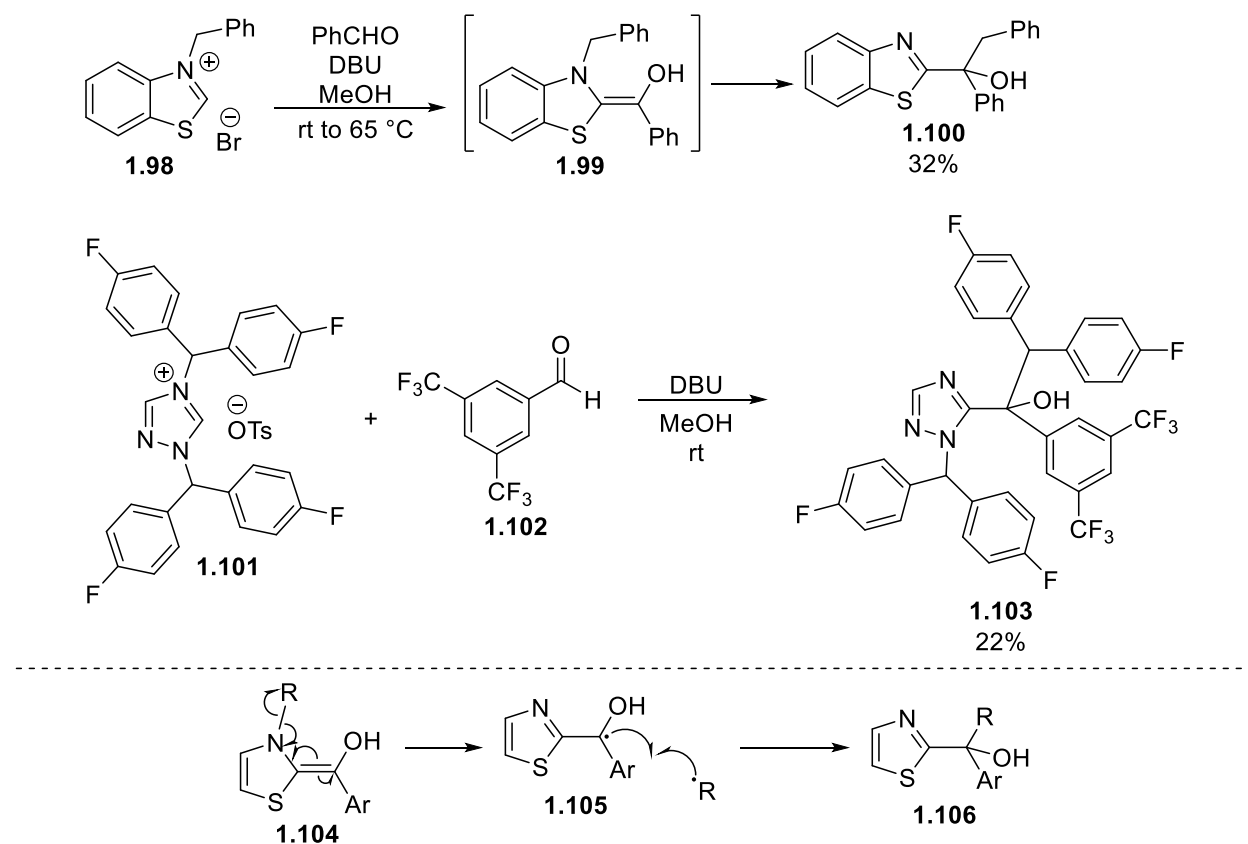
reaction. ^1H NMR spectral evidence also showed that under identical conditions, Breslow intermediate **1.95** and radical pair **1.96** coexisted, possibly in equilibrium. In a follow-up experiment, they prepared an *O*-methylated Breslow intermediate and mixed it with an aldehyde. This mixture was EPR-active, suggesting the formation of radical pair **1.96**, and lending evidence to the hypothesis that Breslow intermediate **1.95** can be formed by homolytic bond cleavage of the benzylic C-H bond in **1.94**. Based on these experiments, they concluded that there is evidence for an alternate mechanism that invokes radical pair **1.96** as a key intermediate, where benzoin is formed by SET radical recombination of **1.96**.



Scheme 1.7: Rehbein's proposed SET mechanism of the benzoin condensation.

The SET mechanism is further supported by the work of McIntosh et al.,⁴⁸ who have recently reported the discovery of radical [1,3]-rearrangements of Breslow intermediates

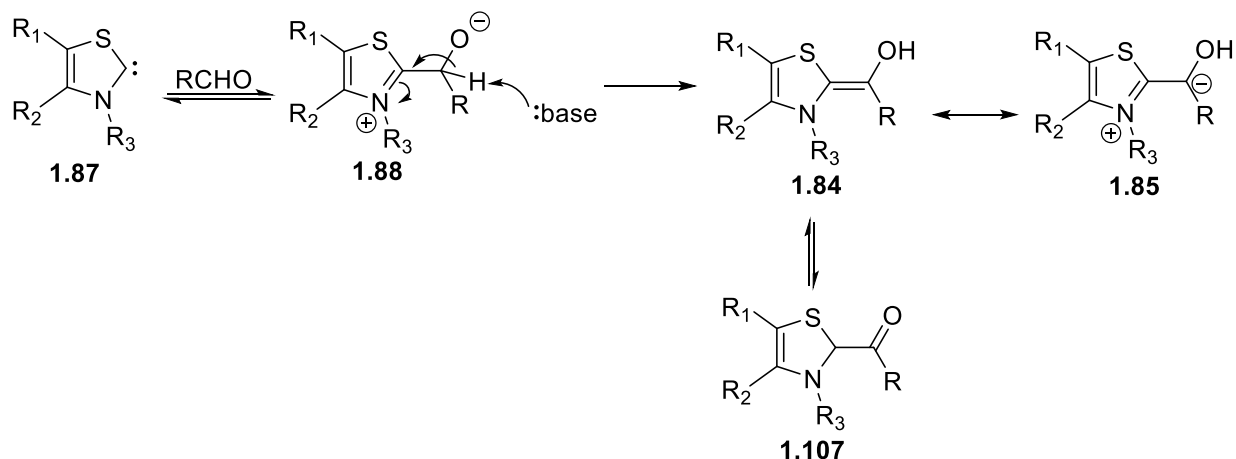
(Scheme 1.8). *N*-benzyl-substituted thiazole and 1,2,4-triazole Breslow intermediates, generated *in situ*, undergo a [1-3]-rearrangement process where the *N*-substituent migrates to the former carbonyl carbon, forming tertiary alcohol products. Based on EPR evidence and computations, they attribute this reaction to occur by spontaneous homolysis of the C-N bond, followed by radical recombination to form the tertiary alcohol. For *N*-diarylmethyl substrates, the enthalpies of homolysis are as low as 6.6 kcal/mol, due to resonance stabilization of the diarylmethyl radical.



Scheme 1.8: Radical [1,3]-rearrangements of Breslow intermediates.

1.1.3.2 The Breslow intermediate

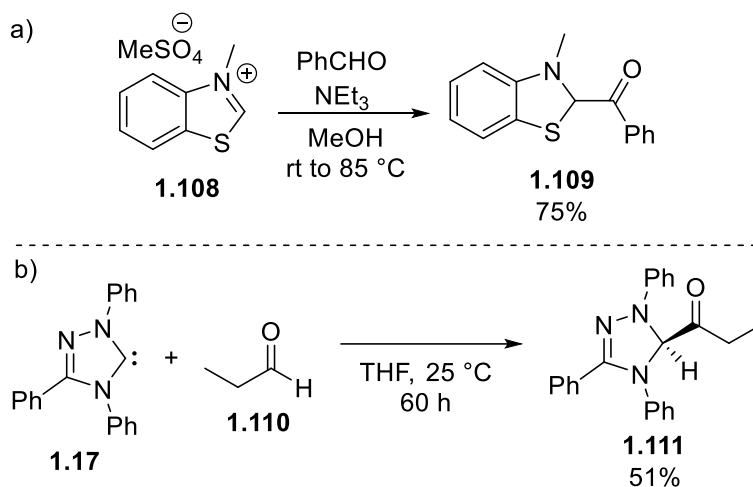
Since Breslow's initial proposal of the Breslow intermediate, he and other researchers have made attempts at isolating the Breslow intermediate and its analogues. Breslow's early attempts to isolate the Breslow intermediate from benzoin condensation reaction conditions proved to be unsuccessful, presumably due to its labile nature and reactivity. Formation of the Breslow intermediate is reversible, and since it is an enol, the Breslow intermediate exists in equilibrium with its keto tautomer (Scheme 1.9). These properties of the Breslow intermediate have made it a challenging compound to isolate and characterize; however, success has been achieved in the isolation and characterization of structural analogues of the Breslow intermediate.



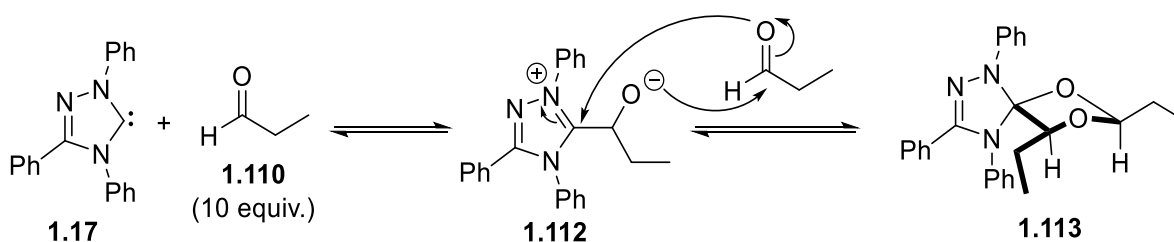
Scheme 1.9: Generation, resonance forms, and tautomers of the Breslow intermediate.

Early work by Jordan et. al reported the first synthesized structural analogues of the Breslow intermediate and studies of their physical properties.⁴⁹ Their work provided strong evidence that the neutral resonance structure **1.84** was a predominant contributor for any thiamine-bound intermediate. In 1964, Metzger reported on the synthesis of the keto-tautomer of

the Breslow intermediate from the condensation of benzaldehyde with a benzothiazolium salt⁵⁰ (Scheme 1.10a). More recently, Berkessel et. al reported on the synthesis and isolation of a triazolium-derived keto-tautomer of the Breslow intermediate⁵¹ (Scheme 1.10b). Their attempts to generate the Breslow intermediate or an *O*-silylated Breslow intermediate were unsuccessful. However, in that same work, they found that the resting state for that system under catalytic conditions was a spirocyclic dioxolane **1.113**, resulting from the condensation of the carbene with two molecules of aldehyde. The observation of this resting state also illustrates the electrophilic nature of the former carbene atom in the initial carbene-aldehyde adduct **1.112**.



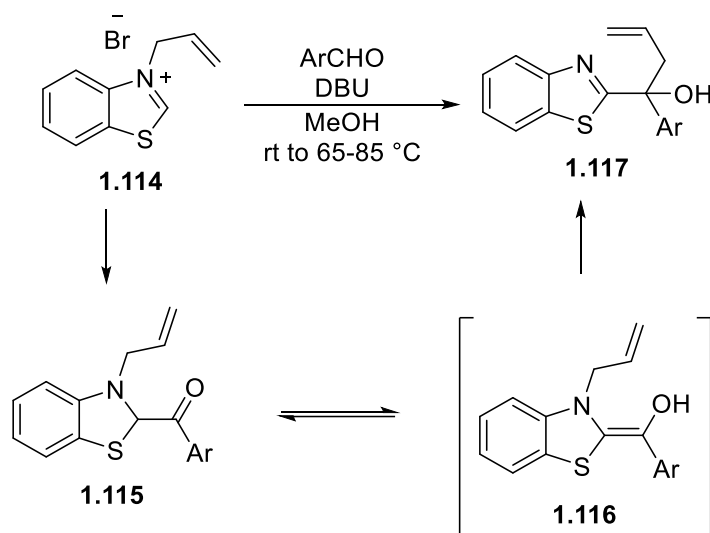
Scheme 1.10: Synthesis of keto-Breslow intermediates by a) Metzger and b) Berkessel.



Scheme 1.11: Formation of spirocyclic dioxolane resting state by Berkessel.

Electrophilic and nucleophilic trapping of transient intermediates is a common practice used to provide evidence for the existence of those intermediates. To date, there has been only

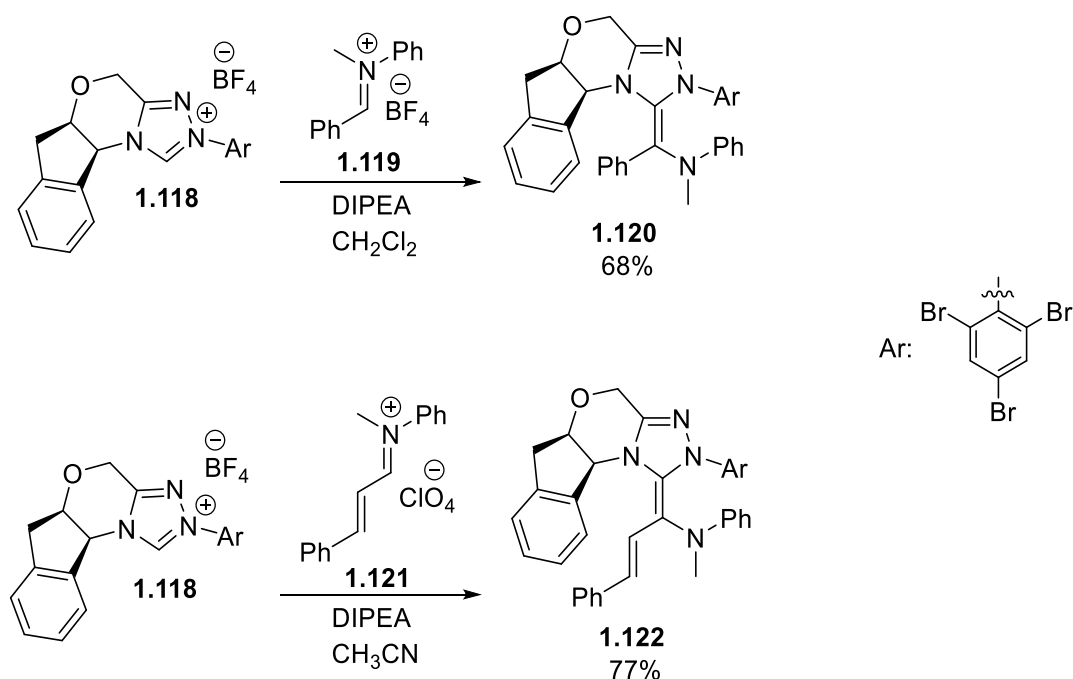
one example of such a strategy being used to indirectly confirm the existence of the Breslow intermediate. By using an *N*-allyl benzothiazolium salt, McIntosh's group was able to capture generated Breslow intermediates *in situ* via a thermal Claisen rearrangement⁵² (Scheme 1.12). They found that the reaction was specific to aromatic aldehydes, and that electron-poor aldehydes reacted faster than their electron-rich or electron-neutral counterparts.



Scheme 1.12: Trapping of Breslow intermediates via a thermal Claisen rearrangement.

In 2012, Rovis' group was successful in synthesizing, isolating, and characterizing the first Breslow intermediate analogue⁵³ (Scheme 1.13). They postulated that aldehyde-derived Breslow intermediates were difficult to isolate due to the relative acidity of the enol functionality. By replacing the aldehyde electrophile with an electronically similar but chemically different iminium species, the -OH functionality was replaced with a more stable -NR₂ functionality. Another design consideration was crystallinity of the isolated product, so they chose a sterically hindered catalyst to increase the chances of isolating a crystalline product. Acyl anion equivalent **1.120** was isolated in 68% yield, and homoenolate equivalent **1.122** was isolated in 77% yield. They demonstrated that **1.120** was a catalytically relevant species by

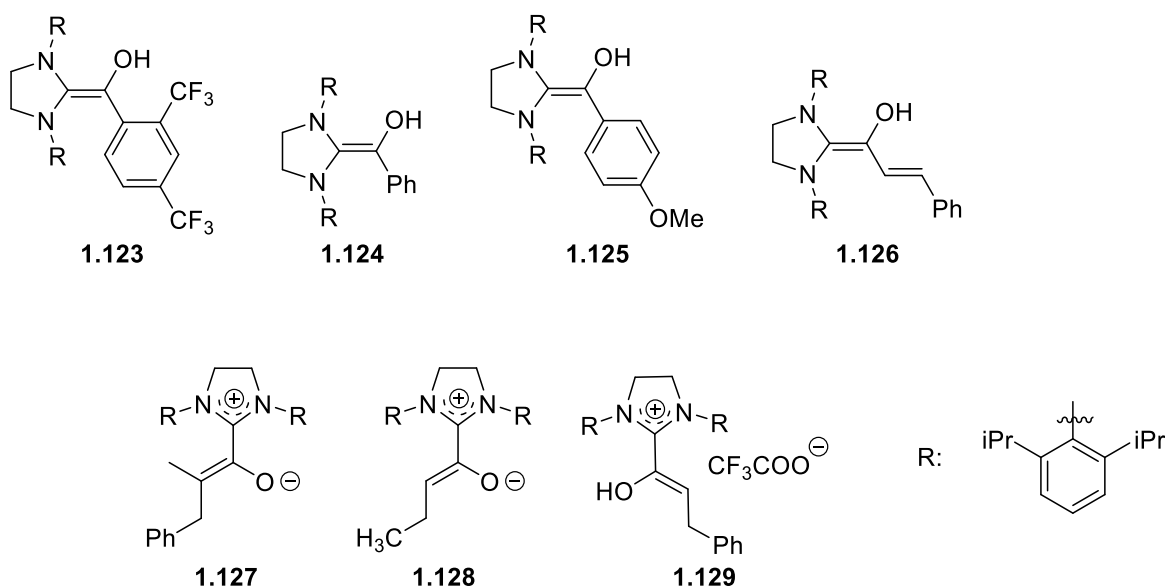
adding 10 mol% with 10 mol% acetic acid, and observing 99% yield in an intramolecular Stetter reaction. The homoenolate activity of **1.122** was confirmed by subjecting it to a deuterium source, and they observed full deuterium incorporation at the γ -position.



Scheme 1.13: Aza-Breslow analogues prepared and characterized by Rovis's group.

A year later, Berkessel et. al were successful in preparing, isolating, and characterizing by NMR and X-ray diffraction a variety of Breslow intermediates, homoenolate equivalents, and azolium enolates, derived from a saturated imidazolidyl carbene⁵⁴ (Scheme 1.14). Reaction monitoring experiments showed that the Breslow intermediate is rapidly formed, and then gradually converts to the azolium enolate. Unlike in Rovis' study, the prepared Breslow intermediates and azolium enols were not subjected to reaction conditions, and so the specific catalytic activity is unknown. Compared to 1,2,4-triazolium carbene precursors, imidazolinium precursors are not widely used in NHC organocatalysis, due to much higher activities exhibited by 1,2,4-triazolyl carbenes. It is plausible that the Breslow intermediates and azolium enols

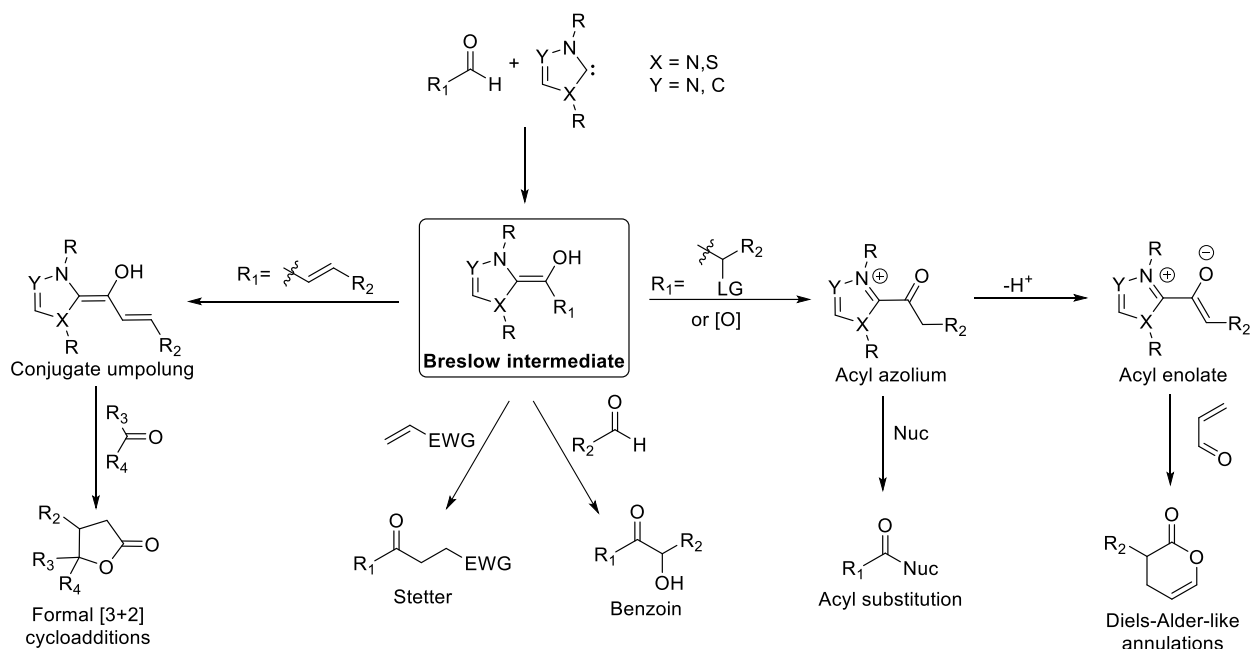
isolated by Berkessel et. al were able to be isolated because of these reactivity differences; imidazolinium-derived Breslow intermediates could simply be more prone to isolation. Both of these studies provide a strong structural basis for the mechanistic analysis of NHC-catalyzed α^1 - α^3 - α^3 umpolung, and validate Breslow's original mechanistic proposal.



Scheme 1.14: Catalytic intermediates prepared and characterized by Berkessel et. al.

1.1.4 Reactions catalyzed by NHCs

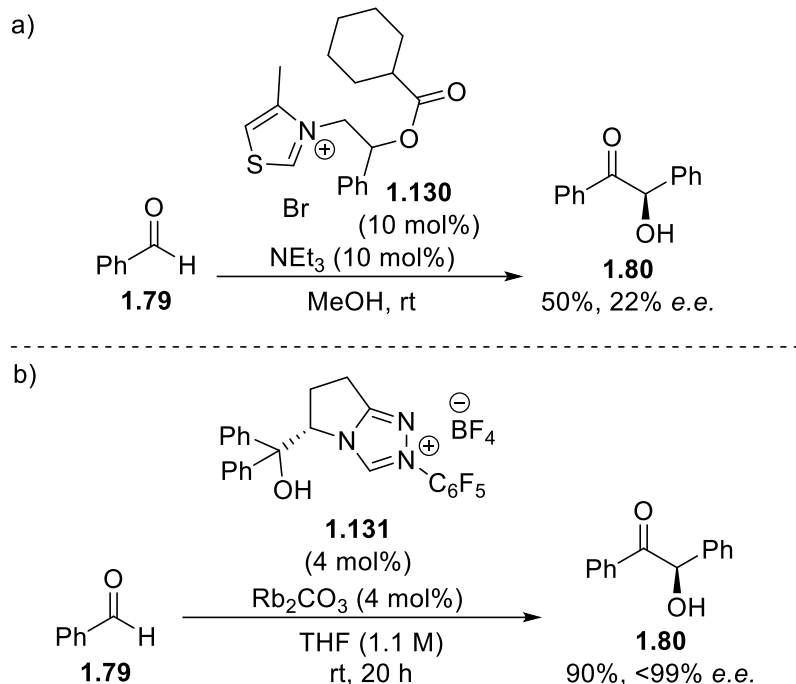
Breslow's benzoin condensation mechanism and the key intermediates he proposed provide a foundation for the major modes of NHC reactivity. From the Breslow intermediate, and depending on reaction conditions and catalyst choice, different pathways can be taken, resulting in a diverse array of products that can be formed under the umbrella of "NHC catalysis" (Scheme 1.15). Such reactions include the asymmetric benzoin reaction, Stetter reaction, reactions involving homoenolates/extended Breslow intermediates, and reactions involving acylazolium intermediates.



Scheme 1.15: Possible NHC reaction pathways from the Breslow intermediate.

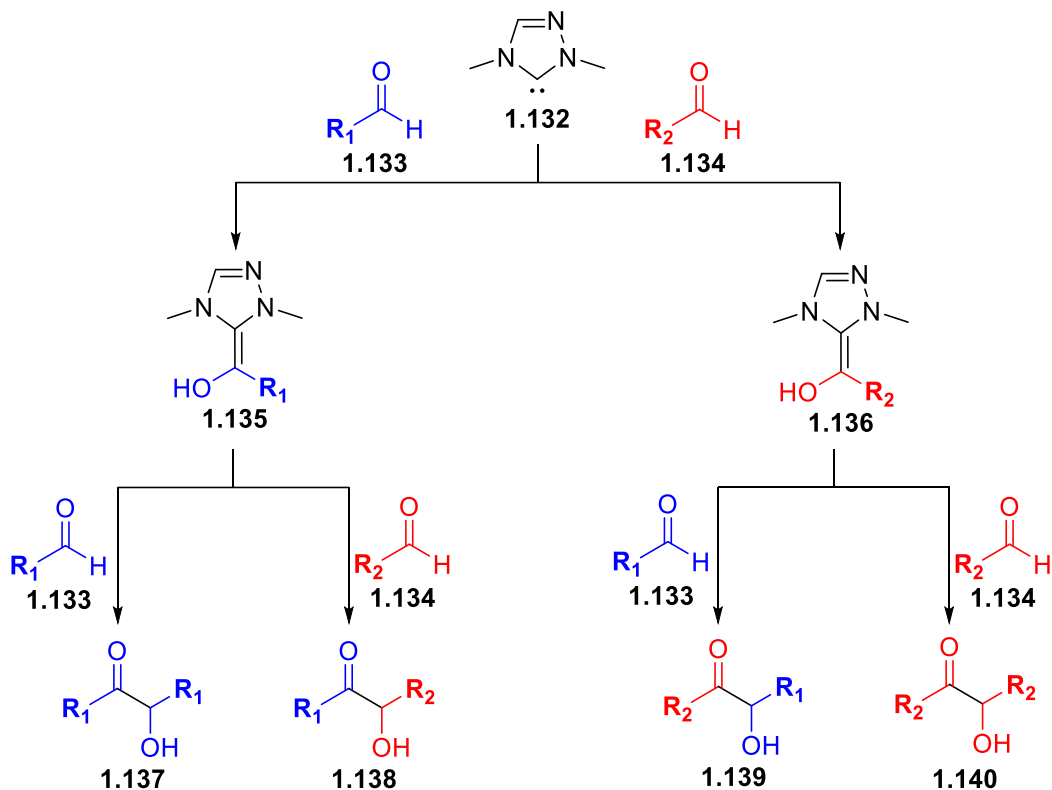
1.1.4.1 The asymmetric benzoin and cross-acyloin condensations

The benzoin reaction, first reported by Wohler and Liebig³⁸ in 1832, is the condensation of two molecules of benzaldehyde to produce an α -hydroxy ketone. Originally catalyzed by cyanide, Ukai et. al discovered that thiazolium salts could also catalyze the benzoin condensation.⁴⁰ The product of the benzoin condensation is an α -hydroxyketone containing a stereogenic center adjacent to the carbonyl. As a result, many chemists have worked towards developing an enantioselective benzoin condensation. The first example of an enantioselective benzoin condensation was reported by Sheehan and Hunneman in 1966, utilizing a chiral thiazolium catalyst, achieving 50% yield and 22% *e.e.*⁵⁵ Since then, many improvements have been made both on yield and enantioselectivity, but Cannon and Zeitler's 2009 report⁵⁶ remains as one of the most efficient enantioselective benzoin condensations: >99% *e.e.* and 90% yield.



Scheme 1.16: a.) The first report of an asymmetric benzoin condensation. b.) Cannon and Zeitler's enantioselective benzoin condensation.

The cross-benzoin and cross-acyloin condensations are another widely studied class of benzoin condensation reactions. In the cross-benzoin condensation, both aldehydes are aromatic; in the cross-acyloin condensation, at least one of the aldehydes is aliphatic. The intermolecular condensation of two aldehydes can potentially give four possible products: two homo- and two cross-benzoin/acyloin products (Scheme 1.17).

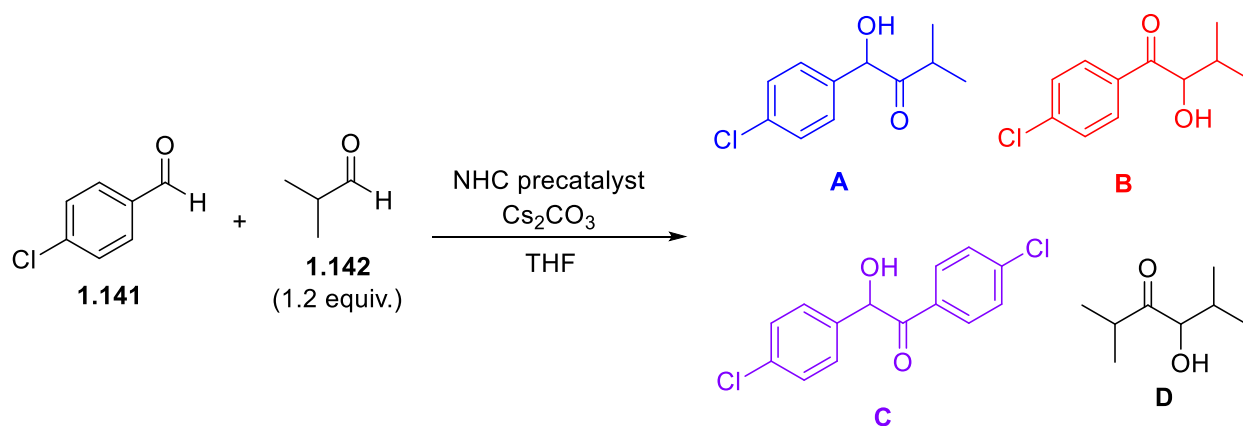


Scheme 1.17: Possible products in the cross-benzoin condensation.

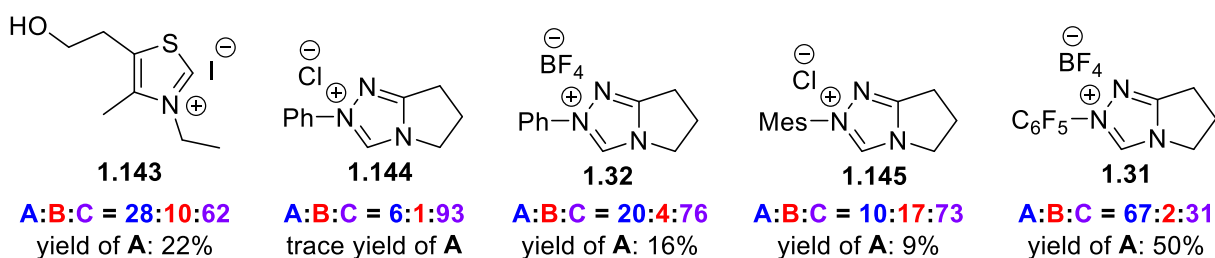
There are two main challenges in controlling this reaction: ensuring the carbene catalyst preferentially attacks one aldehyde over the other, and for the Breslow intermediate to preferentially attack the second aldehyde. In cross-benzoin products, the functionality adjacent to the carbonyl comes from the aldehyde that was attacked by the carbene, and the functionality adjacent to the alcohol comes from the aldehyde that was attacked by the Breslow intermediate. To ensure that the generated Breslow intermediate attacks the desired second aldehyde, a large excess (10-15 equiv.) of second aldehyde is often included in the reaction.^{57,58} This method works when the excess aldehyde is readily available, but can be problematic if it is a specialty chemical or the product of a multi-step synthesis.

In the cross-benzoin and cross-acyloin condensations, proper catalyst choice plays a significant role in determining the major product. The azolium core, *N*-substituent, and even

counterion of the catalyst can play a role in determining relative product ratios. Scheme 1.18 shows an example of divergent selectivities between thiazolium and 1,2,4-triazolium salt catalyst precursors in the cross-acyloin condensation of an aromatic and aliphatic aldehyde.⁵⁸ This reaction produces four possible products: cross-acyloin products **A** and **B**, and homo-acyloin products **C** and **D**. Of all the azolium salts tested, none of them produced homo-acyloin product **D**. Thiazolium salt **1.143** and 1,2,4-triazolium salts **1.31**, **1.32**, **1.144**, and **1.145** all favor product **C**, but to different extents. Even among NHC precursors of the same class, the differences in selectivity can be significant. Comparing triazoliums **1.144** and **1.32**, switching the counterion from tetrafluoroborate to chloride results in an approximately 20% increase in selectivity, and chloride salt **1.144** gives almost exclusively product **C**. The *N*-substituent plays a significant role as well in determining relative product ratios. *N*-mesityl-substituted NHC precursor **1.145** exhibits similar selectivities as *N*-phenyl-substituted NHC precursor **1.32**. *N*-C₆F₅-substituted NHC precursor **1.31**, however, shows a preference for product **A**.



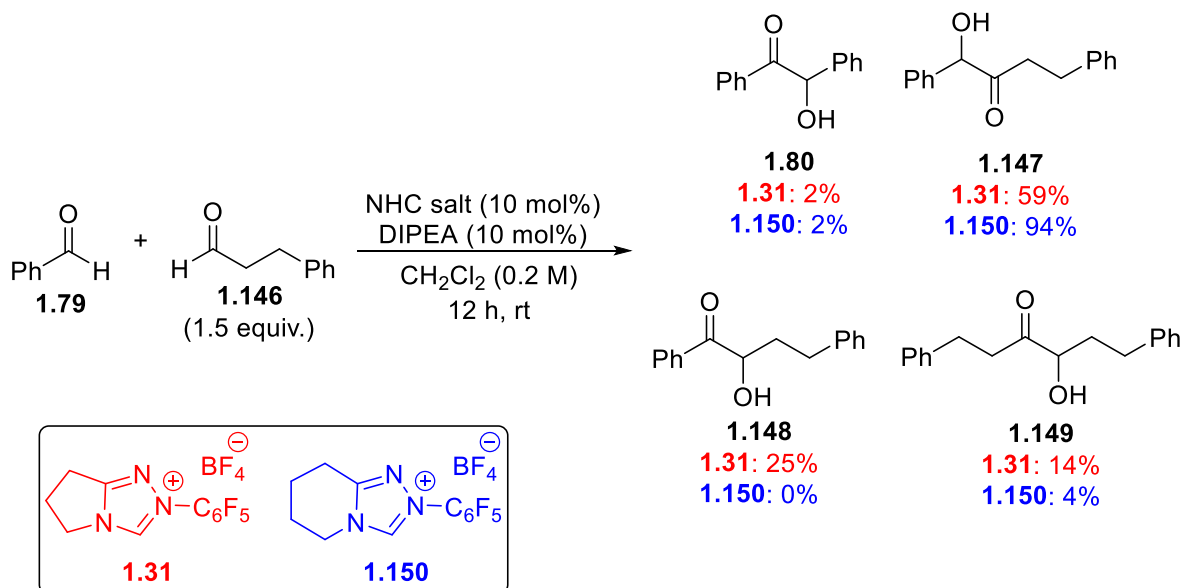
NHC precatalysts:



Scheme 1.18: Divergent selectivities between thiazolium and 1,2,4-triazolium salt NHC catalyst precursors in the cross-acyloin condensation.⁵⁸

Gravel's group was able to greatly enhance selectivity in the cross-benzoin condensation simply by expanding the fused ring of the triazolium salt precatalyst by one carbon.⁵⁹ Scheme 1.19 shows an excerpt from their catalyst optimization experiments. Catalyst **1.31**, which is generally regarded as a superior benzoin condensation catalyst, shows a preference for cross-benzoin products, but the selectivity between the two is poor. Catalyst **1.150**, on the other hand, shows exceptional selectivity for only one cross-benzoin product, with only 6% homo-benzoin product. This reaction is also performed with only 1.5 equivalents of the second aldehyde, which is a large improvement over the 10 equivalents previously used. Crossover experiments also showed that the chemoselective reaction was under kinetic control, as subjecting benzoin and

hydrocinnamaldehyde to the reaction conditions did not result in any cross-benzoin product being formed.

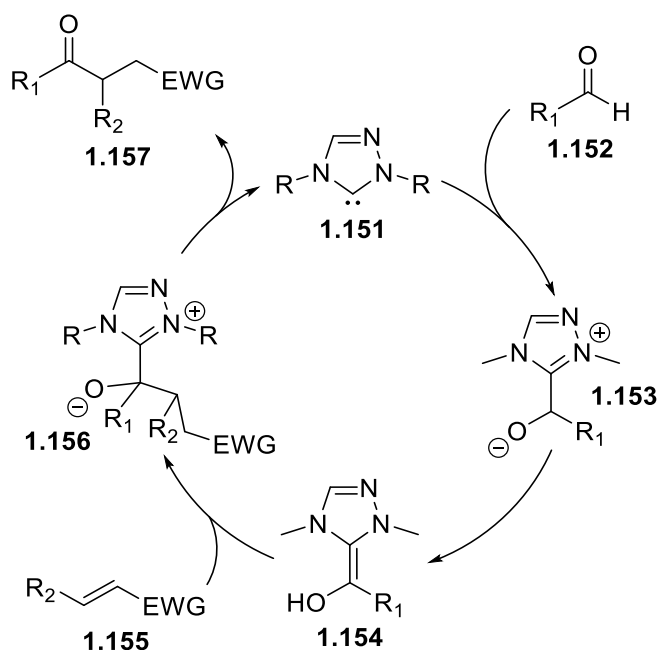


Scheme 1.19: Enhanced chemoselectivity in the cross-benzoin reaction reported by Gravel's group.

1.1.4.2 The Stetter reaction

The Stetter reaction is the NHC-catalyzed umpolung of aldehydes with electrophilic carbon-carbon bonds (Michael acceptors). It is similar to the benzoin condensation in that the Breslow intermediate directly attacks the Michael acceptor. Like the benzoin condensation, the Stetter reaction was first discovered to be catalyzed by the cyanide ion,⁶⁰ and then later found to be catalyzed by thiazolium salts in the presence of base.⁶¹ The products of the Stetter reaction are 1,4-bifunctional compounds such as γ -ketones, γ -ketonitriles, and γ -ketoesters, synthetically useful intermediates which can be challenging to construct via more traditional methods. The electrophilic coupling partners used in the Stetter reaction often have electron-withdrawing groups to allow for nucleophilic attack by the Breslow intermediate, but recently some groups

have shown that unactivated alkenes can work in the reaction.⁶² The original work by Stetter in the 1970s dealt with the symmetric intermolecular variant, and it wasn't until 1995 that a general intramolecular Stetter reaction was reported by Ciganek,⁶³ with an enantioselective variant reported by Enders the following year.⁶⁴

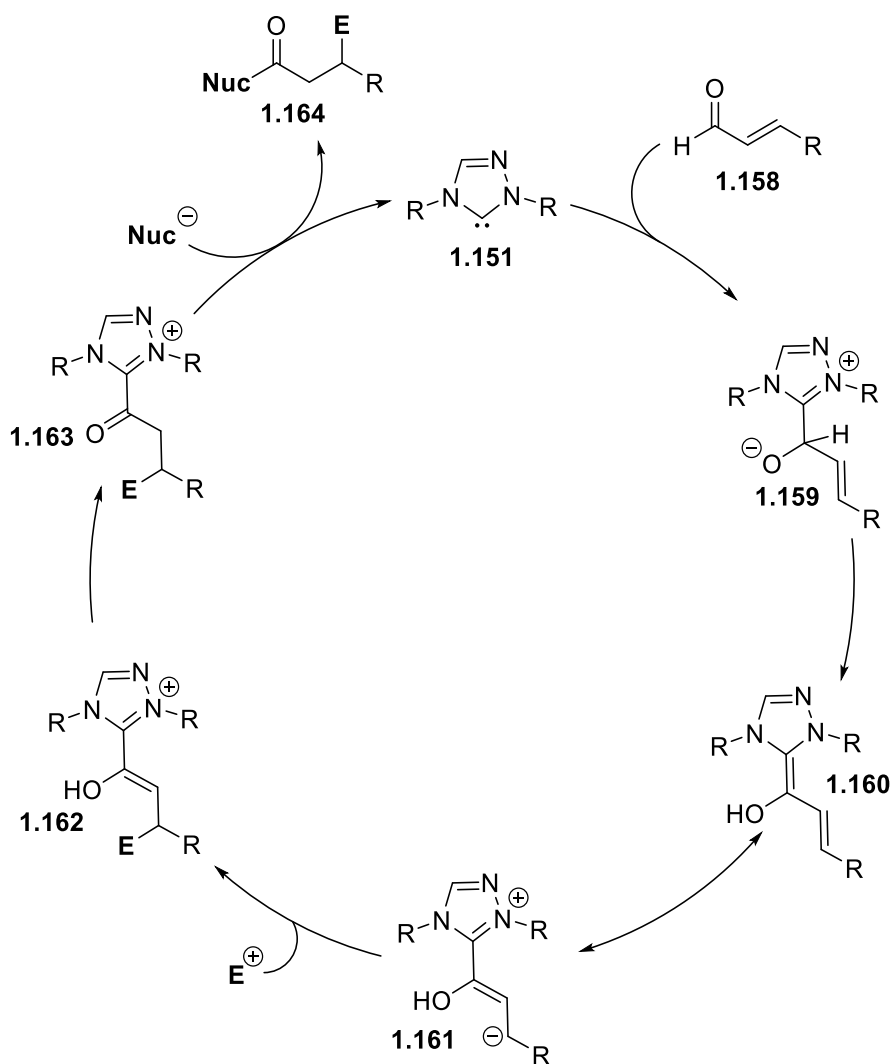


Scheme 1.20: Mechanism of the Stetter reaction.

The mechanism for the Stetter reaction is shown in Scheme 1.20. Similar to the benzoin reaction, the free carbene catalyst **1.151** attacks aldehyde substrate **1.152**, forming a tetrahedral adduct **1.153** which isomerizes to the Breslow intermediate **1.154**. Instead of another aldehyde substrate, the Breslow intermediate then attacks an activated alkene **1.155** to give adduct **1.156**. From this adduct, the carbonyl is re-formed, and product **1.157** and free carbene catalyst are released.

1.1.4.3 A³-d³ umpolung: extended Breslow intermediates

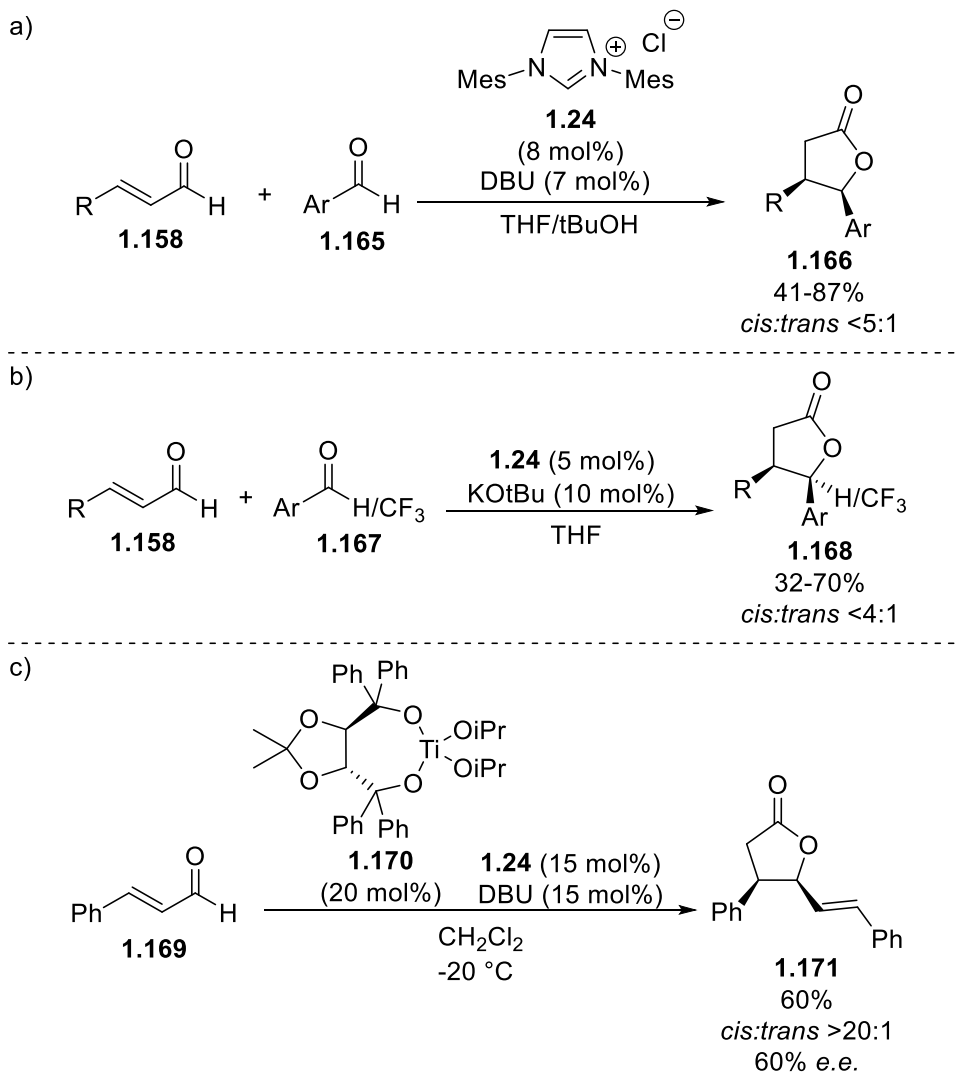
When an α,β -unsaturated aldehyde is employed as an electrophile in NHC catalysis, new avenues of reactivity are opened up. The β -position of the aldehyde, originally a potential electrophilic Michael acceptor, undergoes a polarity inversion and becomes a unique nucleophilic site in an a³ to d³ umpolung (also called conjugate umpolung). The final result of this polarity inversion is a β -functionalized carbonyl compound. The prototypical mechanism for this type of activity is given in Scheme 1.21. The carbene **1.151** attacks the carbonyl of α,β -unsaturated aldehyde **1.158**, forming tetrahedral intermediate **1.159**. This tetrahedral intermediate undergoes proton transfer to give conjugated Breslow intermediate **1.160**, commonly called an “extended” Breslow intermediate or homoenolate equivalent. The extended Breslow intermediate **1.160** is in resonance with zwitterionic **1.161**, which has a formal negative charge at the formerly β -carbon; these resonance structures help to demonstrate the nucleophilic nature of that carbon. The extended Breslow intermediate/homoenolate equivalent then attacks an electrophile giving enol azolium **1.162**, which tautomerizes to acyl azolium **1.163**. This is then captured by a nucleophile, releasing product **1.164** and regenerating the carbene catalyst.



Scheme 1.21: Prototypical mechanism for reactions involving an extended Breslow intermediate.

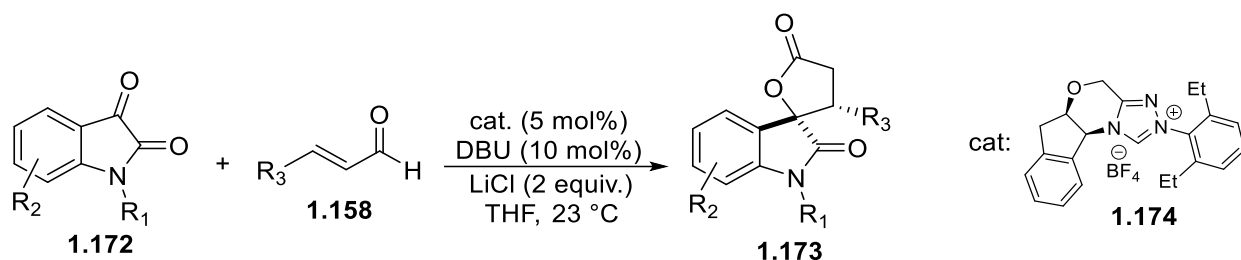
The first examples of NHC-catalyzed conjugate umpolung were reported independently in 2004 by Bode⁶⁵ and Glorius⁶⁶ (Scheme 1.22a & b). Using bis-mesityl-substituted imidazolium precatalyst **1.24** (commonly referred to as IMes), both researchers were able to catalyze the annulation of α,β -unsaturated aldehydes with aromatic aldehydes, selectively producing γ -butyrolactones, instead of homo- or cross-benzoin products. Glorius extended the scope of the reaction by demonstrating that aryl trifluoromethyl ketones act as electrophiles in the reaction, generating a quaternary carbon stereocenter. In addition, Glorius found that utilizing a chiral

imidazolium salt precatalyst resulted in stereoselective products up to 25% *e.e.* Scheidt's group improved on the enantioselectivity of this reaction by incorporating a chiral Lewis acid to act cooperatively with the NHC catalyst⁶⁷ (Scheme 1.22). By employing chiral Ti-TADDOL (**1.170**) and achiral IMes, they were able to achieve chiral γ -butyrolactone **1.171** in 60% yield, with >20:1 dr and 60% *e.e.*



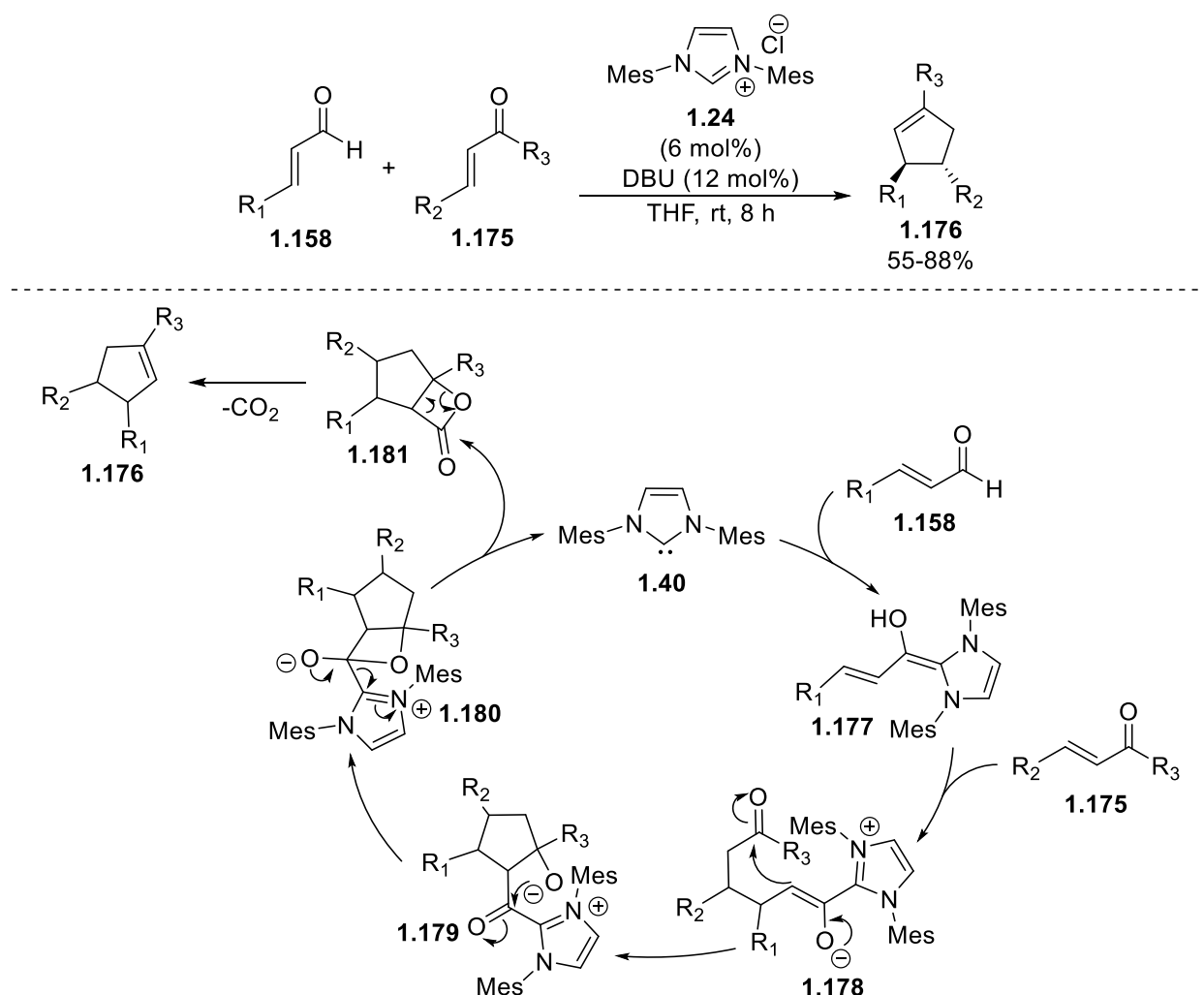
Scheme 1.22: Synthesis of γ -butyrolactones by NHC homoenolate catalysis. a) Bode's first report of NHC homoenolate activity.⁶⁵ b) Glorius's simultaneous report of NHC homoenolate activity⁶⁶. c) Schiedt's improvement of γ -butyrolactone enantioselectivity by NHC/Lewis acid cooperative catalysis.⁶⁷

In NHC-catalyzed homoenolate reactions, the choice of electrophile is not limited to other aldehydes. Nair et. al demonstrated that 1,2-dicarbonyl compounds such as cyclohexanedione and isatins reacted with homoenolate equivalents to give spirocyclic γ -butyrolactones in up to 98% yield, albeit with low diastereoselectivity.⁶⁸ Scheidt's group improved upon this reaction by employing cooperative Lewis acid catalysis with a chiral NHC, achieving up to 20:1 diastereoselectivity and 91% *e.e.* in 86% yield.⁶⁹ They also improved upon the scope of the reaction, showing that a wide range of aldehydes and isatins could be employed in the reaction (Scheme 1.23).



Scheme 1.23: Synthesis of spirocyclic γ -butyrolactones by NHC-catalyzed homoenolate addition to isatins.

Nair et. al also demonstrated that chalcones are efficient electrophilic annulation partners with homoenolates.⁷⁰ However, instead of the expected cyclopentanone products, they found that 3,4-*trans*-disubstituted cyclopentenones were the only products formed (Scheme 1.24).

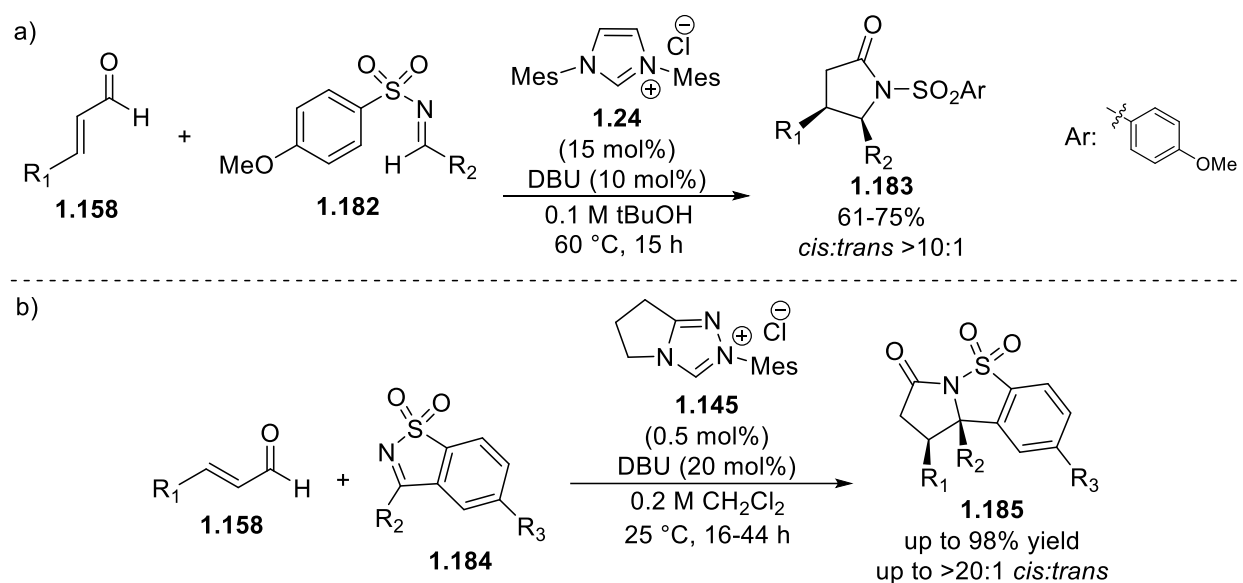


Scheme 1.24: Synthesis and proposed mechanism of *trans*-cyclopentenones by NHC-catalyzed homoenolate addition to chalcones.

They propose that instead of cyclization to the expected cyclopentanone, the NHC homoenolate equivalent annulates with the chalcone to form a bicyclic β -lactone, which undergoes a [2+2]-cycloreversion, ejecting CO₂ and forming the observed cyclopentene.

Bode's group showed that γ -lactams could be made by annulation of the homoenolate equivalent with *N*-sulfonylimines, producing products in ratios of *cis*:*trans* up to 10:1⁷¹ (Scheme 1.25a). However, this reaction is limited to *N*-4-methoxybenzenesulfonyl imines. Three years

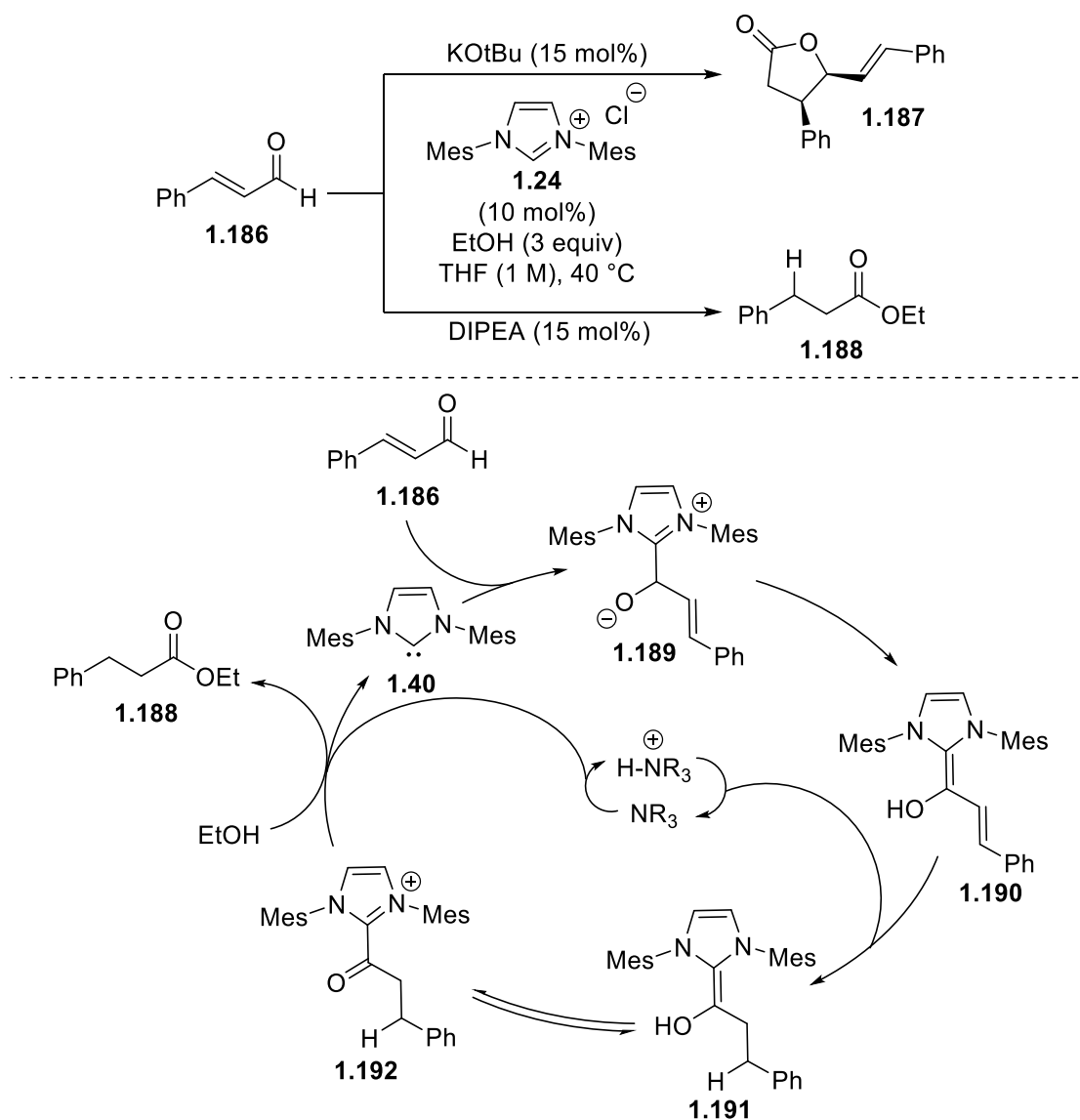
later, Bode's group then reported that cyclic sulfonyl ketimines were superior electrophiles in the reaction, giving high yields and diastereoselectivities⁷² (Scheme 1.25b). This report was also the first time a triazolium precatalyst was employed in homoenolate addition, and catalyst loading was as low as 0.5%.



Scheme 1.25: a) Bode's synthesis of γ -lactams via homoenolate addition to *N*-sulfonylimines. b) Bode's use of cyclic ketimines as superior electrophiles.

When the homoenolate equivalent **1.160** is generated, there are two general possibilities of electrophile that it can react with. The homoenolate can react with an sp^2 electrophile as described above, or simply be protonated at the β -position, generating a saturated acyl azolium species. Bode's group found that the choice of base is crucial in determining which pathway the homoenolate reacts.⁷³ They found that when strong bases such as KOtBu or DBU are used, protonation of the homoenolate equivalent is disfavored and the expected lactone products are formed. When a weaker amine base is used, such as triethylamine or DIPEA, protonation of the homoenolate is favored, resulting in a saturated acyl azolium species that can be trapped by an

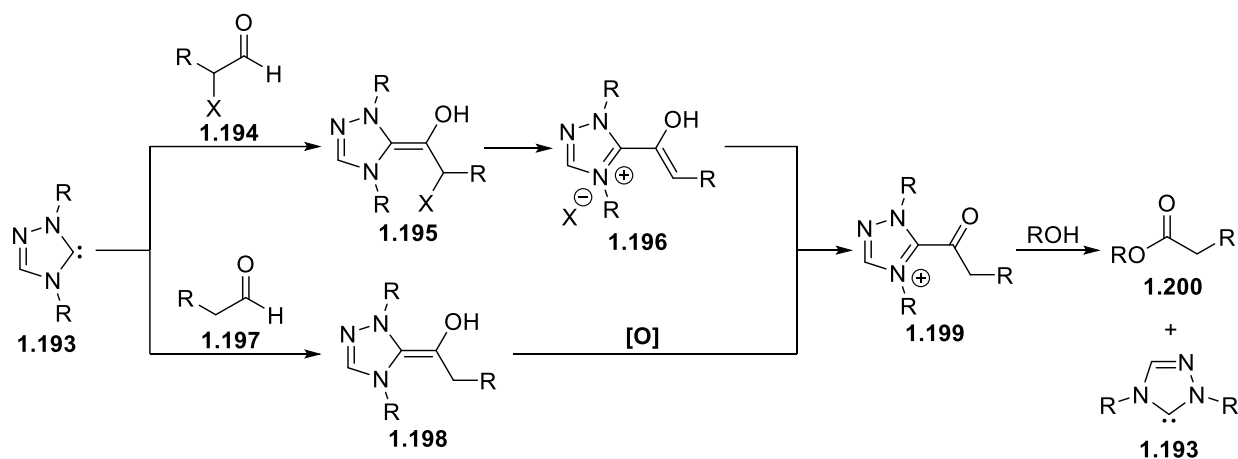
alcohol nucleophile, resulting in a redox esterification of the starting aldehyde (Scheme 1.26). They postulate that the low pK_a of the conjugate acid of the amine base allows for reversible deprotonation, and for the base to act as a catalytic proton shuttle. Stronger bases irreversibly deprotonate the azolium, favoring carbon-carbon bond formation over homoenolate protonation.



Scheme 1.26: Choice of base determines product formation in homoenolate NHC catalysis.

1.1.4.4 Acyl azolium catalysis

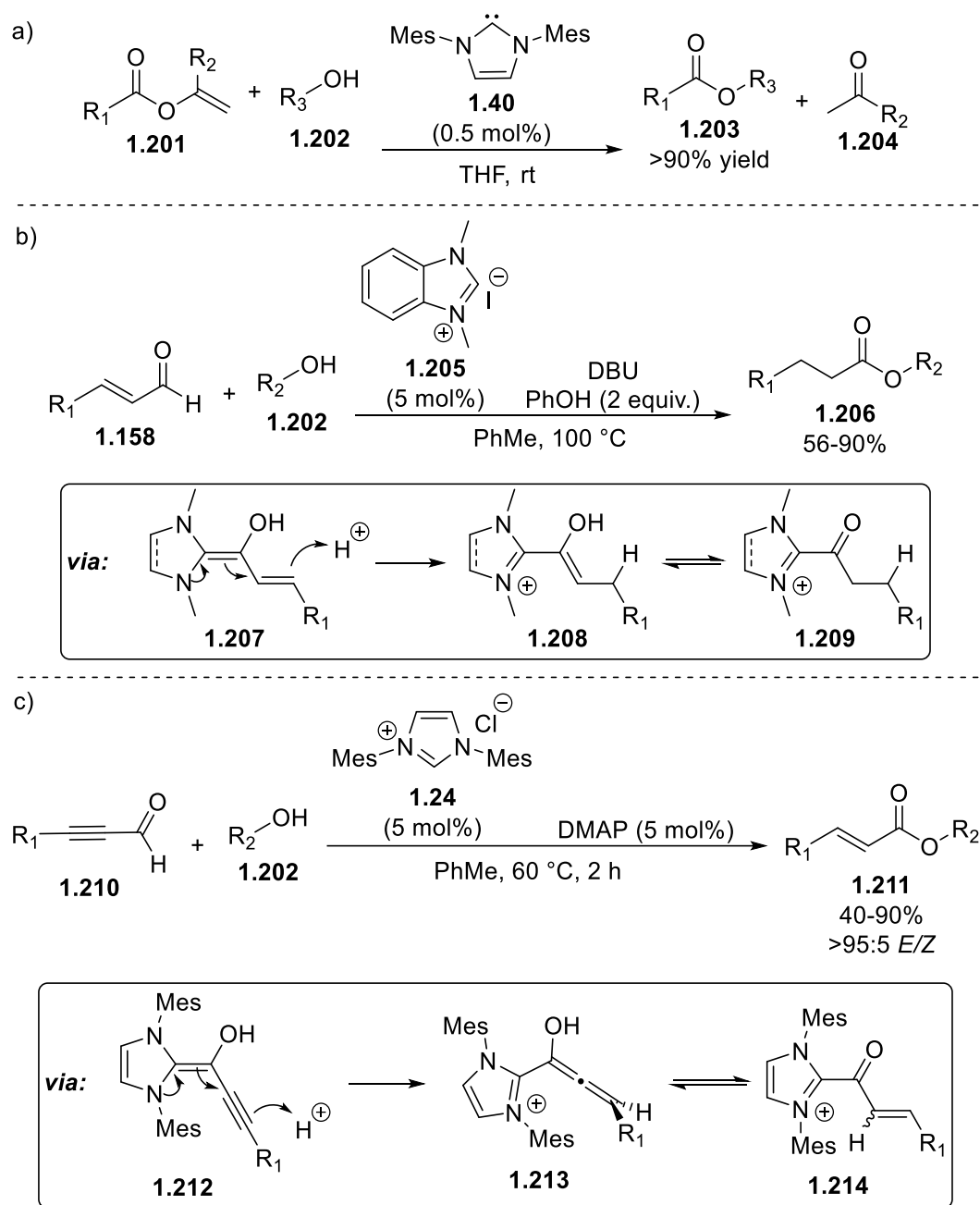
In addition to being efficient umpolung catalysts, NHCs also exhibit competency in non-umpolung processes. The most prevalent of these processes involve the generation of an acyl azolium intermediate, where the NHC acts as a superior leaving group, activating the carbonyl for attack by a nucleophile. The acyl azolium can be accessed via an internal redox reaction of aldehydes with α -leaving groups, or by oxidation of the Breslow intermediate by an external oxidant (Scheme 1.27). Once the acyl azolium is generated, it is captured by a nucleophile, usually an alcohol, to give ester products and regenerate the catalyst.



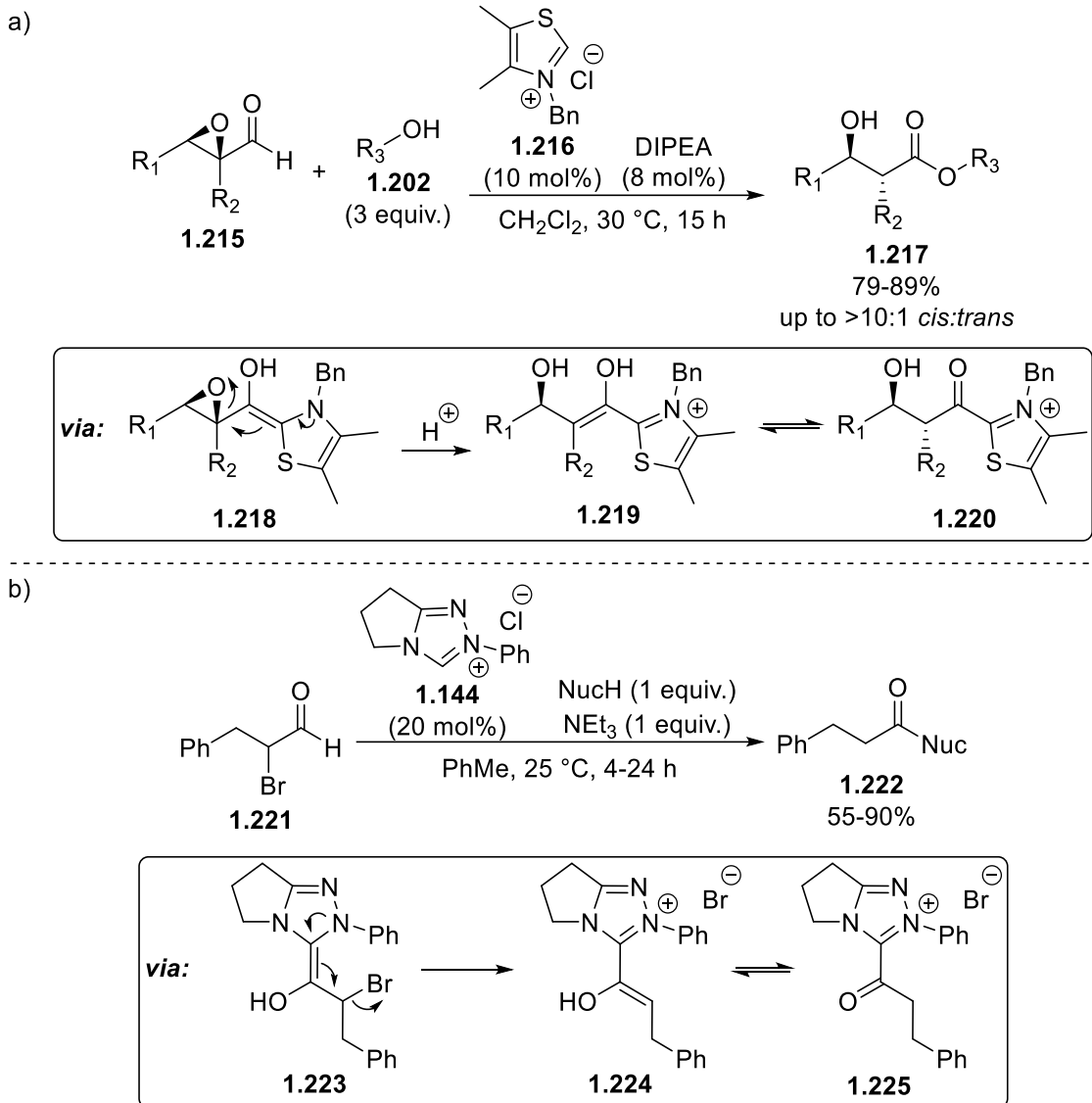
Scheme 1.27: Different methods of accessing acyl azolium intermediates.

As early as 2003, NHCs were reported to facilitate the transesterification of simple esters with primary alcohols, via an acyl azolium intermediate⁷⁴ (Scheme 1.28a). In 2005, Scheidt's group reported the synthesis of saturated esters from α,β -unsaturated aldehydes, generating the acyl azolium intermediate via β -protonation of the NHC-bound homoenolate equivalent⁷⁵ (Scheme 1.28b). Zeitler showed that when alkynyl aldehydes are used as substrates, the β -position can be protonated to give an α,β -unsaturated acyl azolium intermediate, giving α,β -unsaturated esters in high *E/Z* stereoselectivities⁷⁶ (Scheme 1.28c). Bode's group has shown that

chiral formylcyclopropanes and epoxy aldehydes provide a unique intramolecular redox handle to access chirally diverse esters^{77,78} (Scheme 1.29a). Rovis's group has demonstrated that α -haloaldehydes give access to the acyl azolium intermediates, and saturated esters as final products⁷⁹ (Scheme 1.29b).



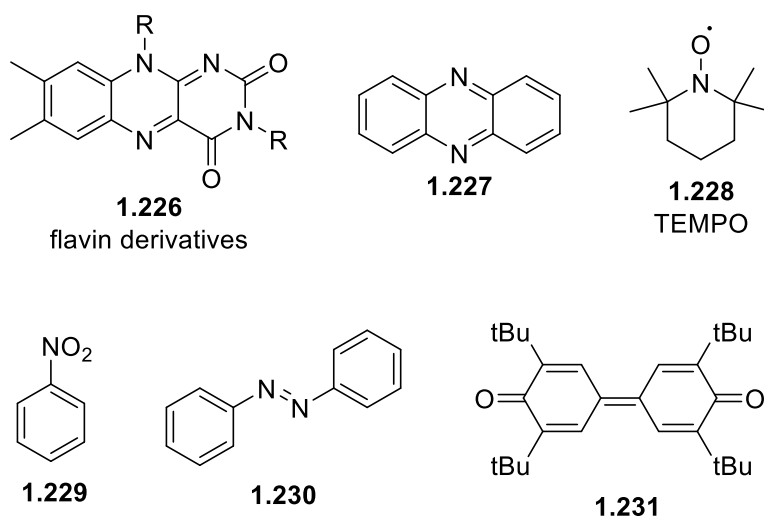
Scheme 1.28: Examples of NHC-catalyzed reactions that proceed through an acyl azolium intermediate.



Scheme 1.29: NHC-catalyzed generation of acyl azoliums via internal redox reaction.

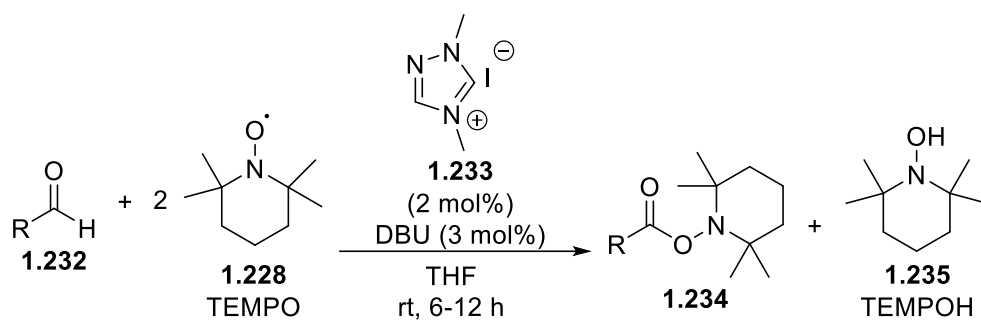
A much more common method of generating acyl azolium intermediates is via oxidation of the Breslow intermediate with an external oxidant, and generating esters via oxidative esterification. Stoichiometric MnO_2 has been used to facilitate this reaction, as well as molecular oxygen. Organic oxidants are much more common, and examples of nitro compounds, flavins, and azobenzenes have been demonstrated as external organic oxidants in NHC-catalyzed oxidative esterifications (Scheme 1.30). Bisquinone compound **1.75** has become the standard

oxidant used in NHC oxidative chemistry, due to its easy preparation and removal from reaction mixtures. In its reduced bisphenol form, it can potentially act as a competitive nucleophile and form unwanted products. However, the steric bulk of the *tert*-butyl groups prevent that from happening, adding to its success and usefulness as an oxidant in NHC-catalyzed reactions.

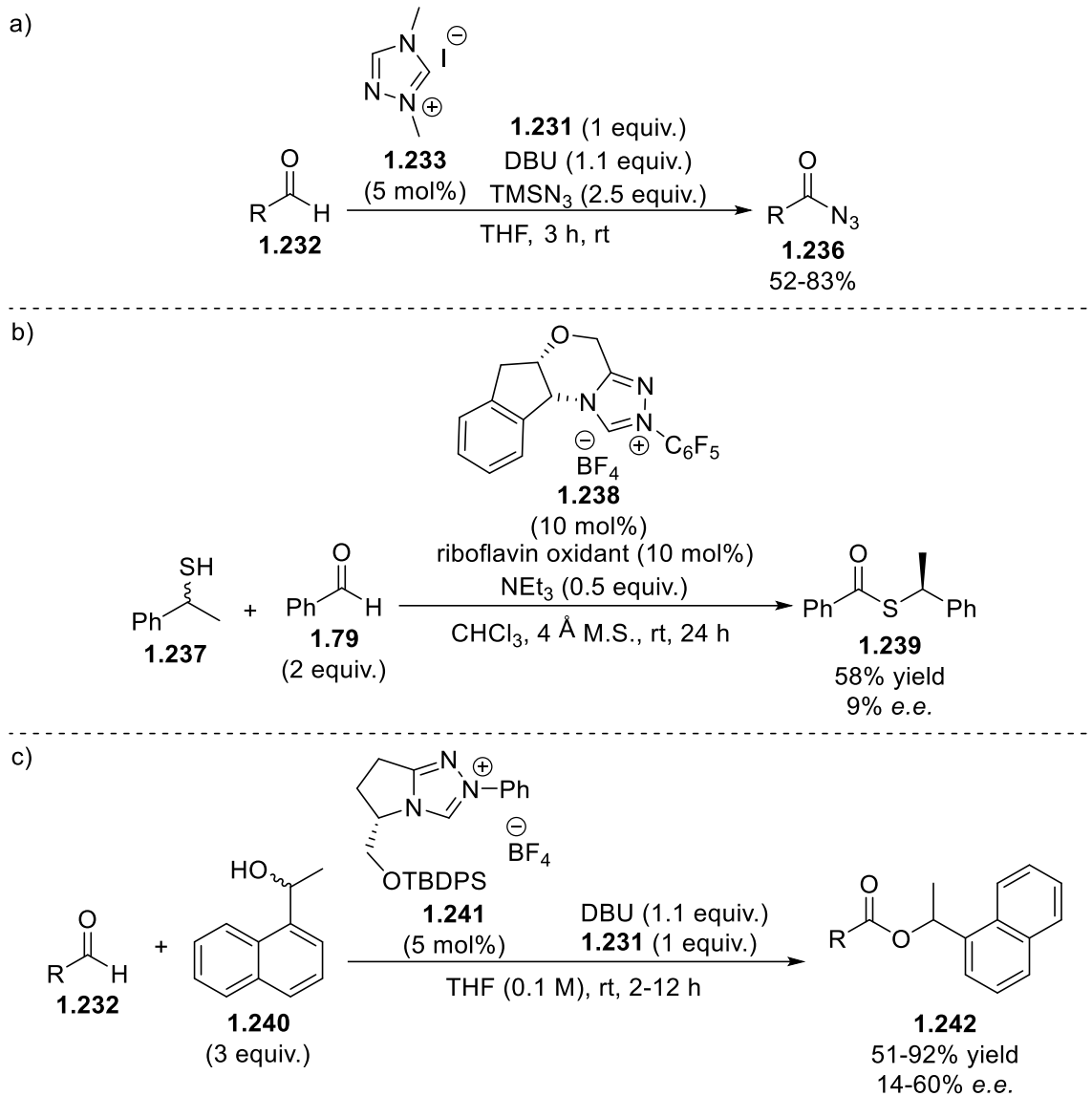


Scheme 1.30: Organic oxidants used in NHC catalysis.

In 2008, Studer's group reported on the use of TEMPO as a single-electron biomimetic organic oxidant for the oxidative esterification of aldehydes⁸⁰ (Scheme 1.31). While this protocol provides the desired TEMPO esters in high yields with high catalytic efficiency, the choice of nucleophile substrate is limited only to TEMPO[•]. The TEMPO esters can be converted to their corresponding carboxylic acid derivatives by treatment with aqueous HCl, and to their corresponding methyl esters by treatment with methanolic HCl. In a later paper, the same group developed a more general protocol for NHC-catalyzed oxidative esterification using bisquinone oxidant **1.231** instead of TEMPO.⁸¹ Similar protocols allow for the oxidative azidation⁸² and thioesterification⁸³ of aldehydes, and using chiral NHC catalysts, kinetic resolutions of chiral alcohols⁸⁴ (Scheme 1.32).



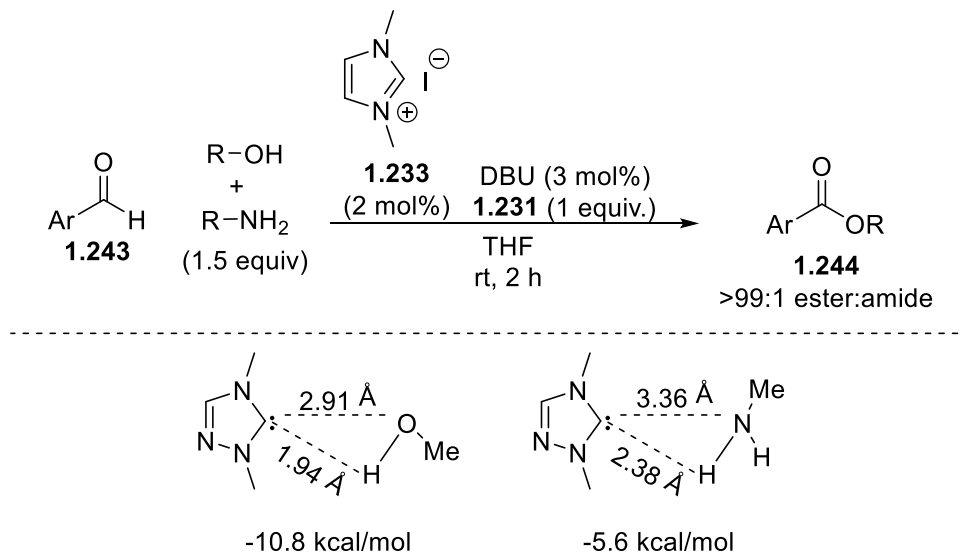
Scheme 1.31: Studer's biomimetic oxidation with TEMPO.



Scheme 1.32: a) NHC-catalyzed oxidative azidation. b) NHC-catalyzed oxidative thioesterification. c) NHC-catalyzed kinetic resolution of chiral alcohols.

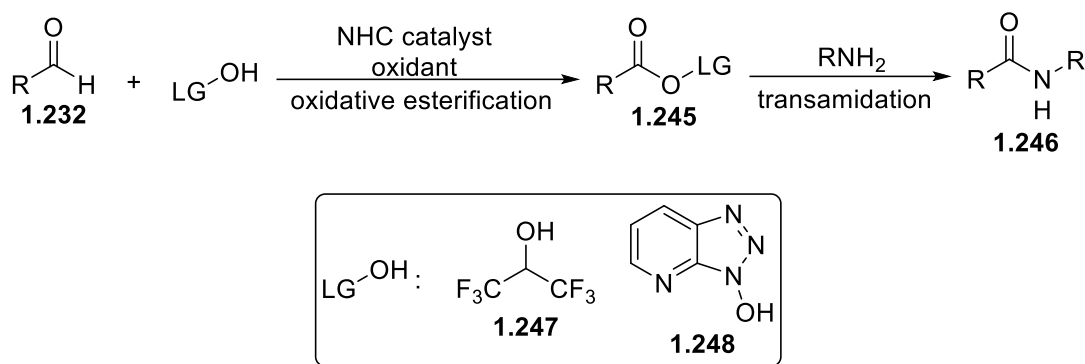
A logical extension of this methodology would be to apply it to amine nucleophiles, however attempts at direct oxidative amidations give low conversions of the desired amide product. In fact, Studer's group found that in the presence of amines, alcohols will selectively undergo oxidative esterification rather than amidation⁸¹ (Scheme 1.33a). Mechanistic and computational studies suggested that the chemoselectivity could be explained by cooperative

NHC catalysis. DFT calculations showed that there was a positive H-bonding interaction between the carbene and MeOH with a bond dissociation energy of ~11 kcal/mol, and an elongation of the MeOH O-H bond (Scheme 1.33b). A similar computation with MeNH₂ found the binding energy to be halved, and that the carbene-MeNH₂ complex does not bind as tight as the carbene-MeOH complex.



Scheme 1.33: a) Studer's chemoselective oxidative esterification in the presence of amines. b) Binding energy calculations performed between carbene and MeOH/MeNH₂.

While direct NHC-catalyzed oxidative amidations are not as efficient or high-yielding as other NHC-catalyzed processes, researchers have developed more indirect methods of oxidative amidation. Using a weak alcohol nucleophile such as hexafluoroisopropanol (HFIP) or HOAt allows for the generation of an activated ester, which when exposed to the desired amine nucleophile, undergoes transamidation (Scheme 1.34). HFIP and HOAt act as good leaving groups for the transamidation reaction. Other additives such as DMAP or imidazole, which are common nucleophilic co-catalysts for this type of reaction, gave desired product, but in low yields.

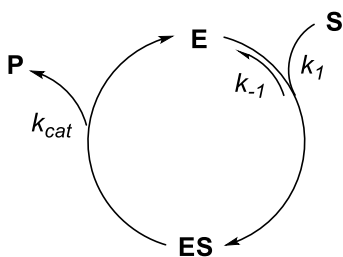


Scheme 1.34: Strategies for NHC-catalyzed oxidative amidation.

1.2 Kinetic analysis by reaction monitoring

1.2.1 Michaelis-Menten kinetics

The Michaelis-Menten model of enzyme kinetics is one of the standard models of catalytic reactions. While it was originally developed to describe enzymatic processes, the concepts it developed apply to organic reaction mechanisms as well. The Michaelis-Menten model utilizes the enzymatic mechanism depicted in Scheme 1.35. Substrate (**S**) reversibly binds with the enzyme (**E**) to form an enzyme-substrate complex (**ES**) with forward and backwards rate constants k_1 and k_{-1} , respectively. The enzyme-substrate complex then releases product (**P**) and enzyme back into the cycle with rate constant k_{cat} .



Scheme 1.35: Simple enzymatic mechanism.

The rate of product formation is given by the equation:

$$\frac{d[P]}{dt} = k_{cat}[ES] \quad (1.2)$$

By the law of mass balance, the initial enzyme concentration ($[E]_0$) is given by the equation:

$$[E]_0 = [E] + [ES] \quad (1.3)$$

It is assumed by the steady-state approximation that $[ES]$ does not change:

$$\frac{d[ES]}{dt} = k_1[S]([E]_0 - [ES]) - k_{-1}[ES] - k_{cat}[ES] = 0 \quad (1.4)$$

Solving for $[ES]$ and substituting into Equation 1.2 gives the Michaelis-Menten equation:

$$\frac{d[P]}{dt} = V = \frac{V_{max}[S]}{K_M + [S]} \quad (1.5)$$

where

$$V_{max} = k_{cat}[E]_0, \quad K_M = \frac{k_{cat} + k_{-1}}{k_1}$$

V_{max} is the maximum rate of product formation, when the enzyme is saturated with substrate. K_M is referred to as the Michaelis constant, and is an inverse measure of substrate binding affinity: a low K_M indicates high affinity for the substrate. V_{max} , k_{cat} , and K_M are all measurable constants, but only when the Michaelis-Menten equation is linearized. Taking the reciprocal of Equation 1.5 gives the Lineweaver-Burk equation:

$$\frac{1}{V} = \frac{K_M}{V_{max}} \frac{1}{[S]} + \frac{1}{V_{max}} \quad (1.6)$$

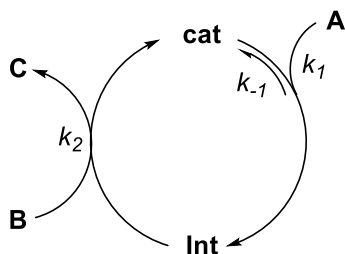
A plot of $\frac{1}{V}$ as a function of $\frac{1}{[S]}$ will yield a linear trend, and V_{max} , K_M , and k_{cat} can be inferred from the data. The Lineweaver-Burk equation provides a powerful mathematical tool for chemists to deconvolute complex kinetic data from catalytic systems, and to extract relevant constants from that data. While this technique is certainly powerful, it does suffer from some

drawbacks. Reaction rates can change over the course of a reaction, due to factors such as catalyst deactivation or product inhibition, and so these plots are generated from initial rate data (10-15% conversion) with increasing substrate concentration. By focusing on only the initial stages of reaction, any potential surprising catalytic behavior later on is completely ignored. In addition, since the Lineweaver-Burk plot is generated by plotting the reciprocals of V and $[S]$, any error in measurement is magnified, especially at low values of V and $[S]$.

1.2.2 Reaction progress kinetic analysis

Reaction progress kinetic analysis (RPKA) is a methodological framework developed by Prof. Donna Blackmond that enables researchers to effectively and efficiently perform a mechanistic analysis using reaction monitoring and simple data manipulation. Like the Lineweaver-Burk plot, the concepts put forward in RPKA are tools to help deconvolute and make sense of complex kinetic data. One of these tools is the graphical rate equation, where rate of reaction is plotted against substrate concentration. From this graphical rate equation, rate constants can be extracted, and the data can be mathematically manipulated and replotted to determine order in substrate. In addition, RPKA suggests a minimum baseline set of experiments that are designed to extract as much kinetic information as possible.

The majority of organic chemists are interested in putting molecules together, and so the reactions of greatest interest will often involve two substrates. The simplest model for a catalytic 2-substrate reaction is shown in Scheme 1.36.



Scheme 1.36: Mechanism for a simple catalytic reaction involving two substrates (A, B), one intermediate (Int), and one product (C).

The overall steady-state rate expression for this mechanism can be expressed as:

$$v = \frac{k_1 k_2 [A][B][\text{cat}]_{\text{total}}}{k_{-1} + k_1 [A] + k_2 [B]} \quad (1.7)$$

If both the numerator and denominator are divided by the reverse rate constant k_{-1} , Equation 1.7 becomes

$$v = \frac{a[A][B][\text{cat}]_{\text{total}}}{1 + b[A] + c[B]} \quad (1.8)$$

$$a = \frac{k_1}{k_{-1}} k_2, \quad b = \frac{k_1}{k_{-1}}, \quad c = \frac{k_2}{k_{-1}}$$

Equation 1.8 is called the “one-plus” form of the steady-state rate equation. As it can be seen, both $[A]$ and $[B]$ appear as additive terms in the denominator, and are multiplied together in the numerator. This complexity suggests that the idea of an integer reaction order in either $[A]$ or $[B]$ is, at best, an approximation. Such an approximation would be to perform kinetic analyses using a large excess of one substrate, approximating zero-order behavior in that substrate. As described previously in this chapter, such an approximation is not synthetically relevant.

To deconvolute this complexity, the concept of “excess” can be introduced. “Excess” ($[e]$) is defined as the difference in the initial concentrations of the two substrates:

$$[e] = [B]_0 - [A]_0 \quad (1.9)$$

Although both $[A]$ and $[B]$ change with time, the manner in which they change is linked to the reaction stoichiometry: every time one molecule of A is converted into one molecule of C, one molecule of B must also be converted as well. With this knowledge, we can assume that $[e] = [B] - [A]$, and an expression for $[B]$ can be written in terms of $[A]$ and $[e]$:

$$[B] = [e] + [A] \quad (1.10)$$

Equation 1.10 can be substituted into Equation 1.8:

$$v = a' \frac{[e][A] + [A]^2}{1 + b'[A]} [\text{cat}]_{\text{total}} \quad (1.11)$$

$$a' = \frac{k_1 k_2}{k_{-1} + k_2 [e]}, \quad b' = \frac{k_1 + k_2}{k_{-1} + k_2 [e]}$$

As all the rate constants, $[e]$, and $[\text{cat}]_{\text{total}}$ are all constants, the steady-state rate expression is simplified such that it is dependent on one variable, $[A]$, and it eliminates the need to run experiments with large excesses of one reactant to approximate zero-order behavior in that reactant. In short, the concept of “excess” allows for kinetic data to be obtained at synthetically relevant substrate concentrations.

When performing a kinetic analysis using RPKA, two types of excess experiments are performed: different excess and same excess. Different excess experiments are designed to determine reaction order in substrate, while same excess experiments are designed to determine if the catalyst is plagued by catalyst deactivation or product inhibition. For the reaction shown in Scheme 1.36, Table 1.1 shows an example set of experiments that would be performed as part of the RPKA protocol to perform a kinetic analysis.

Experiment	$[A]_0$ (mM)	$[B]_0$ (mM)	$[cat]_{total}$ (mM)	$[e]$ (mM)
1	100	100	5	0
2	100	130	5	30
3	120	100	5	-20
4	75	75	5	0

Table 1.1: Example set of experiments for RPKA.

As it can be seen, $[e]$ can be positive, negative, or zero. The magnitude of $[e]$ should be chosen to be a reasonable value; 10% of “standard conditions” is usually a good starting point. Comparing experiments 1 & 2, $[A]_0$ is constant, while $[B]_0$ changes, which means that any rate increase seen in experiment 2 is due to **B** only, and so the reaction will be positive order in **B**. Conversely, if there was no change in reaction rate between the two experiments, the reaction would be zero order in **B**. Comparing experiments 1 & 3, $[B]_0$ is constant while $[A]_0$ changes. Any rate increase observed in experiment 3 is due to **A**, showing positive order in **A**, and no rate increase would show zero order in **A**.

As experiments 1 & 4 have the same value of $[e]$ but different $[A]_0$ and $[B]_0$, these experiments are referred to as “same excess” experiments, and are used to probe catalyst deactivation or product inhibition. The substrate concentrations in experiment 4 are lower than in experiment 1, but catalyst concentration is the same. In experiment 1, by the time substrate concentration reaches 75 mM (the initial concentration in experiment 4), the catalyst has already completed five turnovers. The progress curve for experiment 1 can be time-adjusted and overlaid with the progress curve for experiment 4 at the time where $[A] = 75$ mM. If the two curves overlay after that time, then the activity of the catalyst is unchanged over the course of the reaction. If the curves do not overlay, then something is happening to the catalyst during those

first five turnovers. Product inhibition can be easily probed by performing a third experiment, where a small amount of product **C** is added at the start of the reaction, and comparing the reaction progress profiles to see if they overlay. By following this protocol, an initial kinetic analysis can be performed with few experiments, and interrogation of the kinetic data can be used to propose further experiments for a full kinetic analysis.

One drawback of RPKA is that it works best with “well-behaved” reactions: reactions that form minimal side products, and go to high conversion (>90%). The graphical analysis used in RPKA falls short when multiple side products are formed, or when overall reaction conversion is low. As a result, RPKA is often performed on reactions that have already been optimized through solvent, temperature, substrate, and additive screens. However, for reactions that go to low conversion, or produce undesired side products, the tenets of RPKA can be useful during reaction optimization to understand why a reaction might not reach 100% conversion, or why side products are being formed. Taking a “bottom-up” approach by creating reaction progress curves during the optimization process can provide the chemist with valuable data about the progress of a reaction that simply cannot be obtained from an optimization table.

1.2.3 Reaction monitoring techniques

1.2.3.1 Fourier transform infrared spectroscopy (FTIR)

FTIR is an instrumentation method that many chemists associate with structure identification. In fact, FTIR is often the first method of structure elucidation taught at the undergraduate level, alongside NMR. While Beer’s Law can be used to obtain concentration data from an IR absorbance, placing a compound between two KBr salt plates cannot provide an accurate path length, and is completely impractical in the context of reaction monitoring. To

obtain accurate concentrations, an attenuated total reflectance (ATR) sampling method needs to be used. As many modern commercial IR spectrometers come equipped with ATR modules, IR as an analytical tool is commonplace in the modern research laboratory.

As a reaction monitoring technique, FTIR is advantageous due to its non-invasive, non-destructive nature. Many ReactIR setups, like those from Mettler-Toledo, have probes that can be inserted into the reaction mixture, or flow cells that the reaction mixture can flow through. Both the probe and the flow cell are fitted with an ATR gold-sealed diamond sensor, with a spectral range of 4000-650 cm^{-1} . ReactIR probes are often used for online monitoring of batch processes in an industrial setting, but the flow cell can also be used to monitor batch processes, when it is part of a continuous circulation set up.

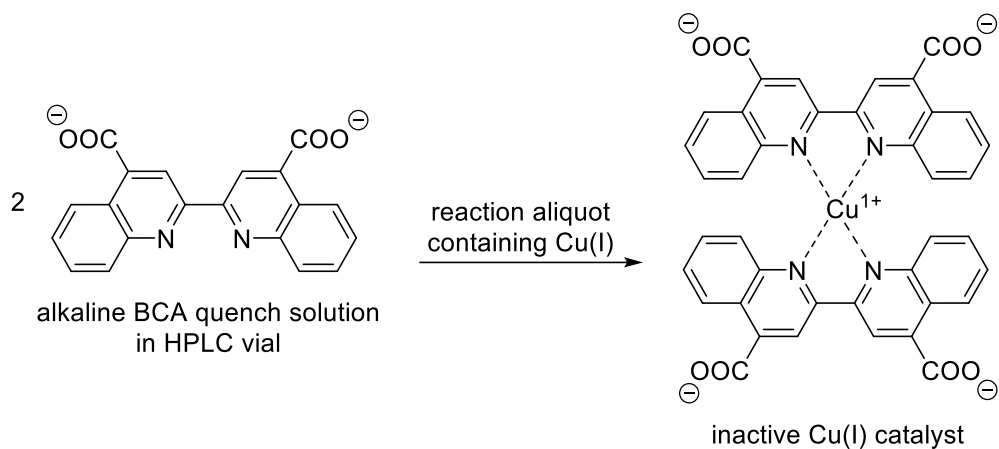
ReactIR is a technique best suited for when the reaction of interest has a substrate with a strong, characteristic absorption, such as a carbonyl stretch (1740-1630 cm^{-1}) or other carbon-heteroatom stretches. It is possible for peaks to overlap, especially if the substrates, products, or byproducts of interest have similar functional groups and stretching vibrations. In that case, the data can be deconvoluted mathematically by using principal component analysis, which is included as a part of Mettler-Toledo's icIR software package. However, common IR vibrations such as sp^2 - or sp^3 -hybridized C-H stretches (3100-2850 cm^{-1}) may be difficult to deconvolute and can be unreliable. While the advertised spectral window for ReactIR is from 4000-650 cm^{-1} , the diamond ATR window has a chemical "blind spot" from 2250-1950 cm^{-1} due to the C-C stretching vibrations of diamond, which overlaps with alkene C=C stretches (2000-1900 cm^{-1}). Due to these limitations, ReactIR is best suited for monitoring sp^3 - and sp^2 -hybridized carbon-heteroatom stretching frequencies.

The physical state of the reaction being analyzed by ReactIR is also important to consider. ReactIR is best suited for homogeneous mixtures, as accurate concentrations of analytes can only be determined by IR if they are in solution. Heterogeneous mixtures can be analyzed by ReactIR, but an orthogonal method such as HPLC should be used in conjunction with ReactIR to obtain accurate mass balance. In addition, the formation of solids in the reaction vessel can be problematic. The ReactIR probe can potentially act as a nucleation site, obscuring the diamond window and preventing accurate data acquisition. In the data, this would appear as a flat reaction progress curve, with no change over time. This limitation can be addressed by thorough mechanical stirring and close observation by the researcher, ensuring that solids do not deposit on the tip of the ReactIR probe.

1.2.3.2 High performance liquid chromatography (HPLC)

As an analytical tool, HPLC-MS is used for the separation, identification, and quantification of target analytes in a mixture. Analyzing a reaction by HPLC is usually done in an offline fashion, and it is useful as a validation of other *in situ* or online methods (IR, calorimetry). Many detection methods are available for HPLC, including fluorescence and evaporative light scattering (ELSD), but the most common method by far is ultraviolet (UV) absorbance. Commercial UV flow cells, such as those provided by Agilent, have wavelength ranges from 200-600 nm. Many HPLC systems are coupled to a mass spectrometer (MS), which allows the user to separate the components of a reaction and identify target masses of interest. Both UV and MS detectors are very sensitive, and so chemical species that would be undetectable by other methods (NMR, IR) can be observed by HPLC-MS.

A key factor when considering using HPLC as a reaction monitoring technique is proper choice of reaction quench. In many cases, simple dilution of the reaction mixture into methanol is sufficient, as the massive drop in concentration is large enough to effectively stop the reaction. If a reaction is acid- or base-catalyzed, quenching into a buffer should be sufficient, depending on the system being analyzed. However, in the case of transition metal-catalyzed systems, where reactions can proceed with extremely low catalyst loadings, there is a risk of continued reaction in the HPLC vial between the time the aliquot is taken and the sample is analyzed. In the Hein lab, Cu-catalyzed azide-alkyne cycloadditions (CuAAC) are commonly studied using HPLC sampling.⁸⁵ To ensure that reactions do not continue in the HPLC vial after an aliquot is taken, an alkaline solution of bicinehonic acid (BCA) is used as a quench solution (Scheme 1.37). Two molecules of BCA bind tightly to Cu(I), creating a stable complex that is no longer reactive, allowing for a true snapshot of the reaction at that particular time point. The ability to properly quench a reaction for HPLC is particularly important when a high volume of samples are required. Samples that are not properly quenched towards the end of the reaction can appear to have incorrectly higher concentrations of product, and this can lead to incorrect interpretation of kinetic data.



Scheme 1.37: Cu(I) deactivation via BCA quench solution.

HPLC is best used for monitoring homogeneous reactions. Reactions involving slurries can give inaccurate concentration data, due to the potentially non-homogeneous distribution of solid particles in a slurry. In addition, solid particles in an HPLC vial can damage the column, and so any solids need to be filtered before analysis. Some commercial slurry sampling solutions are available, such as the Mettler-Toledo EasySampler, but it is limited to twelve samples, and is not practical for monitoring reaction progress.

As with any laboratory tool, there are some drawbacks and limitations of HPLC. First and foremost, HPLC can be time-consuming. Depending on the method, column, and LC system being used, a single sample can take a long time to run, making reactions that require many samples prohibitive to run on what is often a shared instrument. For reactions that produce multiple products, transient intermediates, stable catalytic intermediates, or all of the above, developing an adequate separation method can be time-consuming and is not always intuitive. While starting materials and products will usually separate easily on an HPLC column, undesired side products can be chemically similar to the starting materials or products, or chemically similar to each other, and peaks may overlap. Method development often requires a substantial

amount of time, as many different columns may need to be tried for difficult separations, as well as different starting solvent mixtures and gradients. In addition, each trial method developed during a method development needs to be tested on a reaction mixture to verify if separation is achieved. LC is an offline analysis method, and so for reactions that require frequent sampling, the full HPLC analysis can be very time-consuming on what is often a shared instrument. Some of these time-related drawbacks can be resolved by using an ultra-high performance liquid chromatography (UHPLC) system, which uses much higher pressures and faster eluent flow rates, resulting in faster method times. In addition, shorter, more efficient columns with higher theoretical plates have become more standard, further decreasing method time.

One of the key advantages of HPLC is its inherent ability for quantitation, however there are some caveats. The relative response factors (RRFs) for organic molecules are not the same, and so construction of calibration curves is required for every species of interest in a reaction. For starting materials and major products, calibration curves can be generated with ease. For minor products, side products, and unknown byproducts, this can be challenging and time-consuming. Those compounds need to be identified, and enough quantities need to be synthesized to create the calibration curves. Unfortunately, transient catalytic species generally cannot be quantified in this manner, due to their ephemeral nature. In most cases, internal standards need to be used as well, both in the reaction and to create calibration curves. These internal standards must be inert to the reaction conditions, and must absorb at a wavelength that every other chemical species of interests absorbs at. However, if a reaction is being sampled by a robot liquid handler that can accurately and precisely dispense a desired volume, an internal standard may not be required.

1.2.3.3 Nuclear magnetic resonance (NMR) spectroscopy

NMR spectroscopy is often a first choice to analyze a reaction of interest, due to the wide availability of spectrometers in most chemistry departments. Monitoring reactions by ^1H NMR is by far the most common, but ^{19}F and ^{31}P are common nuclei used for monitoring reactions involving fluorinated substrates, catalytic systems with phosphine ligands, and biological processes. NMR has a distinct advantage over other monitoring techniques in that it is intrinsically quantitative, avoiding the need for calibration curves. If the time and effort are taken to calculate nuclei relaxation times, and volumetric glassware is used to prepare reactions, the initial concentration of reactants can be used to determine concentration data throughout the reaction.⁸⁶ Modern NMR spectrometers come with software packages that facilitate the automatic acquisition of spectra over time, simplifying the data acquisition process. NMR is not intrusive, and the potential is there to characterize every NMR-active compound in the reaction, provided enough signal is present. For high-field spectrometers (500 MHz), μmol quantities of material are easily detected by ^1H NMR spectroscopy. Two-dimensional NMR techniques such as COSY, TOCSY, HSQC, and HMBC can also be employed to help deconvolute a reaction mixture and identify previously unknown reactive species.

While NMR is an extremely useful tool to monitor reaction progress, there are some drawbacks that must be addressed. The cheapest deuterated solvents (CDCl_3 , D_2O , and DMSO-d_6) are not always optimal solvents for a reaction, and deuterated versions of the optimal solvent can be prohibitively expensive. For reactions that exhibit solvent effects, this can be especially problematic. Fortunately, researchers may be able to get around this limitation by using solvent suppression pulse sequences (usually included as part of the NMR software package), or “No-D” techniques, allowing the user to analyze the reaction by ^1H NMR using non-deuterated

solvents.⁸⁷ pH changes during a reaction can cause peaks of interest to drift and overlap with other peaks; fortunately, programs like MestreNova can solve this problem using the Global Spectral Deconvolution algorithm. For fast organic reactions (under 5 minutes), the time between reactant mixing and the start of data acquisition is detrimental to collecting good data, as the initial phase of the reaction can be lost. A solution to this problem is to use stopped-flow NMR techniques, which has been reported by the Landis group.⁸⁸ By using a specialized probe and injecting reactions into the NMR detection region directly, the initial time delay is greatly reduced, and early regimes of reactions where reaction rate is highest can be observed. However, this approach uses a specialized probe and may not be practical for use in a shared instrument facility. Finally, since agitation with a stir bar is impossible inside the NMR spectrometer, a potential cause for concern is that the reaction profile generated from a bench top reaction may be different than one generated using a standard NMR setup. A study by Foley et. al at Pfizer compared the reaction profiles between three different setups: static NMR tubes, online NMR (a flowing stream of the reaction mixture from the reaction vessel is transferred to the NMR probe), and periodically inverting the NMR tubes between acquisitions.⁸⁹ For both heterogeneous and homogeneous reactions, the reaction profiles generated using the three different methods are indeed different. While the reaction profiles generated using each method are comparable to each other, the kinetic analysis derived using these methods may not scale up to larger, stirred reactions that are synthetically relevant.

Chapter 2: Mesoionic 1,2,3-Triazolyl *N*-Heterocyclic Carbene

Organocatalysts

2.1 Introduction

This chapter focuses on the design, synthesis, and application of mesoionic 1,2,3-triazolylidenes as *N*-heterocyclic carbene organocatalysts in the oxidative esterification of aldehydes with alcohol nucleophiles. Using reaction progress monitoring techniques, the catalytic mechanism of this reaction was studied in detail, including identification of reaction orders in each component, and an identification of the catalyst resting state. In addition, a catalytic intermediate was synthesized, isolated, and characterized by single-crystal X-ray diffraction.

2.1.1 Mesoionic *N*-heterocyclic carbenes

Classical *N*-heterocyclic carbenes, such as imidazolylidene **2.1**, triazolylidene **2.2**, and thiazolylidene **2.3** are characterized by the carbene center being flanked by two heteroatoms, at least one of which is a nitrogen. The presence of two flanking heteroatoms help to stabilize the carbene, due to the donation of electrons from the nitrogen into the vacant p orbital of the carbene center.⁸ In the context of organometallic chemistry, *N*-heterocyclic carbenes are widely used as ligands due to the relatively high covalent contribution to the metal-NHC bond, as well as their strong σ -donor properties. The inductive effect of the two nitrogen atoms adjacent to the carbene affect the σ -donation properties of the carbene,⁹⁰ and so efforts have been made to

develop ligands with different placements of stabilizing heteroatoms, altering the electronic structure. These efforts have led to the development of so-called remote carbenes (rNHCs) and abnormal/mesoionic carbenes (MICs) (Figure 2.1). The stabilizing heteroatoms of remote NHCs are not adjacent to the carbene center, while for mesoionic carbenes, a single heteroatom is adjacent to the carbene center. Moreover, mesoionic carbenes are further classified by their canonical resonance structure – they are carbenes for which no uncharged resonance structure can be drawn.

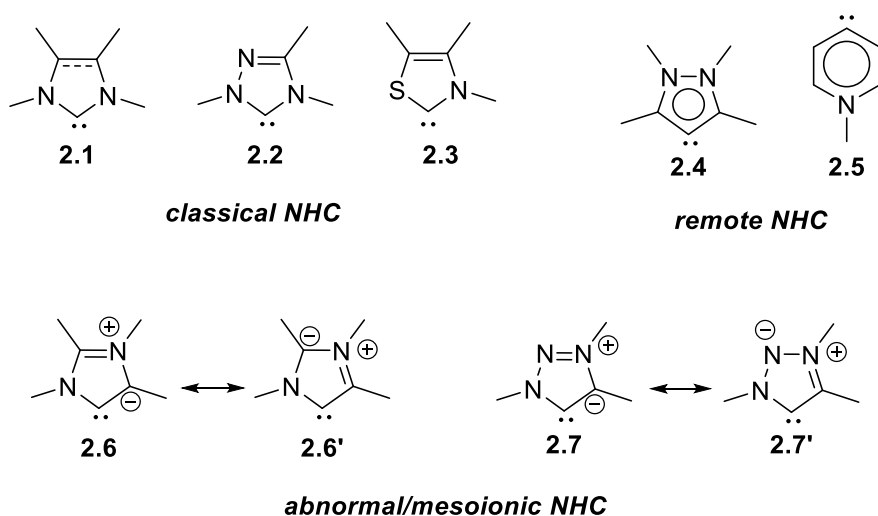
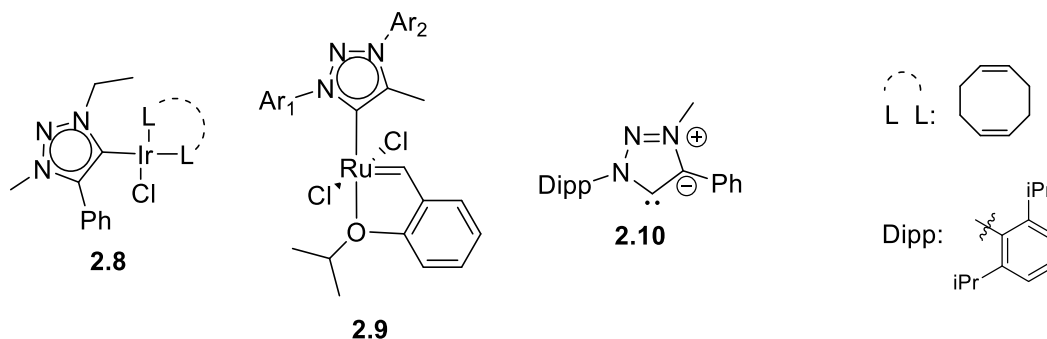


Figure 2.1: Classical, remote, and mesoionic *N*-heterocyclic carbenes.

Mesoionic NHCs derived from 1,2,3-triazolium salts were first developed as ligands for a variety of late transition metal complexes⁹¹ (Scheme 2.1, **2.8**), and later developed as ligands for Ru-catalyzed olefin metathesis⁹² (Scheme 2.1, **2.9**). In 2010, Bertrand et. al prepared the first stable crystalline 1,2,3-triazol-5-ylidene⁹³ (Scheme 2.1, **2.10**). Theoretical computations and experimental IR data on complexes **2.8** and **2.9** and an Ir complex of **2.10** suggest that the carbenes have stronger σ -donor properties than their classical NHC analogues. At the time this work was started, there were no reports of mesoionic carbenes being used as organocatalysts.

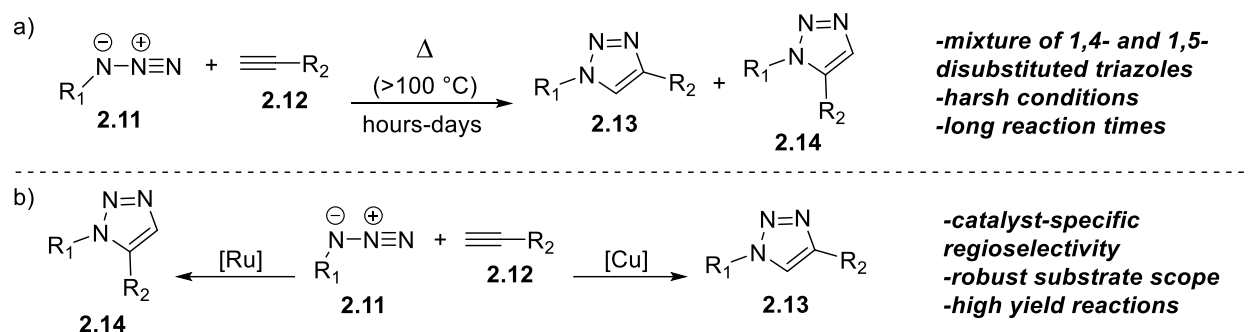
This fact, combined with the superior σ -donor properties of abnormal carbenes, provided the primary motivations for investigating mesoionic carbenes as potential organocatalysts.



Scheme 2.1: Examples of mesoionic 1,2,3-triazolyliidenes found in the literature.

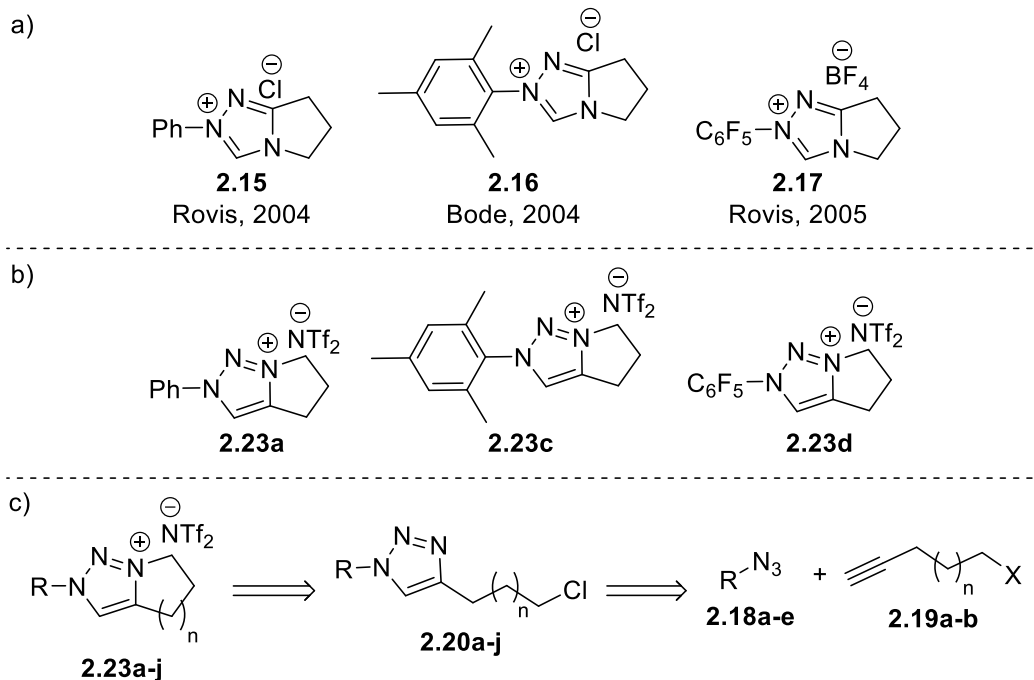
2.2 Design and synthesis of 1,2,3-triazolium salt precatalysts

The synthetic strategy employed in the literature to make 1,2,3-triazolium salt precursors to mesoionic carbenes involves alkylation of 1,4-disubstituted 1,2,3-triazoles.⁹⁴ 1,2,3-triazoles are prepared via the Huisgen 1,3-dipolar cycloaddition of an azide and an alkyne.⁹⁵ When this reaction is performed under uncatalyzed, thermal conditions, a mixture of 1,4- and 1,5-disubstituted 1,2,3-triazole isomers is formed (Scheme 2.2a). When this reaction is catalyzed by ruthenium, the 1,5-regioisomer is selectively formed,⁹⁶ whereas when a copper(I) catalyst is used, the 1,4-regioisomer is exclusively produced.⁹⁷ The Cu(I)-catalyzed azide/alkyne cycloaddition (CuAAC) has become a prime example of “click” chemistry, due to high catalytic efficiency, high yields, mild conditions, and extremely wide substrate scope with respect to both azide and alkyne. The robustness of the CuAAC reaction makes it a prime synthetic strategy for rapidly building a library of potential 1,2,3-triazolium organocatalyst precursors with various electronic and steric properties.



Scheme 2.2: Synthetic methods towards 1,2,3-triazoles.

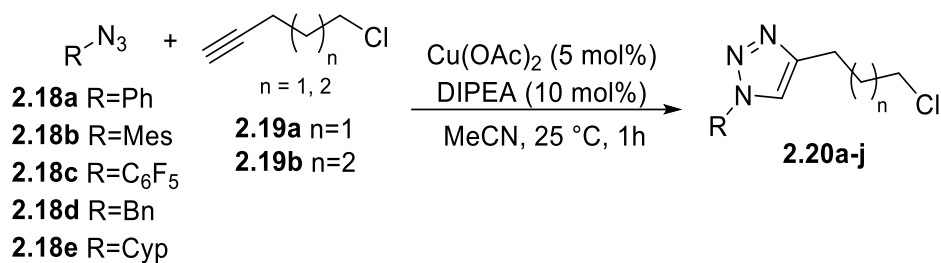
The initial target 1,2,3-triazolium salts **2.23a**, **2.23c**, and **2.23d** were chosen because they are the 1,2,3-triazolium analogues of NHC precatalysts previously described by Rovis³⁵ and Bode⁷³ (Scheme 2.3a). *N*-mesityl substituted **2.16** and *N*-pentafluorophenyl-substituted **2.17** have shown great activity in the benzoin condensation and homoenolate reactions, and the most active and widely used NHC catalysts bear mesityl and pentafluorophenyl *N*-substituents.²¹ Prior to this work, there were no reports of *N*-alkyl-substituted NHCs that exhibit organocatalytic activity, so a series of 1,2,3-triazolium salts bearing *N*-benzyl and *N*-cyclopentyl substituents were included in the planned triazolium library. The size of the fused saturated ring has been shown to play a role in catalytic activity in the benzoin condensation,⁵⁹ and so 1,2,3-triazolium salts with six-membered fused rings were also synthesized. The general synthetic strategy for these 1,2,3-triazolium salts is presented in Scheme 2.3c.



Scheme 2.3: a) Common 1,2,4-triazolium NHC precatalysts found in the literature. b) Proposed 1,2,3-triazolium analogues of common 1,2,4-triazolium NHC precatalysts. c) Synthetic strategy towards 1,2,3-triazolium NHC precatalysts.

2.2.1 Scope of synthesized triazoles and triazolium salts

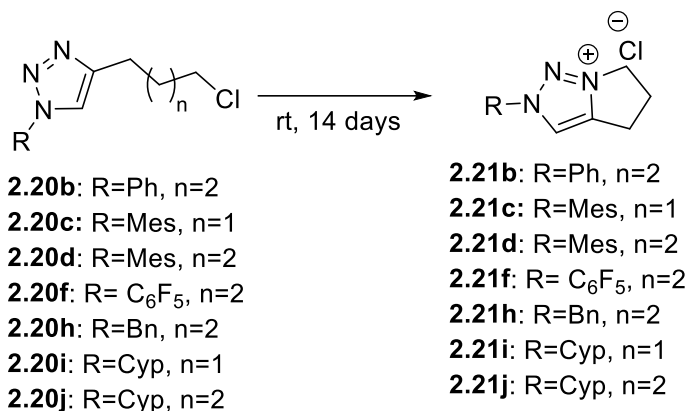
The candidate triazole precursors were synthesized *via* the Cu-catalyzed azide-alkyne cycloaddition of azides **2.18a-e** with either 5-chloro-1-pentyne (**2.19a**) or 6-chloro-1-hexyne (**2.19b**) (Table 2.1).



Entry	R	n	Yield ^a
a	Ph	1	90%
b	Ph	2	81%
c	Mes	1	72%
d	Mes	2	73%
e	C ₆ F ₅	1	90%
f	C ₆ F ₅	2	53%
g	Bn	1	85%
h	Bn	2	79%
i	Cyp	1	59%
j	Cyp	2	50%

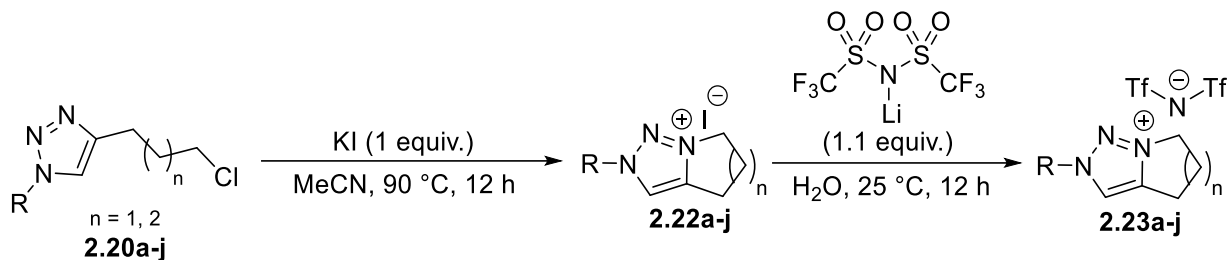
Table 2.1: Scope of 1,2,3-triazolium salt precursors. ^aIsolated yield determined after purification by flash chromatography or recrystallization.

The stability of these triazoles at room temperature is dependent on the physical state of the compound. Compounds **2.20b**, **2.20c**, **2.20d**, **2.20f**, **2.20h**, **2.20i**, and **2.20j**, which are oils at room temperature, spontaneously cyclize to form their corresponding 1,2,3-triazolium chloride salts upon standing at room temperature for approximately two weeks (Scheme 2.4). Triazoles **2.20a**, **2.20e**, and **2.20g** are solids at ambient laboratory conditions, and are not prone to spontaneous cyclization.



Scheme 2.4: Spontaneous cyclization of 1,2,3-triazole oils.

To access the required 1,2,3-triazolium salts, a one-pot Finkelstein reaction and cyclization strategy was employed, followed by ion exchange with lithium bis(trifluoromethane)sulfonamide (LiNTf₂). This choice of anion was made to increase the solubility of triazolium salts **2.23** in organic solvents. The bis(trifluoromethane)sulfonamide counterion was advantageous for purification as well; iodide salts **2.22** are highly water-soluble, allowing for easy separation of organic impurities and reaction by-products by liquid-liquid extraction. Addition of LiNTf₂ to the water extract resulted in separation of triazolium salts **2.23** from the aqueous solvent, either as a precipitate (**2.23b-f**) or as an immiscible ionic liquid (**2.23a**, **2.23g-j**). This simple two-step protocol allowed for rapid, clean synthesis of triazolium salts **2.23** on a multi-gram scale.

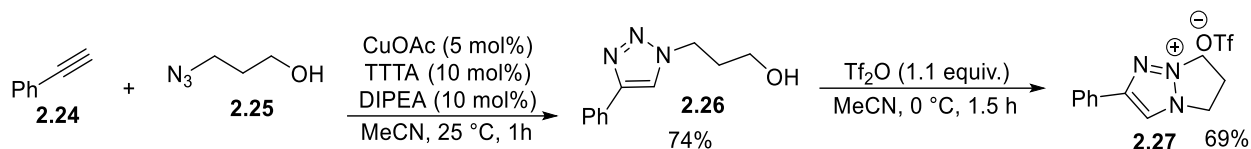


Entry	R	n	Yield
a	Ph	1	56% ^a
b	Ph	2	67% ^b
c	Mes	1	78% ^b
d	Mes	2	78% ^b
e	C ₆ F ₅	1	34% ^b
f	C ₆ F ₅	2	90% ^b
g	Bn	1	68% ^a
h	Bn	2	62% ^a
i	Cyp	1	52% ^a
j	Cyp	2	62% ^a

Table 2.2: Scope of synthesized 1,2,3-triazolium salts **2.19a-j**. ^aIsolated yield after liquid-liquid extraction and removal of solvent. ^bIsolated yield after precipitation from water, vacuum filtration, and drying under high vacuum.

In addition to these 1,3,4-trisubstituted 1,2,3-triazolium salts, a 1,2,4-trisubstituted regioisomer of **2.23a** was synthesized (Scheme 2.5). To access this regioisomer, an aromatic alkyne **2.24** was coupled with hydroxyl-substituted azide **2.25** using copper(I) acetate as catalyst, and tris((1-*tert*-butyl-1*H*-1,2,3-triazolyl)methyl)amine (TTTA) as ligand to obtain triazole **2.26** in 74% yield after recrystallization from toluene. The hydroxyl group on **2.26** was converted to

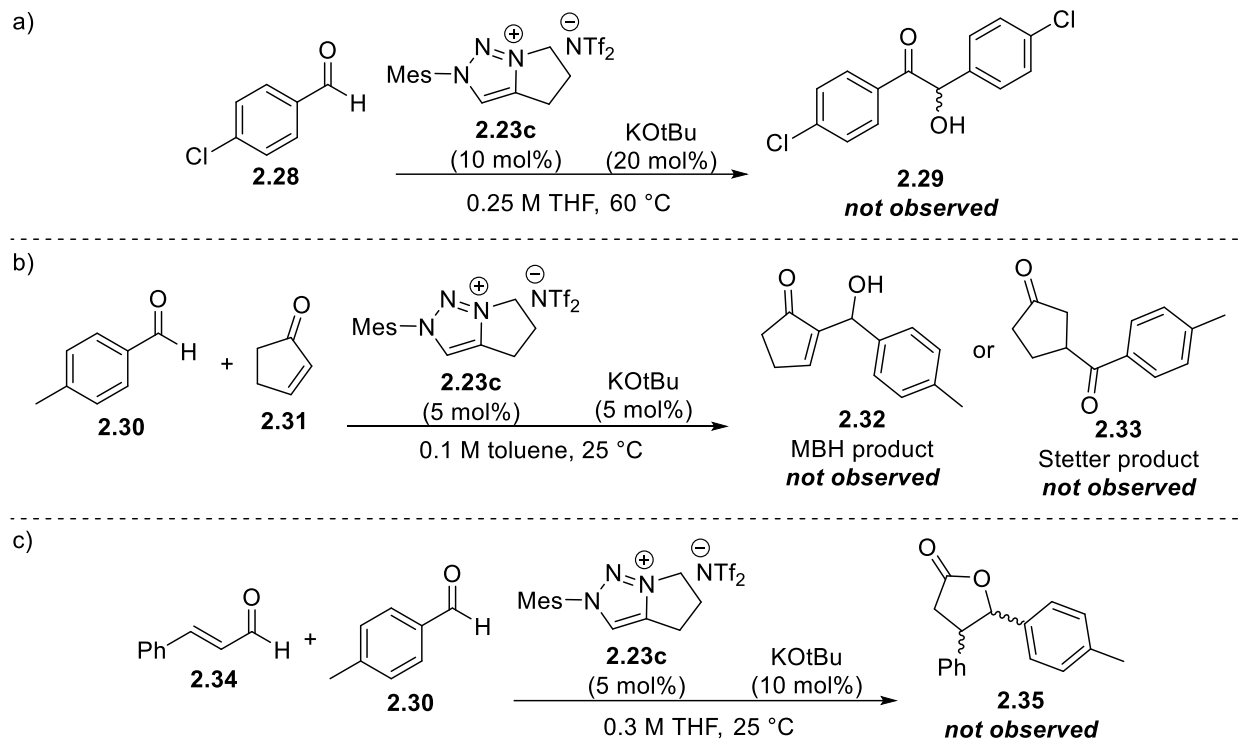
the triflate with Tf₂O, which underwent spontaneous cyclization to give triflate salt **2.27** in 69% yield.



Scheme 2.5: Synthesis of 1,2,4-trisubstituted 1,2,3-triazolium regioisomer 2.27.

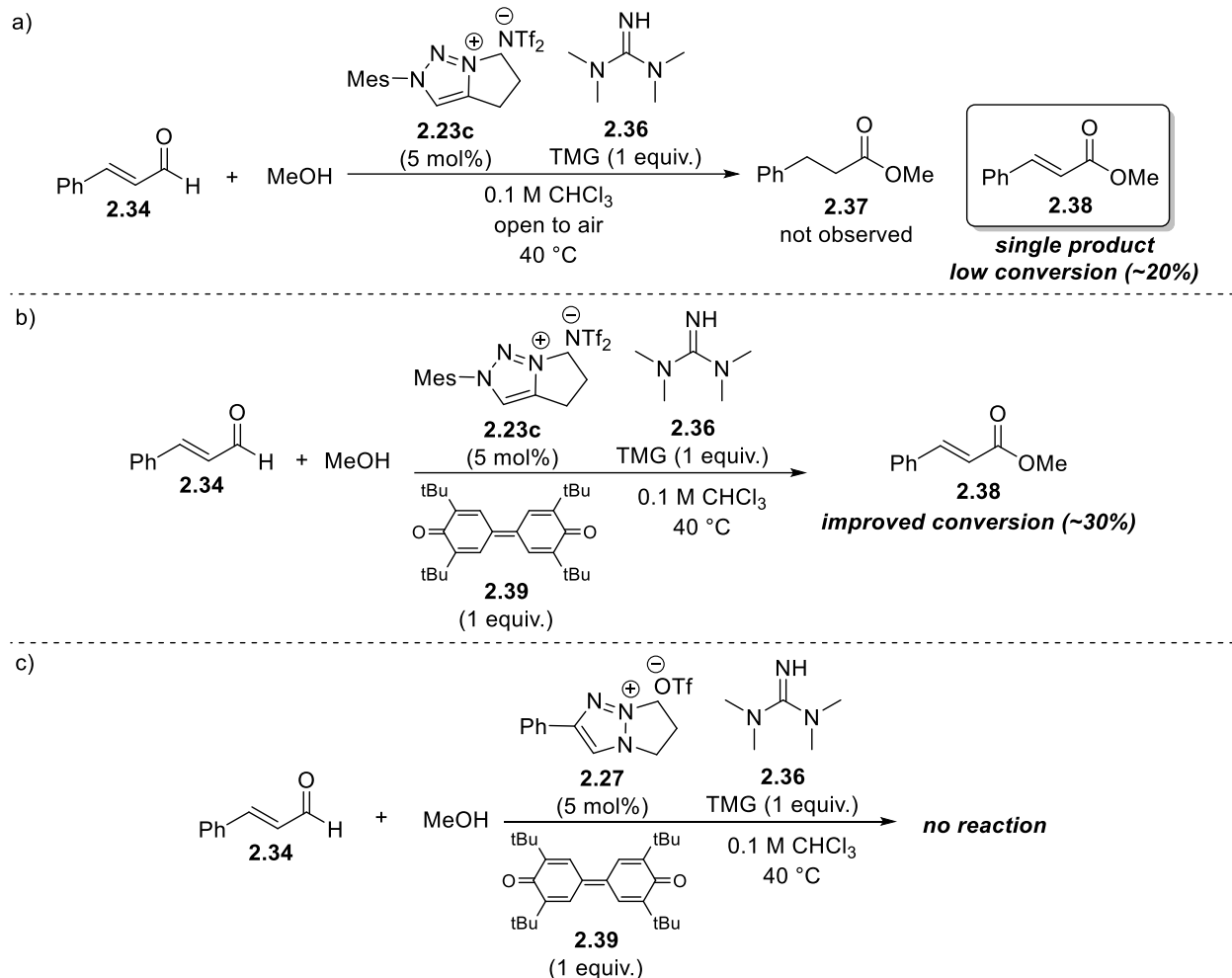
2.3 Initial reaction trials

With a library of triazolium precatalysts in hand, we set out to test them for catalytic activity. Triazolium salt **2.23c** was chosen for testing, due to its similarities to Bode's successful catalyst **2.16**.⁷³ 1,2,3-triazolium salt **2.23c** was tested for catalytic activity in the benzoin condensation, Stetter/Morita-Baylis-Hillman (MBH) reaction, and in conditions to produce lactone **2.35** (Scheme 2.6).



Scheme 2.6: Reaction trials with 1,2,3-triazolium NHC precatalysts: a) benzoin condensation; b) Morita-Baylis-Hillman/Stetter reaction; c) homoienolate lactonization. Each reaction trial did not show evidence of expected product formation.

Unfortunately, each reaction depicted in Scheme 2.6 showed no evidence of product formation. Bode's catalyst **2.16**, the 1,2,4-triazolium analogue of **2.23c**, has been shown to be a very efficient catalyst for the redox esterification of α,β -unsaturated aldehydes,⁷³ and so **2.23c** was subjected to Bode's reaction conditions (Scheme 2.7).



Scheme 2.7: a) Successful reaction trial with 1,2,3-triazolium precatalyst **2.23c**. The observed product of the reaction is the oxidative esterification product, rather than the redox esterification product. b) Improved conversion observed in the oxidative esterification reaction after addition of chemical oxidant **2.39**. c)

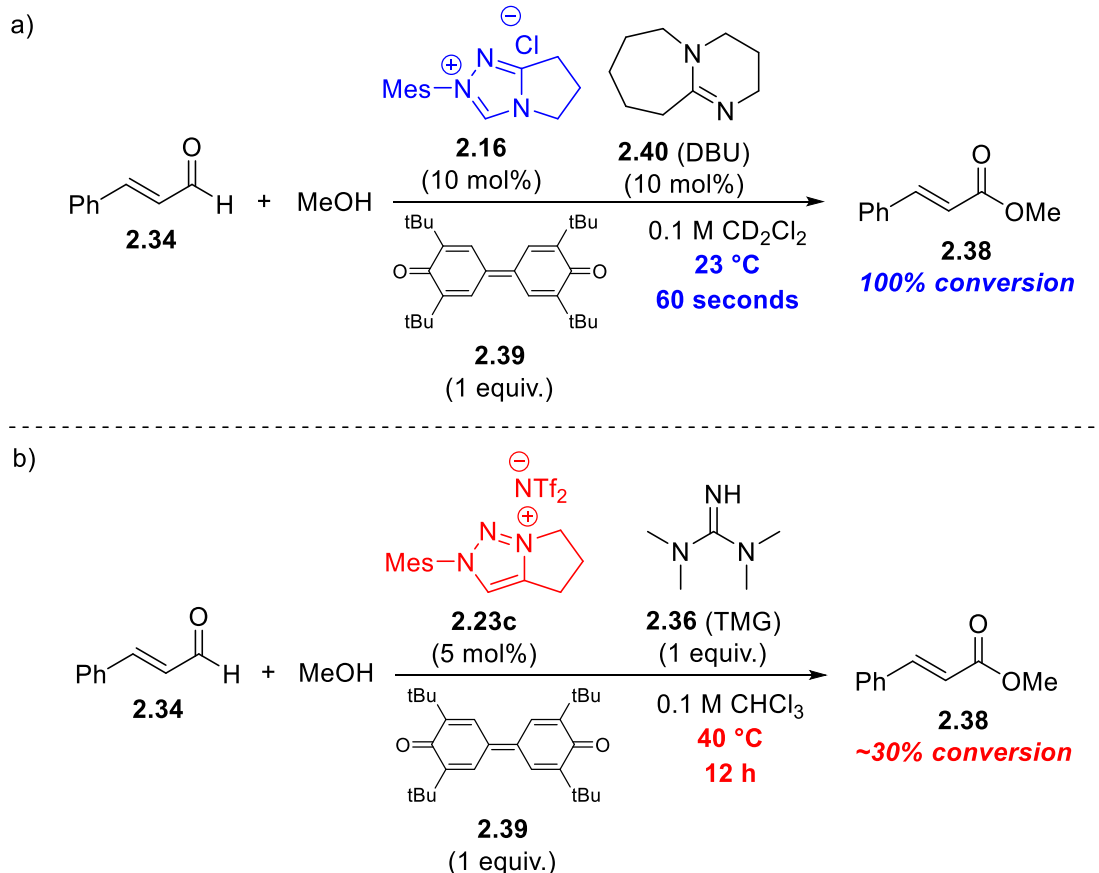
Unsuccessful reaction trial with 1,2,3-triazolium precatalyst **2.27**.

Precatalyst **2.23c** was found to facilitate only the oxidative esterification, not the redox esterification, of cinnamaldehyde **2.34**, presumably using ambient molecular oxygen as stoichiometric oxidant (Scheme 2.7a). Introduction of bisquinone oxidant **2.39** helped to improve conversion of cinnamaldehyde **2.34** to methylcinnamate **2.38**, albeit slightly (Scheme 2.7b).

1,2,4-trisubstituted triazolium salt **2.27** was evaluated as a precatalyst for this reaction, but no catalytic activity was observed (Scheme 2.7c).

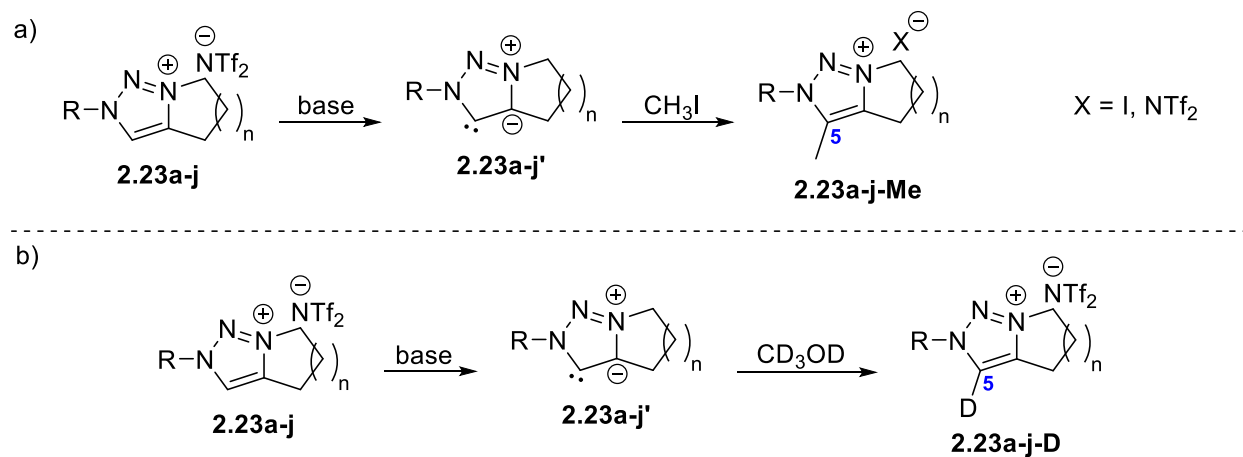
2.4 Methylation and acidity measurements

Bode's *N*-mesityl-substituted 1,2,4-triazolium salt **2.16**, the 1,2,4-triazolium analogue of **2.23c**, has been shown to facilitate the oxidative esterification of cinnamaldehyde with a high degree of efficiency: 100% conversion to product within 60 seconds at room temperature⁹⁸ (Scheme 2.8a). Under similar reaction conditions, 1,2,3-triazolium precatalyst **2.23c** only gave approximately 30% conversion to product in 12 hours, at 40 °C (Scheme 2.8b). It was hypothesized that this lower degree of activity in **2.23c** could be attributed to one of two possibilities: a low degree of nucleophilicity in the *in situ*-generated free carbene, or low acidity of the 1,2,3-triazolium precatalyst, limiting the concentration of active carbene catalyst in solution.



Scheme 2.8: a) Highly efficient oxidative esterification of cinnamaldehyde by 1,2,4-triazolium precatlyst **2.16 reported by Bode.⁹⁸ b) Relatively poor performance in the oxidative esterification of cinnamaldehyde by 1,2,3-triazolium precatlyst **2.23c**.**

To probe carbene nucleophilicity, a series of methylation studies were conducted, subjecting 1,2,3-triazolium salts **2.23a-j** to an excess of methyl iodide in the presence of base, and monitoring the rates of 1,2,3-triazolium consumption and methyl incorporation at the C-5 position by HPLC (Scheme 2.9a). To probe the relative acidities of 1,2,3-triazoliums **2.23a-j**, the rate of deuterium incorporation at the C-5 position was monitored by ^1H NMR (Scheme 2.9b). The structures of each 1,2,3-triazolium salt used in these studies is shown in Figure 2.2.



Scheme 2.9: a) Studies to probe the nucleophilicity of carbenes **2.23a-j'** by monitoring the rate of methyl incorporation at C5. b) Studies to probe the relative acidities of **2.23a-j** by monitoring the rate of deuterium incorporation at C5 by ¹H NMR.

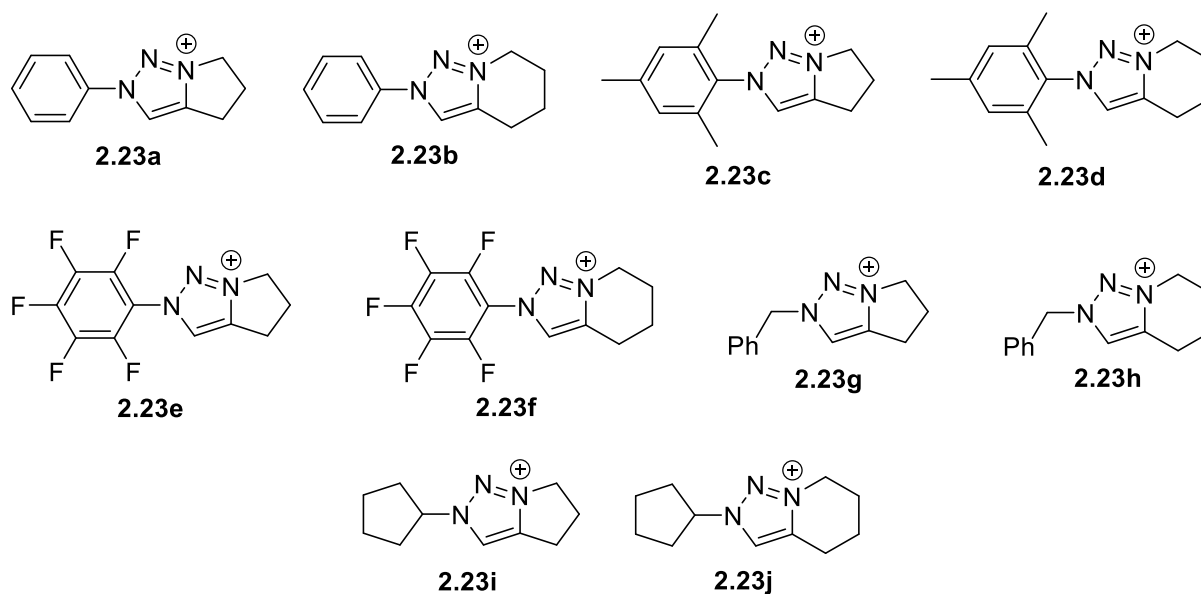
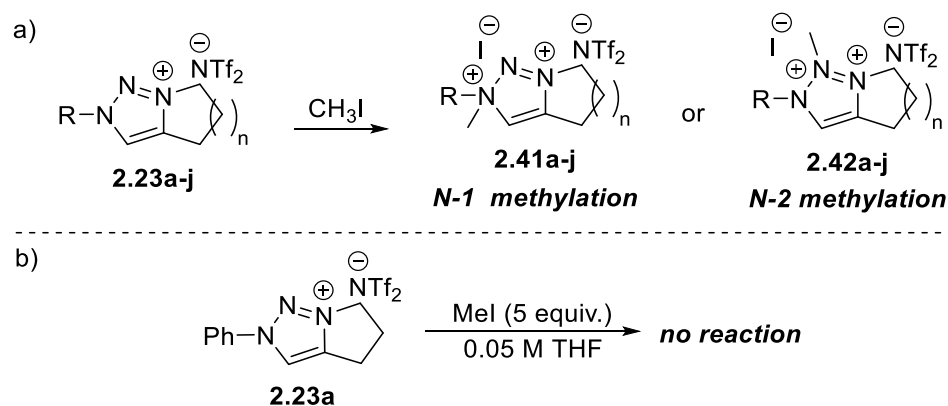


Figure 2.2: 1,2,3-triazolium salts used in methylation and acidity studies. Counterion for all salts is NTf₂⁻.

2.4.1 Methylation studies

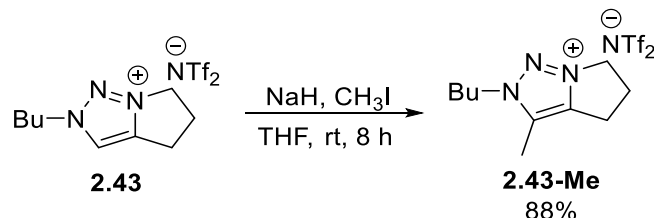
Due to the electrophilic character of methyl iodide, it is plausible to envision methylation at N-1 or N-2 of the triazolium salts **2.23a-j** in the absence of base, potentially forming dicationic species of the type **2.41** or **2.42** (Scheme 2.10a). To test if *N*-methylation was possible, a control experiment was performed, subjecting triazolium salt **2.23a** to an excess of methyl iodide in the absence of base (Scheme 2.10b). No methylation or chemical transformation of triazolium salt **2.23a** was observed by HPLC.



Scheme 2.10: a) Possible *N*-methylation of triazolium salts **2.23a-j** by methyl iodide. c) Methylation control experiment, showing that triazolium salt **2.23a** shows no evidence of chemical transformation in the presence of methyl iodide.

Before conducting the proposed methylation studies, the choice of base used to deprotonate the 1,2,3-triazolium salts needed to be considered. From the initial successful reaction trials (Scheme 2.7), 1,1,3,3-tetramethylguanidine (TMG, **2.36**) proved to be sufficiently basic enough to generate the carbene for catalytic activity. However, during an initial trial run, it was found that methyl iodide preferentially alkylates TMG, and methylation at C-5 of the 1,2,3-triazolium salt. Similar results were observed when amine bases 1,8-diazabicyclo[5.4.0]undec-7-

ene (DBU, **2.40**), triethylamine, and *N,N*-diisopropylethylamine were used. The successful synthesis of C-5-methylated bicyclic 1,2,3-triazolium salts has previously been reported by Tseng et. al using sodium hydride⁹⁹ (Scheme 2.11). However, due to institutional difficulties in acquiring sodium hydride, this was not an option, so potassium *tert*-butoxide (K⁺OT⁻Bu) was chosen as the base for the methylation studies.



Scheme 2.11: Synthesis of C-5-methylated bicyclic 1,2,3-triazolium salts by Tseng et. al.⁹⁹

Figure 2.3 shows reaction progress curves for the methylation of *N*-phenyl and *N*-mesityl substituted triazolium salts **2.23a-d**. The consumption curves for each 1,2,3-triazolium salt **2.23a-d** correlate well with their respective formation curves for **2.23a-d-Me**, indicating that the *in situ*-generated carbenes are sufficiently nucleophilic. *N*-phenyl substituted triazolium with 6-membered bicyclic ring **2.23b** showed fastest conversion to product, with complete conversion within 30 minutes. Conversely, *N*-phenyl substituted triazolium with 5-membered bicyclic ring **2.23a** showed slowest conversion to product. For triazolium salts **2.23a-d**, there is no clear nucleophilicity trend, with respect to both *N*-substituent and size of the saturated fused ring.

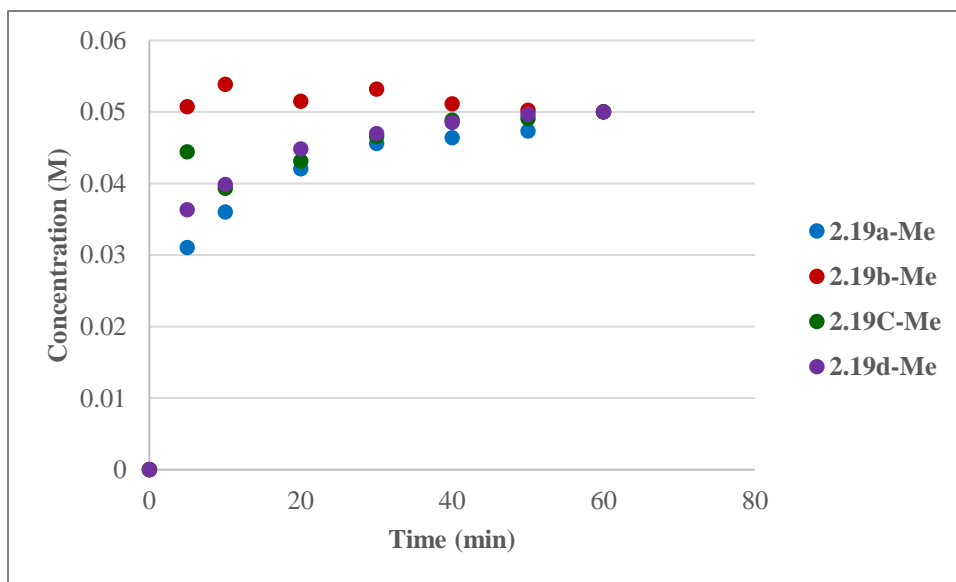
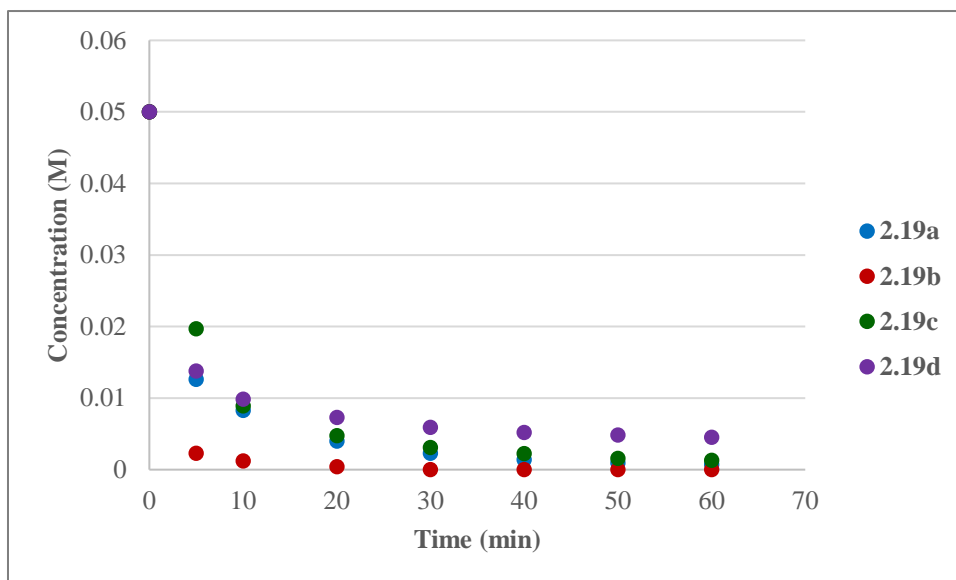
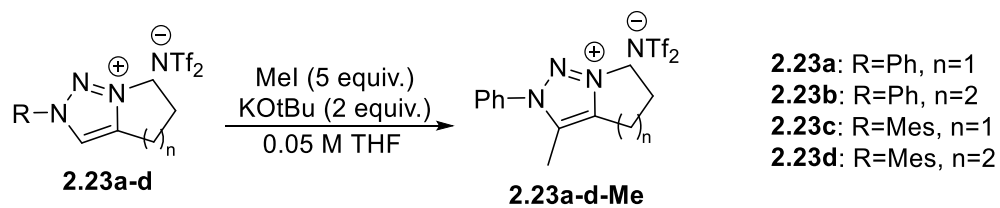


Figure 2.3: Reaction progress curves for the methylation of 1,2,3-triazoliums 2.23a-d.

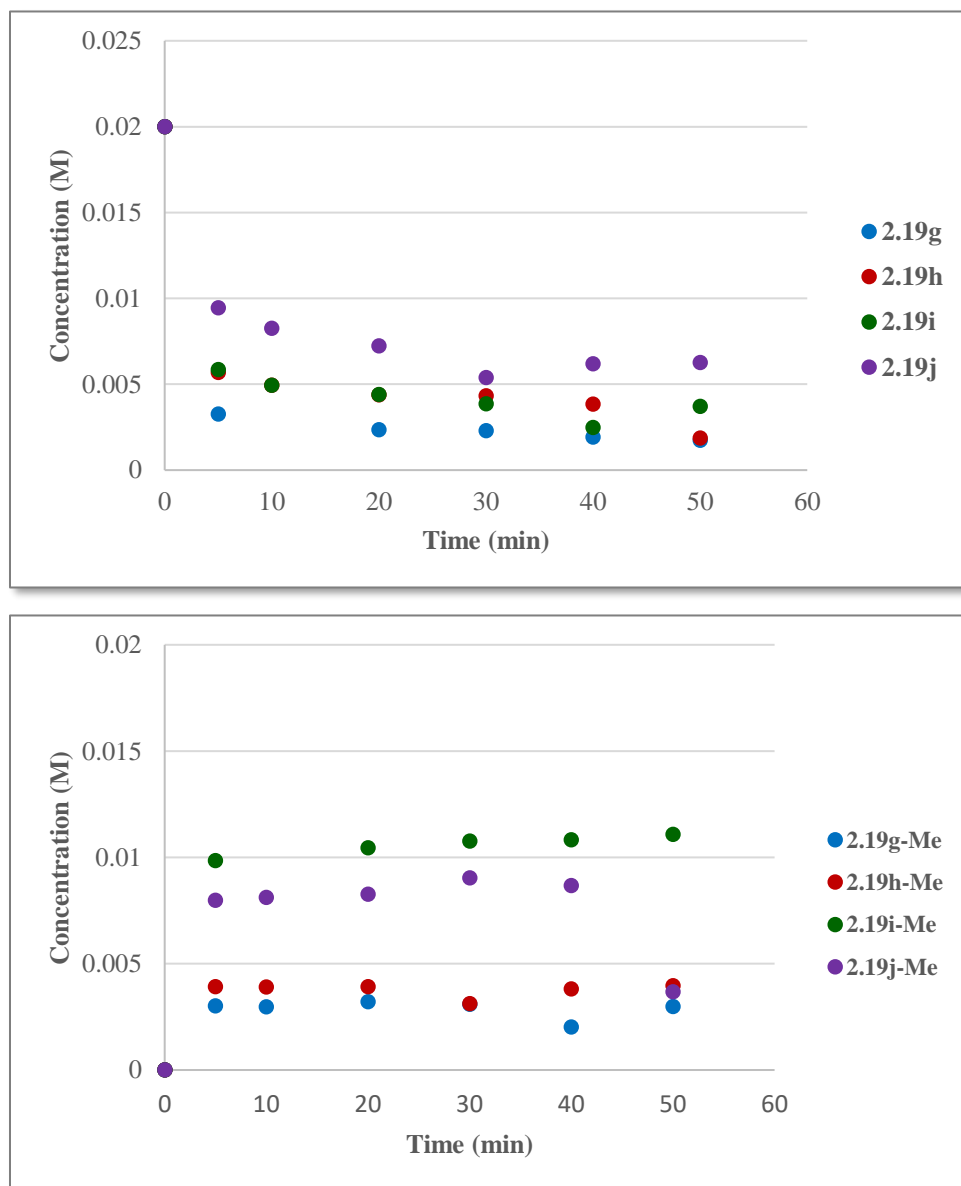
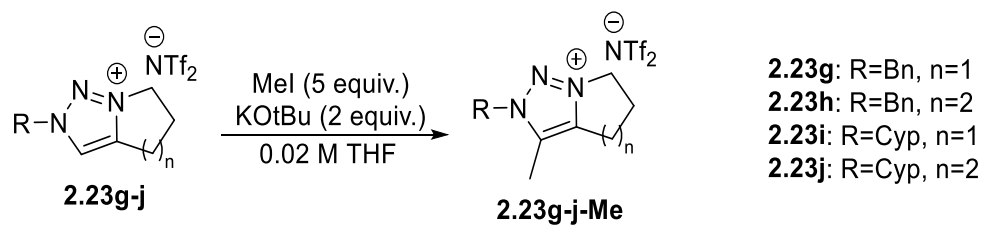
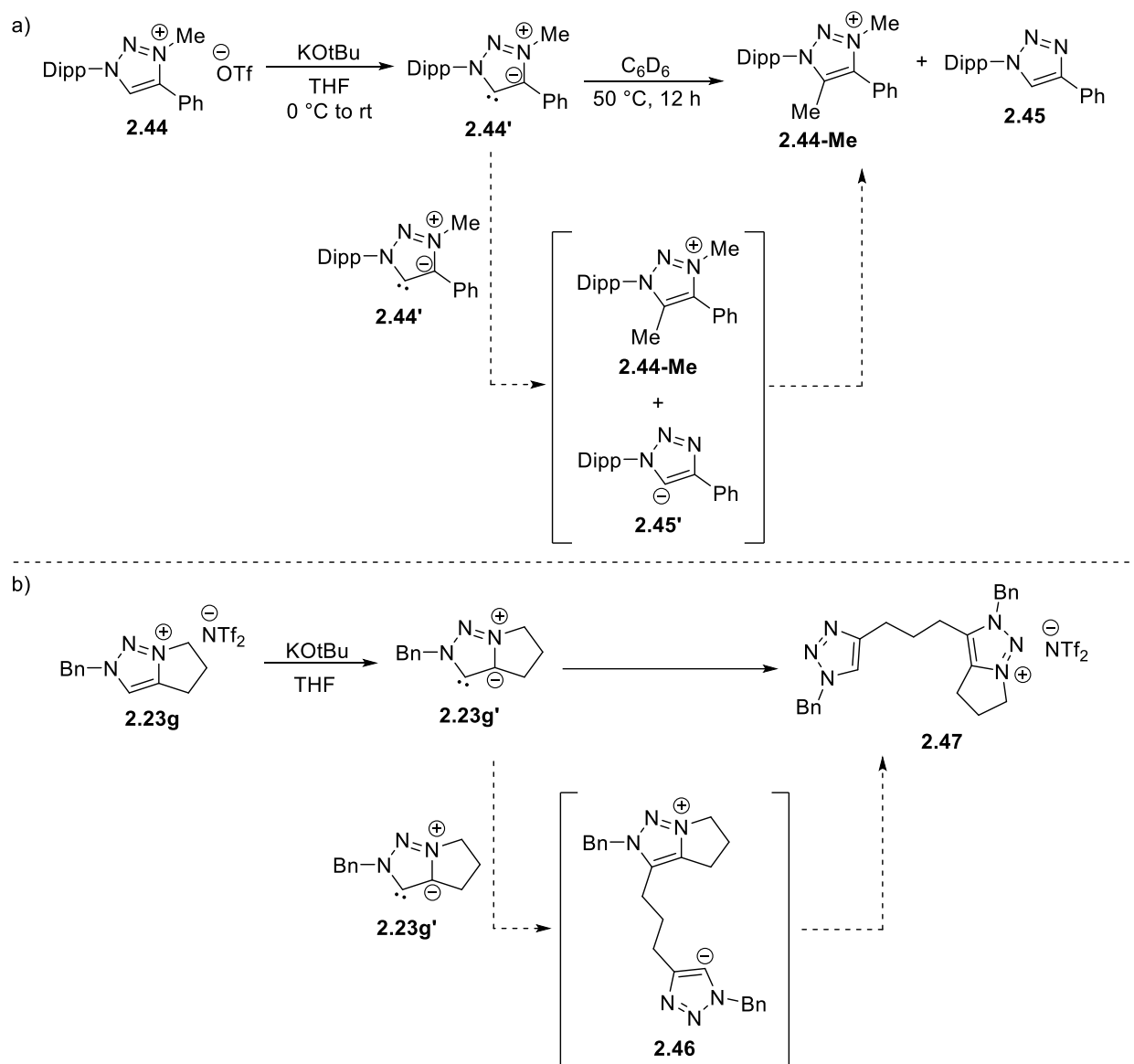


Figure 2.4: Reaction progress curves for the methylation of triazoliums 2.23g-j.

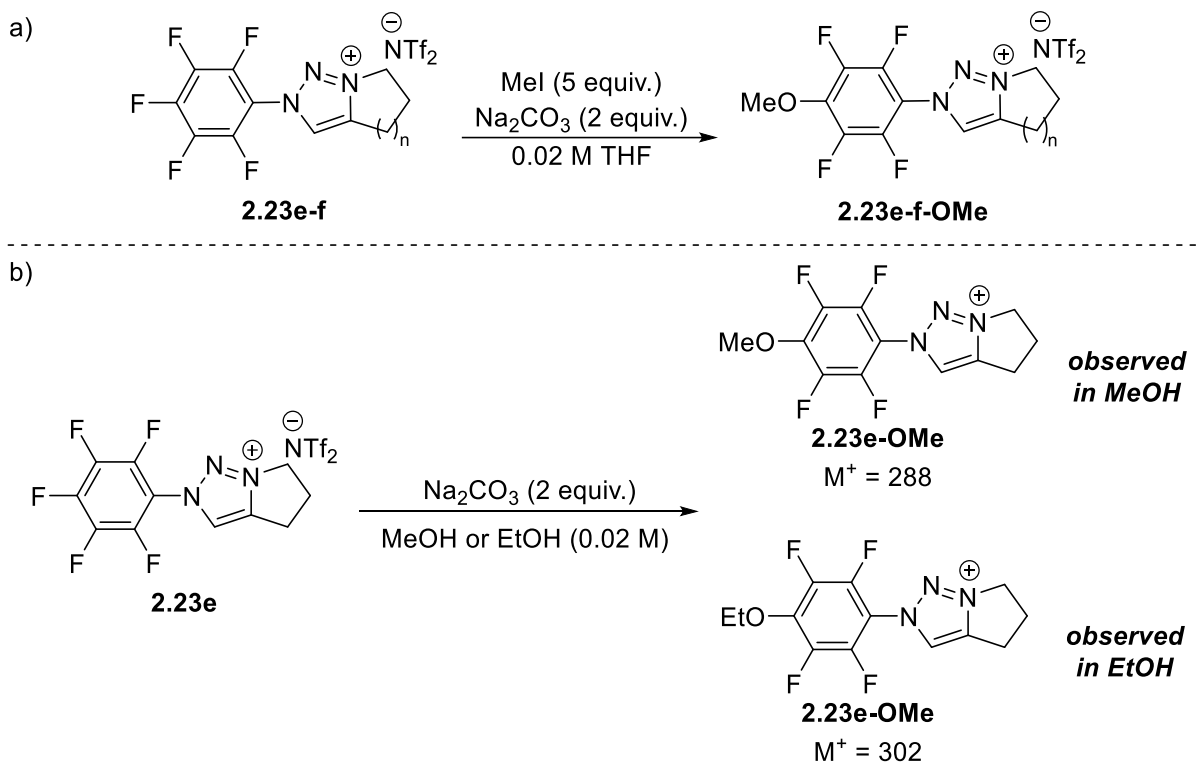
Figure 2.4 shows reaction progress curves for the methylation of *N*-benzyl (Bn) and *N*-cyclopentyl (Cyp) substituted triazolium salts **2.23g-j**. These triazoliums do not show the same extent of product conversion as the *N*-aromatic substituted triazoliums **2.23a-d**. For all four of these triazolium salts, multiple products other than the methylation products **2.23g-j-Me** were detected, suggesting decomposition of the triazolium as well as methylation. A decomposition pathway for 1,2,3-triazolium salts in the presence of strong base has previously been described by Bouffard et. al⁹² (Scheme 2.12a). A possible analogous decomposition pathway for triazolium salts **2.23g-j** is shown in Scheme 2.12b, using triazolium salt **2.23g** as an example. This decomposition pathway involves nucleophilic attack of the carbene on to the methylene group adjacent to the triazolium ring, opening the 5-membered exocyclic ring to form species **2.46**, which then gets protonated to form species **2.47**. This decomposition pathway is a mere possibility; the actual structures of the decomposition products are still unknown.



Scheme 2.12: a) Decomposition of 1,2,3-triazolium salts described by Bouffard et. al.⁹² b) Possible decomposition pathway for triazolium salts 2.23g-j.

When *N*-pentafluorophenyl substituted triazolium salts **2.23e** and **2.23f** were submitted for the methylation study, addition of KOtBu to the reaction mixture resulted in rapid decomposition of both triazoliums into unidentifiable products. To prevent this decomposition, the base used was switched from KOtBu to Na₂CO₃. However, methylation was not observed.

Instead, these triazoliums underwent S_NAr substitution with MeOH, the HPLC/MS quench solvent (Scheme 2.13a).



Scheme 2.13: Nucleophilic aromatic substitution reaction of triazoliums **2.23e and **2.23f**.**

To confirm this observation that nucleophilic aromatic substitution was occurring, two experiments were performed where triazolium salt **2.23e** was subjected to Na₂CO₃ in methanol or ethanol (Scheme 2.13b). HPLC/MS analysis of the methanol reaction mixture showed the presence of a compound with a molecular ion of m/z 288, consistent with **2.23e-OMe**, the product of methanol incorporation into **2.23e**. Analysis of the ethanol reaction mixture showed the presence of a compound with a molecular ion of m/z 302, consistent with **2.23e-OEt**, the product of ethanol incorporation into **2.23e**. These observations suggest that the triazolium functionality is a sufficient activating group for nucleophilic aromatic substitution, and that addition of methanol can occur with a weak base, such as Na₂CO₃.

2.4.2 Acidity measurements by ^1H NMR

With a library of potential 1,2,3-triazolium NHC precursors, we wished to gain insight into the relative acidities of each triazolium salt. As mentioned in Chapter 1, deprotonation of the NHC precatalysts is an essential first step to generate the active carbene catalyst. To evaluate the relative acidities of each triazolium salt, *in situ* ^1H NMR spectroscopy was used to monitor the rate of deuterium incorporation at the C-5 position starting from the protonated azolium precatalyst in the presence of DIPEA and CD_3OD (Figure 2.5). Using this method, the rate of deuterium incorporation can be used to infer how acidic a particular triazolium is – triazoliums that incorporate deuterium faster can be considered more acidic.

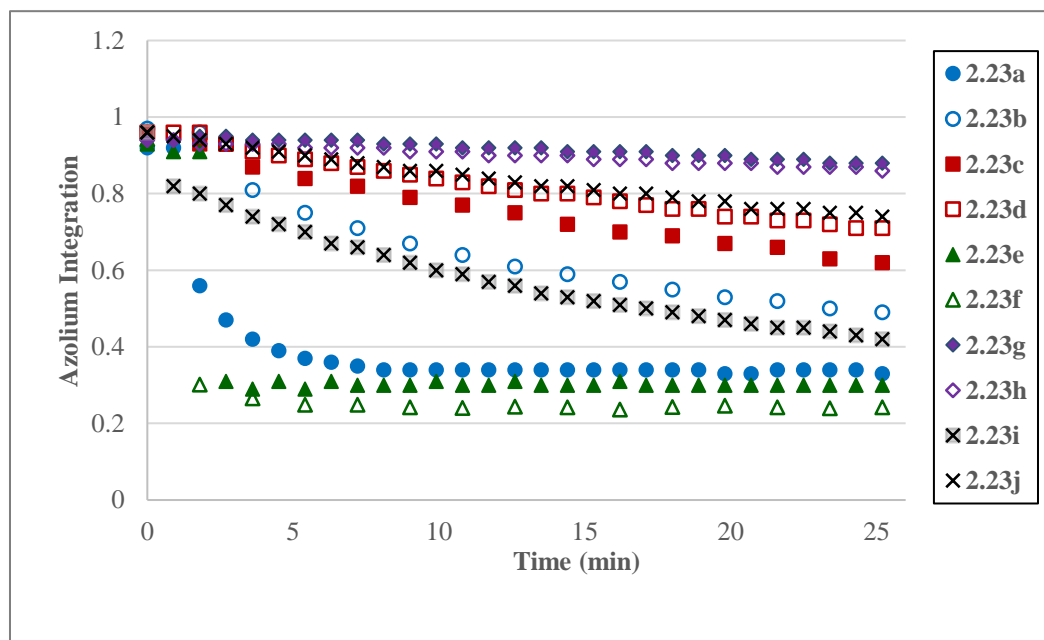
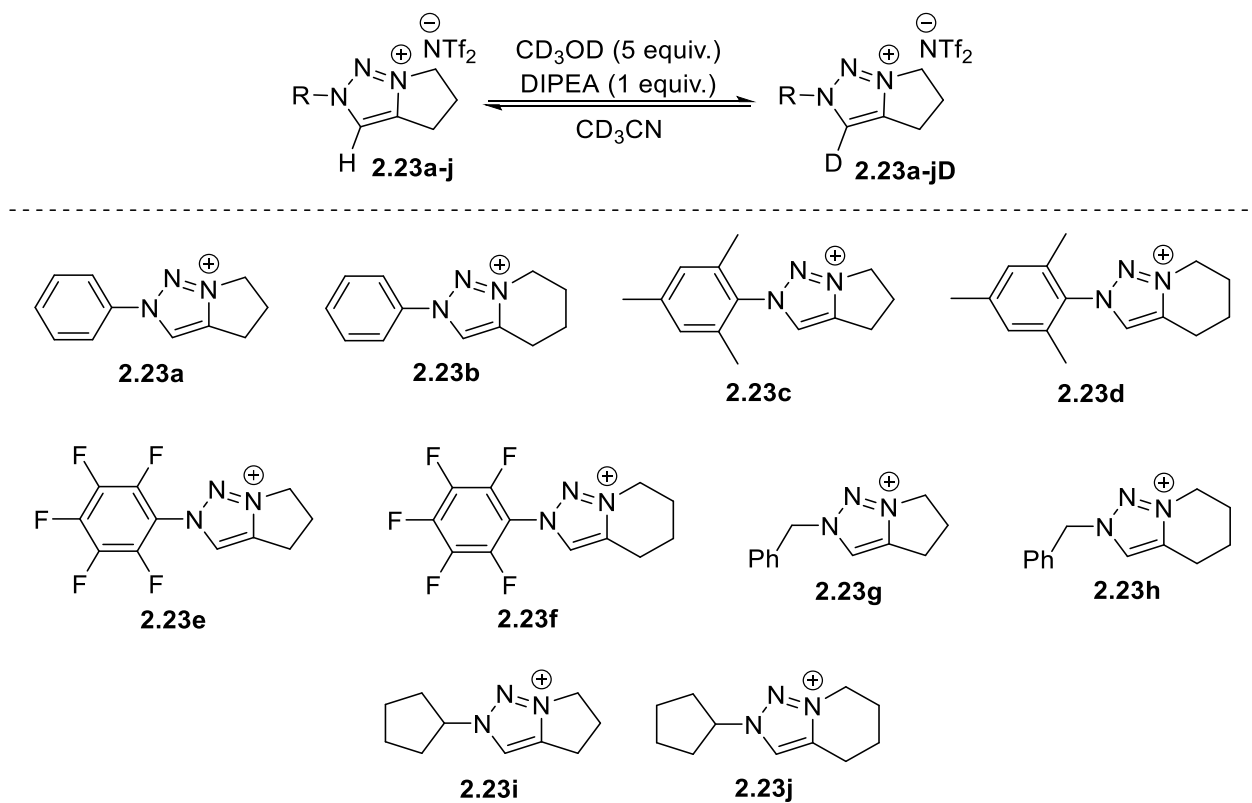


Figure 2.5: Progress curves of deuterium incorporation into triazolium salts 2.23a-j.

This experiment demonstrates that both the *N*-substituent and exocyclic ring size impact the relative acidity of the azolium C-H. Precatalysts with strongly electron-withdrawing pentafluorophenyl substituents (**2.23e** and **2.23f**) show the fastest rate of deuterium incorporation, whereas species with the more electron-rich *N*-mesityl substitution (**2.23c** and **2.23d**) and aliphatic *N*-benzyl substitution (**2.23g** and **2.23h**) display the slowest rates of deuterium incorporation. The nature of the *N*-substituent plays the largest role in determining the acidity of the triazolium C-H. However, the size of the saturated fused ring also has an impact. Except for *N*-pentafluorophenyl substituted triazoliums **2.23e** and **2.23f**, triazoliums bearing a five-membered ring display faster rates of deuterium incorporation than their corresponding six-membered analogues. It is reasonable to assume that triazoliums bearing a five-membered ring are more planar than their six-membered analogues, and hence deprotonation at the C-5 position is less hindered for triazoliums with five-membered saturated rings.⁹⁹

2.4.3 Catalytic activity

Following the methylation and acidity surveys, a study of catalyst activity was conducted, focusing on initial rates, overall product formation, and observing any catalyst deactivation. Individually, each 1,2,3-triazolium salt **2.23** was evaluated as a catalyst for the oxidative esterification of cinnamaldehyde with methanol, and reaction progress curves were generated by HPLC (Figure 2.6). Triazolium **2.23c** exhibits the fastest initial reaction rate, as well as the greatest extent of product formation, reaching ~43% conversion over 50 hours. *N*-pentafluorophenyl-substituted triazoliums **2.23e** and **2.23f** exhibit rapid catalyst deactivation, as no new product is formed after ten hours. These triazoliums are prone to decomposition in the presence of strong base, which can explain the observed deactivation. *N*-alkyl substituted

triazoliums **2.23i** and **2.23j** show very little catalytic activity, only achieving <5% conversion to product. With the exception of **2.23e** and **2.23f**, triazoliums with aromatic *N*-substituents are the best catalysts for this reaction. The size of the saturated fused ring plays a role in catalytic activity as well. Triazoliums with 5-membered rings show both faster initial rate and higher conversion to product over their 6-membered counterparts. This observation may be due to lower steric encumbrance adjacent to the carbene center in triazoliums bearing the 5-membered ring, resulting in enhanced catalytic activity.

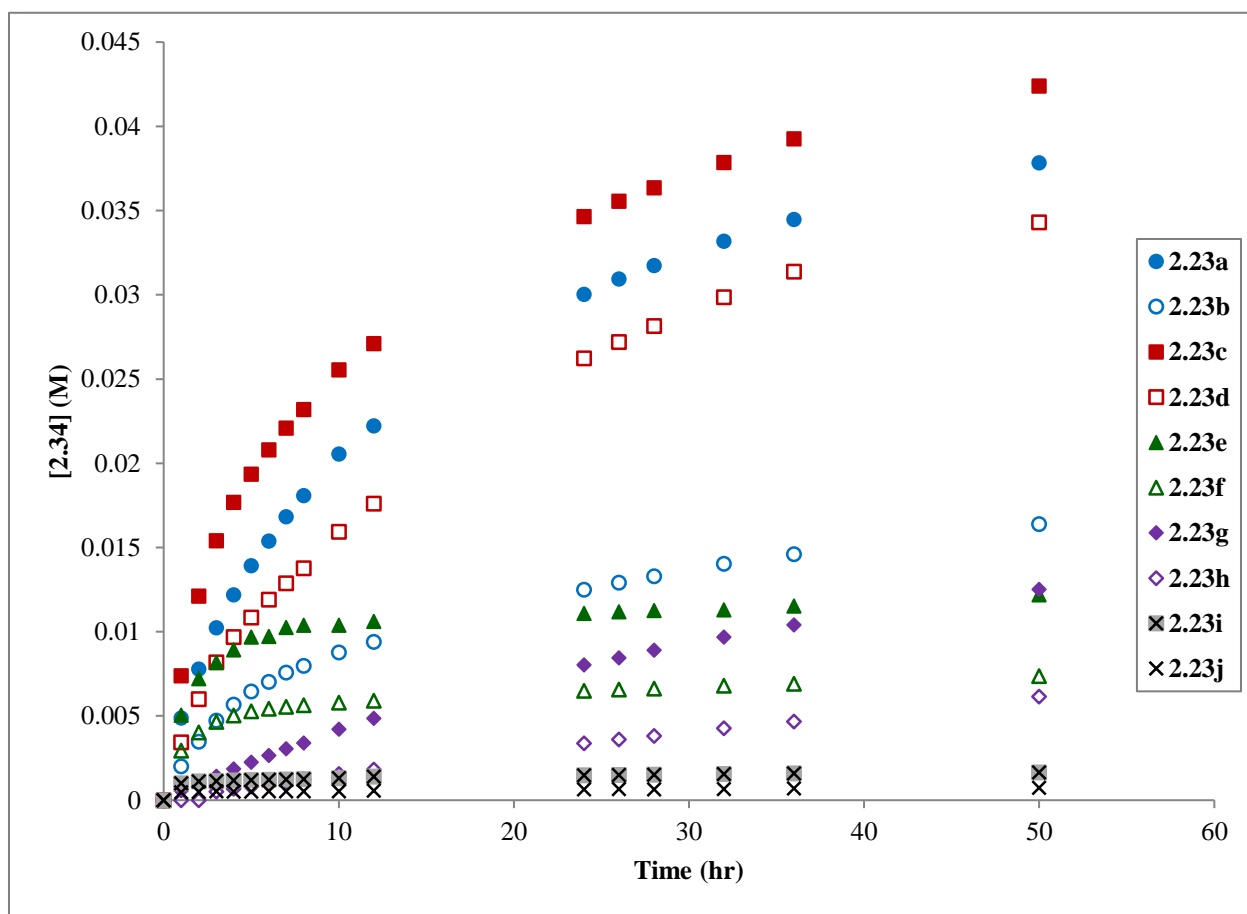
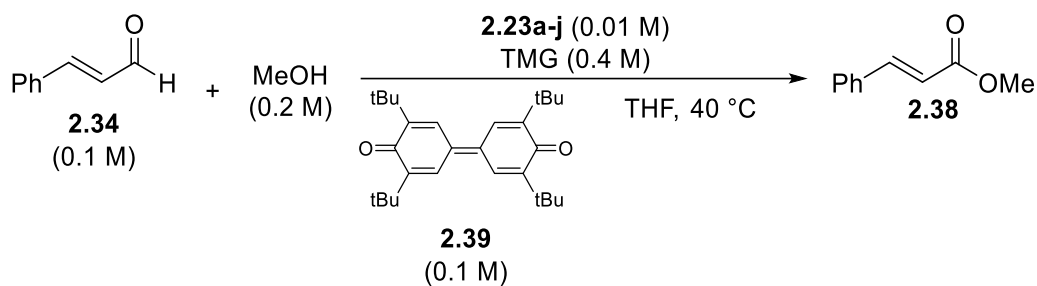


Figure 2.6: Product formation curves of 2.38 with varying 1,2,3-triazolium precatalysts.

2.4.4 Correlations between nucleophilicity, acidity, and reactivity

With a suite of surveys studying the nucleophilicity, acidity, and catalytic performance of each 1,2,3-triazolium precatalyst, they can be ranked according to each metric, and correlations

can be made. Figure 2.7 shows each triazolium ranked in order of increasing nucleophilicity, acidity, and catalytic performance. There are no obvious trends between triazolium nucleophilicity and acidity, with the exception that triazoliums **2.23g** and **2.23h** are both the least nucleophilic and the least acidic. Comparing triazolium nucleophilicity and catalytic activity, triazoliums **2.23a-d**, which are *N*-phenyl and *N*-mesityl substituted, exhibit both the highest degree of nucleophilicity and catalytic activity. However, this is not a one-to-one correlation; the most nucleophilic triazolium **2.23b** exhibits the lowest degree of catalytic activity of these four triazoliums, and triazolium **2.23a** shows the second-best catalytic activity while being the least nucleophilic.

When comparing triazolium acidity to catalytic activity, it appears that the two are inversely proportional to each other. *N*-pentafluorophenyl substituted triazoliums **2.23d** and **2.23d**, which showed the highest degree of deuterium incorporation, and therefore the highest acidity, performed very poorly. *N*-mesityl substituted triazolium **2.23c**, which displayed relatively much lower acidity than triazoliums **2.23d** and **2.23e**, displayed the highest amount of catalytic activity. Moreover, triazoliums **2.23e** and **2.23f** displayed no further conversion after 10 hours, leading to the conclusion that catalyst deactivation is the root cause of the poor performance of these species. The most likely cause of this deactivation is base-mediated decomposition of the catalyst. During the initial methylation studies of **2.23e** and **2.23f**, it was observed that both triazoliums rapidly decomposed in the presence of K₂OtBu, a strong base. TMG, the base used for the oxidative esterification reaction, is a weaker base than K₂OtBu, so it is plausible that the catalyst could participate in a few catalytic turnovers before decomposing. In general, catalytic efficiency is determined by both ring size and the nature of the *N*-substituent,

but *N*-substituent plays less of a role. In addition, the catalytic efficiency and relative acidity appear to be inversely proportional to each other.

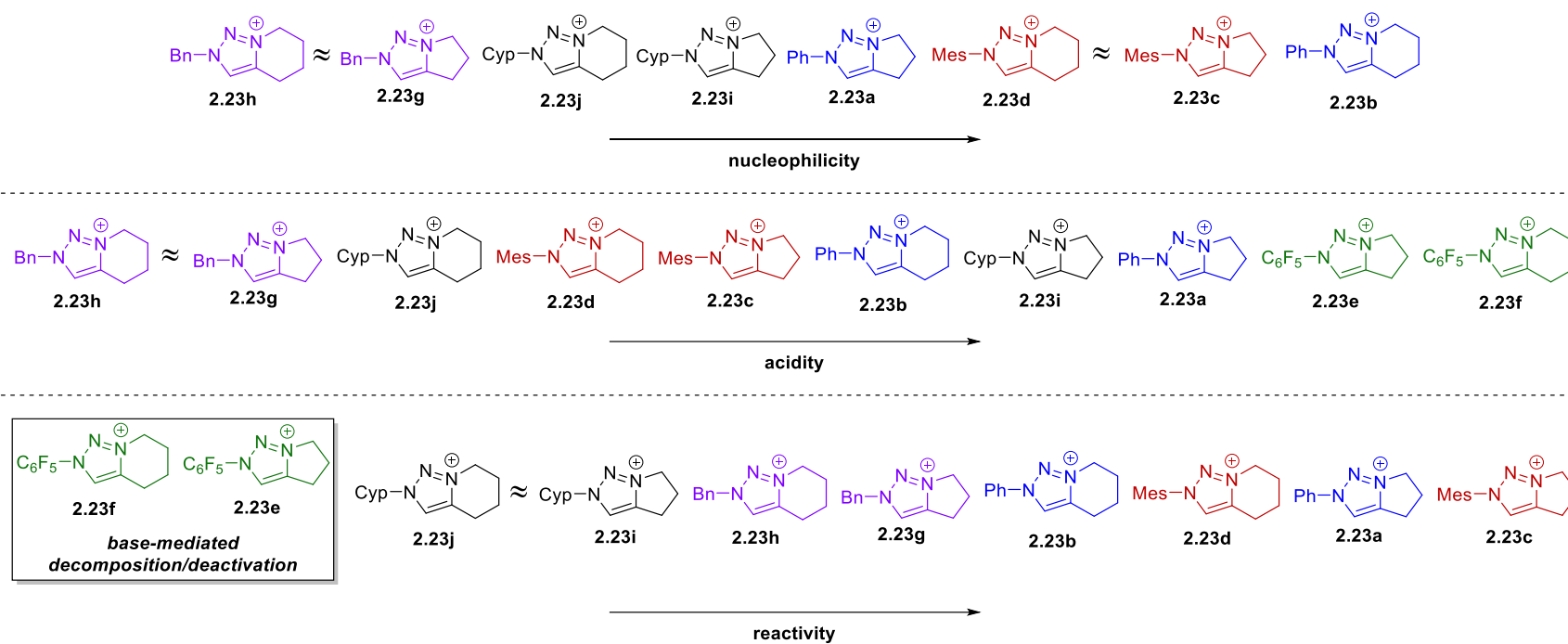


Figure 2.7: Triazoliums 2.23a-j ranked in order of increasing nucleophilicity, acidity, and reactivity. Relative nucleophilicities for triazoliums 2.23e and 2.23f were not able to be determined due to decomposition in the presence of base.

2.5 Application of 1,2,3-triazolium precatalysts to the oxidative esterification of aldehydes – scope and limitations

With a better understanding of the reactivity and acidity patterns of the full library of 1,2,3-triazolium precatalysts, the reaction conditions were optimized and the substrate scope of the reaction was examined. From the previous study, triazolium salt **2.23c** was identified to be the optimal precatalyst for the oxidative esterification reaction. However, these optimization studies were performed before the catalyst optimization, and so triazolium salt **2.23a** was used for these optimization studies. Triazolium salt **2.23a** is the second-best catalyst for this reaction, and it has a similar kinetic profile as the optimal catalyst **2.23c**. For the purposes of solvent and base optimization, it serves as an acceptable analogue to optimize with. Ideally, catalyst and base optimization would have been performed first.

To identify the optimal solvent and base, reaction progress curves were generated using HPLC, and both initial rates of reaction and overall conversion to product were observed. Figure 2.8 shows reaction progress curves for the formation of methylcinnamate **2.38** in different reaction solvents. Methyl *tert*-butyl ether (MTBE) showed the highest conversion to product (62%) after 48 hours, as well as exhibiting the fastest initial rate of product formation. Acetonitrile, dichloromethane (DCM), and methyl ethyl ketone (MEK) show approximately the same productive catalytic activity in the first twelve hours, but then diverge after that timepoint. Methanol (MeOH) shows less than 5% total conversion over 48 hours. This is most likely due to the very low solubility of oxidant **2.39** in methanol, limiting the amount of oxidant that is available to react. While MTBE was identified as the optimal solvent for this reaction, due to cost, THF was used going forward.

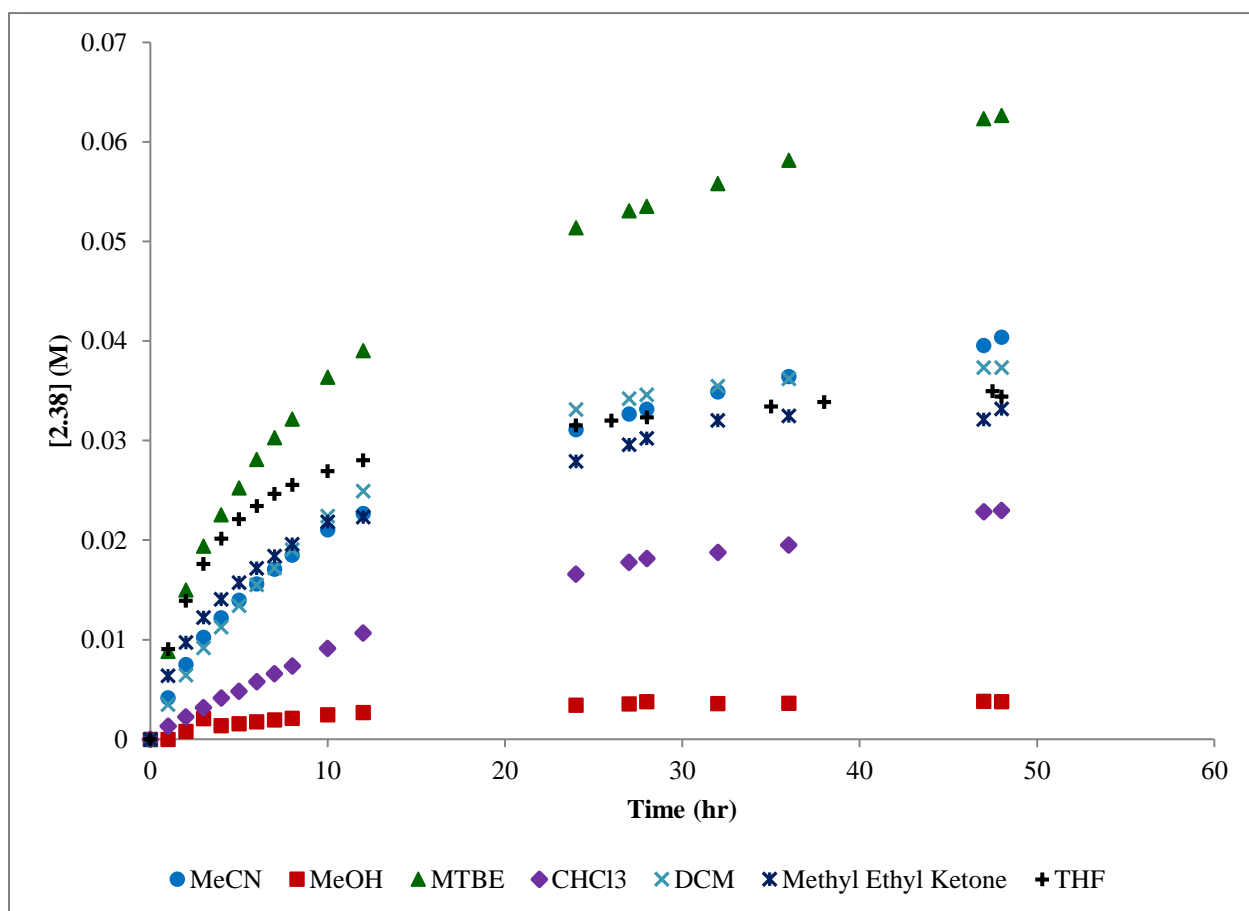
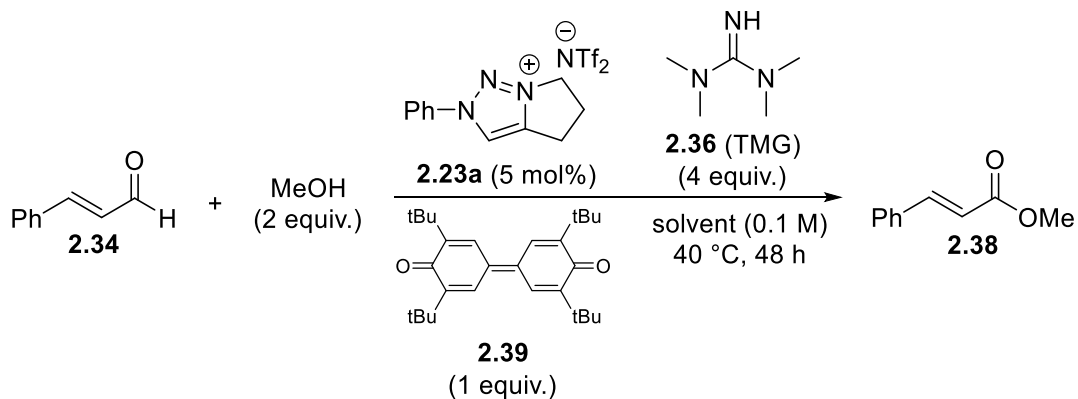


Figure 2.8: Product formation curves for the oxidative esterification of cinnamaldehyde with methanol. Each curve represents a different reaction solvent.

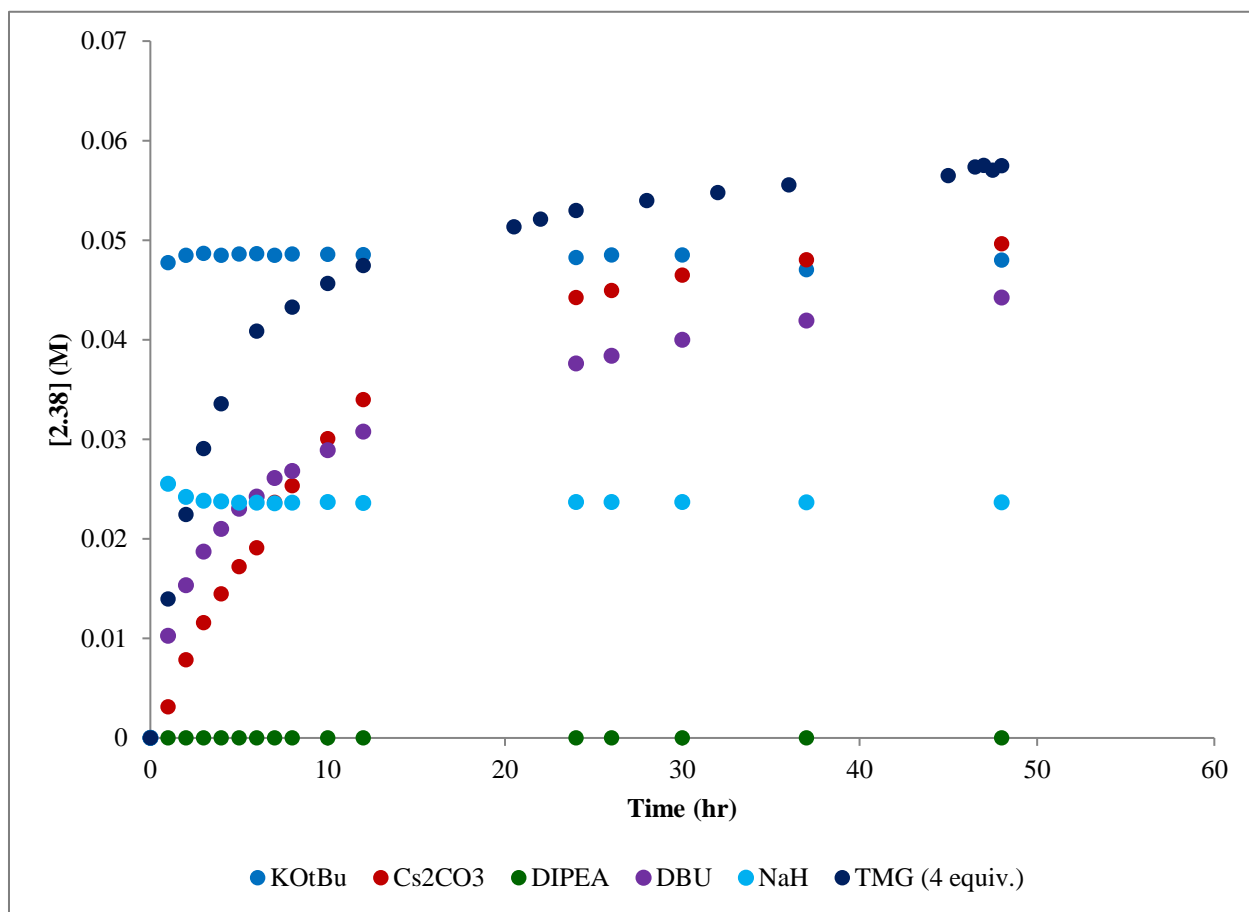
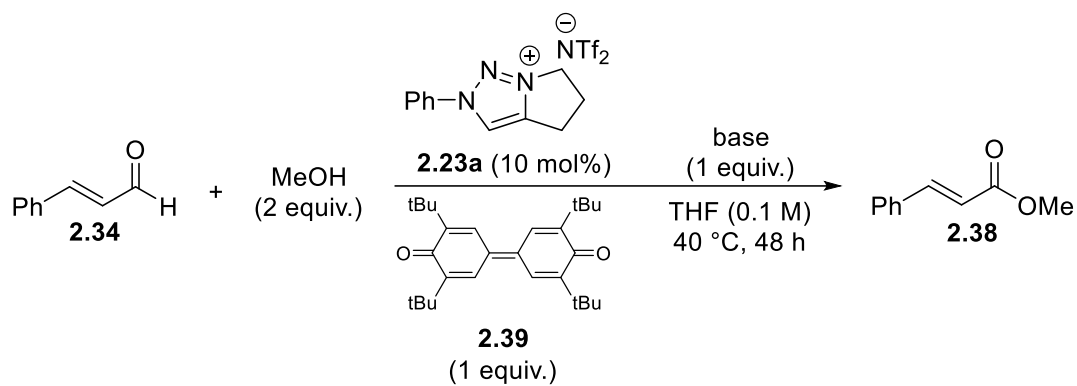
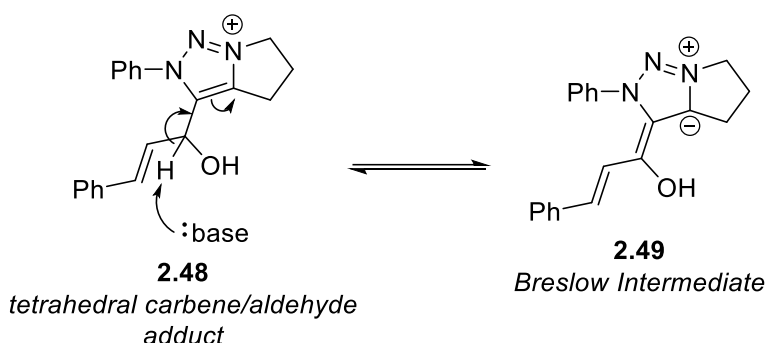


Figure 2.9: Product formation curves for the oxidative esterification of cinnamaldehyde with methanol. Each curve represents a different base.

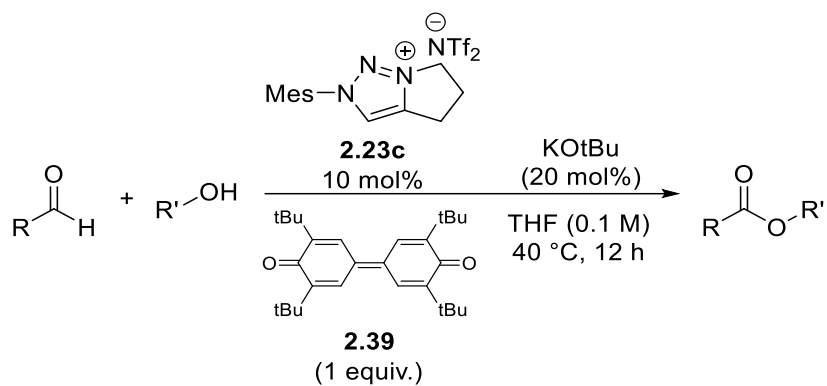
Figure 2.9 shows reaction progress curves for the formation of methylcinnamate **2.38**, using different bases to deprotonate 1,2,3-triazolium precatalyst **2.23a**. Strong bases sodium

hydride (NaH) and potassium *tert*-butoxide (KOtBu) showed extremely rapid product formation, with reaction completion within one hour. However, KOtBu showed a two-fold increase over NaH, achieving 48% conversion, whereas NaH only went to 24% conversion. When Cs₂CO₃ was utilized as the base, the reaction achieved the same conversion as KOtBu, but at a much slower rate (48 hours instead of 1). *N,N*-diisopropylethylamine (DIPEA), a weak nitrogen base, did not facilitate the reaction at all, despite being able to facilitate deuterium exchange in the earlier ¹H NMR acidity study (Section 2.4.2). DIPEA may not be basic enough to facilitate the isomerization of the initial carbene-aldehyde intermediate to the required Breslow intermediate, which may explain the lack of product formation for when this base is used (Scheme 2.14).



Scheme 2.14: Base-mediated isomerization of tetrahedral intermediate 2.48 to Breslow intermediate 2.49.

From the results of this study, KOtBu was chosen as the optimal base for this reaction, due to the relatively high conversion to product in the least amount of time. In addition, higher conversion to product was observed with an increase of catalyst to 10 mol%. The amount of base was reduced to 20 mol% to avoid base-catalyzed hydrolysis of the ester products, and to ensure that some excess base (with respect to catalyst) was present in the reaction, to ensure proper catalytic turnover. With the optimal reaction conditions identified, a brief substrate scope was examined (Table 2.3).



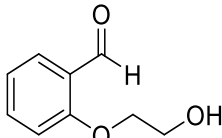
Entry	R	R'	Yield ^a
1	PhCH=CH	Me	82%
2	PhCH=CH	iPr	12%
3	PhCH=CH	Bn	63%
4	4-Cl-C ₆ H ₄	Me	11%
5	4-NO ₂ -C ₆ H ₄	Me	86%
6	4-OMe-C ₆ H ₄	Me	N/A
7	2-pyridyl	Me	74%
8	2-naphthyl	Me	57%
9			12%

Table 2.3: Substrate scope of 1,2,3-triazolylium-catalyzed oxidative esterification of aldehydes. ^aIsolated yield after purification by flash column chromatography.

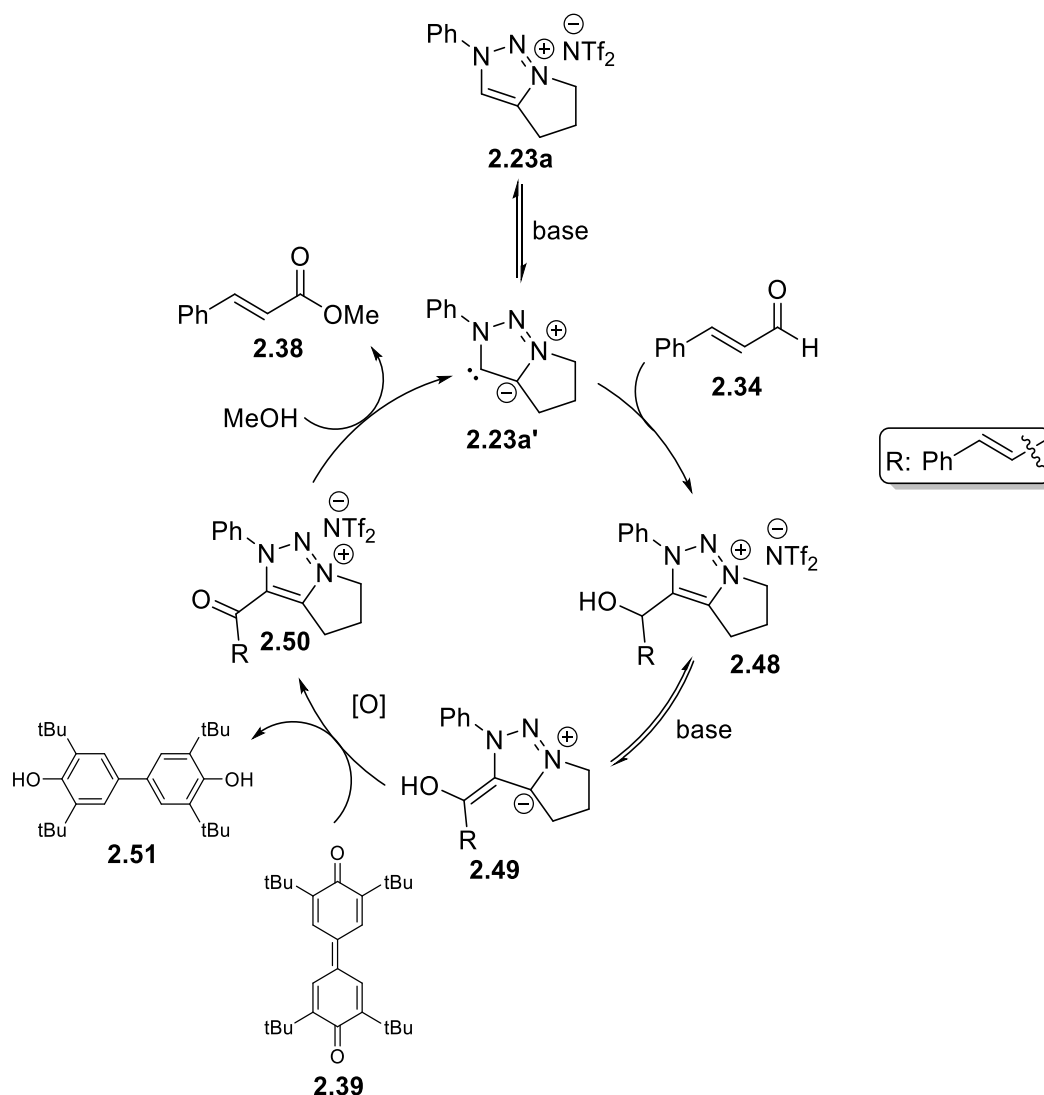
This reaction is compatible only with aromatic aldehydes; aliphatic aldehydes did not show any traces of product when attempted. Aliphatic aldehydes possess an enolizable α -carbon, so side aldol reactions are possible which may contribute to the lack of desired ester product. The reaction works best with primary alcohols (Table 2.3, Entries 1 & 3), while secondary alcohols

are far less reactive (Entry 2). Steric encumbrance most likely plays a role in the observed reduced reactivity of secondary alcohols, as a reaction using *tert*-butyl alcohol (tBuOH) as alcohol nucleophile did not show any traces of product. Reaction trials with phenol were also unsuccessful. With respect to the aldehyde substrate, moderately electron-withdrawing groups on the aromatic ring are not well-tolerated (Entry 4), while aldehydes with strongly electron-withdrawing groups perform well (Entry 5). Electron-donating groups are not tolerated at all (Entry 6). *N*-heterocyclic aldehydes gave good yields (Entry 7), and intramolecular cyclizations can be achieved, albeit in low yields (Entry 9).

2.6 Mechanistic analysis and identification of resting state

A catalytic mechanism for this chemical transformation can be proposed (Scheme 2.15), based on previously proposed mechanisms for NHC-catalyzed oxidative esterifications.⁸⁰ The active catalyst **2.23a'** is generated by deprotonation of the 1,2,3-triazolium precatalyst **2.23a**. Free carbene **2.23a'** adds to the aldehyde in a nucleophilic fashion to form tetrahedral intermediate **2.48**, which then isomerizes to Breslow intermediate **2.49** through base-mediated proton transfer. Intermediate **2.49** is then oxidized to acyl azolium **2.50** by **2.39**, giving bisphenol **2.51** as a byproduct. Acyl azolium **2.50** is then captured by methanol, releasing product and free carbene **2.23a'** back into the catalytic cycle. While this mechanism is a reasonable first assumption, it does not offer any detailed mechanistic information about the reaction, such as reaction orders in each substrate, catalyst resting state, or whether oxidation of Breslow intermediate **2.49** by **2.39** occurs via a two-electron or SET pathway. To answer these questions, a detailed kinetic analysis was performed, monitoring reaction progress by HPLC. To study the effect of reaction rate by each component, multiple reactions were run in parallel with varying

initial concentrations of aldehyde, methanol, oxidant, and base. These mechanistic studies were performed before the base optimization study in Figure 2.9, so it is important to note that TMG (2.36) was used as the base instead of KOtBu. It is also important to note that these experiments were not run in duplicate or triplicate, so it is possible that user error is present. However, attempts were made at minimizing systematic errors by the use of volumetric glassware and syringes, and consistent sampling methods.



Scheme 2.15: Proposed catalytic cycle for the oxidative esterification of aldehydes by 1,2,3-triazolylidene organocatalysts.

2.6.1 Reaction order with respect to aldehyde

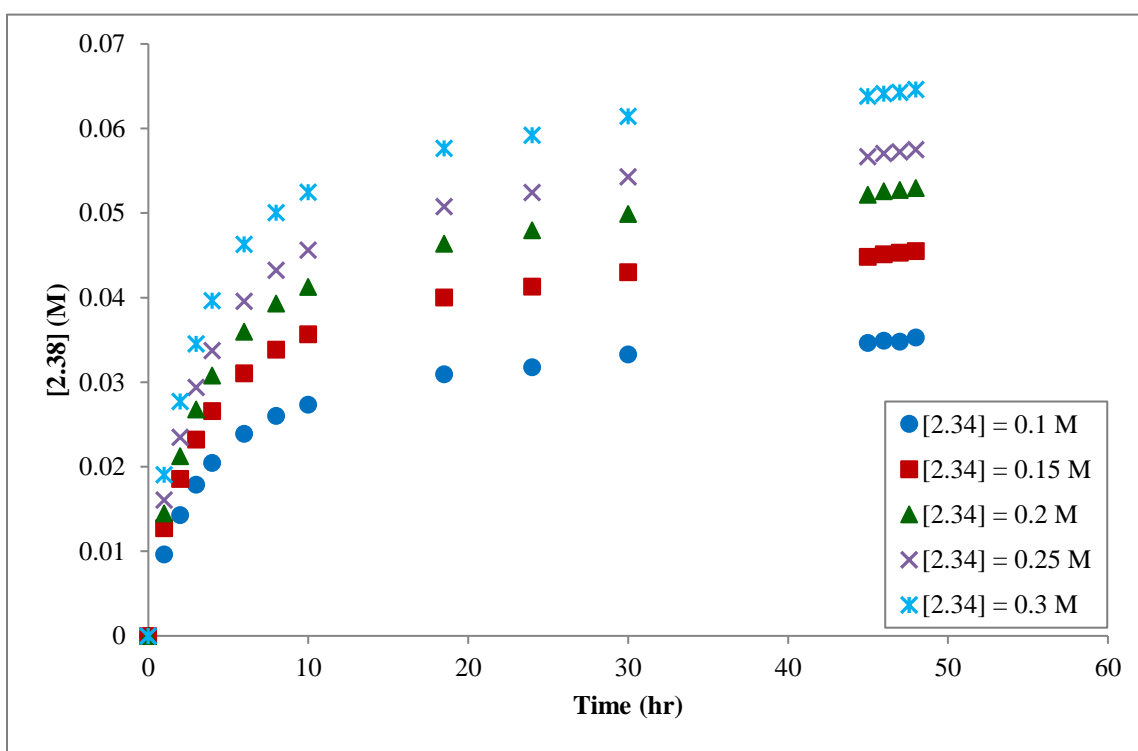
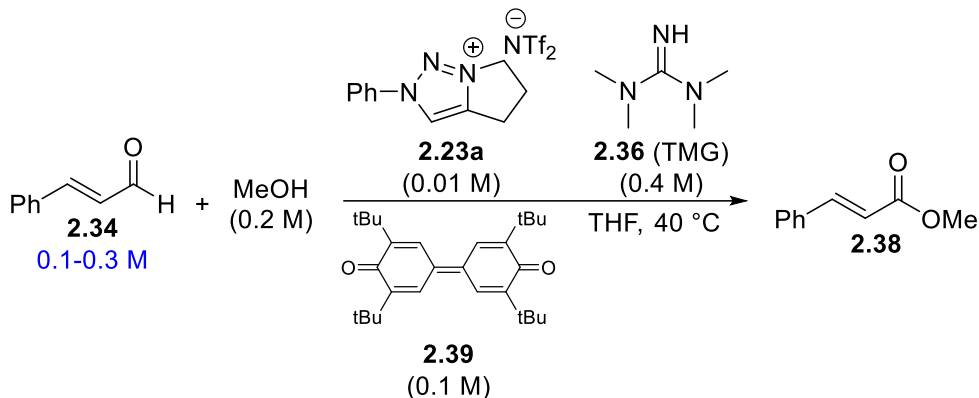


Figure 2.10: Product formation curves for the oxidative esterification of cinnamaldehyde (2.34**) with methanol. Each curve represents a different initial concentration of cinnamaldehyde.**

Figure 2.10 shows product formation curves of methylcinnamate (**2.38**) for different reactions with different initial concentrations of cinnamaldehyde (**2.34**). As the initial concentration of cinnamaldehyde increases, both the initial rate and overall conversion to

product increase. This rate dependence on initial aldehyde concentration indicates that the reaction is positive order with respect to aldehyde.

2.6.2 Reaction order with respect to methanol

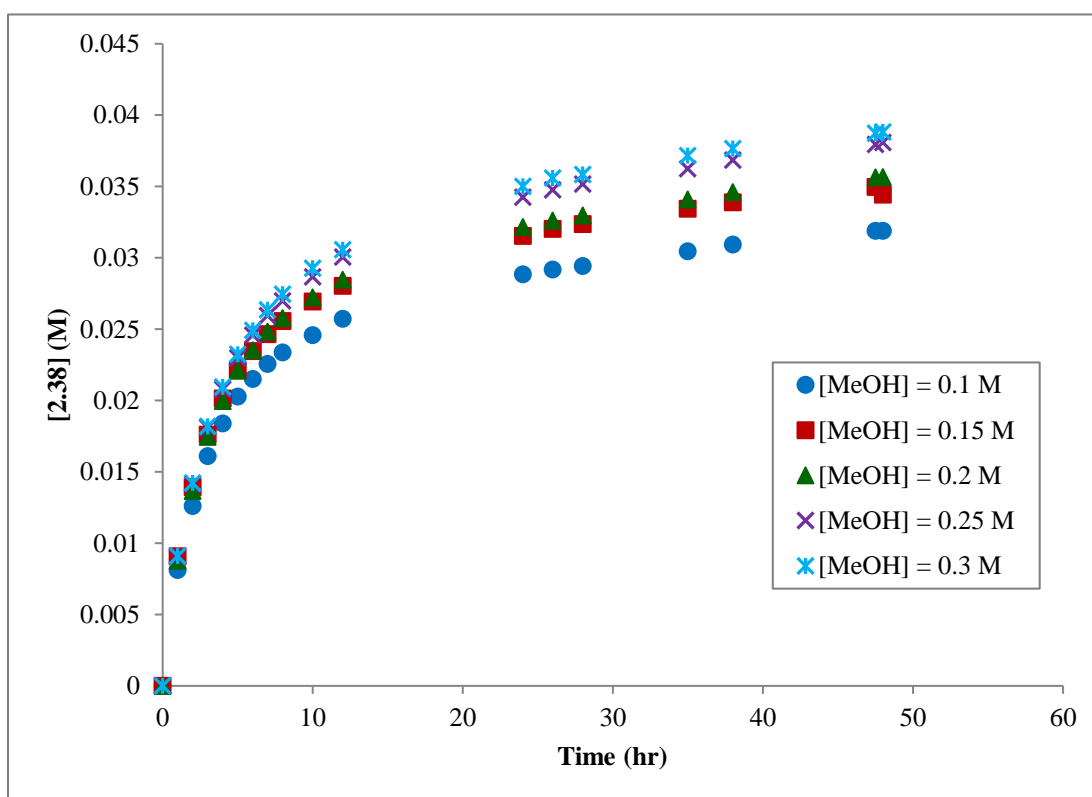
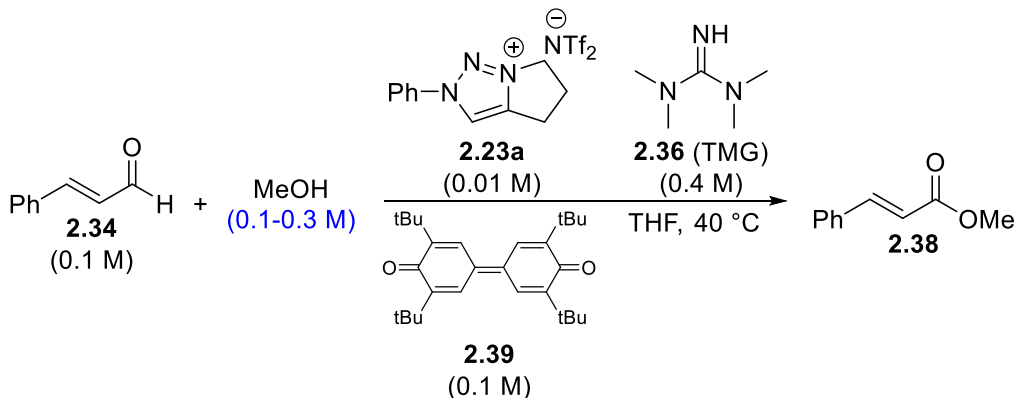


Figure 2.11: Product formation curves for the oxidative esterification of cinnamaldehyde (2.34**) with methanol. Each curve represents a different initial concentration of methanol.**

Figure 2.11 shows product formation curves for different reactions with different initial concentrations of methanol. Examining the product formation curves, they overlay for the first five hours, suggesting there is a zero-order relationship with respect to methanol during that

initial phase of the reaction. However, later in the reaction, the curves do not overlay, suggesting a positive-order relationship with respect to methanol. This can be explained by considering both the hygroscopic nature of the solvent and the long reaction time. THF is a hygroscopic solvent, and in this reaction, water can act as a competing nucleophile to form cinnamic acid instead of the desired product. During the first five hours of reaction, the concentration of exogenous water is low, formation of **2.38** dominates, and the reaction appears zero order with respect to methanol. As the reaction progresses, the solvent picks up more water, which acts as a competing nucleophile. In reactions with a higher initial concentration of methanol, there is more of the desired nucleophile (methanol), resulting in formation of more of the desired product **2.38**, and an observed positive order dependence on methanol.

2.6.3 Reaction order with respect to base

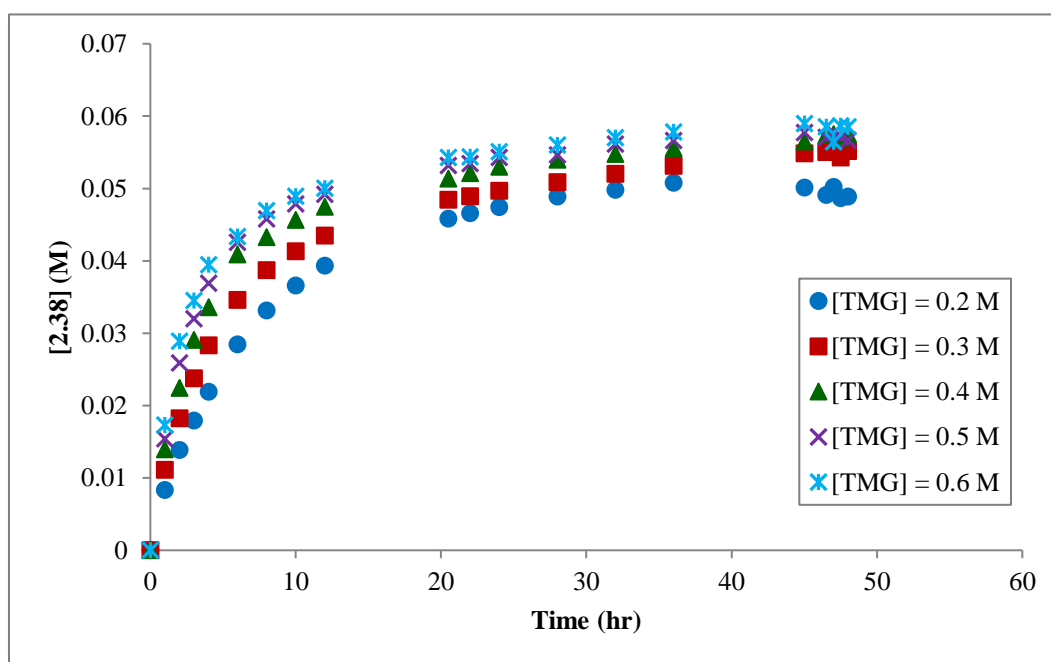
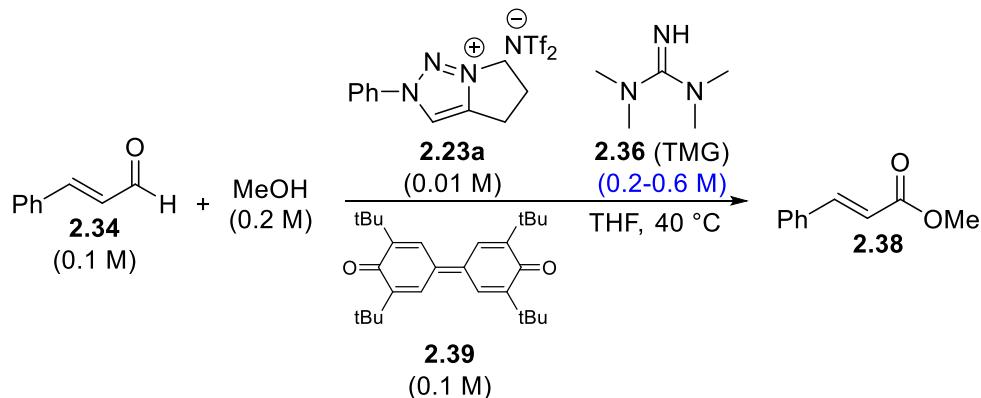


Figure 2.12: Product formation curves for the oxidative esterification of cinnamaldehyde (2.34**) with methanol. Each curve represents a different initial concentration of 1,1,3,3-tetramethylguanidine (TMG).**

Figure 2.12 shows product formation curves for different reactions with different initial concentrations of TMG. As the initial concentration of TMG is increased, the initial rate of reaction increases as well, indicating a positive order dependence. At higher concentrations of TMG ([TMG] = 0.5, 0.6 M), the product formation curves overlay. At these high concentrations

of TMG, the reaction reaches a saturation limit where increasing the concentration of TMG will no longer affect the reaction rate. TMG is involved in two key steps in the catalytic mechanism (Scheme 2.15): deprotonation of the 1,2,3-triazolium precatalyst **2.23a**, and isomerization of tetrahedral intermediate **2.48** to Breslow intermediate **2.49**. From the data, it is not possible to determine which of these steps is slower and contributes to the observed rate dependence on TMG.

2.6.4 Reaction order with respect to oxidant

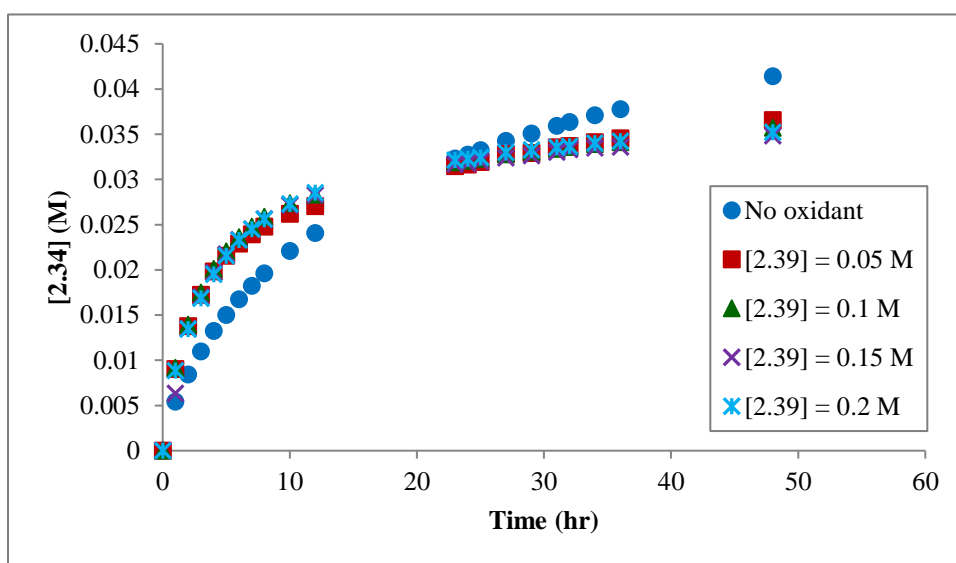
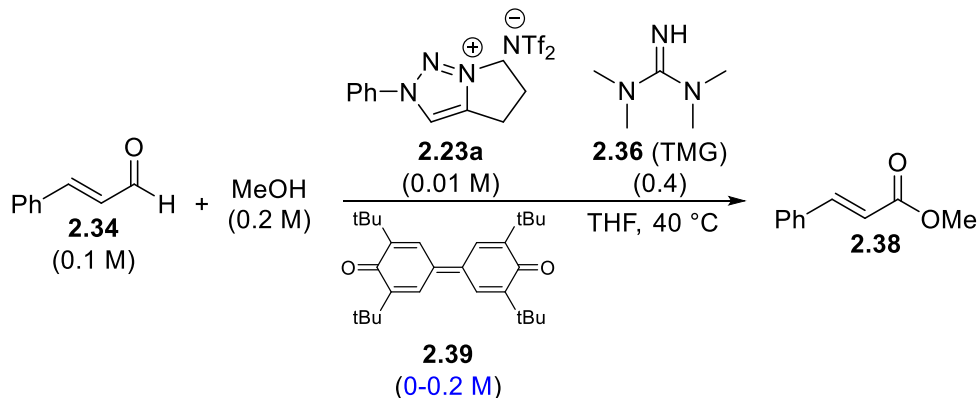


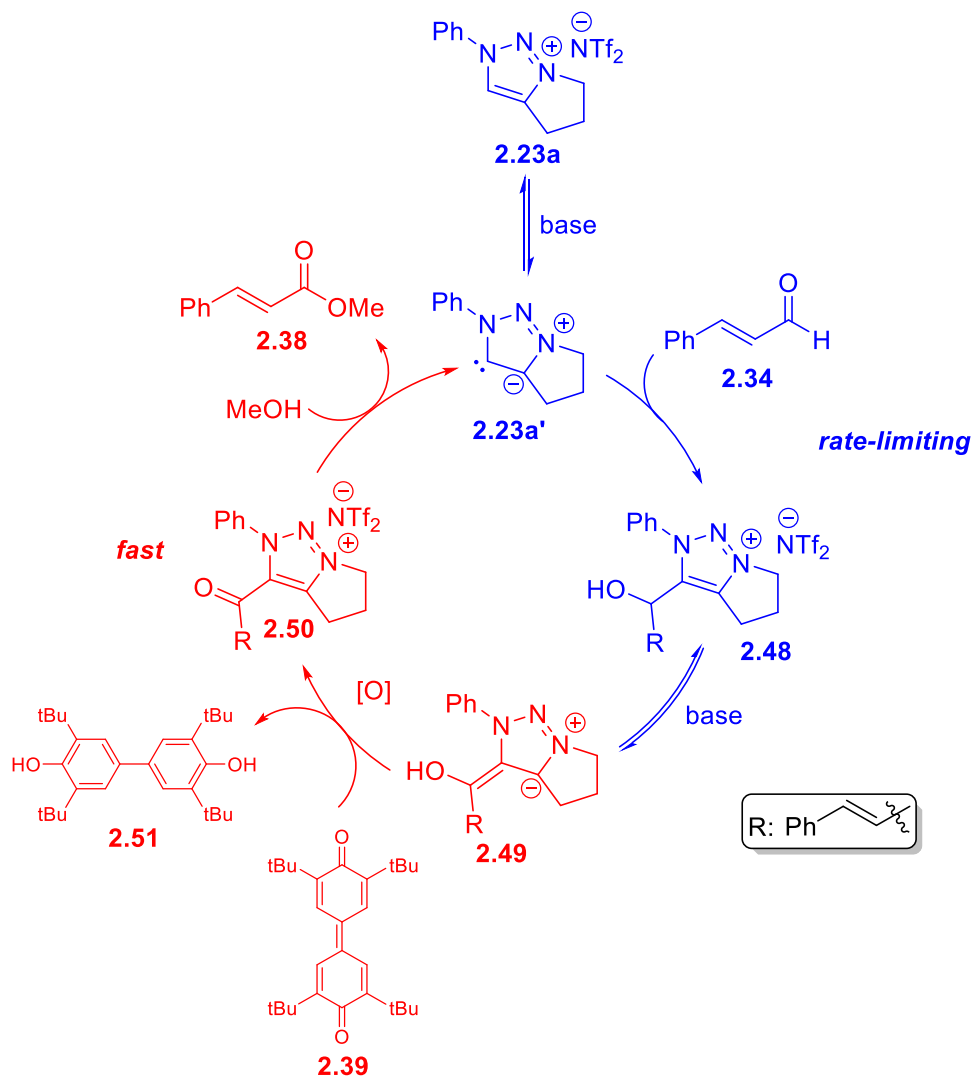
Figure 2.13: Product formation curves for the oxidative esterification of cinnamaldehyde (2.34**) with methanol. Each curve represents a different initial concentration of oxidant **2.39**.**

Figure 2.13 shows product formation curves for different reactions with different initial concentrations of oxidant **2.39**. For concentrations of **2.39** from 0.05 M to 0.2 M, the product formation curves overlay, indicating a zero-order dependence on oxidant. When oxidant **2.39** is omitted, the reaction is still productive, due to atmospheric molecular oxygen acting as the oxidant. In this special case, the initial rate is slower than when oxidant **2.39** is present, but more product is formed later in the reaction (30+ hr). The slower initial rate in the absence of oxidant

2.39 is expected, due to the low concentration of O₂ present in the solvent. In addition, the O₂ molecule has an inherent rate of diffusion into the solvent from the atmosphere, which could be slower than other steps in the catalytic cycle, rendering the oxidation step as the rate-limiting step, and the reaction diffusion-controlled. However, when oxidant **2.39** is used, the reaction is zero-order with respect to oxidant.

2.6.5 Revised mechanism

The results of this kinetic analysis can be analyzed and interpreted within the context of the catalytic cycle (Scheme 2.16).



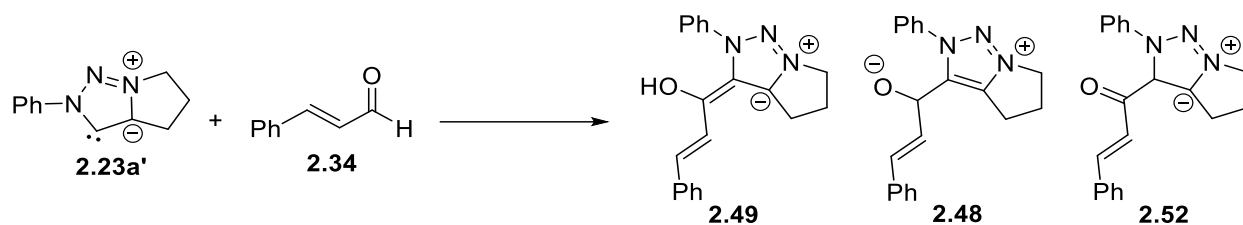
Scheme 2.16: Proposed catalytic cycle for the oxidative esterification of aldehydes by 1,2,3-triazolylidene organocatalysts, with fast and slow steps highlighted.

Since both alcohol and oxidant do not affect the initial reaction rate, it can be concluded that both the oxidation and nucleophilic substitution steps are not inherently rate limiting (Scheme 2.16, **2.49** \rightarrow **2.50** and **2.50** \rightarrow **2.23a'**, respectively). However, there are some caveats to these

conclusions. In the cases where oxidant concentration is very low, the oxidation step can be rate limiting. This is seen when atmospheric molecular oxygen is used as oxidant – low solubility of molecular oxygen in the solvent can result in a slow oxidation step (**2.49** → **2.50**). The second caveat is that while the rate of reaction is not dependent on initial concentration of methanol early in the reaction, it does exhibit a methanol dependence later in the reaction. This observation can be rationalized by build-up of water over long reaction times. In reactions with higher concentrations of methanol, more ester product **2.38** is formed because the methanol concentration is much higher than that of the exogenous water present in the reaction. The reaction shows a positive-order dependence in both TMG and aldehyde, suggesting that the resting state of the catalyst is not clearly defined as a single intermediate, and that there is no single turnover-limiting step for this catalytic system. Instead, it is possible that the rate constants for the formation of free carbene **2.23a'**, addition of aldehyde to generate **2.48** and isomerization to Breslow intermediate **2.49** all have similar magnitude under these reaction conditions. While mathematical simulations were not performed to estimate the magnitude of the individual rate constants in this reaction, software modeling packages such as COPASI could be used to fit the data and generate a mathematical model to extract the individual rate constants.

2.7 Identification and isolation of a catalytically active intermediate

During the course of this kinetic analysis, an intermediate was observed by HPLC/MS with a mass that corresponds to a carbene-aldehyde adduct. It was hypothesized that this compound could be one of three tautomeric forms arising from the nucleophilic addition of free carbene catalyst with the aldehyde (Scheme 2.17): Breslow intermediate **2.49**, tetrahedral intermediate **2.48**, or the keto tautomer of the Breslow-like intermediate (**2.52**).



Scheme 2.17: Possible tautomeric forms of carbene-aldehyde adduct observed by HPLC/MS.

In hopes of isolating this intermediate for further identification, a series of screening reactions were carried out where oxidant was omitted. This screen revealed that 1,2,3-triazolium precatalyst **2.23c**, 4-chlorobenzaldehyde (**2.28**), sodium hydroxide, and ethanol were the optimal conditions to maximize conversion of aldehyde to the desired adduct (Figure 2.14a). Using these conditions, this compound was successfully isolated and characterized by single-crystal X-ray diffraction, revealing that it is in fact the benzylic alcohol carbene-aldehyde adduct (Figure 2.14b).

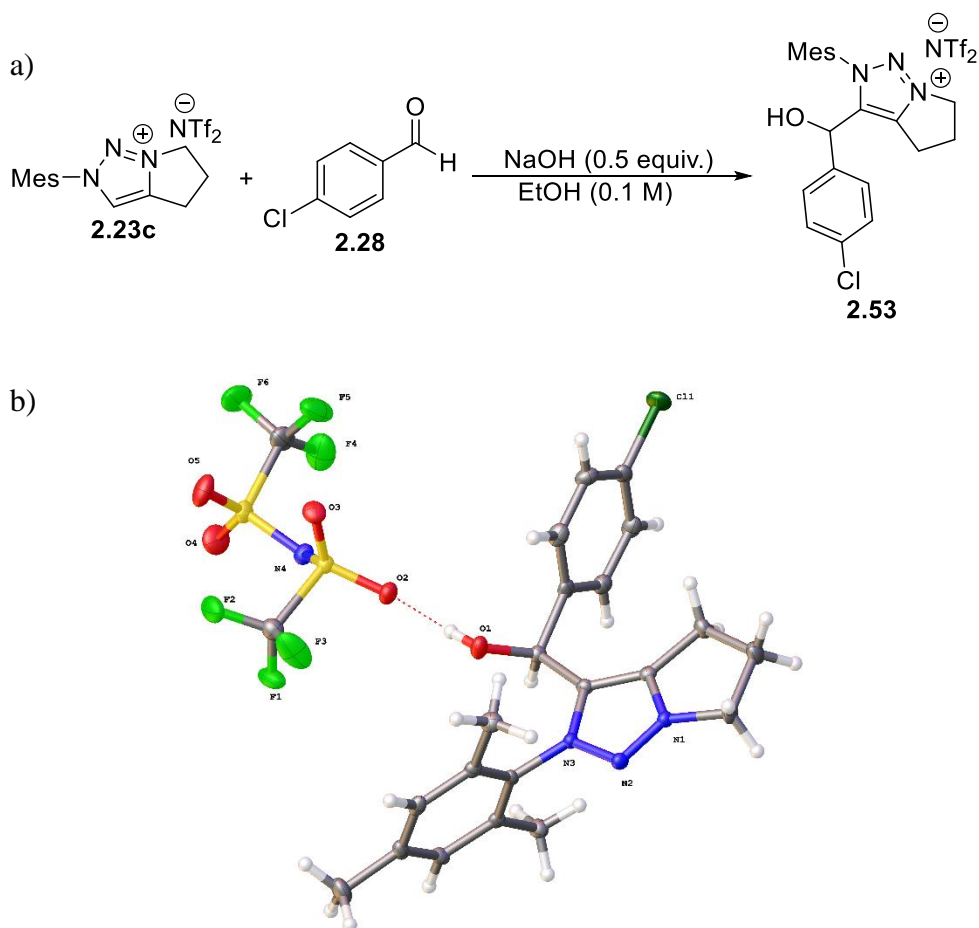
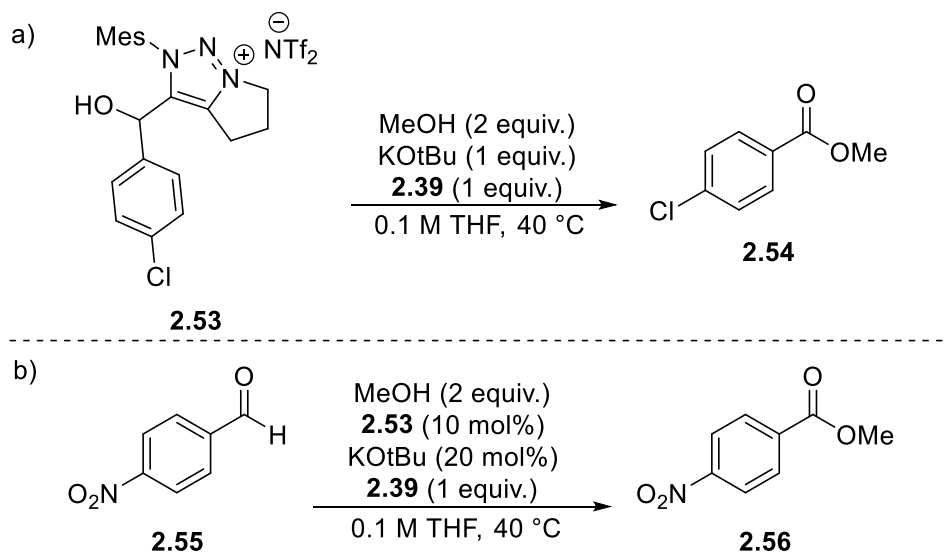


Figure 2.14: a) Conditions used to synthesize carbene-aldehyde adduct **2.53**. b) X-ray crystal structure of **2.53**, showing hydrogen bonding between the hydroxyl group and the NTf₂ counterion.

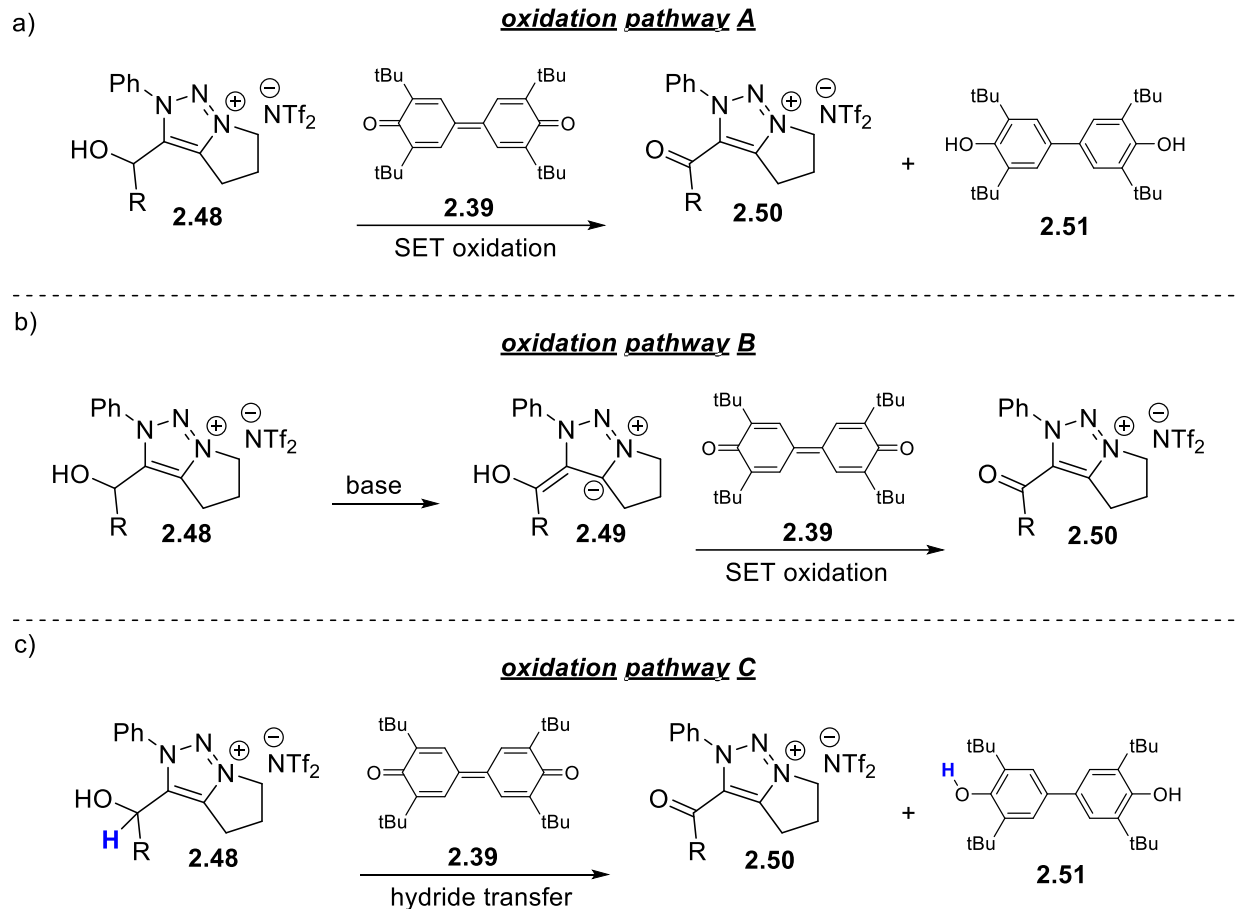
Isolation and identification of **2.53** allows for further refinement of the proposed mechanistic interpretation, and to explain some previously observed reactivity trends. When 4-chlorobenzaldehyde (**2.28**) is used as an aldehyde substrate, the isolated yield is a meager 11% (Table 2.3, Entry 4). As adduct **2.53** is a required catalytic intermediate for that transformation, the remarkable stability of this adduct that allows for its isolation explains why the yield of ester is low. Upon treatment with base, **2.53** reverts back to free carbene and 4-chlorobenzaldehyde (**2.28**), as observed by HPLC. Subjecting **2.53** to the oxidative esterification reaction conditions results in complete conversion to the expected ester (Scheme 2.18a). **2.53** also exhibits catalytic

activity, converting a stoichiometric amount of 4-nitrobenzaldehyde (**2.50**) to its corresponding methyl ester (Scheme 2.18b). These experiments provide strong evidence to support our proposed catalytic mechanism.

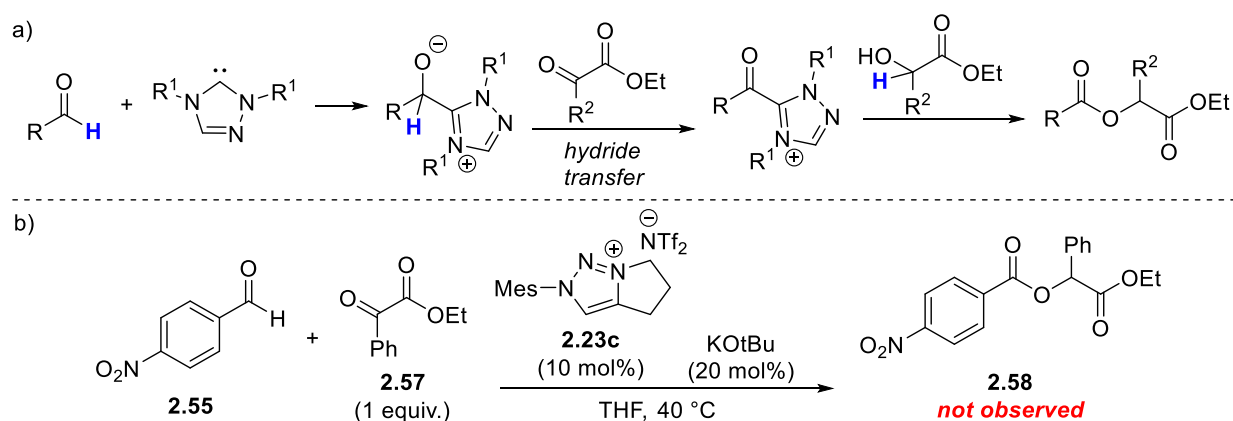


Scheme 2.18: Experiments demonstrating the catalytic activity of 2.53.

While the kinetic analysis gave great insight into the oxidative esterification reaction, a question remained regarding the exact method of generating acyl azolium species **2.50**. There are three possible pathways to generate acyl azolium species **2.50** (Scheme 2.19). Pathway A involves oxidation of tetrahedral intermediate **2.48** by **2.39** via single-electron transfer (SET). Pathway B involves base-mediated isomerization of **2.48** to Breslow intermediate **2.49**, then SET oxidation to **2.50** by **2.39**. Pathway C involves oxidation of **2.48** by transfer of the benzylic hydride to **2.39**. While Pathway C is unlikely due to the steric bulk of the *tert*-butyl groups on **2.39**, a similar mechanism was proposed by Schiedt et. al for the NHC-catalyzed hydroacylation of activated ketones¹⁰⁰ (Scheme 2.20a). To probe the hydride transfer pathway, an experiment was performed using 1,2,3-triazolium precatalyst **2.23c** and the expected product **2.58** was not observed, ruling out oxidation pathway C.

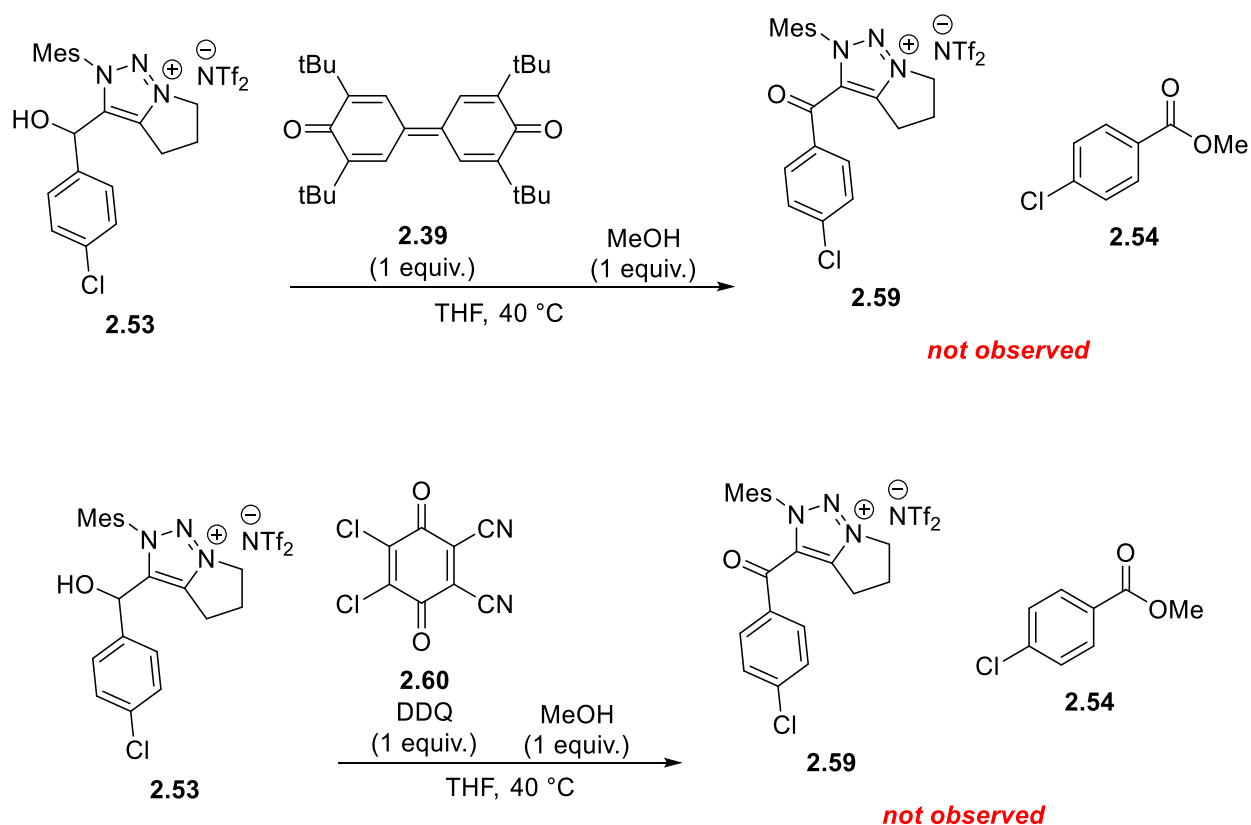


Scheme 2.19: Possible oxidation pathways to acyl azolium intermediate 2.50.



Scheme 2.20: a) Scheidt's proposed mechanism of hydride transfer in the NHC-catalyzed hydroacylation of activated ketones.¹⁰⁰ b) Experiment to probe the hydride transfer pathway for 1,2,3-triazolylidene catalysts.

To probe oxidation pathway A, direct oxidation of **2.53** was attempted with both bisquinone oxidant **2.39** and DDQ (**2.60**), a known SET oxidant,¹⁰¹ in the presence of methanol (Scheme 2.21). In both cases, neither acyl azolium **2.59** or ester **2.54** were detected by HPLC/MS. This experiment rules out oxidation pathway A, leaving oxidation pathway B as the most plausible oxidation pathway. This is further supported by the previously observed catalytic activity of **2.53** in the presence of base and oxidant **2.39**: if **2.53** is unreactive in the absence of base, then that implies a base-mediated isomerization to Breslow intermediate **2.49** is first required, and oxidation to acyl azolium species **2.50** occurs from **2.49**, not **2.48**.



Scheme 2.21: Attempts to oxidize **2.53** by quinone oxidants **2.39** and DDQ.

2.8 Conclusions

In this chapter, the design, synthesis, and application of 1,2,3-triazolium salts as mesoionic carbene precatalysts has been described. These catalysts have been found to facilitate the oxidative esterification of aromatic aldehydes. The catalytic activity of these triazolium salts are governed both by the nature of the *N*-substituent and the size of the fused saturated ring, with ring size being the biggest factor. These triazolium salts show an inverse acidity/activity relationship, with the most acidic triazoliums being the least efficient catalysts. A full mechanistic study using reaction progress monitoring methodology showed the reaction to be zero order with respect to oxidant, and an initial zero-order dependence on nucleophile, which transitions to a positive-order dependence as the reaction proceeds. The resting state of the catalyst cannot be clearly defined as a single intermediate, as the reaction shows rate dependence upon both aldehyde and base. Instead, it is possible that the rate constants for triazolium deprotonation, nucleophilic addition, and isomerization to Breslow intermediate **2.49** have similar magnitudes under these reaction conditions. In addition, a carbene-aldehyde adduct **2.53** was successfully synthesized and characterized by single-crystal X-ray crystallography. Unsuccessful attempts at oxidation of the benzylic center of **2.53** suggest that the oxidation to acyl azolium species **2.50** occurs from Breslow intermediate **2.49**, and not direct oxidation from the initial carbene-aldehyde adduct **2.48**. However, these 1,2,3-triazolylienes do not exhibit the same reactivity as their 1,2,4-triazolyliene brethren, as they only facilitate the oxidative esterification reaction and no other reactions that are proposed to proceed through a Breslow intermediate. A possibility for this discrepancy in reactivity is that oxidation of **2.49** by **2.39** has a lower activation energy than nucleophilic attack of **2.49** to an electrophile.

2.9 Experimental

2.9.1 General considerations

Unless otherwise specified, all reactions were performed open to ambient atmosphere; no extra steps were taken to ensure oxygen-free reactions. All chemicals were purchased from Fisher Scientific, Acros Organics, TCI America, Aldrich, or AK Scientific. Aldehydes were purified by vacuum distillation or washing with saturated aqueous sodium bicarbonate. THF was purified using an Innovative Technologies PS-Micro solvent system. Flash chromatography was carried out using SorbtechTM silica gel 60 Å (230 × 400 mesh), eluting with the indicated solvent mixtures. Thin layer chromatography (TLC) was performed on SorbtechTM precoated silica gel plates (UV254) and was visualized by irradiation with UV light, KMnO₄ stain, or iodine. ¹H (400 & 600 MHz), ¹³C (100 & 150 MHz), and ¹⁹F (375 MHz) were recorded on Varian and Bruker spectrometers at 295K. Chemical shifts (δ) are reported in parts per million, relative to residual solvent peaks as internal standards. Coupling constants (J) are measured in hertz (Hz).

Abbreviations are: s, singlet; d, doublet; t, triplet; q, quartet; p, pentet; m, multiplet. IR was performed on a Jasco FTIR 4100 (ATR set up) and a Thermo Scientific Nicolet 300 (KBr disc). HPLC/MS was performed on an Agilent 1260 Infinity with an Agilent Eclipse XDB C18 (3.5 μm, 3.0 × 7.5 mm) column, eluting with a water/acetonitrile (0.05% TFA additive) gradient. HPLC samples were prepared by taking 10 μL aliquots of reaction mixtures and diluting with 1 mL methanol.

2.9.2 Synthesis of 1,2,3-triazoles

General procedure: To a solution of azide **2.18** (1 equivalent) in acetonitrile (0.3 M), alkyne **2.19** (1 equiv.) and copper(II) acetate (0.05 equiv.) were added, and vigorously stirred

until complete dissolution of copper(II) acetate. DIPEA (0.1 equiv.) was added via syringe, and the solution was stirred at room temperature for 1 hour. Solvent was removed under reduced pressure on a rotary evaporator, and the crude product was purified by flash chromatography (hexanes/EtOAc).

4-(3-chloropropyl)-1-phenyl-1H-1,2,3-triazole (2.20a): The title compound was prepared according to the general procedure using azide **2.18a** (3.05 g, 25.6mmol) and alkyne **2.19a** (2.62 g, 25.6 mmol), and purified using 1:1 hexanes:EtOAc to afford **2.20a** (5.12 g, 23.1 mmol, 90% yield) as an off-white solid. Analytical data for **2.20a**: $^1\text{H NMR}$ (400 MHz, CDCl_3) δ 7.75 (s, 1H), 7.68 (dt, $J = 3.2, 2.0$ Hz, 2H), 7.52 – 7.44 (m, 2H), 7.39 (ddd, $J = 7.4, 3.8, 1.0$ Hz, 1H), 3.59 (t, $J = 6.4$ Hz, 2H), 2.95 (t, $J = 7.3$ Hz, 2H), 2.27 – 2.14 (m, 2H); $^{13}\text{C NMR}$ (100 MHz, CDCl_3) δ 147.2, 137.3, 129.9, 128.8, 120.6, 119.5, 44.3, 32.0, 22.8; **IR** (ATR): 3130, 1600, 1504, 1237, 760 cm^{-1} ; **LRMS** (ESI): Calcd. for $\text{C}_{11}\text{H}_{13}\text{ClN}_3$ ($[\text{M}+\text{H}]^+$): 222.1, Found: 222.1.

4-(4-chlorobutyl)-1-phenyl-1H-1,2,3-triazole (2.20b): The title compound was prepared according to the general procedure using azide **2.18a** (0.479g, 4.02 mmol) and alkyne **2.19b** (0.471 g, 4.02 mmol), and purified using 2:1 hexanes:EtOAc to afford **2.20b** (0.764 g, 3.24 mmol, 81% yield) as a clear oil. Analytical data for **2.20b**: $^1\text{H NMR}$ (400 MHz, CDCl_3) δ 7.70 (d, $J = 0.6$ Hz, 1H), 7.57 (ddd, $J = 6.4, 1.8, 0.8$ Hz, 2H), 7.37 – 7.29 (m, 2H), 7.26 – 7.19 (m, 1H), 3.41 (dd, $J = 7.2, 5.2$ Hz, 2H), 2.66 (dd, $J = 8.1, 5.9$ Hz, 2H), 1.81 – 1.61 (m, 4H); $^{13}\text{C NMR}$ (100 MHz, CDCl_3) δ 148.1, 148.1, 137.0, 129.8, 129.3, 128.5, 128.1, 120.3, 119.9, 119.2, 118.9, 44.6, 31.8, 26.4, 24.7; **IR** (thin film): 3142, 2947, 1598, 1000, 689 cm^{-1} ; **LRMS** (ESI): Calcd. for $\text{C}_{12}\text{H}_{15}\text{ClN}_3$ ($[\text{M}+\text{H}]^+$): 236.1, Found: 236.1.

4-(3-chloropropyl)-1-mesityl-1H-1,2,3-triazole (2.20c): The title compound was prepared according to the general procedure using azide **2.18b** (5.87 g, 36.4 mmol) and alkyne **2.19a** (3.73

g, 36.4 mmol), and purified using 2:1 hexanes:EtOAc to afford **2.20c** (6.92 g, 26.2 mmol, 72% yield) as a yellow oil. Analytical data for **2.20c**: $^1\text{H NMR}$ (400 MHz, CDCl_3) δ 7.35 (s, 1H), 6.95 (s, 1H), 3.59 (t, $J = 6.4$ Hz, 2H), 2.97 (t, $J = 7.3$ Hz, 2H), 2.32 (s, 3H), 2.23 (dt, $J = 13.4, 6.6$ Hz, 2H), 1.92 (s, 6H); $^{13}\text{C NMR}$ (100 MHz, CDCl_3) δ 146.2, 140.1, 135.2, 133.8, 129.2, 123.2, 44.4, 32.0, 22.9, 21.3, 17.4; **IR** (thin film): 2923, 1443, 1228, 989, 580 cm^{-1} ; **LRMS** (ESI): Calcd. for $\text{C}_{14}\text{H}_{19}\text{ClN}_3$ ($[\text{M}+\text{H}]^+$): 264.1, Found: 264.1.

4-(4-chlorobutyl)-1-mesityl-1H-1,2,3-triazole (2.20d): The title compound was prepared according to the general procedure using azide **2.18b** (3.01 g, 18.67 mmol) and alkyne **2.19b** (2.177 g, 18.67 mmol), and purified using 4:1 hexanes:EtOAc to afford **2.20d** (3.8 g, 13.68 mmol, 73% yield) as a colorless oil. Analytical data for **2.20c**: $^1\text{H NMR}$ (400 MHz, CDCl_3) δ 7.31 (s, 1H), 6.93 (s, 2H), 3.54 (t, $J = 6.3$ Hz, 2H), 2.82 (t, $J = 7.0$ Hz, 2H), 2.30 (s, 3H), 1.98 – 1.77 (m, 10H); $^{13}\text{C NMR}$ (100 MHz, CDCl_3) δ 147.2, 139.8, 135.0, 133.6, 129.1, 128.8, 122.8, 44.6, 32.0, 26.6, 24.8, 17.1; **IR** (thin film): 3349, 2960, 1574, 1489, 848 cm^{-1} ; **LRMS** (ESI): Calcd. for $\text{C}_{15}\text{H}_{21}\text{ClN}_3$ ($[\text{M}+\text{H}]^+$): 278.1, Found: 278.2.

4-(3-chloropropyl)-1-(perfluorophenyl)-1H-1,2,3-triazole (2.20e): The title compound was prepared according to the general procedure using azide **2.18c** (0.889 g, 4.25 mmol) and alkyne **2.19a** (0.451 mL, 4.25 mmol), and purified using 7:1 hexanes:EtOAc to afford **2.20e** (1.20 g, 3.84 mmol, 90% yield) as a colorless solid. Analytical data for **2.20e**: $^1\text{H NMR}$ (600 MHz, CDCl_3) δ 7.67 (s, 1H), 3.64 (t, $J = 6.3$ Hz, 2H), 3.02 (t, $J = 7.4$ Hz, 2H), 2.33 – 2.20 (m, 2H); $^{13}\text{C NMR}$ (150 MHz, CDCl_3) δ 146.9, 143.3, 143.2, 143.0, 141.6, 141.5, 141.3, 138.9, 137.2, 123.6, 44.0, 44.0, 31.5, 22.5; $^{19}\text{F NMR}$ (375 MHz, Acetone- d_6) δ -150.92, -150.95, -151.00, -151.03, -155.55, -155.55, -155.61, -155.61, -155.67, -164.76, -164.78, -164.80, -164.82, -164.84, -164.84,

-164.85, -164.87, -164.89, -164.90, -164.92. **IR** (ATR): 3075, 1524, 1241, 1058, 994 cm^{-1} ;

LRMS (ESI): Calcd. for $\text{C}_{11}\text{H}_8\text{ClF}_5\text{N}_3$ ($[\text{M}+\text{H}]^+$): 312.0, Found: 312.1.

4-(4-chlorobutyl)-1-(perfluorophenyl)-1H-1,2,3-triazole (2.20f): The title compound was prepared according to the general procedure using azide **2.18c** (2 g, 9.57 mmol) and alkyne **2.19b** (1.115 g, 9.57 mmol), and purified using 4:1 hexanes:EtOAc to afford **2.20f** (1.65 g, 5.07 mmol, 53%) as a clear oil. Analytical data for **2.20f**: **^1H NMR** (600 MHz, CDCl_3) δ 7.67 (s, 1H), 3.53 (t, $J = 5.9$ Hz, 2H), 2.81 (t, $J = 7.0$ Hz, 2H), 1.85 (d, $J = 3.5$ Hz, 4H); **^{13}C NMR** (150 MHz, CDCl_3) δ 148.0, 143.25, 143.22, 143.16, 143.14, 142.9, 141.55, 141.52, 141.46, 141.4, 141.2, 138.9, 138.8, 138.7, 137.2, 137.1, 137.0, 123.4, 44.6, 31.8, 26.2, 24.6; **^{19}F NMR** (375 MHz, Acetone- d_6) δ -151.38, -151.41, -151.45, -151.48, -156.22, -156.28, -156.34, -165.36, -165.39, -165.44, -165.44, -165.49, -165.52; **IR** (thin film): 2950, 1536, 1231, 997, 837 cm^{-1} ; **LRMS** (ESI): Calcd. for $\text{C}_{12}\text{H}_{10}\text{ClF}_5\text{N}_3$ ($[\text{M}+\text{H}]^+$): 326.0, Found: 326.1.

1-benzyl-4-(3-chloropropyl)-1H-1,2,3-triazole (2.20g): The title compound was prepared according to the general procedure using azide **2.18d** (0.333 g, 2.5 mmol) and alkyne **2.19a** (0.257 g, 2.5 mmol), and purified using 4:1 hexanes:EtOAc to afford **2.20g** (0.499 g, 2.12 mmol, 85%) as an off-white solid. Analytical data for **2.20g**: **^1H NMR** (400 MHz, CDCl_3) δ 7.36 – 7.28 (m, 3H), 7.24 – 7.17 (m, 3H), 5.44 (s, 2H), 3.50 (t, $J = 6.4$ Hz, 2H), 2.80 (t, $J = 7.3$ Hz, 2H), 2.16 – 2.01 (m, 2H); **^{13}C NMR** (100 MHz, CDCl_3) δ 146.7, 134.8, 129.2, 128.84, 128.77, 128.4, 128.1, 127.7, 121.2, 120.7, 54.0, 44.1, 31.9, 31.8, 22.7; **IR** (ATR): 2957, 1496, 1216, 1049, 722 cm^{-1} ; **LRMS** (ESI): Calcd. for $\text{C}_{12}\text{H}_{15}\text{ClN}_3$ ($[\text{M}+\text{H}]^+$): 236.1, Found: 236.1.

1-benzyl-4-(4-chlorobutyl)-1H-1,2,3-triazole (2.20h): The title compound was prepared according to the general procedure using azide **2.18d** (0.418 g, 3.14 mmol) and alkyne **2.19b** (0.366 g, 3.14 mmol), and purified using 4:1 hexanes:EtOAc to afford **2.20h** (0.619 g, 2.48

mmol, 79%) as a clear oil. Analytical data for **2.20h**: $^1\text{H NMR}$ (400 MHz, CDCl_3) δ 7.20 (ddd, J = 9.5, 8.1, 4.3 Hz, 6H), 5.39 (s, 2H), 3.57 – 3.29 (m, 2H), 2.63 (dd, J = 8.6, 5.4 Hz, 2H), 1.72 (dt, J = 9.1, 3.3 Hz, 4H); $^{13}\text{C NMR}$ (100 MHz, CDCl_3) δ 147.8, 134.9, 129.2, 128.7, 128.3, 128.1, 127.6, 121.0, 120.4, 53.9, 44.6, 31.9, 26.5, 24.8; **IR** (thin film: 2939, 1550, 1456, 1216, 1052, 697 cm^{-1} ; **LRMS** (ESI): Calcd. for $\text{C}_{13}\text{H}_{17}\text{ClN}_3$ ($[\text{M}+\text{H}]^+$): 250.1, Found: 250.1.

4-(3-chloropropyl)-1-cyclopentyl-1H-1,2,3-triazole (2.20i): The title compound was prepared according to the general procedure using azide **2.18e** (0.5 g, 4.5 mmol) and alkyne **2.19a** (0.462 g, 4.5 mmol), and purified using 4:1 hexanes:EtOAc to afford **2.20i** (0.570 g, 2.67 mmol, 59%) as a clear oil. Analytical data for **2.20i**: $^1\text{H NMR}$ (400 MHz, CDCl_3) δ 7.00 (s, 1H), 4.59 – 4.42 (m, 1H), 3.18 (t, J = 6.5 Hz, 2H), 2.46 (t, J = 7.4 Hz, 2H), 1.89 – 1.71 (m, 4H), 1.68 – 1.57 (m, 2H), 1.54 – 1.43 (m, 2H), 1.41 – 1.29 (m, 2H); $^{13}\text{C NMR}$ (100 MHz, CDCl_3) δ 145.8, 119.8, 119.2, 61.6, 61.3, 44.1, 33.2, 31.8, 23.9, 22.6; **IR** (thin film): 2872, 1550, 1444, 1049, 806, 650 cm^{-1} ; **LRMS** (ESI): Calcd. for $\text{C}_{10}\text{H}_{17}\text{ClN}_3$ ($[\text{M}+\text{H}]^+$): 214.1, Found: 214.1.

4-(4-chlorobutyl)-1-cyclopentyl-1H-1,2,3-triazole (2.20j): The title compound was prepared according to the general procedure using azide **2.18e** (0.346 g, 3.11 mmol) and alkyne **2.19b** (0.363 g, 3.11 mmol), and purified using 2:1 hexanes:EtOAc to afford **2.20j** (0.354 g, 1.55 mmol, 50%) as a clear oil. Analytical data for **2.20j**: $^1\text{H NMR}$ (400 MHz, CDCl_3) δ 7.15 (s, 1H), 4.74 – 4.47 (m, 1H), 3.37 – 3.12 (m, 2H), 2.43 (t, J = 7.0 Hz, 2H), 1.91 (qd, J = 7.0, 1.2 Hz, 2H), 1.80 – 1.63 (m, 2H), 1.64 – 1.32 (m, 8H); $^{13}\text{C NMR}$ (100 MHz, CDCl_3) δ 146.8, 119.5, 119.0, 61.33, 61.29, 44.5, 33.0, 31.7, 26.4, 24.6, 23.8; **IR** (thin film): 2955, 1550, 1446, 1215, 1051, 731 cm^{-1} ; **LRMS** (ESI): Calcd. for $\text{C}_{11}\text{H}_{19}\text{ClN}_3$ ($[\text{M}+\text{H}]^+$): 228.1, Found: 228.1.

3-(4-phenyl-1H-1,2,3-triazol-1-yl)propan-1-ol (2.26): Azide **2.25** (1.2398 g, 12.26 mmol), phenylacetylene (1.35 mL, 12.29 mmol), copper(I) acetate (0.075 g, 0.613 mmol), and tris((1-*tert*-butyl-1H-1,2,3-triazolyl)methyl)amine (TTTA)¹⁰² (0.527 g, 1.23 mmol) were dissolved in acetonitrile (40 mL) in a 100 mL round bottom flask. DIPEA (0.214 mL, 1.226 mmol) was added via syringe, and the solution was stirred overnight. Solvent was removed under reduced pressure, and the crude product was recrystallized from toluene to afford triazole **2.26** (1.83 g, 9.02 mmol, 74%) as a white solid. Analytical data for **2.26**: ¹H NMR (600 MHz, CDCl₃) δ 7.88 (s, 1H), 7.83 (d, *J* = 7.5 Hz, 2H), 7.43 (t, *J* = 7.6 Hz, 2H), 7.35 (t, *J* = 7.4 Hz, 1H), 4.58 (t, *J* = 6.8 Hz, 2H), 3.70 (t, *J* = 5.8 Hz, 2H), 3.16 (s, 1H), 2.24 – 2.12 (m, 2H); ¹³C NMR (150 MHz, CDCl₃) δ 130.2, 128.92, 128.91, 128.4, 125.8, 58.6, 47.2, 32.6; IR (ATR): 3200, 2932, 1463, 1218, 1078, 762 cm⁻¹; LRMS (ESI): Calcd. for C₁₁H₁₄N₃O ([M+H]⁺): 204.1, Found: 204.1.

2.9.3 Synthesis of 1,2,3-triazolium salts

General procedure: to a solution of triazole **2.20** in acetonitrile (2 M), potassium iodide (1.1 equivalent) was added, and the mixture was refluxed at 75 °C overnight. Solids were filtered on a pad of celite, and solvent was removed under reduced pressure. The resulting residue was reconstituted in dichloromethane (30 mL) and extracted with H₂O (3×75 mL). The aqueous layers were combined and lithium bis(trifluoromethane)sulfonimide (LiNTf₂, 1.1 equivalent) was added, and the solution was stirred overnight. The final product was isolated either by filtration or extraction with dichloromethane (3×30 mL) and removal of solvent under reduced pressure.

2-phenyl-2,4,5,6-tetrahydropyrrolo[1,2-*c*][1,2,3]triazol-7-ium

bis(trifluoromethyl)sulfonamide (2.23a): The title compound was prepared according to the

general procedure using triazole **2.20a** (5.12 g, 23.1 mmol) to afford triazolium salt **2.23a** (5.99 g, 12.83 mmol, 56%) as a yellow oil. Analytical data for **2.23a**: $^1\text{H NMR}$ (600 MHz, CDCl_3) δ 8.44 (s, 1H), 7.82 – 7.69 (m, 2H), 7.64 – 7.47 (m, 3H), 4.76 – 4.60 (m, 2H), 3.31 – 3.14 (m, 2H), 2.98 – 2.74 (m, 2H); $^{13}\text{C NMR}$ (150 MHz, CDCl_3) δ 148.29, 148.28, 148.27, 135.5, 131.9, 130.35, 130.34, 130.33, 122.9, 122.8, 121.6, 120.8, 118.6, 116.5, 50.9, 26.0, 22.3; $^{19}\text{F NMR}$ (375 MHz, Acetone- d_6) δ -84.25; **IR** (ATR): 3135, 1501, 1336, 1176, 1048, 761 cm^{-1} ; **LRMS** (ESI): Calcd. for $\text{C}_{11}\text{H}_{12}\text{N}_3$ (M^+): 186.1, Found: 186.1.

2-phenyl-4,5,6,7-tetrahydro-2H-[1,2,3]triazolo[1,5-a]pyridin-8-ium

bis(trifluoromethyl)sulfonamide (2.23b): The title compound was prepared according to the general procedure using triazole **2.20b** (3.67 g, 15.57 mmol) to afford triazolium salt **2.23b** (5.01 g, 10.43 mmol, 67%) as a yellow oil. Analytical data for **2.23b**: $^1\text{H NMR}$ (400 MHz, CDCl_3) δ 8.48 (s, 1H), 7.86 – 7.68 (m, 2H), 7.67 – 7.44 (m, 3H), 4.56 (t, $J = 6.2$ Hz, 2H), 3.04 (t, $J = 6.4$ Hz, 2H), 2.28 – 2.12 (m, 2H), 2.06 – 1.92 (m, 2H); $^{13}\text{C NMR}$ (100 MHz, CDCl_3) δ 141.7, 135.1, 132.1, 130.5, 125.6, 121.8, 49.6, 21.4, 20.2, 17.9; $^{19}\text{F NMR}$ (375 MHz, CDCl_3) δ 33.42; **IR** (ATR): 3127, 1332, 1049, 762 cm^{-1} ; **LRMS** (ESI): Calcd. for $\text{C}_{12}\text{H}_{14}\text{N}_3$ (M^+): 200.1, Found: 200.2.

2-mesityl-2,4,5,6-tetrahydropyrrolo[1,2-c][1,2,3]triazol-7-ium

bis(trifluoromethyl)sulfonamide (2.23c): The title compound was prepared according to the general procedure using triazole **2.20c** (6.92 g, 26.2 mmol) to afford triazolium salt **2.23c** (10.46 g, 20.57 mmol, 78%) as an off-white solid. Analytical data for **2.23c**: $^1\text{H NMR}$ (400 MHz, CDCl_3) δ 7.99 (s, 1H), 7.00 (s, 2H), 4.86 – 4.67 (m, 2H), 3.37 (t, $J = 7.5$ Hz, 2H), 3.06 – 2.85 (m, 2H), 2.34 (s, 3H), 2.00 (s, 6H); $^{13}\text{C NMR}$ (100 MHz, CDCl_3) δ 148.5, 142.8, 134.7, 132.2,

130.0, 126.8, 51.4, 26.1, 22.8, 21.3, 17.2; **¹⁹F NMR** (375 MHz, CDCl₃) δ 28.25; **IR** (ATR): 3113, 1348, 1177, 1054, 610 cm⁻¹; **LRMS** (ESI): Calcd. for C₁₄H₁₈N₃ (M⁺): 228.1, Found: 228.0.

2-mesityl-4,5,6,7-tetrahydro-2H-[1,2,3]triazolo[1,5-a]pyridin-8-ium

bis(trifluoromethyl)sulfonamide (2.23d): The title compound was prepared according to the general procedure using triazole **2.20d** (2.7 g, 9.72 mmol) to afford triazolium salt **2.23d** (3.95 g, 7.56 mmol, 78%) as a yellow oil. Analytical data for **2.23d**: **¹H NMR** (400 MHz, CDCl₃) δ 8.07 (s, 1H), 6.98 (s, 2H), 4.60 (t, *J* = 6.2 Hz, 2H), 3.12 (t, *J* = 6.4 Hz, 2H), 2.31 (s, 3H), 2.30 – 2.22 (m, 2H), 2.06 (dtd, *J* = 9.5, 6.4, 2.9 Hz, 2H), 1.97 (s, 6H); **¹³C NMR** (100 MHz, CDCl₃) δ 142.4, 141.4, 134.3, 131.3, 130.5, 129.9, 129.5, 129.1, 124.5, 121.3, 118.1, 114.9, 49.5, 21.2, 20.9, 20.0, 17.6, 16.9; **¹⁹F NMR** (375 MHz, CDCl₃) δ -79.06; **IR** (ATR): 3088, 1578, 1348, 1049, 739 cm⁻¹; **LRMS** (ESI): Calcd. for C₁₅H₂₀N₃ (M⁺): 242.2, Found: 242.2.

2-(perfluorophenyl)-2,4,5,6-tetrahydropyrrolo[1,2-c][1,2,3]triazol-7-ium

bis(trifluoromethyl)sulfonamide (2.23e): The title compound was prepared according to the general procedure using triazole **2.20e** (4.27 g, 13.7 mmol) to afford triazolium salt **2.23e** (2.59 g, 4.65 mmol, 34%) as a white solid. Analytical data for **2.23e**: **¹H NMR** (600 MHz, Acetone-d₆) δ 9.04 (s, 1H), 5.22 – 4.97 (m, 2H), 3.53 (t, *J* = 7.6 Hz, 2H), 3.12 (dt, *J* = 15.2, 7.6 Hz, 2H); **¹³C NMR** (150 MHz, Acetone-d₆) δ 149.58, 149.56, 145.0, 144.0, 143.9, 143.3, 142.2, 139.2, 137.5, 128.8, 128.5, 52.2, 26.2, 22.8; **¹⁹F NMR** (375 MHz, Acetone-d₆) δ -80.02, -147.04, -147.06, -147.07, -147.08, -147.09, -147.12, -147.12, -147.13, -147.14, -147.15, -147.16, -148.76, -148.77, -148.79, -148.82, -148.83, -148.84, -148.88, -148.89, -148.90, -161.28, -161.30, -161.31, -161.33, -161.35, -161.36, -161.37, -161.38, -161.41, -161.41, -161.44; **IR** (ATR): 3150, 1537, 1351, 1052, 876 cm⁻¹; **LRMS** (ESI): Calcd. for C₁₁H₇F₅N₃ (M⁺): 276.1, Found: 276.1.

2-(perfluorophenyl)-4,5,6,7-tetrahydro-2H-[1,2,3]triazolo[1,5-a]pyridin-8-ium

bis(trifluoromethyl)sulfonamide (2.23f): The title compound was prepared according to the general procedure using triazole **2.20f** (1.65 g, 5.07 mmol) to afford triazolium salt **2.23f** (2.61 g, 4.57 mmol, 90%) as a white solid. Analytical data for **2.23f**: $^1\text{H NMR}$ (400 MHz, Acetone- d_6) δ 9.01 (s, 1H), 4.90 (t, $J = 6.2$ Hz, 2H), 3.26 (t, $J = 6.3$ Hz, 2H), 2.48 – 2.30 (m, 2H), 2.16 (ddd, $J = 15.8, 7.9, 4.5$ Hz, 2H); $^{13}\text{C NMR}$ (100 MHz, Acetone- d_6) δ 145.4, 144.3, 142.8, 142.5, 141.7, 139.6, 137.1, 131.0, 130.6, 124.8, 121.6, 118.4, 115.2, 50.4, 21.0, 20.1, 17.5; $^{19}\text{F NMR}$ (375 MHz, Acetone- d_6) δ -80.03, -147.06, -147.07, -147.07, -147.10, -147.12, -147.12, -148.95, -149.00, -149.01, -149.06, -149.07, -161.33, -161.34, -161.38, -161.38, -161.39, -161.43. **IR** (ATR): 3142, 1527, 1347, 1137, 998 cm^{-1} ; **LRMS** (ESI): Calcd. for $\text{C}_{12}\text{H}_9\text{F}_5\text{N}_3$ (M^+): 290.1, Found: 290.1.

2-benzyl-2,4,5,6-tetrahydropyrrolo[1,2-c][1,2,3]triazol-7-ium

bis(trifluoromethyl)sulfonamide (2.23g): The title compound was prepared according to the general procedure using triazole **2.20g** (3.32 g, 14.1 mmol) to afford triazolium salt **2.23g** (4.6 g, 9.58 mmol, 68%) as a pale yellow oil. Analytical data for **2.23g**: $^1\text{H NMR}$ (400 MHz, CDCl_3) δ 7.96 (s, 1H), 7.38 (s, 5H), 5.59 (s, 2H), 4.74 – 4.38 (m, 2H), 3.12 (t, $J = 7.5$ Hz, 2H), 2.90 – 2.67 (m, 2H); $^{13}\text{C NMR}$ (100 MHz, CDCl_3) δ 147.7, 131.2, 130.2, 129.7, 129.4, 124.5, 58.2, 50.8, 26.2, 22.4; $^{19}\text{F NMR}$ (375 MHz, CDCl_3) δ 33.42; **IR** (thin film): 3127, 1583, 1332, 1051, 514 cm^{-1} ; **LRMS** (ESI): Calcd. for $\text{C}_{12}\text{H}_{14}\text{N}_3$ (M^+): 200.1, Found: 200.1.

2-benzyl-4,5,6,7-tetrahydro-2H-[1,2,3]triazolo[1,5-a]pyridin-8-ium

bis(trifluoromethyl)sulfonamide (2.23h): The title compound was prepared according to the general procedure using triazole **2.20h** (3.178 g, 12.73 mmol) to afford triazolium salt **2.23h** (3.88 g, 7.85 mmol, 62%) as a pale yellow oil. Analytical data for **2.23h**: $^1\text{H NMR}$ (400 MHz,

CDCl₃) δ 8.01 (s, 1H), 7.49 – 7.29 (m, 5H), 5.58 (s, 2H), 4.45 (t, J = 6.2 Hz, 2H), 2.91 (t, J = 6.4 Hz, 2H), 2.26 – 2.06 (m, 2H), 2.02 – 1.85 (m, 2H); ¹³C NMR (100 MHz, CDCl₃) δ 140.6, 130.8, 130.2, 129.7, 129.6, 129.2, 129.1, 126.8, 124.5, 121.3, 118.1, 114.9, 57.4, 49.0, 21.1, 19.8, 17.7; ¹⁹F NMR (375 MHz, CDCl₃) δ -79.01; IR (thin film) 3122, 2967, 1577, 1351, 1056, 741, 514 cm⁻¹; LRMS (ESI): Calcd. for C₁₃H₁₆N₃ (M⁺): 214.1, Found: 214.1.

2-cyclopentyl-2,4,5,6-tetrahydropyrrolo[1,2-c][1,2,3]triazol-7-ium

bis(trifluoromethyl)sulfonamide (2.23i): The title compound was prepared according to the general procedure using triazole **2.20i** (4.6 g, 21.5 mmol) to afford triazolium salt **2.23i** (5.12 g, 11.17 mmol, 52%) as a pale yellow oil. Analytical data for **2.23i**: ¹H NMR (400 MHz, CDCl₃) δ 8.03 (s, 1H), 5.15 – 4.87 (m, 1H), 4.68 – 4.45 (m, 2H), 3.16 (t, J = 7.5 Hz, 2H), 2.97 – 2.71 (m, 2H), 2.29 (td, J = 13.7, 7.5 Hz, 2H), 2.05 (ddd, J = 9.8, 7.5, 4.4 Hz, 2H), 1.93 – 1.80 (m, 2H), 1.79 – 1.67 (m, 2H); ¹³C NMR (100 MHz, CDCl₃) δ 147.4, 123.7, 67.0, 50.6, 33.2, 26.3, 24.0, 22.4; ¹⁹F NMR (375 MHz, CDCl₃) δ -84.24; IR (thin film): 2970, 1584, 1352, 1056, 789, 514 cm⁻¹; LRMS (ESI): Calcd. for C₁₀H₁₆N₃ (M⁺): 178.1, Found: 178.2.

2-cyclopentyl-4,5,6,7-tetrahydro-2H-[1,2,3]triazolo[1,5-a]pyridin-8-ium

bis(trifluoromethyl)sulfonamide (2.23j): The title compound was prepared according to the general procedure using triazole **2.20j** (2.62 g, 11.5 mmol) to afford triazolium salt **2.23j** (3.34 g, 7.07 mmol, 62%) as a pale yellow oil. Analytical data for **2.23j**: ¹H NMR (400 MHz, CDCl₃) δ 8.11 (s, 1H), 5.14 – 4.88 (m, 1H), 4.45 (t, J = 6.2 Hz, 2H), 2.97 (t, J = 6.4 Hz, 2H), 2.29 (dt, J = 13.1, 6.6 Hz, 2H), 2.22 – 2.13 (m, 2H), 2.07 (td, J = 14.3, 6.8 Hz, 2H), 1.98 (dt, J = 12.1, 6.3 Hz, 2H), 1.87 (dd, J = 9.8, 5.9 Hz, 2H), 1.74 (dd, J = 10.0, 5.4 Hz, 2H); ¹³C NMR (100 MHz, CDCl₃) δ 140.6, 126.4, 66.3, 49.2, 33.1, 24.1, 21.5, 20.1, 18.1; ¹⁹F NMR (375 MHz, CDCl₃) δ

28.22; **IR** (thin film): 3164, 2967, 1449, 1351, 1186, 1058, 616, 514 cm^{-1} ; **LRMS** (ESI): Calcd. for $\text{C}_{11}\text{H}_8\text{N}_3$ (M^+): 192.1, Found: 192.2.

2-phenyl-6,7-dihydro-5H-pyrazolo[1,2-a][1,2,3]triazol-8-ium trifluoromethanesulfonate

(2.27): In a 50 mL round bottom flask, triazole **2.26** (0.638 g, 3.14 mmol) and DIPEA (0.602 mL, 3.45 mmol) were dissolved in dichloromethane (15 mL). The flask was placed in an ice bath, fitted with a rubber septum, and purged with N_2 gas for 15 minutes. Triflic anhydride (0.581 mL, 3.45 mmol) was added via syringe, and the solution was stirred for 1.5 hours. Solvent was removed under reduced pressure to afford triazolium salt **2.27** (0.723 g, 2.16 mmol, 69%) as a white solid. Analytical data for **2.27**: **^1H NMR** (600 MHz, Acetone- d_6) δ 9.32 (s, 1H), 8.04 – 7.88 (m, 2H), 7.68 – 7.44 (m, 3H), 5.20 – 4.96 (m, 4H), 3.44 – 3.23 (m, 2H); **^{13}C NMR** (150 MHz, Acetone- d_6) δ 153.6, 130.7, 130.6, 129.4, 127.4, 126.2, 126.1, 124.4, 123.2, 122.3, 120.2, 51.59, 51.56, 51.54, 50.42, 50.39, 50.36, 25.2; **IR** (ATR): 3141, 1226, 1034, 767, 637 cm^{-1} ; **LRMS** (ESI): Calcd. for $\text{C}_{11}\text{H}_{12}\text{N}_3$ (M^+): 186.1, Found: 186.1.

2.9.4 General procedure for methylation experiments

For triazolium salts **2.23a-d**, 0.1 mmol of triazolium salt was dissolved in 2 mL THF in a 5 mL scintillation vial with a stir bar, and an initial timepoint HPLC sample was taken. Methyl iodide (5 equiv.) was added via syringe, immediately followed by KOtBu (2 equiv.), and HPLC timepoints were taken at 5, 10, 20, 30, 40, and 50 minutes. For triazolium salts **2.23e** and **2.23f**, this procedure was modified by using 0.04 mmol of triazolium salt, and 2 equivalents of Na_2CO_3 . For triazolium salts **2.23g-j**, this procedure was modified by using 0.4 mmol of triazolium salt.

2.9.5 General procedure for NMR exchange experiments

Triazolium salt (**2.23a-j**, 0.035 mmol) was dissolved in CD₃CN (0.7 mL) and transferred to a screw-cap NMR tube with septum. The sample was locked and shimmed, and an initial ¹H NMR spectrum was taken. The sample was ejected, and CD₃OD (5 equiv.) was injected by syringe, inverting the tube three times to ensure adequate mixing. The sample was re-inserted into the NMR, and an array was programmed to take spectra every 90 seconds for 20 minutes. The sample was then ejected again, and DIPEA (1 equiv.) was injected by syringe, inverting the tube three times to ensure adequate mixing. The sample was re-inserted into the NMR spectrometer, and another array was programmed to take spectra every 90 seconds for 25 minutes. The FIDs were imported and processed in MestreNova.

2.9.6 General procedure for reaction monitoring experiments

A stock solution was prepared by dissolving catalyst **2.23c** (46 mg, 0.09 mmol), methanol (146 μ L, 3.6 mmol), oxidant **2.39** (0.736 g, 1.8 mmol), and 2-methoxynaphthalene (0.285 g, 1 equiv.) in THF (18 mL). Five 20-dram scintillation vials with septa caps were charged with 3 mL aliquots of stock solution. Different amounts of cinnamaldehyde were added to each vial (38 μ L, 0.3 mmol, 1 equiv.; 57 μ L, 0.45 mmol, 1.5 equiv.; 76 μ L, 0.6 mmol, 2 equiv.; 94 μ L, 0.75 mmol, 2.5 equiv.; 113 μ L, 0.9 mmol, 3 equiv.) and an initial t=0 sample was taken. The vials were stirred and heated to 40 °C, then TMG (151 μ L, 1.2 mmol) was added to each vial, and timepoints were taken at 1, 2, 3, 4, 6, 8, 10, 18.5, 24, 30, 45, 46, 47, and 48 hours.

2.9.7 General procedure for the oxidative esterification of aldehydes

In a 20-dram scintillation vial, aldehyde (0.5 mmol), **2.39** (0.204 g, 0.5 mmol), **2.23c** (0.025 g, 0.05 mmol), and alcohol (1.0 mmol) were dissolved in THF (5 mL). The solution was heated to 40 °C, and KOtBu (11 mg, 0.1 mmol) was added. The solution was stirred and heated overnight, then solvent was removed under reduced pressure and the crude mixture was purified by silica gel flash chromatography.

Methyl cinnamate (Table 2.3, entry 1): Prepared from cinnamaldehyde (63 μ L) and methanol (40 μ L) using the general procedure and purified using 10:1 hexanes:ethyl acetate to afford methyl cinnamate (66.5 mg, 0.41 mmol, 82%) as a yellow solid. Spectroscopic data is identical to that of an authentic sample.

Isopropyl cinnamate (Table 2.3, entry 2): Prepared from cinnamaldehyde (63 μ L) and 2-propanol (76 μ L) using the general procedure and purified using 10:1 hexanes:ethyl acetate to afford isopropyl cinnamate (11 mg, 0.06 mmol, 12%) as a clear oil. Spectroscopic data is identical to that of an authentic sample.

Benzyl cinnamate (Table 2.3, entry 3): Prepared from cinnamaldehyde (63 μ L) and benzyl alcohol (104 μ L) using the general procedure and purified using 10:1 hexanes:ethyl acetate to afford benzyl cinnamate (75 mg, 0.315 mmol, 63%) as a yellow oil. Spectroscopic data is identical to that of an authentic sample.

Methyl 4-chlorobenzoate (Table 2.3, entry 4): Prepared from 4-chlorobenzaldehyde (70 mg) and methanol (40 μ L) using the general procedure and purified using 15:1 hexanes:MTBE to afford methyl 4-chlorobenzoate (9 mg, 0.055 mmol, 11%) as a white solid. Spectroscopic data was identical to that of an authentic sample.

Methyl 4-nitrobenzoate (Table 2.3, entry 5): Prepared from 4-nitrobenzaldehyde (76 mg) and methanol (40 μ L) using the general procedure and purified using 4:1 hexanes:ethyl acetate to afford methyl 4-nitrobenzoate (78 mg, 0.43 mmol, 86%) as a yellow solid. Spectroscopic data was identical to that of an authentic sample.

Methyl picolinate (Table 2.3, entry 7): Prepared from 2-pyridinecarboxaldehyde (60 μ L) and methanol (40 μ L) using the general procedure and purified using 2:1 hexanes:ethyl acetate to afford the methyl picolinate (51 mg, 0.37 mmol, 74%) as a yellow oil. Spectroscopic data is consistent with the literature.¹⁰³

Methyl 2-naphthoate (Table 2.3, entry 8): Prepared from 2-naphthaldehyde (78 mg) and methanol (40 μ L) using the general procedure and purified using 15:1 hexanes:MTBE to afford methyl 2-naphthoate (53 mg, 0.29 mmol, 57%) as a yellow solid. Spectroscopic data is consistent with the literature.¹⁰⁴

2,3-Dihydro-5H-benzo[e][1,4]dioxepin-5-one (Table 2.3, entry 9): Prepared from 2-(2-hydroxyethoxy)benzaldehyde (83 mg) using the general procedure and purified using 15:1 hexanes:MTBE to afford the product (16 mg, 0.06 mmol, 12%) as a yellow oil. Spectroscopic data is consistent with the literature.¹⁰⁵

Chapter 3: *N*-Heterocyclic Carbene-Catalyzed Oxidative *N*-Acylation of Electron-Poor *N*-Nucleophiles

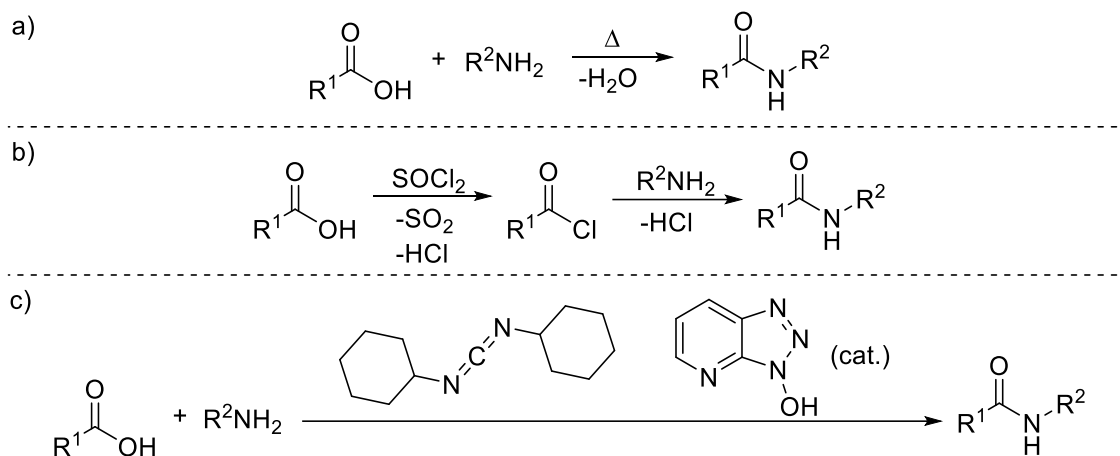
3.1 Introduction

Throughout the development of NHC catalysis, much of the spotlight has been directed towards catalyst development and improvement, with a focus on the products of the reaction itself, instead of a deep mechanistic understanding of the catalyst and how it changes or decomposes during a reaction. With respect to NHC catalysis, much of the mechanistic work has been focused on confirming the existence of the Breslow intermediate^{51,53,54} and investigating the relationship between catalyst structure and reactivity/selectivity.^{59,20,106,98,107} While these kinds of studies are vital to the advancement of the field as a whole, understanding all of the potential off-cycle pathways a catalyst can engage in is critical. This chapter focuses on two main topics: the development and mechanistic understanding of the NHC-catalyzed oxidative acylation of aldehydes with electron-poor *N*-nucleophiles, and catalyst deactivation pathways in the NHC-catalyzed direct oxidative amidation of aldehydes with electron-rich amines.

3.1.1 Current methods of NHC-catalyzed oxidative amidation

The synthesis of amides is of great importance to the general chemistry community, due to their presence in pharmaceuticals, and as the basic backbone of peptides and higher order proteins. On paper, amide synthesis is a trivial reaction: the coupling of a carboxylic acid and an amine, with removal of water (Scheme 3.1a). In practice, combining a carboxylic acid and an amine in solution will form a carboxylate-ammonium salt instead of the desired amide. To solve

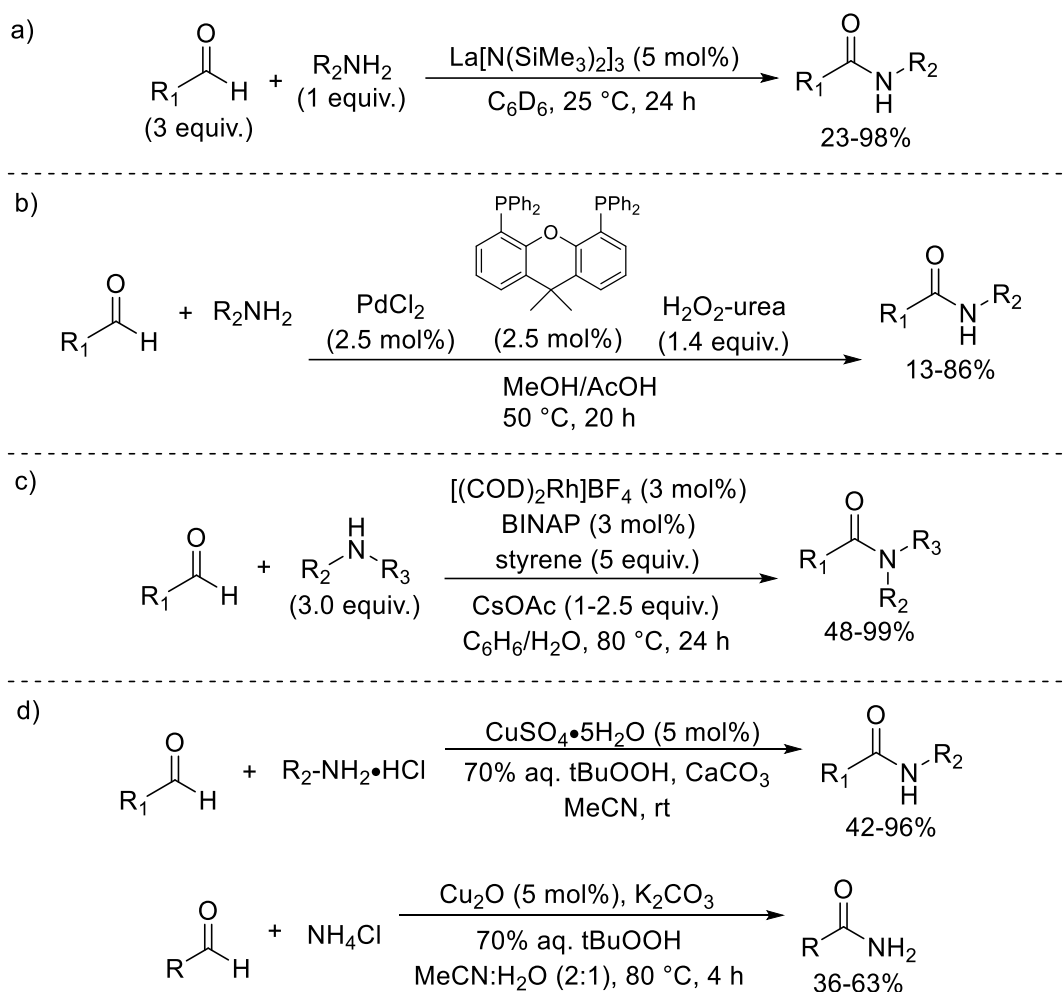
the challenges created by this limitation, practical amide synthesis strategies have been developed that involve activation of the carboxylate group, by transformation of the -OH into a good leaving group. A simple application of this strategy is conversion of a carboxylic acid to its corresponding acyl chloride, followed by nucleophilic acyl substitution by the amine (Scheme 3.1b). While this strategy works well for simple amides, these conditions are not amenable for peptide synthesis, due to the potential for acid-catalyzed racemization at the α -amino center. Retaining the absolute configuration of amino acids in peptide synthesis is crucial, especially for peptides that are to be used as potential drug candidates. To address this drawback, a plethora of coupling reagents have been developed specifically for peptide synthesis, such as carbodiimide and hydroxytriazole reagents¹⁰⁸ (Scheme 3.1c). While these methods are valuable for a wide range of amides and peptides, the atom economy of these coupling reagents is quite low.



Scheme 3.1: Synthetic methods for amides.

Another strategy for amide synthesis is via oxidative amidation of aldehydes, usually by metal-mediated catalysis (Scheme 3.2). Such strategies include lanthanide catalysis¹⁰⁹ (Scheme 3.2a), palladium catalysis¹¹⁰ (Scheme 3.2b), rhodium catalysis¹¹¹ (Scheme 3.2c), and copper catalysis¹¹² (Scheme 3.2d). These methods suffer from some drawbacks, such as a requirement

for large excess in one substrate, or expensive transition metal catalysts and ligands. In addition, these methods involve transition metal catalysts, which can pose potential environmental hazards after disposal. By employing relatively inexpensive, earth-abundant catalysts, such as *N*-heterocyclic carbenes, some of these drawbacks can be addressed.



Scheme 3.2: Select examples of metal-mediated oxidative amidations of aldehydes.

NHC-catalyzed oxidative esterifications of aldehydes with alcohols are fast, efficient, and high-yielding reactions.¹¹³ A logical extension of that reactivity would be NHC-catalyzed oxidative amidations of aldehydes with amines. However, direct NHC-catalyzed oxidative amidations perform quite poorly, suffering from low yields.⁸² In addition, if given a choice

a)

$\text{Ar}-\text{C}(=\text{O})\text{H} + \text{F}_3\text{C}-\text{CH}(\text{OH})-\text{CF}_3 \xrightarrow[\text{THF, rt, 2 h}]{\text{DBU (20 mol\%)}, \text{ (5 mol\%)}, \text{ (1 equiv.)}}$ $\left[\text{Ar}-\text{C}(=\text{O})-\text{O}-\text{CH}(\text{CF}_3)_2 \right] \xrightarrow[\text{rt, 12 h}]{\text{RNH}_2 \text{ (2.5 equiv.)}}$ $\text{Ar}-\text{C}(=\text{O})-\text{NH}-\text{R}$ 78-93%



3.2 Discovery of NHC-catalyzed oxidative coupling of 4-chlorobenzaldehyde with 1,1,3,3-tetramethylguanidine

1,1,3,3-tetramethylguanidine (TMG, **3.1**) is commonly used as a substitute for non-nucleophilic bases 1,8-diazabicyclo[5.4.0]undec-7-ene (DBU, **3.2**) and 1,5-diazabicyclo[4.3.0]non-5-ene (DBN, **3.3**), due to its lower cost and ease of handling (Figure 3.1). Like DBU and DBN, TMG has traditionally been considered a non-nucleophilic base.¹¹⁴ In NHC catalysis, DBU is one of the most common bases used to deprotonate the azolium salt precatalyst to generate the active carbene catalyst.

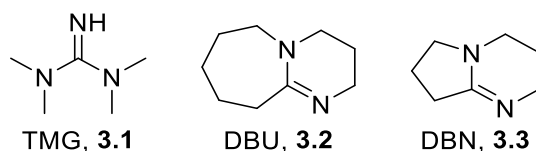
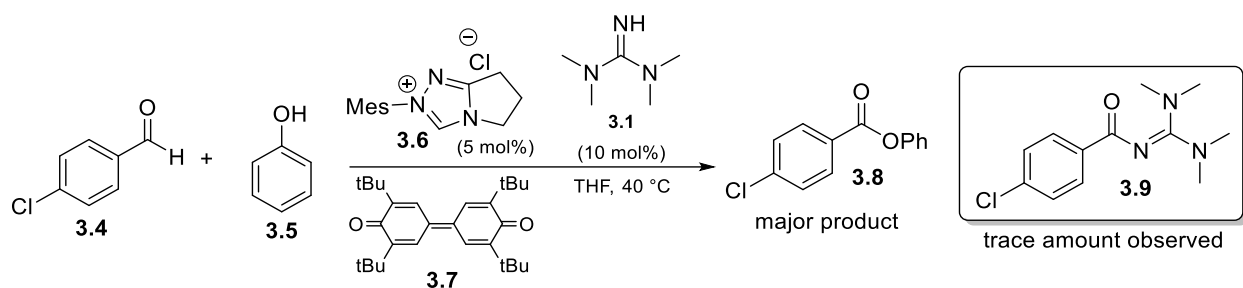
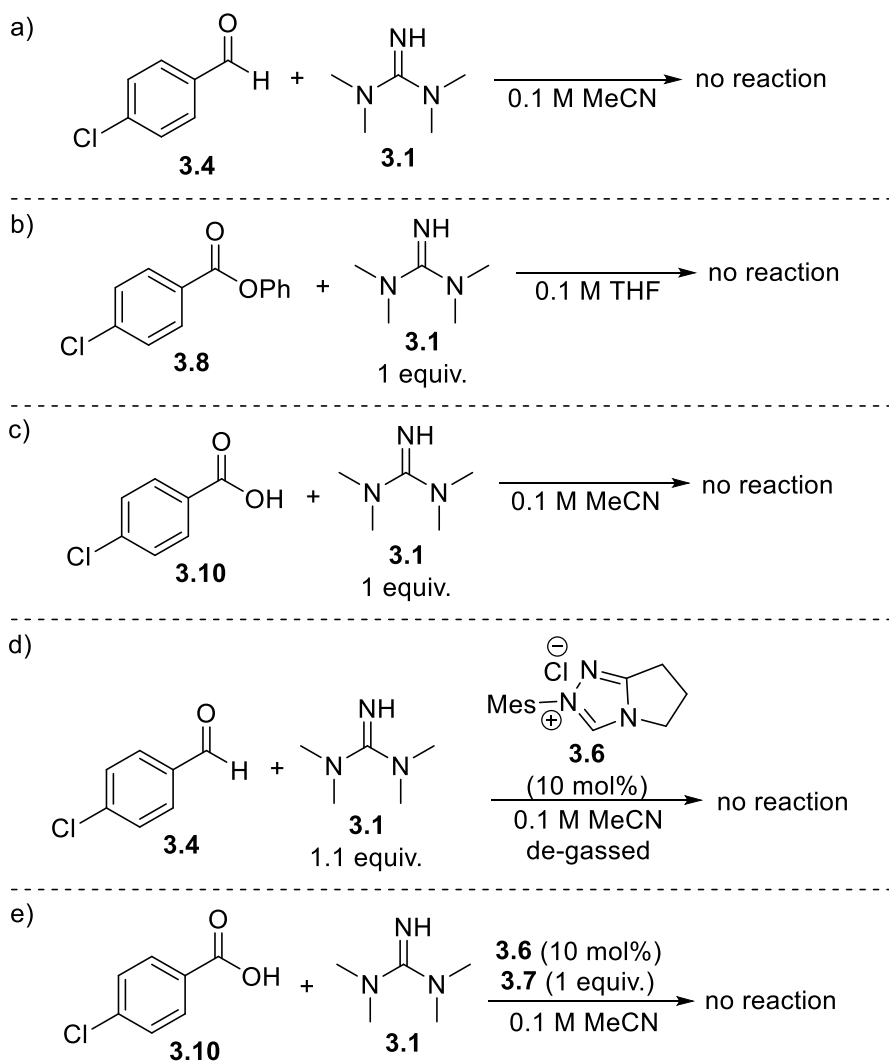


Figure 3.1: Structures of the non-nucleophilic bases TMG, DBU, and DBN.

Due to the relatively high viscosity of DBU, and the similar pK_as of DBU and TMG,¹¹⁵ we believed that making a substitution would be acceptable for the purposes of studying the oxidative esterification aldehydes with phenols by 1,2,4-triazolylidene catalysts (Scheme 3.4). However, HPLC/MS analysis of the reaction mixture in Scheme 3.4 showed trace amounts of aldehyde-TMG adduct **3.9**. Under these reaction conditions, we believed that **3.9** was being formed by nucleophilic capture of TMG with the *in situ*-generated acyl azolium intermediate. To prove this, a series of control experiments were carried out to rule out other possible pathways to form **3.7** (Scheme 3.5).



Scheme 3.4: Observation of aldehyde-guanidine adduct.

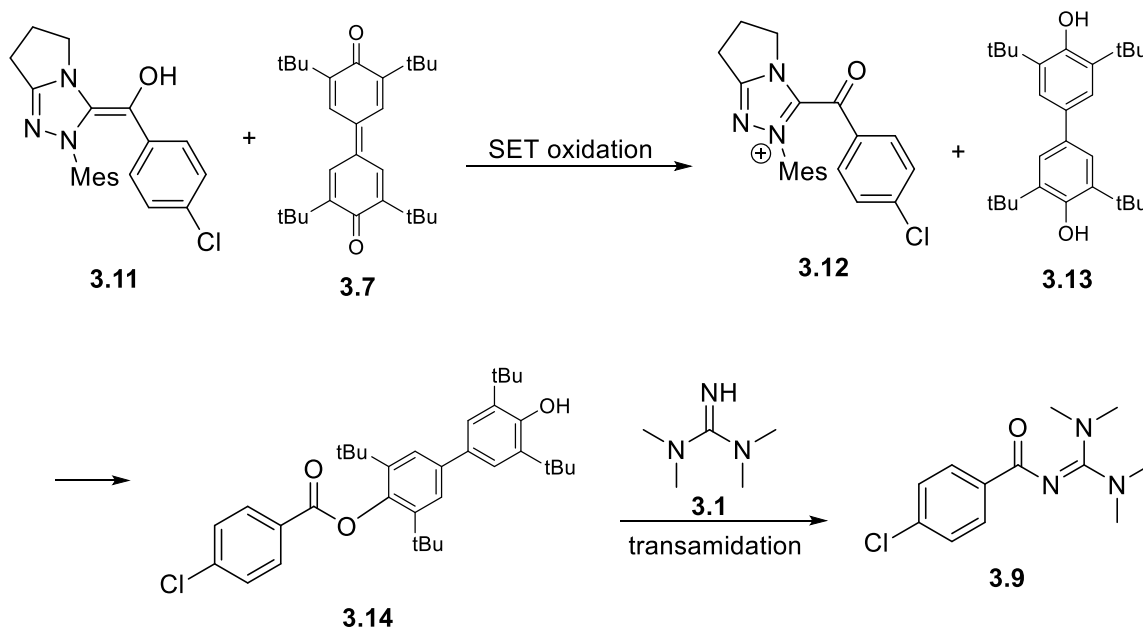


Scheme 3.5: Control experiments to rule out non-NHC-catalyzed pathways to form *N*-acylguanidine **3.9.**

Mixing 4-chlorobenzaldehyde (**3.4**) or 4-chlorobenzoic acid (**3.10**) with one equivalent of TMG (Scheme 3.5a, 3.3c respectively) did not show any trace of *N*-acylguanidine **3.9**. To rule

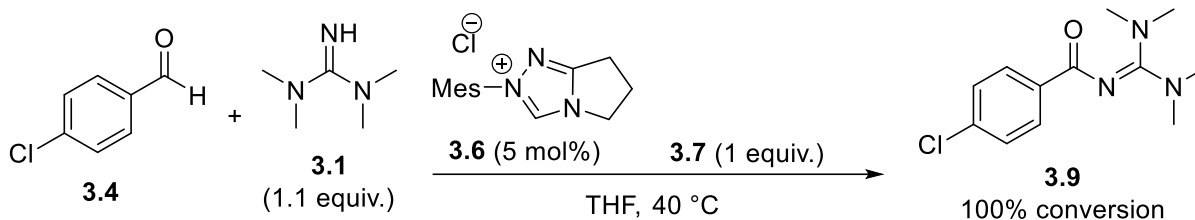
out transamidation, phenyl 4-chlorobenzoate (**3.8**) was mixed with one equivalent of TMG (Scheme 3.5b), and no product formation was observed. To verify that oxidant was required, a reaction was run in degassed solvent without oxidant **3.7**, and no product formation was observed (Scheme 3.5d). Finally, a reaction was run using 4-chlorobenzoic acid (**3.10**) as starting material, and no product formation was observed as well (Scheme 3.5e).

Another possible pathway to the formation of **3.9** is via transamidation of ester **3.14**, the product of oxidative coupling between 4-chlorobenzaldehyde **3.4** and *tert*-butyl-substituted biphenol **3.13**, the byproduct of oxidation of Breslow intermediate **3.11** with oxidant **3.7** (Scheme 3.6). However, the two adjacent *tert*-butyl groups to the phenolic oxygen provide a great amount of steric bulk, rendering the phenolic oxygen non-nucleophilic. In fact, the non-nucleophilic nature of **3.13** is the reason why **3.7** is commonly chosen as an oxidant in NHC catalysis.¹¹³ In addition, we did not observe esters of the type **3.14** in any of our experiments.



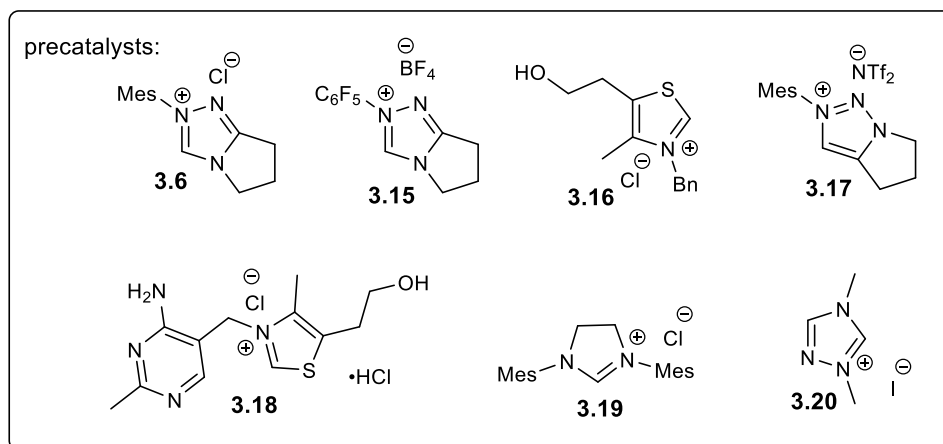
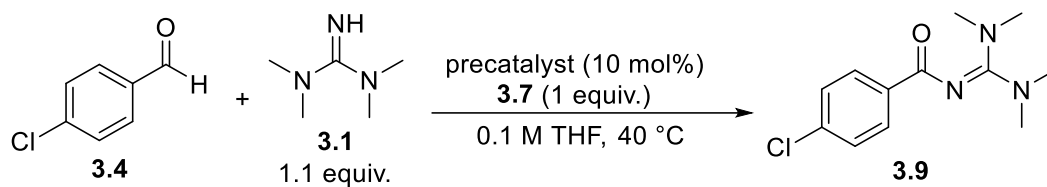
Scheme 3.6: Possible transamidation pathway to form **3.9**.

The results of these control experiments provide sufficient evidence that *N*-acylguanidine **3.9** forms via NHC-catalyzed oxidative coupling of TMG to 4-chlorobenzaldehyde. To see if *N*-acylguanidine **3.9** could be synthesized as the desired product, an experiment was performed using a stoichiometric amount of TMG. After ten minutes of reaction time, full conversion of aldehyde to the desired product **3.9** was observed (Scheme 3.7), determined by HPLC.

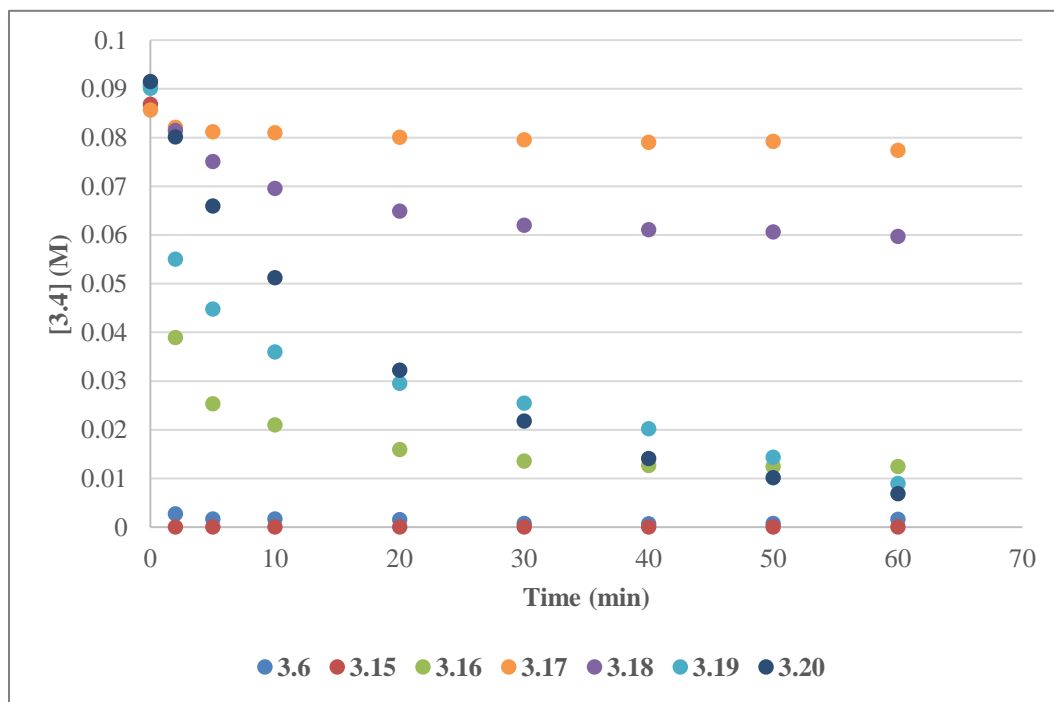


Scheme 3.7: Synthesis of 3.9 using stoichiometric TMG.

With this development, a series of reaction monitoring experiments by HPLC/MS were performed to determine the optimal catalyst for this transformation (Figure 3.2), tracking both consumption of aldehyde **3.4** and formation of *N*-acylguanidine **3.9**.



a)



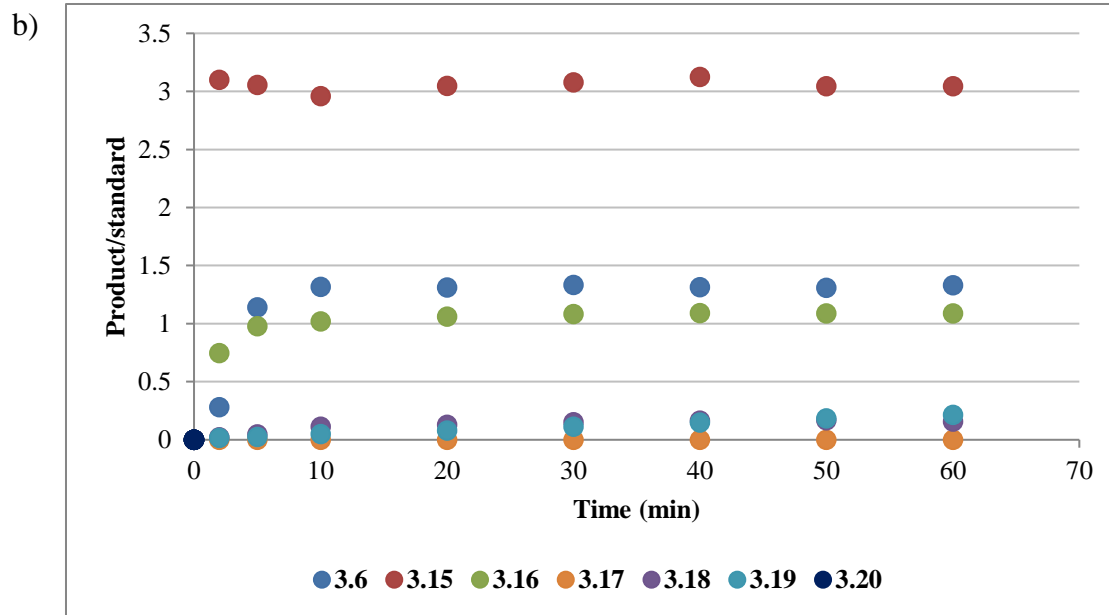


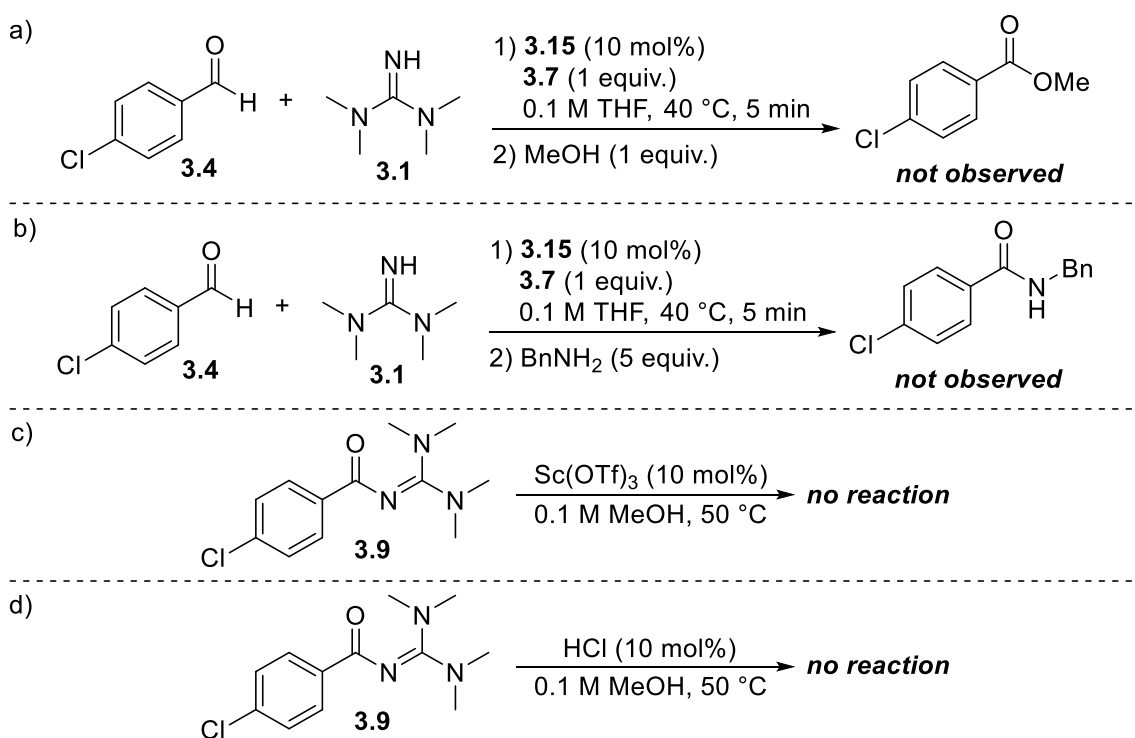
Figure 3.2: a) Aldehyde consumption curves for each precatalyst. b) Product formation curves for each precatalyst.

From Figure 3.2a, both bicyclic 1,2,4-triazolium precatalysts **3.6** and **3.15** show complete aldehyde consumption within the first ten minutes of reaction. *N,N*-dimethyl-substituted 1,2,4-triazolium salt **3.20** also shows high aldehyde consumption and *N*-acylguanidine formation, but at a much slower rate than its *N*-mesityl and *N*-perfluorophenyl analogues. Interestingly, the aldehyde consumption profiles for 1,2,4-triazolium precatalysts **3.6** and **3.15** did not match their respective **3.9** formation profiles, while the reaction profiles for **3.20** did. In addition to differences in reaction rate between these three similar catalysts, they also display unique chemoselectivity.

Precatalyst **3.15** shows the highest amount of *N*-acylguanidine formation, within the fastest time (2 minutes). Thiazolium precatalyst **3.16** shows similar *N*-acylguanidine formation as **3.6**, but less aldehyde consumption. Thiamine hydrochloride (**3.18**) as a precatalyst did not perform well at all. 1,2,3-triazolium precatalyst **3.17** did not produce any *N*-acylguanidine

product. From this optimization study, precatalysts **3.6** and **3.15** appeared to be the best catalyst candidates for further reaction optimization. **3.15** was chosen as the optimal catalyst going forward, due to its rapid reactivity and higher product conversion over **3.6**. In addition, from a practical standpoint, the synthesis of **3.15** is easier than that of **3.6**, due to the stability of the perfluorophenyl hydrazine precursor.³⁵

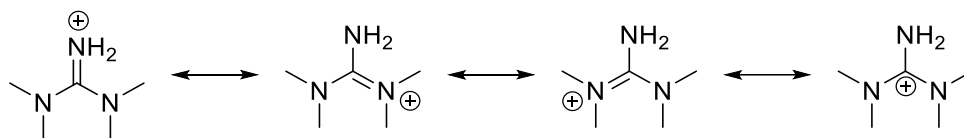
With the optimal catalyst chosen, *N*-acyl guanidine **3.9** was successfully prepared in 93% isolated yield. Since guanidines are commonly employed as nucleophilic organocatalysts,¹¹⁴ it was hypothesized that the guanidine group could be cleaved and replaced with another nucleophile, akin to NHC-catalyzed oxidative amidation/esterification via an active ester. To test this, a series of experiments were performed (Scheme 3.8).



Scheme 3.8: Experiments probing the formation and stability of *N*-acyl guanidine **3.9.**

To probe whether the *N*-acylguanidine could function as an active ester, two separate reactions were run where the *N*-acylguanidine was allowed to form initially, and then MeOH (1 equiv.) or benzylamine (5 equiv.) were added (Scheme 3.8a and Scheme 3.8b, respectively). In both cases, only **3.9** was observed, and no transesterification/transamidation occurred. To probe the stability of **3.9**, a previously prepared sample was subjected to catalytic Sc(OTf)₃ in MeOH, but no transesterification or breakdown was observed (Scheme 3.8c). When **3.9** was subjected to aqueous HCl in MeOH, no breakdown products or transesterification products were detected (Scheme 3.8d). In addition, **3.9** is stable on a C₁₈-capped silica HPLC column with a 0.05% trifluoroacetic acid water/acetonitrile mobile phase, suggesting that **3.9** is resilient to stronger Brønsted acids.

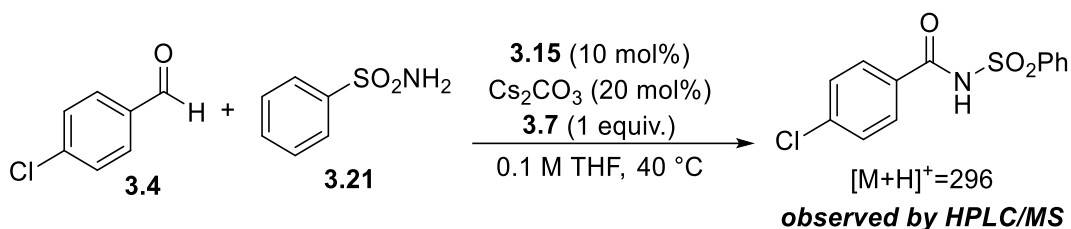
As it has previously been mentioned in this chapter, direct oxidative amidation by NHC catalysis results in low yields, and nucleophilic additives need to be employed for successful amidations. However, the discovery of **3.9** by oxidative NHC catalysis suggests that NHC-catalyzed direct oxidative amidation is possible under certain conditions. In fact, TMG behaves as an exceptional nucleophile in this reaction. The strong basicity of TMG arises from the resonance stability of its conjugated base, due to delocalization of six π -electrons across the molecule¹¹⁴ (Scheme 3.9). However, despite being strong bases, guanidines are traditionally considered non-nucleophilic. It stands to reason that if electron delocalization is a factor in the observed reactivity, other substrates with a degree of electron delocalization would work as well. With that hypothesis, we set out to see if this chemistry was effective towards sulfonamides, which also have significant electron delocalization across the -SO₂NH₂ group.



Scheme 3.9: Resonance structures of the conjugate acid of 1,1,3,3-tetramethylguanidine (TMG).

3.3 Extension to sulfonamides and other electron-poor nucleophiles

To test the applicability of our oxidative *N*-acylation chemistry to other nucleophiles, we ran an initial test reaction with 4-chlorobenzaldehyde (**3.4**) and benzenesulfonamide (**3.21**), using **3.15** as catalyst and Cs₂CO₃ as base (Scheme 3.10). HPLC/MS analysis of the reaction mixture revealed a product with mass $[M+H]^+=296$, the same mass of the expected product. With a successful hit, we performed a series of reactions to optimize the reaction conditions, namely with respect to base and solvent.



Scheme 3.10: Observation of *N*-acyl benzenesulfonamide by HPLC/MS.

To optimize the reaction conditions, reaction progress monitoring by HPLC/MS was used to observe relative rate and conversion as a function of base and solvent (Figure 3.3). These reactions were optimized using propionaldehyde (**3.22**) and benzenesulfonamide (**3.21**) as substrates, giving *N*-acylsulfonamide product **3.23**. **3.23** was detectable by HPLC/MS, both by the UV and MS detector, giving $[M+H]^+ = 214$ in the mass spectrum. Unfortunately, propionaldehyde was not an ideal substrate to optimize the reaction with, due to **3.23** being formed in very low conversions, and not isolable by column chromatography. Regardless, the

information gained from these optimization experiments was useful in applying the chemistry to other aldehyde substrates.

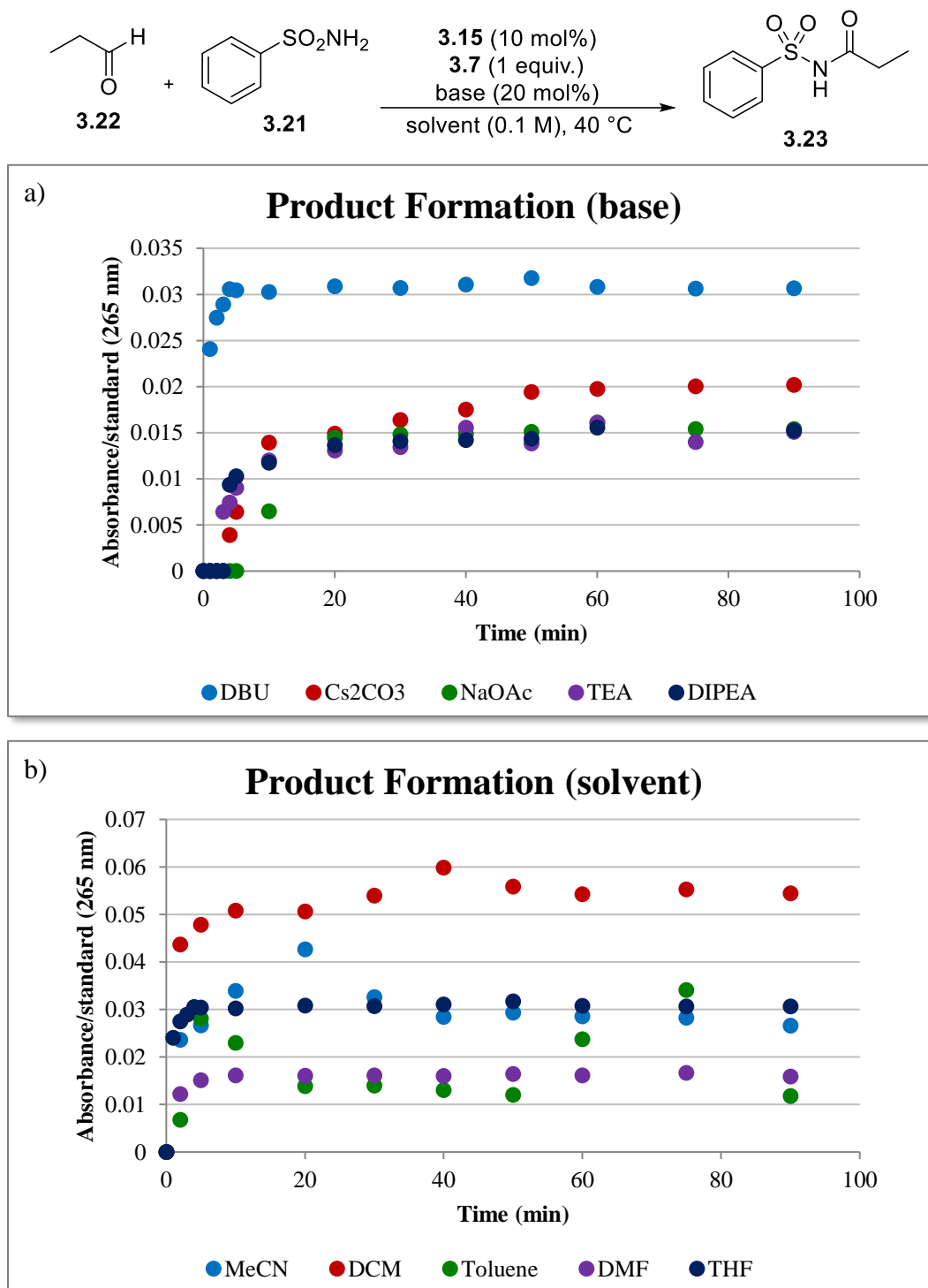
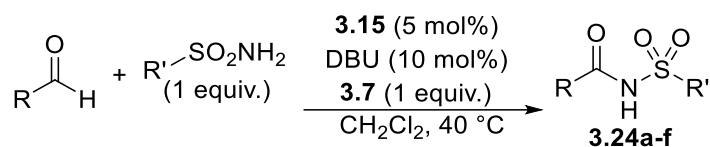


Figure 3.3: a) Product formation curves generated by HPLC with different bases. b) Product formation curves generated by HPLC with different solvents.

From Figure 3.3a, DBU clearly gives both the fastest initial rate, and highest conversion to product. However, the reaction stops forming new product after five minutes, suggesting catalyst deactivation. Sodium acetate, triethylamine, and *N,N*-diisopropylethylamine all have essentially identical rate profiles. Cs_2CO_3 has a similar rate profile to these bases at the start of the reaction, but goes to a higher conversion at the end of the reaction. Of all the bases screened, DBU is the strongest base (conjugate acid $\text{pK}_a \sim 13.5$ ¹¹⁵). The pK_a of precatalyst **3.15** is 16.5,²¹ so the acid/base equilibrium involving **3.15** and DBU will favor the carbene, resulting in faster rates of reaction when DBU is used. It is also important to note that the *N*-acylsulfonamide product **3.23** has an acidic N-H ($\text{pK}_a \sim 5.5$). When the product is present in solution, it will also exist in a dynamic equilibrium with the free carbene, and due to the pK_a difference, the protonated azolium **3.15** will be favored. This can explain why catalyst deactivation occurs when DBU is used as base.

From Figure 3.3b, dichloromethane (DCM) appears to be the optimal solvent for this reaction, producing twice as much product as the reaction run in THF, the solvent used for the base screen. THF and DMF are both hygroscopic solvents,¹¹⁶ which may explain the low conversion to product; exogenous water can trap the *in situ*-generated acyl azolium intermediate, forming propionic acid as a byproduct. The low product conversions in toluene and acetonitrile can be attributed to solubility differences; benzenesulfonamide **3.21** exhibits a low solubility in toluene, while oxidant **3.7** exhibits a low solubility in acetonitrile. Finally, we found that lowering the catalyst loading to 5 mol% and base loading to 10 mol% proved to be similarly as efficient as 10 mol% catalyst and 20 mol% base. With these optimized conditions, we examined the tolerability of different substrates to the reaction.

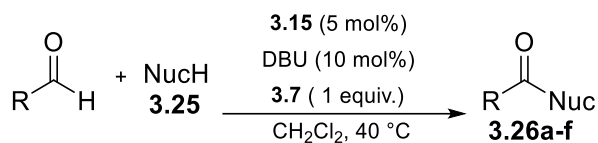
Table 3.1 shows the tolerability of this reaction to aldehyde substrates. This reaction is only efficient with aromatic aldehydes. Propionaldehyde as a substrate shows a trace amount of product by HPLC/MS, but attempts at isolating the product were unsuccessful. The reaction is tolerant to heteroaromatic aldehydes (Entries 5 & 6). Electron-poor 4-nitrobenzaldehyde (Entry 8) showed high conversion of aldehyde, but attempts at isolation were unsuccessful. After silica gel chromatography, only benzenesulfonamide and 4-nitrobenzoic acid were isolated, suggesting that the electron-poor nitro *N*-acysulfonamide is quite susceptible to acid-catalyzed hydrolysis. Aromatic sulfonamides are the only nucleophiles that work, as a reaction with methanesulfonamide gave no traces of product, even after 24 hours of reaction time (Entry 7).



Entry	R	R'	Time (hr)	Yield ^a
1	Ph	Ph	12	96%
2	4-Cl-C ₆ H ₄	Ph	12	54%
3	PhCH=CH	Ph	12	93%
4	Ph	4-Me-C ₆ H ₄	12	50%
5	2-pyridyl	Ph	12	87%
6	2-furyl	Ph	12	46%
7	Ph	Me	24	0%
8	4-NO ₂ -C ₆ H ₄	Ph	12	0%

Table 3.1: Substrate scope for the NHC-catalyzed oxidative acylation of primary sulfonamides. ^a Isolated yield after purification by column chromatography.

Following this initial survey, we then examined a substrate scope of other electron-poor *N*-nucleophiles (Table 3.2). A secondary sulfonamide nucleophile (Entry 1) performed moderately well, and *N*-benzyl *O*-benzyl hydroxylamine and succinimide went to complete conversion, but gave moderate yields (Entries 2 & 4). The hydroxylamine substrate (Entry 2) is notable because it is more electron-rich than the other nucleophiles presented, and seems to contradict the previous observation of electron-rich *N*-nucleophiles performing poorly in this reaction. Amidine and 2-aminobenzothiazole (Entries 5 & 6) were exceptional nucleophiles in this reaction, going to 100% conversion within 5 minutes.



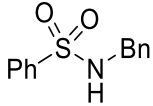
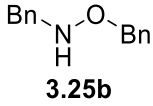
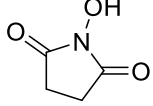
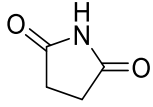
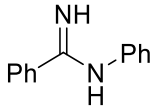
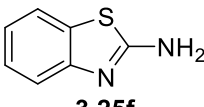
Entry	R	Nuc	Time	Conversion ^a	Yield ^b
1	Ph	 3.25a	12 hr	100%	73%
2	Ph	 3.25b	12 hr	95%	54%
3	4-Cl-C ₆ H ₄	 3.25c	12 hr	100%	88%
4	4-Cl-C ₆ H ₄	 3.25d	12 hr	100%	46%
5	4-Cl-C ₆ H ₄	 3.25e	10 min	100%	65%
6	4-Cl-C ₆ H ₄	 3.25f	10 min	100%	48%

Table 3.2: Substrate scope of NHC-catalyzed oxidative acylation of aldehydes with electron-poor nucleophiles. ^aDetermined by HPLC analysis of the reaction mixture, focusing on aldehyde consumption.

^bIsolated yield after purification by column chromatography.

3.4 Mechanistic investigations

With a general idea of the types of compounds compatible with this reaction, we wanted to uncover the reason why direct oxidative amidation with electron-poor nucleophiles was successful, while direct oxidative amidation with electron-rich *N*-nucleophiles performed poorly. To achieve this, ^1H NMR was used to generate a full mechanistic profile of this 1,2,4-triazolium-based NHC system. The use of ^1H NMR as a reaction monitoring technique allows for much higher data density and does not require the use of quench solvents, which are required when HPLC is used. Understanding the detailed mechanistic profile of this system is also advantageous because it allows for a comparison to the mechanistic profile of the 1,2,3-triazolylidene-catalyzed system described in Chapter 2.

To perform a full detailed mechanistic analysis by ^1H NMR, a system amenable to reaction progress analysis by ^1H NMR was required. Benzaldehyde (**3.27**) and *p*-toluenesulfonamide (**3.28**) were found to be ideal coupling partners, due to the increased solubility of **3.28** in CD_2Cl_2 and the presence of the methyl groups on **3.28** and **3.24d**. The singlet ^1H NMR resonances that arise from these methyl groups can act as NMR handles, and these resonances can be integrated and converted to concentration data for **3.28** and **3.24d** over the course of the reaction. However, due to the acidity of **3.24d**, the solution pH changes throughout the course of the reaction, resulting in resonances corresponding to **3.24d** shifting over the course of the reaction and overlapping with other resonances. Unfortunately, the methyl resonances corresponding to **3.28** and **3.24d** overlap with one another throughout the course of the reaction, and determining concentration data from these resonances was possible. The aromatic region of the ^1H NMR spectrum also exhibited peak overlap as the reaction progressed, but to a lesser extent (Figure 3.4).

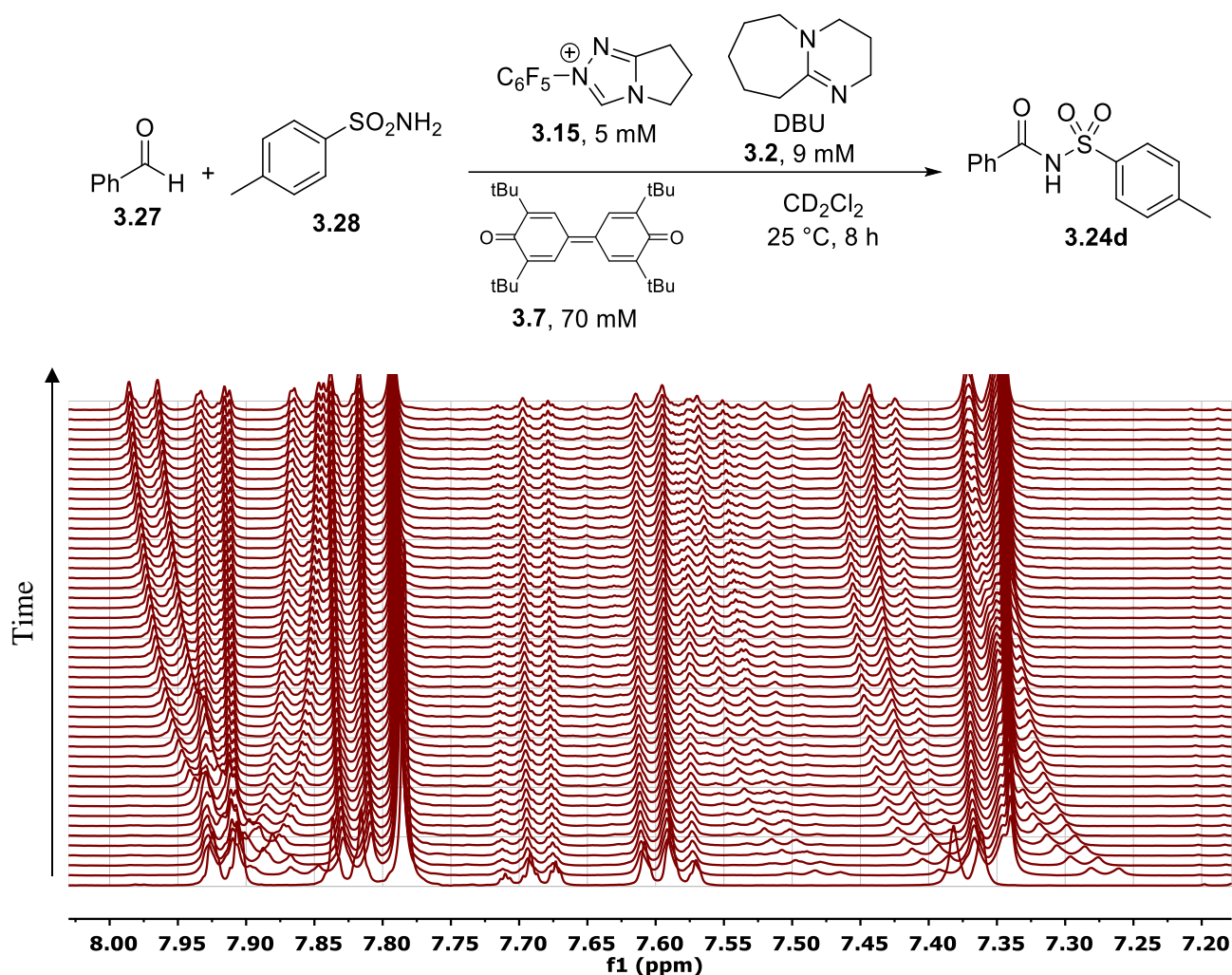


Figure 3.4: Top: model reaction used for studying the NHC-catalyzed oxidative amidation of aldehydes with sulfonamides. Bottom: stacked ^1H NMR spectra of the reaction mixture. Each spectrum represents ten minutes of reaction time. The aromatic region ($\delta = 7\text{--}8$ ppm) is shown to emphasize peak overlap as the reaction proceeds.

As shown in Figure 3.4, there is a triplet resonance signal that increases in intensity as the reaction proceeds, shifting from $\delta = 7.37$ to $\delta = 7.47$ ppm over the course of the reaction. This signal is clear and unobscured by other resonances in the latter parts of the reaction, but it is obscured in the initial phase of the reaction. Similarly, the doublet that shifts from $\delta = 7.27$ to $\delta \sim 7.35$ ppm is clear and unobscured by other resonances in the initial phase of reaction, but is

obscured in the latter phase of the reaction. To generate overall product curves, the unobscured parts of these two phases were integrated and spliced together (Figure 3.5). During the first 60 minutes of reaction, the doublet corresponding to H_a (blue) is unobscured and can be integrated reliably, whereas the signal corresponding to H_b (red) does not give an accurate integration. As the pH of the reaction changes with time, the peaks shift, and H_b can be reliably integrated during the later parts of the reaction. The two curves can then be spliced together to create an overall product formation curve.

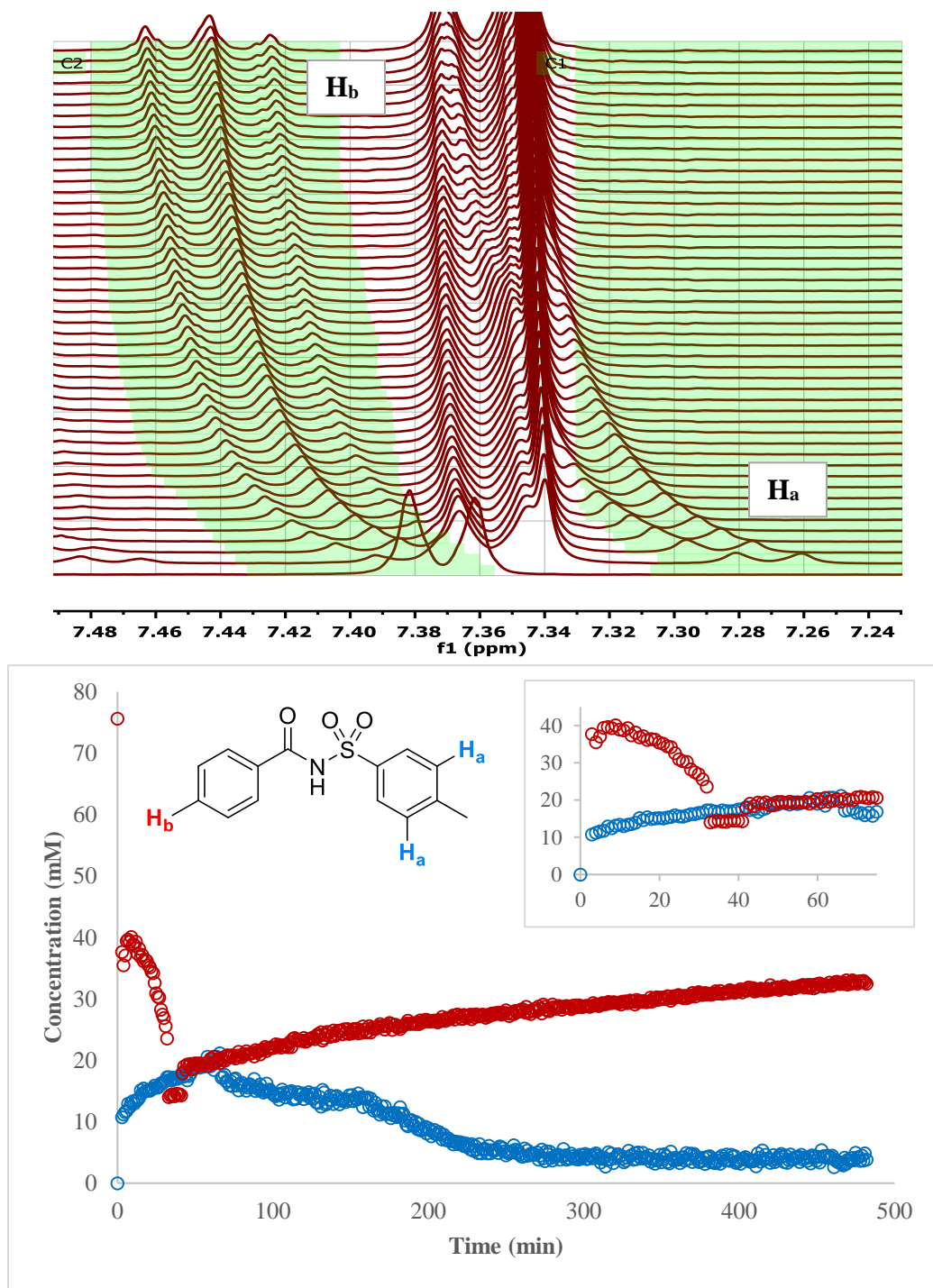


Figure 3.5: Top: magnification of the aromatic region used for integration to generate overall product curves.

Because of overlap after 60 minutes, the integration limits for H_a are set only for the first 60 minutes.

Bottom: the individual integration curves for H_a and H_b spliced together.

To generate these curves, the raw NMR data was processed using MestReNova 11.0's Reaction Monitoring plugin. This plugin converts NMR signal to concentration, provided the concentration of one species at one timepoint is already known. To account for this, solutions were prepared using volumetric glassware, and the initial concentration of aldehyde was set in the program to calculate the concentration factor. Using this processing method, the concentration of the major species present in the reaction can be monitored over time (Figure 3.6).

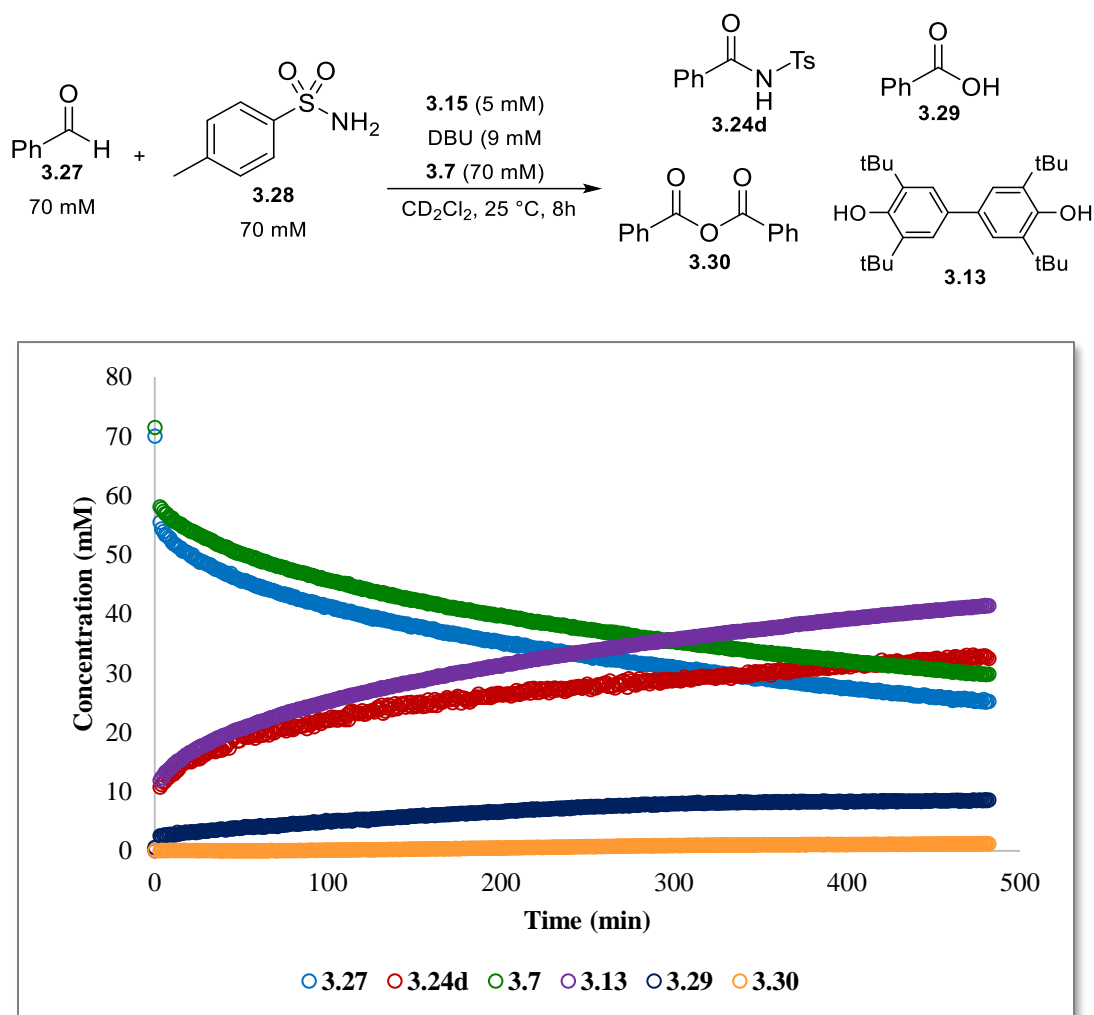


Figure 3.6: Reaction progress curves showing all species present in the reaction.

As shown in Figure 3.6, benzaldehyde (**3.27**), oxidant (**3.7**), and product (**3.24d**) can be monitored by ^1H NMR, as well as major byproduct of oxidant reduction **3.13**. *p*-Toluenesulfonamide (**3.28**) is not shown because both the aromatic and methyl signals overlap with signals corresponding to the product **3.24d** and byproduct **3.13**. Benzoic acid (**3.29**) can also be seen as a minor side product, generated by nucleophilic capture of exogenous water by the *in situ*-generated acyl azolium intermediate, or by oxidation of benzaldehyde. In addition, benzoic anhydride (**3.30**) can be detected in low concentrations, generated by nucleophilic capture of the acyl azolium intermediate with benzoic acid. This analysis by ^1H NMR allows us to monitor the individual rates of reaction for each species in parallel.

The presence of anhydride **3.30** is an interesting observation, as there have been no previous reports of anhydride formation by NHC catalysis. To prove that benzoic anhydride formation was a side reaction in the oxidative acylation, an experiment was performed with one equivalent of benzoic acid as the nucleophile (Figure 3.7). As expected, benzoic anhydride is formed as the sole product. However, unlike with sulfonamide nucleophiles, there seems to be an initial induction period, rather than a rapid burst of product formation. This initial induction period coincides with an increase in benzoic acid concentration, which is most likely formed from capture of the *in situ*-generated acyl azolium intermediate by water, or by oxidation of benzaldehyde by molecular oxygen.

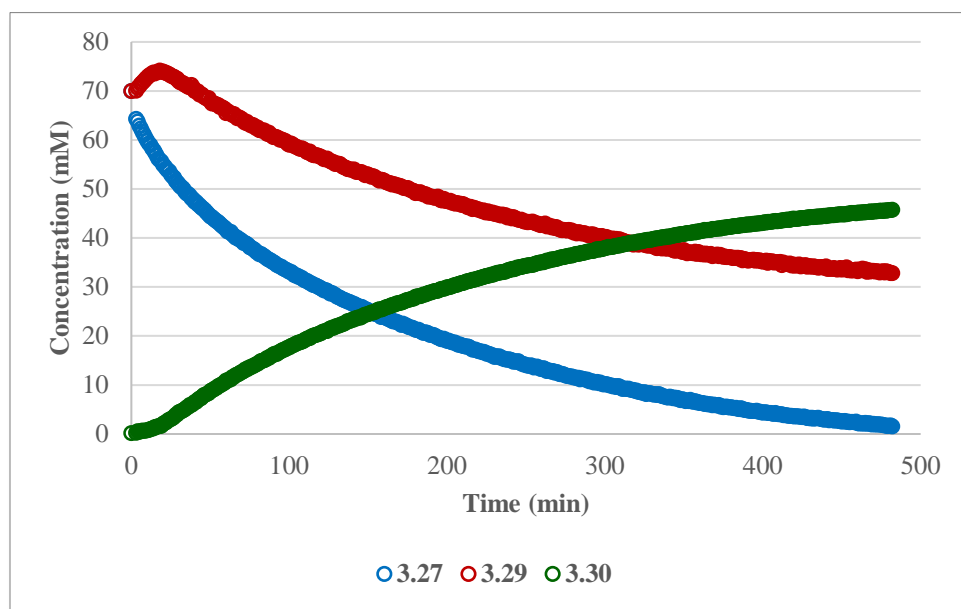
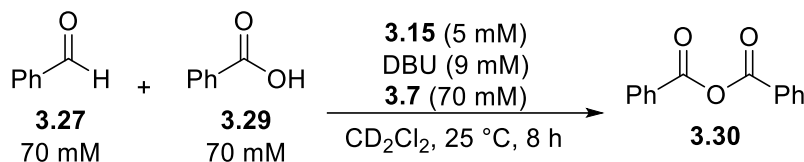


Figure 3.7: Reaction progress curves showing benzoic anhydride formation when benzoic acid is used as nucleophile.

One of the key features of the oxidative sulfonamidation reaction is the presence of two distinct regimes: Regime I (0-2 minutes) and Regime II (2 minutes onwards) (Figure 3.8). For the reaction in Figure 3.8, 32.5 mM of product **3.24d** is formed, corresponding to a yield of 46%. During Regime I, 10 mM of **3.24d** is formed within two minutes, whereas in Regime II, 22.5 mM of **3.24d** is formed over the course of eight hours. The rate of product formation is drastically slower in Regime II than in Regime I, suggesting that the intrinsic kinetics in each regime is different. The causes of the drastic rate difference between both regimes are analyzed and explained in the following sections.

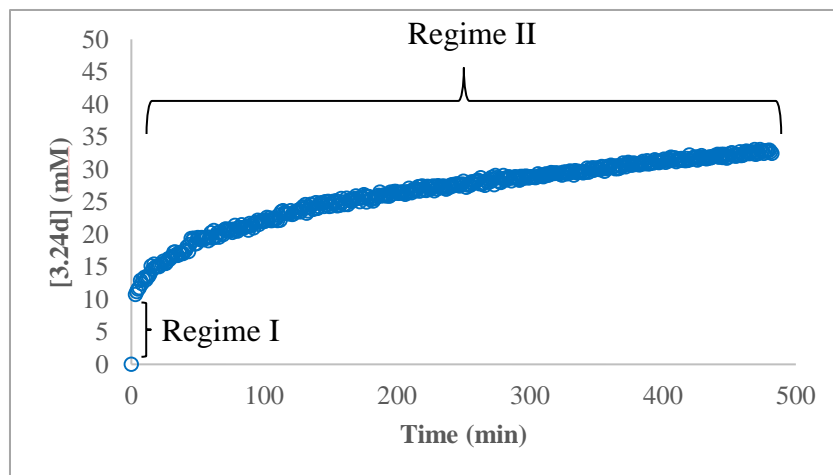
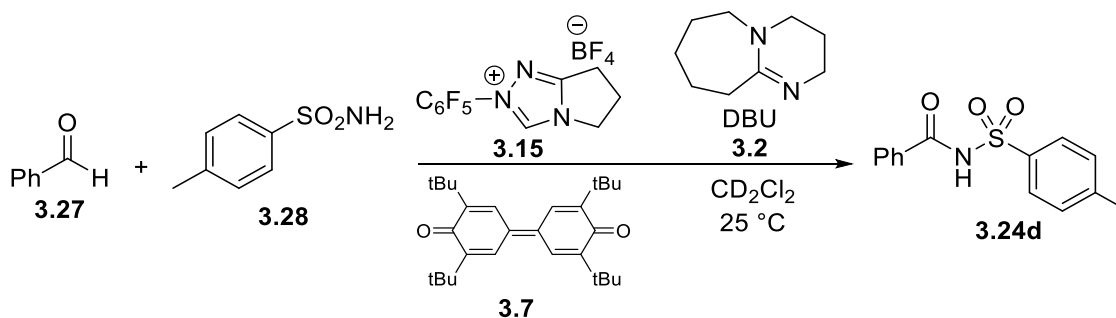


Figure 3.8: Product formation curve of 3.24d generated by ^1H NMR, emphasizing both reaction regimes.

3.4.1 Same “excess” experiments to probe catalyst deactivation

To determine if the oxidative sulfonamidation reaction was suffering from catalyst deactivation or product inhibition, the “same excess” protocol (Section 1.2.2) developed by Baxter and Blackmond^{117,118} was employed. An explanation of this protocol in the context of the reaction shown in Scheme 3.11 follows.



Scheme 3.11: Overall scheme for the reaction studied by reaction progress analysis methodology.

For a reaction exhibiting 1:1 stoichiometry between two substrates, such as the reaction in Scheme 3.11, mass balance dictates that for every molecule of **3.27** consumed, one molecule of **3.28** is consumed as well. This relationship is expressed mathematically in equation 3.1. The

reaction “excess” [e] is defined as the difference in initial concentrations of these two substrates (equation 3.2).

$$[\mathbf{3.27}]_0 - [\mathbf{3.27}] = [\mathbf{3.28}]_0 - [\mathbf{3.28}] \quad (3.1)$$

$$\text{excess} = [\mathbf{e}] = [\mathbf{3.27}]_0 - [\mathbf{3.28}]_0 \quad (3.2)$$

Substituting equation 3.2 into equation 3.1, an expression for [3.28] can be written in terms of only [3.27] and [e] (a constant):

$$[\mathbf{3.28}] = [\mathbf{e}] + [\mathbf{3.27}] \quad (3.3)$$

The simplest rate equation for the system in Scheme 3.11 is given in equation 3.4:

$$\text{rate} = k[\mathbf{3.27}]^x[\mathbf{3.28}]^y[\text{cat}]^z \quad (3.4)$$

where x, y, and z are reaction orders in aldehyde (3.27), sulfonamide (3.28), and catalyst, respectively. It is important to note that for this rate expression, the assumption is made that the concentration of active catalyst ([cat]) does not change, i.e. there is no product inhibition or catalyst deactivation. The assumption must also be made that [3.7] and [DBU] do not change, and these terms can be incorporated into k, effectively making it k_{obs} . In addition, since [cat] is assumed to be unchanging, it can be considered a constant, and incorporated into k_{obs} , simplifying the equation further. Rearranging equation 3.3 and substituting into equation 3.4, an expression for rate involving only [3.27] can be constructed:

$$\text{rate} = k[\mathbf{3.27}]^x([\mathbf{e}] + [\mathbf{3.27}])^y \quad (3.5)$$

From the mathematical relationship derived in equation 3.5, for all reactions with the same value of [e], the same rate of reaction should be obtained at the same concentration of [3.27], regardless of the initial concentration of [3.27]. For example, if one reaction starts at [3.27] = 0.1 M and a second reaction starts at [3.27] = 0.08 M, the instantaneous rates of reaction should be identical when [3.27] = 0.06 M in each system. If the rates of reaction are not identical, then

something other than the intrinsic kinetics of the system is influencing the reaction rate, usually catalyst deactivation or product inhibition. In other words, a reaction with “fresh” catalyst should exhibit the same rate profile as a reaction that has already had 20 catalytic turnovers. While this method cannot intrinsically reveal the nature of catalyst deactivation or product inhibition, it is a useful tool for glean information about catalyst stability from a few experiments.

Figure 3.9 shows aldehyde consumption curves for two “same excess” experiments, run at 50 and 70 mM initial concentrations of **3.27** and **3.28**. Visual inspection of Figure 3.9 reveals three key features of this reaction. First, there is a period of rapid aldehyde consumption (Regime I) between the first two data points (~3 min) followed by a vastly slower period of aldehyde consumption (Regime II) for the rest of the reaction. Second, examining the beginning of Regime II for both reactions, the 70 mM reaction (blue curve) appears to be faster than the 50 mM reaction (red curve). Third, late in the reaction (>300 min), both curves appear to be parallel, suggesting that both reactions have the same kinetic profile.

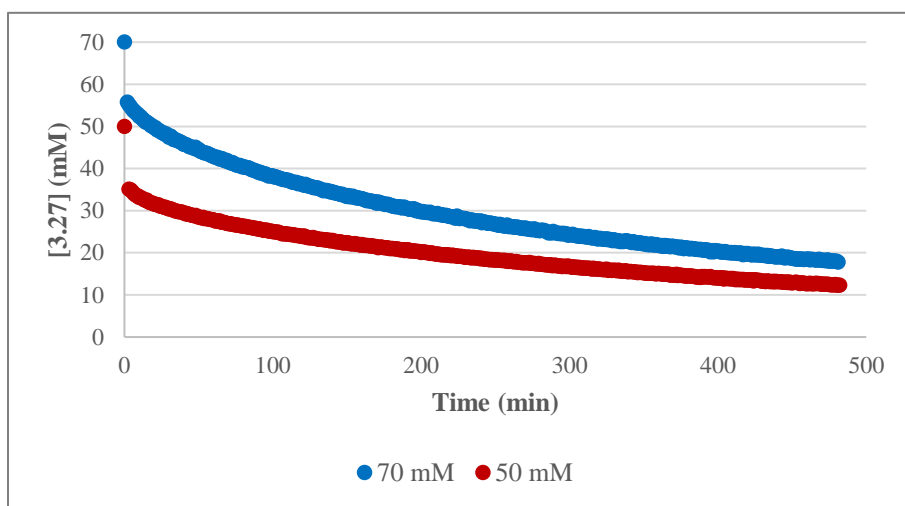
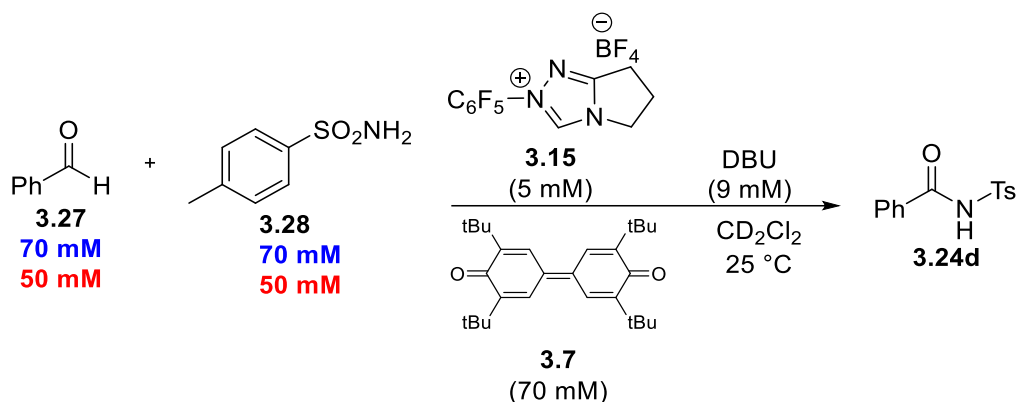


Figure 3.9: Reaction progress curves of aldehyde consumption, run at the same $[e]=0$.

To see if catalyst deactivation or product inhibition was affecting this reaction, the time domain of the 50 mM curve was mathematically manipulated such that the beginning of Regime II of the 50 mM curve overlaid a point on the 70 mM curve (Figure 3.10). The point of overlay is where the concentration of benzaldehyde (**3.27**) is equal to 35 mM. For the 70 mM reaction (blue curve), the catalyst has completed seven turnovers at this point, while for the 50 mM reaction (red curve), the catalyst has completed only three turnovers. If there was no irreversible catalyst death or product inhibition, the two curves in Figure 3.10 should overlay. This is not the case, and so catalyst deactivation or product inhibition is occurring.

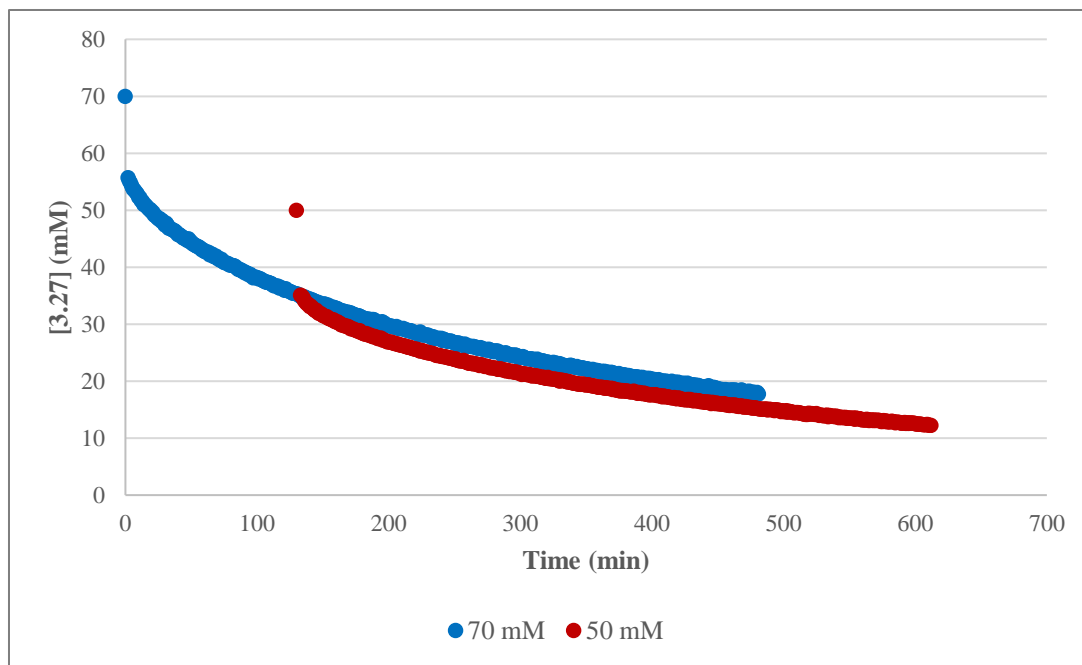
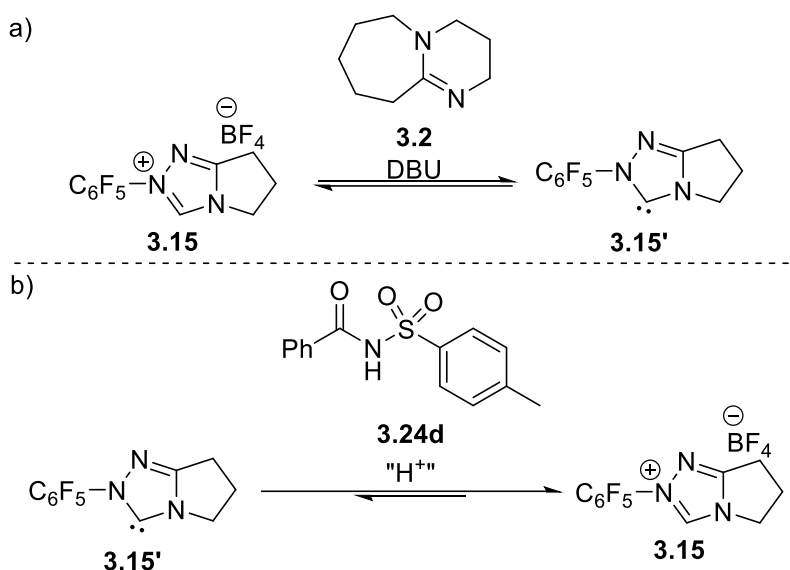


Figure 3.10: Benzaldehyde consumption curves from Figure 3.9, mathematically manipulated in the time domain so that the start of Regime II in the 50 mM reaction (red curve) overlays at a point on the 70 mM reaction (blue curve). The point where the two curves overlay is at approximately 35 mM.

Upon closer inspection of Figure 3.10, at the point of intersection (where $[3.27] = 35$ mM), the red 50 mM curve shows faster consumption of **3.27** than the blue 70 mM curve, but then the two curves become parallel, which indicates that both reactions are exhibiting similar kinetics after a certain point. An explanation for this observation lies in a discussion of the acid/base dynamic of NHC catalysis and the effect of product **3.24d** on solution pH. Generation of the active carbene catalyst **3.15'** requires deprotonation of the azolium precatalyst **3.15** by a base, such as DBU (Scheme 3.12a). The N-H proton of *N*-acylsulfonamide **3.24d** is quite acidic ($pK_a \sim 5$), so as **3.24d** is produced throughout the reaction, the solution pH lowers, and the active carbene catalyst can potentially be protonated (Scheme 3.12b). At the point of intersection in Figure 3.10, the concentration of benzaldehyde **3.27** is 35 mM. By mass balance, this means that

for the red 50 mM curve, the concentration of **3.24d** at the point of intersection must be 15 mM, while for the blue 70 mM curve, it must be 36 mM. For the red 50 mM curve, the lower concentration of **3.24d** results in a higher solution pH, and so the rate of reaction is higher due to less product inhibition. As the concentration of **3.24d** increases and the solution pH lowers, the reaction reaches a saturation point of catalyst inhibition by **3.24d** and both curves become parallel. This product inhibition and its role in the overall reaction will be discussed in greater detail in the next section.



Scheme 3.12: a) Generation of active carbene catalyst by DBU. b) Inhibition of catalyst by product.

3.4.2 Different “excess” experiments to determine order in each reaction component

The basic rate equation for this catalytic system is

$$\text{rate} = k_{\text{obs}}[\mathbf{3.21}]^a[\mathbf{3.22}]^b[\mathbf{3.9}]^c[\mathbf{3.4}]^d[\text{DBU}]^e \quad (3.6)$$

where a, b, c, d, and e are the orders in aldehyde, sulfonamide, catalyst, oxidant, and base, respectively. k_{obs} can be considered the overall rate constant, and it incorporates all of the rate constants for each elementary step of the reaction. To determine the reaction orders in each

component, classical kinetic techniques would use a large excess of one or more components, and vary the initial concentration of the component of interest (pseudo first-order techniques). Our method involves using practical amounts of each component, and varying the concentration of the component of interest, and monitoring the rate profile of the reaction. Curves that overlay indicate that the component with differing initial concentrations does not affect the overall reaction rate, and therefore it is zero order in that component. Conversely, curves that do not overlay indicate that that component affects the overall rate of reaction, and therefore the reaction has a positive order in that component.

Using this methodology, a detailed mechanistic analysis was performed, analyzing and identifying the reaction order in each component. Since the 1,2,4-triazolium precatalysts are direct analogues of the 1,2,3-triazolium salt precatalysts studied in Chapter 2, similar behavior was expected for the 1,2,4-triazolium precatalysts. Figure 3.11 shows product formation curves as a function of time when initial aldehyde concentration is increased from 50 mM to 90 mM.

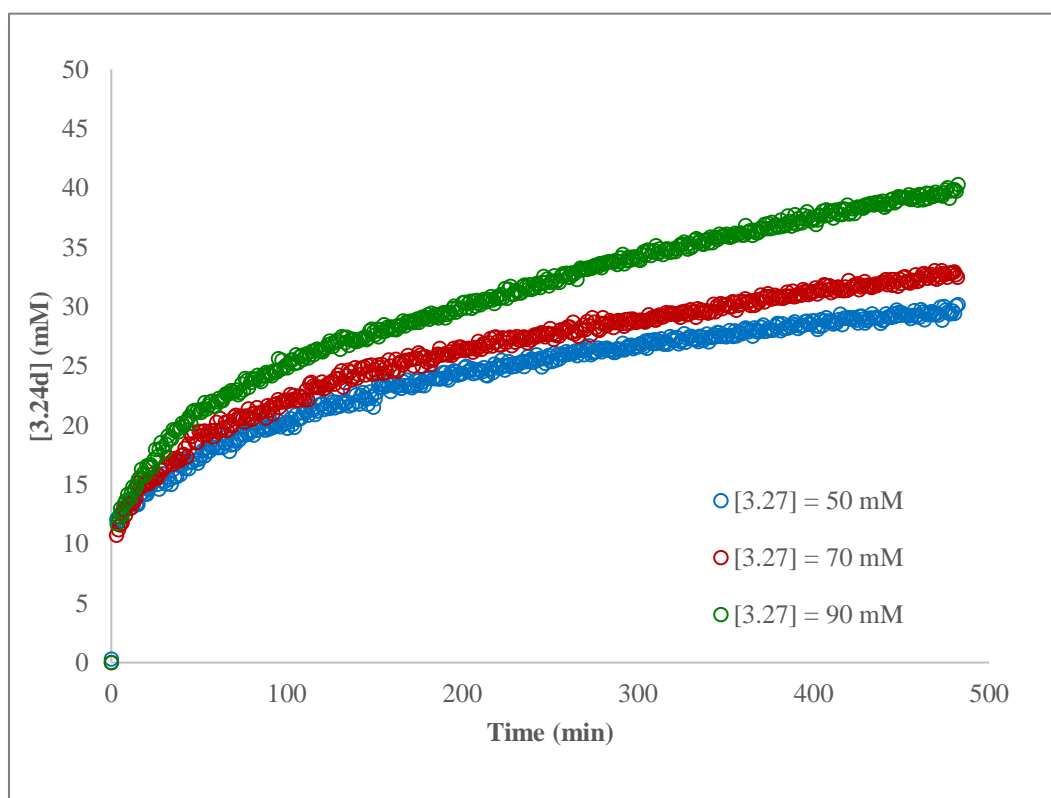
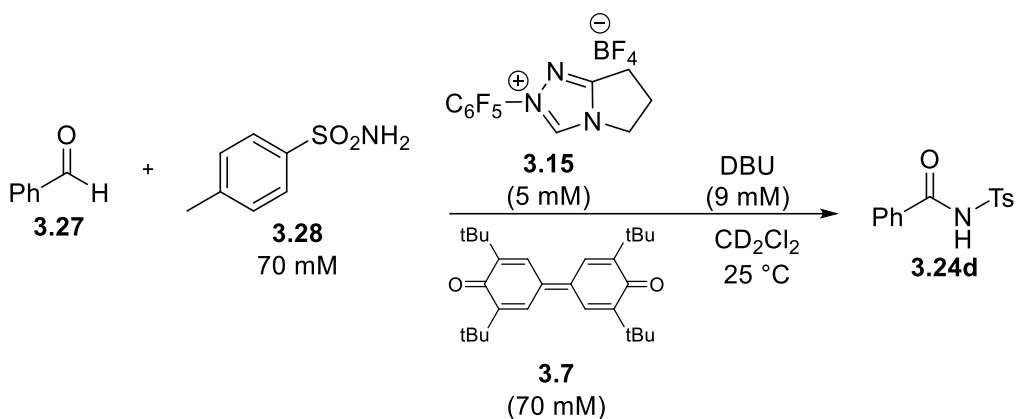


Figure 3.11: Product formation curves with differing initial concentrations of benzaldehyde (3.27**). $[\text{3.28}]_0 = 70 \text{ mM}$, $[\text{3.7}]_0 = 70 \text{ mM}$, $[\text{3.15}]_0 = 5 \text{ mM}$, $[\text{DBU}]_0 = 9 \text{ mM}$.**

For each initial concentration of aldehyde, the same amount of product is rapidly produced during Regime I. In Regime II, the rate of formation of product increases as a function

of initial aldehyde concentration, indicating a small positive (but not first) order relationship with respect to aldehyde.

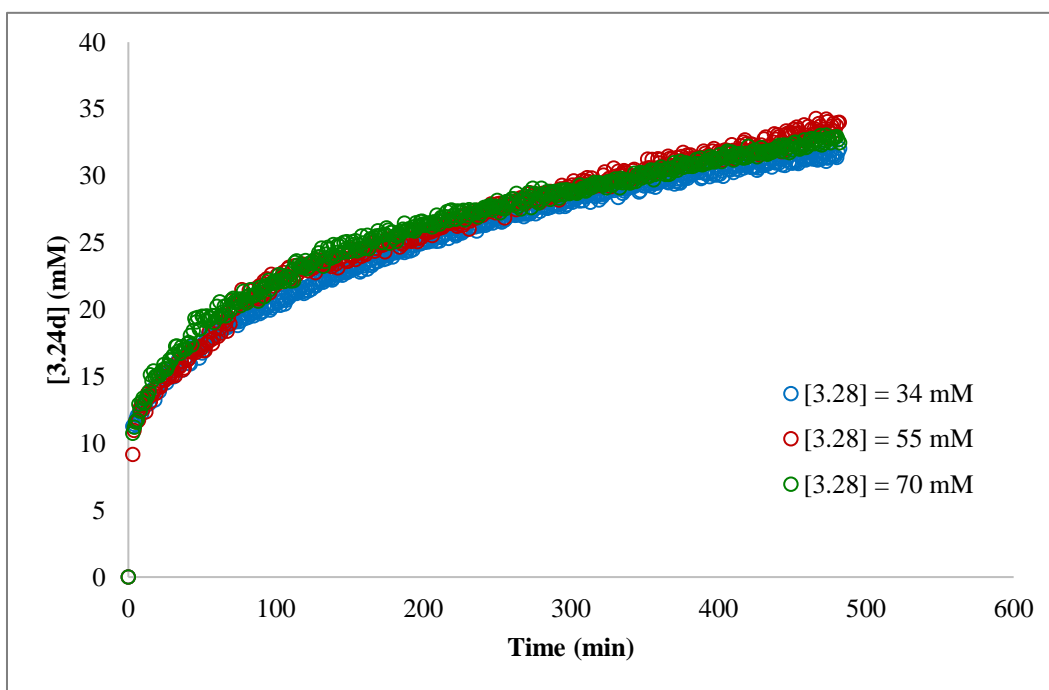
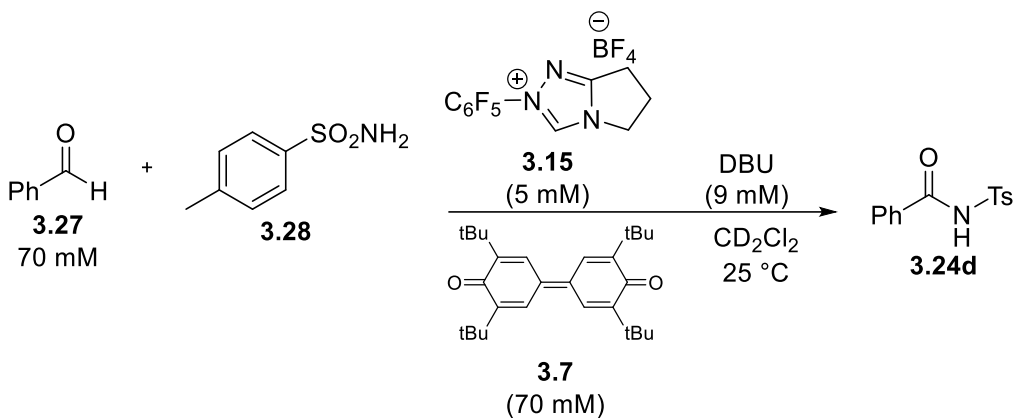


Figure 3.12: Product formation curves with different initial concentrations of *p*-toluenesulfonamide (**3.28**).

$$[\text{3.27}]_0 = 70 \text{ mM}, [\text{3.7}]_0 = 70 \text{ mM}, [\text{3.15}]_0 = 5 \text{ mM}, [\text{DBU}]_0 = 9 \text{ mM}.$$

Figure 3.12 shows product formation curves as a function of time when the concentration of sulfonamide **3.28** is increased from 34 mM to 70 mM. In Regime I, the same amount of product is rapidly formed for each initial concentration of sulfonamide. In Regime II, the product

curves overlay. Overlaying curves indicate that each reaction is effectively the same, and the reaction is zero-order with respect to sulfonamide nucleophile.

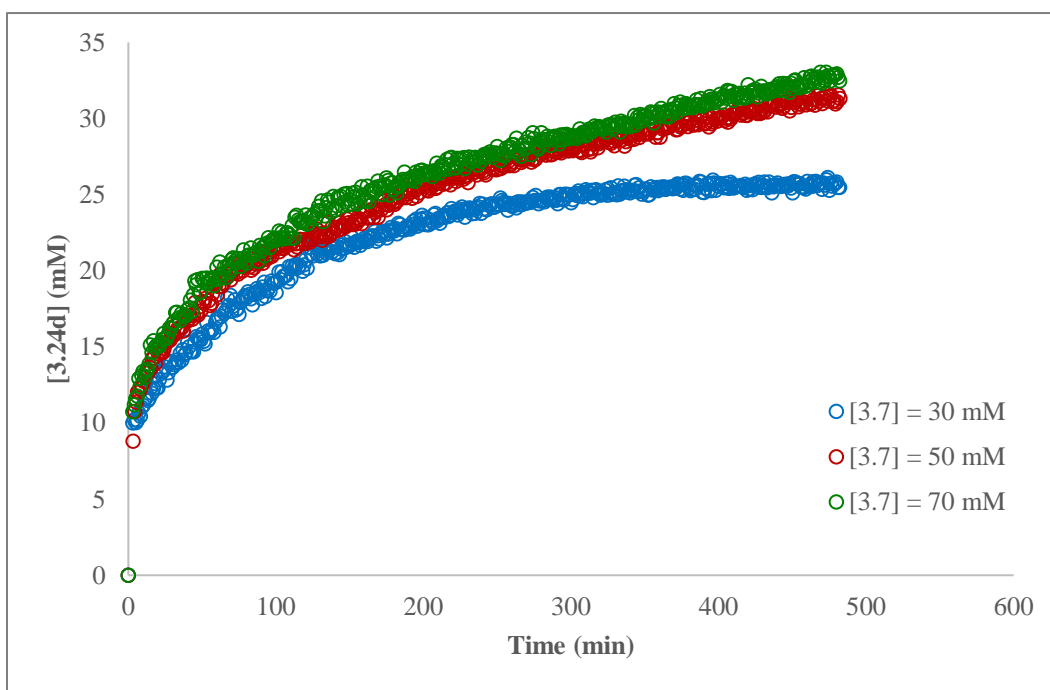
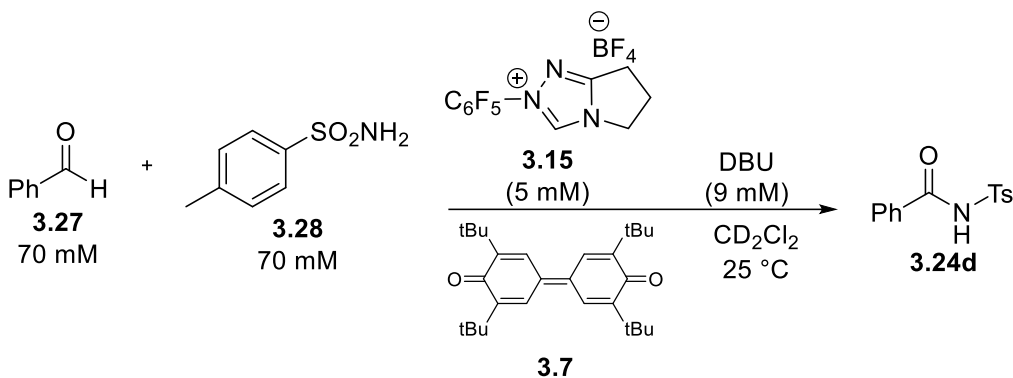


Figure 3.13: Product formation curves with differing initial concentrations of oxidant (3.7**). $[\text{3.27}]_0 = 70 \text{ mM}$, $[\text{3.28}]_0 = 70 \text{ mM}$, $[\text{3.15}]_0 = 5 \text{ mM}$, $[\text{DBU}]_0 = 9 \text{ mM}$.**

Figure 3.13 shows product formation curves as a function of time when oxidant **3.7** is varied from 30 mM to 70 mM. Like experiments varying aldehyde and sulfonamide, during Regime I the amount of product formed is the same across all three reactions. During Regime II,

the 50 mM and 70 mM reactions overlay, indicating a zero-order relationship with respect to oxidant. However, the 30 mM reaction deviates from this behavior. This observation can be attributed to the much lower concentration of oxidant; the concentration of oxidant is much lower than aldehyde or sulfonamide, and so it becomes limiting in the case of the 30 mM reaction.

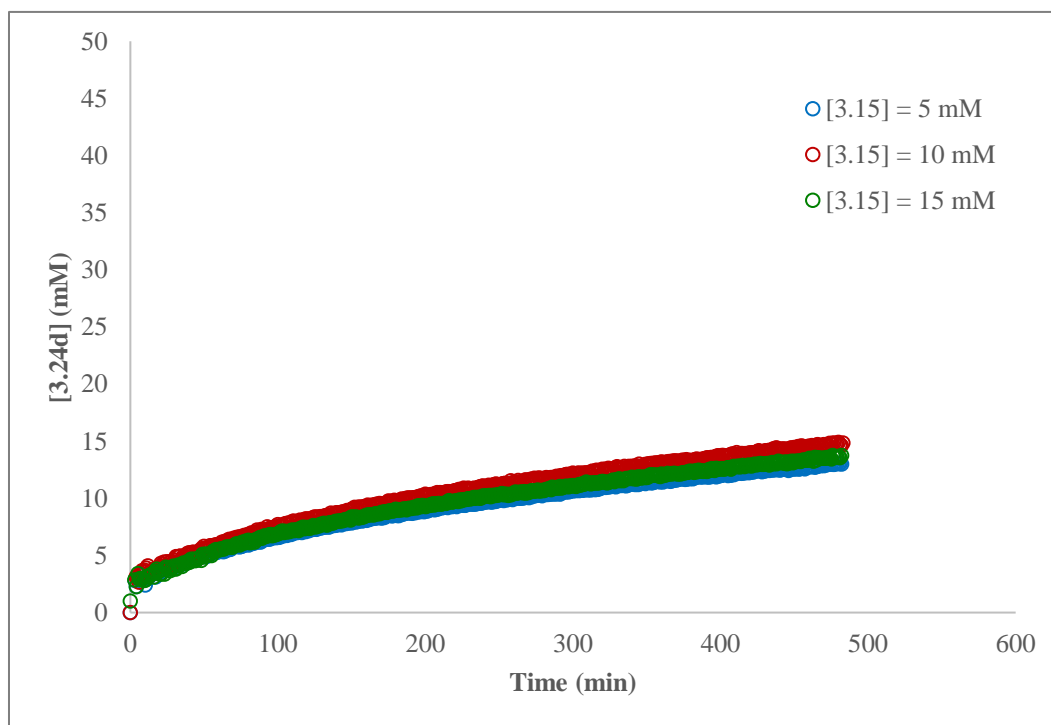
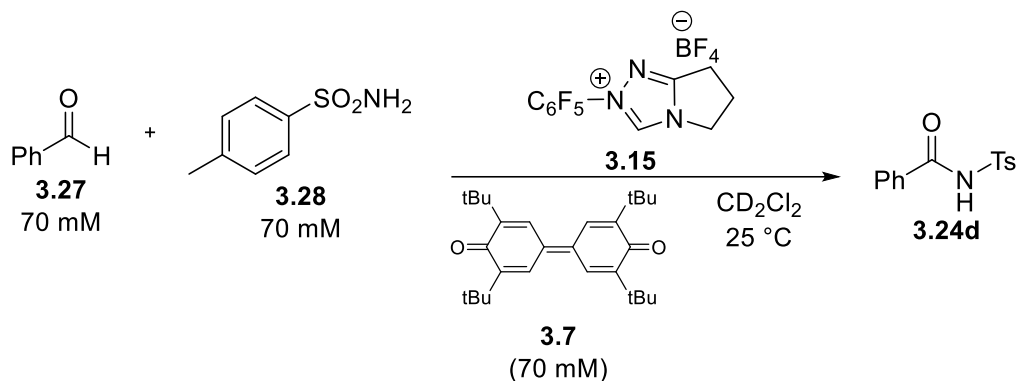
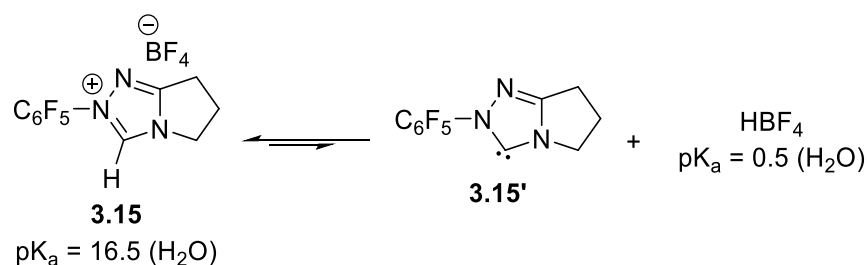


Figure 3.14: Product formation curves with different initial concentrations of triazolium pre-catalyst (3.15**).**

$[\text{3.27}]_0 = 70 \text{ mM}$, $[\text{3.28}]_0 = 70 \text{ mM}$, $[\text{3.7}]_0 = 70 \text{ mM}$. DBU was omitted for this set of experiments.

To measure the relative order in catalyst only, reactions were run without DBU (Figure 3.14). The reaction is drastically slower and only proceeds to ~20% conversion, but the active catalyst is still able to be generated in the absence of base. This observation suggests that there is a solution equilibrium between triazolium precatalyst **3.15** and active carbene catalyst **3.15'** (Scheme 3.13). Due to the massive pK_a difference between **3.15** and HBF_4 , this equilibrium lies far to the left in favor of **3.15**; nevertheless, a small amount of **3.15'** is able to be generated and the reaction can proceed, albeit with low catalytic turnover. Bode's group has reported similar catalytic activity of *N*-mesityl-substituted 1,2,4-triazolium salts in the absence of base, in both enantioselective Claisen rearrangements¹¹⁹ and redox esterifications of enals.⁹⁸



Scheme 3.13: Proposed acid/base equilibrium between triazolium **3.15 and carbene **3.15'**. pK_a values for **3.15**²¹ and HBF_4 ¹²⁰ were determined experimentally.**

The product formation curves in Figure 3.14 appear to overlay, suggesting that there is no measurable difference in reaction rate when initial precatalyst concentration is equal to 5, 10, or 15 mM; this would imply that the reaction is zero order in catalyst. However, a catalyst-mediated reaction cannot truly be zero order in catalyst; there must be a concentration dependence on catalyst. For this reaction in the absence of base, the concentration of active catalyst is solely dependent on the equilibrium shown in Scheme 3.13. Small changes in concentration of **3.15** have minimal effect on the concentration of **3.15'**, and so the reaction appears zero order in

catalyst, despite the logical requirement that there must be a concentration dependence on catalyst.

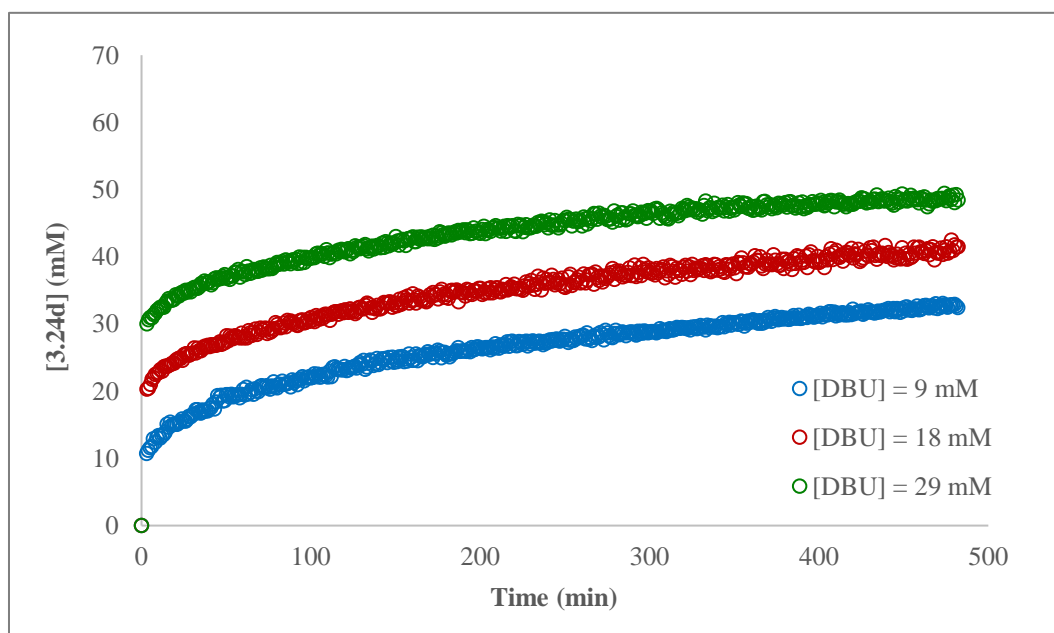
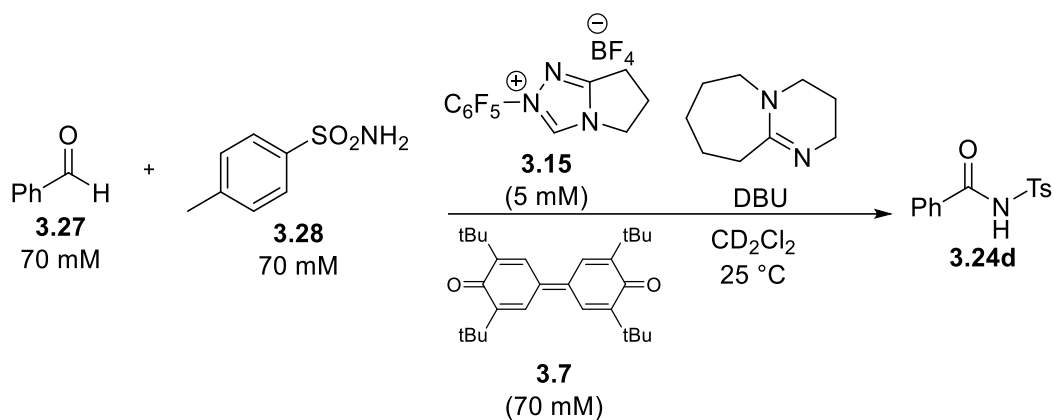


Figure 3.15: Product formation curves of **3.24d** with different initial concentrations of DBU. $[\text{3.27}]_0 = 70 \text{ mM}$, $[\text{3.28}]_0 = 70 \text{ mM}$, $[\text{3.7}]_0 = 70 \text{ mM}$, $[\text{3.15}]_0 = 5 \text{ mM}$.

Figure 3.15 shows reaction progress curves of **3.24d** as a function of time, with initial DBU concentrations increasing from 9 mM to 29 mM. Regime I for all three reactions is drastically different. As initial DBU concentration increases, the concentration of product formed during Regime I increases, corresponding to the initial concentration of DBU for each reaction.

The shape of the curves during Regime II appear to be parallel to each other, so to examine the contribution of Regime II only, Regime I was subtracted from each curve and Regime II for each reaction was plotted (Figure 3.16).

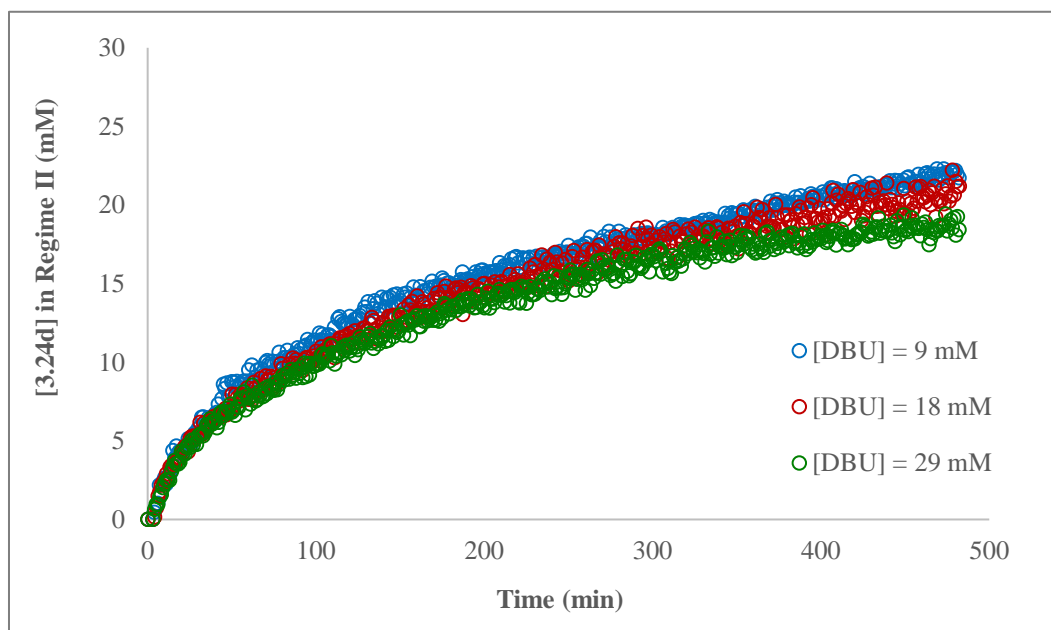


Figure 3.16: Product formation of 3.24d during Regime II only when the initial concentration of DBU is varied. $[3.27]_0 = 70$ mM, $[3.28]_0 = 70$ mM, $[3.7]_0 = 70$ mM, $[3.15]_0 = 5$ mM.

The product formation curves for **3.24d** in Figure 3.16 overlay, indicating that during Regime II, the reaction is zero order with respect to DBU. On the contrary, the product formation curves of **3.24d** in Figure 3.15 show a rate dependence on DBU during Regime I, indicating that the reaction is positive order in DBU during Regime I. From these observations, it was hypothesized that if a full equivalent of DBU was used in the reaction, full conversion of **3.27** to **3.24d** would be observed in a matter of minutes, instead of hours. Figure 3.17a shows reaction progress curves for **3.27** and **3.24d** when a full equivalent of DBU was utilized in the reaction (70 mM). As predicted, the reaction goes to full conversion within five minutes. The slope of a first-order rate plot (Figure 3.17b) reveals k_{obs} for this reaction to be 1.1 s^{-1} .

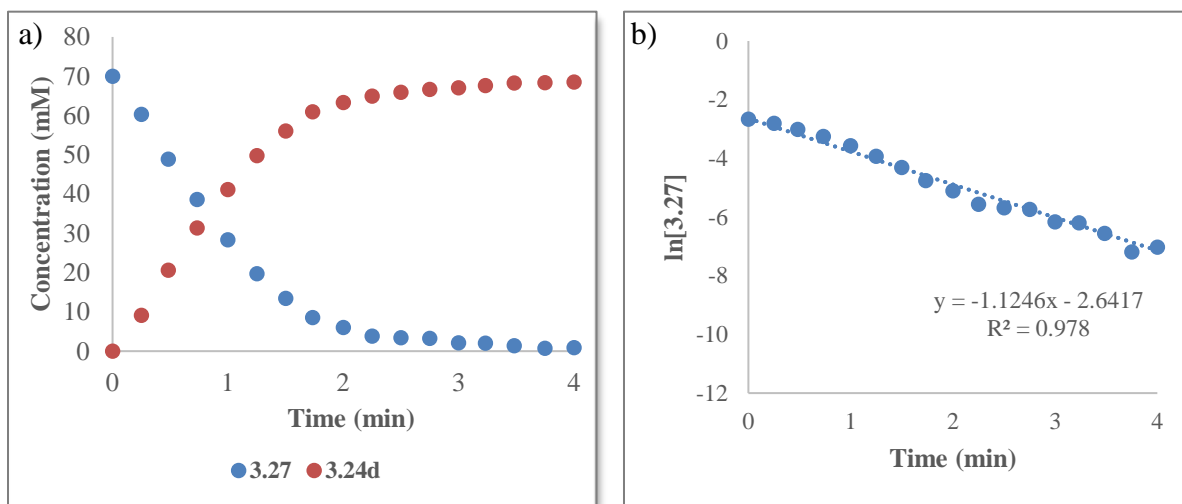
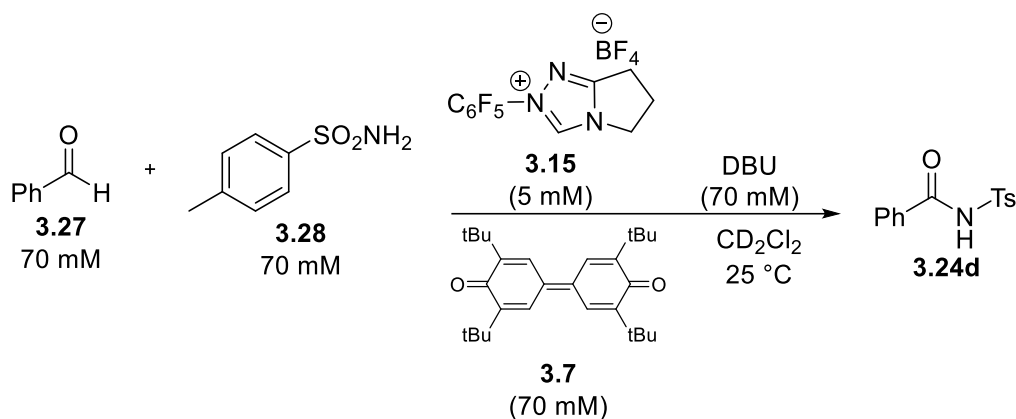
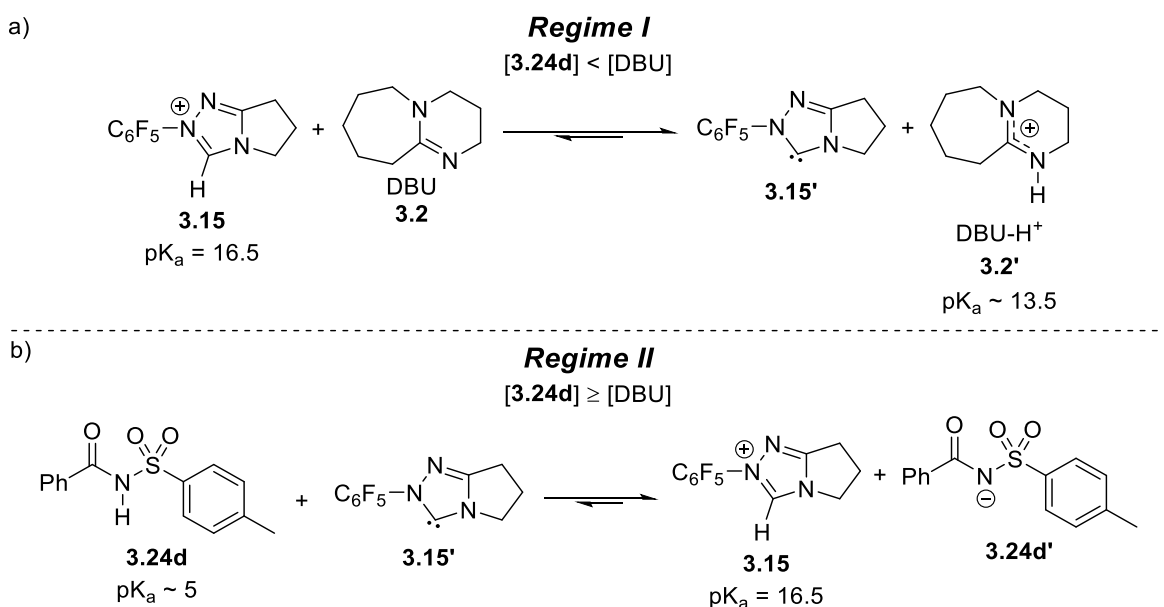


Figure 3.17: a) Reaction progress curves generated by ReactIR of **3.27** and **3.24d** when one equivalent of DBU is used. $[\text{3.27}]_0 = 70 \text{ mM}$, $[\text{3.28}]_0 = 70 \text{ mM}$, $[\text{3.7}]_0 = 70 \text{ mM}$, $[\text{3.15}]_0 = 5 \text{ mM}$, $[\text{DBU}]_0 = 70 \text{ mM}$. b) First order rate plot of $\ln[\text{3.27}]$ as a function of time.

The drastic rate dependence on DBU concentration in this reaction can be explained in the context of the relative pK_a s of the major species in the reaction. The triazolium salt precatalyst **3.15** has a calculated pK_a of 16.5,²¹ which is deprotonated by DBU to give free carbene **3.15'** and DBU-H^+ , which has a pK_a of ~ 13.5 .¹¹⁵ The predicted pK_a of *N*-acylsulfonamide **3.24d** is approximately 5. During Regime I (Scheme 3.14a), when rapid product formation occurs, the **3.15/3.15'** equilibrium favors **3.15'**, due to an excess of DBU relative to

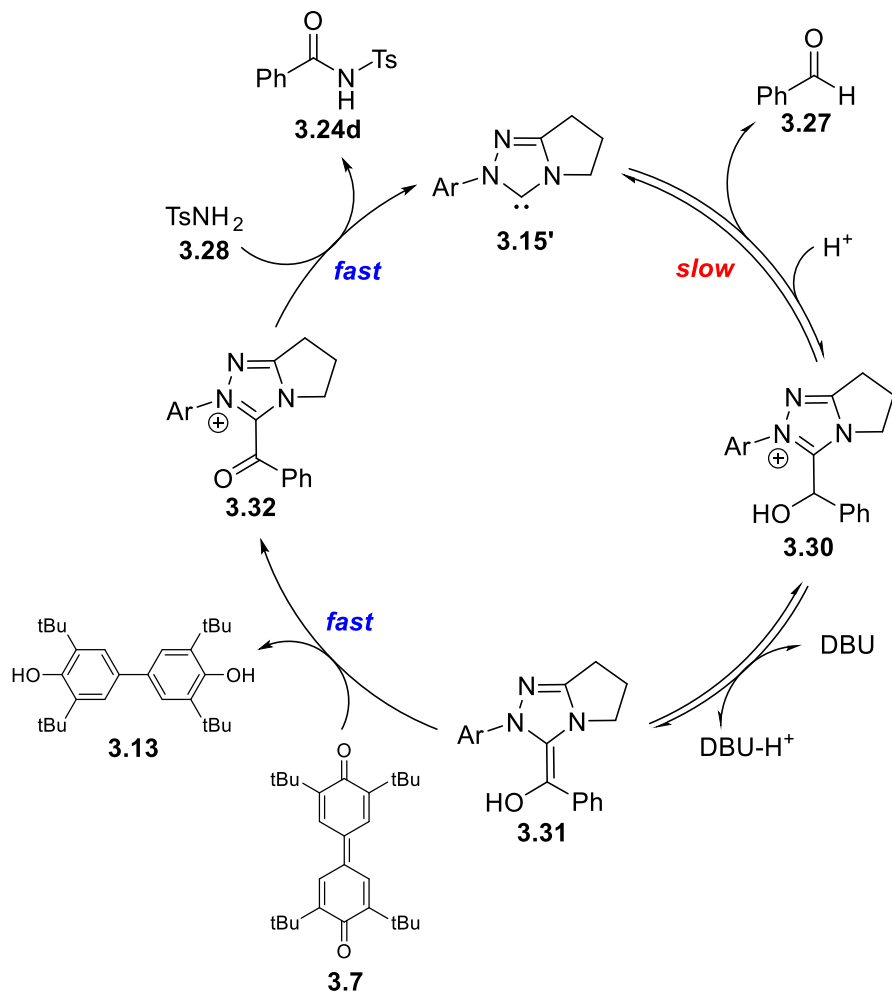
3.15. DBU acts as a buffer in Regime I, ensuring that the pH of the solution is high enough to favor carbene **3.15'**, which continues to facilitate rapid formation of **3.24d**. As soon as the concentration of **3.24d** equals the initial concentration of DBU, the solution pH is lowered to a point where **3.15** is favored, and the reaction shifts into Regime II (Scheme 3.14b). In Regime II, as more **3.24d** is formed, the solution pH is lowered, protonating **3.15'** and increasingly pushing the **3.15/3.15'** equilibrium towards **3.15**, effectively inhibiting the active catalyst. Benzoic acid (**3.29**, $pK_a = 4.2^{121}$) is also formed as a minor side product in low concentrations and can contribute to the low solution pH. However, the amount formed is negligible, and **3.24d** is the major contributor to low solution pH.



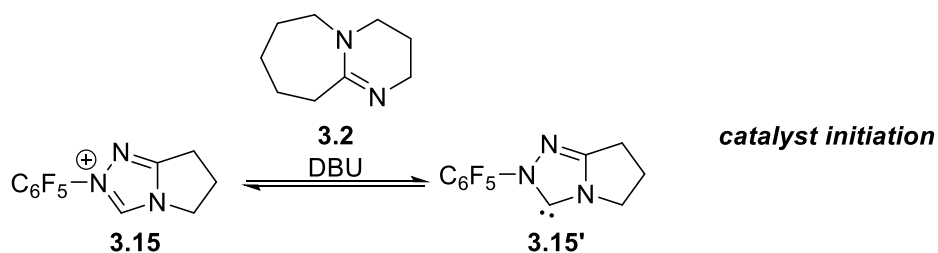
Scheme 3.14: Dominant acid/base equilibria present during a) Regime I and b) Regime II.

The reaction progress data can be analyzed within the context of the proposed catalytic mechanism (Scheme 3.15a).

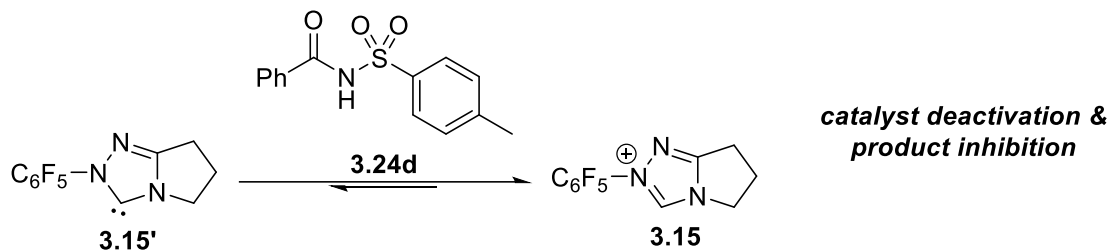
a)



b)



c)



Scheme 3.15: a) Proposed catalytic cycle; b) catalyst initiation pathway; c) catalyst deactivation pathway.

From the data, this reaction shows zero-order behavior in oxidant **3.7** and sulfonamide nucleophile **3.28**, and positive order behavior in benzaldehyde **3.27** and DBU. The reaction appears to be zero order in catalyst in the absence of DBU, but this observation is due to a solution equilibrium between **3.15** and **3.15'**, which was not affected by the small increases in concentration of **3.15** in our experiments. When DBU concentration is high (Regime I), i.e. more DBU is present in solution than *N*-acylsulfonamide product **3.24d**, DBU acts as a buffer to ensure that the equilibrium between **3.15** and **3.15'** is favored towards free carbene **3.15'**, allowing for rapid formation of **3.24d**. When the concentration of **3.24d** is greater than or equal to [DBU] (Regime II), the buffering ability of DBU diminishes, and the higher concentration of acidic **3.24d** lowers the solution pH, which in turn pushes the **3.15/3.15'** equilibrium towards **3.15**, deactivating the active catalyst (Scheme 3.15c). This creates a reversible off-cycle reservoir of catalyst species **3.15**, and the turnover-limiting step in this case is the formation of **3.15'**.

3.5 Catalyst deactivation pathways

NHC-catalyzed direct oxidative amidations of aldehydes with primary, electron-rich amines suffer from low yields,⁸² suggesting an unknown catalyst deactivation pathway is present. With a detailed understanding of the oxidative chemistry with electron-poor nucleophiles, we turned to studying electron-rich substrates in an effort to identify these unknown catalyst deactivation pathways.

In a first effort, the direct oxidative amidation of 4-chlorobenzaldehyde (**3.4**) with benzylamine (**3.33**) was monitored by ¹H NMR (Figure 3.18). Examination of the product formation curves reveals that amide formation is initially rapid, but then stops at the 5-minute

mark. It can also be seen that imine **3.35** is being formed competitively alongside the oxidation products of amide **3.34** and 4-chlorobenzoic acid **3.10**.

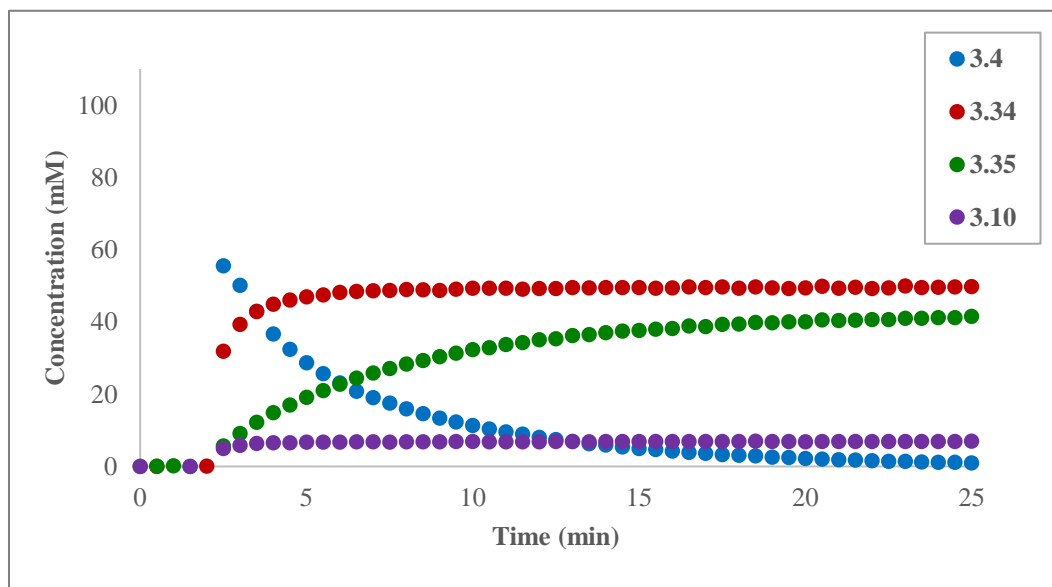
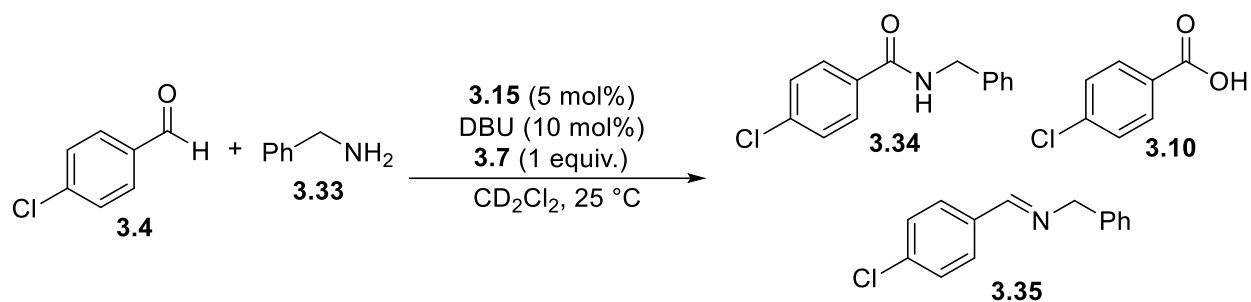
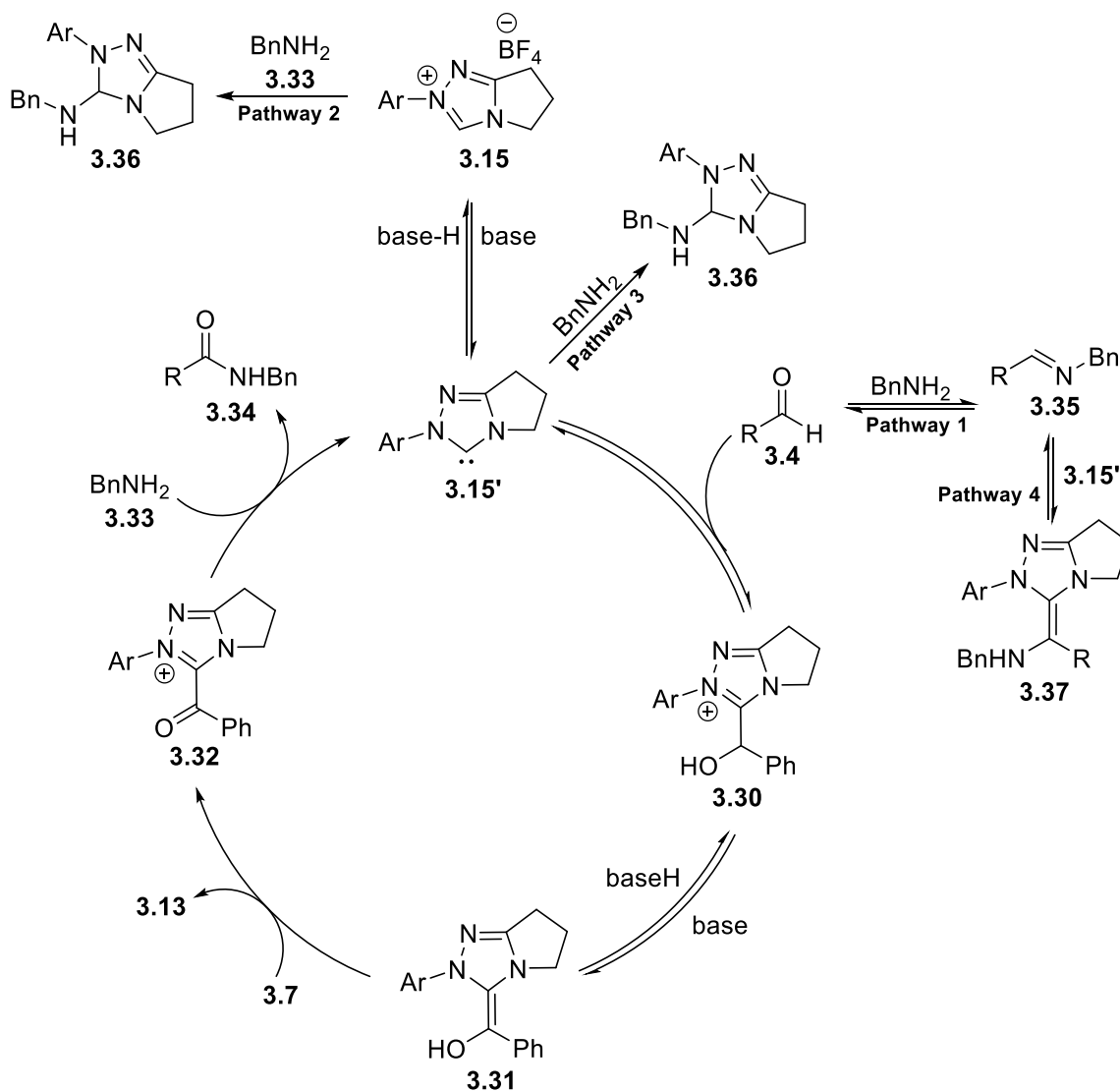


Figure 3.18: Reaction progress curves generated in the oxidative amidation of 4-chlorobenzaldehyde with benzylamine.

The observed rapid catalyst deactivation could occur through four possible pathways (Scheme 3.16).



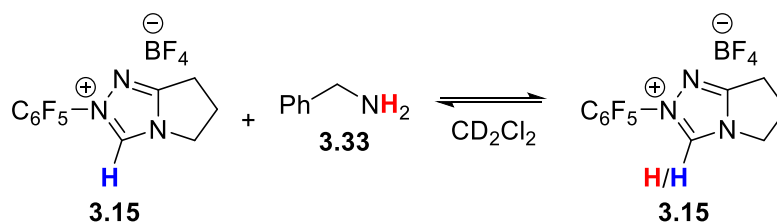
Scheme 3.16: Possible carbene deactivation pathways in the direct oxidative amidation of aldehydes with benzylamine.

Pathway 1 involves the side reaction of imine formation, by condensation of benzylamine with 4-chlorobenzaldehyde. This side reaction consumes both starting materials, and so less material is available for desired amide formation, slowing the reaction down. Pathway 2 involves nucleophilic attack of benzylamine onto the azolium precatalyst to form off-cycle species **3.36**, preventing formation of carbene **3.15'** and slowing the rate of product formation. Pathway 3 also involves formation of **3.36**, but via insertion of the carbene into the benzylamine N-H bond.

Pathway 4 involves nucleophilic attack of carbene onto the imine side product **3.35** formed via Pathway 1, forming off-cycle species **3.37**, which can be considered an aza-Breslow intermediate.⁵³ Pathway 1 can be ruled out because amide formation ceases before the majority of imine is formed. Because the imine concentration is low (~15 mM) at the time amidation stops (~50 mM at 5 minutes), imine formation does not sufficiently deplete the starting material to a point where it causes amide formation to cease. Pathway 4 can be ruled out because at imine concentrations equivalent to catalyst concentration (~5 mM), the rate of amide formation is still significant, suggesting that catalyst is not binding to imine in an irreversible manner. In addition, no carbene-imine adducts are observable by ¹H NMR.

3.5.1 *In situ* identification of a carbene-amine adduct

With pathways 1 and 4 ruled out, the possibilities of pathways 2 and 3 were probed using ¹H NMR and reaction progress monitoring. **3.15** and benzylamine in CD₂Cl₂ showed no evidence of nucleophilic attack of benzylamine at the C-5 position. However, upon addition of benzylamine, the azolium C-5 resonance disappears, while the ring CH₂ resonances remain the same. The disappearance of this signal suggests that the azolium was deprotonated by benzylamine to form the free carbene. However, this is unlikely, as the ring CH₂ resonances of the free carbene would have different chemical shifts, which was not observed. In addition, there is no resonance in the ¹³C spectrum that could be attributed to the carbenic carbon. Instead, it is likely that the azolium C-5 proton and benzylamine NH₂ protons exchange rapidly (Scheme 3.17). This exchange would happen faster than the NMR timescale, and so the signal would average out into the baseline of the spectrum.



Scheme 3.17: Observed proton exchange between 3.15 and benzylamine 3.33.

When DBU was added to this solution, new signals corresponding to the ring CH₂ protons appeared, with a high degree of J-coupling. This high order J-coupling suggested that these new CH₂ signals have a diastereotopic relationship with one another, implying that a new stereocenter like the one found in **3.36** was forming. However, the resonances attributed to DBU overlapped with the new peaks of interest. To resolve these signals, the solvent for this study was changed to CDCl₃, and DBU was replaced with TMG, simplifying the spectrum (Figure 3.19a). The resonances from 2.2-2.6 ppm and at 3.2 ppm (Figure 3.19a, highlighted boxes) have high-order J-coupling, suggesting that these signals arise from protons bearing a diastereotopic relationship to each other. When this reaction was monitored (Figure 3.19b), it could be seen that 6.04 ppm rapidly forms and then reaches an equilibrium concentration, and slowly decomposes. Similarly, the signals at 2.04 ppm, 4.64 ppm, and 7.82 ppm form at the same rate that 6.04 ppm is consumed, suggesting two things: 2.04, 4.64, and 7.82 ppm are resonances of the same compound, and 6.04 ppm decomposes to this compound. To identify these species, a full suite of 1D and 2D NMR techniques, including HSQC, HMBC, and selective 1D-TOCSY, were carried out on the mixture.

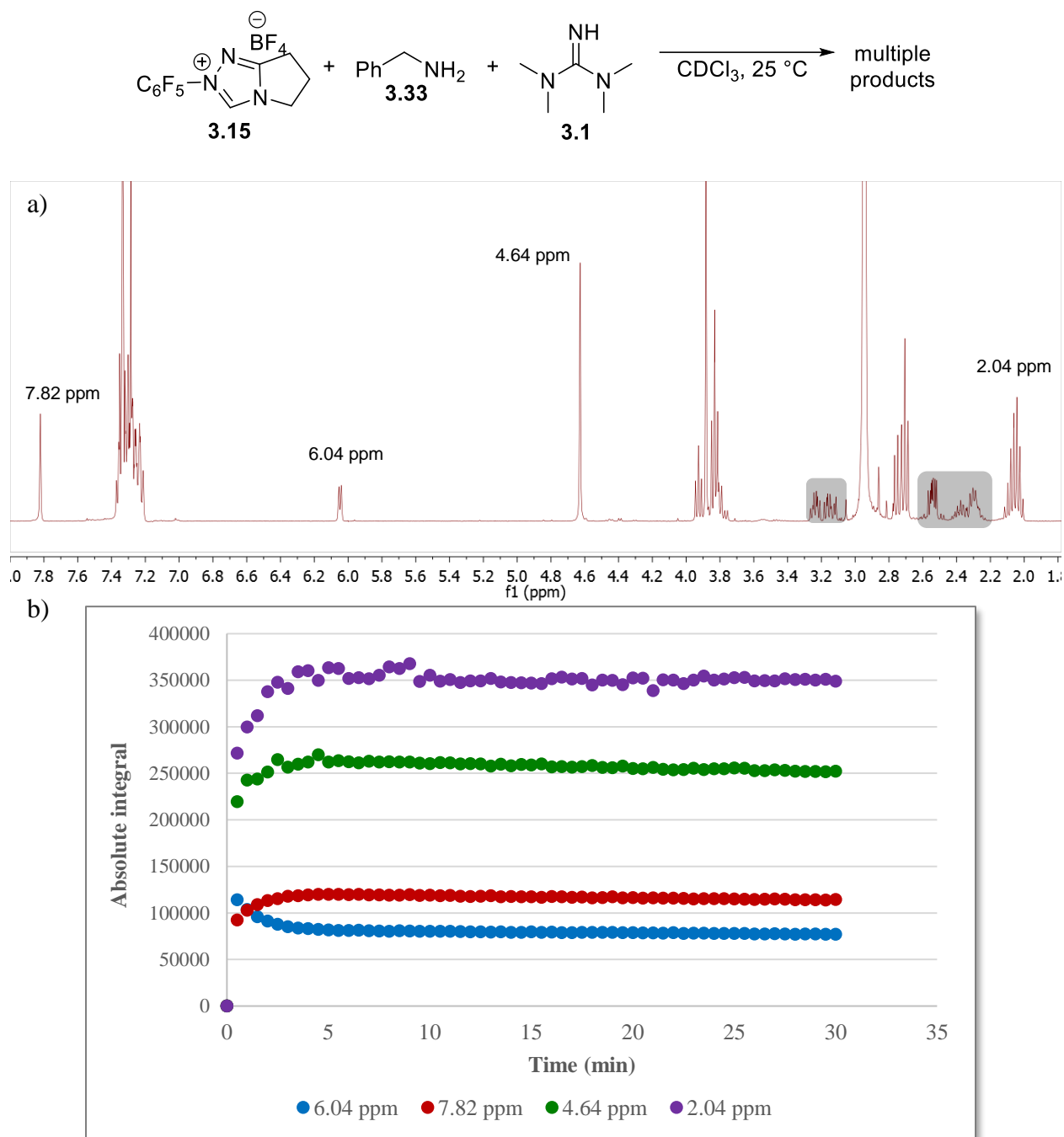


Figure 3.19: a) ^1H NMR spectra of reaction mixture after 30 minutes. b) Reaction progress curves of key ^1H NMR resonances.

Figure 3.20 shows the determined structures of **3.36** and **3.38**, as well as ^1H and ^{13}C NMR assignments determined from both HSQC (Figure 3.21) and HMBC (Figure 3.22). A detailed analysis of the evidence in support of these structures and assignments follows.

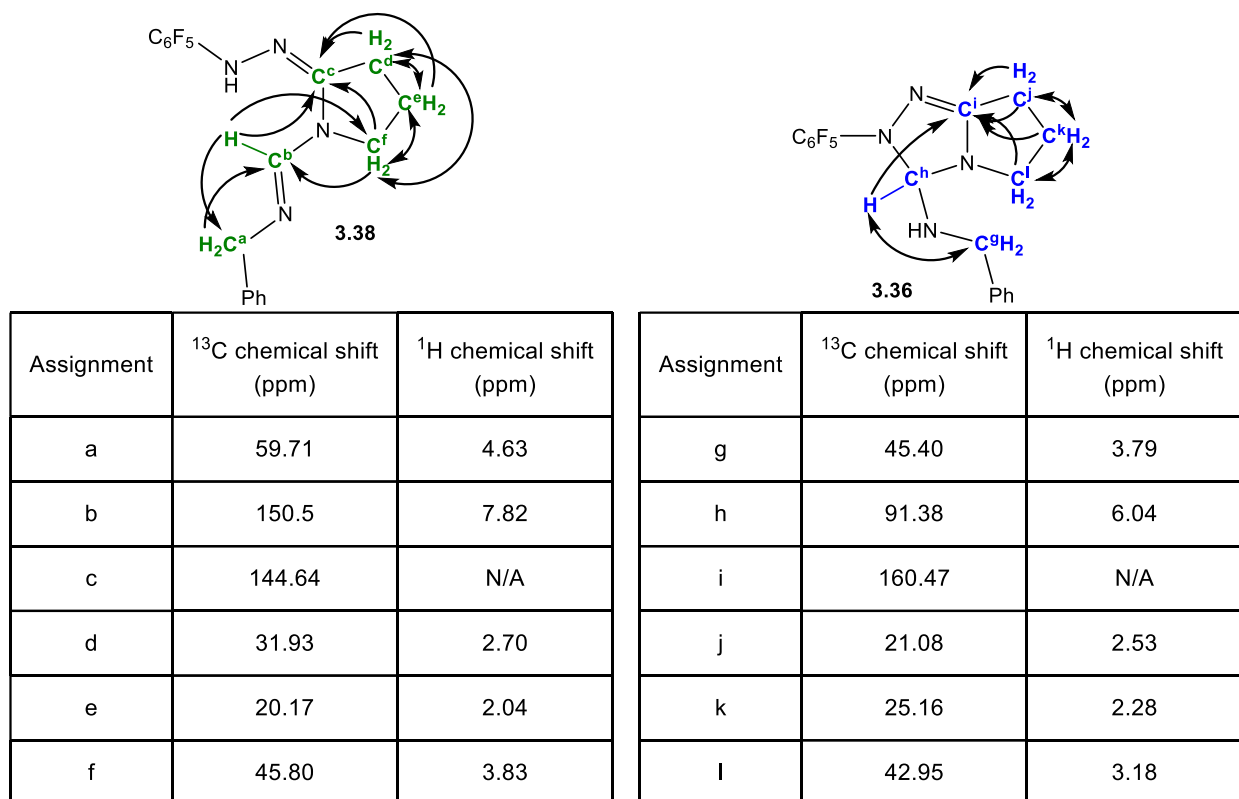


Figure 3.20: ^1H and ^{13}C NMR assignments for key resonances in **3.36** and **3.38**, obtained from HSQC (Figure 3.21) and HMBC (Figure 3.22). The black arrows show observed HMBC correlations.

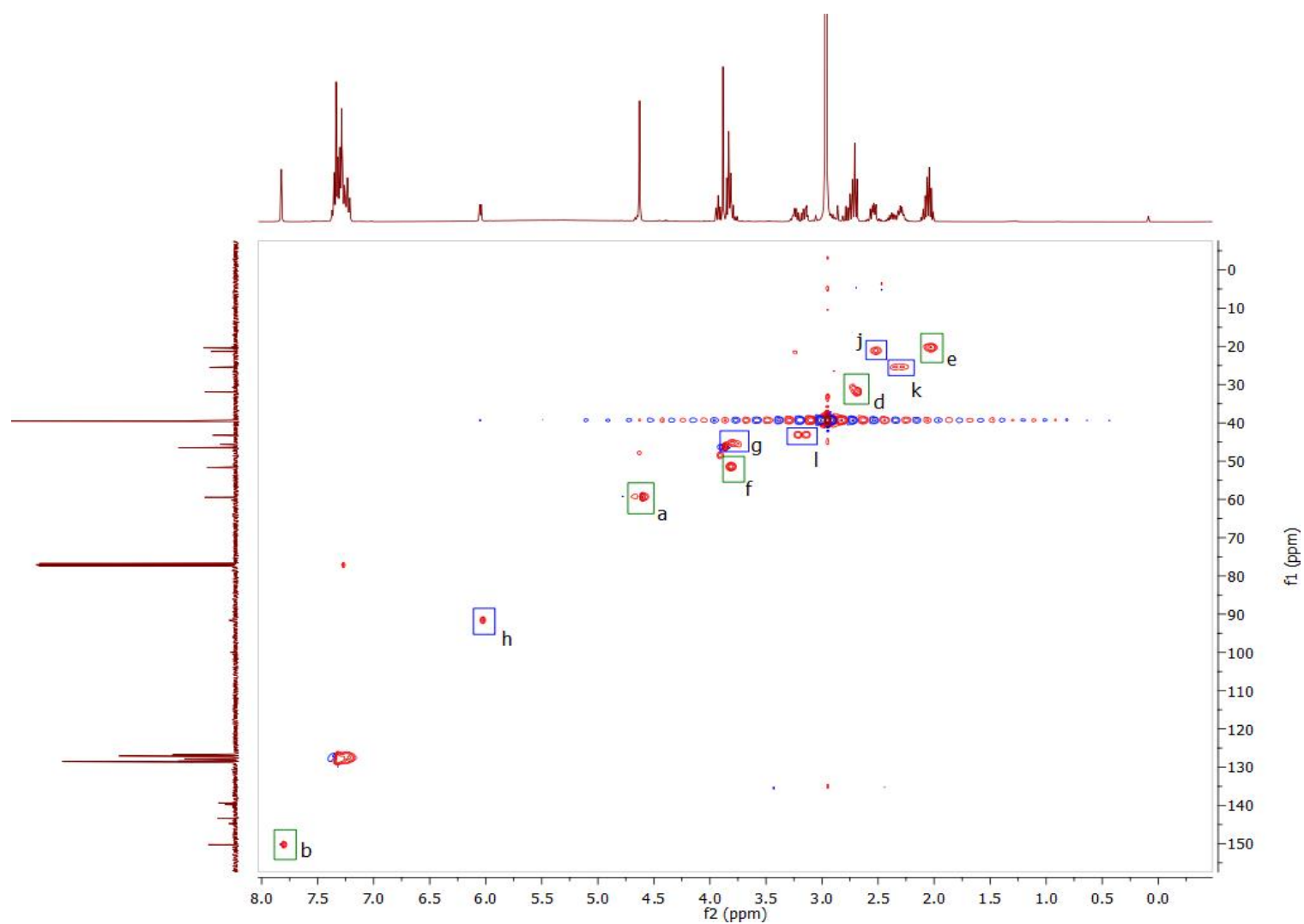


Figure 3.21: HSQC spectra of reaction mixture after 30 minutes containing 1 equiv each of 3.15, benzylamine, and TMG in CDCl_3 . Blue boxes show HSQC correlations for 3.36, green boxes show HSQC correlations for 3.38.

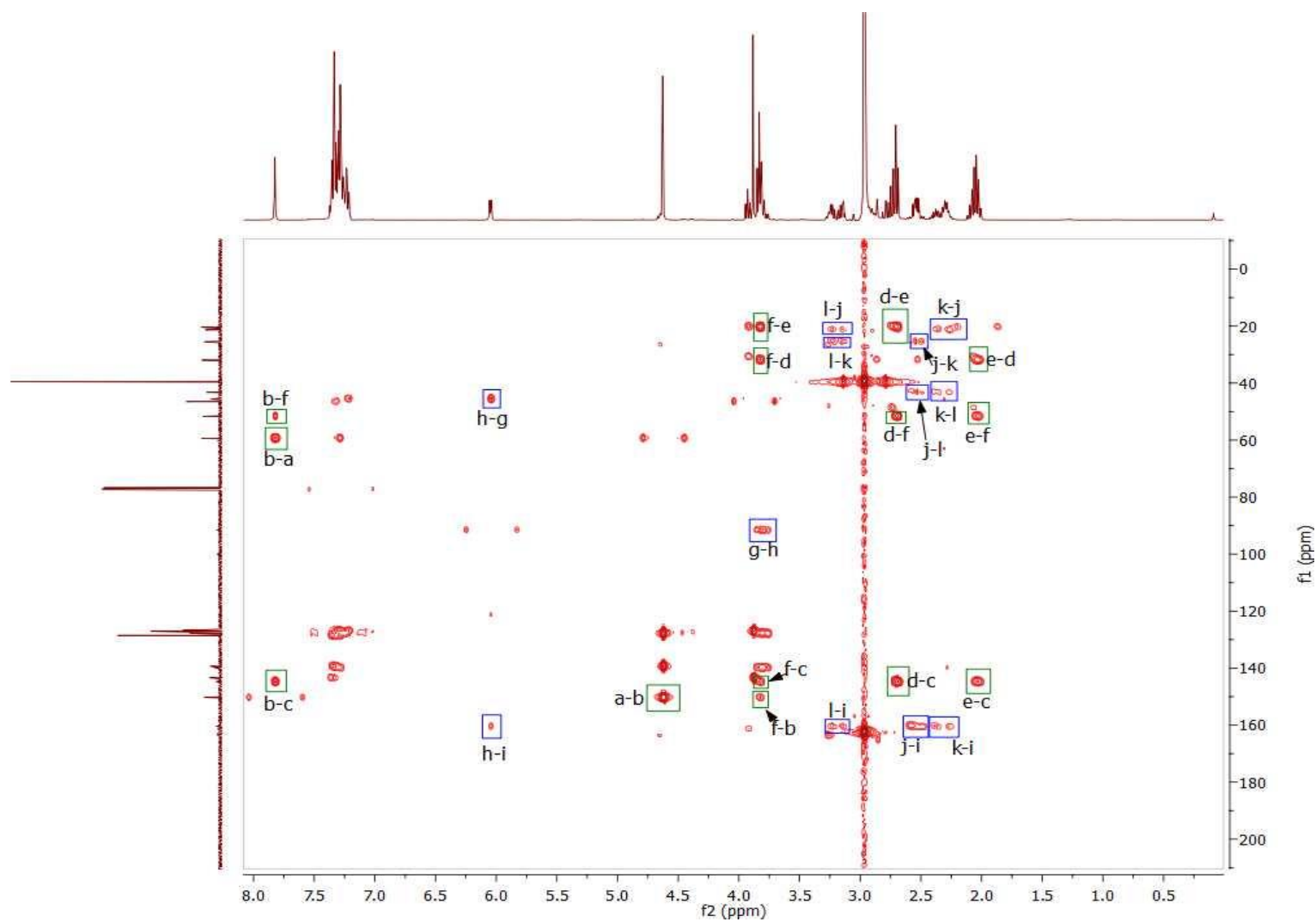


Figure 3.22: HMBC spectra of reaction mixture after 30 minutes containing 1 equiv each of 3.15, benzylamine, and TMG in CDCl_3 . Blue boxes show HMBC correlations for 3.36, green boxes show HMBC correlations for 3.38.

From Figure 3.22, the singlet at $\delta_{\text{1H}} = 7.82$ ppm shows an HSQC correlation at $\delta_{\text{13C}} = 150.5$ ppm, corresponding to the imine functionality in **3.38** (C^{b}). This same resonance shows HMBC correlations to C^{f} ($\delta_{\text{13C}} = 51.74$ ppm), C^{a} ($\delta_{\text{13C}} = 59.71$ ppm), and C^{c} ($\delta_{\text{13C}} = 144.64$ ppm). The singlet at $\delta_{\text{1H}} = 4.63$ ppm shows an HSQC correlation at $\delta_{\text{13C}} = 59.71$ ppm, corresponding to the benzylic CH_2 protons in **3.38** (C^{a}). C^{a} shows HMBC correlations to the aromatic carbons of the benzyl group ($\delta_{\text{13C}} = 127.71$ and 139.52 ppm), as well as C^{b} ($\delta_{\text{13C}} = 150.15$ ppm). The three methylene groups of the pyrrolidinimine ring in **3.38** (C^{d} , C^{e} , and C^{f}) have the following HSQC correlations: C^{d} ($\delta_{\text{1H}} = 2.70$ ppm, $\delta_{\text{13C}} = 31.93$ ppm); C^{e} ($\delta_{\text{1H}} = 2.04$ ppm, $\delta_{\text{13C}} = 20.17$ ppm); C^{f} ($\delta_{\text{1H}} = 3.83$ ppm, $\delta_{\text{13C}} = 51.74$ ppm). The resonance for C^{e} ($\delta_{\text{1H}} = 2.04$ ppm) is a pentet, while the resonances for C^{d} ($\delta_{\text{1H}} = 2.70$ ppm) and C^{f} ($\delta_{\text{1H}} = 3.83$ ppm) are triplets; this splitting pattern is consistent with the proposed structure of **3.38**. Finally, C^{d} , C^{e} , and C^{f} all show HMBC correlations to C^{b} ($\delta_{\text{13C}} = 144.64$ ppm). From this data, the structure of **3.38** can be assigned with confidence.

To help in identification of the structure of **3.36**, selective 1D-TOCSY (Figure 3.23) was used to identify the isolated spin systems in the reaction mixture. This experiment identified a total of three unique spin systems. The resonances in Figure 3.23d are attributed to the ring methylene protons in **3.38**, which were identified from the previous HSQC/HMBC analysis. Figure 3.23b shows the complex multiplet at ~ 3.2 ppm is coupled to two other high-order multiplets at 2.53 ppm and 2.35 ppm. Figure 3.23c shows the doublet at 6.04 ppm is coupled to a complex multiplet at 3.81 ppm, and what appears to be a quartet at 2.30 ppm. Our initial conclusion from this data is that it supports the structure of **3.36**. We assigned the doublet at 6.04

ppm to the methine C-H (C^h) and the higher-order multiplets in Figure 3.23b to the ring methylene protons (C^j , C^k , and C^l).

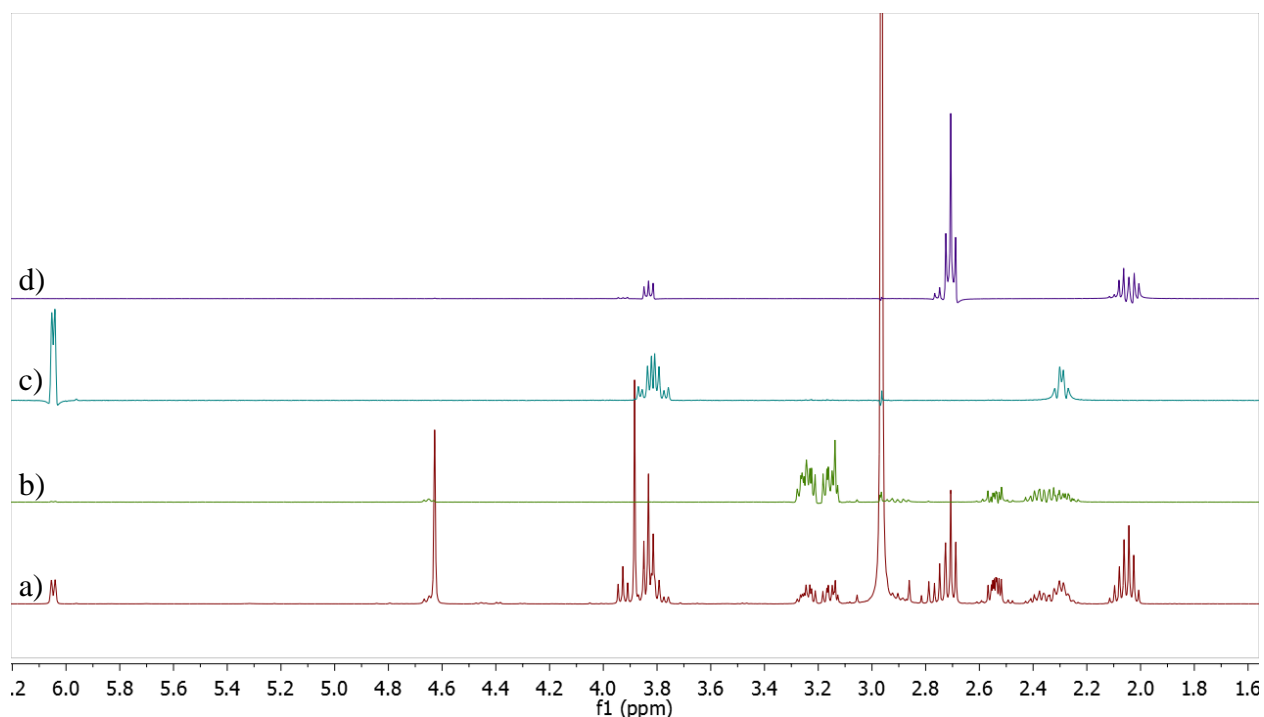


Figure 3.23: Selective 1D-TOCSY spectra showing three unique spin systems in the reaction mixture.

The HSQC and HMBC spectra support this as well, as the doublet at 6.04 ppm and the high-order multiplets in Figure 3.23b all show HMBC correlations with a carbon at 160.47 ppm (Figure 3.22, h-i, l-i, j-i, k-i), which is consistent with the sp^2 carbon in the 1,2,4-triazole ring. However, assignment of the benzylic methylene protons still presented a challenge. To aid in this assignment, selective 1D-TOCSY spectra of the doublet at 6.04 ppm were taken with different mixing times, and the integrals plotted as a function of mixing time (Figure 3.24). As mixing time increases, energy from the selective pulse at 6.04 ppm transfers out to the other protons in the spin system, and their respective resonances will have more signal and higher integrations. As it can be seen in Figure 3.24, the resonance at 2.30 ppm increases in signal faster with shorter mixing time than the resonance at 3.81 ppm, indicating that the proton corresponding to 2.30

ppm is physically closer to the protons corresponding to 6.04 ppm, while the protons corresponding to 3.81 ppm are more distant.

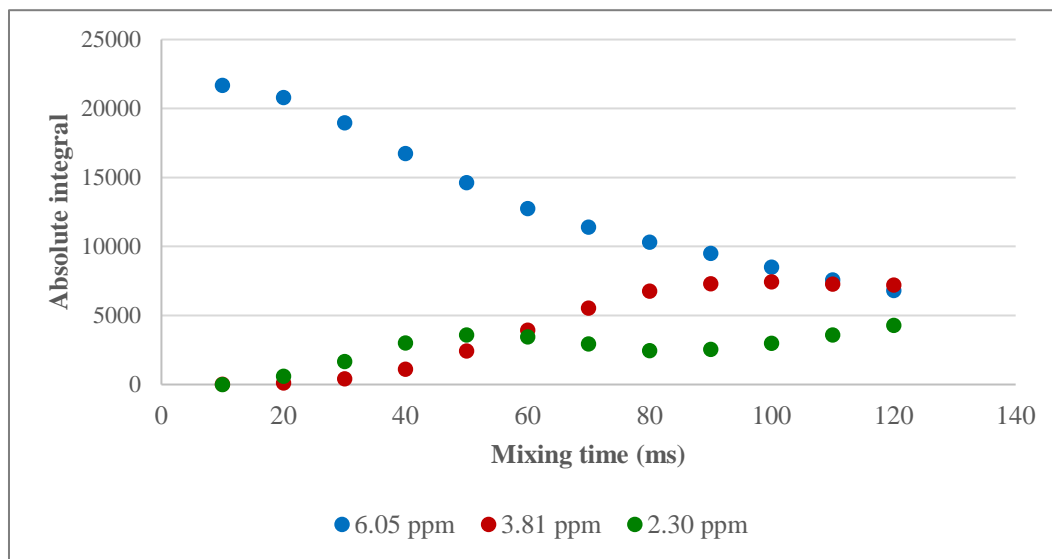


Figure 3.24: 1D-selective TOCSY spectra integrals as a function of time. The doublet at 6.05 ppm is selectively pulsed.

This data supports the assignment of the complex multiplet at 3.81 ppm to be the benzyl methylene protons in **3.36**, the quartet at 2.30 ppm to be the N-H proton, and the doublet at 6.04 ppm to be the methine proton in **3.36**. Figure 3.25 summarizes these assignments for both **3.36** and **3.38** in the ^1H NMR of the reaction mixture.

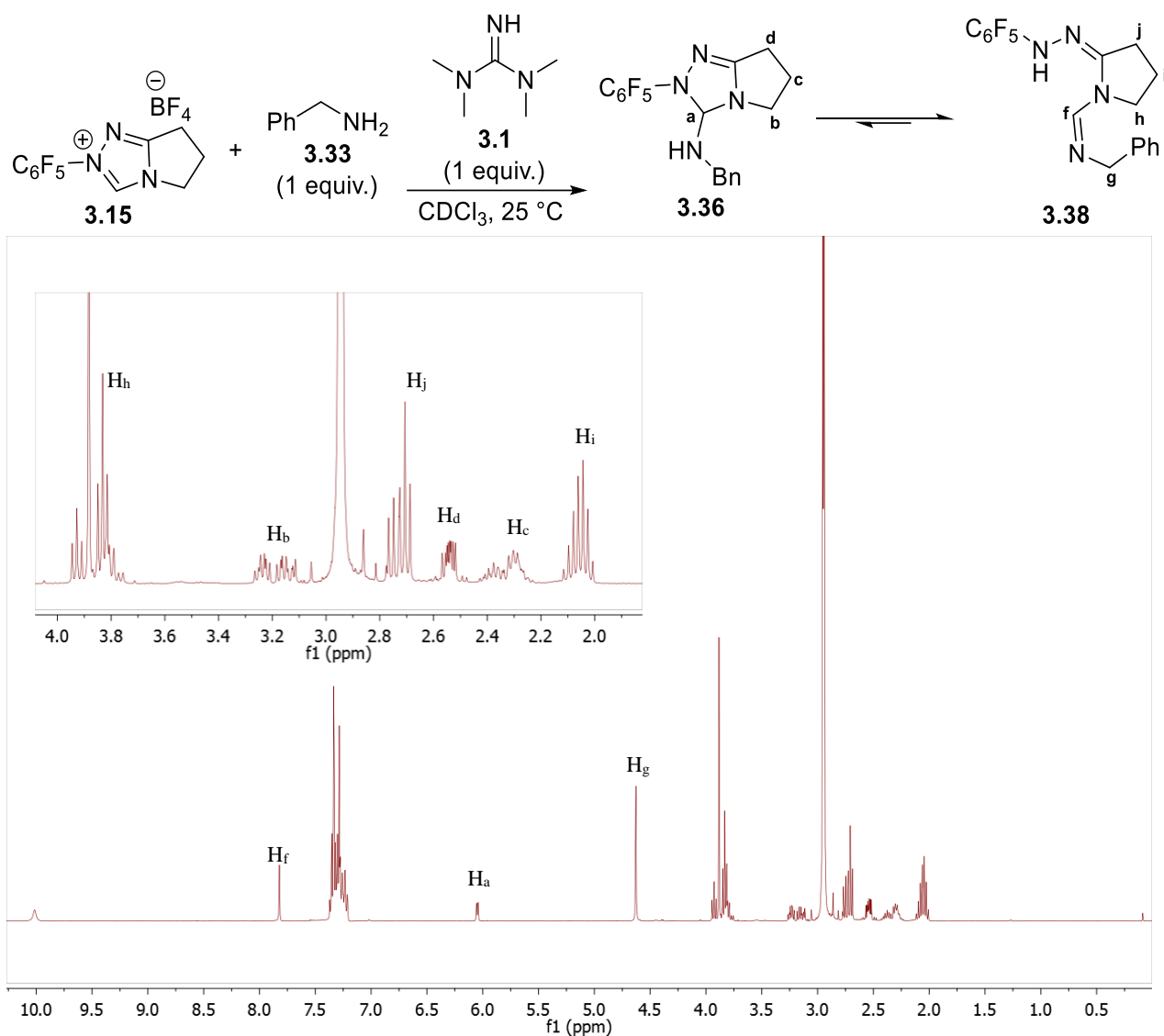
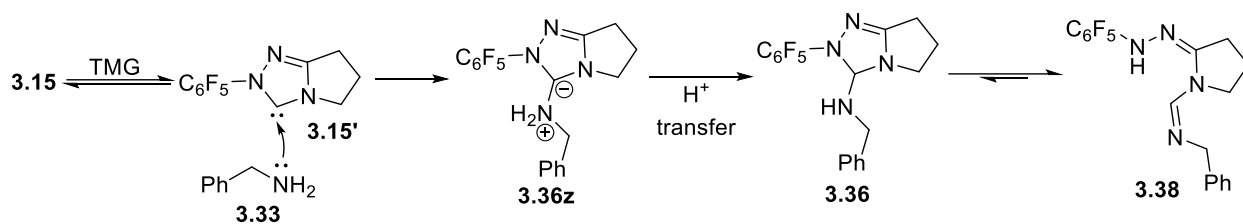


Figure 3.25: ^1H NMR spectrum of reaction mixture containing **3.29** and **3.30**. Key resonances are labeled.

With confirmed structures of **3.36** and **3.38**, a mechanism of formation can be proposed (Scheme 3.18). After deprotonation of triazolium salt **3.15** by TMG, a lone pair on benzylamine attacks the vacant p orbital of the carbene, forming zwitterionic species **3.36z**. The perfluorophenyl group, with its strong electron-withdrawing character, helps to stabilize the negative charge generated in intermediate **3.36z**. It also helps to increase the electrophilicity of

the carbene center for nucleophilic attack by benzylamine. Proton transfer of the zwitterionic intermediate leads to **3.36**, which ring-opens to give **3.38** in an equilibrium concentration.



Scheme 3.18: Proposed mechanism for the formation of **3.36** and **3.38**.

3.5.2 Isolation and characterization of a carbene-carbene adduct

During our attempts to identify the root cause of catalyst deactivation, a few attempts were made at isolating the carbene-benzylamine adduct before it was characterized *in situ*. While none of these attempts resulted in isolation of the carbene-benzylamine intermediate, a very unexpected carbene self-condensation product was isolated and characterized by X-ray crystallography (Figure 3.26). The most striking feature of this compound is the nitrile functionality, which requires the cleavage of a stable N-N bond.

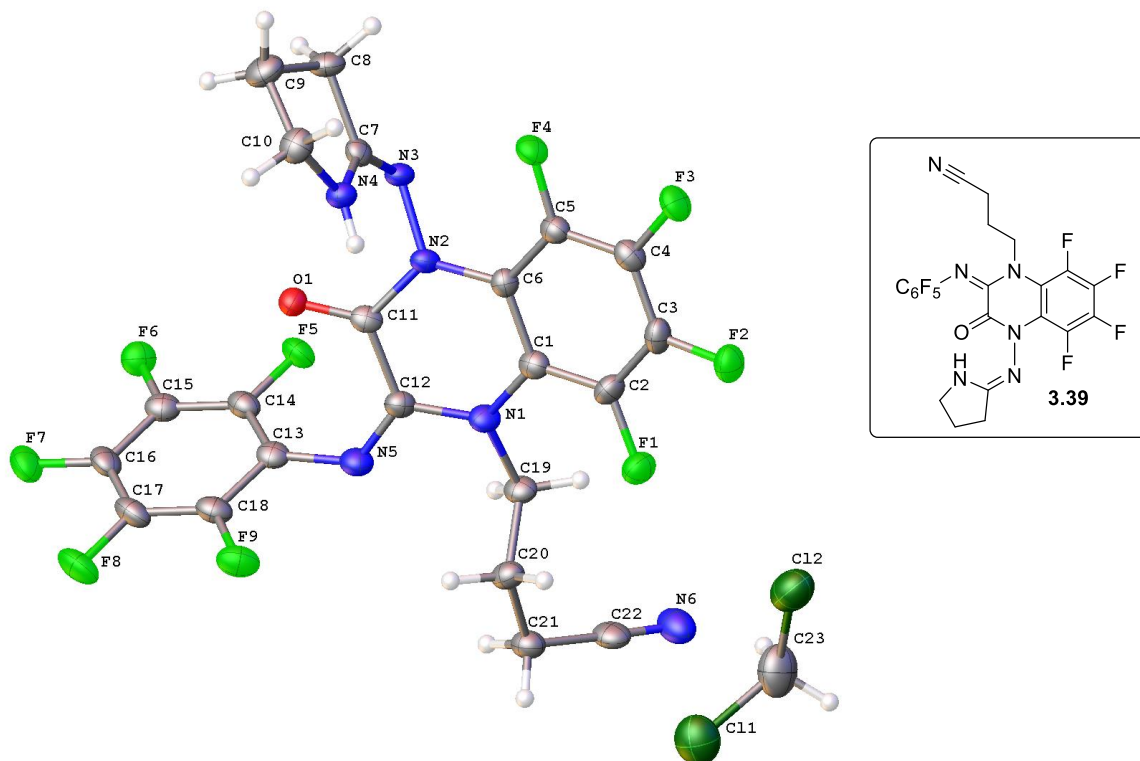
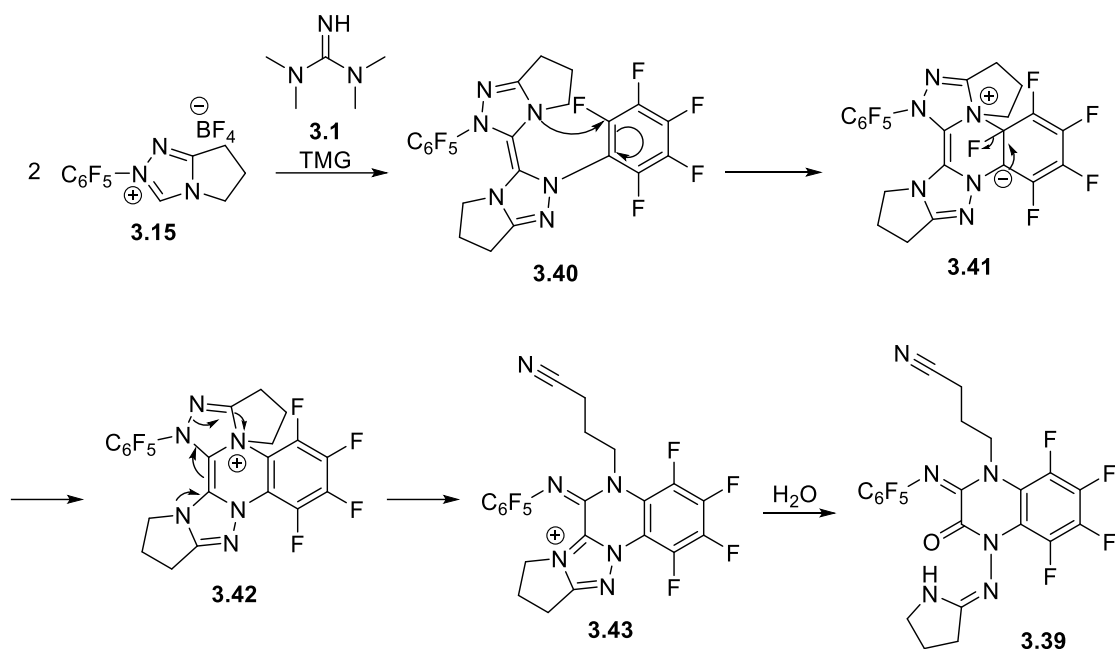


Figure 3.26: X-ray crystal structure of 3.39.

A plausible mechanism to form this catalyst byproduct is detailed in Scheme 3.19. Upon deprotonation of triazolium salt **3.15**, the carbene forms the Wanzlick dimer¹ **3.40**. The dimer then undergoes an intramolecular S_NAr reaction, followed by an unprecedented triazole ring-opening to produce nitrile **3.43**. The resulting 1,2,4-triazolium salt undergoes iminium hydrolysis to give **3.39**. While this transformation is quite interesting, the isolated yield of **3.39** was a meager 7%; the isolation of this catalytic byproduct represents a minor pathway of catalyst deactivation.



Scheme 3.19: Proposed mechanism for the formation of 3.39.

3.6 Conclusions

In this chapter, oxidative acylation of aldehydes with sulfonamides and electron-poor *N*-nucleophiles was demonstrated, and mechanistic studies were conducted using ¹H NMR reaction monitoring techniques. From these studies, oxidative acylation with sulfonamides and electron-poor *N*-nucleophiles is successful because the catalyst exists in a reservoir of reversible off-cycle species, and the nucleophiles used are not strong enough to attack the empty p-orbital of the free carbene. On the contrary, benzylamine has been shown to form 2 carbene-benzylamine adducts that exist in equilibrium. These adducts are formed by nucleophilic attack of benzylamine into the empty p-orbital of the free carbene, which is possible due to the electron-withdrawing pentafluorophenyl group, increasing the electrophilicity of the ambiphilic carbene. In addition, a carbene-carbene condensation byproduct was isolated, demonstrating a possible catalyst deactivation pathway that does not involve benzylamine.

3.7 Experimental

3.7.1 General considerations

All chemicals and solvents were purchased from Fisher, Acros, TCI America, Aldrich, and AK Scientific, and were used without further purification unless otherwise stated. Solvents were purified on an Innovative Technologies PS-Micro solvent system prior to use. Aldehydes were purified by redistillation or washing with aqueous saturated NaHCO₃ prior to use. ¹H (400 MHz) and ¹³C (100 MHz) NMR spectra were recorded on a Bruker AV400sp at 295 K.

Chemical shifts (δ) are reported in parts per million relative to residual solvent peaks as internal standards. Abbreviations are: s, singlet; d, doublet; t, triplet; q, quartet; p, pentet; m, multiplet.

HPLC was performed on an Agilent 1260 Infinity with an Agilent Eclipse XDB C18 (3.5 μm, 3.0 × 7.5 mm) column, eluting with a water/acetonitrile (0.05% TFA additive) gradient. HPLC samples were prepared by taking 10 μL aliquots of reaction mixtures and diluting with 1 mL methanol. Flash chromatography was performed using Sorbtech silica gel 60 Å (230 × 400 mesh), eluting with the indicated solvent mixtures. Thin layer chromatography (TLC) was performed on Sorbtech precoated silica gel plates (UV254) and was visualized by irradiation with UV light or staining with KMnO₄ solution.

3.7.2 Synthesis of *N*-(bis(dimethylamino)methylene)-4-chlorobenzamide (**3.9**)

4-chlorobenzaldehyde (0.070 g, 0.5 mmol), oxidant **3.7** (0.204 g, 0.5 mmol), and azolium precatalyst **3.15** (9 mg, 0.025 mmol) were dissolved in THF (5 mL) in a 20 mL scintillation vial, and heated to 40 °C. 1,1,3,3-tetramethylguanidine (69 μL, 0.55 mmol) was added via syringe, and the reaction stirred for 1h. Solvent was then removed under vacuum, and the crude mixture was purified by flash silica chromatography (1:1 DCM:acetone) to give **3.9** (0.118 g, 0.47 mmol,

93% yield) as a yellow oil. Analytical data for **3.7**: $^1\text{H NMR}$ (400 MHz, CDCl_3) δ 7.98 (d, J = 8.6 Hz, 2H), 7.19 (d, J = 8.6 Hz, 2H), 2.85 (s, 12H); $^{13}\text{C NMR}$ (100 MHz, CDCl_3) δ 170.4, 168.1, 136.7, 135.9, 130.5, 127.8, 40.1.

3.7.3 General procedure for oxidative *N*-acylation of sulfonamides

Aldehyde (1 equivalent), sulfonamide (1 equivalent), oxidant **3.7** (1 equivalent), and azolium precatalyst **3.15** (0.05 equivalents) were dissolved in dichloromethane (5 mL) in a 20 mL scintillation vial and heated to 40 °C. DBU (0.1 equivalents) was added via syringe, and the solution was stirred at 40 °C overnight. Upon reaction completion, solvent was removed under reduced pressure, and the crude mixture was purified by flash silica chromatography (EtOAc/hexanes or DCM/acetone).

***N*-(phenylsulfonyl)benzamide (3.24a)**: The title compound was prepared according to the general procedure from benzaldehyde (53 mg, 0.5 mmol) and benzenesulfonamide (79 mg, 0.5 mmol), and purified with 9:1 DCM:acetone to afford **3.24a** (125 mg, 0.48 mmol, 96% yield) as a white solid. Analytical data for **3.24a**: $^1\text{H NMR}$ (400 MHz, CDCl_3) δ 8.16 (d, J = 7.6 Hz, 2H), 8.16 (d, J = 7.6 Hz, 1H), 7.82 (d, J = 7.5 Hz, 2H), 7.82 (d, J = 7.5 Hz, 1H), 7.64 (t, J = 7.4 Hz, 1H), 7.64 (t, J = 7.4 Hz, 1H), 7.54 (t, J = 7.8 Hz, 3H), 7.54 (t, J = 7.8 Hz, 1H), 7.40 (t, J = 7.8 Hz, 2H), 7.40 (t, J = 7.8 Hz, 1H); $^{13}\text{C NMR}$ (100 MHz, CDCl_3) δ 164.6, 138.5, 134.0, 133.5, 131.1, 129.0, 128.9, 128.5, 127.9; **LRMS** (ESI): Calcd. for $\text{C}_{13}\text{H}_{10}\text{NO}_3\text{S}+\text{H}$: 262.1, found: 262.1.

4-chloro-*N*-(phenylsulfonyl)benzamide (3.24b): The title compound was prepared according to the general procedure from 4-chlorobenzaldehyde (70 mg, 0.5 mmol) and benzenesulfonamide (79 mg, 0.5 mmol), and purified with 9:1 DCM:acetone to afford **3.24b** (72 mg, 0.27 mmol, 54% yield) as a white solid. Analytical data for **3.24b**: $^1\text{H NMR}$ (300 MHz, Acetone- d_6) δ 8.28 – 8.05

(m, 2H), 8.04 – 7.89 (m, 2H), 7.84 – 7.34 (m, 5H); ^{13}C NMR (75 MHz, Acetone-*d*₆) δ 163.9, 139.7, 138.9, 133.7, 130.7, 130.0, 128.9, 128.8, 128.3; **LRMS** (ESI): Calcd. for $\text{C}_{13}\text{H}_{10}\text{ClNO}_3\text{S}+\text{H}$: 296.0, found: 296.0.

***N*-(phenylsulfonyl)cinnamamide (3.24c)**: The title compound was prepared according to the general procedure from cinnamaldehyde (63 μL , 0.5 mmol) and benzenesulfonamide (79 mg, 0.5 mmol), and purified with 4:1 hexanes:EtOAc to afford **3.24c** (134 mg, 0.47 mmol, 93% yield) as a white solid. Analytical data for **3.24c**: ^1H NMR (400 MHz, CDCl_3) δ 8.21 – 8.10 (m, 1H), 7.71 (d, *J* = 15.7 Hz, 1H), 7.66 – 7.58 (m, 1H), 7.56 – 7.49 (m, 1H), 7.46 (dd, *J* = 7.8, 1.5 Hz, 1H), 7.40 – 7.28 (m, 2H), 6.51 (d, *J* = 15.7 Hz, 1H); ^{13}C NMR (100 MHz, CDCl_3) δ 163.8, 146.1, 138.6, 134.0, 133.7, 130.9, 129.0, 128.9, 128.5, 128.3, 117.5; **LRMS** (ESI): Calcd. for $\text{C}_{15}\text{H}_{13}\text{NO}_3\text{S}+\text{H}$: 288.1, found: 288.1.

***N*-(phenylsulfonyl)picolinamide (3.24d)**: The title compound was prepared according to the general procedure from pyridine-2-carboxaldehyde (48 μL , 0.5 mmol) and benzenesulfonamide (79 mg, 0.5 mmol), and purified with 4:1 DCM:acetone to afford **3.24d** (114 mg, 0.44 mmol, 87% yield) as a yellow oil. Analytical data for **3.24d**: ^1H NMR (400 MHz, $\text{DMSO}-d_6$) δ 8.76 (s, 1H), 8.13 (d, *J* = 7.6 Hz, 1H), 7.94 (t, *J* = 7.4 Hz, 2H), 7.89 (d, *J* = 6.5 Hz, 2H), 7.54 (s, 1H), 7.44 (d, *J* = 7.1 Hz, 3H); ^{13}C NMR (100 MHz, $\text{DMSO}-d_6$) δ 169.2, 154.2, 149.8, 145.1, 138.7, 131.2, 128.7, 126.9, 126.4, 124.3; **LRMS** (ESI): Calcd. for $\text{C}_{12}\text{H}_{10}\text{N}_2\text{O}_3\text{S}+\text{H}$: 263.0, found: 263.1.

***N*-(phenylsulfonyl)furan-2-carboxamide (3.24e)**: The title compound was prepared according to the general procedure from furfural (41 μL , 0.5 mmol) and benzenesulfonamide (79 mg, 0.5 mmol). The crude mixture was purified using 4:1 hexanes:EtOAc to afford **3.24e** (57 mg, 0.23 mmol, 46% yield) as a yellow oil. Analytical data for **3.24e**: ^1H NMR (400 MHz, CDCl_3) δ 8.27 – 8.02 (m, 2H), 7.63 (t, *J* = 7.4 Hz, 1H), 7.53 (t, *J* = 7.7 Hz, 2H), 7.22 (d, *J* = 3.5 Hz, 1H), 6.50

(dd, $J = 3.6, 1.7$ Hz, 1H); ^{13}C NMR (100 MHz, CDCl_3) δ 154.6, 146.0, 145.1, 138.5, 134.0, 128.9, 128.4, 118.1, 112.9; LRMS (ESI): Calcd. for $\text{C}_{11}\text{H}_9\text{NO}_4\text{S}+\text{H}$: 252.0, found: 252.1.

4-methyl-*N*-(phenylsulfonyl)benzamide (3.24f): The title compound was prepared according to the general procedure from benzaldehyde (51 μL , 0.5 mmol) and *p*-toluenesulfonamide (86 mg, 0.5 mmol). The crude mixture was purified using 9:1 DCM:acetone to afford **3.24f** (107 mg, 0.39 mmol, 78% yield) as a white solid. Analytical data for **3.24f**: ^1H NMR (400 MHz, CDCl_3) δ 9.69 (s, 1H), 8.07 (d, $J = 8.3$ Hz, 2H), 7.86 (d, $J = 7.5$ Hz, 2H), 7.54 (t, $J = 7.4$ Hz, 1H), 7.41 (t, $J = 7.7$ Hz, 2H), 7.35 (d, $J = 8.1$ Hz, 2H), 2.44 (s, 3H); ^{13}C NMR (100 MHz, CDCl_3) δ 164.6, 145.2, 135.5, 133.4, 131.1, 129.6, 128.8, 128.6, 128.0, 21.7; LRMS (ESI): Calcd. for $\text{C}_{14}\text{H}_{13}\text{NO}_3\text{S}+\text{H}$: 276.1, found: 276.0.

3.7.4 General procedure for the oxidative coupling of aldehydes to electron-poor nucleophiles

Aldehyde (1 equivalent), *N*-nucleophile (1 equivalent), oxidant **3.7** (1 equivalent), and azolium precatalyst **3.15** (0.05 equivalents) were dissolved in DCM (5 mL) in a 20 mL scintillation vial and heated to 40 °C. DBU (0.1 equivalents) was added via syringe, and the solution was stirred at 40 °C overnight. Upon reaction completion, solvent was removed under reduced pressure, and the crude mixture was purified by flash silica chromatography (EtOAc/hexanes or DCM/acetone).

***N*-benzyl-*N*-(phenylsulfonyl)benzamide (3.26a):** The title compound was prepared according to the general procedure from benzaldehyde (51 μL , 0.5 mmol) and *N*-benzylbenzenesulfonamide (124 mg, 0.5 mmol), and purified using 10:1 hexanes:EtOAc to afford **3.26a** (127 mg, 0.37 mmol, 73% yield) as a white solid. Analytical data for **3.26a**: ^1H

NMR (400 MHz, CDCl₃) δ 7.75 – 7.66 (m, 2H), 7.56 – 7.48 (m, 1H), 7.46 – 7.34 (m, 5H), 7.34 – 7.25 (m, 2H), 7.25 – 7.13 (m, 5H), 5.00 (s, 2H); **¹³C NMR** (100 MHz, CDCl₃) δ 171.5, 138.9, 136.1, 134.8, 133.6, 131.7, 128.7, 128.6, 128.4, 128.21, 128.18, 127.9, 127.8, 51.3; **LRMS** (ESI): Calcd. for C₂₀H₁₇NO₃S+H: 352.1, found: 352.1.

***N*-benzyl-*N*-(benzyloxy)benzamide (3.26b):** The title compound was prepared according to the general procedure from benzaldehyde (51 μ L, 0.5 mmol) and *N*-benzyl-*O*-benzylhydroxylamine (107 mg, 0.5 mmol), and purified using 3:1 hexanes:EtOAc to afford **3.26b** (86 mg, 0.27 mmol, 54% yield) as a white solid. Analytical data for **3.26b**: **¹H NMR** (400 MHz, CDCl₃) δ 7.78 – 7.69 (m, 2H), 7.57 – 7.22 (m, 11H), 7.00 (d, *J* = 6.7 Hz, 2H), 4.98 (s, 2H), 4.59 (s, 2H); **¹³C NMR** (100 MHz, CDCl₃) δ 170.2, 136.4, 134.4, 134.1, 130.6, 129.5, 128.8, 128.7, 128.6, 128.45, 128.36, 128.0, 127.9, 77.1, 51.5; **LRMS** (ESI): Calcd. for C₂₁H₁₉NO₂+H: 318.1, found: 318.2.

2,5-dioxopyrrolidin-1-yl 4-chlorobenzoate (3.26c): The title compound was prepared according to the general procedure from 4-chlorobenzaldehyde (70 mg, 0.5 mmol) and *N*-hydroxysuccinimide (58 mg, 0.5 mmol), and purified using 4:1 hexanes:EtOAc to afford **3.26c** (55 mg, 0.23 mmol, 46% yield) as a white solid. Analytical data for **3.26c**: **¹H NMR** (400 MHz, CDCl₃) δ 8.07 (d, *J* = 8.8 Hz, 2H), 7.49 (d, *J* = 8.8 Hz, 2H), 2.91 (s, 4H); **¹³C NMR** (100 MHz, CDCl₃) δ 169.1, 161.1, 141.7, 131.9, 129.3, 123.5, 25.7; **LRMS** (ESI): Calcd. for C₁₁H₈ClNO₄+H: 254.0, found: 254.1.

1-(4-chlorobenzoyl)pyrrolidine-2,5-dione (3.26d): The title compound was prepared according to the general procedure from 4-chlorobenzaldehyde (70 mg, 0.5 mmol) and succinimide (50 mg, 0.5 mmol), and purified using 4:1 hexanes:EtOAc to afford **3.26d** (55 mg, 0.23 mmol, 46% yield) as a white solid. Analytical data for **3.26d**: **¹H NMR** (400 MHz, CD₂Cl₂) δ 7.86 – 7.72 (m, 2H), 7.57 – 7.44 (m, 2H), 2.92 (s, 4H); **¹³C NMR** (100 MHz, CD₂Cl₂) δ 174.5, 166.8, 141.5,

131.7, 130.1, 129.3, 29.1; **HRMS** (ESI): Calcd. for $C_{11}H_8ClNO_3+Na$: 260.0090, found: 260.0093.

(E)-4-chloro-N-(phenyl(phenylamino)methylene)benzamide (3.26e): The title compound was prepared according to the general procedure from 4-chlorobenzaldehyde (70 mg, 0.5 mmol) and *N*-phenylbenzimidamide (98 mg, 0.5 mmol), and purified using 4:1 hexanes:EtOAc to afford **3.26e** (108 mg, 0.33 mmol, 65% yield) as a white solid. Analytical data for **3.26e**: **1H NMR** (400 MHz, $CDCl_3$) δ 8.27 (d, J = 8.5 Hz, 2H), 7.79 – 6.77 (m, 12H); **^{13}C NMR** (100 MHz, $CDCl_3$) δ 178.3, 165.3, 138.45, 138.37, 135.6, 134.3, 131.2, 131.1, 129.5, 129.1, 128.41, 128.39, 125.8, 123.7; **LRMS** (ESI): Calcd. for $C_{20}H_{15}ClN_2O+H$: 335.1, found: 335.1.

N-(benzo[d]thiazol-2-yl)-4-chlorobenzamide (3.26f): The title compound was prepared according to the general procedure from 4-chlorobenzaldehyde (70 mg, 0.5 mmol) and 2-aminobenzothiazole (75 mg, 0.5 mmol). The product precipitated out of solution and **3.26f** (70 mg, 0.24 mmol, 48% yield) was collected as a white solid by vacuum filtration. No further purification was required. Analytical data for **3.26f**: **1H NMR** (400 MHz, $DMSO-d_6$) δ 12.97 (s, 1H), 8.13 (d, J = 8.6 Hz, 2H), 7.99 (d, J = 7.8 Hz, 1H), 7.76 (d, J = 8.0 Hz, 1H), 7.61 (d, J = 8.5 Hz, 2H), 7.53 – 7.39 (m, 1H), 7.38 – 7.24 (m, 1H); **^{13}C NMR** (100 MHz, $DMSO-d_6$) δ 165.6, 138.2, 130.7, 126.7, 148.7, 131.8, 124.2, 131.2, 129.2, 138.2, 122.2, 148.7, 120.7, 131.8, 122.2; **HRMS** (ESI): Calcd. for $C_{14}H_9ClN_2OS+H$: 289.0197, found: 289.0198.

Chapter 4: Development of a New Synthetic Method for Isothiourea

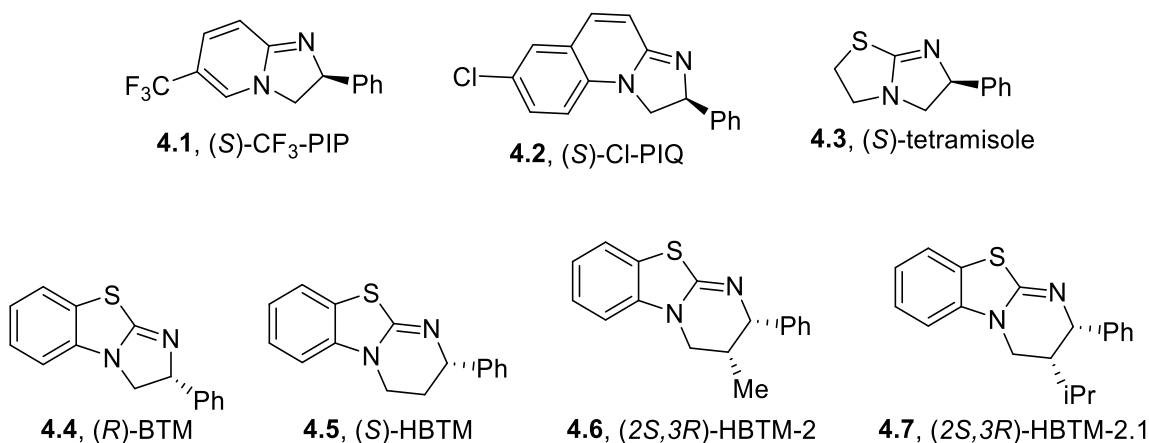
Organocatalyst Precursors

4.1 Introduction

4.1.1 Overview of isothiurea Lewis base catalysts

As early as 1901, pyridine has been used as a catalyst for the esterification of alcohols with anhydrides or acyl chlorides. In 1978, dimethylaminopyridine (DMAP) was developed as a more active pyridine catalyst, for alcohols that could not be esterified using the pyridine method.¹²² Chiral pyridine derivatives were developed in the late 1990s and early 2000s, however the enantioselectivities of these catalysts are moderate ($s < 50$).^{123,124} In 2004, Birman developed the first generation of chiral amidine organocatalysts CF₃-PIP (**4.1**), which performed the kinetic resolution of secondary aryl alcohols with enantioselectivities of up to 85%.¹²⁵ The following year, Birman developed the second generation of enantioselective amidine organocatalysts Cl-PIQ (**4.2**), which gave faster reaction rates and enantioselectivities ($s \leq 113$) than CF₃-PIP.¹²⁶ In 2006, Birman developed the third generation of enantioselective catalysts, namely the isothiurea (ITU) organocatalysts tetramisole (**4.3**) and benzotetramisole (BTM, **4.4**).¹²⁷ Tetramisole, a commercial compound, proved to be less active than the amidine organocatalysts, but demonstrated comparable enantioselectivities ($s \leq 31$). BTM, on the other hand, proved to be a remarkably better catalyst ($s \leq 355$). In 2008, Birman reported on the ring-expanded analogue of BTM, homobenzotetramisole (HBTM, **4.5**).¹²⁸ HBTM shows increased catalytic activity compared to BTM as well as a modified substrate selectivity profile, giving high levels of selectivity ($s \leq 107$) for aryl cyclohexanols. In 2009, Birman and Smith independently developed HBTM-2 (**4.6**) and HBTM-2.1 (**4.7**), respectively, improving catalyst

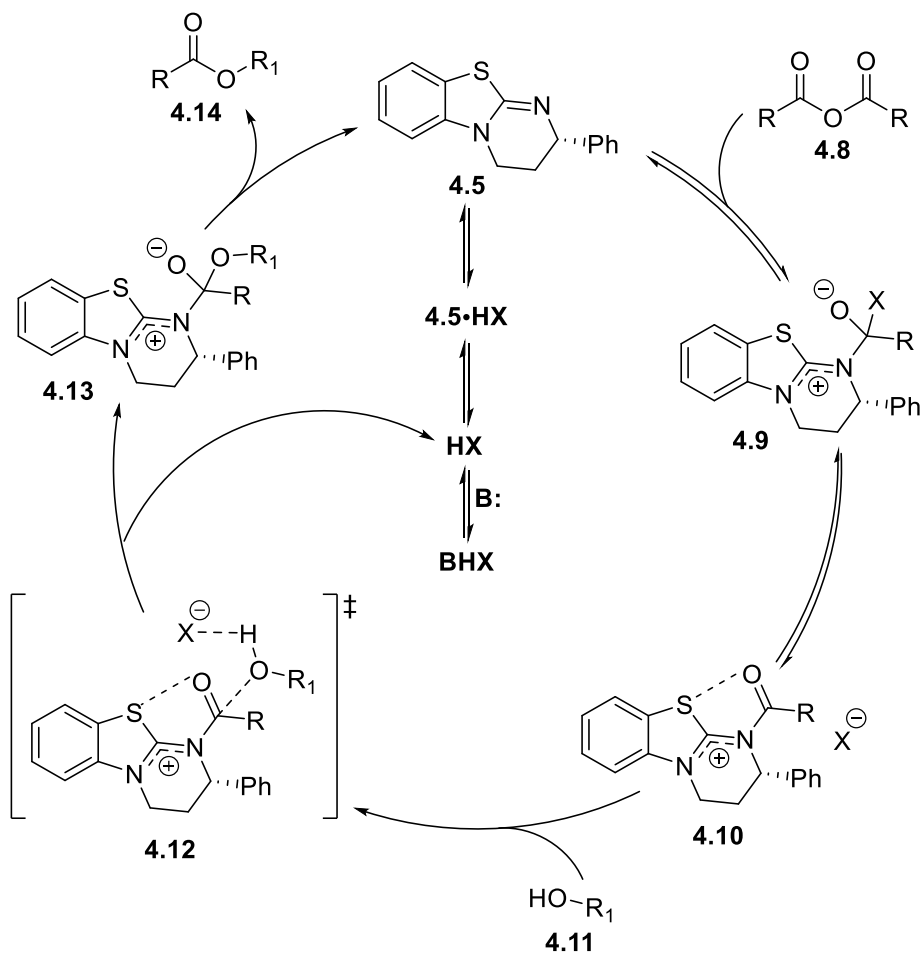
enantioselectivities further by adding more steric bulk adjacent to the nucleophilic sp^2 nitrogen.^{129,130}



Scheme 4.1: Amidine and isothioureia organocatalysts.

The feature common to these amidine and isothioureia catalysts is the presence of a stereocenter, adjacent to the sp^2 -hybridized nucleophilic nitrogen that is central to the catalytic activity. Scheme 4.2 shows a generalized mechanism for an ITU-catalyzed kinetic resolution of a chiral alcohol. The ITU catalyst attacks the acylating agent, usually an anhydride, forming tetrahedral intermediate **4.9** which collapses to form acylated catalyst **4.10**. This intermediate is then captured by the alcohol nucleophile via a transition state **4.12** to give tetrahedral intermediate **4.13**, which collapses to release product and catalyst. Mechanistic studies by Wagner et al.¹³¹ have shown that for HBTM, the kinetic resolution reaction is first order in catalyst, acylating agent, and alcohol, and the rate-limiting step is nucleophilic attack of alcohol to acylated catalyst **4.10**. They showed that a rapid pre-equilibrium exists between HBTM **4.5**, anhydride **4.8**, and acylated HBTM **4.10**, with a $K_{eq} < 1$. The reaction does not display a Michaelis-Menten relationship between HBTM **4.5** and anhydride **4.8**, where the dominant catalytic species in the reaction would be **4.10**. Instead, the catalyst is not saturated with

substrate, leading to a first-order dependence on anhydride **4.8**. This rapid pre-equilibrium explains why the reaction can exhibit first-order kinetics in HBTM **4.5**, anhydride **4.8**, and alcohol **4.11**.



Scheme 4.2: General mechanism for HBTM-catalyzed acyl transfer reactions.

A common motif among amidine and ITU-catalyzed enantioselective acylations is the selectivity of substrate. Among all three generations of catalysts that have been developed by Birman, secondary alcohols with aryl substituents adjacent to the chiral center give the highest selectivities. To explain these reactivity trends, transition states have been proposed where the π system of the benzylic alcohol stacks with the π system of the amidine/ITU catalyst, providing

stabilizing interactions (Figure 4.1). For catalysts with an annulated benzene ring, these interactions are further stabilized via π - π and cation- π interactions. The conformation of the *N*-acyl isothiuronium species **4.10** is also important in determining selectivity. Calculations have shown that there is a stabilizing interaction between the carbonyl oxygen lone pair and the $\sigma^*_{\text{S-C}}$ orbital.¹³² This stabilizing interaction places the carbonyl group in close proximity to the sulfur atom and helps to lock in the conformation of acyl isothiuronium species **4.10**, as well as helping to stabilize the formation of tetrahedral intermediate **4.13**. In addition, steric repulsion between the acyl group and the R group of the alcohol nucleophile contribute to the observed enantioselectivity, and the orientation of the phenyl group on the ring ensures that nucleophilic attack preferentially occurs from one side of the catalyst.

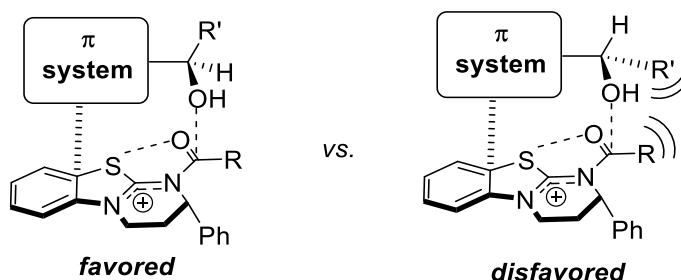
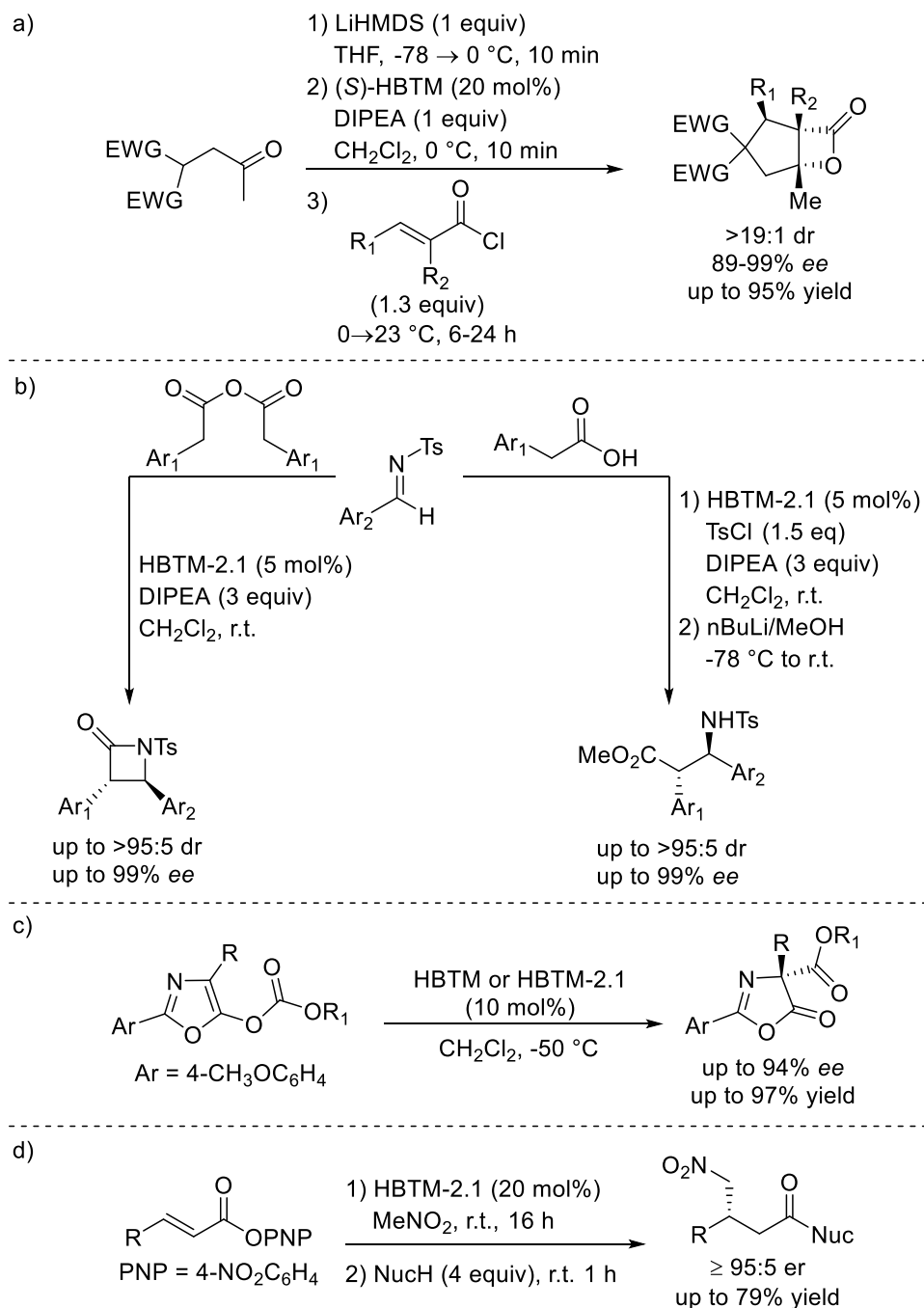


Figure 4.1: Proposed transition state and mode of chiral recognition for chiral ITU catalysts.

While the origins of ITU organocatalysis lie in enantioselective kinetic resolutions, they have proven to be versatile catalysts for enantioselective synthesis. The mode of activation remains the same – formation of a stabilized acyl isothiuronium intermediate via nucleophilic attack with an acylating agent – but the choice of nucleophile is different, allowing for diverse chemical scaffolds to be created. Romo's group described a Michael-aldol- β -lactonization organocascade process for the synthesis of highly functionalized cyclopentanes in excellent

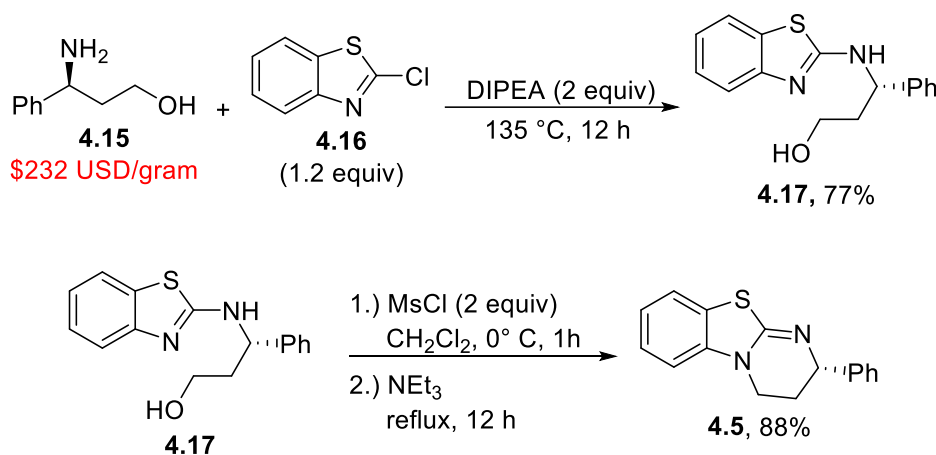
yields and enantioselectivities, using HBTM as a catalyst to form the required chiral α,β -unsaturated acyl isothiuronium intermediates for conjugate addition¹³³ (Scheme 4.3a). Smith's group described the enantioselective formal [2+2] cycloadditions between *N*-sulfonyl aldimines and aryl anhydrides or carboxylic acids, to give anti β -lactams or anti β -amino esters, respectively¹³⁴ (Scheme 4.3b). In some cases, the substrates themselves come as a packaged all-in-one nucleophile/acylating agent, allowing for enantioselective ITU-catalyzed rearrangements. Smith's group reported the HBTM- or HBTM-2.1-catalyzed enantioselective Steglich rearrangement of oxazolyl carbonates to give 4-carboxyazlactones¹³⁵ (Scheme 4.3c). In this reaction, the aryloxycarbonyl group is transferred to the ITU catalyst, generating an azlactone enolate which undergoes preferential C-carboxylation to give the product. Using a similar strategy, the Smith group reported the enantioselective Michael addition of nitroalkanes to α,β -unsaturated *p*-nitrophenyl esters¹³⁶ (Scheme 4.3d).



Scheme 4.3: Select examples of enantioselective isothiurea catalysis. a) HBTM-catalyzed synthesis of complex cyclopentanes.¹³³ b) HBTM-2.1-catalyzed synthesis of β -lactams or β -amino esters.¹³⁴ c) HBTM-2.1-catalyzed Steglich rearrangement.¹³⁵ d) HBTM-2.1-catalyzed Michael additions of nitroalkanes to α,β -unsaturated p-nitrophenyl esters.¹³⁶

4.1.2 Synthesis of HBTM

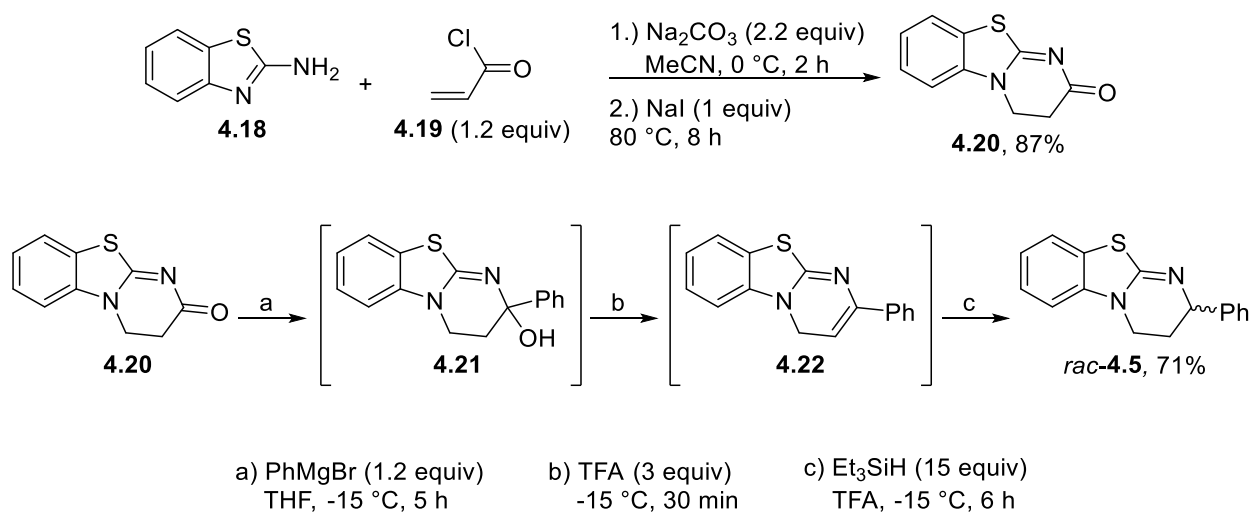
When Birman's group first reported their synthesis of HBTM and its utility as an acyl transfer catalyst, they utilized a S_NAr /cyclization strategy to synthesize the desired catalyst (Scheme 4.4).¹²⁸ While this strategy produced enantiopure HBTM in good yields, it suffers from some drawbacks. To obtain enantiopure HBTM, the synthesis must start with enantiopure amino alcohol **4.15**, which is commercially expensive, or prepared via a 5-step synthesis involving a resolution. In addition, the first step of the HBTM synthesis is performed neat at 135 °C in a pressure tube, which is not conducive for large-scale production.



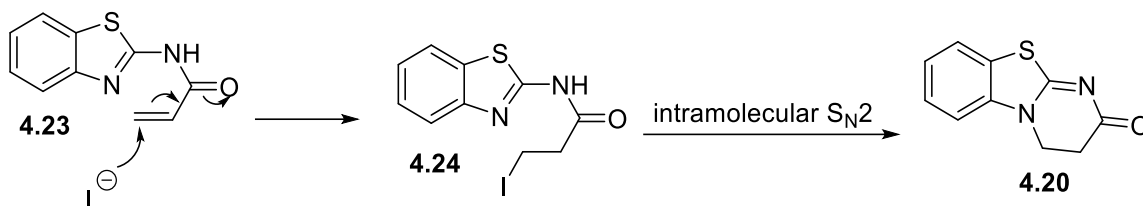
Scheme 4.4: Birman's synthesis of HBTM.

In 2013, Romo's group reported an alternate route towards HBTM (Scheme 4.5).¹³⁷ This method involved the one-pot acylation of 2-aminobenzothiazole **4.18** with acryloyl chloride **4.19** and subsequent NaI-promoted cyclization to key intermediate dihydropyrimidone (DHP) **4.20**. The proposed mechanism for the NaI-promoted cyclization involves conjugate addition of iodide ion to *in situ*-generated acrylamide **4.23**, followed by S_N2 cyclization to DHP **4.20** (Scheme 4.6). The DHP intermediate is then subjected to a one-pot Grignard addition/elimination/reduction sequence to yield racemic HBTM in good yields. This method is advantageous over Birman's for

two key reasons: substitution of the α,β -unsaturated acid chloride allows for greater structural diversity on the saturated ring, and the wide availability of Grignard reagents allows for greater structural diversity at the α -position to the nucleophilic nitrogen. However, this method also has its disadvantages. Since the synthesis is racemic, a resolution of the final product is required. Romo achieved this with high enantiopurity (>99% *ee*) by using preparative supercritical fluid chromatography (SFC), a method that is not commonly available to most chemists, and is limited by batch size (~5 g maximum). The synthesis of DHP **4.20** is also problematic, as it is an extremely polar compound and purification by column chromatography requires a 9:1 CH_2Cl_2 :acetone mixture mobile phase for a clean purification. Acryloyl chloride **4.19** can also pose a synthetic challenge, due to its susceptibility to hydrolysis, Michael addition, and polymerization.¹³⁸ Romo's initial attempts at substituting acryloyl chloride **4.19** with 3-chloropropionyl chloride resulted in poor yields of DHP **4.20**. In collaboration with the Romo lab, the work presented in this chapter was done in an effort to find a better, optimized route towards DHP **4.20**.



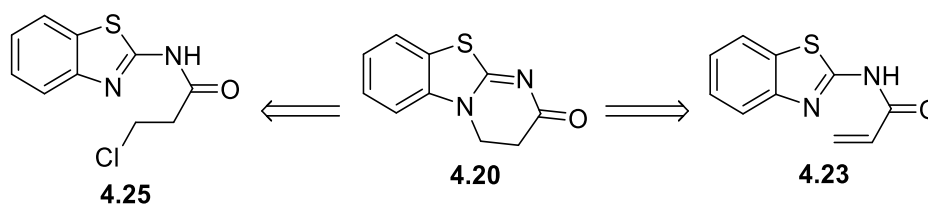
Scheme 4.5: Romo's synthesis of racemic HBTM.



Scheme 4.6: Proposed mechanism of NaI conjugate addition to form 4.20.

4.2 Initial synthetic attempts to access key dihydropyrimidinone intermediate

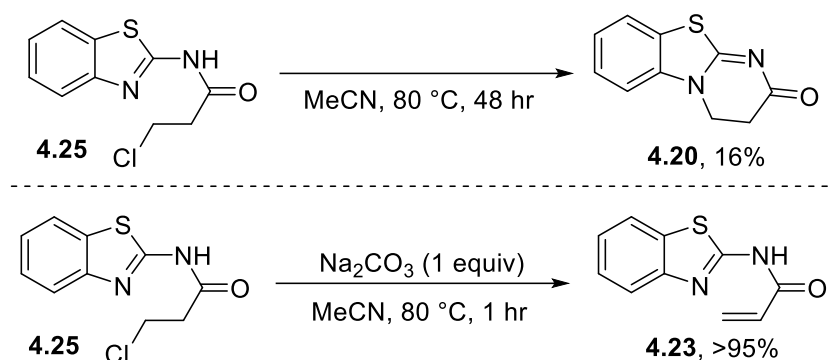
The strategy to access the key DHP intermediate **4.20** was a relatively simple one: **4.20** can be accessed via intramolecular S_N2 cyclization of chloroamide **4.25**, or via intramolecular conjugate addition to the double bond of acrylamide **4.23** (Scheme 4.7).



Scheme 4.7: Synthetic strategy towards DHP 4.20.

Chloroamide **4.25** was prepared by addition of 3-chloropropionyl chloride to a solution of 2-aminobenzothiazole and Na_2CO_3 at 0 °C. Taking pure chloroamide **4.25** and heating it in refluxing acetonitrile only produced the desired DHP product in 16% yield, even after a prolonged reaction time of 48 hours. It was hypothesized that HCl formed during the cyclization was protonating the thiazole functionality, rendering it non-nucleophilic. To remedy this, one equivalent of Na_2CO_3 was added to neutralize any possible HCl being formed. Notably, the chloroamide **4.25** selectively underwent elimination to give acrylamide **4.23** in quantitative

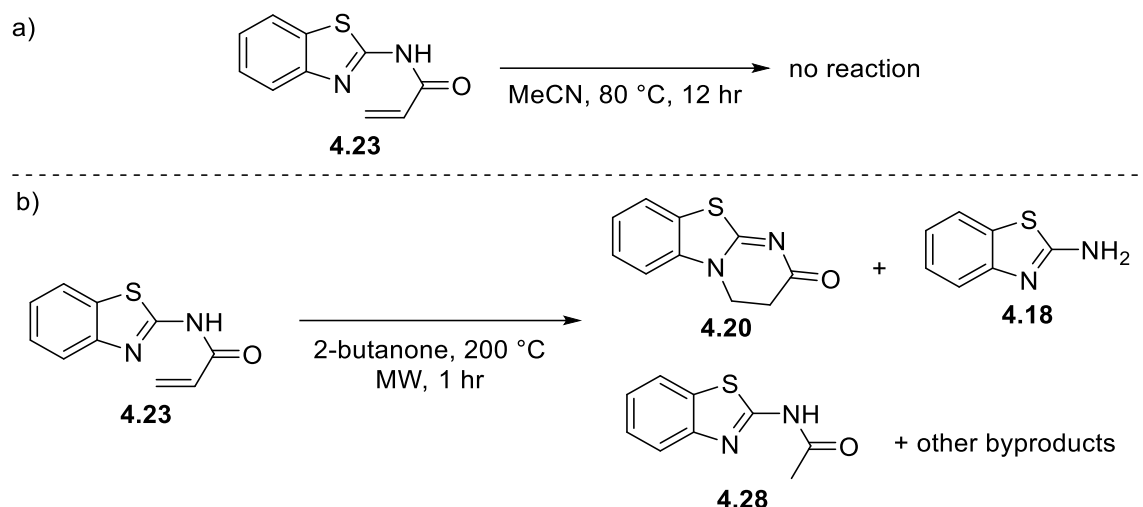
yields, instead of cyclization. Since acrylamide **4.23** was easily attainable this way, we then focused our efforts on methods to convert **4.23** to **4.20** via intramolecular conjugate addition.



Scheme 4.8: Synthetic attempts towards DHP **4.20** from chloroamide **4.25**.

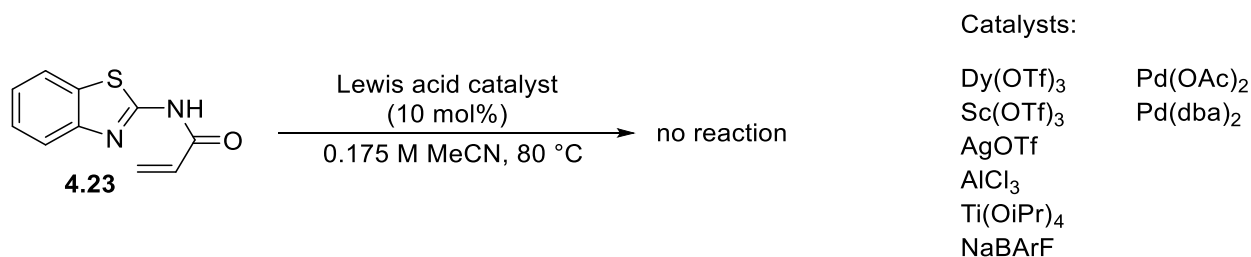
4.3 Lewis acid and NaI-catalyzed cyclization of acrylamide to DHP

In an initial experiment, acrylamide **4.23** was heated in refluxing acetonitrile overnight in an attempt to produce DHP **4.20** via simple thermal isomerization of **4.23** (Scheme 4.9a). Unfortunately, after twelve hours, no reaction was observed. Hypothesizing that a temperature of 80 °C provided insufficient energy to promote cyclization, acrylamide **4.23** was heated to 200 °C in a microwave reactor in an attempt to achieve the desired transformation (Scheme 4.9b). After one hour of microwave heating, LCMS analysis showed that the desired product **4.20** was formed, but many other byproducts were formed as well, including amine **4.18** and amide **4.28**. The presence of these products demonstrates the harshness of these conditions, as amine **4.18** is formed by thermal hydrolysis of the acrylamide, and **4.28** is most likely formed by a transamidation reaction with the solvent itself. In addition, at the end of this reaction, carbon black was detected at the bottom of the microwave tube. It may be possible that cyclization of **4.23** to **4.20** is achievable at temperatures between 80 and 200 °C, however no such attempt was made.



Scheme 4.9: Synthetic attempts towards DHP 4.20 from acrylamide 4.23. a) Attempt at thermal isomerization of acrylamide 4.23 in refluxing acetonitrile. b) Microwave heating of acrylamide 4.23.

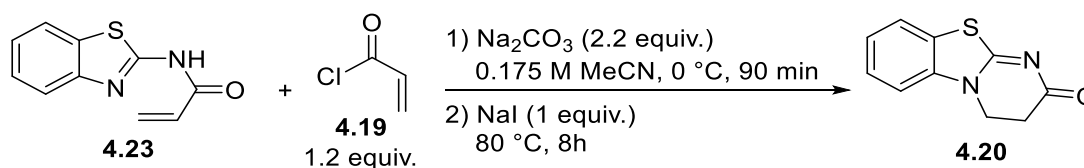
With thermal and microwave heating proving to be unsuccessful, it was hypothesized that a Lewis acid catalyst would help activate the acryloyl moiety of **4.23** for conjugate addition (Scheme 4.10). Initially, the Lewis acids Dy(OTf)₃, Sc(OTf)₃, and NaBARF₄ proved to be unsuccessful. Unfortunately, every Lewis acid tried, including AlCl₃, Ti(OiPr)₄, and Pd(OAc)₂, were unsuccessful in generating the desired DHP product. The organocatalysts DABCO and DMAP were also unsuccessful at catalyzing the transformation via conjugate addition to the double bond.



Scheme 4.10: Unsuccessful attempts at cyclization via Lewis acid activation.

In Romo's synthesis of DHP **4.20**, NaI is used as an additive, presumably by conjugate addition of iodide to *in situ*-generated **4.23** followed by cyclization (Scheme 4.6). With multiple failures at cyclization through Lewis acid catalysis, the role of NaI in the cyclization was investigated. Surprisingly, heating acrylamide **4.23** with one equivalent of NaI in acetonitrile overnight resulted in no product formation. From this experiment, it was clear that the presence of acryloyl chloride **4.19** was critical in the formation of **4.20**, beyond just the acylation of aminobenzothiazole **4.18**.

To probe the exact role of acryloyl chloride in the reaction, a series of experiments were performed. First, an experiment replicating Romo's conditions using acrylamide **4.23** in place of aminobenzothiazole **4.18** showed high conversion to DHP **4.20** by LCMS. While this experiment confirmed the critical role of acryloyl chloride in producing DHP **4.20**, it was unclear exactly what that role was.



Scheme 4.11: Experiment to probe the role of acryloyl chloride.

Next, a crossover experiment was performed using Romo's conditions (Figure 4.2), starting from methyl-substituted 2-aminobenzothiazole **4.26**, and dosing acrylamide **4.23** in after 90 minutes at 0 °C, after acylation of **4.26** was presumably complete. The use of methyl-tagged aminobenzothiazole **4.26** as starting material allowed for the easy separation and identification (by MS) of critical species present in the reaction. We hypothesized that after dosing the reaction with **4.23** and NaI, we would observe the formation of both **4.20** and methyl-labeled DHP **4.33a** after overnight reflux.

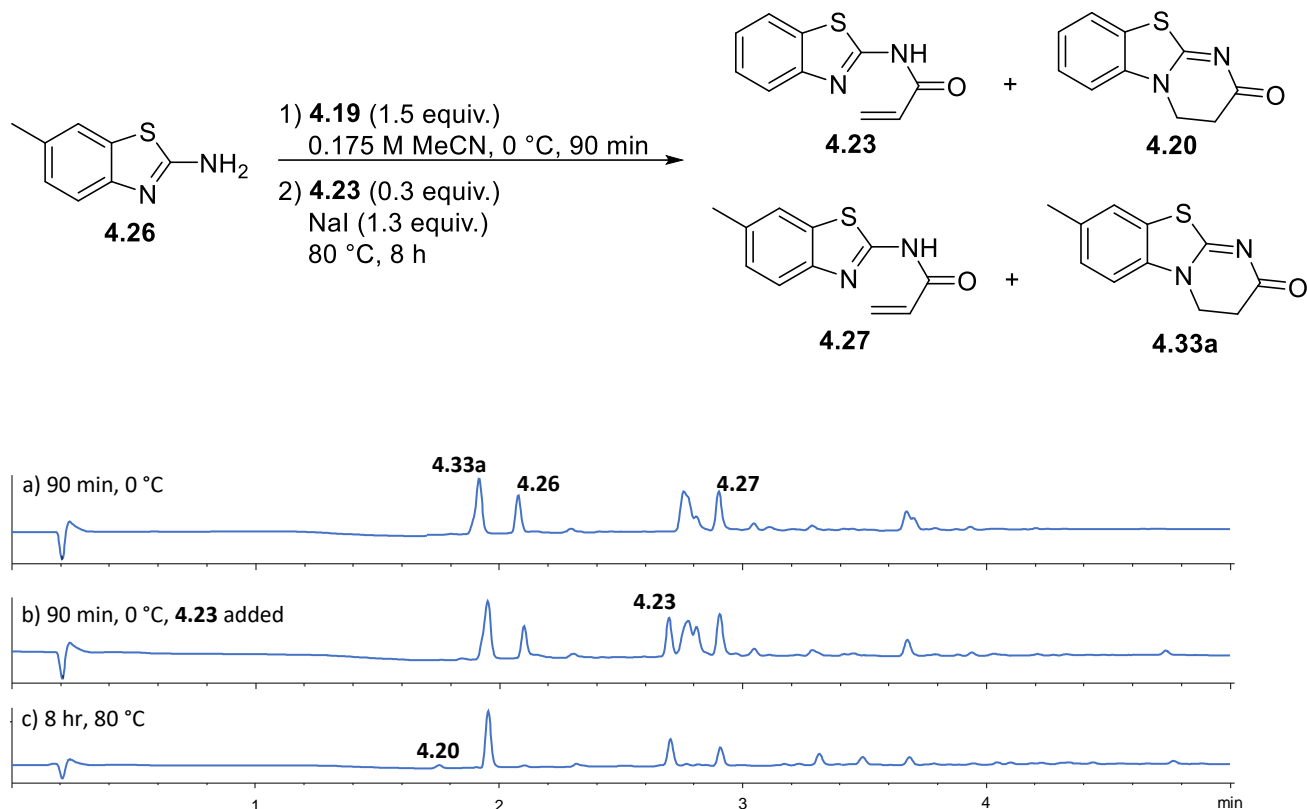


Figure 4.2: HPLC traces of the crossover experiment taken at different intervals.

As Figure 4.2a shows, a large amount of methyl-labeled DHP **4.33a** is formed within the first 90 minutes reaction at 0 °C, along with methyl-labeled acrylamide **4.27**. After dosing the reaction with acrylamide **4.23** and overnight reflux, a very small amount of **4.20** was formed from **4.23**, but the vast majority of **4.23** remained unreacted. From this series of experiments, a number of conclusions can be made. First, it is clear that higher temperatures are not important in this reaction, as the majority of DHP **4.20** or **4.33a** is formed during the first 90 minutes at 0 °C (Figure 4.2a). Secondly, an *in situ*-generated catalyst does not facilitate the cyclization of acrylamides **4.23** or **4.27** to **4.20** or **4.33a**. In the crossover experiment (Figure 4.2), the conversion of **4.23** to **4.20** is very low; if a catalyst was generated *in situ*, we would expect this conversion to be much higher. Finally, acryloyl chloride **4.19** appears to be crucial in the

cyclization from **4.23** to **4.20**. DHP **4.20** is *only* formed when acryloyl chloride **4.19** is added to starting material, whether it be acrylamide **4.23** or aminobenzothiazole **4.18**. Attempts at cyclization of **4.23** via thermal and microwave heating, as well as Lewis acid catalysis, also support the notion that acryloyl chloride **4.19** is crucial.

The observation that the majority of methyl-labeled DHP **4.33a** is formed during the initial acryloyl chloride addition at 0 °C was grounds for further investigation with a faster rate of sampling. However, due to the heterogeneous nature of the reaction, our lab's previously developed method for automated solution sampling¹³⁹ was unable to be implemented. Instead, a Mettler-Toledo EasySampler system coupled to a Gilson 215 liquid handler was used to monitor the reaction by preparing HPLC samples for offline analysis at ten minute intervals (Figure 4.3).

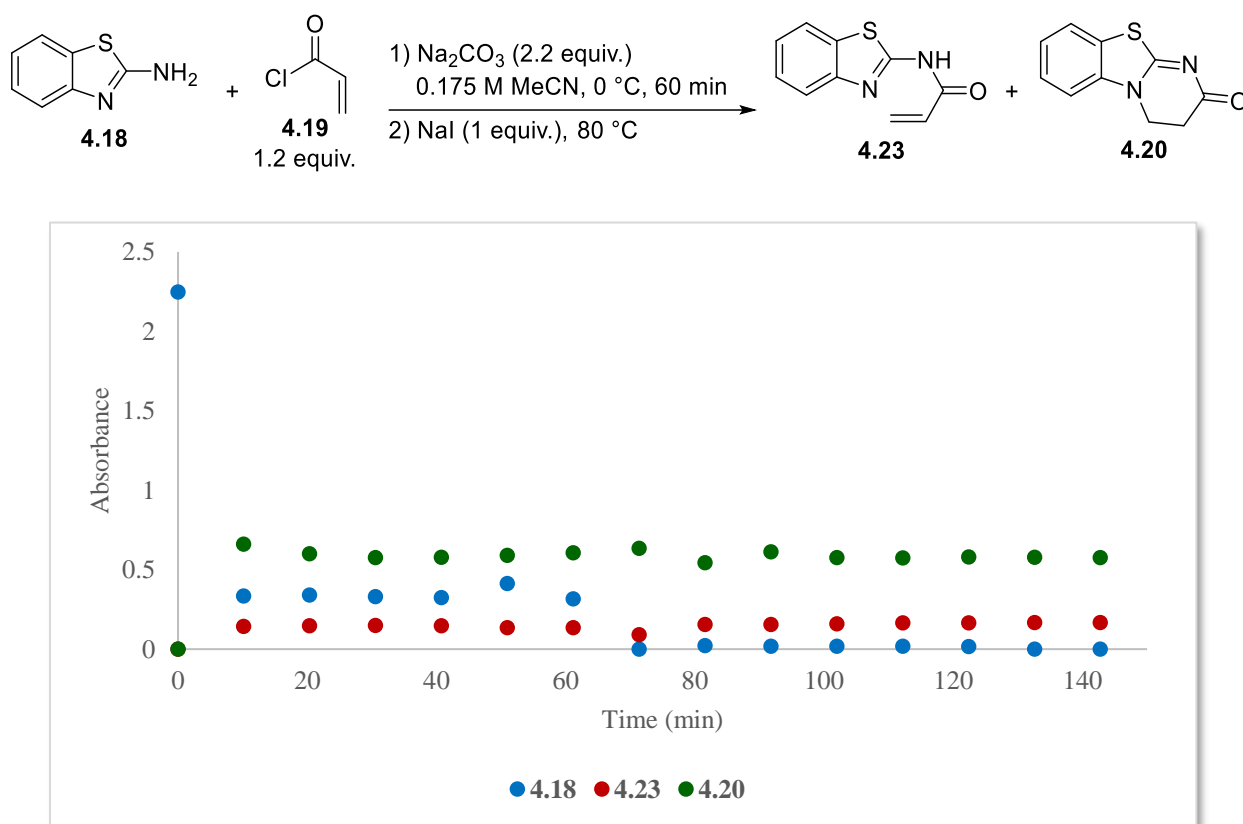
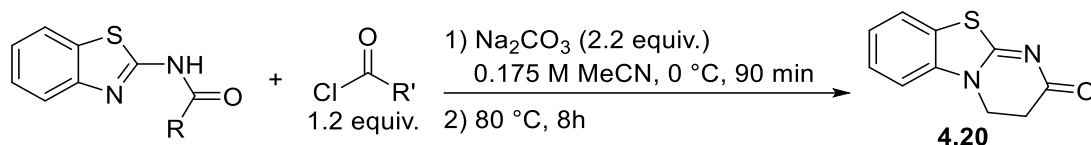


Figure 4.3: Reaction progress profiles of **4.18**, **4.23**, and **4.20** in a reaction using Romo's conditions.

From Figure 4.3, it can be seen that all product formation occurs within the first 10 minutes of reaction time, during and immediately after the dropwise addition of acryloyl chloride. In addition, all acrylamide **4.23** that is formed during the reaction forms during this 10 minute window as well. Aminobenzothiazole **4.18** is fully consumed after NaI addition and within the first ten minutes of heating to 80 °C, however the exact byproducts that are formed are unknown. As expected, the presence of NaI did not affect the conversion of **4.23** to **4.20**, leading to the conclusion that NaI is unnecessary in this chemical transformation, and that acryloyl chloride is the only component necessary to convert both aminobenzothiazole **4.18** and acrylamide **4.23** into DHP **4.20**.

These developments led to questions about acid chloride selectivity: can cyclization of acrylamide **4.23** be achieved when a different acid chloride is employed? Can a different amide be used while using acryloyl chloride? To answer these questions, a series of experiments was performed, systematically varying the amide substituent and acid chloride used. Experiments were also performed with and without the addition of NaI, to understand how it affected the reaction, if at all (Table 4.1).



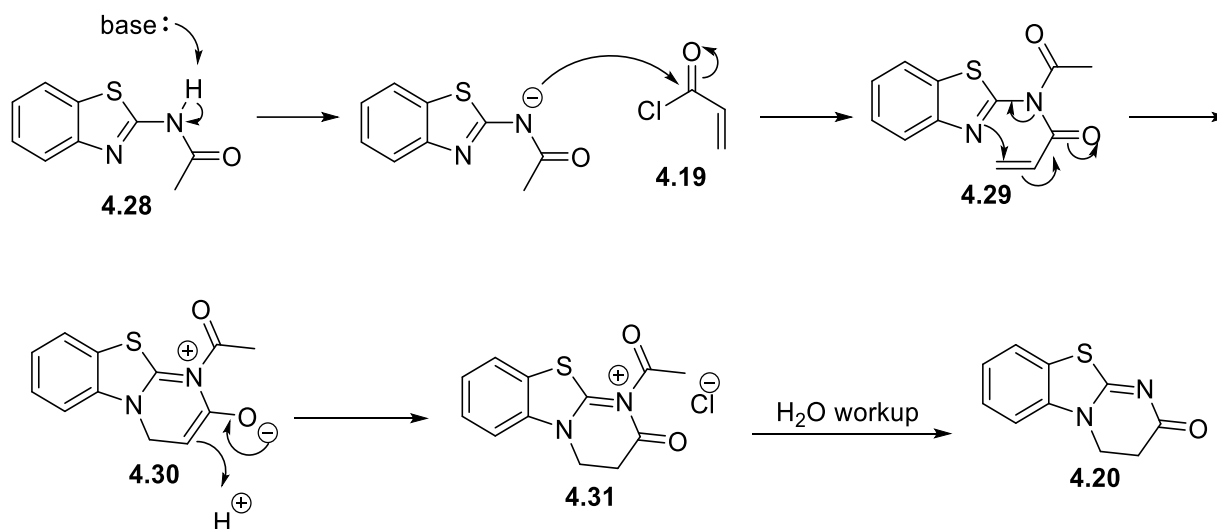
Entry	R	R'	NaI added (Y/N)	Conversion ^a
1	CH ₂ =CH ₂	CH ₂ =CH ₂	Y	>75%
2	CH ₂ =CH ₂	CH ₃	Y	0%
3	CH ₃	CH ₂ =CH ₂	Y	>75%
4	CH ₂ =CH ₂	CH ₂ =CH ₂	N	98%
5	CH ₂ =CH ₂	CH ₃	N	95%
6	CH ₃	CH ₂ =CH ₂	N	100% (87% isolated yield)

Table 4.1: Systematic variation of amide, acid chloride, and NaI addition. ^a Conversion determined by HPLC.

When acryloyl chloride is used, regardless of if NaI is used or not, cyclization is achieved (Table 4.1, entries 1,3,4,6). When both acetyl chloride and NaI are used, no cyclization occurs (Table 4.1, entry 2). However, when NaI is omitted from this reaction, the reaction proceeds efficiently and **4.20** can be isolated in 87% yield (Table 4.1 entry 6). NaI appears to decompose acetyl chloride *in situ*, however the exact mechanism of decomposition is unknown. This result is not duplicated when using acryloyl chloride. From these experiments, the best conditions were determined to be those from entry 6, starting from the acetamide and using acryloyl chloride as acylating agent.

From these results, a mechanistic proposal can be put forth (Scheme 4.12). In the presence of base, amide **4.28** is deprotonated and undergoes nucleophilic acyl substitution with acryloyl chloride to form imide intermediate **4.29**. The presence of the acetyl group activates the

acryloyl moiety for conjugate addition, and allows for cyclization to enolate **4.30**, which gets protonated to form acetylated DHP **4.31**. Upon aqueous workup, the acetyl group is hydrolyzed to give free DHP **4.20**.



Scheme 4.12: Proposed mechanism for the formation of DHP **4.20 from amide **4.28**.**

Up to this point, imide intermediate **4.29** had not been detected by HPLC/MS. However, during a reaction monitoring experiment where triethylamine was used in place of Na_2CO_3 as base, a transient intermediate was detected (Figure 4.4, green curve). This intermediate had an ionized mass of $[M+H]^+ = 247$, which is consistent with the proposed imide intermediate **4.29**. This intermediate is present in UV-detectable concentrations during the first phase of the reaction at 0 °C, but it is rapidly consumed once the temperature reaches 80 °C (approximately 60 minutes, indicated by the vertical black bar in Figure 4.4). At high temperatures, **4.29** reaches a low steady-state concentration. A plausible explanation for why imide **4.29** is detectable when triethylamine is used but not with Na_2CO_3 is due to triethylamine acting as an acylation catalyst. With Na_2CO_3 , the imide **4.29** is formed in an uncatalyzed manner at 80 °C, and then rapidly

cyclizes to acylated DHP **4.31**. In both cases, imide **4.29** exhibits steady-state behavior at high temperatures.

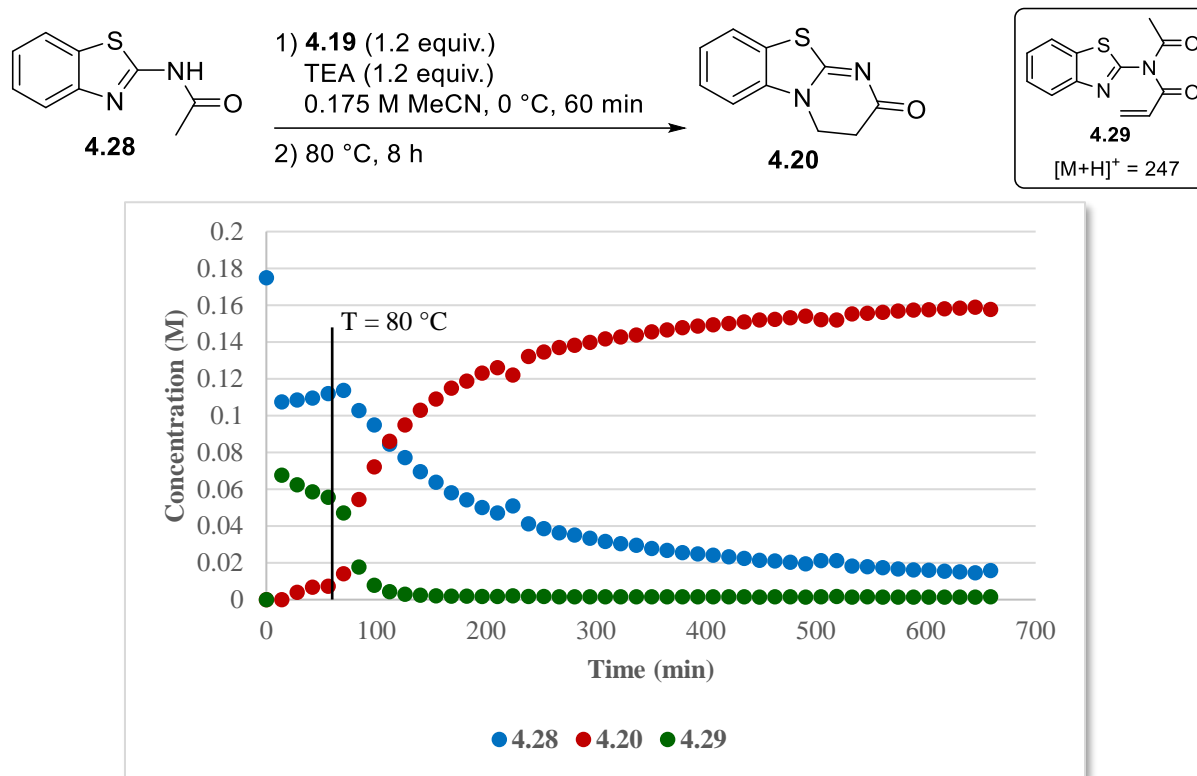


Figure 4.4: Reaction progress profiles generated by HPLC showing rapid generation and consumption of imide **4.29**. The vertical black bar indicates the time when the thermostat was changed from 0 to 80 °C.

4.4 Computational results

One of the key questions that remained to be answered was an explanation for why direct cyclization from acrylamide **4.23** was disfavored over cyclization from imide **4.29**. To help answer this question, we collaborated with the Cheong group at Oregon State University to perform calculations on the different reaction pathways. Figure 4.5 shows the potential energy differences between the direct cyclization pathway (red) and imide cyclization (blue). ΔG^\ddagger for the direct cyclization pathway was calculated to be 33.2 kcal/mol. In comparison, ΔG^\ddagger for the

imide cyclization pathway was calculated to be 25.6 kcal/mol, a 7.6 kcal/mol difference.

Geometry optimization calculations found that for the imide cyclization pathway, there is a stabilizing (~ 6 kcal/mol) $S\cdots O$ interaction between the benzothiazole sulfur and acetyl group carbonyl. Similar stabilizing $S\cdots O$ interactions are implicated in enantioselectivity-determining steps for related isothiurea organocatalysts.¹³² While a 33 kcal/mol barrier for direct cyclization is not prohibitively high, the 7.6 kcal/mol difference between direct and imide cyclization is significant, and explains why imide cyclization occurs readily, while direct acrylamide cyclization is only achievable at very high temperatures.

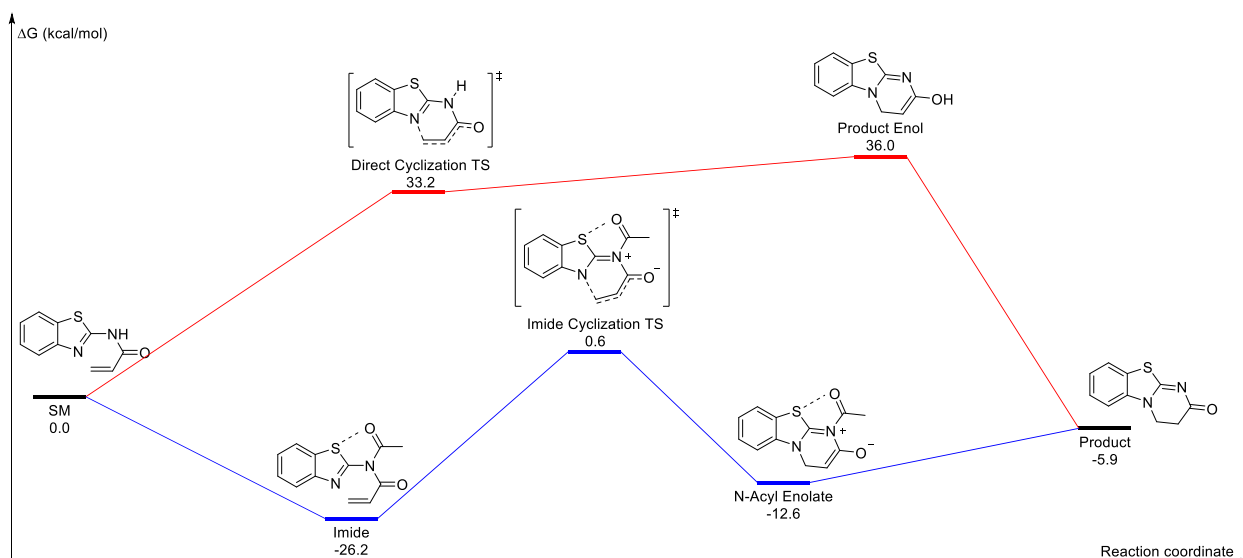


Figure 4.5: Reaction coordinate diagram showing energy barrier differences between direct acrylamide cyclization (red) and imide cyclization (blue). Level of theory: SCS-MP2/def2- ∞ //B3LYP/6-31G* with solvation at B3LYP/6-31+G/PCM(MeCN). Calculations performed by the Cheong group at Oregon State University.**

4.5 Extension of cyclization chemistry to other substrates and limitations

With a solid mechanistic foundation for this cyclization chemistry, a number of dihydropyrimidones were prepared with differing substituents on the benzothiazole ring, as well as dihydropyrimidones derived from benzimidazole, benzoxazole, and 4-substituted thiazole substrates (Figure 4.6). The reaction is amenable to substrates with both electron-poor and electron-rich substituents at the C8 position of the aromatic ring. The reaction is not specific to benzothiazole derivatives, as benzoxazole derivative **4.33g** was successfully prepared in 93% yield. When an analogous *N*-methyl benzimidazole was prepared, it underwent *in situ* oxidation to give a mixture of expected dihydropyrimidone **4.33h** and α,β -unsaturated product **4.33h'**. This chemistry was extended to 3-substituted thiazoles as well (**4.33i** and **4.33j**). However, reaction times for these compounds were longer (24-48 hrs) and required a larger excess of acryloyl chloride. The most likely explanation for this is due to the lack of aromatic electron density found on the benzothiazoles; the fused benzothiazole rings have greater electron density, allowing for faster rates of reaction.

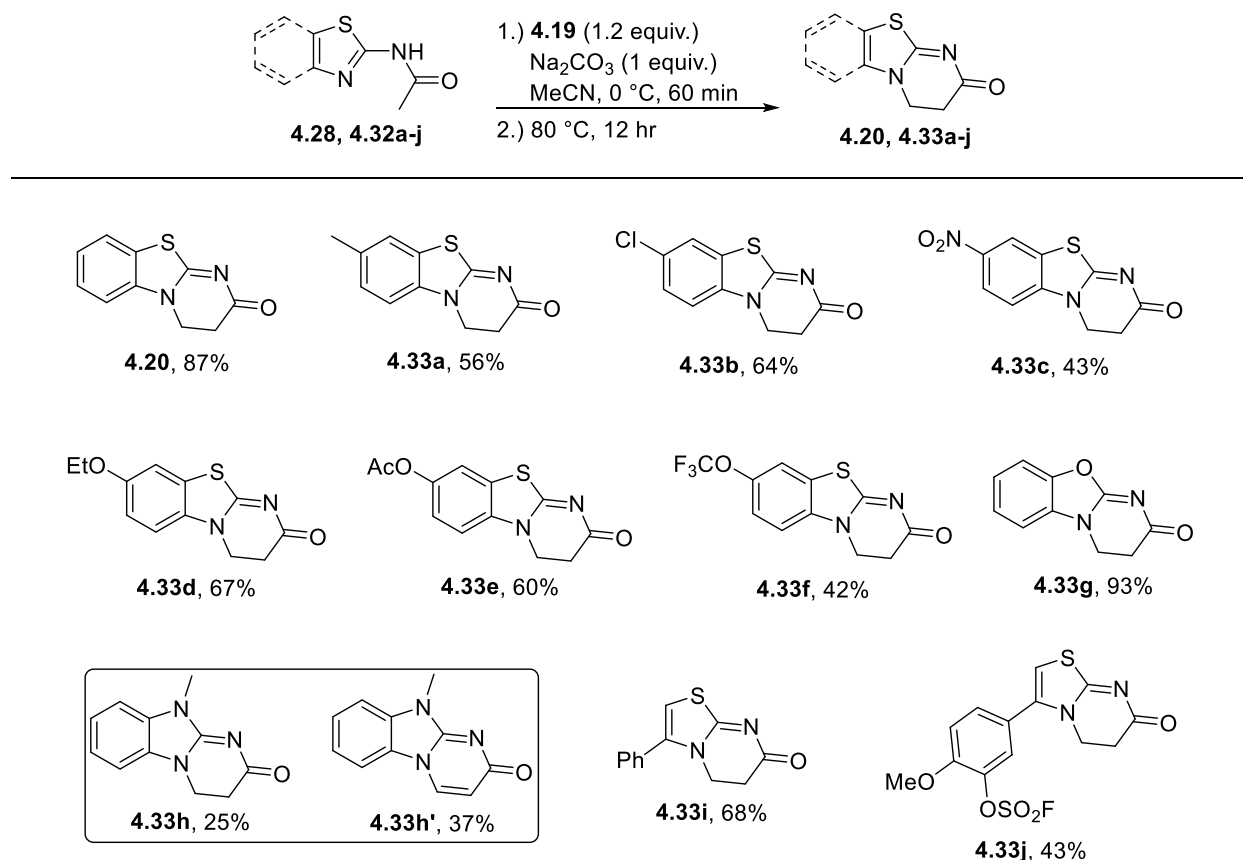
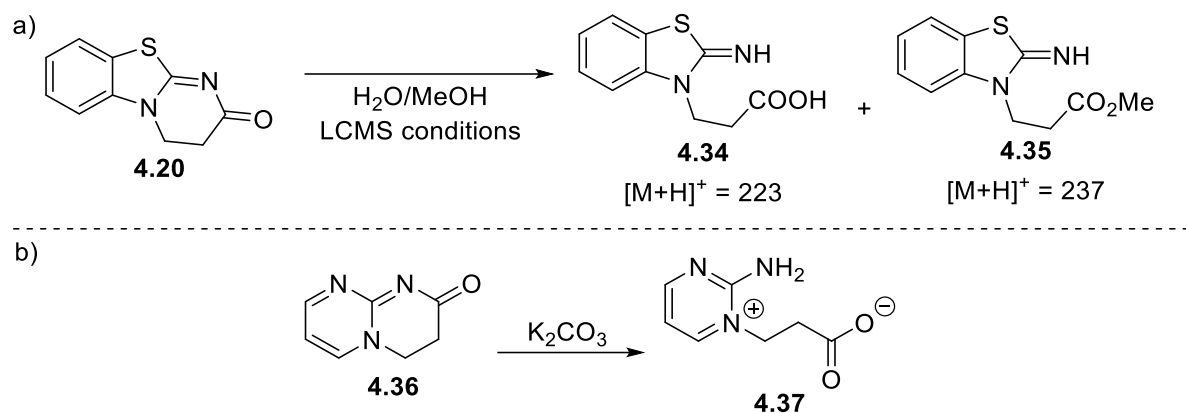


Figure 4.6: Substrate scope. Isolated yields determined after purification by column chromatography.

As shown in Figure 4.6, this reaction suffers from low to moderate isolated yields. When the reaction conditions for the formation of **4.20** are sampled by HPLC/MS, two additional peaks appear with masses of $[\text{M}+\text{H}]^+ = 223$ and 237. These masses are consistent with adducts of **4.20** with water and methanol, respectively. The most likely structures of these two adducts are **4.34** and **4.35**, results of hydrolysis/methanolysis of **4.20** in the HPLC vial (Scheme 4.13a). Since workup of this reaction involves an aqueous wash, it is possible that formation of acid **4.34** contributes to the moderate to low yields of reaction. There is also literature precedence for this byproduct formation; Greco and Warchol¹⁴⁰ observed a similar transformation of related DHP **4.36** to betaine **4.37** in the presence of equimolar K_2CO_3 (Scheme 4.13).



Scheme 4.13: a) Proposed decomposition of 4.20 under HPLC conditions. b) Decomposition of 4.36 to betaine 4.37 observed by Greco and Warchol.¹⁴⁰

4.6 Preliminary mechanistic studies

In an effort to probe the dependence of electronic structure on relative rates of cyclization between different amides, we monitored by HPLC a series of competition experiments between amide **4.28**, electron-rich ethoxy-substituted **4.32d**, and electron-poor trifluoromethoxy-substituted **4.32f** (Figure 4.7).

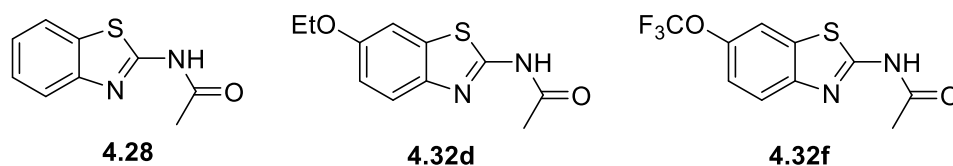


Figure 4.7: Amide starting materials used in competition experiments.

The first competition reaction performed was between **4.28** and ethoxy-substituted **4.32d**. Due to the electron-donating nature of the ethoxy group, we predicted a faster rate of reaction for **4.32d**. However, the product formation curves in Figure 4.8 appear to have similar rates of product formation, suggesting that the electron-donating properties of the ethoxy group have minimal

effect on the rate of reaction. As a control experiment, we monitored the rate of formation of **4.33d** on its own.

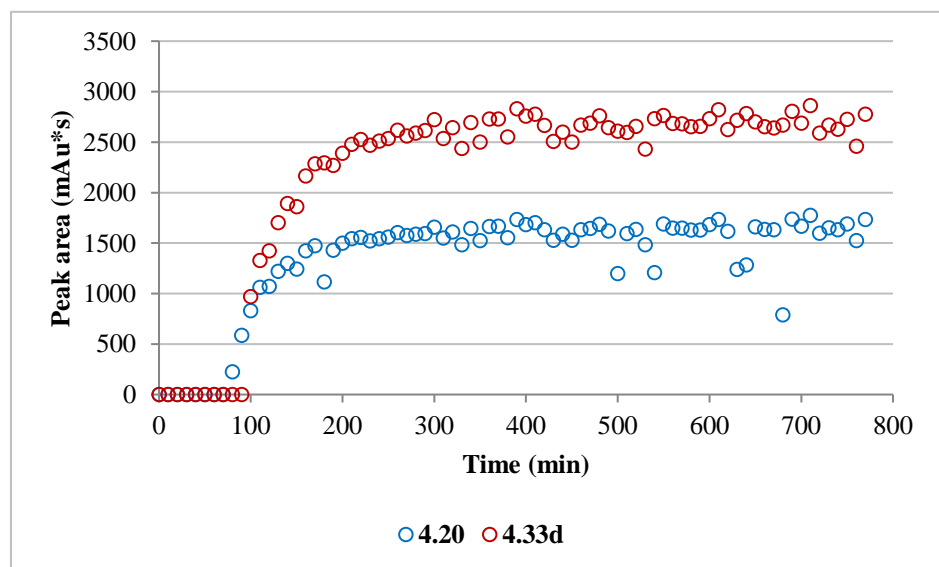
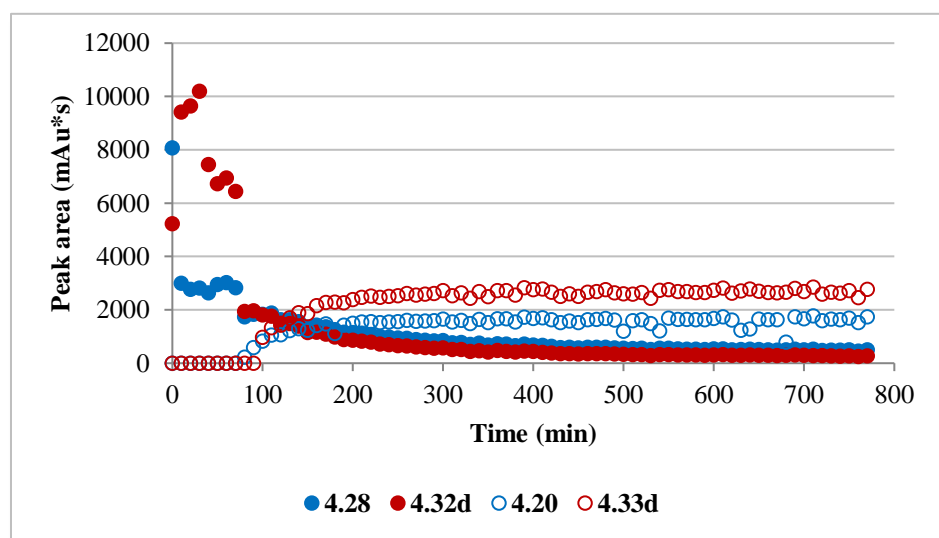
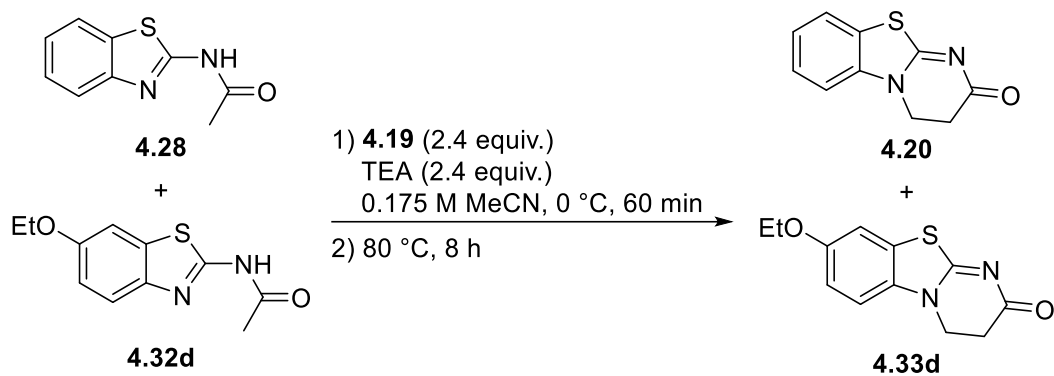


Figure 4.8: Reaction progress curves for the competition reaction between 4.28 and 4.32d.

Comparing the product formation curves of **4.33d** in both the competition and control experiments (Figure 4.9, left) revealed a surprising result: the rate of formation of **4.33d** in the competition experiment is faster than in the control experiment. To see if this was also true for **4.20**, a similar comparison was performed (Figure 4.9, right), and the rate of formation of **4.20** in the competition reaction is identical to the rate of formation of **4.20** in a control experiment; the curves overlay perfectly. The reason for this discrepancy is not immediately clear; in the competition experiment, 2.4 equivalents of acryloyl chloride are used, compared to the 1.2 equivalents used in the control experiments. The larger concentration of acryloyl chloride could explain the increased rate difference between the competition and control experiments for **4.33d**, similar behavior would be expected for **4.20** between the competition and control experiments, which is not observed. In Figure 4.8, it can be seen that a small amount of **4.20** is formed before **4.33d**. Since dihydropyrimidone **4.20** is structurally similar to HBTM, an acyl transfer catalyst, one possibility is that **4.20** facilitates the acyl transfer of the acryloyl moiety to **4.32d**, accelerating the formation of the required 4-ethoxy imide that is required to form **4.33d**. If this is the case, the formation of **4.20** in the control experiment would be self-catalytic, resulting in identical rate profiles for the formation of **4.20** in both the competition and control experiments. To get a better idea of the rate of cyclization differences for **4.28** and **4.32d**, the product formation curves in standalone experiments were compared (Figure 4.10). The curves overlay well, suggesting the rates of product formation are the same. However, it is important to note that calibration curves were not made for these compounds, and these curves are not true concentration profiles. However, the general shape of these curves are very similar, and there does not appear to be any significant rate differences in product formation when standalone

reactions are compared. It can be concluded from this that the effect of electron-donating substituents on the benzothiazole ring is negligible.

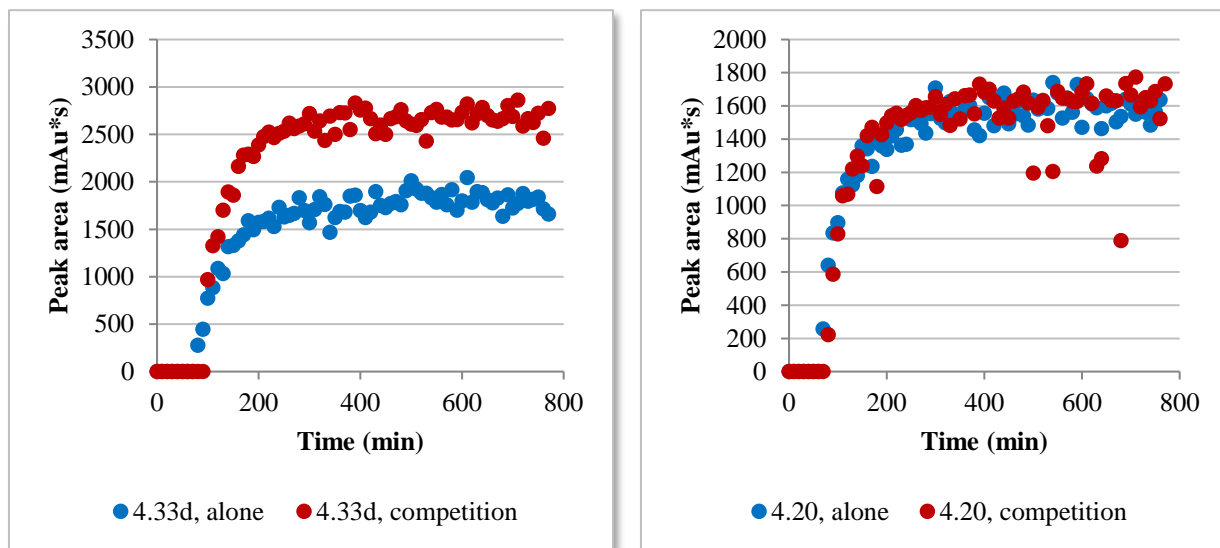


Figure 4.9: Comparison of product formation curves for 4.33d and 4.20 in both competition and standalone reactions.

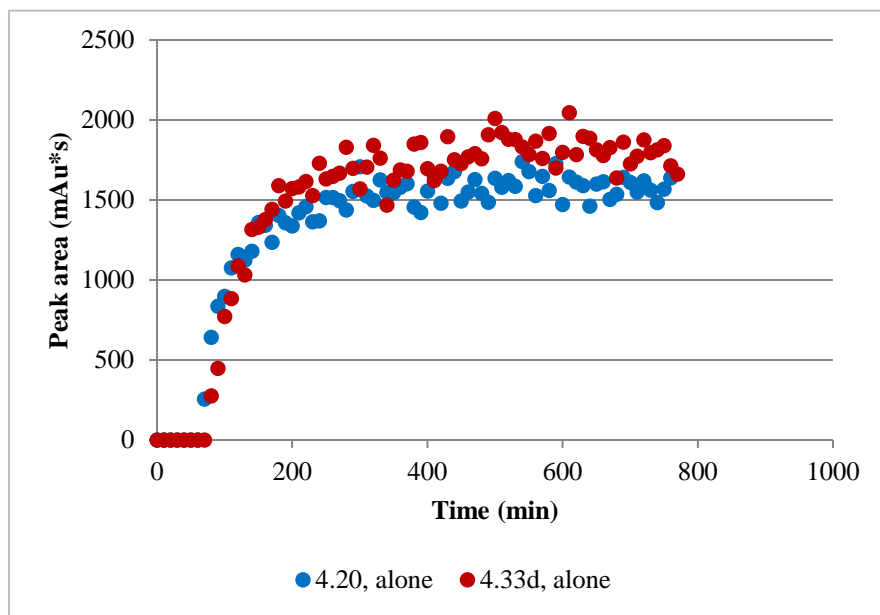


Figure 4.10: Comparison of product formation curves for 4.20 and 4.33d in standalone reactions only.

To probe the rate differences of electron-poor substrates, a competition experiment between **4.28** and 4-trifluoromethoxy-substituted **4.32f** was performed (Figure 4.11). Due to the electron-withdrawing properties of the trifluoromethoxy group, the formation of **4.33f** would be expected to be slower than the formation of **4.20**, and that is exactly what is observed. **4.28** is consumed much more rapidly than **4.32f**, stopping at around 300 minutes. The rate profiles of the formation of **4.20** and **4.33f** show that **4.20** is formed faster than **4.33f**, which is expected. However, the amount of both products decreases in the later portion of the reaction (>300 min), suggesting product decomposition.

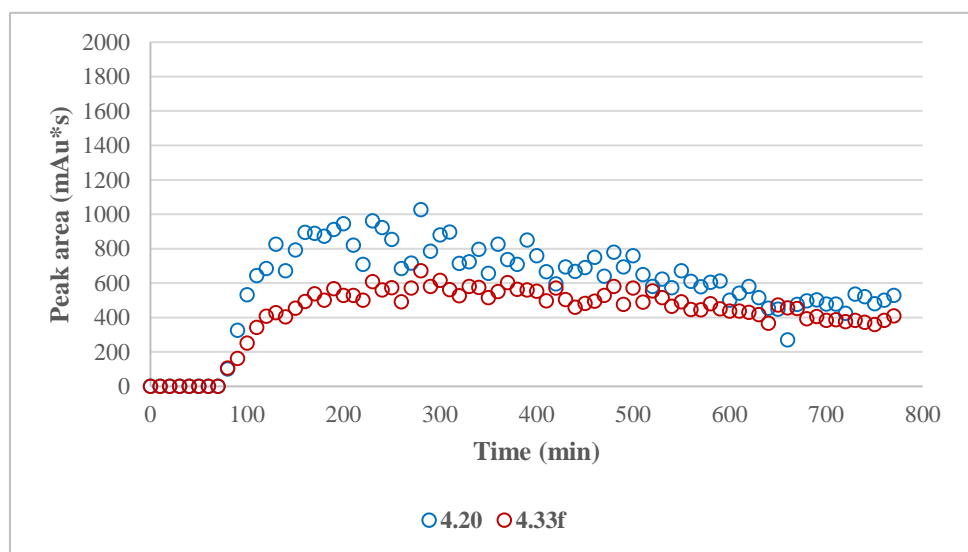
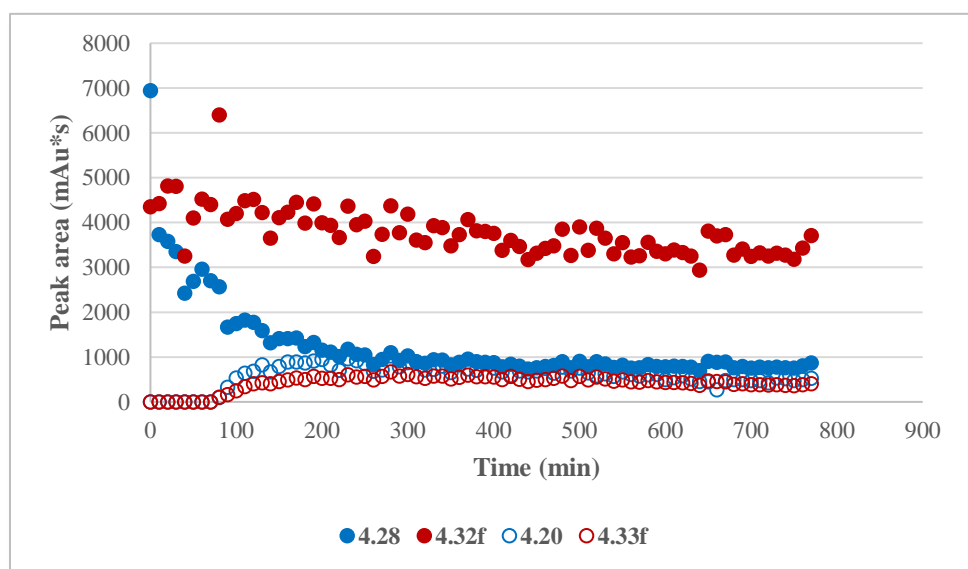
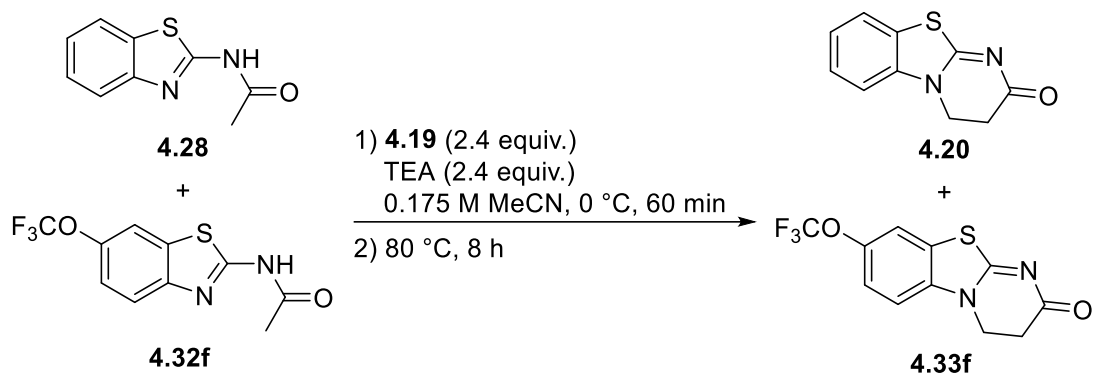


Figure 4.11: Reaction progress curves in the competition reaction between 4.28 and 4.32f.

4.7 Conclusion

To summarize, a new method of synthesizing dihydropyrimidones has been developed, by acylation of 2-acetamidobenzothiazoles with acryloyl chloride and subsequent intramolecular conjugate addition. Moreover, investigations into the original synthetic methods of these types of dihydropyrimidones revealed that the addition of NaI as an additive was unnecessary, and that the original synthesis most likely proceeded via an intramolecular conjugate addition to the acryloyl moiety of a mixed imide. Calculations showed that this imide cyclization mechanism is favored over direct acrylamide cyclization by 7.6 kcal/mol, helping to explain the initial failed attempts at direct acrylamide cyclization, and successes with the imide cyclization. Preliminary mechanistic studies show that substrates with electron-withdrawing substituents react slower, but there appears to be no change in reaction rate for substrates with electron-donating substituents. These preliminary mechanistic studies also suggest that the dihydropyrimidones could act as acyl transfer catalysts, analogous to their structurally similar isothioureia analogue HBTM. However, more thorough mechanistic investigations need to be performed, such as a more thorough study correlating reaction rate with the electronic nature of the ring substituents, and experiments probing the potential of **4.20** acting as an acyl transfer catalyst.

4.8 Experimental

4.8.1 General considerations

All chemicals and solvents were purchased from Fisher, Acros, TCI America, Aldrich, and AK Scientific, and were used without further purification unless otherwise stated.

Acetonitrile was dried over 4 Å molecular sieves prior to use. 6-

(trifluoromethoxy)benzo[*d*]thiazol-2-amine was prepared according to a previously published

procedure.¹⁴¹ ^1H (400 MHz) and ^{13}C (100 MHz) NMR spectra were recorded on a Bruker AV400sp at 295 K. Chemical shifts (δ) are reported in parts per million relative to residual solvent peaks as internal standards. Abbreviations are: s, singlet; d, doublet; t, triplet; q, quartet; p, pentet; m, multiplet. HPLC was performed on an Agilent 1260 Infinity with an Agilent Eclipse XDB C18 (3.5 μm , 3.0×7.5 mm) column, eluting with a water/acetonitrile (0.05% TFA additive) gradient. HPLC samples were prepared by taking 10 μL aliquots of reaction mixtures and diluting with 1 mL methanol. Flash chromatography was performed using Sorbtech silica gel 60 Å (230 \times 400 mesh), eluting with the indicated solvent mixtures. Thin layer chromatography (TLC) was performed on Sorbtech precoated silica gel plates (UV254) and was visualized by irradiation with UV light or staining with KMnO_4 solution.

4.8.2 Synthesis of *N*-(benzo[*d*]thiazol-2-yl)acrylamide (4.23)

In a 100 mL round-bottom flask, *N*-(benzo[*d*]thiazol-2-yl)-3-chloropropanamide (2.12 g, 8.75 mmol) and anhydrous Na_2CO_3 (1.02 g, 9.63 mmol) were suspended in dry acetonitrile (50 mL) with a stir bar. A water condenser was attached, and the mixture was heated to 80 $^\circ\text{C}$ and refluxed for one hour. The mixture was cooled to room temperature, and solvent was removed under reduced pressure. Water (25 mL) and CH_2Cl_2 (25 mL) were added to the flask and transferred to a 125 mL separatory funnel. The organic layer was separated, and the aqueous layer was washed with CH_2Cl_2 (2 \times 25 mL). The combined organic extracts were combined, dried over anhydrous Na_2SO_4 , and solvent was removed under reduced pressure to give a white solid (1.70 g, 8.31 mmol, 95%) that was dried under high vacuum overnight. Analytical data for **4.23**: ^1H NMR (400 MHz, CDCl_3) δ 7.82 (dd, J = 47.7, 8.0 Hz, 2H), 7.41 (dt, J = 42.9, 7.5 Hz, 2H), 6.63 (d, J = 16.9 Hz, 1H), 6.38 (dd, J = 16.9, 10.3 Hz, 1H), 5.89 (d, J = 10.3 Hz, 1H); LRMS (ESI): Calc'd for $\text{C}_{10}\text{H}_8\text{N}_2\text{OS}+\text{H}$: 205.0, found: 205.1.

4.8.3 Synthesis of *N*-(benzo[d]thiazol-2-yl)-3-chloropropanamide (4.25)

In a 100 mL round-bottom flask, 2-aminobenzothiazole (1.31 g, 8.75 mmol) and anhydrous Na₂CO₃ (1.11 g, 10.5 mmol) were suspended in dry acetonitrile (50 mL) with a stir bar. The flask was fitted with a rubber septum, cooled to 0 °C in an ice bath, and the flask was purged with N₂ for 10 minutes. Under a stream of N₂, 3-chloropropanoyl chloride (1.0 mL, 10.5 mmol) was added dropwise via syringe, and the mixture was stirred at 0 °C for 1 hour. Once the reaction was determined to be complete by HPLC, the solvent was removed under reduced pressure. Water (50 mL) was added to the flask, and the solids were triturated for 20 minutes. The white solids were collected by suction filtration and air dried. The crude product was recrystallized from methanol and collected by vacuum filtration as a white powder (1.83 g, 7.61 mmol, 87%). Analytical data for **4.25**: ¹H NMR (400 MHz, DMSO-d₆) δ 7.97 (dd, *J* = 7.9, 0.5 Hz, 1H), 7.73 (d, *J* = 7.9 Hz, 1H), 7.42 (t, 1H), 7.29 (t, 1H), 3.91 (t, *J* = 6.3 Hz, 2H), 3.01 (t, *J* = 6.3 Hz, 2H); ¹³C NMR (101 MHz, DMSO-d₆) δ 169.7, 158.0, 148.9, 131.8, 126.6, 124.0, 122.2, 121.0, 38.7; LRMS (ESI): Calc'd for C₁₁H₁₁ClN₂OS+H: 255.0, found: 255.1.

4.8.4 General procedure for synthesis of acetamides

In a 20 mL scintillation vial with rubber septum, the corresponding 2-aminothiazole (2 mmol) was dissolved in acetic anhydride (2 mL) with a stir bar, and three drops of neat pyridine were added. The solution was stirred and heated at 80 °C for 1 hour. Water (3 mL) was added, and the mixture was stirred for 20 minutes. The resulting precipitate was collected by suction filtration and dried under high vacuum overnight. The acetamides were used without further purification.

***N*-(benzo[d]thiazol-2-yl)acetamide (4.28)**: The title compound was prepared from 2-aminobenzothiazole (0.3 g, 2 mmol) using the general procedure, and isolated as a yellow crystalline solid (0.300 g, 1.56 mmol, 78%). Analytical data for **4.28**: ¹H NMR (400 MHz,

CD₃OD) δ 7.83 (dd, J = 7.9, 0.5 Hz, 1H), 7.72 (d, J = 8.1 Hz, 1H), 7.41 (ddd, J = 8.3, 7.3, 1.2 Hz, 1H), 7.28 (td, J = 7.7, 1.1 Hz, 1H), 2.25 (s, 3H); **LRMS** (ESI): Calc'd for C₉H₈N₂OS+H: 193.0, found: 193.0.

***N*-(6-methylbenzo[*d*]thiazol-2-yl)acetamide (4.32a):** The title compound was prepared from 6-methylbenzo[*d*]thiazol-2-amine (0.328 g, 2 mmol) using the general procedure, and isolated as a white solid (0.293 g, 1.42 mmol, 71%). Analytical data for **4.32a**: **¹H NMR** (400 MHz, CDCl₃) δ 7.67 (dd, J = 4.3, 3.6 Hz, 2H), 7.29 (dd, J = 8.0, 1.3 Hz, 1H), 2.51 (s, 3H), 2.29 (s, 3H); **¹³C NMR** (101 MHz, CDCl₃) δ 168.8, 159.3, 145.4, 134.2, 131.9, 127.9, 121.5, 119.8, 23.5, 21.5; **LRMS** (ESI): Calc'd for C₁₀H₁₀N₂OS+H: 207.1, found: 207.1.

***N*-(6-chlorobenzo[*d*]thiazol-2-yl)acetamide (4.32b):** The title compound was prepared from 6-chlorobenzo[*d*]thiazol-2-amine (0.368 g, 2 mmol) using the general procedure, and isolated as a white powder (0.420 g, 1.86 mmol, 93%). Analytical data for **4.32b**: **¹H NMR** (400 MHz, Acetone-*d*₆) δ 8.01 (d, J = 2.1 Hz, 1H), 7.69 (d, J = 8.6 Hz, 1H), 7.43 (dd, J = 8.6, 2.2 Hz, 1H), 2.33 (s, 4H); **¹³C NMR** (101 MHz, Acetone-*d*₆) δ 169.0, 158.6, 147.9, 133.7, 128.2, 126.4, 121.8, 121.0, 22.1; **LRMS** (ESI): Calc'd for C₉H₇ClN₂OS+H: 227.0, found: 227.1.

***N*-(6-nitrobenzo[*d*]thiazol-2-yl)acetamide (4.32c):** The title compound was prepared from 6-nitrobenzo[*d*]thiazol-2-amine (0.390 g, 2 mmol) using the general procedure, and isolated as a yellow powder (0.308g, 1.3 mmol, 65%). Analytical data for **4.32c**: **¹H NMR** (400 MHz, DMSO-*d*₆) δ 9.03 (d, J = 2.3 Hz, 1H), 8.27 (dd, J = 8.9, 2.4 Hz, 1H), 7.88 (d, J = 8.9 Hz, 1H), 2.26 (s, 3H); **¹³C NMR** (101 MHz, DMSO-*d*₆) δ 170.6, 163.9, 153.9, 143.4, 132.6, 122.2, 121.0, 119.4, 23.3; **LRMS** (ESI): Calc'd for C₉H₇N₃O₃S+H: 238.0, found: 238.0.

***N*-(6-ethoxybenzo[*d*]thiazol-2-yl)acetamide (4.32d):** The title compound was prepared from 6-ethoxybenzo[*d*]thiazol-2-amine (0.389 g, 2 mmol) using the general procedure, and isolated as a beige powder (0.378 g, 1.6 mmol, 80%). Analytical data for **4.32d**: $^1\text{H NMR}$ (400 MHz, DMSO-*d*₆) δ 7.61 (d, *J* = 8.8 Hz, 1H), 7.53 (d, *J* = 2.5 Hz, 1H), 7.00 (dd, *J* = 8.8, 2.6 Hz, 1H), 4.06 (q, *J* = 7.0 Hz, 2H), 2.18 (s, 3H), 1.35 (t, *J* = 7.0 Hz, 3H); $^{13}\text{C NMR}$ (101 MHz, DMSO-*d*₆) δ 169.5, 156.4, 155.8, 143.0, 133.2, 121.5, 115.6, 105.8, 64.1, 23.2, 15.2; **LRMS** (ESI): Calc'd for C₁₁H₁₂N₂O₂S+H: 237.1, found: 237.1.

2-acetamidobenzo[*d*]thiazol-6-yl acetate (4.32e): The title compound was prepared from 2-aminobenzo[*d*]thiazol-6-ol (0.332 g, 2 mmol) using the general procedure, and isolated as a purple powder (0.435 g, 1.74 mmol, 87%). Analytical data for **4.32e**: $^1\text{H NMR}$ (300 MHz, DMSO-*d*₆) δ 7.74 (dd, *J* = 10.6, 5.5 Hz, 2H), 7.17 (dd, *J* = 8.7, 2.4 Hz, 1H), 2.28 (s, 3H), 2.19 (s, 3H); $^{13}\text{C NMR}$ (75 MHz, DMSO-*d*₆) δ 170.1, 158.8, 147.0, 132.6, 121.4, 121.1, 115.4, 23.3, 21.4; **LRMS** (ESI): C₁₁H₁₀N₂O₃S+H: 251.0, found: 251.1.

***N*-(6-(trifluoromethoxy)benzo[*d*]thiazol-2-yl)acetamide (4.32f):** The title compound was prepared from 6-(trifluoromethoxy)benzo[*d*]thiazol-2-amine (0.468 g, 2 mmol) using the general procedure, and isolated as an off-white powder (0.458 g, 1.66 mmol, 83%). Analytical data for **4.32f**: $^1\text{H NMR}$ (300 MHz, Acetone-*d*₆) δ 7.98 (d, *J* = 1.3 Hz, 1H), 7.77 (d, *J* = 8.8 Hz, 1H), 7.38 (dd, *J* = 8.8, 1.5 Hz, 1H), 2.32 (s, 3H); $^{19}\text{F NMR}$ (282 MHz, Acetone-*d*₆) δ -59.25; **LRMS** (ESI): Calc'd for C₁₀H₇F₃N₂O₂S+H: 277.0, found: 277.0.

***N*-(benzo[*d*]oxazol-2-yl)acetamide (4.32g):** The title compound was prepared from 2-aminobenzoxazole (0.268 g, 2 mmol) using the general procedure, and isolated as an off-white solid (0.236 g, 1.34 mmol, 67%). Analytical data for **4.32g**: $^1\text{H NMR}$ (400 MHz, DMSO-*d*₆) δ 7.89 – 7.43 (m, 2H), 7.28 (dq, *J* = 15.1, 7.5, 1.4 Hz, 2H), 2.22 (s, 3H); $^{13}\text{C NMR}$ (101 MHz,

DMSO-d₆) δ 168.7, 155.7, 148.0, 141.2, 124.9, 123.9, 118.6, 110.4, 24.3; **LRMS** (ESI): Calc'd for C₉H₈N₂O₂+H: 177.1, found: 177.2.

***N*-(1-methyl-1*H*-benzo[*d*]imidazol-2-yl)acetamide (4.32h):** The title compound was prepared from 1-methyl-1*H*-benzo[*d*]imidazol-2-amine (0.294 g, 2 mmol) using the general procedure, and isolated as an off-white powder (0.250 g, 1.32 mmol, 66%). Analytical data for **4.32h**: **¹H NMR** (300 MHz, CDCl₃) δ 7.63 – 6.75 (m, 4H), 3.68 (s, 3H), 2.22 (d, *J* = 44.9 Hz, 3H); **LRMS** (ESI): Calc'd for C₁₀H₁₁N₃O+H: 190.1, found: 190.2.

***N*-(4-phenylthiazol-2-yl)acetamide (4.32i):** The title compound was prepared from 4-phenylthiazol-2-amine (0.352 g, 2 mmol) using the general procedure, and isolated as an off-white powder (0.401 g, 1.84 mmol, 92%). Analytical data for **4.32i**: **¹H NMR** (400 MHz, CDCl₃) δ 7.87 – 7.74 (m, 2H), 7.49 – 7.38 (m, 2H), 7.38 – 7.31 (m, 1H), 7.14 (s, 1H), 1.83 (s, 3H); **¹³C NMR** (101 MHz, CDCl₃) δ 168.4, 159.5, 149.4, 134.1, 128.9, 128.4, 126.3, 107.8, 22.7; **LRMS** (ESI): Calc'd for C₁₁H₁₀N₂OS+H: 219.1, found: 219.0.

5-(2-acetamidothiazol-4-yl)-2-methoxyphenyl sulfurofluoridate (4.32j): The title compound was prepared from 5-(2-aminothiazol-4-yl)-2-methoxyphenyl sulfurofluoridate (0.609 g, 2 mmol) using the general procedure, and isolated as a slightly yellow powder (0.547 g, 1.58 mmol, 79%). Analytical data for **4.32j**: **¹H NMR** (300 MHz, CDCl₃) δ 7.83 (dt, *J* = 10.6, 4.3 Hz, 2H), 7.13 (d, *J* = 7.4 Hz, 2H), 4.00 (s, 3H), 2.20 (s, 3H); **¹⁹F NMR** (282 MHz, CDCl₃) δ 40.07; **LRMS** (ESI): Calc'd for C₁₂H₁₁FN₂O₅S₂+H: 347.0, found: 347.1.

4.8.5 General procedure for cyclization of acetamides to dihydropyrimidinones

In a 20 mL scintillation vial with rubber septum, acetamide (0.875 mmol) and anhydrous Na₂CO₃ (0.093 g, 0.875 mmol) were suspended in dry acetonitrile (5 mL) with a stir bar. The mixture was cooled to 0 °C in an ice bath, then acryloyl chloride (85 μ L, 1.05 mmol) was added

dropwise via syringe. The mixture was stirred at 0 °C for 60 minutes, then heated to 80 °C for 8 hours. The reaction was cooled to room temperature, and solvent was removed under reduced pressure. Water (10 mL) and CH₂Cl₂ were added to the crude solids, and the biphasic mixture was transferred to a 125 mL separatory funnel. The organic layer was separated, and the aqueous layer was extracted with CH₂Cl₂ (2 x 10 mL). The combined organic layers were dried over anhydrous Na₂SO₄, and solvent was removed under reduced pressure. The crude products were purified by flash chromatography (9:1 CH₂Cl₂:acetone).

3,4-dihydro-2H-benzo[4,5]thiazolo[3,2-*a*]pyrimidin-2-one (4.20): The title compound was prepared from **4.28** (0.168 g, 0.875 mmol) using the general procedure to give the product as a white crystalline solid (0.155 g, 0.761 mmol, 87%). Analytical data for **4.20**: **¹H NMR** (300 MHz, CDCl₃) δ 7.62 (d, *J* = 7.9 Hz, 1H), 7.57 – 7.40 (m, 1H), 7.42 – 7.25 (m, 1H), 7.20 (d, *J* = 8.1 Hz, 1H), 4.27 (t, *J* = 7.7 Hz, 2H), 2.92 (t, *J* = 7.7 Hz, 2H); **LRMS** (ESI): Calc'd for C₁₀H₈N₂OS+H: 205.0, found: 205.1.

8-methyl-3,4-dihydro-2H-benzo[4,5]thiazolo[3,2-*a*]pyrimidin-2-one (4.33a): The title compound was prepared from **4.32a** (0.181 g, 0.875 mmol) using the general procedure to give the product as a white crystalline solid (0.107 g, 0.49 mmol, 56%). Analytical data for **4.33a**: **¹H NMR** (300 MHz, Acetone-*d*₆) δ 7.57 (s, 1H), 7.41 – 7.14 (m, 2H), 4.32 (t, *J* = 7.7 Hz, 2H), 2.73 (t, *J* = 7.7 Hz, 2H), 2.40 (s, 3H); **HRMS** (ESI): Calc'd for C₁₁H₁₀N₂OS+H: 219.0587, found: 219.0592.

8-chloro-3,4-dihydro-2H-benzo[4,5]thiazolo[3,2-*a*]pyrimidin-2-one (4.33b): The title compound was prepared from **4.32b** (0.198 g, 0.875 mmol) using the general procedure to give the product as a white crystalline solid (0.134 g, 0.56 mmol, 64%). Analytical data for **4.33b**: **¹H NMR** (300 MHz, Acetone-*d*₆) δ 7.92 (d, *J* = 2.0 Hz, 1H), 7.51 (dt, *J* = 19.4, 5.4 Hz, 2H), 4.44 (t,

$J = 7.6$ Hz, 2H), 2.82 (t, $J = 7.6$ Hz, 2H); **HRMS** (ESI): Calc'd for $C_{10}H_7ClN_2OS+H$: 239.0040, found: 239.0045.

8-nitro-3,4-dihydro-2H-benzo[4,5]thiazolo[3,2-*a*]pyrimidin-2-one (4.33c): The title compound was prepared from **4.32c** (0.207 g, 0.875 mmol) using the general procedure to give the product as a yellow crystalline solid (0.094 g, 0.376 mmol, 43%). Analytical data for **4.33c**: **1H NMR** (400 MHz, DMSO) δ 8.88 (d, $J = 2.4$ Hz, 1H), 8.35 (dd, $J = 9.0, 2.4$ Hz, 1H), 7.62 (d, $J = 9.0$ Hz, 1H), 4.36 (t, $J = 7.6$ Hz, 2H), 2.73 (t, $J = 7.6$ Hz, 2H); **HRMS** (ESI): Calc'd for $C_{10}H_7N_3O_3S+H$: 250.0281, found: 250.0285.

8-ethoxy-3,4-dihydro-2H-benzo[4,5]thiazolo[3,2-*a*]pyrimidin-2-one (4.33d): The title compound was prepared from **4.32d** (0.207 g, 0.875 mmol) using the general procedure to give the product as a beige powder (0.145 g, 0.586 mmol, 67%). Analytical data for **4.33d**: **1H NMR** (300 MHz, Acetone- d_6) δ 7.38 (d, $J = 2.5$ Hz, 1H), 7.30 (d, $J = 8.9$ Hz, 1H), 7.05 (dd, $J = 8.9, 2.5$ Hz, 1H), 4.31 (t, $J = 7.7$ Hz, 2H), 4.19 – 3.97 (m, 2H), 2.72 (t, $J = 7.7$ Hz, 2H), 1.38 (t, $J = 7.0$ Hz, 3H); **HRMS** (ESI): Calc'd for $C_{12}H_{12}N_2O_2S+H$: 249.0692, found: 249.0696.

2-oxo-3,4-dihydro-2H-benzo[4,5]thiazolo[3,2-*a*]pyrimidin-8-yl acetate (4.33e): The title compound was prepared from **4.32e** (0.219 g, 0.875 mmol) using the general procedure to give the product as a crystalline purple solid (0.137 g, 0.525 mmol, 60%). Analytical data for **4.33e**: **1H NMR** (400 MHz, $CDCl_3$) δ 7.37 (d, $J = 2.2$ Hz, 1H), 7.18 (dt, $J = 21.8, 5.5$ Hz, 2H), 4.24 (t, $J = 7.7$ Hz, 2H), 2.89 (t, $J = 7.7$ Hz, 2H), 2.35 (s, 3H); **HRMS** (ESI): Calc'd for $C_{12}H_{10}N_2O_3S+H$: 263.0485, found: 263.0495.

8-(trifluoromethoxy)-3,4-dihydro-2H-benzo[4,5]thiazolo[3,2-*a*]pyrimidin-2-one (4.33f): The title compound was prepared from **4.32f** (0.242 g, 0.875 mmol) using the general procedure to give the product as an off-white powder (0.106 g, 0.367 mmol, 42%). Analytical data for **4.33f**:

¹H NMR (400 MHz, CDCl₃) δ 7.49 (d, *J* = 1.4 Hz, 1H), 7.34 (dd, *J* = 8.8, 1.4 Hz, 1H), 7.17 (d, *J* = 8.8 Hz, 1H), 4.26 (t, *J* = 7.7 Hz, 2H), 2.90 (t, *J* = 7.7 Hz, 2H); **¹⁹F NMR** (377 MHz, CDCl₃) δ -58.00; **HRMS** (ESI): Calc'd for C₁₁H₇F₃N₂O₂S+H: 289.0253, found: 289.0261.

3,4-dihydro-2H-benzo[4,5]oxazolo[3,2-*a*]pyrimidin-2-one (4.33g): The title compound was prepared from **4.32g** (0.154 g, 0.875 mmol) using the general procedure to give the product as a crystalline white solid (0.153 g, 0.814 mmol, 93%). Analytical data for **4.33g**: **¹H NMR** (300 MHz, CDCl₃) δ 7.55 – 7.02 (m, 4H), 4.18 (t, *J* = 7.7 Hz, 2H), 2.91 (t, *J* = 7.7 Hz, 2H); **¹³C NMR** (75 MHz, CDCl₃) δ 176.2, 163.8, 144.6, 130.1, 125.5, 124.1, 111.5, 108.8, 38.7, 28.9; **HRMS** (ESI): Calc'd for C₁₀H₈N₂O₂+H: 189.0659, found: 189.0658.

10-methyl-3,4-dihydrobenzo[4,5]imidazo[1,2-*a*]pyrimidin-2(10H)-one (4.33h): The title compound was prepared from **4.32h** (0.166 g, 0.875 mmol) using the general procedure to give the product as a slightly yellow solid (0.044 g, 0.219 mmol, 25%). Analytical data for **4.33h**: **¹H NMR** (300 MHz, CDCl₃) δ 7.45 – 7.03 (m, 4H), 4.16 (t, *J* = 7.5 Hz, 2H), 3.61 (s, 3H), 2.86 (t, *J* = 7.6 Hz, 2H); **LRMS** (ESI): Calc'd for C₁₁H₁₁N₃O+H: 202.1, found: 202.1.

10-methylbenzo[4,5]imidazo[1,2-*a*]pyrimidin-2(10H)-one (4.33h'): The title compound was prepared from **4.32h** (0.166 g, 0.875 mmol) using the general procedure to give the product as a slightly yellow solid (0.065 g, 0.324 mmol, 37%). Analytical data for **4.33h'**: **¹H NMR** (300 MHz, CDCl₃) δ 8.73 (d, *J* = 8.1 Hz, 1H), 8.03 (d, *J* = 6.5 Hz, 1H), 7.55 (dd, *J* = 11.3, 4.3 Hz, 1H), 7.48 – 7.33 (m, 2H), 6.21 (d, *J* = 6.5 Hz, 1H), 3.86 (s, 3H); **¹³C NMR** (75 MHz, CDCl₃) δ 159.58, 154.6, 149.6, 131.8, 126.7, 122.5, 116.0, 110.1, 102.6, 28.6; **LRMS** (ESI): Calc'd for C₁₁H₉N₃O+H: 200.1, found: 200.1.

3-phenyl-5,6-dihydro-7H-thiazolo[3,2-*a*]pyrimidin-7-one (4.33i): The title compound was prepared from **4.32i** (0.191 g, 0.875 mmol) using the general procedure to give the product as an

off-white solid (0.137 g, 0.595 mmol, 68%). Analytical data for **4.33i**: ^1H NMR (300 MHz, CDCl_3) δ 7.67 – 6.98 (m, 5H), 6.38 (s, 1H), 3.96 (t, $J = 7.5$ Hz, 2H), 2.59 (t, $J = 7.5$ Hz, 2H); ^{13}C NMR (75 MHz, CDCl_3) δ 174.7, 173.4, 140.7, 130.3, 129.3, 129.0, 128.9, 103.5, 103.4, 53.7, 43.3, 28.8; LRMS (ESI): Calc'd for $\text{C}_{12}\text{H}_{10}\text{N}_2\text{OS}+\text{H}$: 231.1, found: 231.1.

2-methoxy-5-(7-oxo-6,7-dihydro-5H-thiazolo[3,2-*a*]pyrimidin-3-yl)benzenesulfonyl fluoride

(4.33j): The title compound was prepared from **4.32j** (0.289 g, 0.875 mmol) using the general procedure to give the product as a white crystalline solid (0.129 g, 0.376 mmol, 43%). Analytical data for **4.33j**: ^1H NMR (400 MHz, CDCl_3) δ 7.49 – 7.30 (m, 2H), 7.18 (d, $J = 8.5$ Hz, 1H), 6.40 (s, 1H), 4.10 – 3.87 (m, 5H), 2.67 (t, $J = 7.5$ Hz, 2H); ^{13}C NMR (101 MHz, CDCl_3) δ 174.3, 172.7, 152.7, 138.8, 138.2, 130.3, 123.3, 121.4, 114.0, 104.0, 56.6, 43.1, 28.5; HRMS (ESI): Calc'd for $\text{C}_{13}\text{H}_{11}\text{FN}_2\text{O}_5\text{S}_2+\text{H}$: 359.0166, found: 359.0179.

Chapter 5: Conclusions and Future Work

5.1 Conclusions and future work – 1,2,3-triazolylidene organocatalysts

In Chapter 2, the design and synthesis of 1,2,3-triazolium salt mesoionic carbene precursors was described, as well as their application as organocatalysts in the oxidative esterification of aromatic aldehydes. The activity of these 1,2,3-triazolylidenes are governed both by the nature of the *N*-substituent and the size of the fused saturated ring; catalysts with 5-membered fused rings are more reactive than those with 6-membered rings. The 1,2,3-triazolium salt precursors show an inverse acidity/activity relationship, with the most acidic triazolium salts being the least efficient catalysts. A detailed mechanistic study of the oxidative esterification reaction was conducted using reaction progress monitoring methodology. The reaction shows zero order behavior with respect to oxidant and an initial zero-order dependence on nucleophile, which transitions to a positive-order dependence as the reaction proceeds. The resting state of the catalyst cannot be clearly defined as a single intermediate, as the reaction shows rate dependence upon both aldehyde and base. Instead, it is possible that the rate constants for 1,2,3-triazolium deprotonation, carbene addition, and isomerization to the Breslow intermediate have similar magnitudes under the reaction conditions. In addition, a catalytically active carbene-aldehyde adduct was synthesized and characterized by single-crystal X-ray crystallography.

Experiments performed on the isolated catalytic intermediate show that for the 1,2,3-triazolylidene system, the acyl azolium species is generated by oxidation of the Breslow intermediate, and not by direct oxidation of the benzylic carbene-aldehyde adduct. Despite evidence that the Breslow intermediate is indeed formed in the 1,2,3-triazolylidene system, they do not show other types of NHC reactivity such as the benzoin condensation, Stetter

reaction, or homoenolate equivalent formation from α,β -unsaturated aldehydes. Future work in this aspect should focus on the design of new catalysts that should exhibit more nucleophilicity from the Breslow intermediate. Studies on the nucleophilicity parameters of *N*-heterocyclic carbenes have shown that carbenes bearing electron-donating *N*-substituents show higher degrees of nucleophilicity than carbenes bearing *N*-alkyl substituents. It stands to reason that Breslow intermediates derived from carbenes bearing electron-donating *N*-substituents should exhibit higher degrees of nucleophilicity as well. Figure 5.1 shows a 1,2,3-triazolium salt bearing an electron-donating *N*-substituent and its associated Breslow intermediate that could potentially exhibit classical NHC reactivity.

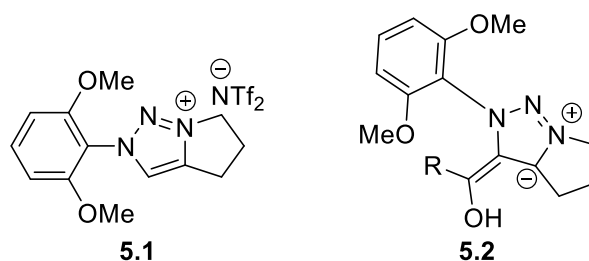


Figure 5.1: Proposed electron-rich 1,2,3-triazolium precatalyst and its associated Breslow intermediate that can potentially participate in classical NHC reactions.

The reaction progress curves for the 1,2,3-triazolyldene-catalyzed oxidative esterification show evidence of catalyst deactivation – the initial rates of reaction are much faster than the later rates of reaction. However, the present work did not investigate the origin of this observed deactivation. A re-examination of the mechanistic profiles of this catalytic system using a high data density collection method – such as NMR, ReactIR, or real-time mass spectrometric analysis – could help gain insight into the origin of the observed catalyst deactivation. Both NMR and real-time mass spectrometric analysis have high detection limits,

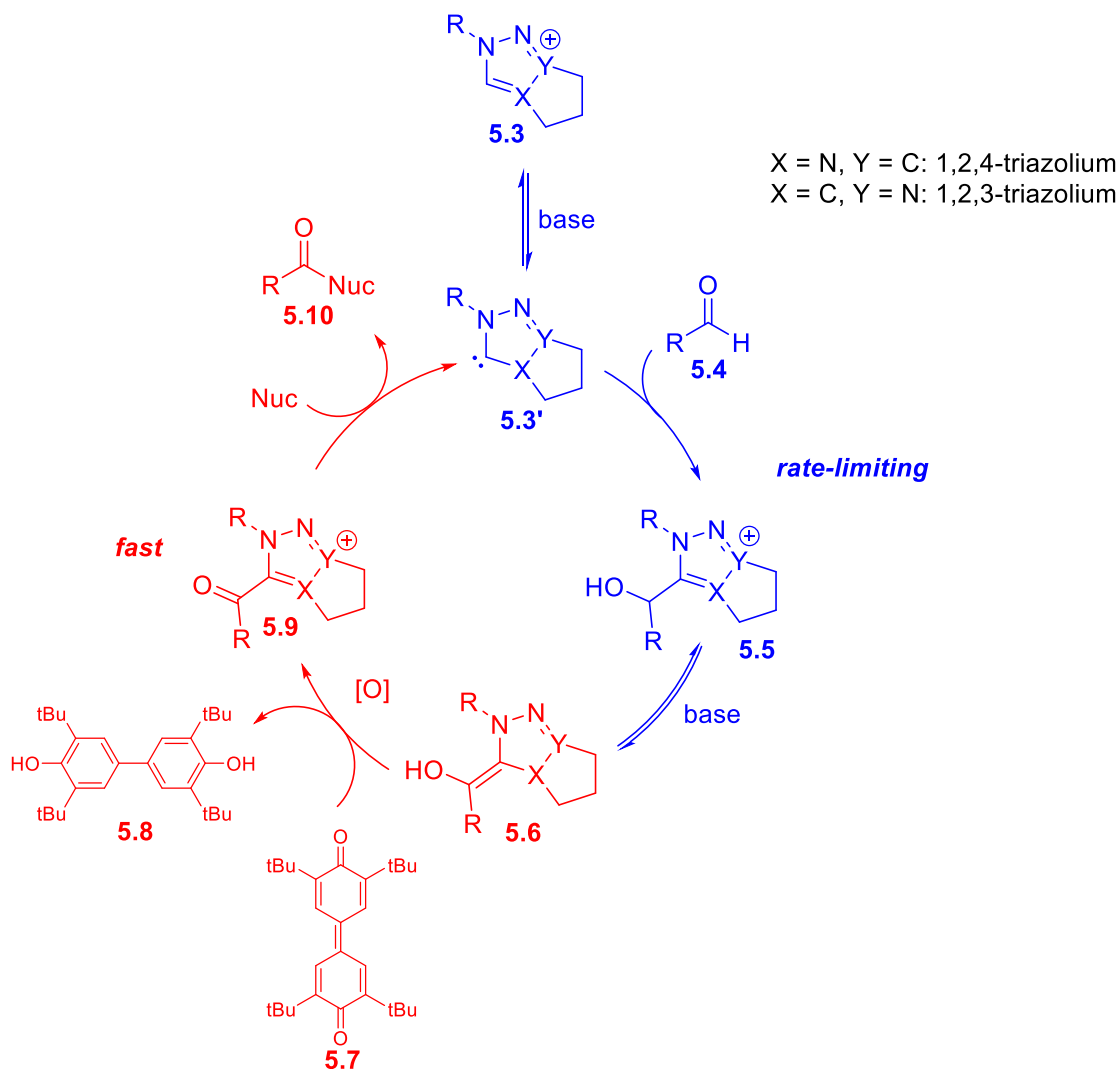
and they would be useful for identifying any potential off-cycle catalyst species that contribute to the observed catalyst deactivation.

5.2 Conclusions and future work – NHC-catalyzed oxidative acylation

In Chapter 3, the NHC-catalyzed oxidative acylation of aromatic aldehydes with sulfonamides and electron-poor *N*-nucleophiles was demonstrated, and mechanistic studies were conducted using ^1H NMR reaction monitoring techniques. From these studies, oxidative acylation with sulfonamides and electron-poor *N*-nucleophiles is successful because the catalyst exists in a reservoir of reversible off-cycle species, and the nucleophiles used are not strong enough to attack the empty p-orbital of the free carbene. On the contrary, benzylamine has been shown to form 2 carbene-benzylamine adducts that exist in equilibrium. These adducts are formed by nucleophilic attack of benzylamine into the empty p-orbital of the free carbene, which is possible due to the electron-withdrawing pentafluorophenyl group, increasing the electrophilicity of the ambiphilic carbene. In addition, a carbene-carbene condensation byproduct was isolated, demonstrating a possible catalyst deactivation pathway that does not involve benzylamine.

From the mechanistic work performed in Chapters 2 & 3, some generalizations can be made about oxidative NHC organocatalysis as a whole. In our work, we found that catalysts with both 1,2,3- and 1,2,4-triazolium scaffolds have similar resting states. Namely, nucleophilic addition of the carbene to the aldehyde substrate and isomerization to the Breslow intermediate are slow steps, whereas oxidation to the acyl azolium and capture by the nucleophile are fast and do not contribute to the observed rate equation. Isomerization of the initial carbene-aldehyde adduct to the Breslow intermediate is assisted by the base as a proton shuttle, which explains the positive order behavior of the base for catalysts with 1,2,3-triazolium scaffolds. Conversely, the same can

be said for catalysts with 1,2,4-triazolium scaffolds, however the massive rate increases observed with additional base were mostly due to the acidic nature of the sulfonamide product. These generalizations are summarized in Scheme 5.1.



Scheme 5.1: Generalized mechanism for oxidative NHC organocatalysis.

The *N*-acylsulfonamide moiety can be considered an isostere of the carboxylic acid functional group; both *N*-acylsulfonamides and carboxylic acids have pK_as in the range of 3.5-4.5, and the presence of N-H or O-H bonds allows for networks of hydrogen bonding. Due to these similarities with carboxylic acids, as well as their stability to hydrolysis, *N*-

acylsulfonamides have become compounds of interest for pharmaceutical development. Drug candidates have been developed that contain the *N*-acylsulfonamide moiety, including potent antibiotics and Hepatitis C virus inhibitors such as Asunaprevir¹⁴² (Figure 5.2). The NHC-catalyzed oxidative acylation of sulfonamides presented in Chapter 3 is a mild and efficient synthetic method that can potentially be used in the production of these drug candidates. One of the drawbacks of the NHC-catalyzed oxidative acylation reported in Chapter 3 is that it is specific for aryl aldehydes and aryl sulfonamides. Under the reported reaction conditions, aliphatic aldehydes are prone to enolization by DBU, and can participate in unwanted aldol reactions. Further work on optimizing this reaction can be done to find an NHC/base system that is amenable to aliphatic aldehydes. Such a system would most likely consist of an acidic NHC precursor with an electron-withdrawing *N*-substituent such as a pentafluorophenyl group, and a weak base such as sodium acetate, to minimize enolization of the aliphatic aldehyde.

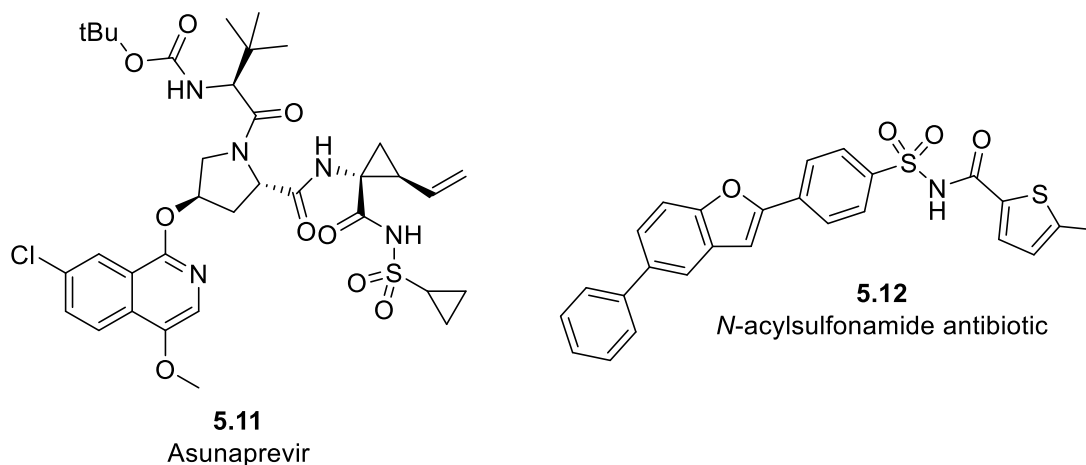


Figure 5.2: Pharmaceuticals containing the *N*-acylsulfonamide functionality.

5.3 Conclusions and future work – dihydropyrimidone synthesis

The work performed in Chapter 4 resulted in the development of a better, cleaner, and arguably more intriguing method of synthesizing precursors for isothioureas organocatalysts. One of the original goals of this work was to develop a resolution method for racemic HBTM, however the research direction was steered towards methodology and mechanistic analysis. The resolution of racemic HBTM is still a challenge that needs to be addressed, and future work can be done to solve this problem by developing salt screens that are amenable to diastereomeric resolution, or coupled preferential crystallization methods.

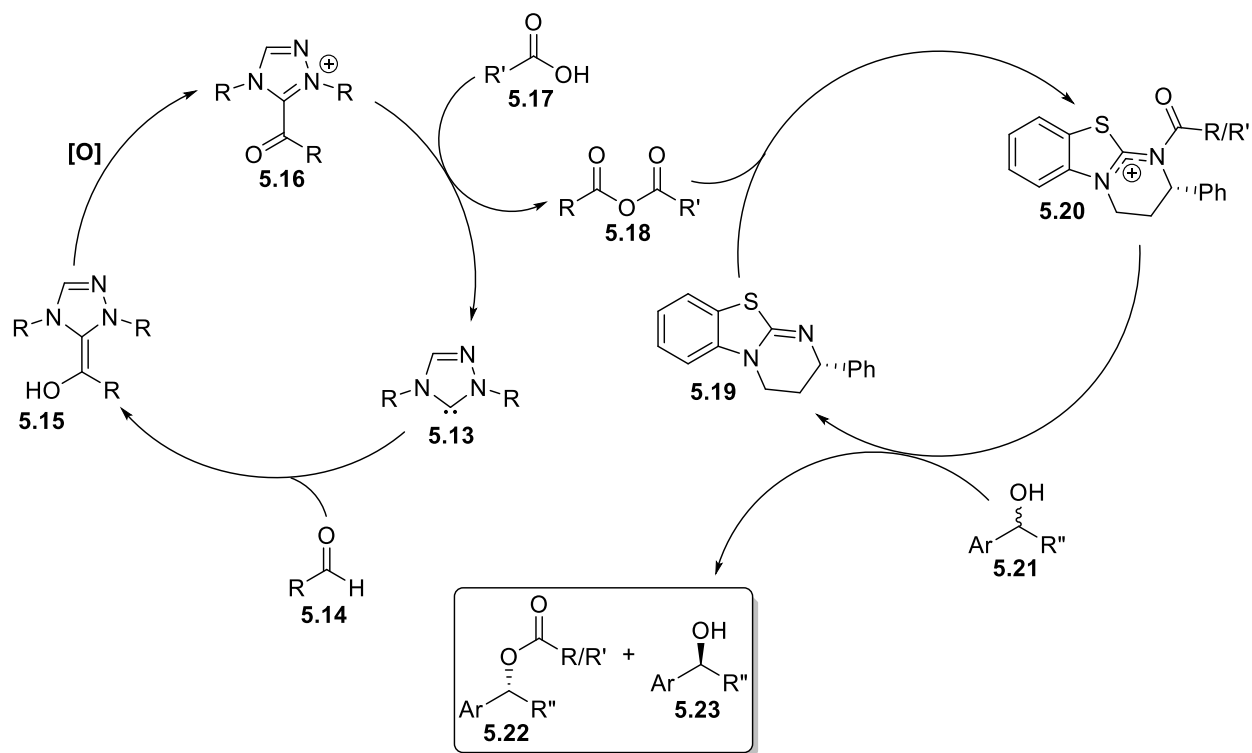
The mechanistic analysis performed in Chapter 4 is very rough and preliminary, and there are more questions that need to be addressed. One of these research questions involves rate differences in cyclization between acrylamide and acetamide starting materials. When acrylamide is used as starting material, it appears that it cyclizes faster than the acetamide, despite a common imide intermediate for both substrates. It is possible that this observation is a result of differing geometries of the starting materials. In the acrylamide, the acryloyl moiety could initially be in close physical proximity to the nucleophilic nitrogen, whereas in the acetamide, a bond rotation might have to take place before cyclization. Geometry optimizations of solvated molecules, and dihedral angle calculations during imide bond rotation could help answer these questions, as well as NOE experiments on imides generated *in situ* in an NMR tube.

5.4 NHC/TTU dual catalysis

Recently, cooperative catalytic systems have become a topic of great interest for researchers. By using two catalysts in the same pot that activate substrates in different ways, new ways of putting molecules together can be achieved. Lewis acid/NHC dual catalytic systems

have been reported, and the addition of a Lewis acid to the NHC system has resulted in enhanced enantioselectivities and reactivities. Lewis acid/ITU dual catalysis has also been reported, leading to chemical transformations that cannot be performed with one single catalyst. Dual NHC/amine organocatalysis is also known, which enables complex chemical transformations without the use of expensive, environmentally unfriendly, rare metal catalysts.

In Chapter 2, it was discovered that benzoic acid works surprisingly well as a weak nucleophile with oxidative NHC chemistry, forming benzoic anhydride *in situ*. This chemistry can be further developed by examining the substrate scope of both aldehyde and carboxylic acid, as well as optimization of catalyst, base, and solvent. This chemistry is particularly interesting due to the potential of generating mixed anhydrides *in situ* under very mild conditions. This also potentially opens up avenues for synergistic NHC/ITU organocatalysis, due to anhydrides being the most common electrophiles used in ITU catalysis. Scheme 5.2 shows a possible mechanistic model for this kind of catalysis. A potential problem lies in the nucleophilic selectivity of the ITU catalyst – with symmetrical anhydrides, only one ester product is possible, whereas with mixed anhydrides two ester products are possible, depending on which anhydride carbonyl the ITU attacks initially. To control this selectivity, selecting R or R' to have sufficient steric bulk will ensure that the ITU attacks the carbonyl with less steric bulk adjacent to it, giving a desired ester product. This also allows for more chemically diverse esters to be made, which can lead to easier separations for kinetic resolutions. To date, there have been no reports of NHC/ITU dual catalysis, and it would be a valuable addition to the established body of literature.



Scheme 5.2: Possible mode of dual catalysis with both NHCs and ITUs.

References

- (1) Wanzlick, H. W. *Angew. Chemie Int. Ed. English* **1962**, *1* (2), 75–80.
- (2) Scholl, M.; Ding, S.; Lee, C. W.; Grubbs, R. H. *Org. Lett.* **1999**, *1* (6), 953–956.
- (3) Voet, D.; Voet, J. G. *Biochemistry*, 3rd editio.; John Wiley & Sons: Hoboken, NJ, 2004.
- (4) Mizuhara, S.; Tamura, R.; Arata, H. *Proc. Jpn. Acad.* **1951**, *27*, 302–308.
- (5) Breslow, R. *J. Am. Chem. Soc.* **1958**, *80* (14), 3719–3726.
- (6) Lemal, D. M.; Lovald, R. A.; Kawano, K. I. *J. Am. Chem. Soc.* **1964**, *86* (12), 2518–2519.
- (7) Denk, M. K.; Hatano, K.; Ma, M. *Tetrahedron Lett.* **1999**, *40* (11), 2057–2060.
- (8) Arduengo, A. J.; Harlow, R. L.; Kline, M. *J. Am. Chem. Soc.* **1991**, *113* (1), 361–363.
- (9) Arduengo, A. J.; Dias, H. V. R.; Harlow, R. L.; Kline, M. *J. Am. Chem. Soc.* **1992**, *114* (14), 5530–5534.
- (10) Arduengo, A. J.; Goerlich, J. R.; Marshall, W. J. *J. Am. Chem. Soc.* **1995**, *117* (44), 11027–11028.
- (11) Arduengo, A. J.; Davidson, F.; Dias, H. V. R.; Goerlich, J. R.; Khasnis, D.; Marshall, W. J.; Prakasha, T. K. *J. Am. Chem. Soc.* **1997**, *119* (52), 12742–12749.
- (12) Enders, D.; Breuer, K.; Raabe, G.; Runsink, J.; Teles, J. H.; Melder, J.; Ebel, K.; Brode, S. *Angew. Chemie Int. Ed. English* **1995**, *34* (9), 1021–1023.
- (13) Chu, Y.; Deng, H.; Cheng, J.-P. *J. Org. Chem.* **2007**, *72* (20), 7790–7793.
- (14) Higgins, E. M.; Sherwood, J. A.; Lindsay, A. G.; Armstrong, J.; Massey, R. S.; Alder, R. W.; O'Donoghue, A. C. *Chem. Commun.* **2011**, *47* (5), 1559–1561.
- (15) Massey, R. S.; Collett, C. J.; Lindsay, A. G.; Smith, A. D.; O'Donoghue, A. C. *J. Am. Chem. Soc.* **2012**, *134* (50), 20421–20432.

- (16) Olmstead, W. N.; Bordwell, F. G. *J. Org. Chem.* **1980**, *45* (16), 3299–3305.
- (17) Trotaş, I.-T.; Zimmermann, T.; Schüth, F. *Chem. Rev.* **2014**, *114* (3), 1761–1782.
- (18) Mayr, H.; Ofial, A. R. *J. Phys. Org. Chem.* **2008**, *21* (7–8), 584–595.
- (19) Maji, B.; Breugst, M.; Mayr, H. *Angew. Chemie Int. Ed.* **2011**, *50* (30), 6915–6919.
- (20) Levens, A.; An, F.; Breugst, M.; Mayr, H.; Lupton, D. W. *Org. Lett.* **2016**, *18* (15), 3566–3569.
- (21) Flanigan, D. M.; Romanov-Michailidis, F.; White, N. A.; Rovis, T. *Chem. Rev.* **2015**, *115* (17), 9307–9387.
- (22) Sheehan, J. C.; Hara, T. *J. Org. Chem.* **1974**, *39* (9), 1196–1199.
- (23) Pesch, J.; Harms, K.; Bach, T. *European J. Org. Chem.* **2004**, *2004* (9), 2025–2035.
- (24) Kuhn, K. M.; Grubbs, R. H. *Org. Lett.* **2008**, *10* (10), 2075–2077.
- (25) Benhamou, L.; César, V.; Gornitzka, H.; Lugan, N.; Lavigne, G. *Chem. Commun.* **2009**, No. 31, 4720.
- (26) Bertogg, A.; Camponovo, F.; Togni, A. *Eur. J. Inorg. Chem.* **2005**, *2005* (2), 347–356.
- (27) Calder, I. C.; Spotswood, T. M.; Sasse, W. H. P. *Tetrahedron Lett.* **1963**, *4* (2), 95–100.
- (28) Arduengo, A. J.; Krafczyk, R.; Schmutzler, R.; Craig, H. A.; Goerlich, J. R.; Marshall, W. J.; Unverzagt, M. *Tetrahedron* **1999**, *55* (51), 14523–14534.
- (29) Glorius, F.; Altenhoff, G.; Goddard, R.; Lehmann, C. *Chem. Commun.* **2002**, No. 22, 2704–2705.
- (30) Bildstein, B.; Malaun, M.; Kopacka, H.; Wurst, K.; Mitterböck, M.; Ongania, K.-H.; Opromolla, G.; Zanello, P. *Organometallics* **1999**, *18* (21), 4325–4336.
- (31) Oertel, A.; Ritleng, V.; Chetcuti, M. *Synthesis (Stuttg.)* **2009**, *2009* (10), 1647–1650.
- (32) Enders, D.; Breuer, K.; Kallfass, U.; Balensiefer, T. *Synthesis (Stuttg.)* **2003**, *2003* (08),

1292–1295.

- (33) Knight, R. L.; Leeper, F. J. *J. Chem. Soc. Perkin Trans. I* **1998**, No. 12, 1891–1894.
- (34) Enders, D.; Kallfass, U. *Angew. Chemie Int. Ed.* **2002**, *41* (10), 1743–1745.
- (35) Kerr, M. S.; Read de Alaniz, J.; Rovis, T. *J. Org. Chem.* **2005**, *70* (14), 5725–5728.
- (36) Struble, J. R.; Bode, J. W. *Org. Synth.* **2010**, *87*, 362.
- (37) Seebach, D. *Angew. Chemie Int. Ed. English* **1979**, *18* (4), 239–258.
- (38) Wöhler, F.; Liebig, J. von. *Ann. der Pharm.* **1832**, *3* (3), 249–282.
- (39) Lapworth, A. *J. Chem. Soc., Trans.* **1903**, *83*, 995–1005.
- (40) Ukai, T.; Tanaka, R.; Dokawa, T. *J. Pharm. Soc. Japan* **1943**, *63*, 296–304.
- (41) Castells, J.; Lopez-Calahorra, F.; Domingo, L. *J. Org. Chem.* **1988**, *53* (19), 4433–4436.
- (42) Castells, J.; López-Calahorra, F.; Geijo, F.; Pérez-Dolz, R.; Bassedas, M. *J. Heterocycl. Chem.* **1986**, *23* (3), 715–720.
- (43) Breslow, R.; Kim, R. *Tetrahedron Lett.* **1994**, *35* (5), 699–702.
- (44) Van Den Berg, H. J.; Challa, G.; Pandit, U. K. *J. Mol. Catal.* **1989**, *51* (1), 1–12.
- (45) López-Calahorra, F.; Rubires, R. *Tetrahedron* **1995**, *51* (35), 9713–9728.
- (46) Breslow, R.; Schmuck, C. *Tetrahedron Lett.* **1996**, *37* (45), 8241–8242.
- (47) Rehbein, J.; Ruser, S.-M.; Phan, J. *Chem. Sci.* **2015**, *6* (10), 6013–6018.
- (48) Alwarsh, S.; Xu, Y.; Qian, S. Y.; McIntosh, M. C. *Angew. Chemie Int. Ed.* **2016**, *55* (1), 355–358.
- (49) Jordan, F.; Kudzin, Z. H.; Rios, C. B. *J. Am. Chem. Soc.* **1987**, *109* (14), 4415–4416.
- (50) Metzger, J.; Larive, H.; Dennilauler, R.; Baralle, R.; Gaurat, C. *Bull. Soc. Chim. Fr.* **1964**, 2857–2867.
- (51) Berkessel, A.; Elfert, S.; Etzenbach-Effers, K.; Teles, J. H. *Angew. Chem. Int. Ed. Engl.*

- 2010**, 49 (39), 7120–7124.
- (52) Alwarsh, S.; Ayinuola, K.; Dormi, S. S.; McIntosh, M. C. *Org. Lett.* **2013**, 15 (1), 3–5.
- (53) DiRocco, D. a; Oberg, K. M.; Rovis, T. *J. Am. Chem. Soc.* **2012**, 134 (14), 6143–6145.
- (54) Berkessel, A.; Yatham, V. R.; Elfert, S.; Neudörfl, J.-M. *Angew. Chemie Int. Ed.* **2013**, 52 (42), 11158–11162.
- (55) Sheehan, J. C.; Hunneman, D. H. *J. Am. Chem. Soc.* **1966**, 88 (15), 3666–3667.
- (56) Baragwanath, L.; Rose, C. A.; Zeitler, K.; Connon, S. J. *J. Org. Chem.* **2009**, 74 (23), 9214–9217.
- (57) Jin, M. Y.; Kim, S. M.; Han, H.; Ryu, D. H.; Yang, J. W. *Org. Lett.* **2011**, 13 (5), 880–883.
- (58) Jin, M. Y.; Kim, S. M.; Mao, H.; Ryu, D. H.; Song, C. E.; Yang, J. W. *Org. Biomol. Chem.* **2014**, 12 (10), 1547–1550.
- (59) Langdon, S. M.; Wilde, M. M. D.; Thai, K.; Gravel, M. *J. Am. Chem. Soc.* **2014**, 136 (21), 7539–7542.
- (60) Stetter, H.; Schreckenberger, M. *Angew. Chemie Int. Ed. English* **1973**, 12 (1), 81–81.
- (61) Stetter, H. *Angew. Chemie Int. Ed. English* **1976**, 15 (11), 639–647.
- (62) Schedler, M.; Wang, D.-S.; Glorius, F. *Angew. Chemie Int. Ed.* **2013**, 52 (9), 2585–2589.
- (63) Ciganek, E. *Synthesis (Stuttg.)*. **1995**, 1995 (10), 1311–1314.
- (64) Enders, D.; Breuer, K.; Runsink, J.; Teles, J. H. *Helv. Chim. Acta* **1996**, 79 (7), 1899–1902.
- (65) Sohn, S. S.; Rosen, E. L.; Bode, J. W. *J. Am. Chem. Soc.* **2004**, 126 (44), 14370–14371.
- (66) Burstein, C.; Glorius, F. *Angew. Chemie Int. Ed.* **2004**, 43 (45), 6205–6208.
- (67) Cardinal-David, B.; Raup, D. E. a; Scheidt, K. a. *J. Am. Chem. Soc.* **2010**, 132 (15), 5345–

- 5347.
- (68) Nair, V.; Vellalath, S.; Poonoth, M.; Mohan, R.; Suresh, E. *Org. Lett.* **2006**, 8 (3), 507–509.
- (69) Dugal-Tessier, J.; O'Bryan, E. A.; Schroeder, T. B. H.; Cohen, D. T.; Scheidt, K. A. *Angew. Chemie Int. Ed.* **2012**, 51 (20), 4963–4967.
- (70) Nair, V.; Vellalath, S.; Poonoth, M.; Suresh, E. *J. Am. Chem. Soc.* **2006**, 128 (27), 8736–8737.
- (71) He, M.; Bode, J. W. *Org. Lett.* **2005**, 7 (14), 3131–3134.
- (72) Rommel, M.; Fukuzumi, T.; Bode, J. W. *J. Am. Chem. Soc.* **2008**, 130 (51), 17266–17267.
- (73) Sohn, S. S.; Bode, J. W. *Org. Lett.* **2005**, 7 (18), 3873–3876.
- (74) Grasa, G. A.; Güveli, T.; Singh, R.; Nolan, S. P. *J. Org. Chem.* **2003**, 68 (7), 2812–2819.
- (75) Chan, A.; Scheidt, K. A. *Org. Lett.* **2005**, 7 (5), 905–908.
- (76) Zeitler, K. *Org. Lett.* **2006**, 8 (4), 637–640.
- (77) Chow, K. Y.-K.; Bode, J. W. *J. Am. Chem. Soc.* **2004**, 126 (26), 8126–8127.
- (78) Sohn, S. S.; Bode, J. W. *Angew. Chem. Int. Ed. Engl.* **2006**, 45 (36), 6021–6024.
- (79) Reynolds, N. T.; Read de Alaniz, J.; Rovis, T. *J. Am. Chem. Soc.* **2004**, 126 (31), 9518–9519.
- (80) Guin, J.; De Sarkar, S.; Grimme, S.; Studer, A. *Angew. Chem. Int. Ed. Engl.* **2008**, 47 (45), 8727–8730.
- (81) De Sarkar, S.; Grimme, S.; Studer, A. *J. Am. Chem. Soc.* **2010**, 132 (4), 1190–1191.
- (82) De Sarkar, S.; Studer, A. *Org. Lett.* **2010**, 12 (9), 1992–1995.
- (83) Iwahana, S.; Iida, H.; Yashima, E. *Chem. a Eur. J.* **2011**, 17 (29), 8009–8013.
- (84) De Sarkar, S.; Biswas, A.; Song, C.; Studer, A. *Synthesis (Stuttg.)* **2011**, 2011 (12), 1974–

- 1983.
- (85) Chung, R.; Vo, A.; Hein, J. E. *ACS Catal.* **2017**, 7 (4), 2505–2510.
- (86) Susanne, F.; Smith, D. S.; Codina, A. *Org. Process Res. Dev.* **2012**, 16 (1), 61–64.
- (87) Hoye, T. R.; Eklov, B. M.; Ryba, T. D.; Voloshin, M.; Yao, L. J. *Org. Lett.* **2004**, 6 (6), 953–956.
- (88) Christianson, M. D.; Tan, E. H. P.; Landis, C. R. *J. Am. Chem. Soc.* **2010**, 132 (33), 11461–11463.
- (89) Foley, D. A.; Dunn, A. L.; Zell, M. T. *Magn. Reson. Chem.* **2016**, 54 (6), 451–456.
- (90) Schuster, O.; Yang, L.; Raubenheimer, H. G.; Albrecht, M. *Chem. Rev.* **2009**, 109 (8), 3445–3478.
- (91) Mathew, P.; Neels, A.; Albrecht, M. *J. Am. Chem. Soc.* **2008**, No. 130, 13534–13535.
- (92) Bouffard, J.; Keitz, B. K.; Tonner, R.; Lavallo, V.; Guisado-Barrios, G.; Frenking, G.; Grubbs, R. H.; Bertrand, G. *Organometallics* **2011**, 30 (9), 2617–2627.
- (93) Guisado-Barrios, G.; Bouffard, J.; Donnadiou, B.; Bertrand, G. *Angew. Chemie* **2010**, 122 (28), 4869–4872.
- (94) Donnelly, K. F.; Petronilho, A.; Albrecht, M. *Chem. Commun.* **2013**, 49 (12), 1145–1159.
- (95) Hein, J. E.; Fokin, V. V. *Chem. Soc. Rev.* **2010**, 39 (4), 1302.
- (96) Zhang, L.; Chen, X.; Xue, P.; Sun, H. H. Y.; Williams, I. D.; Sharpless, K. B.; Fokin, V. V.; Jia, G. .
- (97) Rostovtsev, V. V.; Green, L. G.; Fokin, V. V.; Sharpless, K. B. *Angew. Chemie Int. Ed.* **2002**, 41 (14), 2596–2599.
- (98) Mahatthananchai, J.; Bode, J. W. *Chem. Sci.* **2012**, 3 (1), 192.
- (99) Tseng, M.-C.; Cheng, H.-T.; Shen, M.-J.; Chu, Y.-H. *Org. Lett.* **2011**, 13 (16), 4434–4437.

- (100) Chan, A.; Scheidt, K. a. *J. Am. Chem. Soc.* **2006**, *128* (14), 4558–4559.
- (101) Jang, Y. H.; Youn, S. W. *Org. Lett.* **2014**, *16* (14), 3720–3723.
- (102) Hein, J. E.; Krasnova, L. B.; Iwasaki, M.; Fokin, V. V. *Org. Synth.* **2011**, *88*, 238–246.
- (103) Mamane, V.; Aubert, E.; Fort, Y. *J. Org. Chem.* **2007**, *72* (19), 7294–7300.
- (104) Das, A.; Chaudhuri, R.; Liu, R.-S. *Chem. Commun. (Camb).* **2009**, No. 27, 4046–4048.
- (105) Rose, C. a; Zeitler, K. *Org. Lett.* **2010**, *12* (20), 4552–4555.
- (106) Maji, B.; Mayr, H. *Angew. Chemie Int. Ed.* **2012**, *51* (41), 10408–10412.
- (107) Langdon, S. M.; Legault, C. Y.; Gravel, M. *J. Org. Chem.* **2015**, *80* (7), 3597–3610.
- (108) Valeur, E.; Bradley, M. *Chem. Soc. Rev.* **2009**, *38* (2), 606–631.
- (109) Seo, S.; Marks, T. J. *Org. Lett.* **2008**, *10* (2), 317–319.
- (110) Suto, Y.; Yamagiwa, N.; Torisawa, Y. *Tetrahedron Lett.* **2008**, *49* (40), 5732–5735.
- (111) Wu, Z.; Hull, K. L. *Chem. Sci.* **2016**, *7* (2), 969–975.
- (112) Ghosh, S. C.; Ngiam, J. S. Y.; Seayad, A. M.; Tuan, D. T.; Chai, C. L. L.; Chen, A. J. *Org. Chem.* **2012**, *77* (18), 8007–8015.
- (113) De Sarkar, S.; Biswas, A.; Samanta, R. C.; Studer, A. *Chem. - A Eur. J.* **2013**, *19* (15), 4664–4678.
- (114) Taylor, J. E.; Bull, S. D.; Williams, J. M. J. *Chem. Soc. Rev.* **2012**, *41* (6), 2109.
- (115) Kaupmees, K.; Trummal, A.; Leito, I. *Croat. Chem. Acta* **2014**, *87* (4), 385–395.
- (116) Williams, D. B. G.; Lawton, M. *J. Org. Chem.* **2010**, *75* (24), 8351–8354.
- (117) Baxter, R. D.; Sale, D.; Engle, K. M.; Yu, J.; Blackmond, D. G. **2012**.
- (118) Blackmond, D. G. *Angew. Chem. Int. Ed. Engl.* **2005**, *44* (28), 4302–4320.
- (119) Kaeobamrung, J.; Mahatthananchai, J.; Zheng, P.; Bode, J. W. *J. Am. Chem. Soc.* **2010**, *132* (26), 8810–8812.

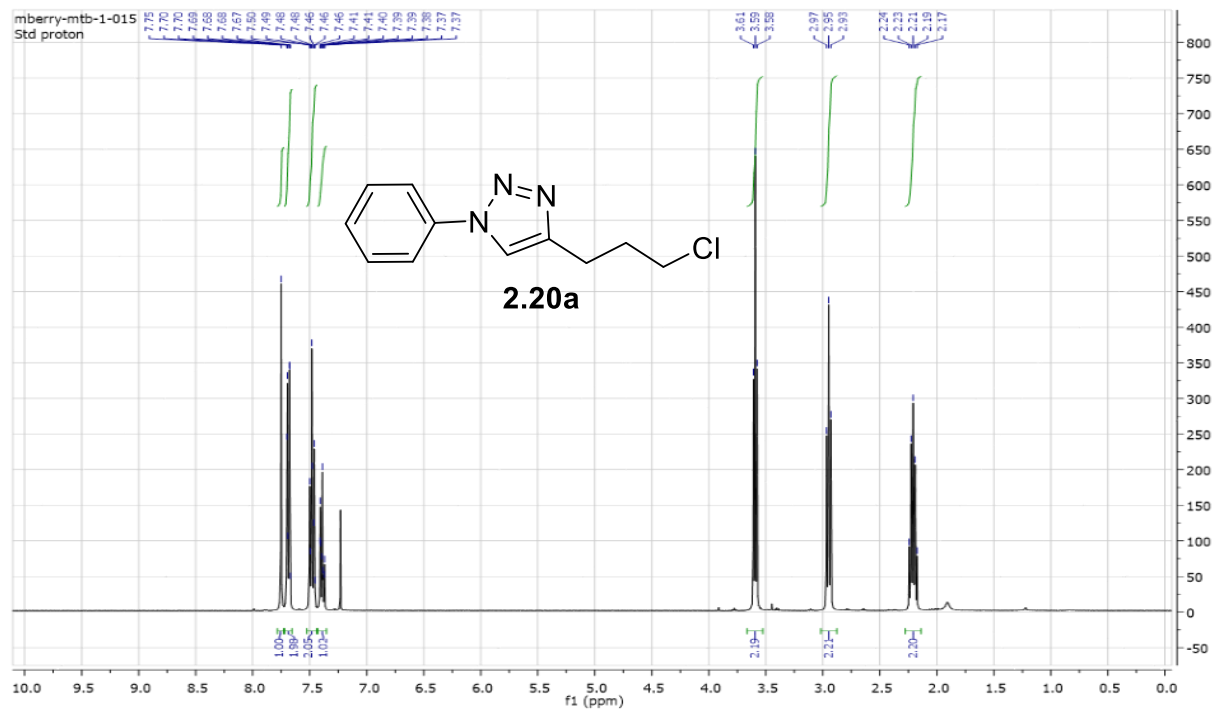
- (120) PERRIN, D. D. In *Ionisation Constants of Inorganic Acids and Bases in Aqueous Solution*; Elsevier, 1982; pp 1–138.
- (121) Harris, D. *Quantitative Chemical Analysis*, 8 ed.; W. H. Freeman and Company: New York, 2010.
- (122) Höfle, G.; Steglich, W.; Vorbrüggen, H. *Angew. Chemie Int. Ed. English* **1978**, *17* (8), 569–583.
- (123) Ruble, J. C.; Latham, H. A.; Fu, G. C. *J. Am. Chem. Soc.* **1997**, *119* (6), 1492–1493.
- (124) Spivey, A. C.; Fekner, T.; Spey, S. E. *J. Org. Chem.* **2000**, *65* (10), 3154–3159.
- (125) Birman, V. B.; Uffman, E. W.; Jiang, H.; Li, X.; Kilbane, C. J. *J. Am. Chem. Soc.* **2004**, *126* (39), 12226–12227.
- (126) Birman, V. B.; Jiang, H. *Org. Lett.* **2005**, *7* (16), 3445–3447.
- (127) Birman, V. B.; Li, X. *Org. Lett.* **2006**, *8* (7), 1351–1354.
- (128) Birman, V. B.; Li, X. *Org. Lett.* **2008**, *10* (6), 1115–1118.
- (129) Zhang, Y.; Birman, V. B. *Adv. Synth. Catal.* **2009**, *351* (14–15), 2525–2529.
- (130) Joannesse, C.; Johnston, C. P.; Concellón, C.; Simal, C.; Philp, D.; Smith, A. D. *Angew. Chemie Int. Ed.* **2009**, *48* (47), 8914–8918.
- (131) Wagner, A. J.; Rychnovsky, S. D. *Org. Lett.* **2013**, *15* (21), 5504–5507.
- (132) Robinson, E. R. T.; Walden, D. M.; Fallan, C.; Greenhalgh, M. D.; Cheong, P. H.-Y.; Smith, A. D. *Chem. Sci.* **2016**, *7* (12), 6919–6927.
- (133) Liu, G.; Shirley, M. E.; Van, K. N.; McFarlin, R. L.; Romo, D. *Nat. Chem.* **2013**, *5* (12), 1049–1057.
- (134) Smith, S. R.; Douglas, J.; Prevet, H.; Shapland, P.; Slawin, A. M. Z.; Smith, A. D. *J. Org. Chem.* **2014**, *79* (4), 1626–1639.

- (135) Joannesse, C.; Johnston, C. P.; Morrill, L. C.; Woods, P. A.; Kieffer, M.; Nigst, T. A.; Mayr, H.; Lebl, T.; Philp, D.; Bragg, R. A.; Smith, A. D. *Chem. - A Eur. J.* **2012**, *18* (8), 2398–2408.
- (136) Matviitsuk, A.; Greenhalgh, M. D.; Antúnez, D.-J. B.; Slawin, A. M. Z.; Smith, A. D. *Angew. Chemie* **2017**, *129* (40), 12450–12455.
- (137) Ranieri, B.; Robles, O.; Romo, D. *J. Org. Chem.* **2013**, *78* (12), 6291–6296.
- (138) Movsisyan, M.; Heugebaert, T. S. A.; Dams, R.; Stevens, C. V. *ChemSusChem* **2016**, *9* (15), 1945–1952.
- (139) Chung, R.; Yu, D.; Thai, V. T.; Jones, A. F.; Veits, G. K.; Read de Alaniz, J.; Hein, J. E. *ACS Catal.* **2015**, *5* (8), 4579–4585.
- (140) Greco, C. V.; Warchol, J. F. *J. Org. Chem.* **1971**, *36* (4), 604–607.
- (141) Khotavivattana, T.; Verhoog, S.; Tredwell, M.; Pfeifer, L.; Calderwood, S.; Wheelhouse, K.; Lee Collier, T.; Gouverneur, V. *Angew. Chemie Int. Ed.* **2015**, *54* (34), 9991–9995.
- (142) Ammazalorso, A.; De Filippis, B.; Giampietro, L.; Amoroso, R. *Chem. Biol. Drug Des.* **2017**, *90* (6), 1094–1105.
- (143) Bruker AXS Inc.: Madison, Wisconsin, USA 1997.
- (144) Krause, L.; Herbst-Irmer, R.; Sheldrick, G. M.; Stalke, D. *J. Appl. Crystallogr.* **2015**, *48* (1), 3–10.
- (145) Sheldrick, G. M. *Acta Crystallogr. Sect. A Found. Adv.* **2015**, *71* (1), 3–8.
- (146) Sheldrick, G. M. *Acta Crystallogr. Sect. C Struct. Chem.* **2015**, *71* (1), 3–8.
- (147) Dolomanov, O. V.; Bourhis, L. J.; Gildea, R. J.; Howard, J. A. K.; Puschmann, H. *J. Appl. Crystallogr.* **2009**, *42* (2), 339–341.

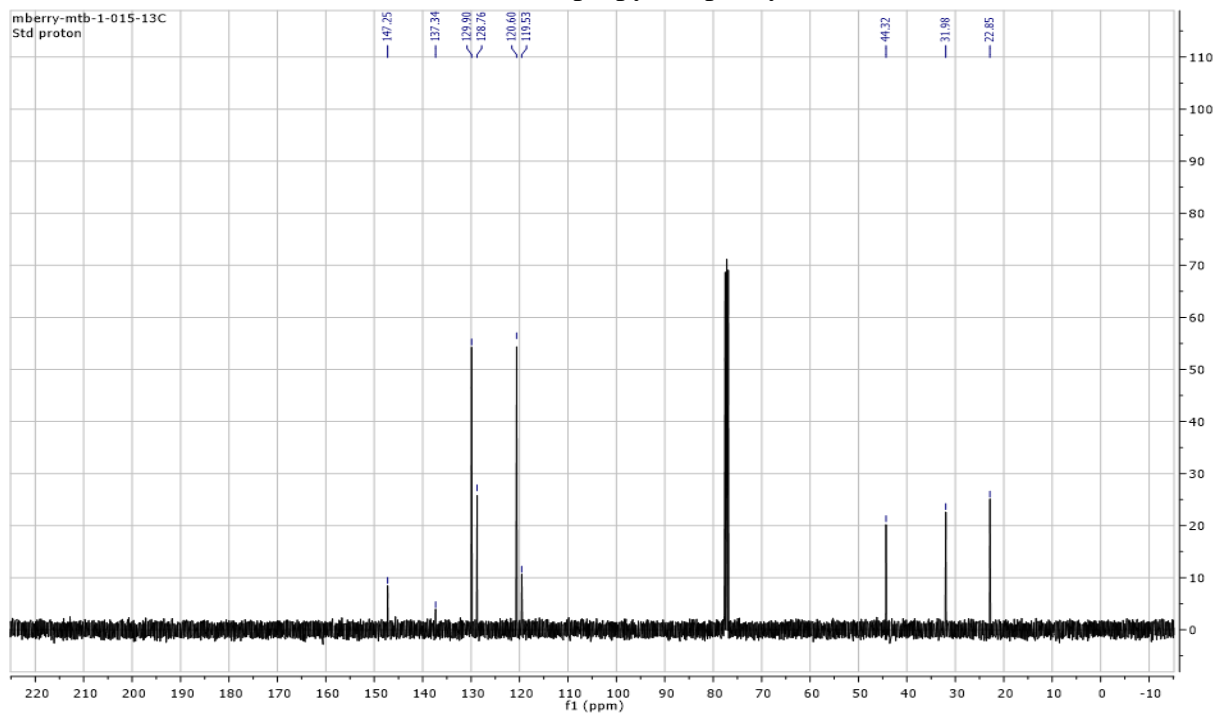
Appendices

Appendix A NMR Spectra from Chapter 2

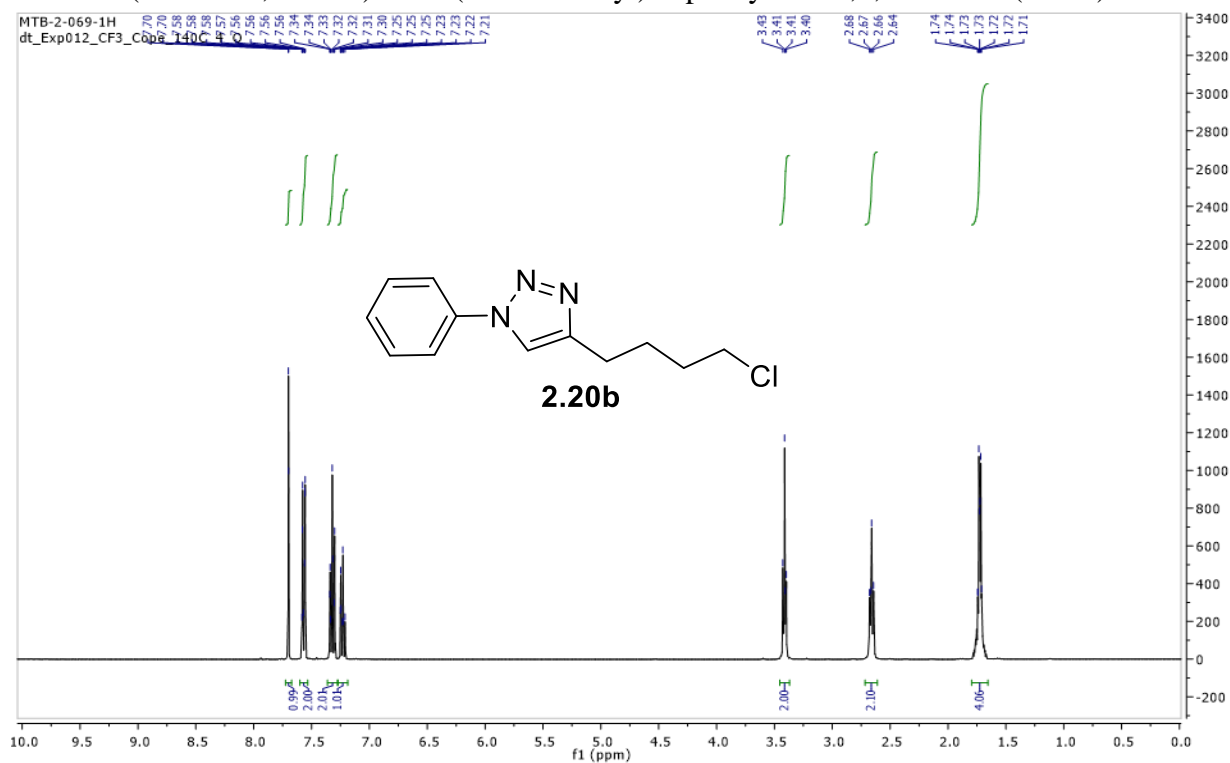
^1H NMR (400 MHz, CDCl_3) for 4-(3-chloropropyl)-1-phenyl-1H-1,2,3-triazole (**2.20a**):



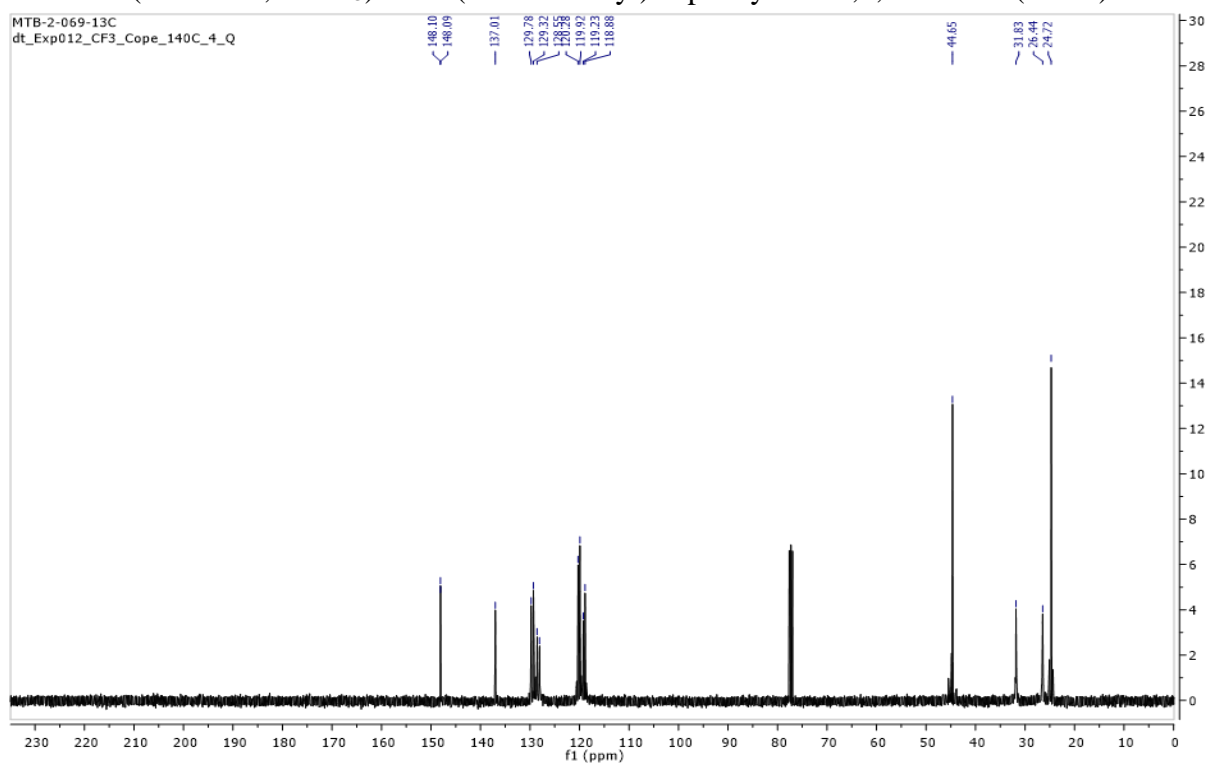
^{13}C NMR (100 MHz, CDCl_3) for 4-(3-chloropropyl)-1-phenyl-1H-1,2,3-triazole (**2.20a**):



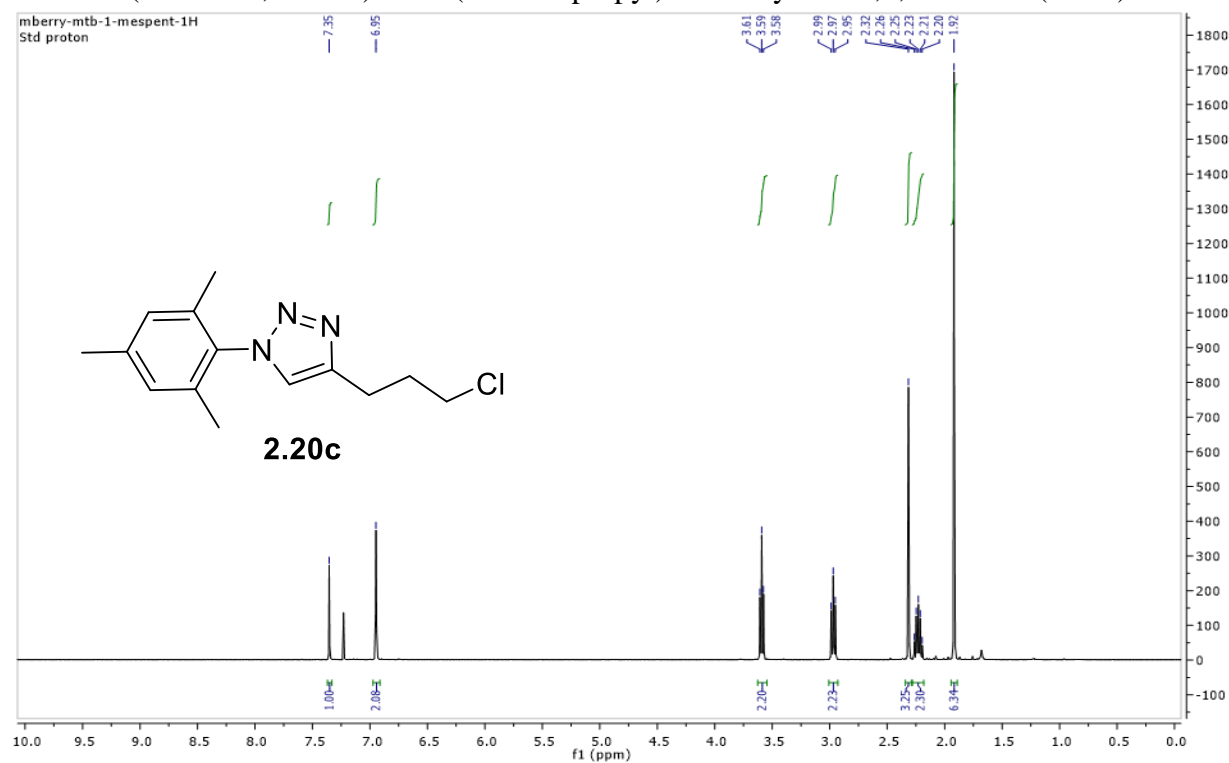
^1H NMR (400 MHz, CDCl_3) for 4-(4-chlorobutyl)-1-phenyl-1H-1,2,3-triazole (**2.20b**):



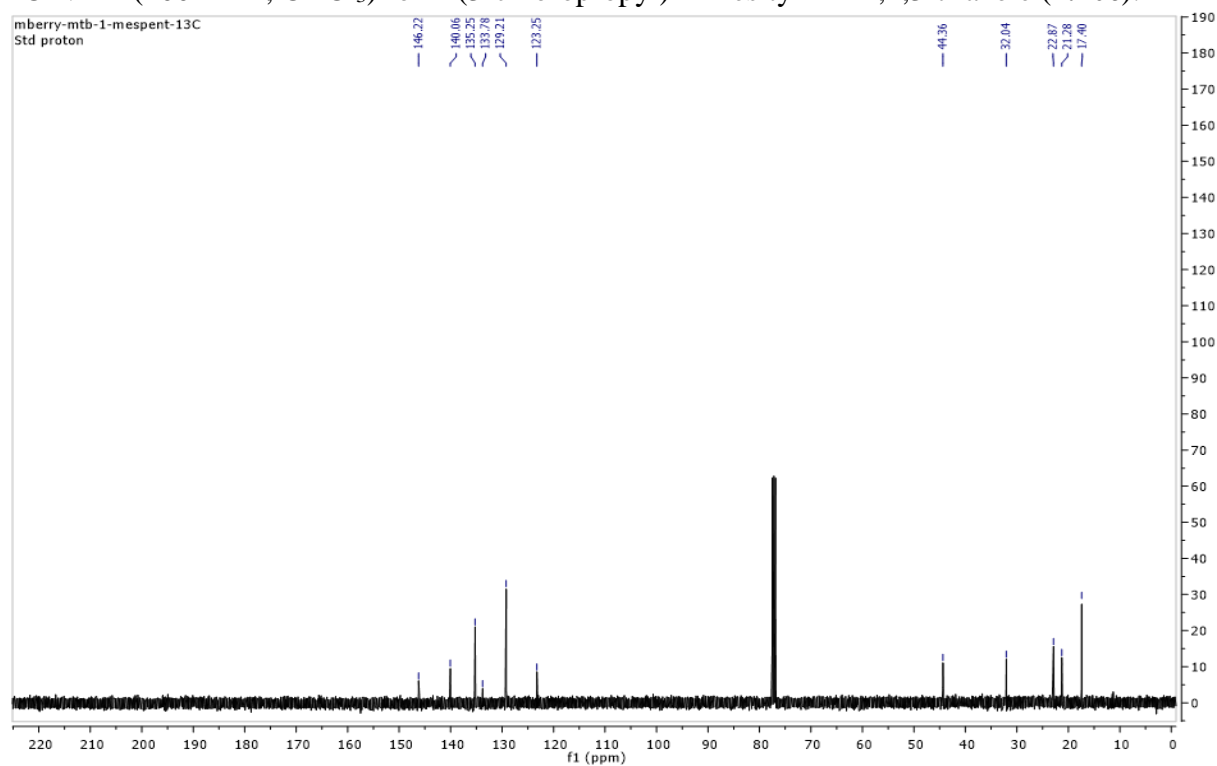
^{13}C NMR (100 MHz, CDCl_3) for 4-(4-chlorobutyl)-1-phenyl-1H-1,2,3-triazole (**2.20b**):



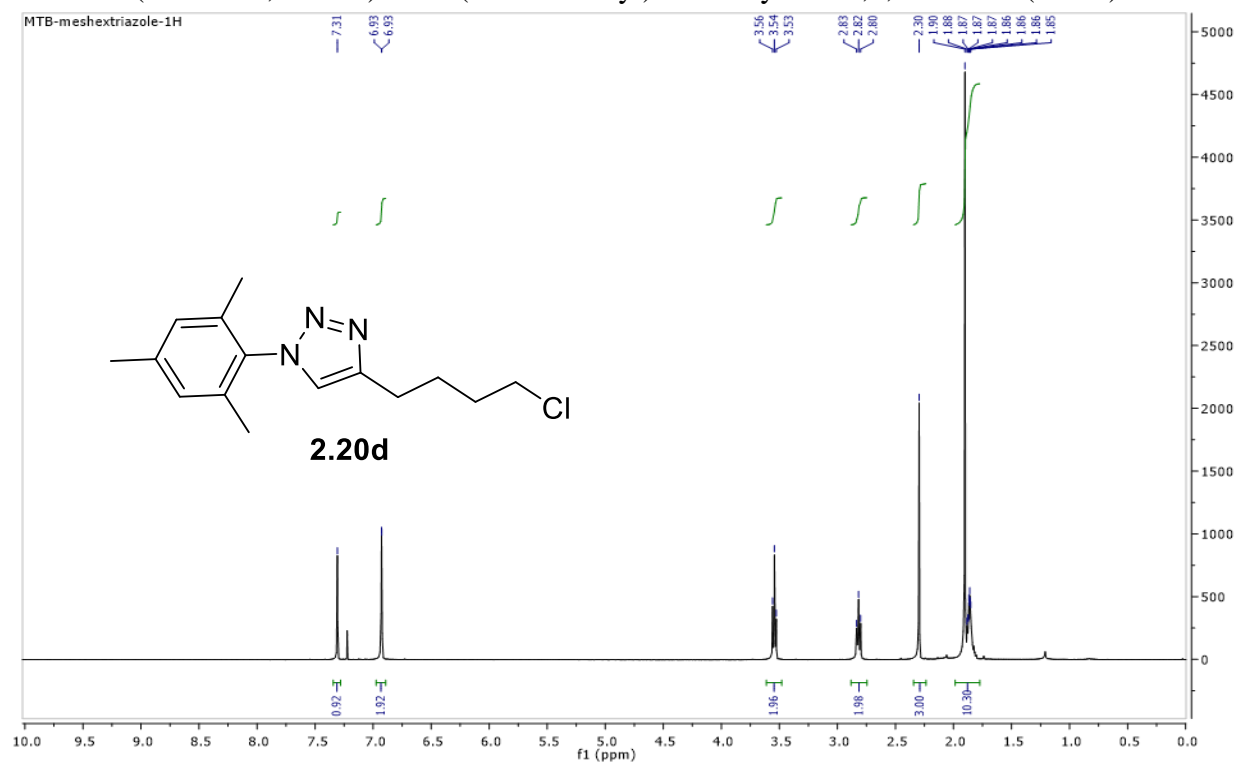
^1H NMR (400 MHz, CDCl_3) for 4-(3-chloropropyl)-1-mesityl-1H-1,2,3-triazole (**2.20c**):



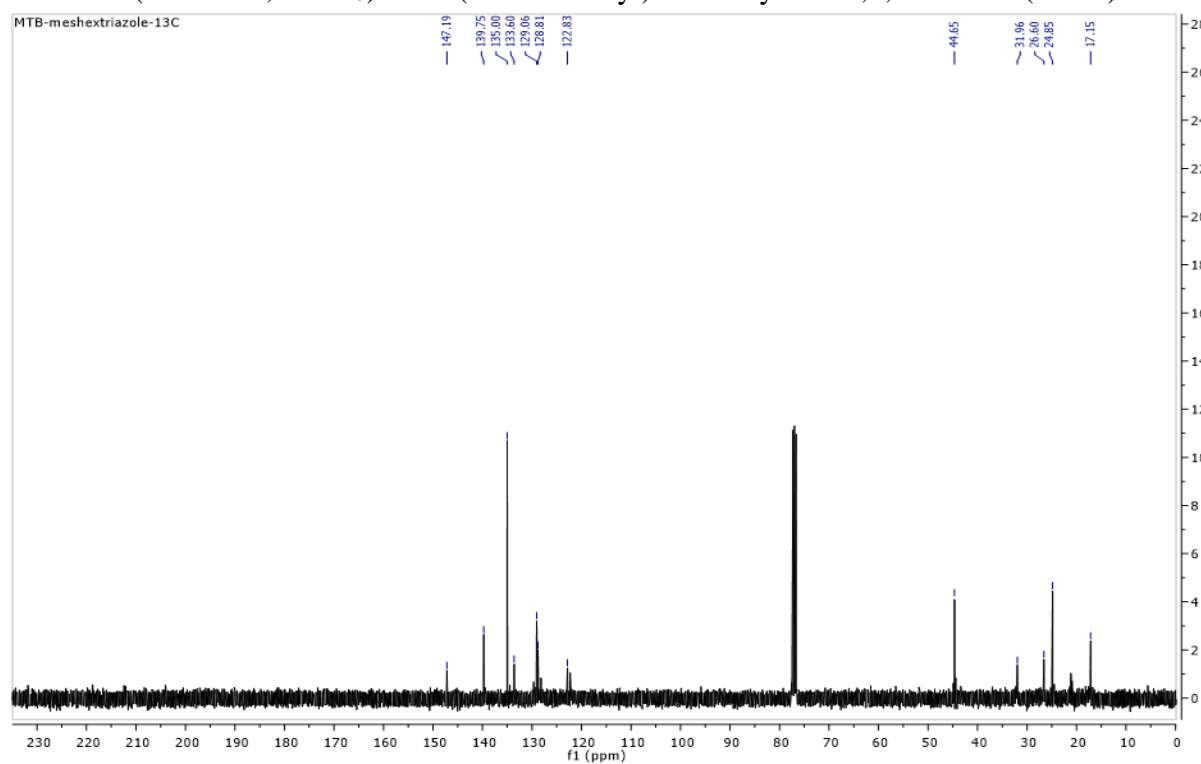
^{13}C NMR (100 MHz, CDCl_3) for 4-(3-chloropropyl)-1-mesityl-1H-1,2,3-triazole (**2.20c**):



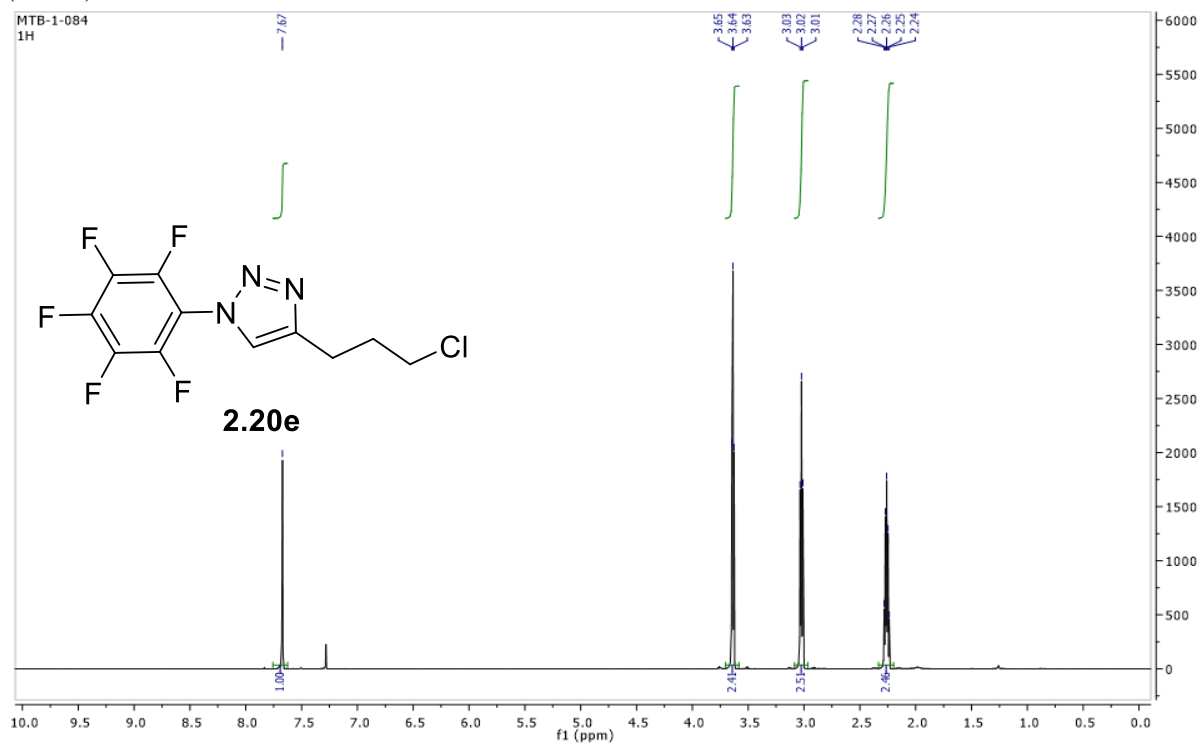
^1H NMR (400 MHz, CDCl_3) for 4-(4-chlorobutyl)-1-mesityl-1H-1,2,3-triazole (**2.20d**):



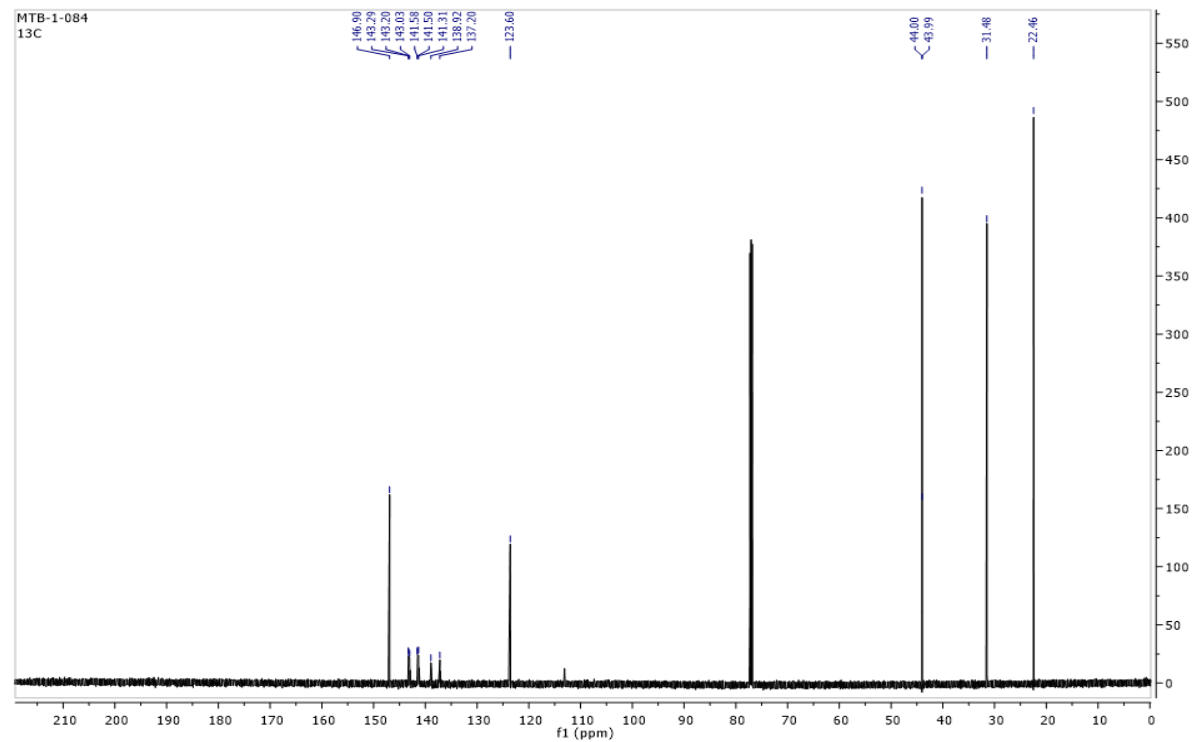
^{13}C NMR (100 MHz, CDCl_3) for 4-(4-chlorobutyl)-1-mesityl-1H-1,2,3-triazole (**2.20d**):



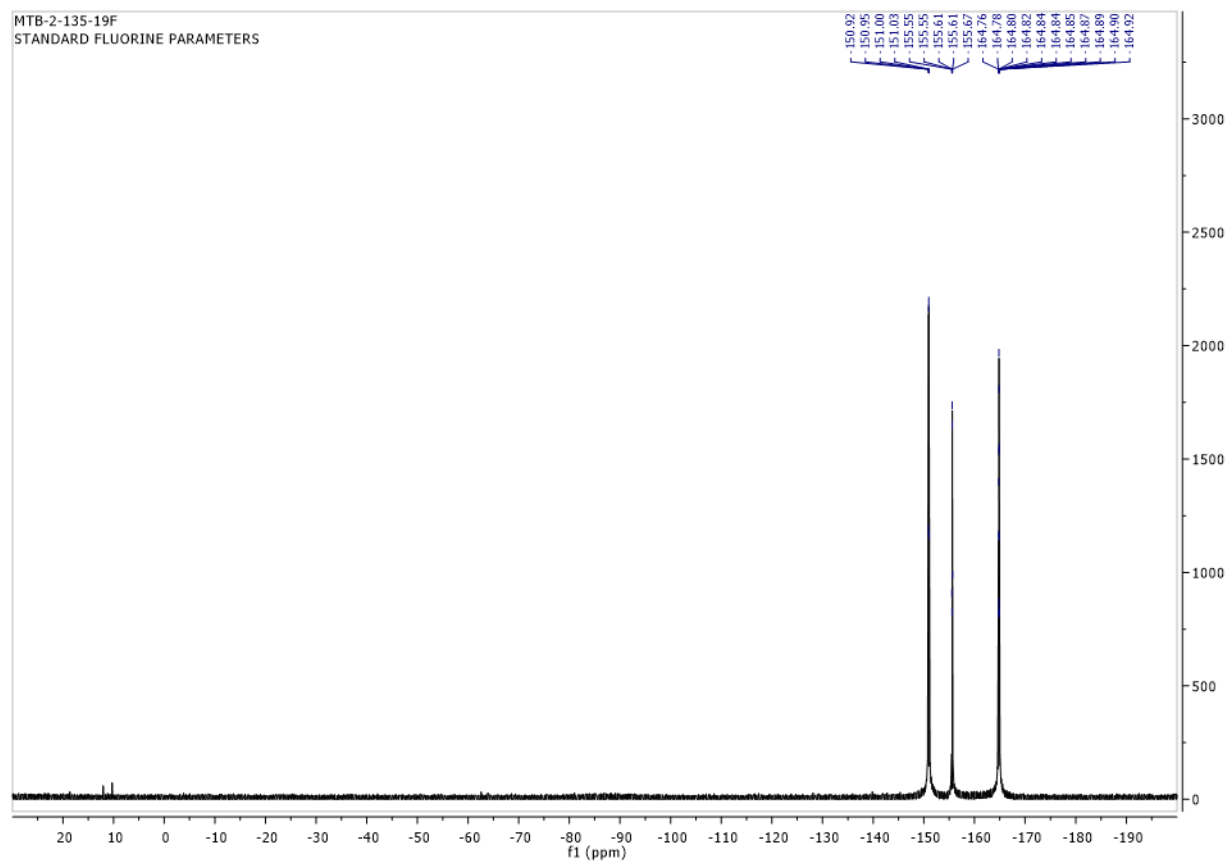
^1H NMR (600 MHz, CDCl_3) for 4-(3-chloropropyl)-1-(perfluorophenyl)-1H-1,2,3-triazole (**2.20e**):



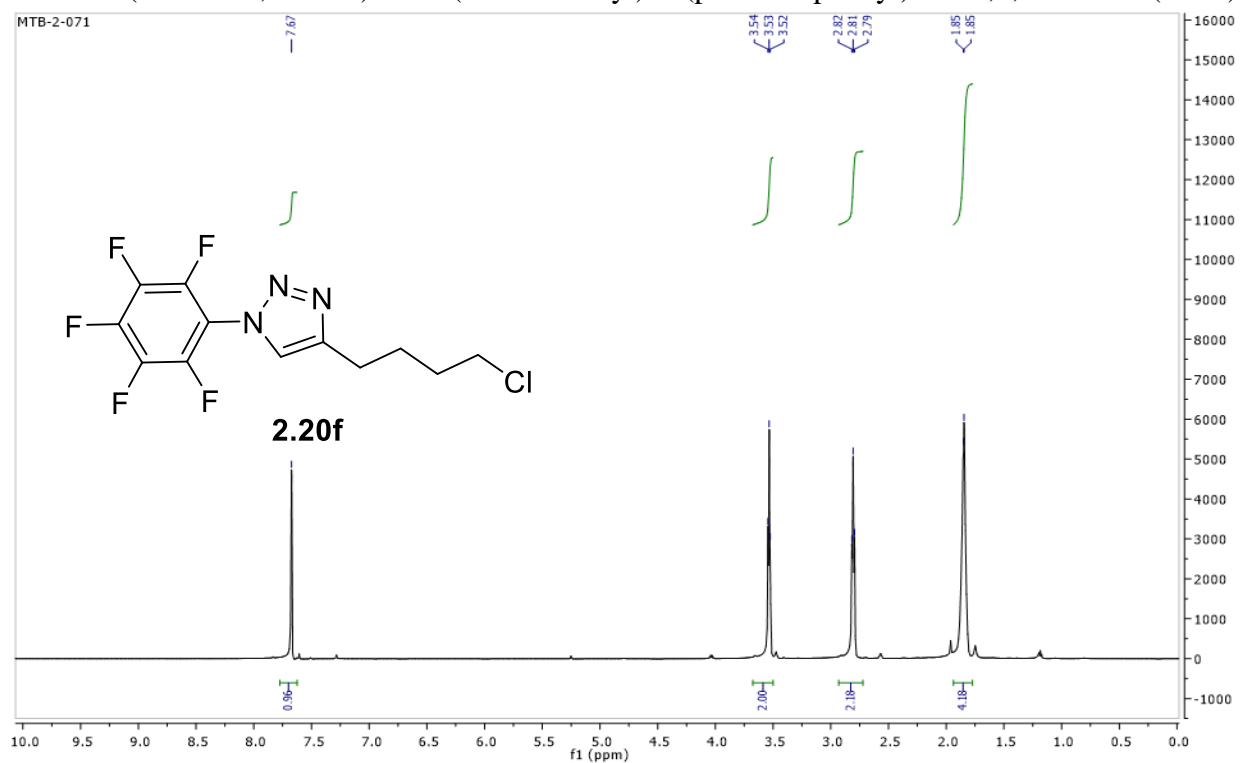
^{13}C NMR (150 MHz, CDCl_3) for 4-(3-chloropropyl)-1-(perfluorophenyl)-1H-1,2,3-triazole (**2.20e**):



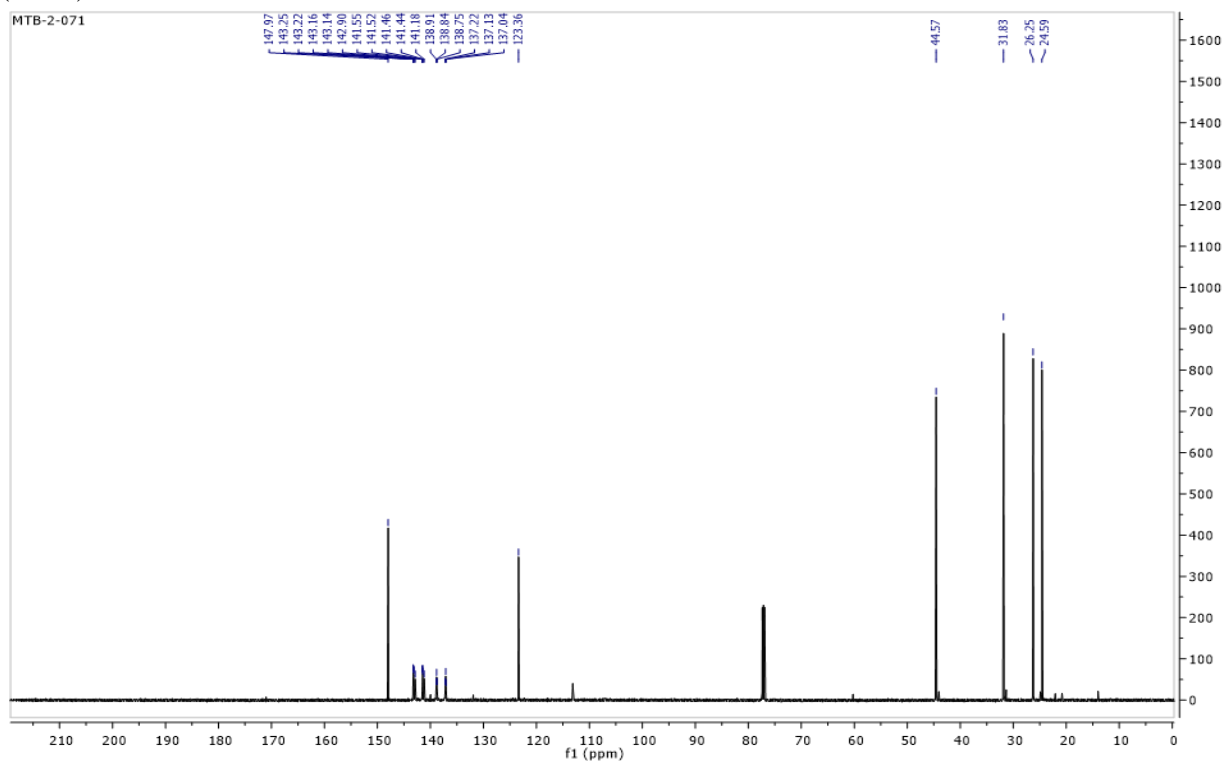
^{19}F NMR (375 MHz, CDCl_3) for 4-(3-chloropropyl)-1-(perfluorophenyl)-1H-1,2,3-triazole (**2.20e**):



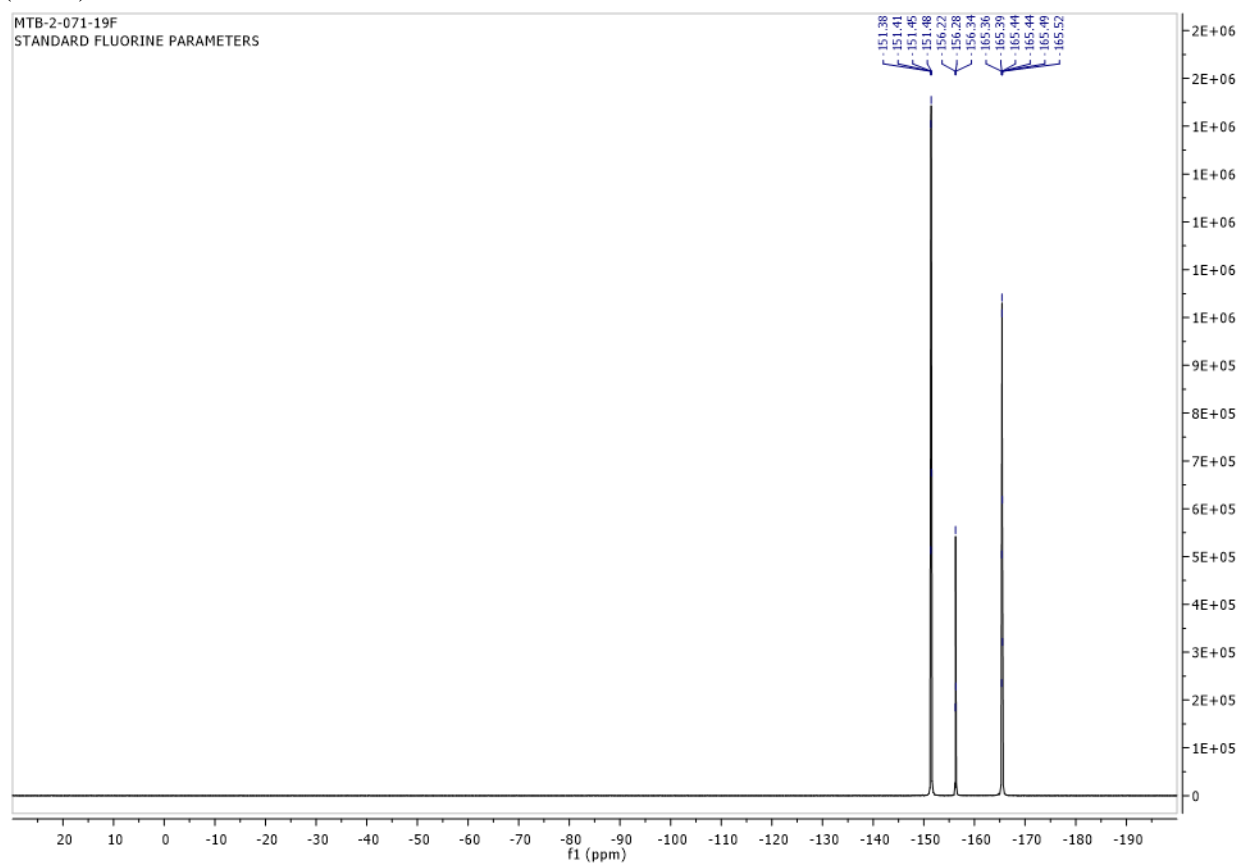
^1H NMR (600 MHz, CDCl_3) for 4-(4-chlorobutyl)-1-(perfluorophenyl)-1H-1,2,3-triazole (**2.20f**):



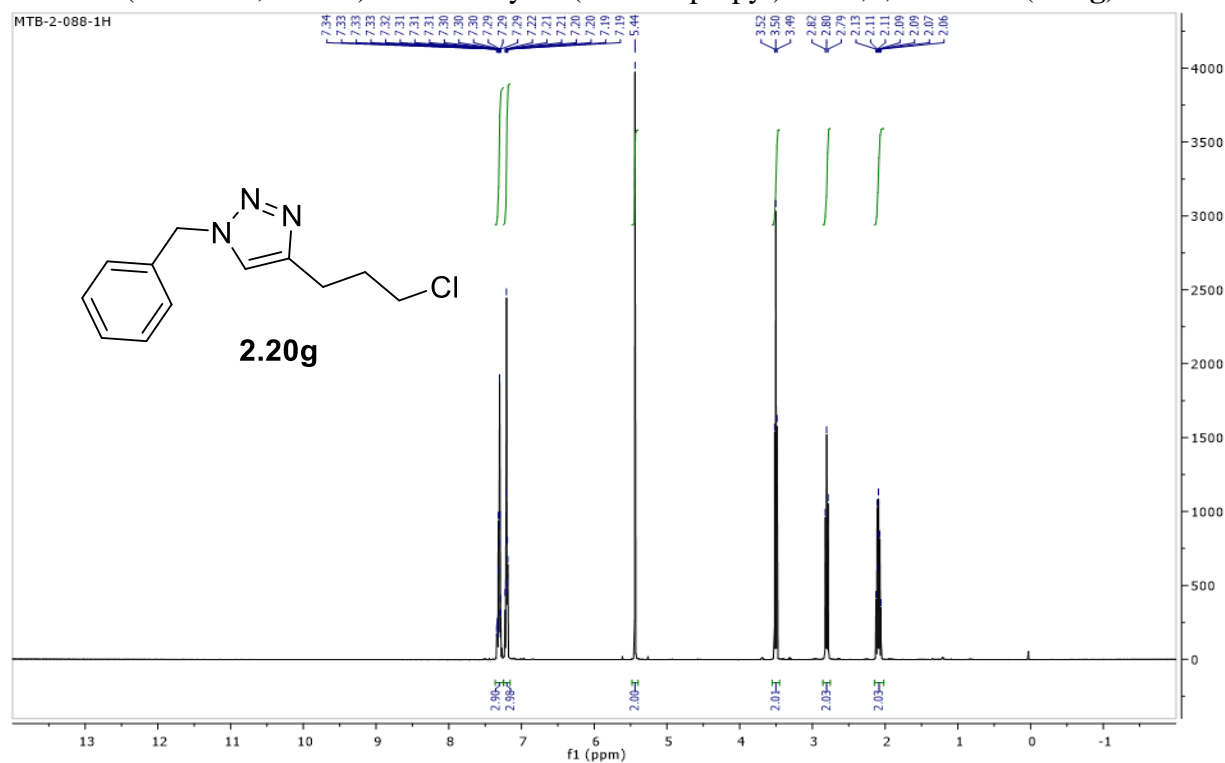
^{13}C NMR (150 MHz, CDCl_3) for 4-(4-chlorobutyl)-1-(perfluorophenyl)-1H-1,2,3-triazole (**2.20f**):



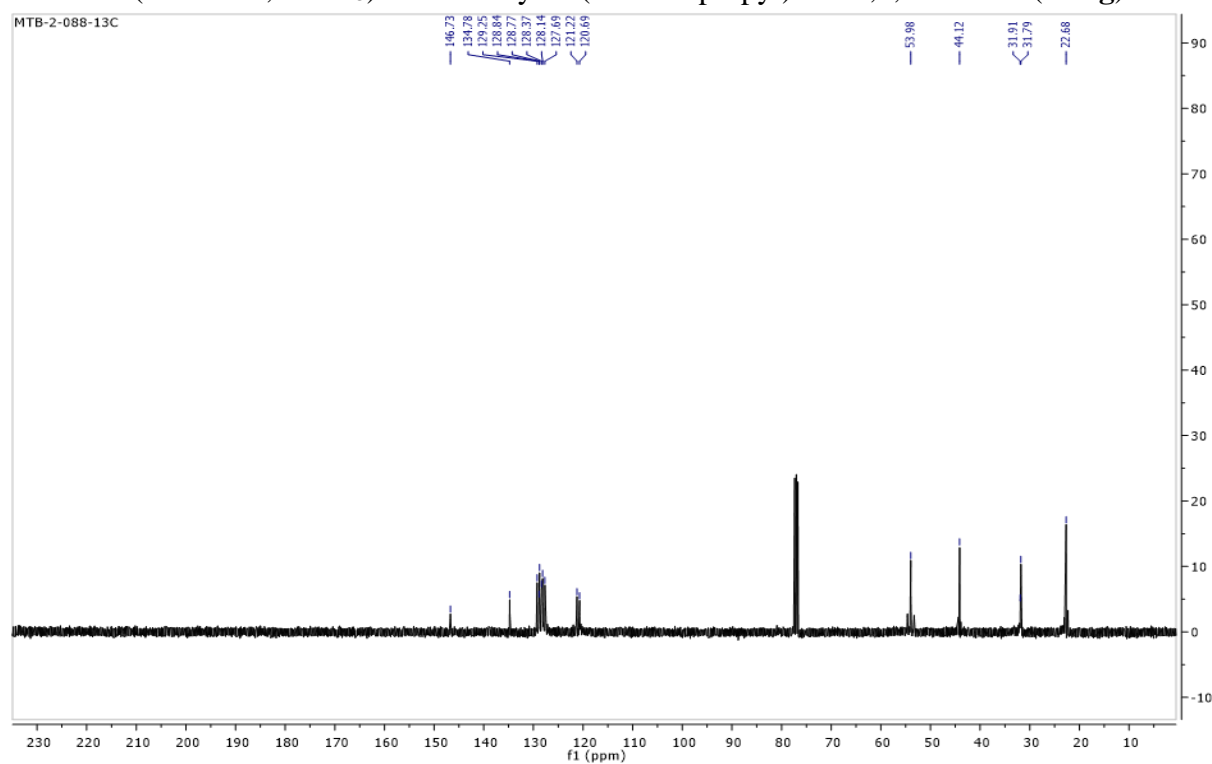
^{19}F NMR (375 MHz, CDCl_3) for 4-(4-chlorobutyl)-1-(perfluorophenyl)-1H-1,2,3-triazole
(**2.20f**):



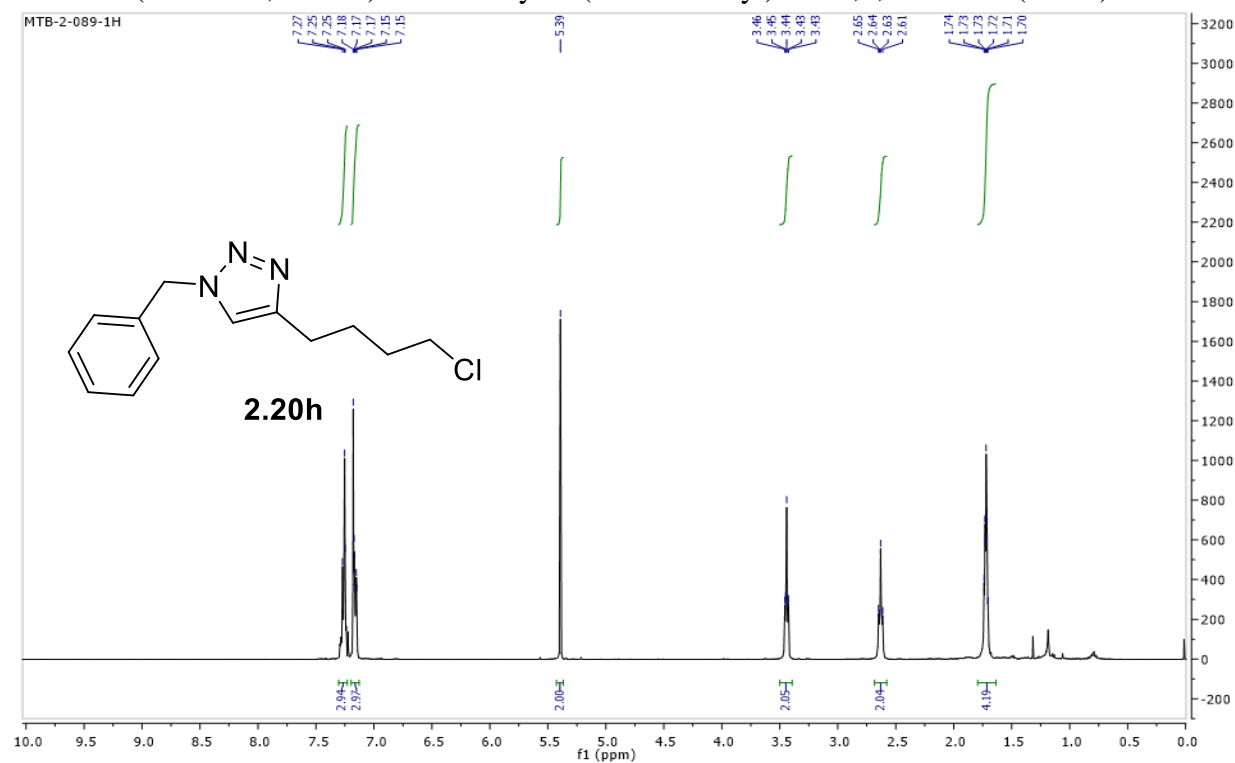
^1H NMR (400 MHz, CDCl_3) for 1-benzyl-4-(3-chloropropyl)-1H-1,2,3-triazole (**2.20g**):



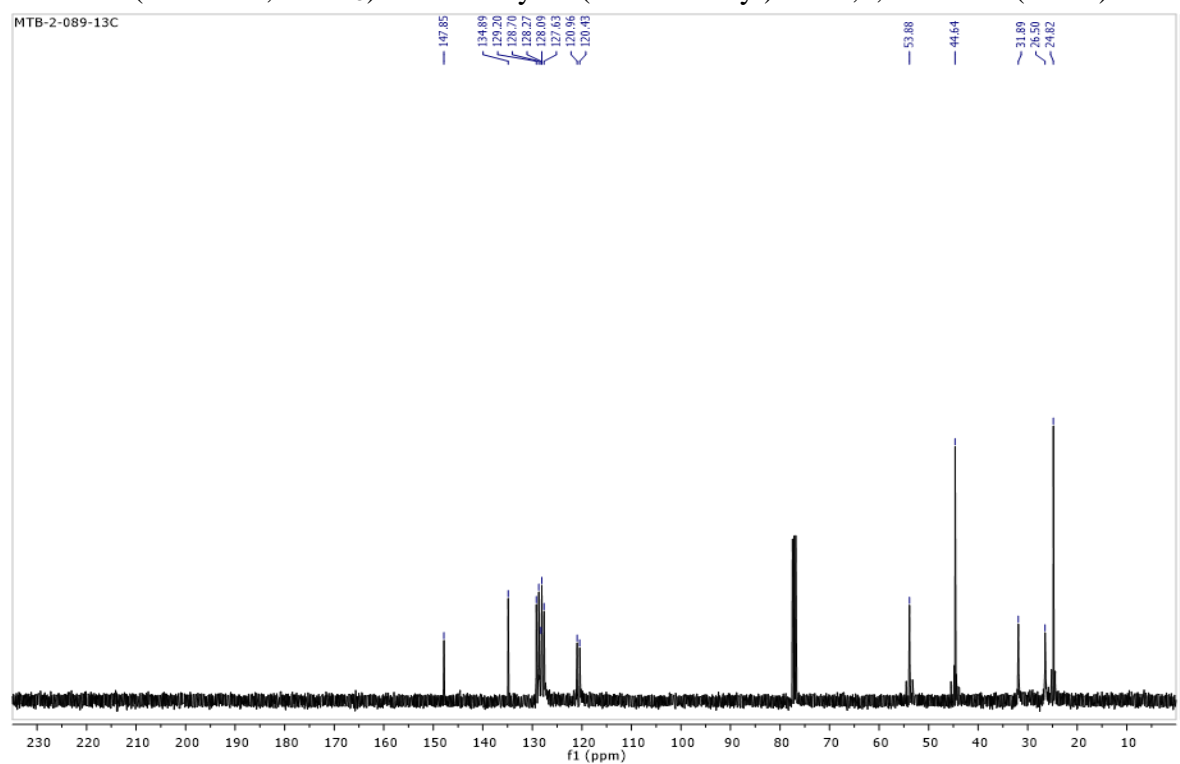
^{13}C NMR (100 MHz, CDCl_3) for 1-benzyl-4-(3-chloropropyl)-1H-1,2,3-triazole (**2.20g**):



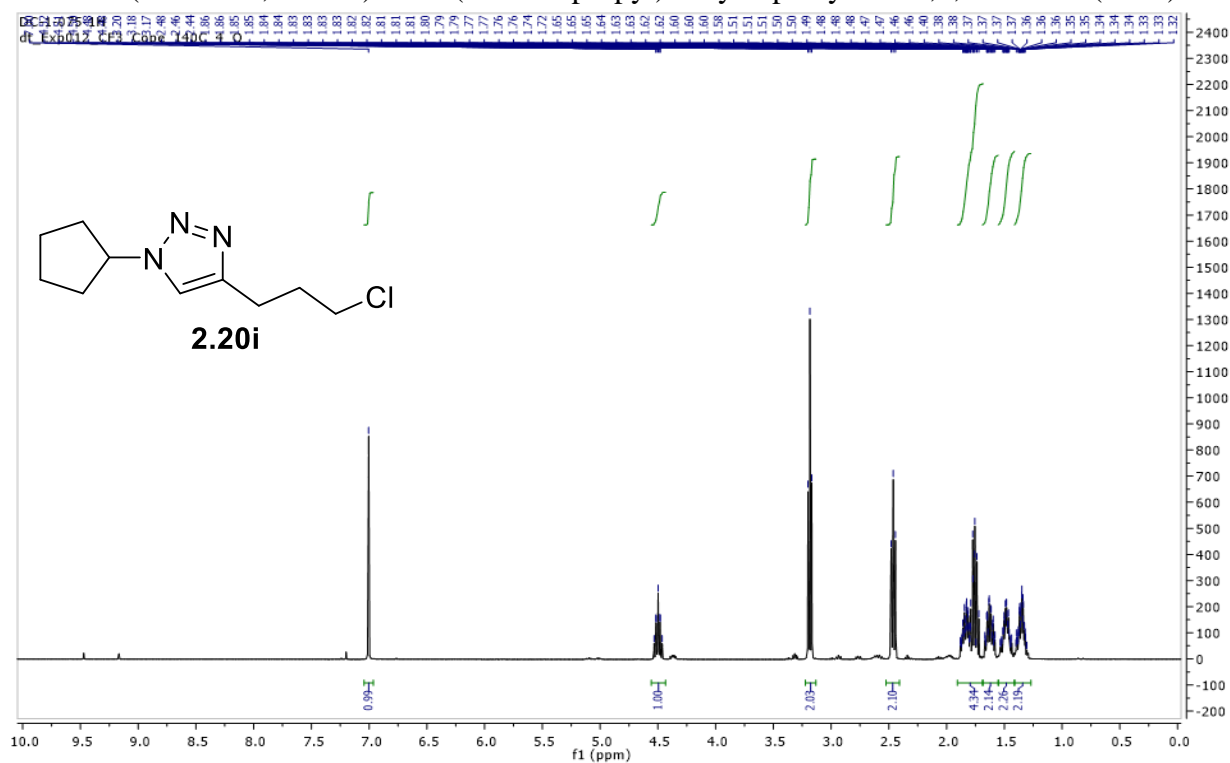
^1H NMR (400 MHz, CDCl_3) for 1-benzyl-4-(4-chlorobutyl)-1H-1,2,3-triazole (**2.20h**):



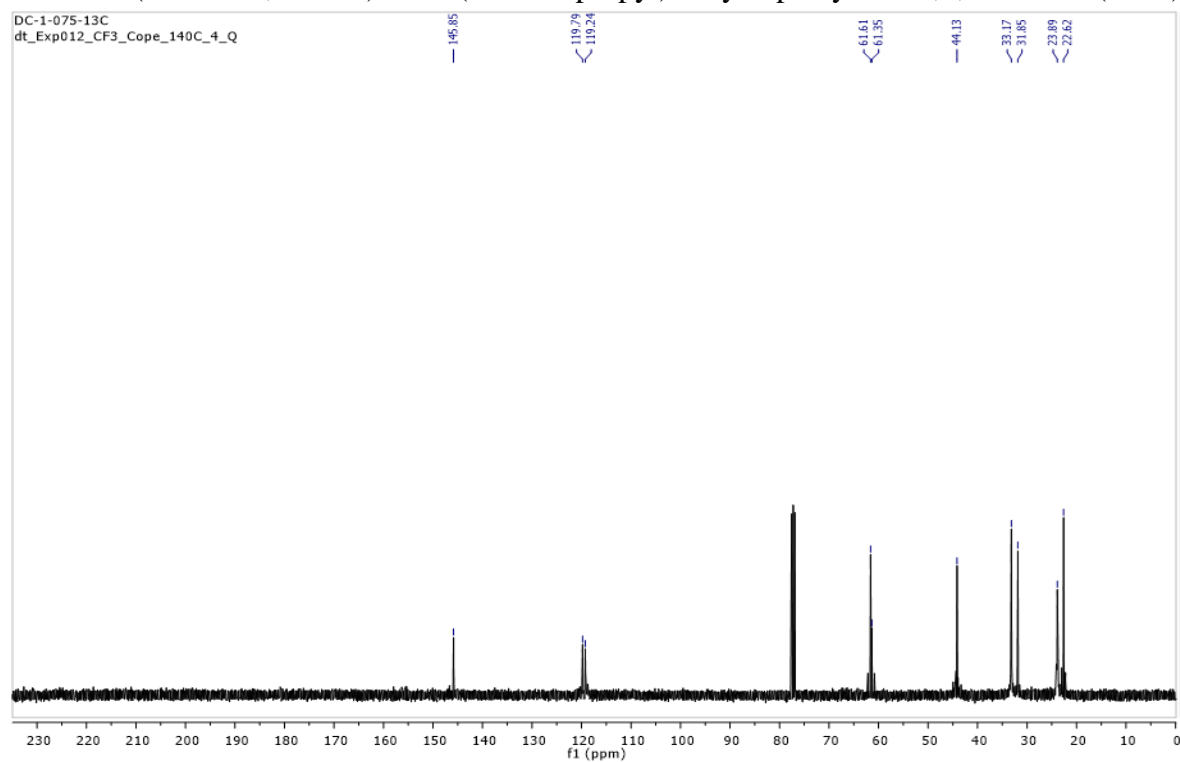
^{13}C NMR (100 MHz, CDCl_3) for 1-benzyl-4-(4-chlorobutyl)-1H-1,2,3-triazole (**2.20h**):



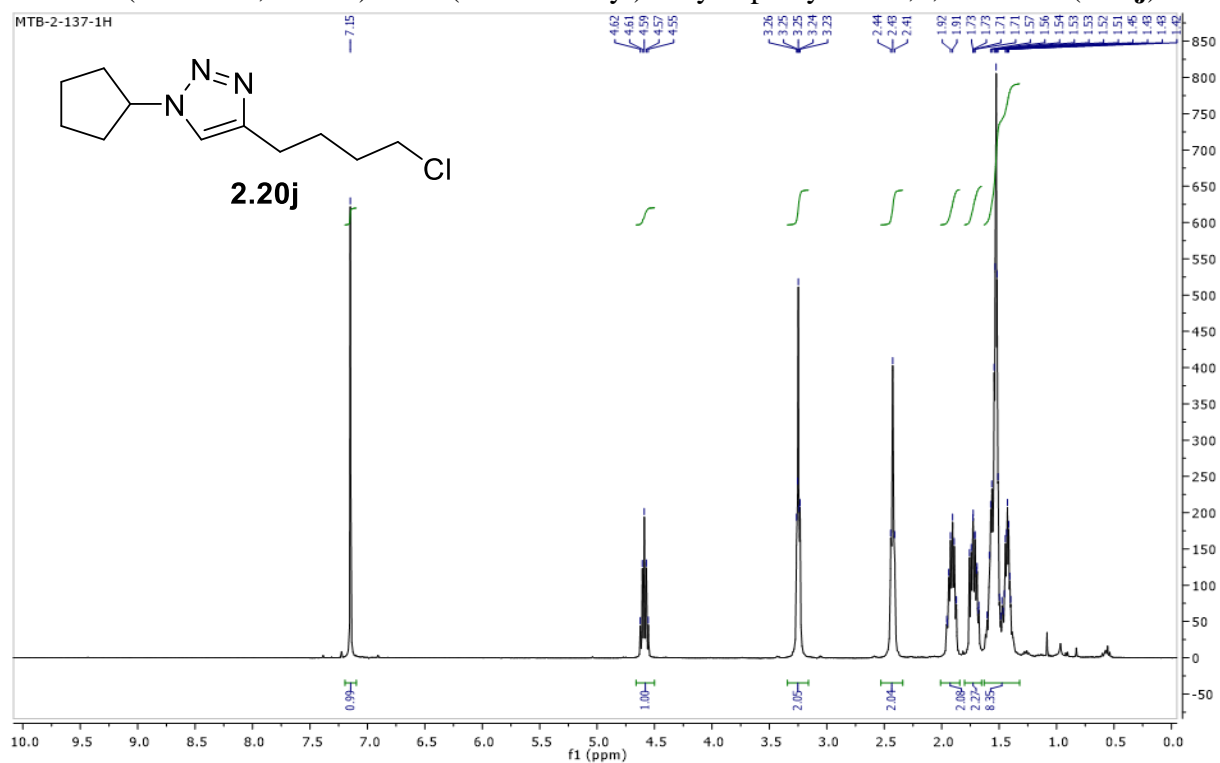
^1H NMR (400 MHz, CDCl_3) for 4-(3-chloropropyl)-1-cyclopentyl-1H-1,2,3-triazole (**2.20i**):



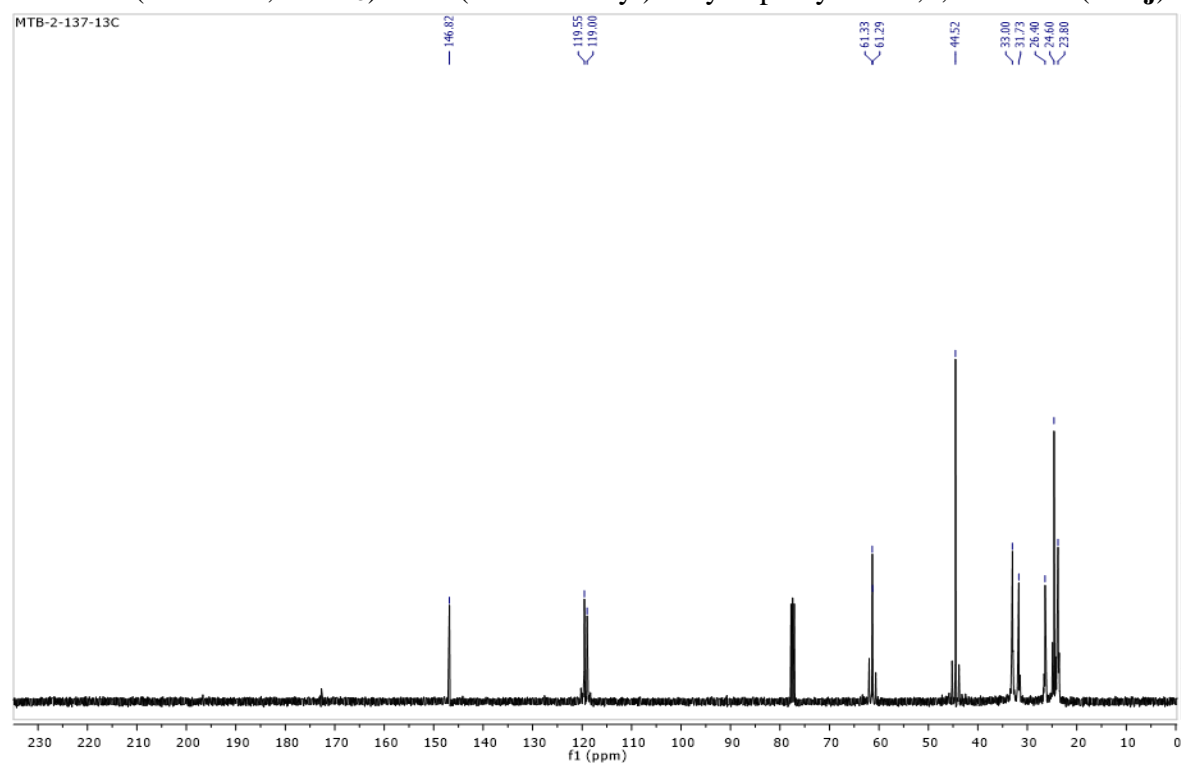
^{13}C NMR (100 MHz, CDCl_3) for 4-(3-chloropropyl)-1-cyclopentyl-1H-1,2,3-triazole (**2.20i**):



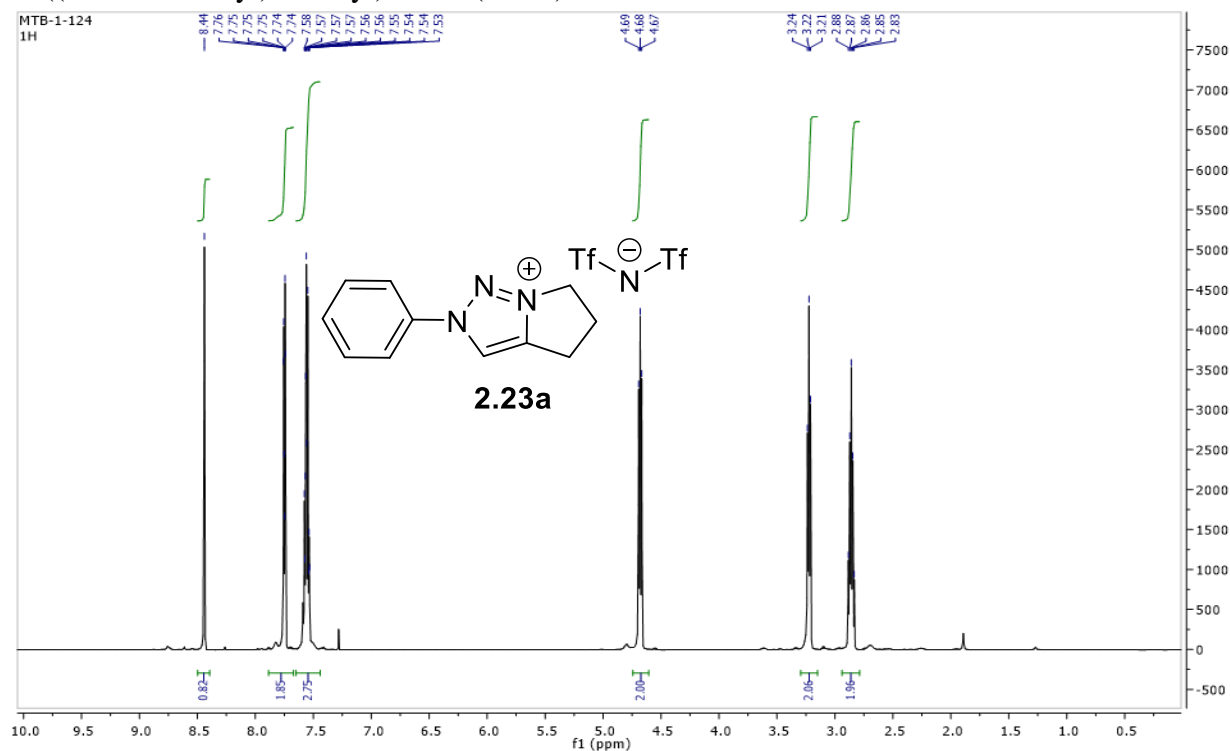
^1H NMR (400 MHz, CDCl_3) for 4-(4-chlorobutyl)-1-cyclopentyl-1H-1,2,3-triazole (**2.20j**):



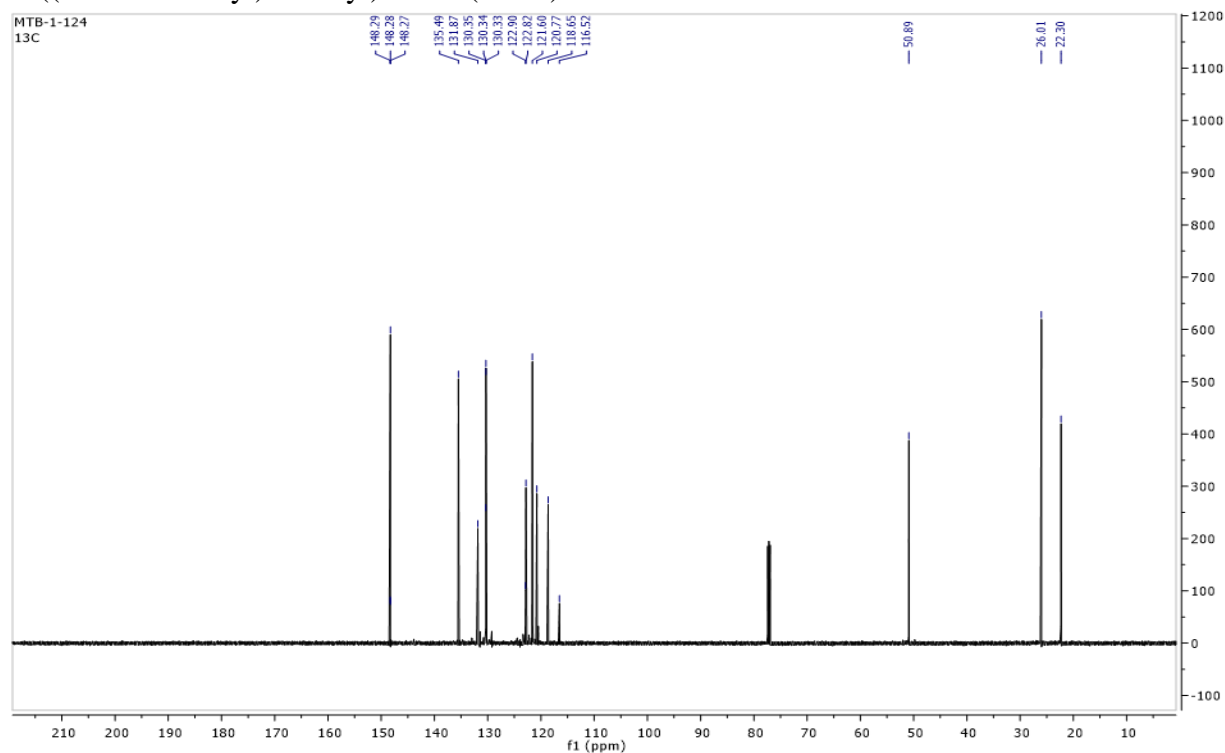
^{13}C NMR (100 MHz, CDCl_3) for 4-(4-chlorobutyl)-1-cyclopentyl-1H-1,2,3-triazole (**2.20j**):



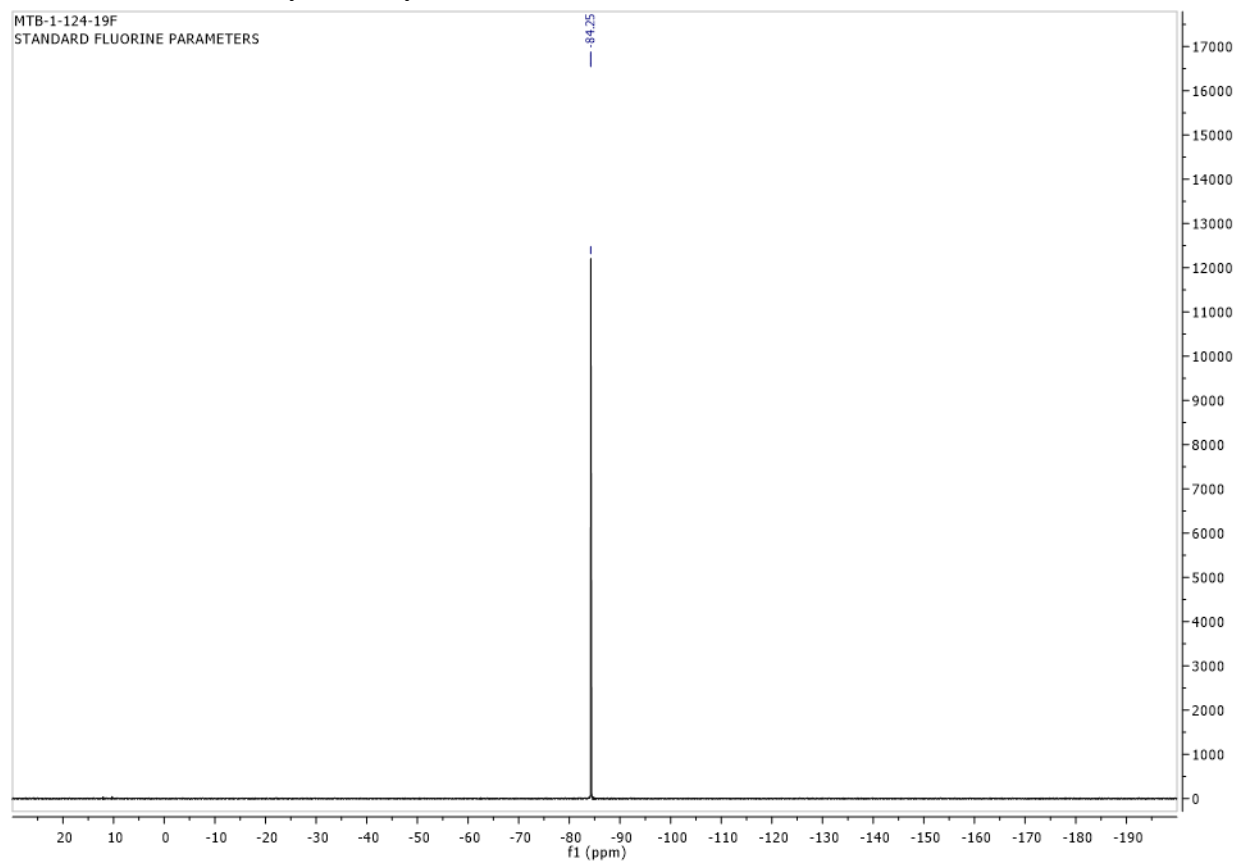
^1H NMR (600 MHz, CDCl_3) for 2-phenyl-2,4,5,6-tetrahydropyrrolo[1,2-c][1,2,3]triazol-7-ium bis((trifluoromethyl)sulfonyl)amide (**2.23a**):



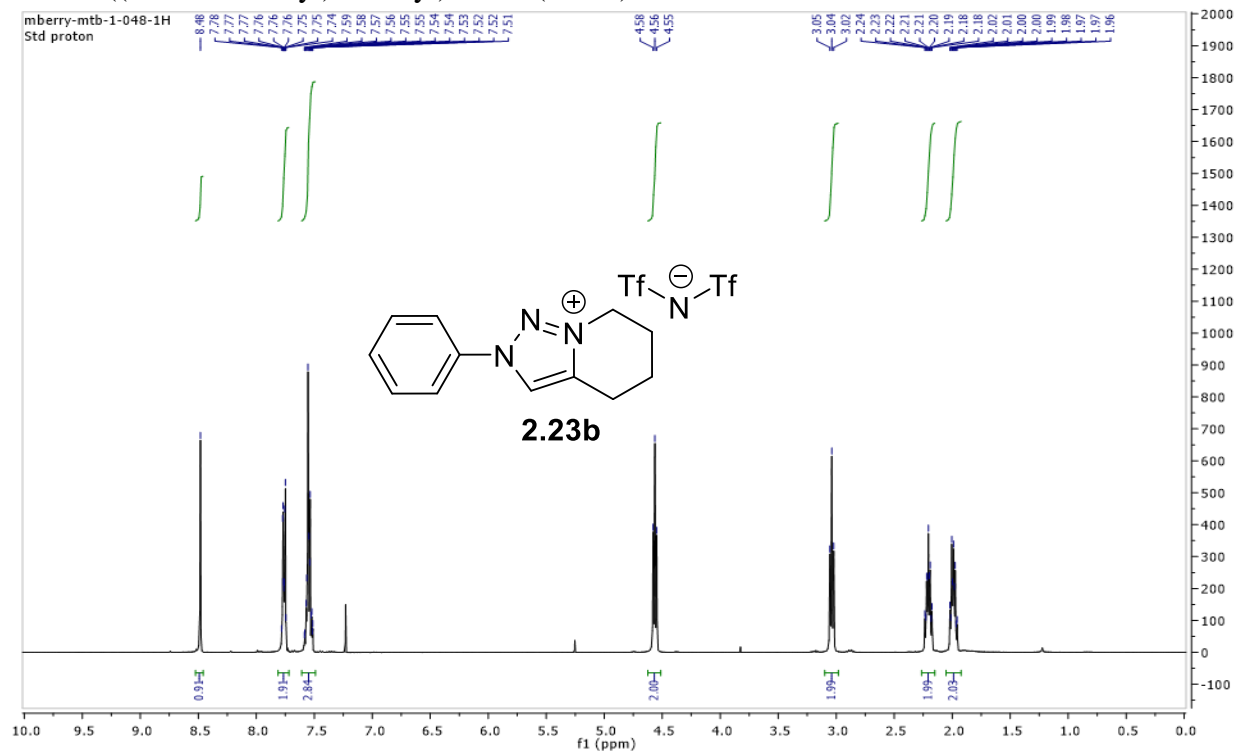
^{13}C NMR (150 MHz, CDCl_3) for 2-phenyl-2,4,5,6-tetrahydropyrrolo[1,2-c][1,2,3]triazol-7-ium bis((trifluoromethyl)sulfonyl)amide (**2.23a**):



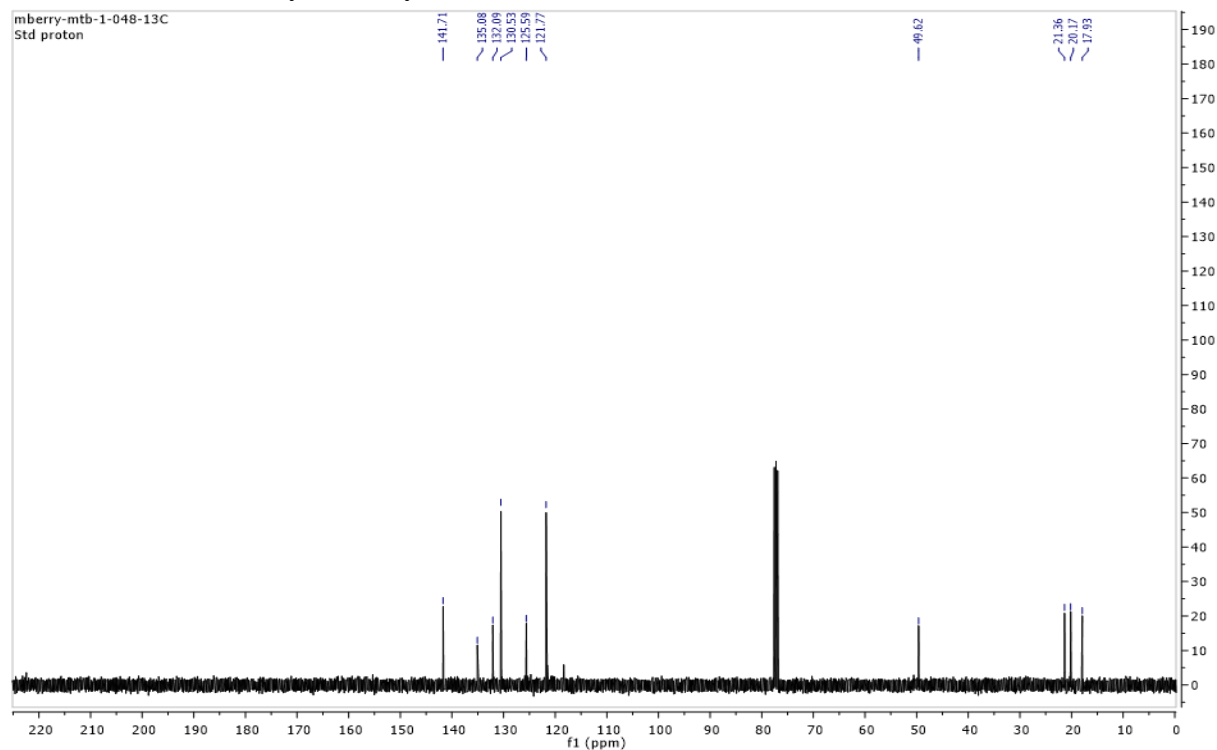
^{19}F NMR (375 MHz, acetone- d_6) for 2-phenyl-2,4,5,6-tetrahydropyrrolo[1,2- c][1,2,3]triazol-7-ium bis((trifluoromethyl)sulfonyl)amide (**2.23a**):



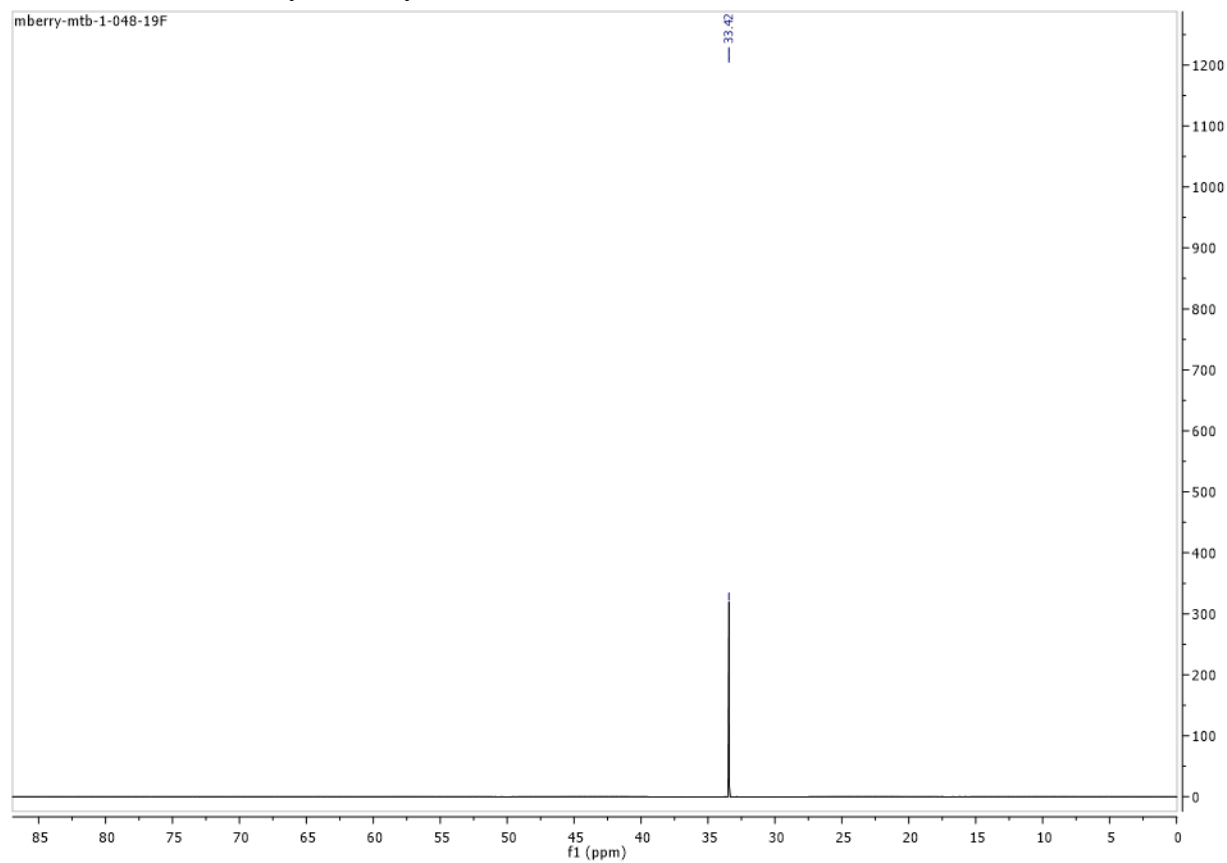
^1H NMR (400 MHz, CDCl_3) for 2-phenyl-4,5,6,7-tetrahydro-2H-[1,2,3]triazolo[1,5-a]pyridin-8-ium bis((trifluoromethyl)sulfonyl)amide (**2.23b**):



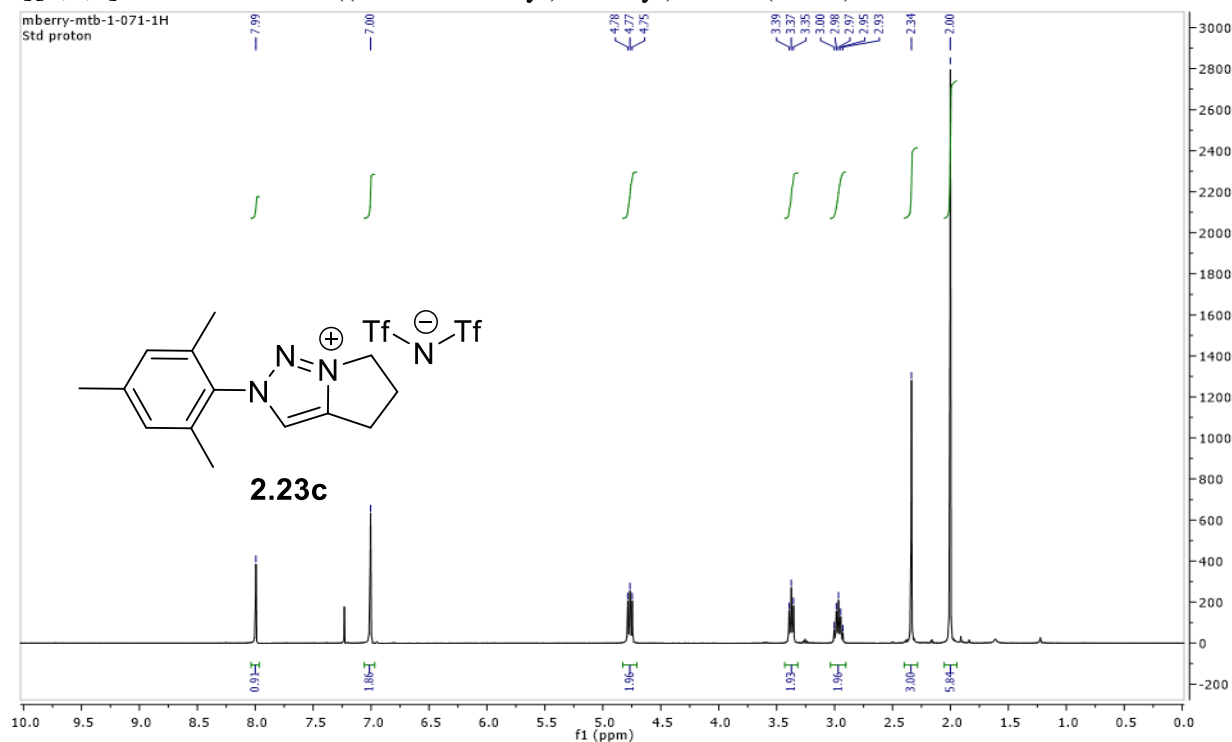
^{13}C NMR (100 MHz, CDCl_3) for 2-phenyl-4,5,6,7-tetrahydro-2H-[1,2,3]triazolo[1,5-a]pyridin-8-ium bis((trifluoromethyl)sulfonyl)amide (**2.23b**):



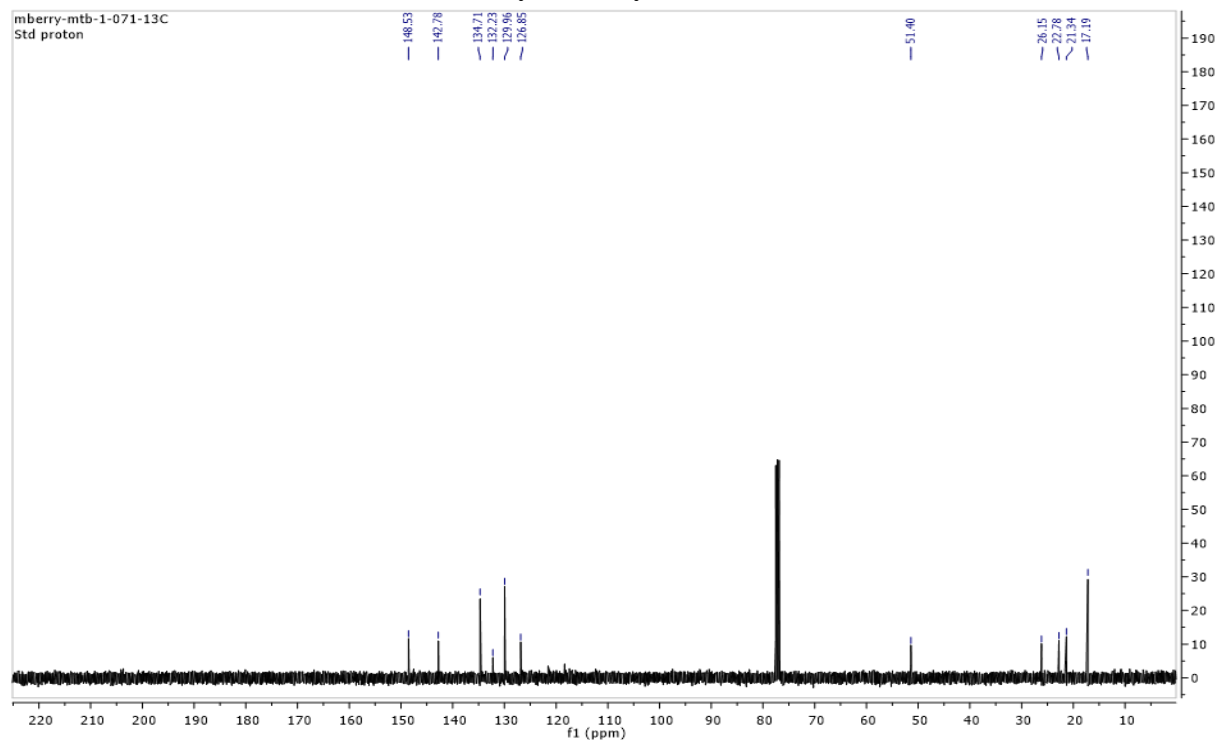
^{19}F NMR (375 MHz, CDCl_3) for 2-phenyl-4,5,6,7-tetrahydro-2H-[1,2,3]triazolo[1,5-a]pyridin-8-ium bis((trifluoromethyl)sulfonyl)amide (**2.23b**):



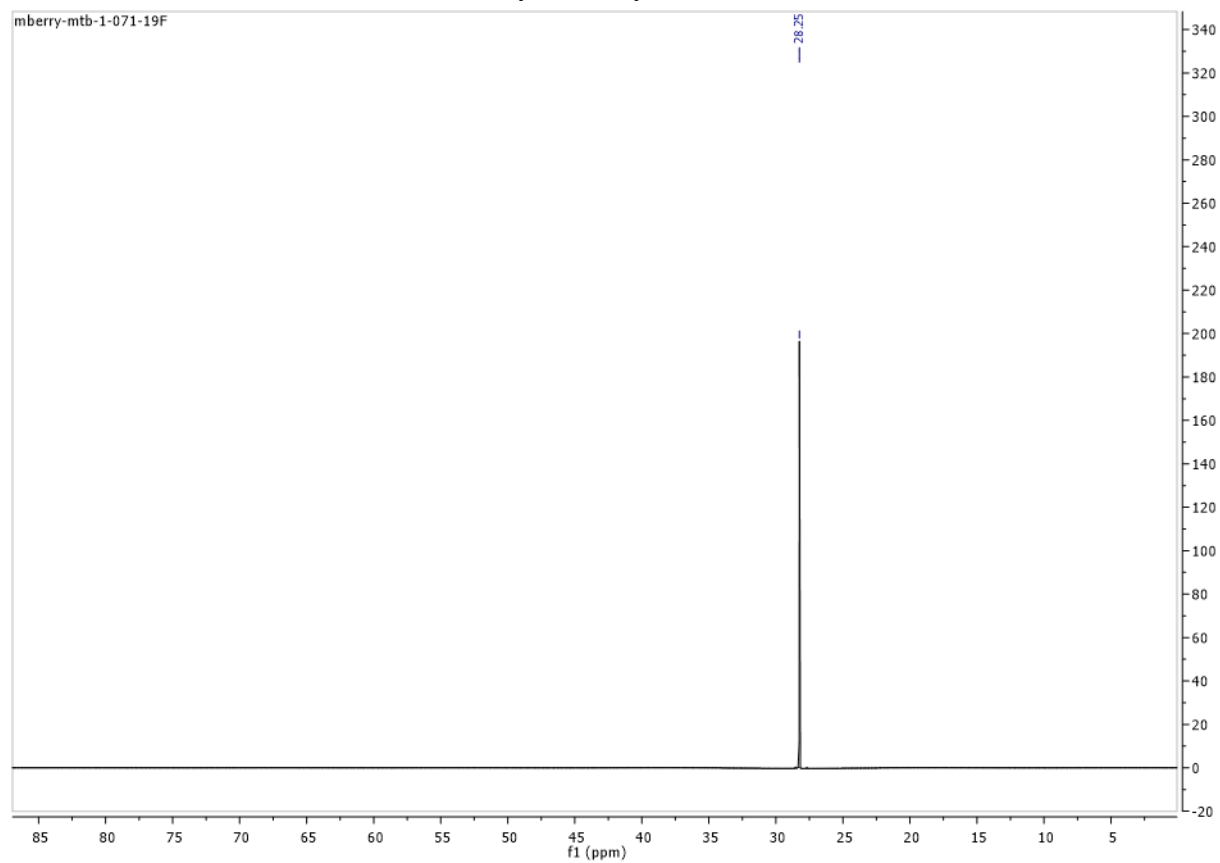
^1H NMR (400 MHz, CDCl_3) spectrum for 2-mesityl-2,4,5,6-tetrahydropyrrolo[1,2-c][1,2,3]triazol-7-ium bis((trifluoromethyl)sulfonyl)amide (**2.23c**):



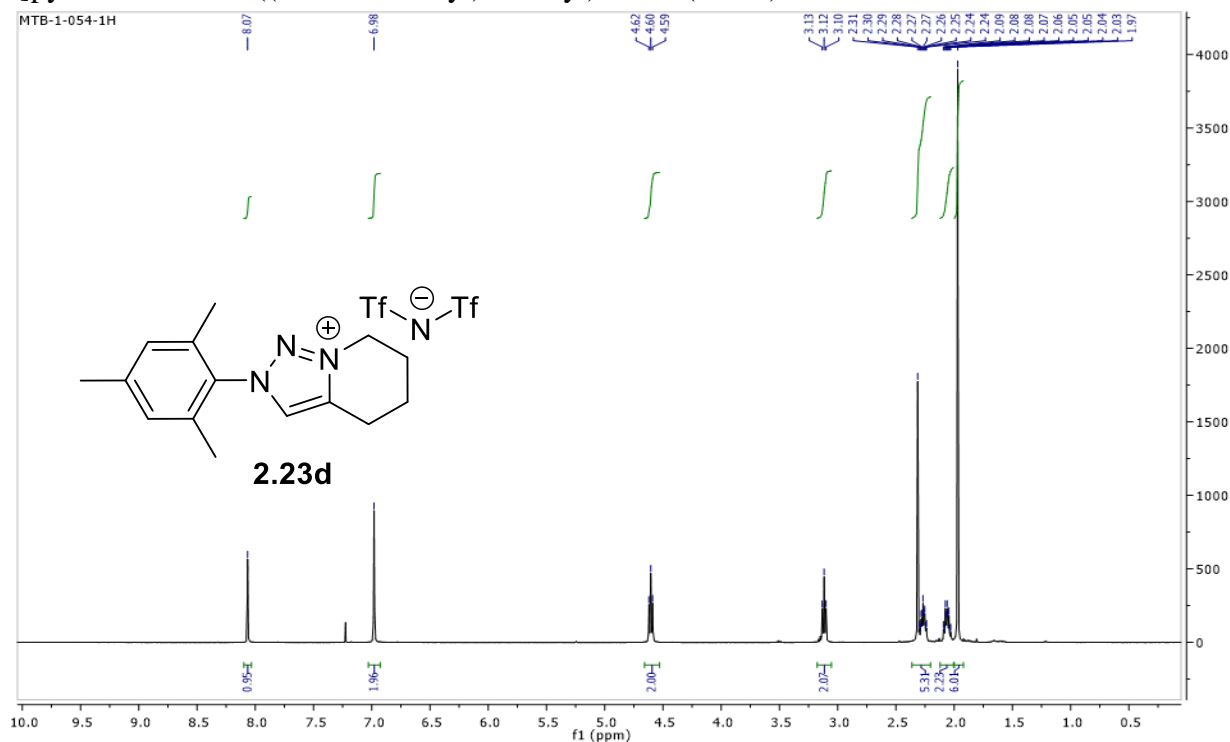
^{13}C NMR (100 MHz, CDCl_3) spectrum for 2-mesityl-2,4,5,6-tetrahydropyrrolo[1,2-c][1,2,3]triazol-7-ium bis((trifluoromethyl)sulfonyl)amide (**2.23c**):



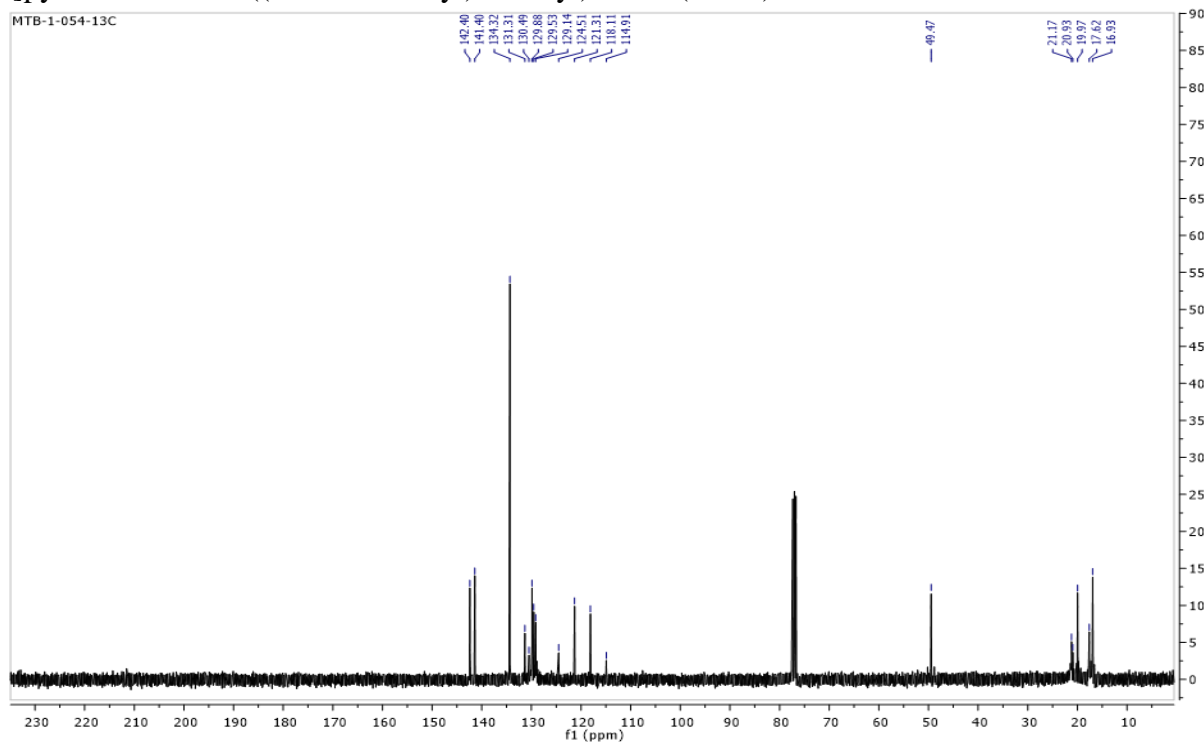
^{19}F NMR (375 MHz, CDCl_3) spectrum for 2-mesityl-2,4,5,6-tetrahydropyrrolo[1,2-c][1,2,3]triazol-7-ium bis((trifluoromethyl)sulfonyl)amide (**2.23c**):



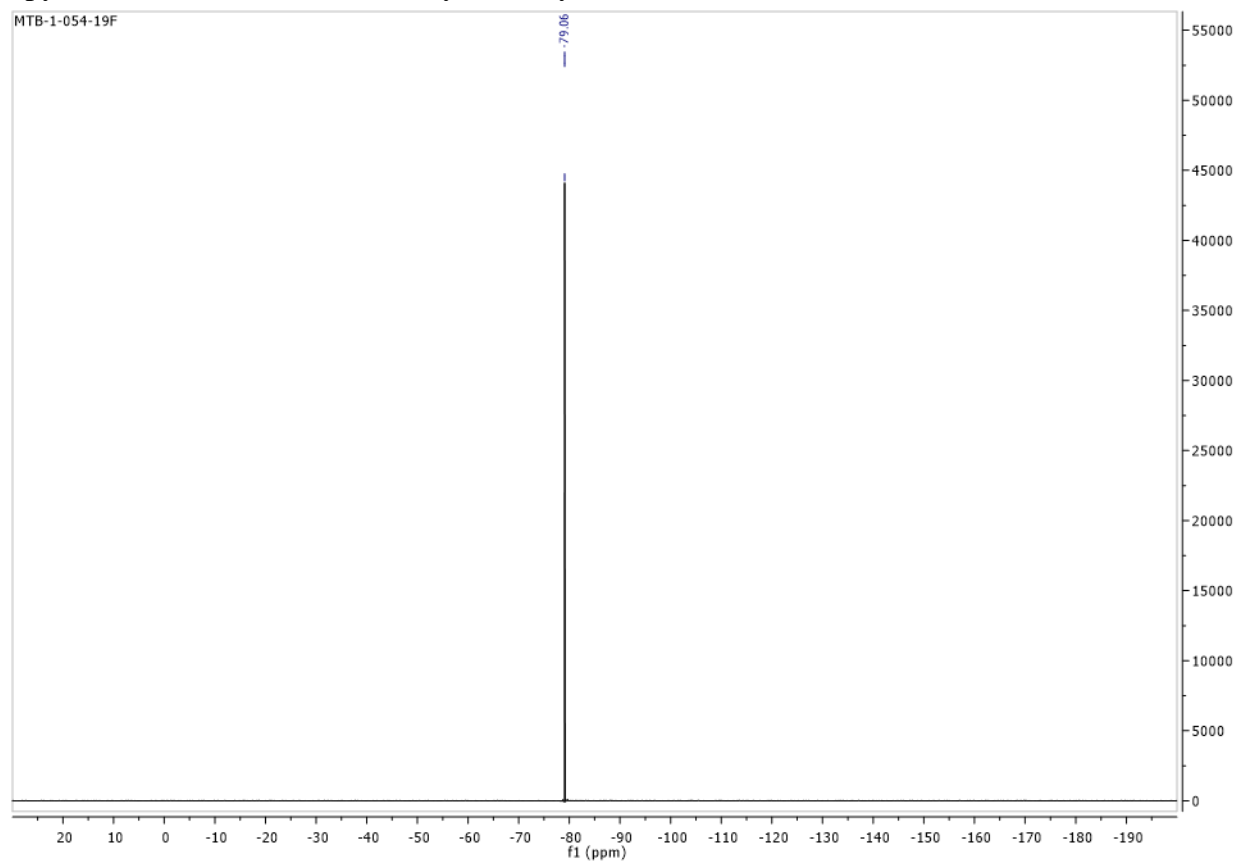
^1H NMR (400 MHz, CDCl_3) spectrum for 2-mesityl-4,5,6,7-tetrahydro-2H-[1,2,3]triazolo[1,5-a]pyridin-8-ium bis((trifluoromethyl)sulfonyl)amide (**2.23d**):



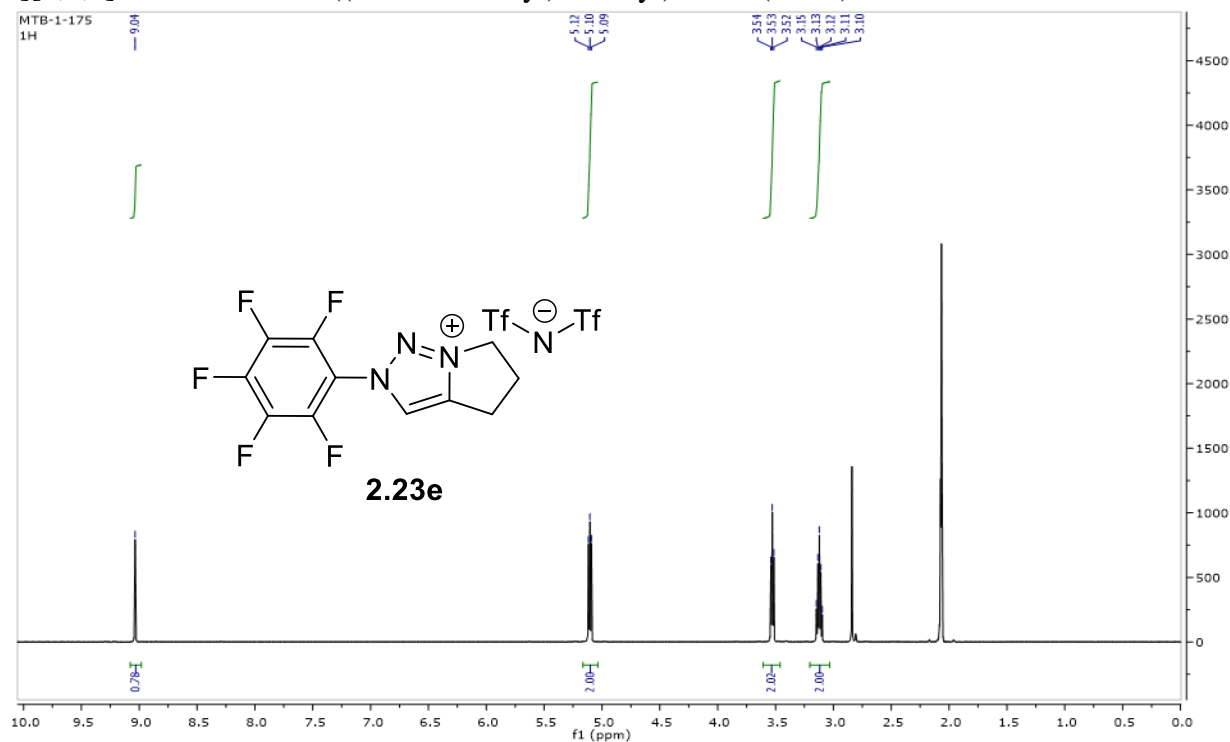
^{13}C NMR (100 MHz, CDCl_3) spectrum for 2-mesityl-4,5,6,7-tetrahydro-2H-[1,2,3]triazolo[1,5-a]pyridin-8-ium bis((trifluoromethyl)sulfonyl)amide (**2.23d**):



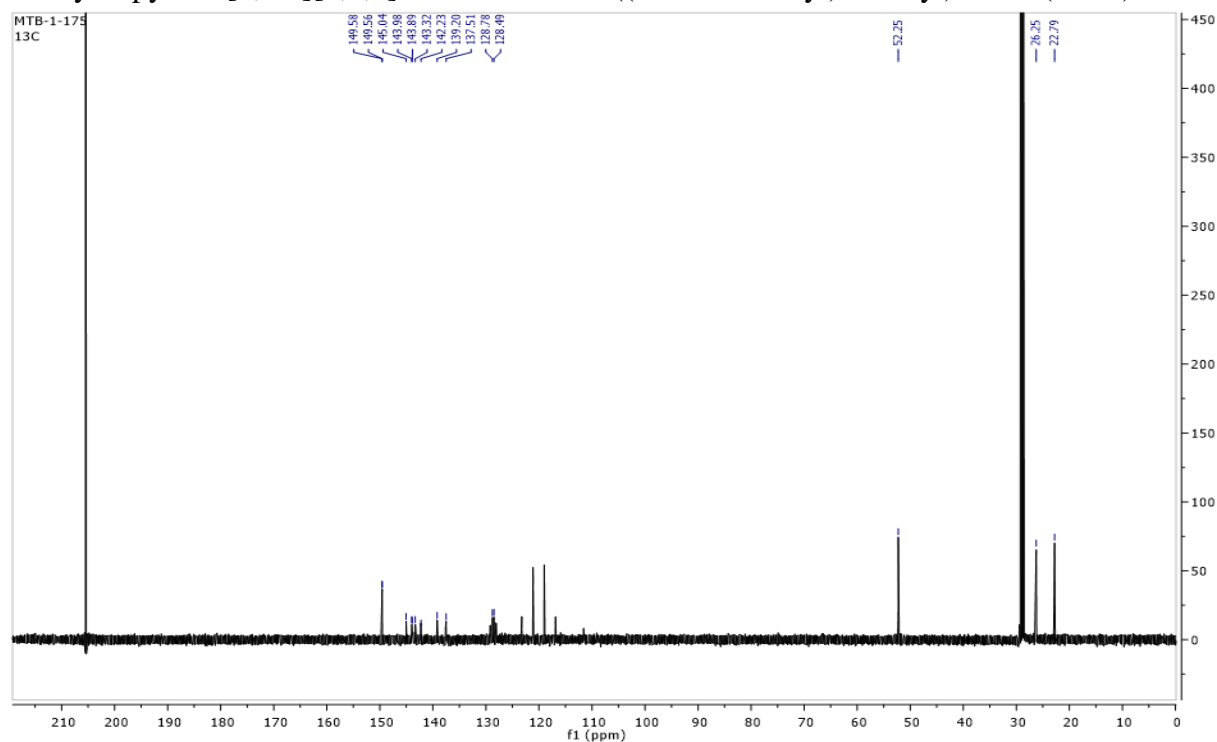
^{19}F NMR (375 MHz, CDCl_3) spectrum for 2-mesityl-4,5,6,7-tetrahydro-2H-[1,2,3]triazolo[1,5-a]pyridin-8-ium bis((trifluoromethyl)sulfonyl)amide (**2.23d**):



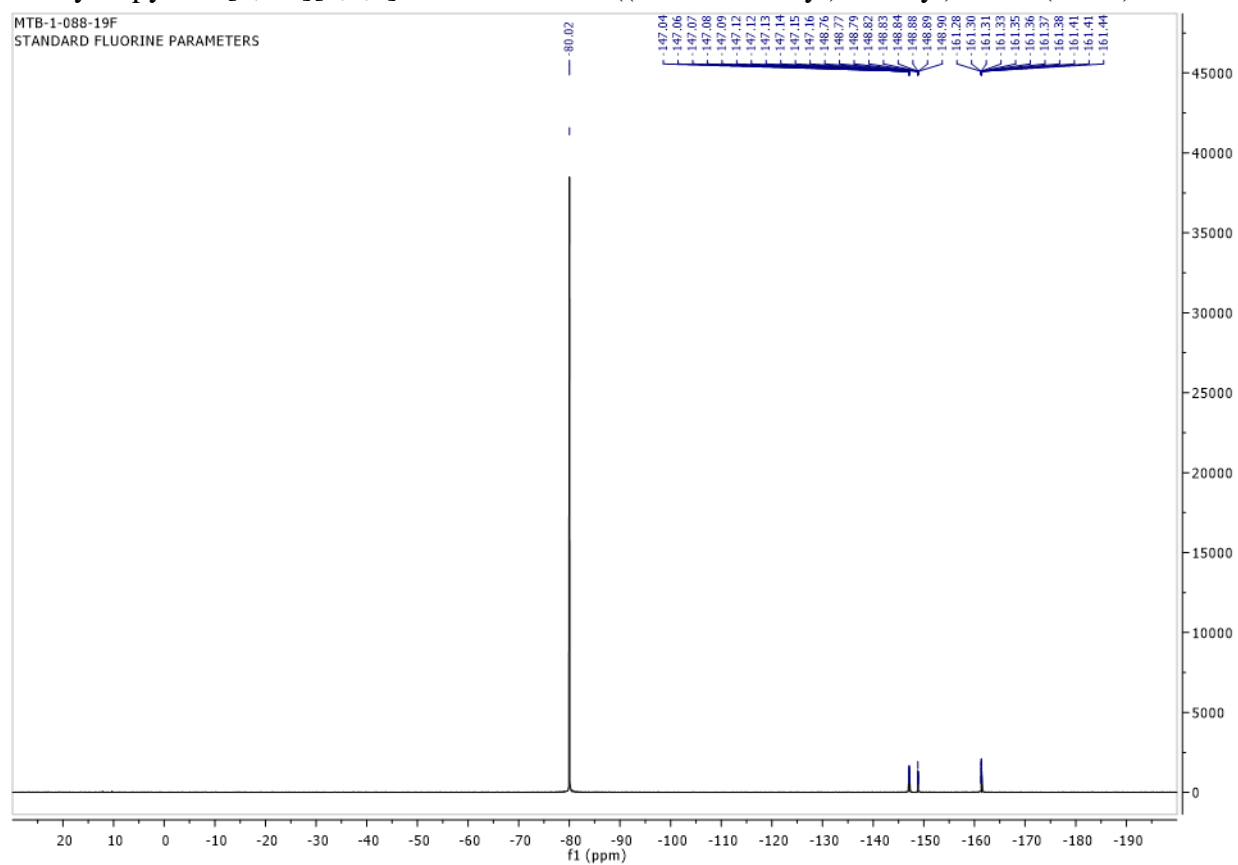
^1H NMR (600 MHz, acetone- d_6) spectrum for 2-(perfluorophenyl)-2,4,5,6-tetrahydropyrrolo[1,2-c][1,2,3]triazol-7-ium bis((trifluoromethyl)sulfonyl)amide (**2.23e**):



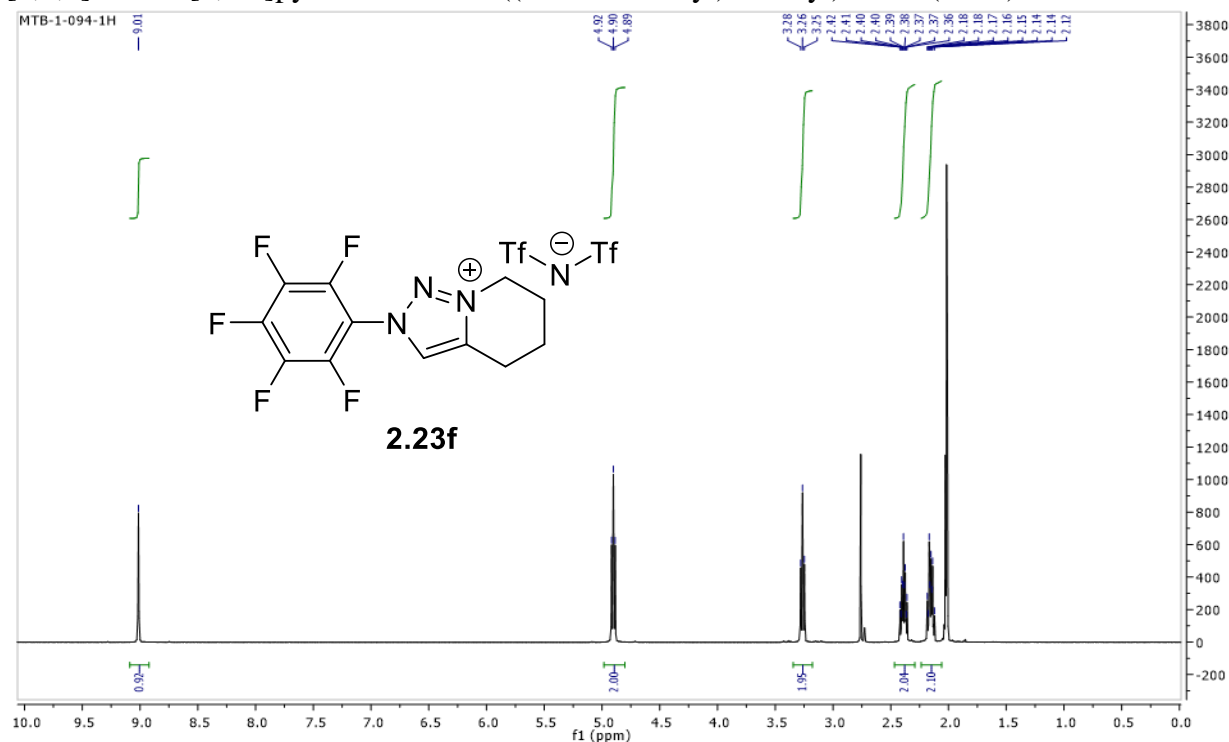
^{13}C NMR (150 MHz, acetone- d_6) spectrum for 2-(perfluorophenyl)-2,4,5,6-tetrahydropyrrolo[1,2-c][1,2,3]triazol-7-ium bis((trifluoromethyl)sulfonyl)amide (**2.23e**):



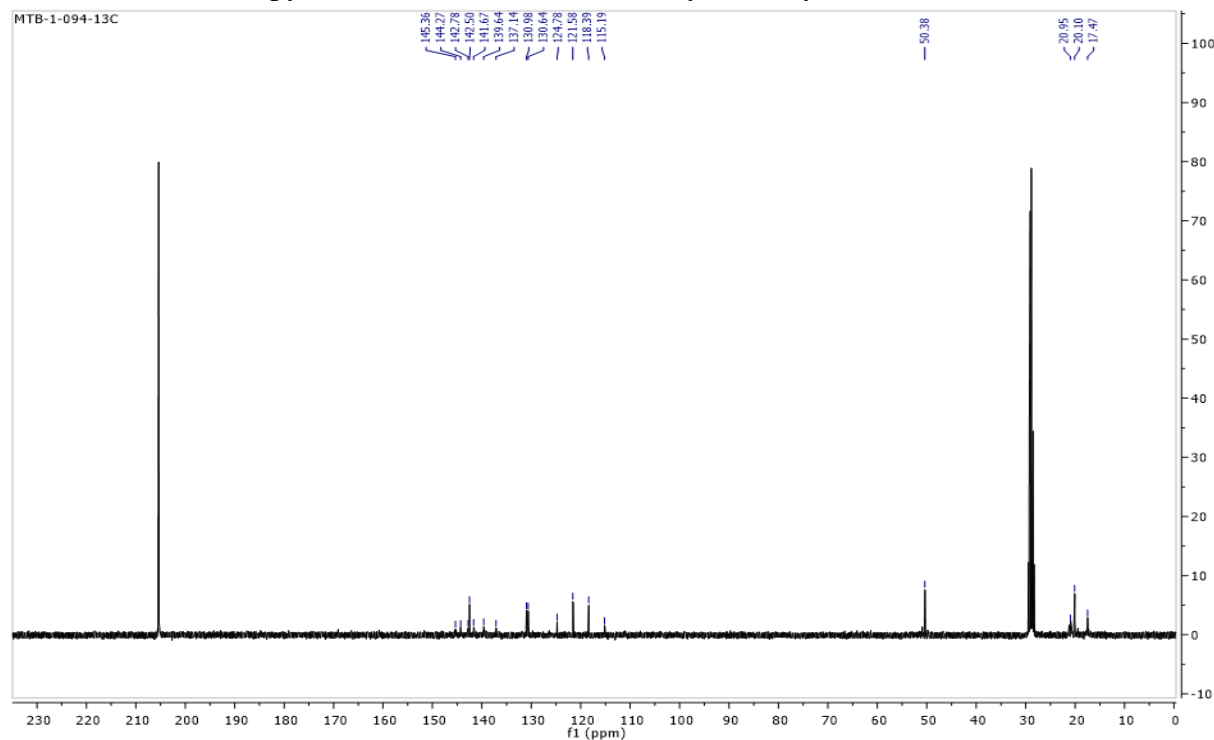
^{19}F NMR (375 MHz, acetone- d_6) spectrum for 2-(perfluorophenyl)-2,4,5,6-tetrahydropyrrolo[1,2-c][1,2,3]triazol-7-ium bis((trifluoromethyl)sulfonyl)amide (**2.23e**):



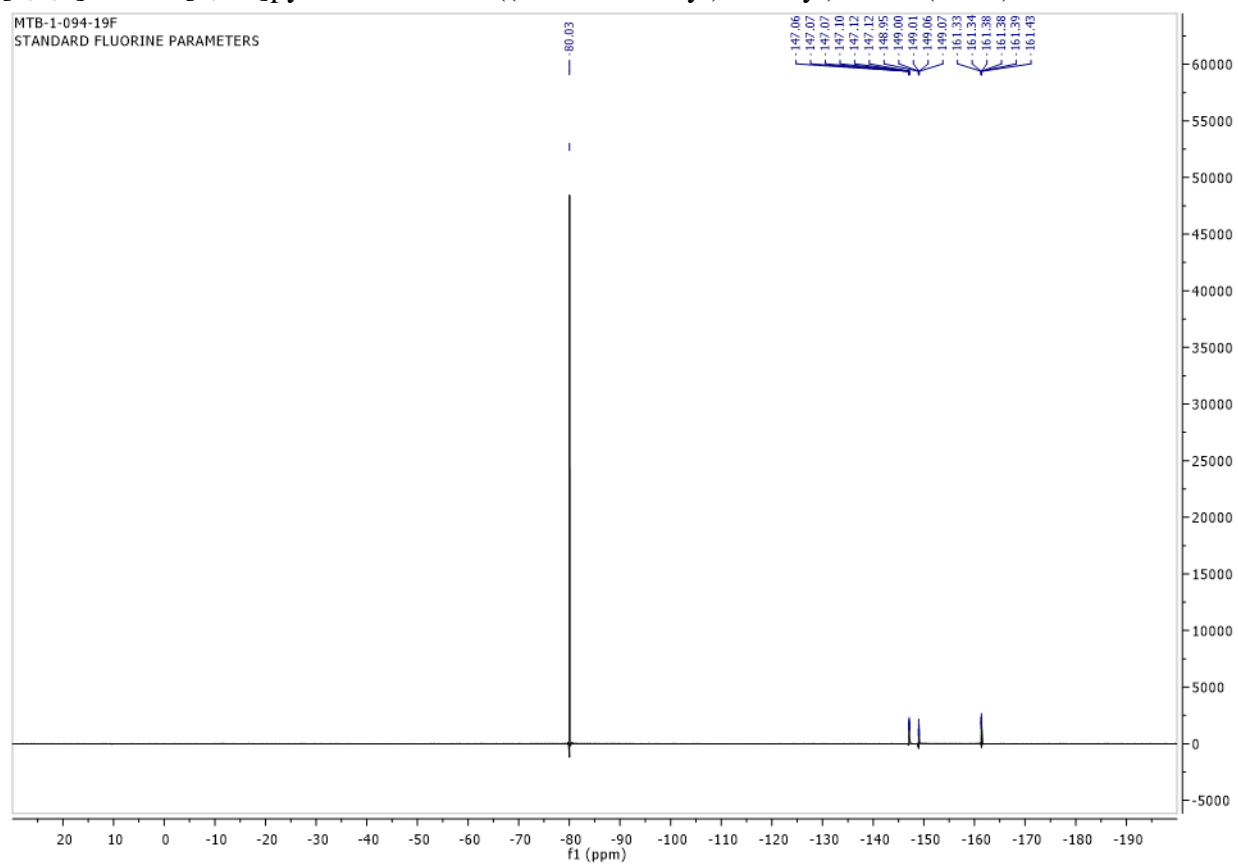
^1H NMR (400 MHz, acetone- d_6) spectrum for 2-(perfluorophenyl)-4,5,6,7-tetrahydro-2H-[1,2,3]triazolo[1,5-a]pyridin-8-ium bis((trifluoromethyl)sulfonyl)amide (**2.23f**):



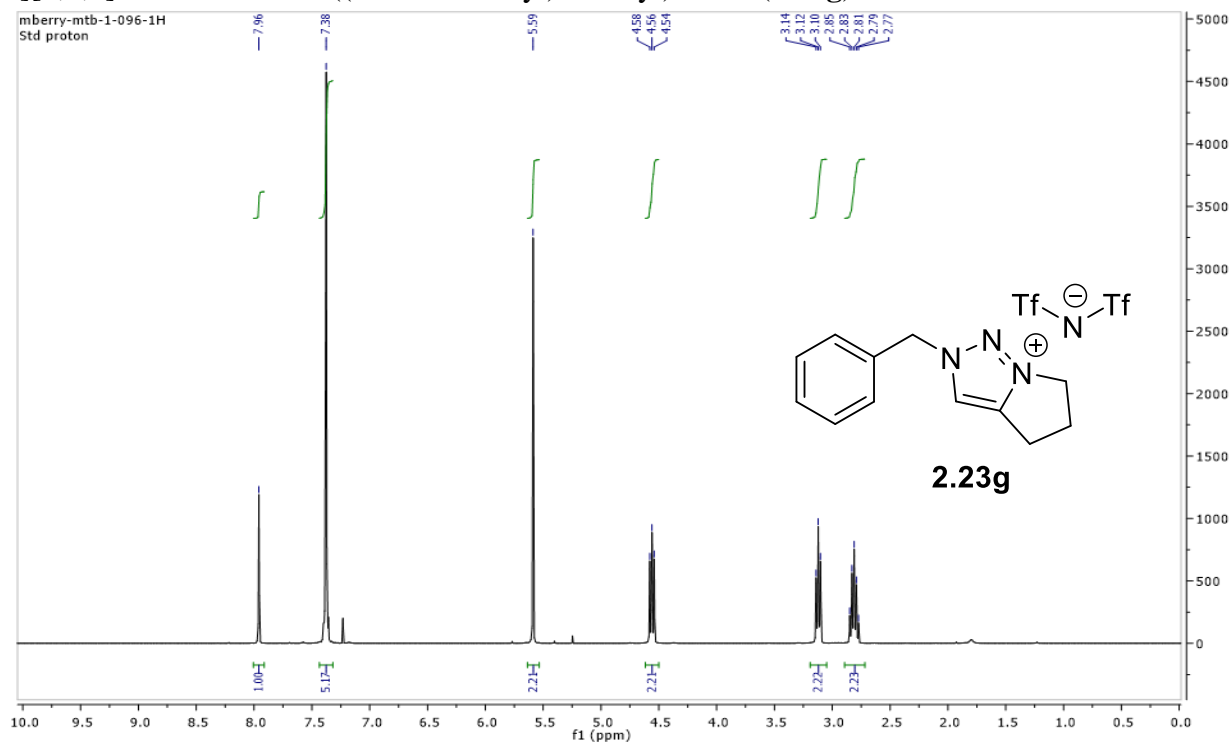
^{13}C NMR (100 MHz, acetone- d_6) spectrum for 2-(perfluorophenyl)-4,5,6,7-tetrahydro-2H-[1,2,3]triazolo[1,5-a]pyridin-8-ium bis((trifluoromethyl)sulfonyl)amide (**2.23f**):



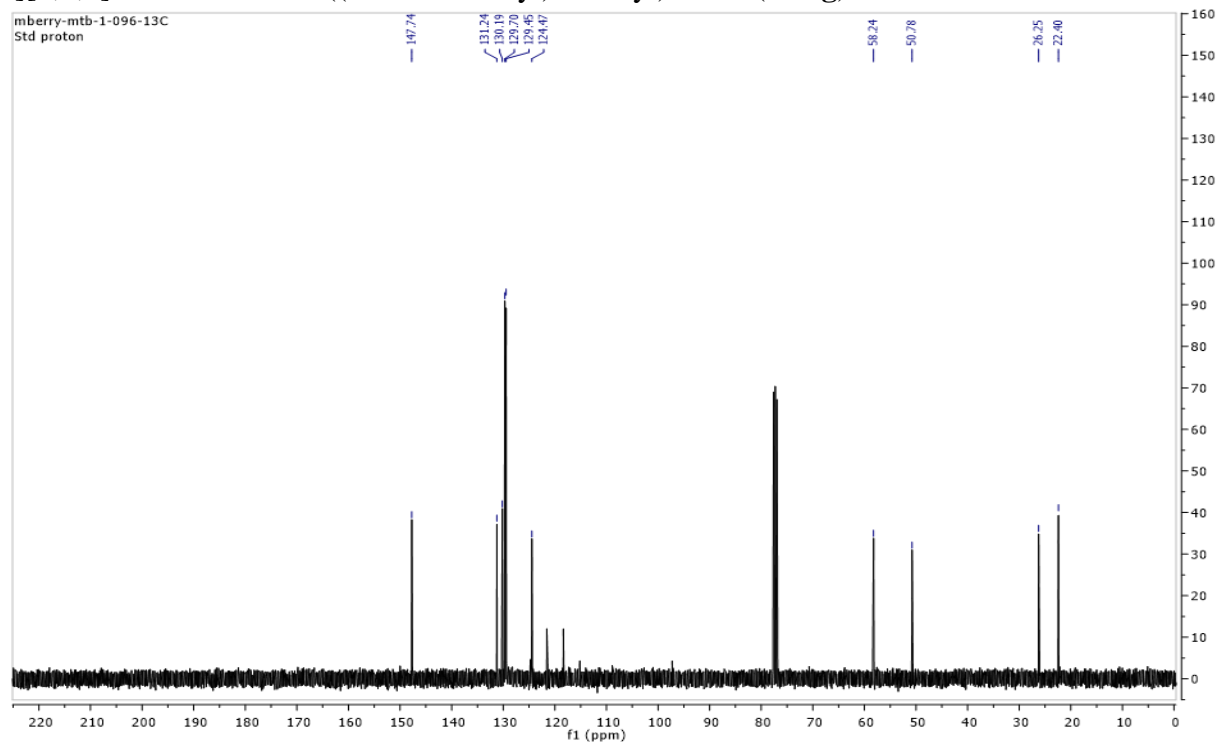
^{19}F NMR (375 MHz, acetone- d_6) spectrum for 2-(perfluorophenyl)-4,5,6,7-tetrahydro-2H-[1,2,3]triazolo[1,5-a]pyridin-8-ium bis((trifluoromethyl)sulfonyl)amide (**2.23f**):



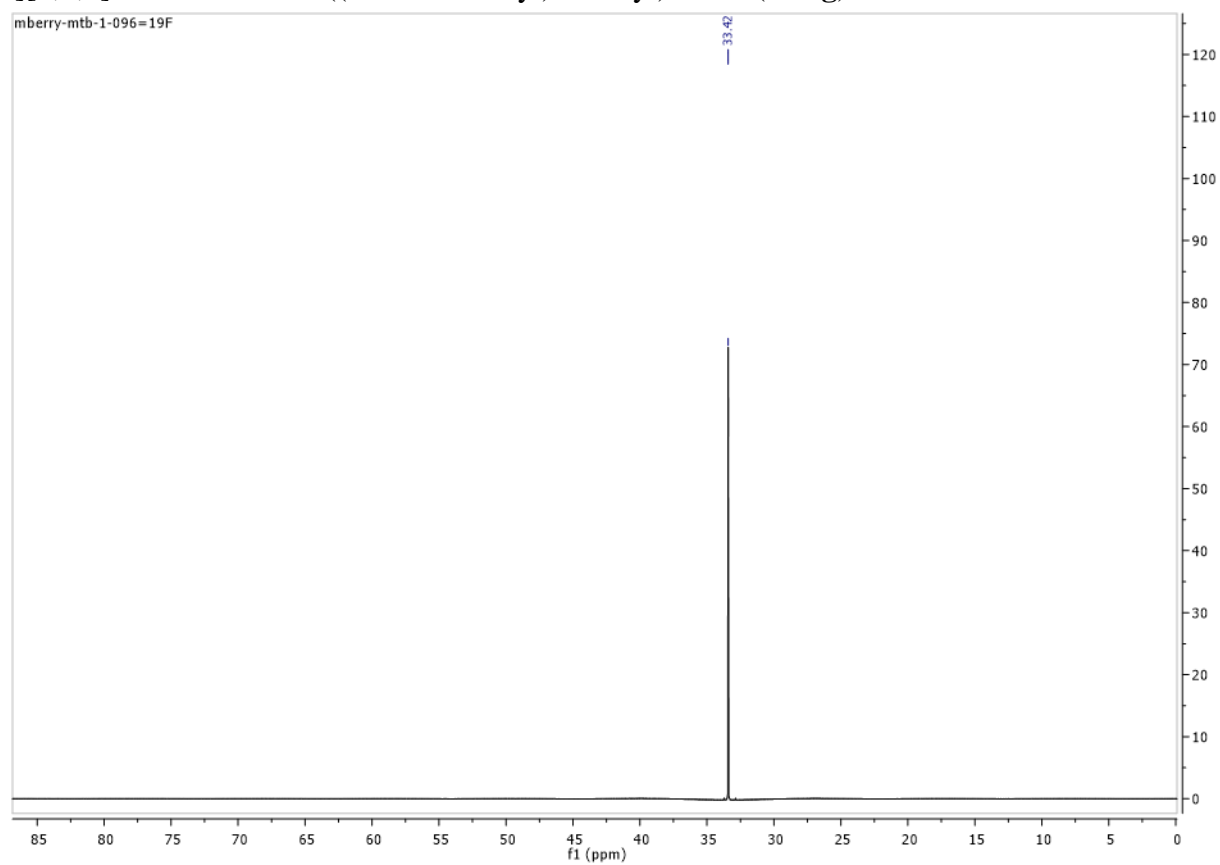
^1H NMR (400 MHz, CDCl_3) spectrum for 2-benzyl-2,4,5,6-tetrahydropyrrolo[1,2-c][1,2,3]triazol-7-ium bis((trifluoromethyl)sulfonyl)amide (**2.23g**):



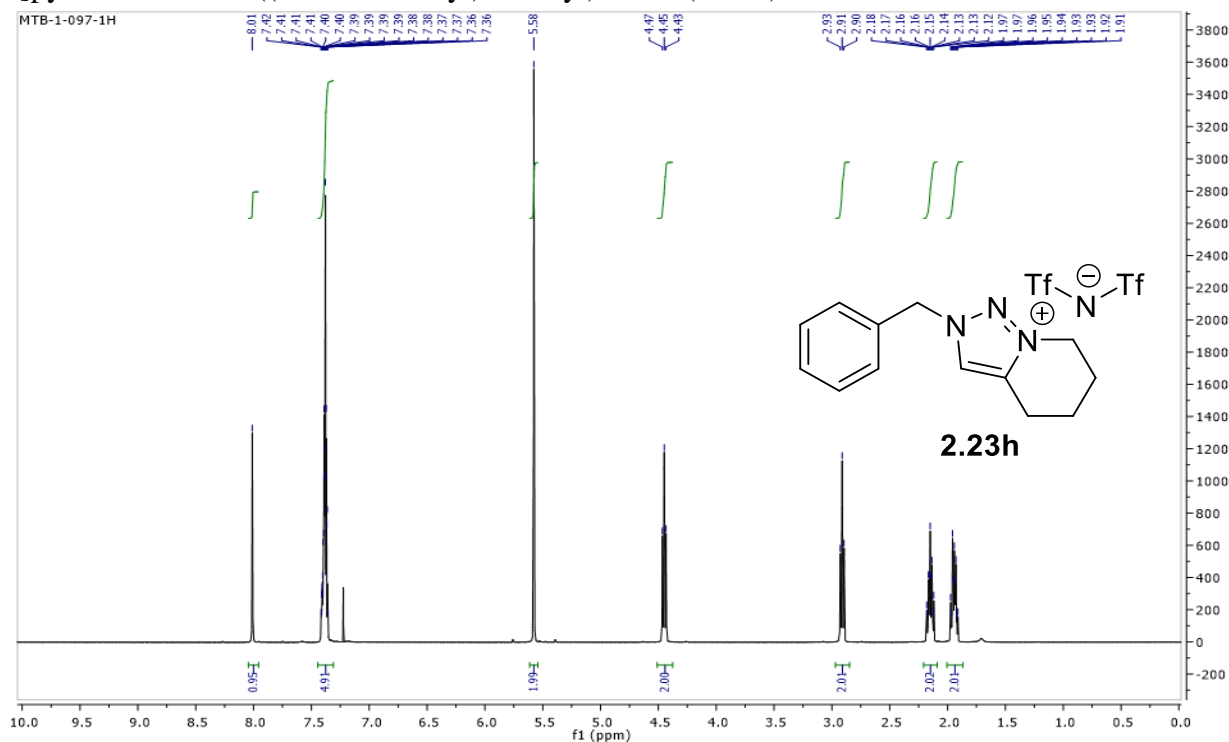
^{13}C NMR (100 MHz, CDCl_3) spectrum for 2-benzyl-2,4,5,6-tetrahydropyrrolo[1,2-c][1,2,3]triazol-7-ium bis((trifluoromethyl)sulfonyl)amide (**2.23g**):



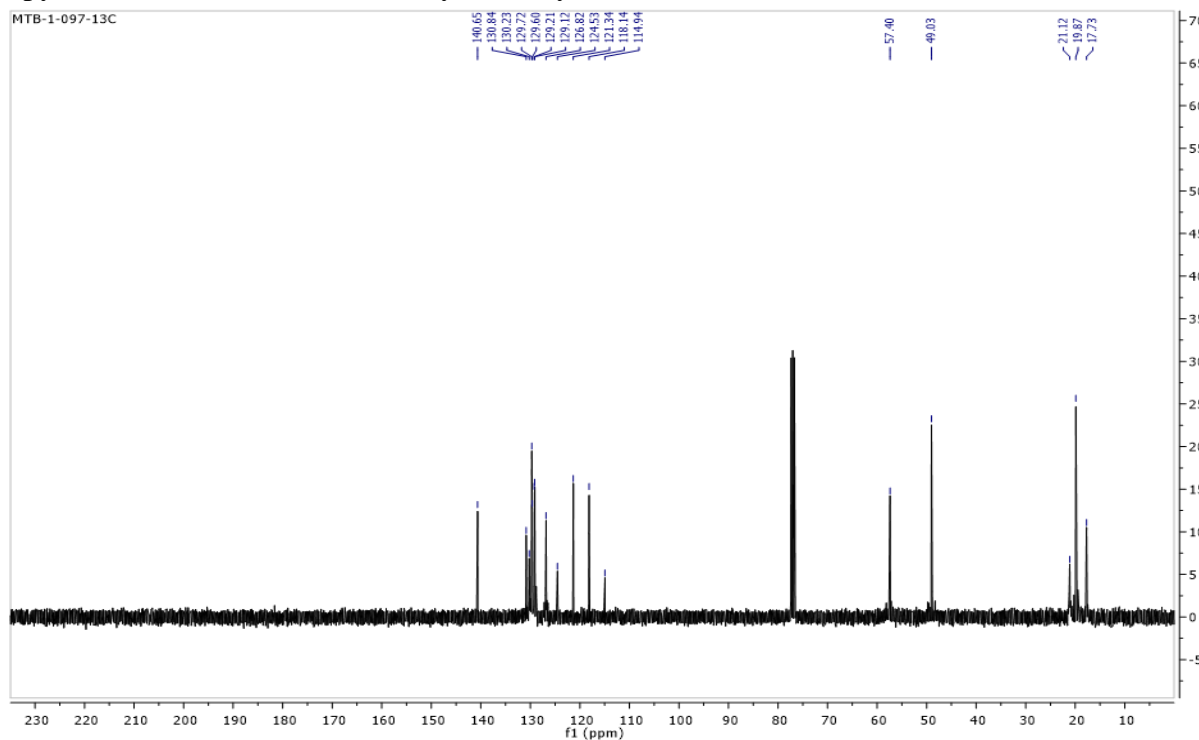
^{19}F NMR (375 MHz, CDCl_3) spectrum for 2-benzyl-2,4,5,6-tetrahydropyrrolo[1,2-c][1,2,3]triazol-7-ium bis((trifluoromethyl)sulfonyl)amide (**2.23g**):



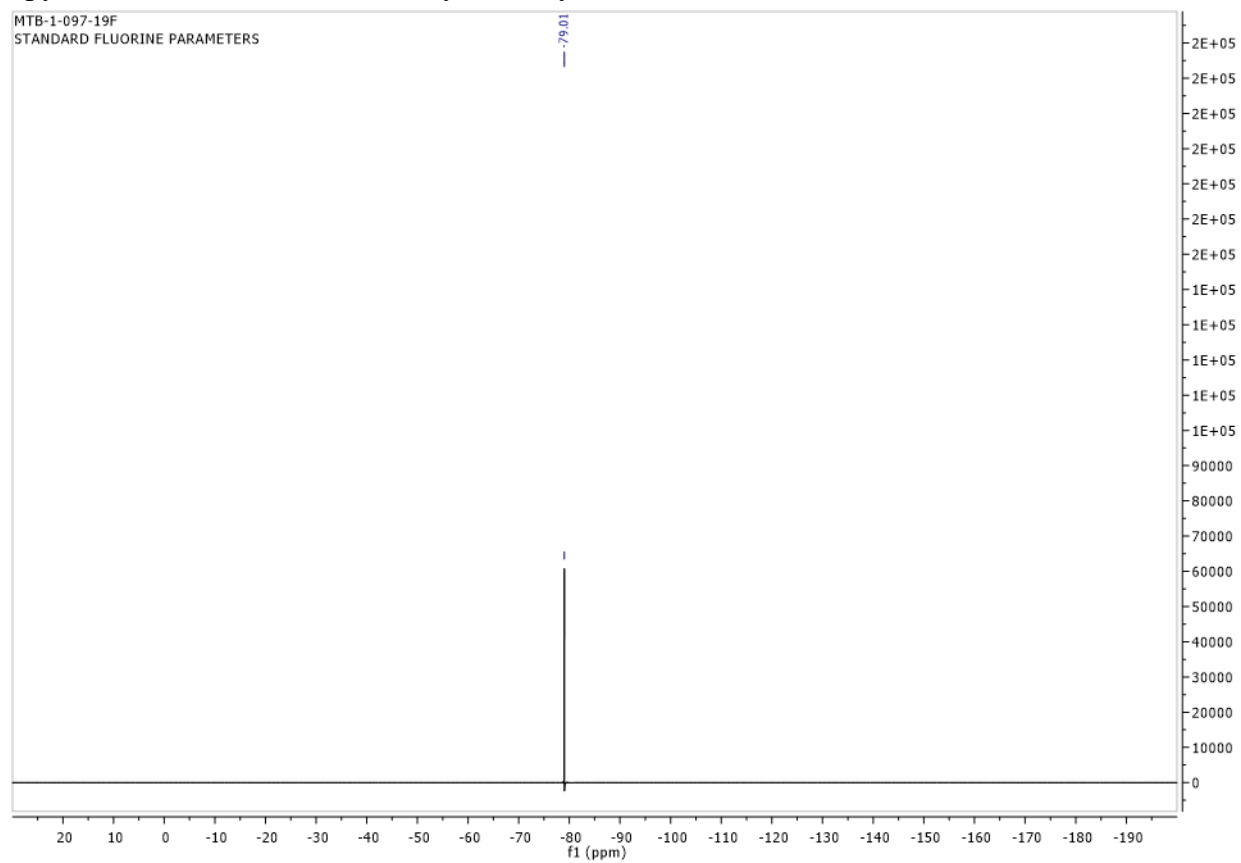
^1H NMR (400 MHz, CDCl_3) spectrum for 2-benzyl-4,5,6,7-tetrahydro-2H-[1,2,3]triazolo[1,5-a]pyridin-8-ium bis((trifluoromethyl)sulfonyl)amide (**2.23h**):



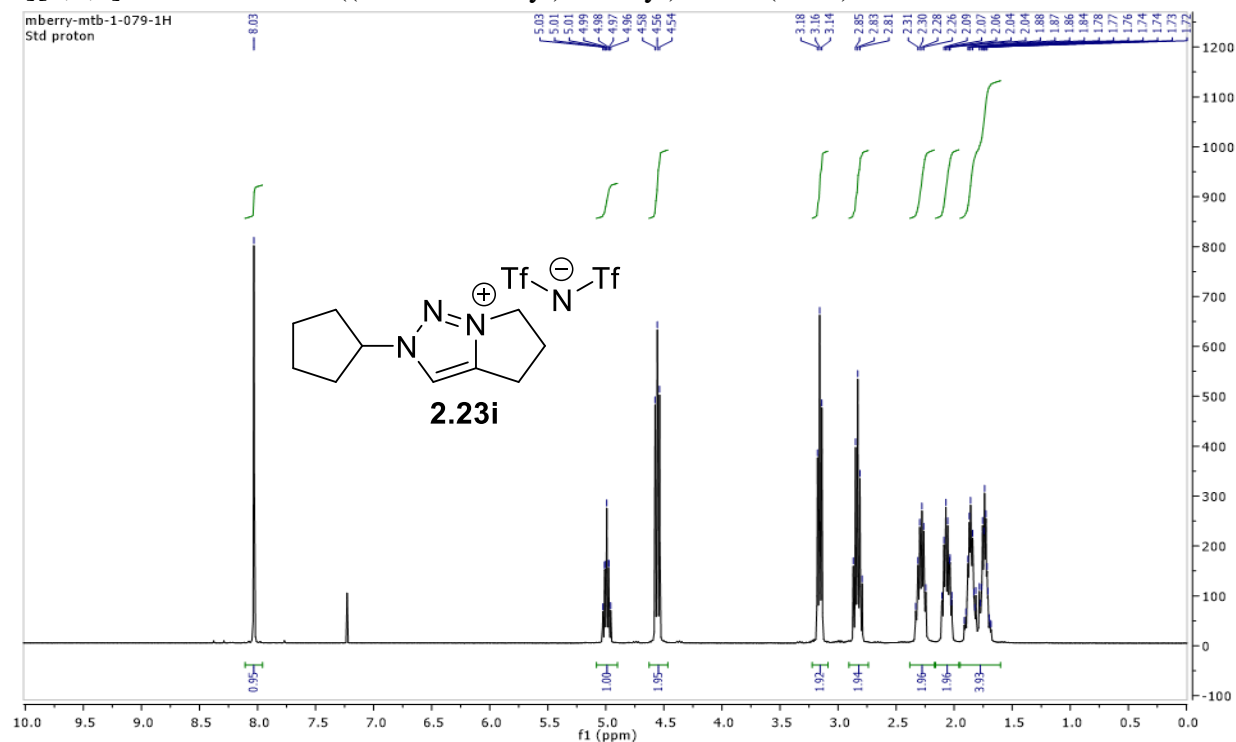
^{13}C NMR (100 MHz, CDCl_3) spectrum for 2-benzyl-4,5,6,7-tetrahydro-2H-[1,2,3]triazolo[1,5-a]pyridin-8-ium bis((trifluoromethyl)sulfonyl)amide (**2.23h**):



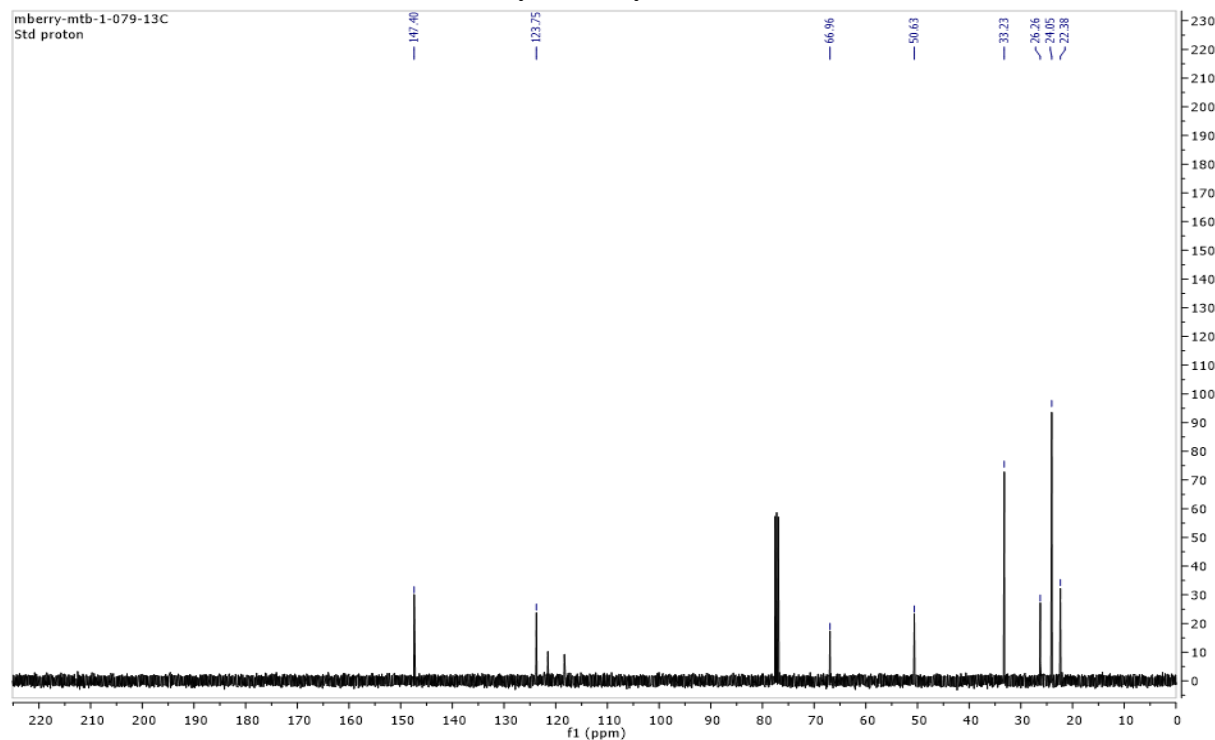
^{19}F NMR (375 MHz, CDCl_3) spectrum for 2-benzyl-4,5,6,7-tetrahydro-2H-[1,2,3]triazolo[1,5-a]pyridin-8-ium bis((trifluoromethyl)sulfonyl)amide (**2.23h**):



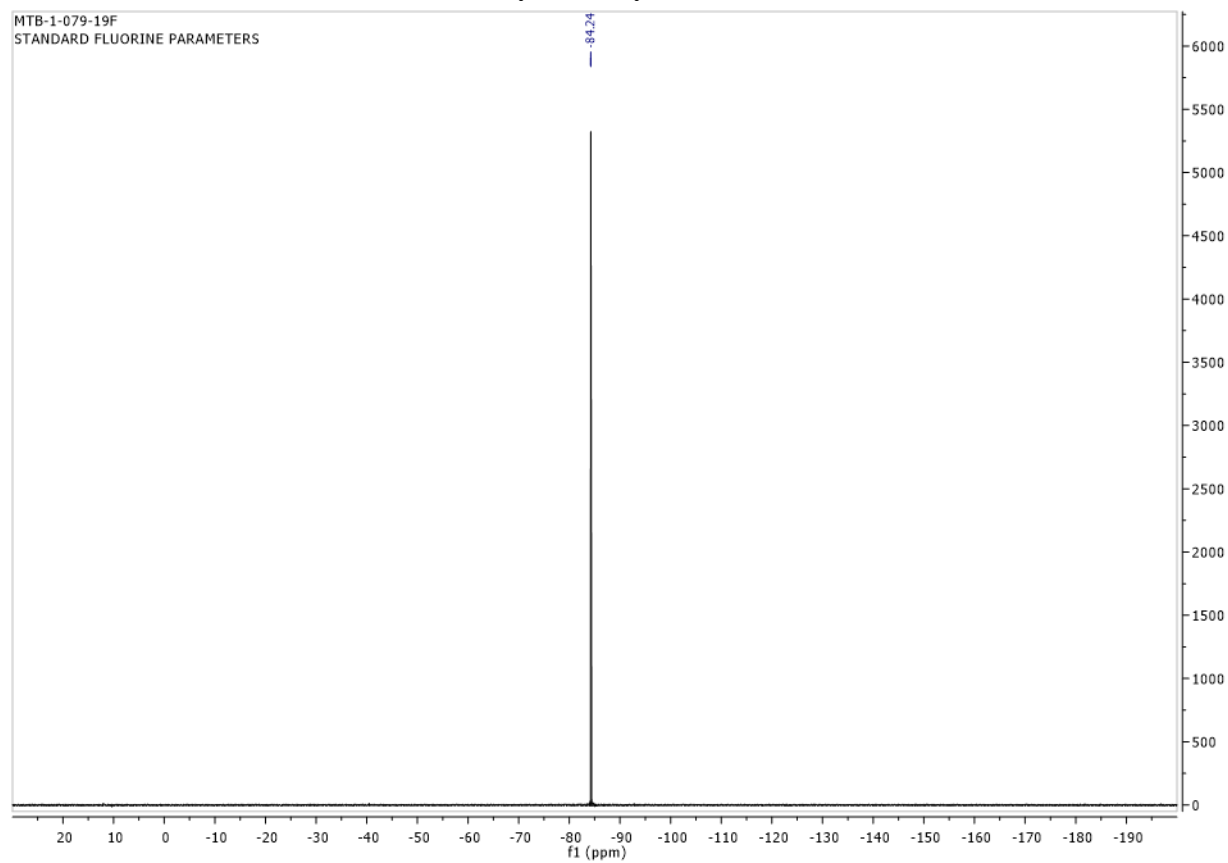
^1H NMR (400 MHz, CDCl_3) spectrum for 2-cyclopentyl-2,4,5,6-tetrahydropyrrolo[1,2-c][1,2,3]triazol-7-ium bis((trifluoromethyl)sulfonyl)amide (**2.23i**):



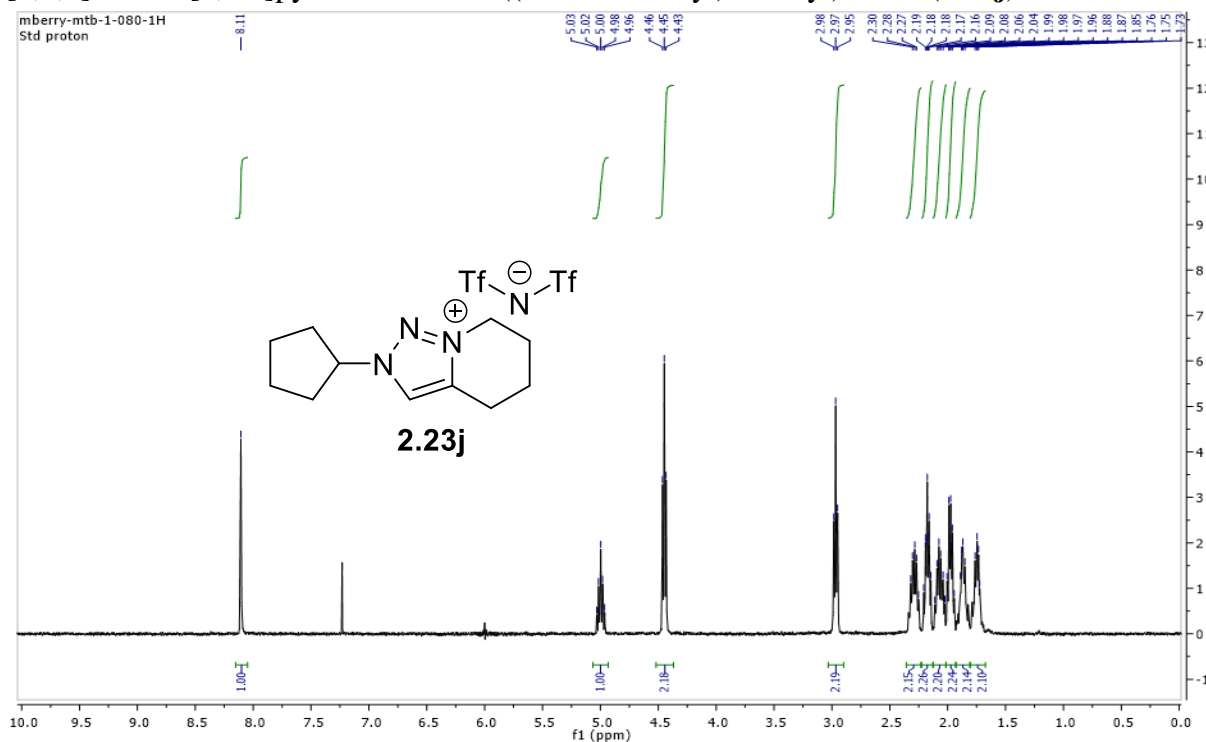
^{13}C NMR (100 MHz, CDCl_3) spectrum for 2-cyclopentyl-2,4,5,6-tetrahydropyrrolo[1,2-c][1,2,3]triazol-7-ium bis((trifluoromethyl)sulfonyl)amide (**2.23i**):



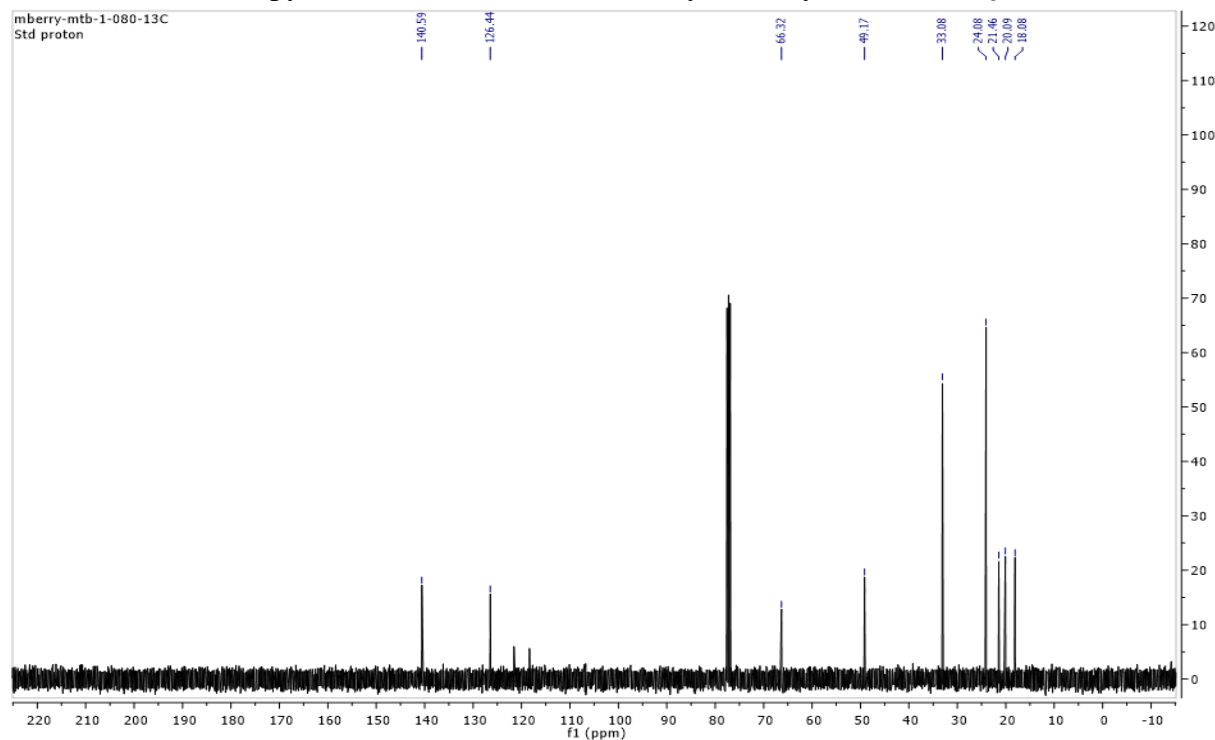
^{19}F NMR (375 MHz, CDCl_3) spectrum for 2-cyclopentyl-2,4,5,6-tetrahydropyrrolo[1,2-c][1,2,3]triazol-7-ium bis((trifluoromethyl)sulfonyl)amide (**2.23i**):



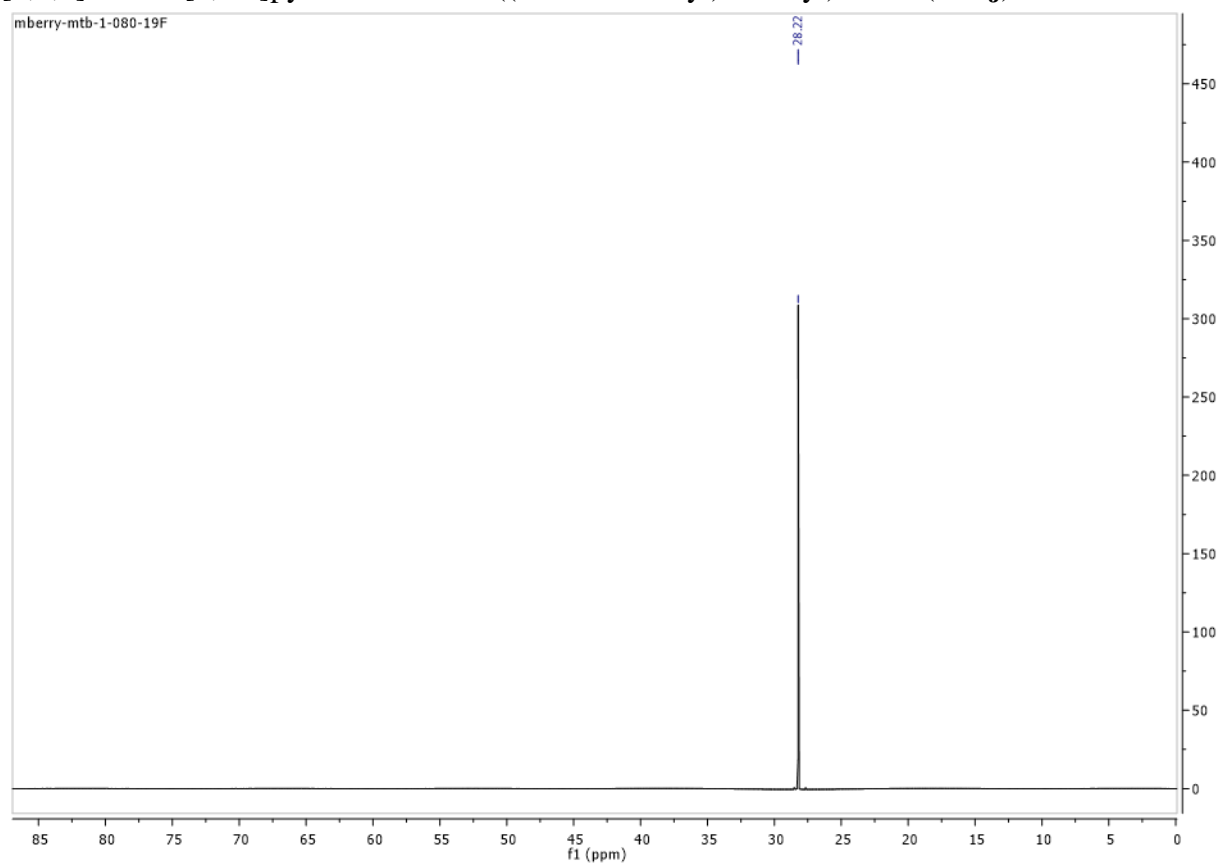
^1H NMR (400 MHz, CDCl_3) spectrum for 2-cyclopentyl-4,5,6,7-tetrahydro-2H-[1,2,3]triazolo[1,5-a]pyridin-8-ium bis((trifluoromethyl)sulfonyl)amide (**2.23j**):



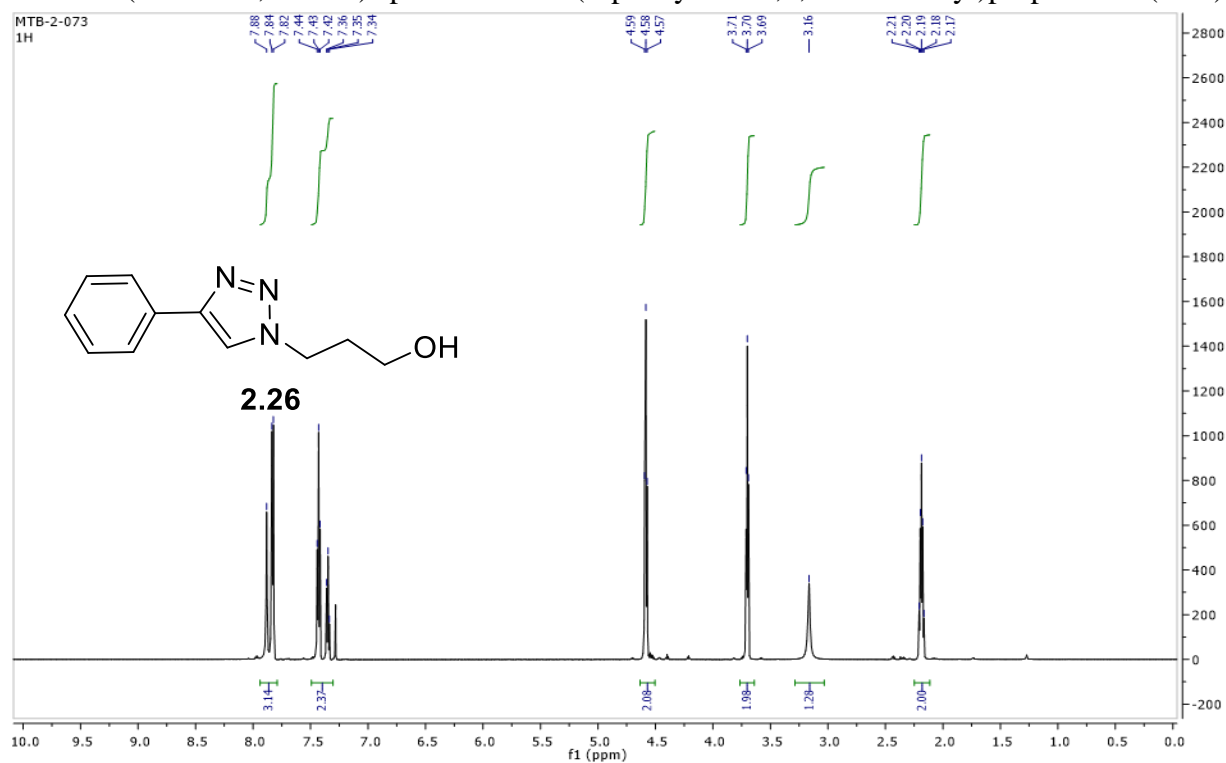
^{13}C NMR (100 MHz, CDCl_3) spectrum for 2-cyclopentyl-4,5,6,7-tetrahydro-2H-[1,2,3]triazolo[1,5-a]pyridin-8-ium bis((trifluoromethyl)sulfonyl)amide (**2.23j**):



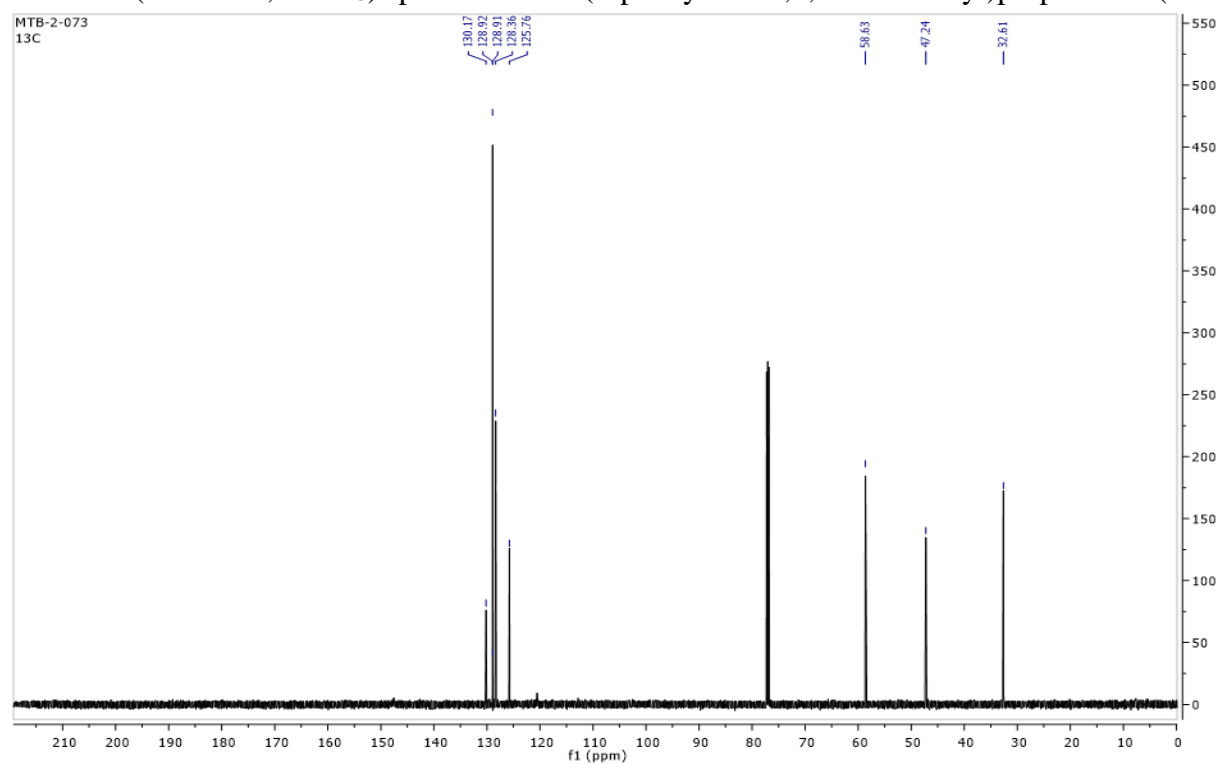
^{19}F NMR (375 MHz, CDCl_3) spectrum for 2-cyclopentyl-4,5,6,7-tetrahydro-2H-[1,2,3]triazolo[1,5-a]pyridin-8-ium bis((trifluoromethyl)sulfonyl)amide (**2.23j**):



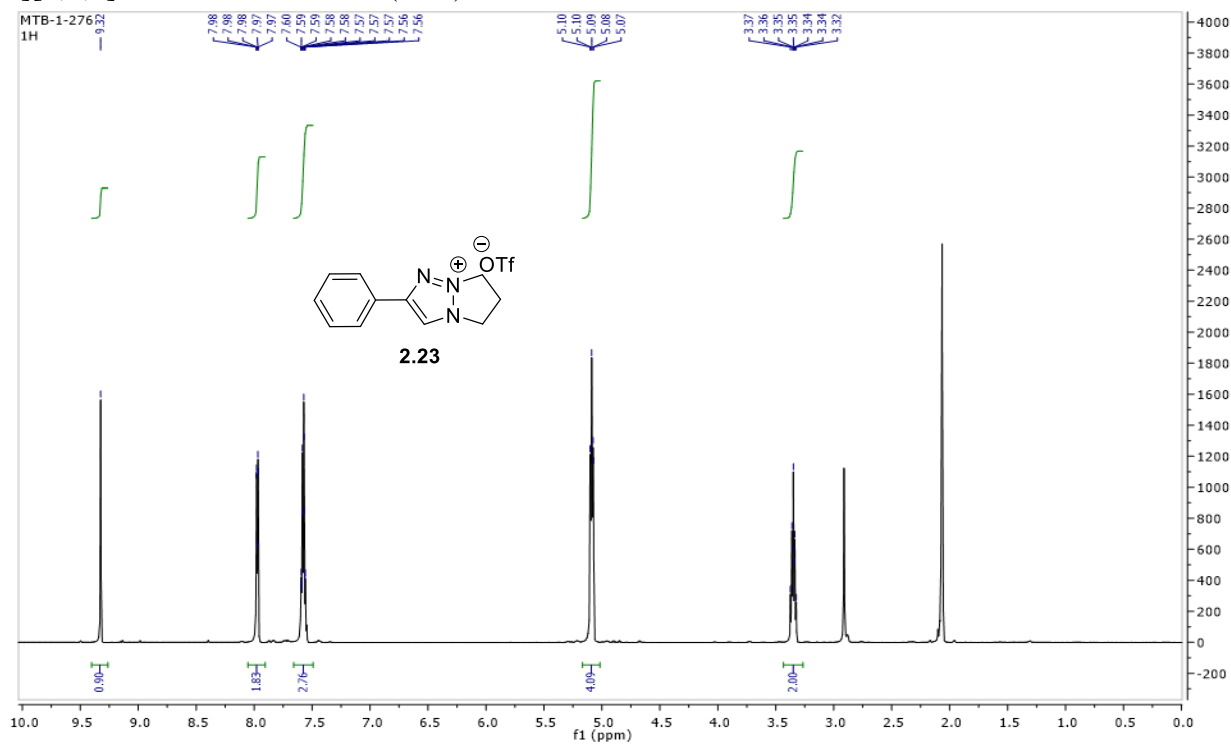
^1H NMR (600 MHz, CDCl_3) spectrum for 3-(4-phenyl-1H-1,2,3-triazol-1-yl)propan-1-ol (**2.26**):



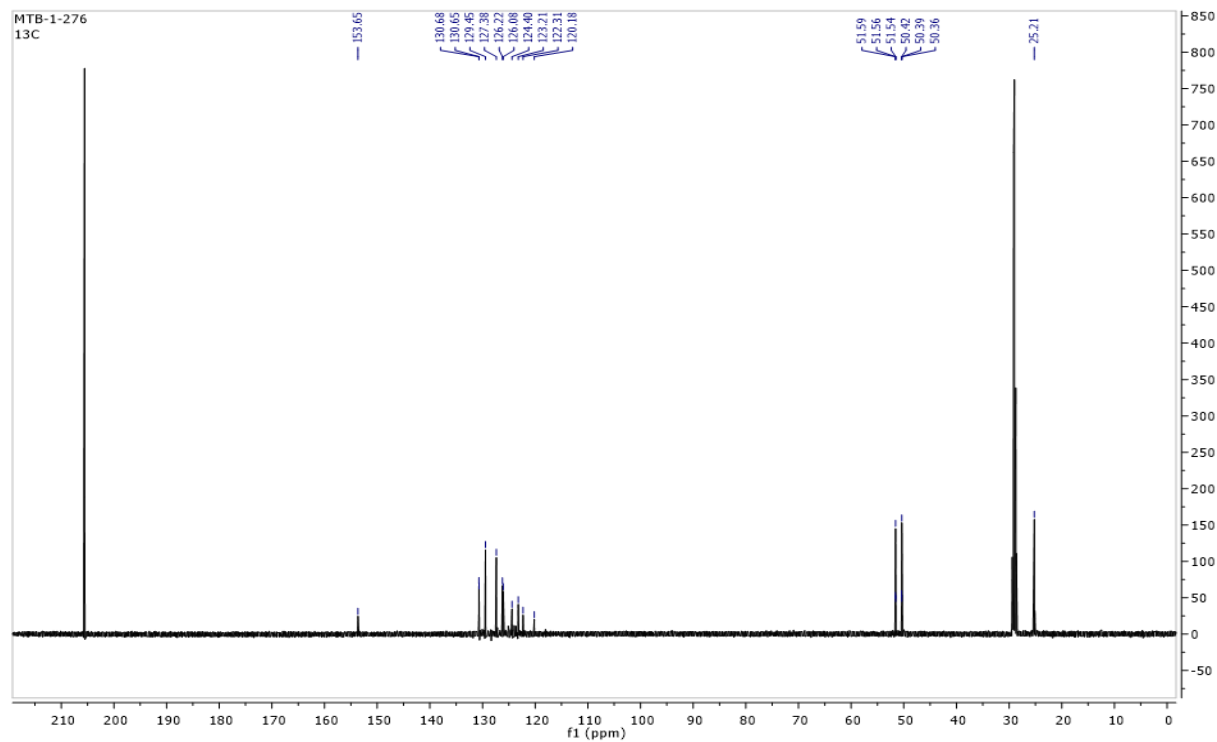
^{13}C NMR (150 MHz, CDCl_3) spectrum for 3-(4-phenyl-1H-1,2,3-triazol-1-yl)propan-1-ol (**2.26**):



^1H NMR (600 MHz, acetone- d_6) spectrum for 2-phenyl-6,7-dihydro-5H-pyrazolo[1,2-a][1,2,3]triazol-8-ium triflate (**2.27**):

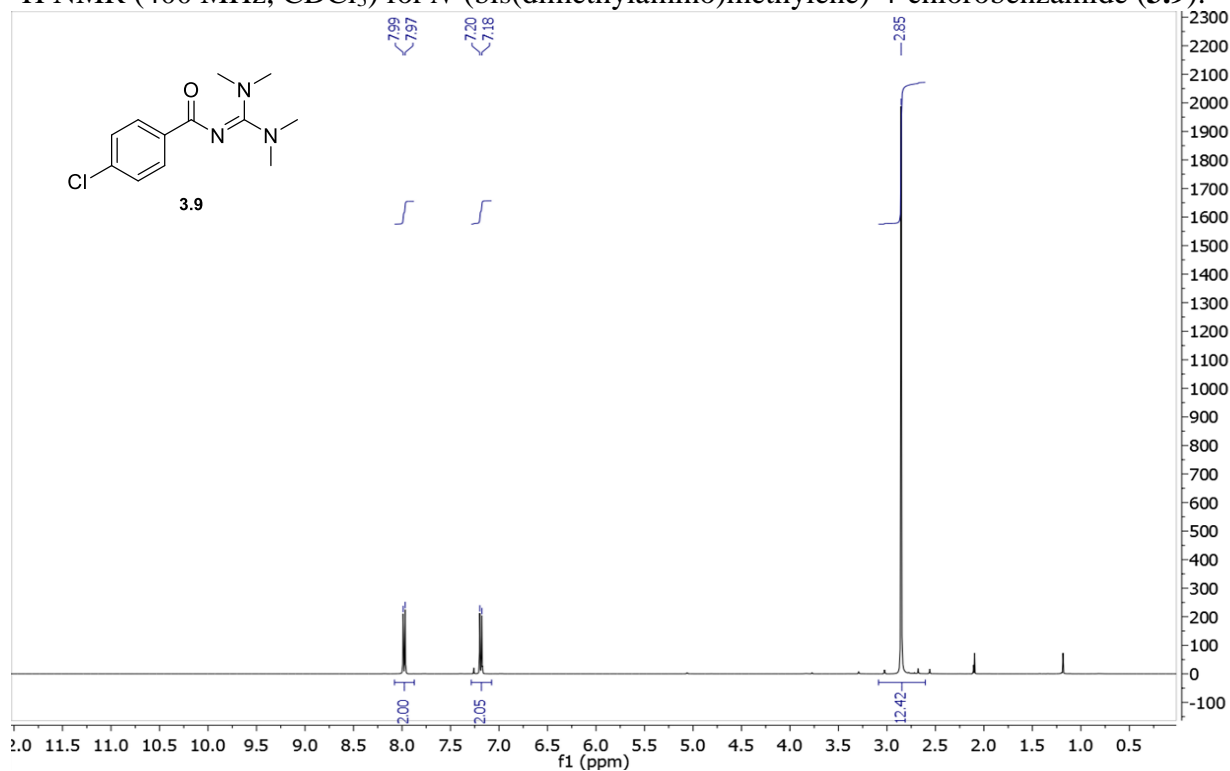


^{13}C NMR (150 MHz, acetone- d_6) spectrum for 2-phenyl-6,7-dihydro-5H-pyrazolo[1,2-a][1,2,3]triazol-8-ium triflate (**2.23**):

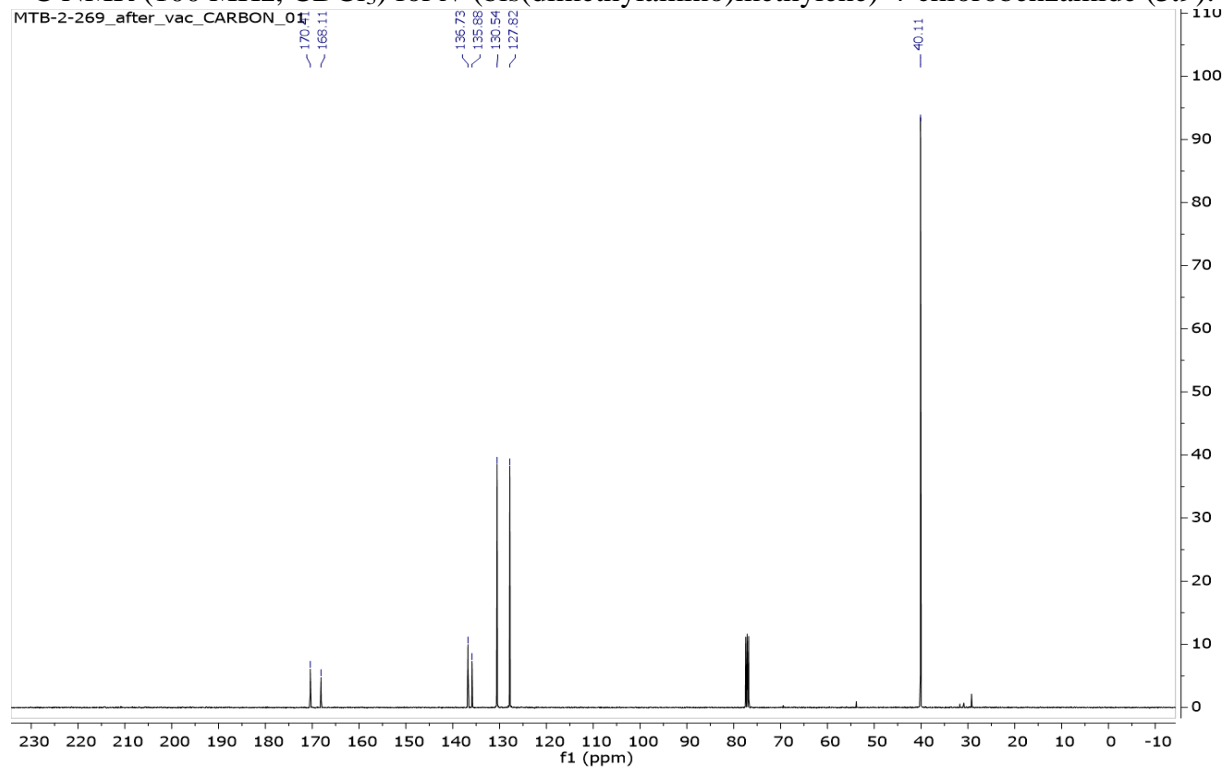


Appendix B NMR spectra from Chapter 3

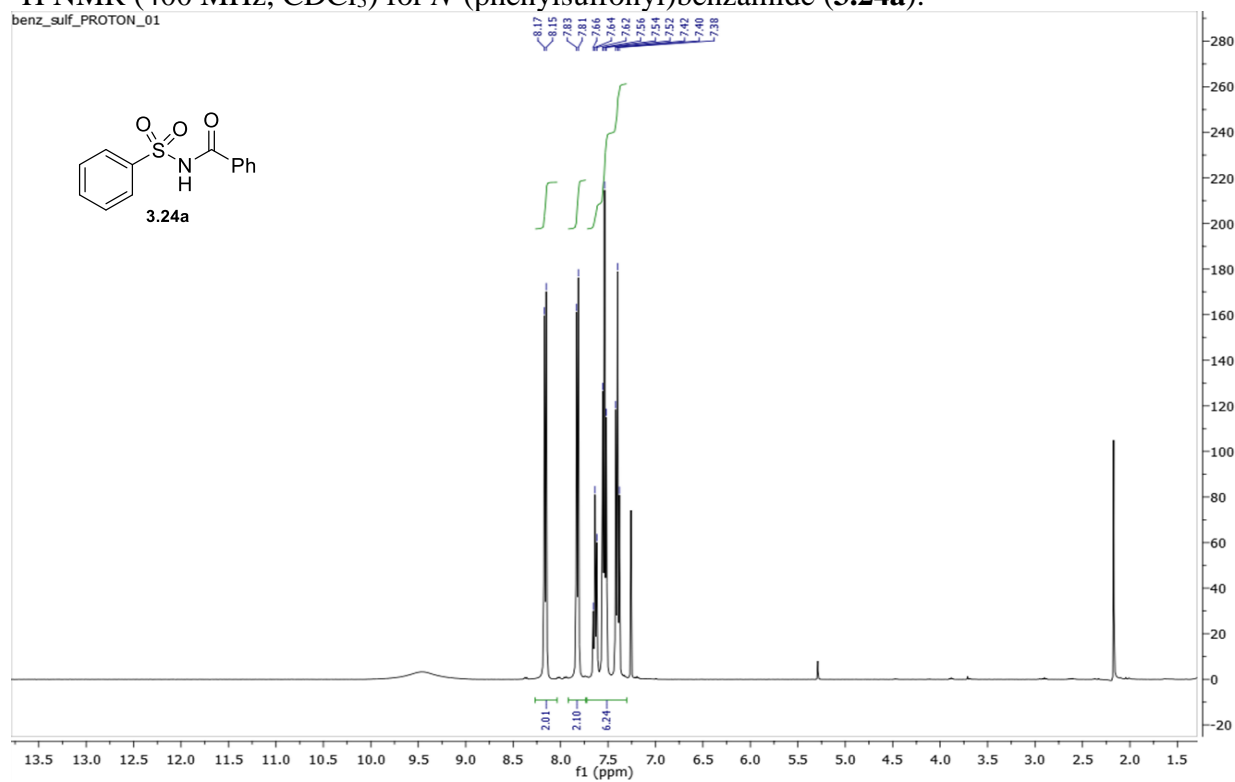
^1H NMR (400 MHz, CDCl_3) for *N*-(bis(dimethylamino)methylene)-4-chlorobenzamide (**3.9**):



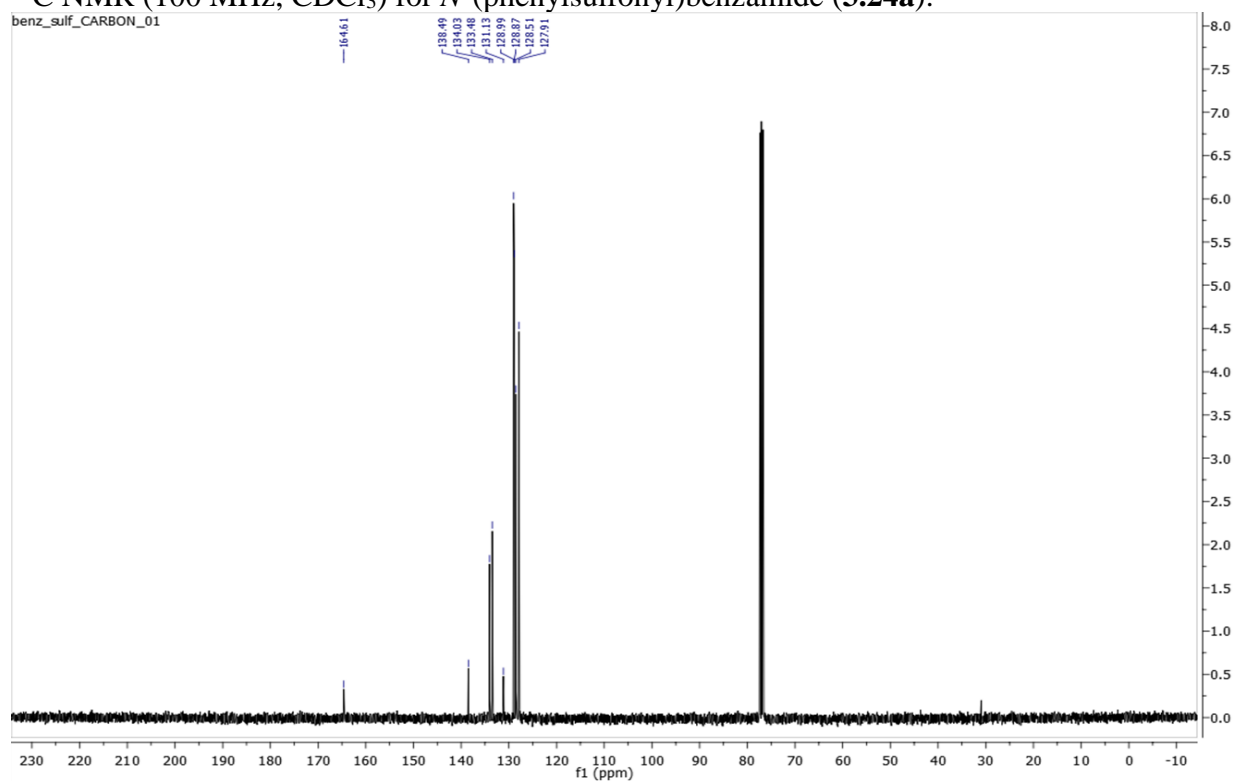
^{13}C NMR (100 MHz, CDCl_3) for *N*-(bis(dimethylamino)methylene)-4-chlorobenzamide (**3.9**):



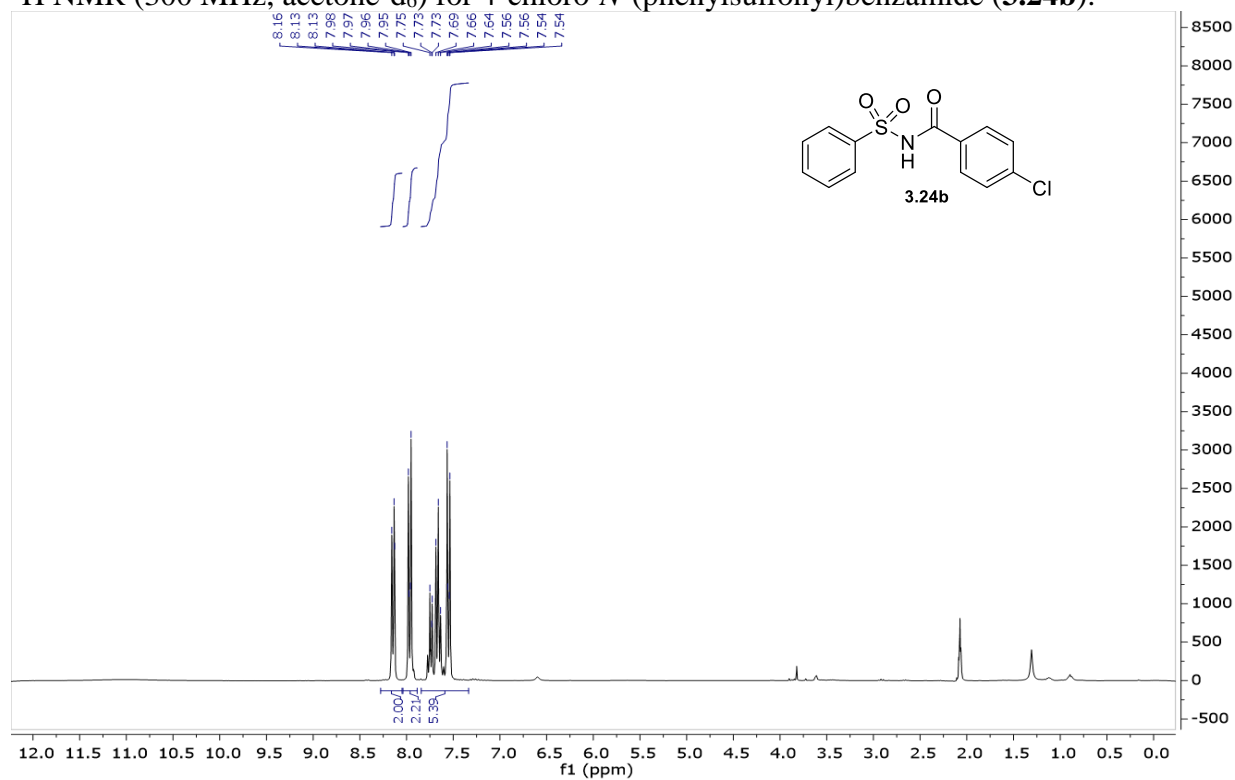
^1H NMR (400 MHz, CDCl_3) for *N*-(phenylsulfonyl)benzamide (**3.24a**):



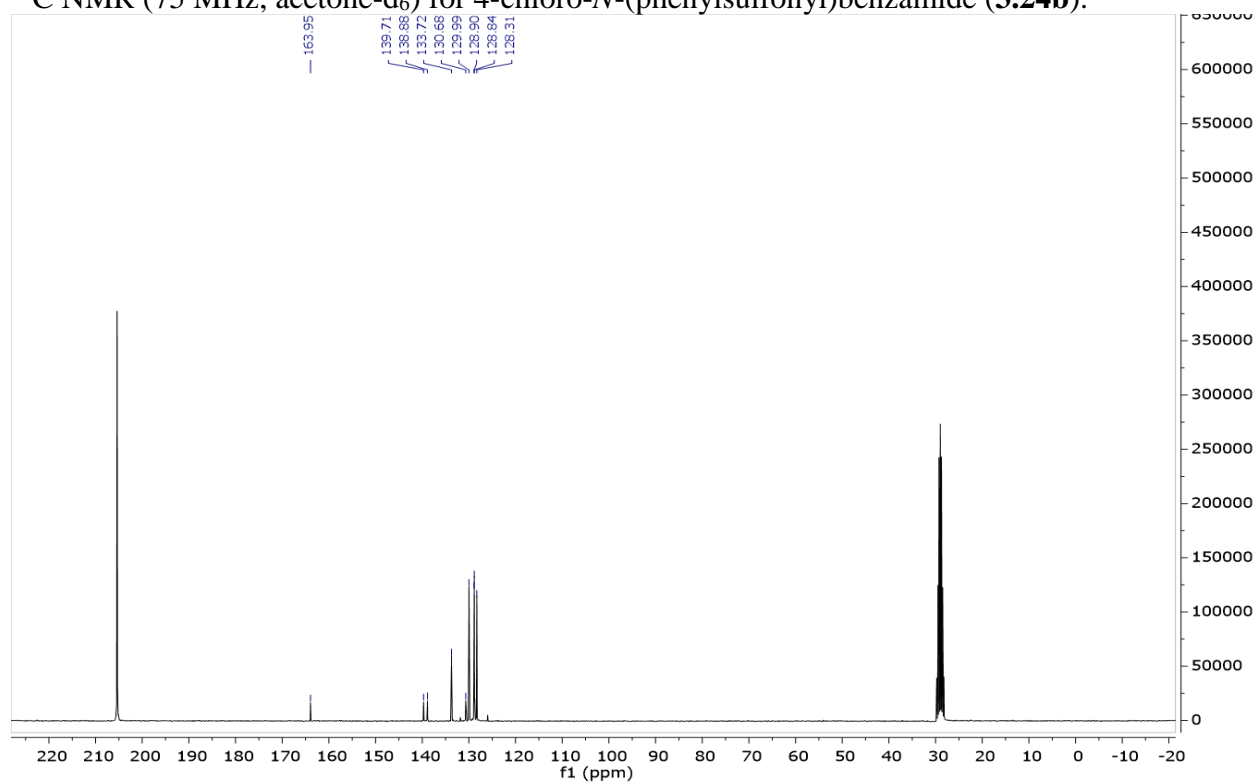
^{13}C NMR (100 MHz, CDCl_3) for *N*-(phenylsulfonyl)benzamide (**3.24a**):



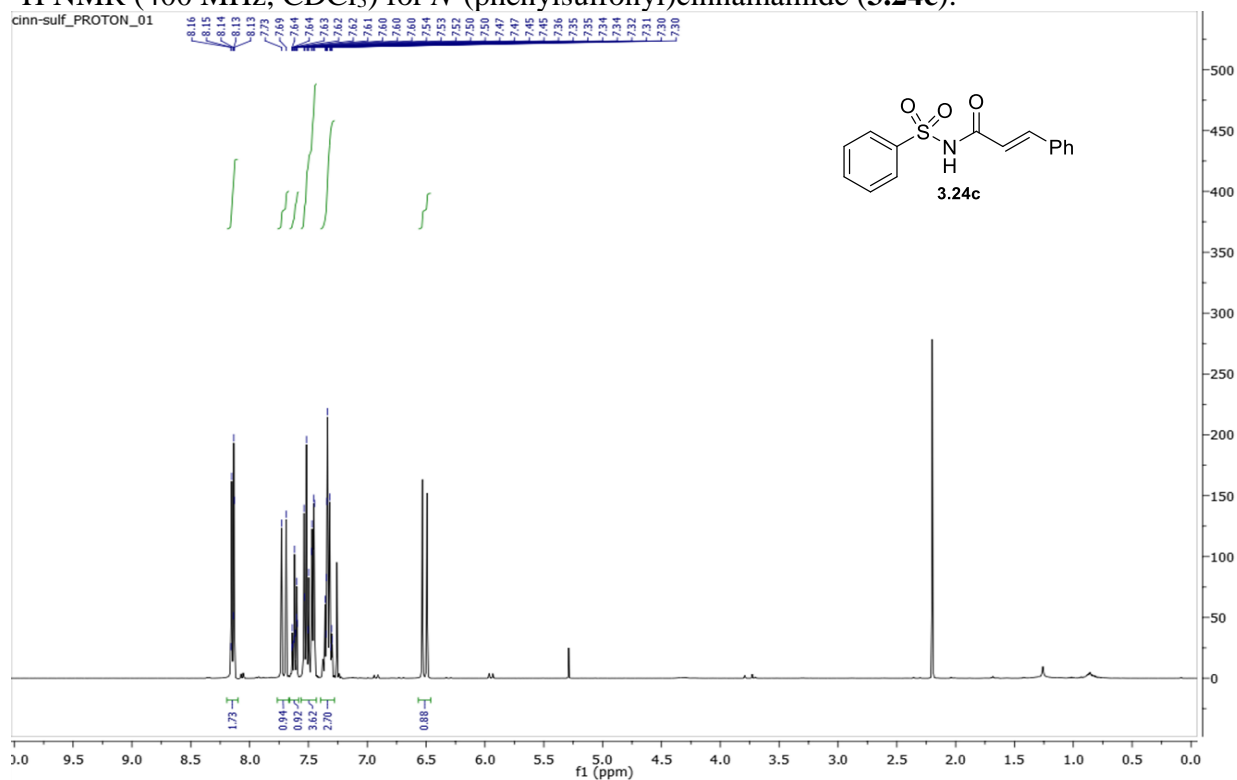
^1H NMR (300 MHz, acetone- d_6) for 4-chloro-*N*-(phenylsulfonyl)benzamide (**3.24b**):



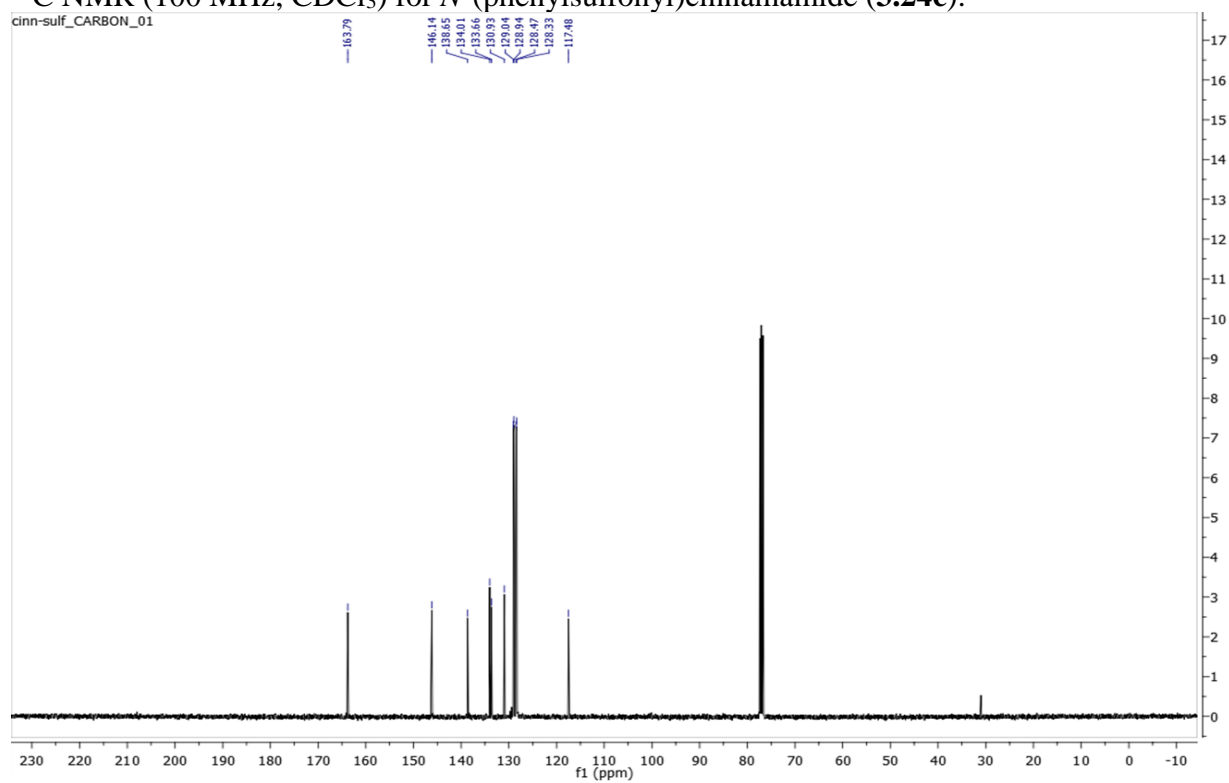
^{13}C NMR (75 MHz, acetone- d_6) for 4-chloro-*N*-(phenylsulfonyl)benzamide (**3.24b**):



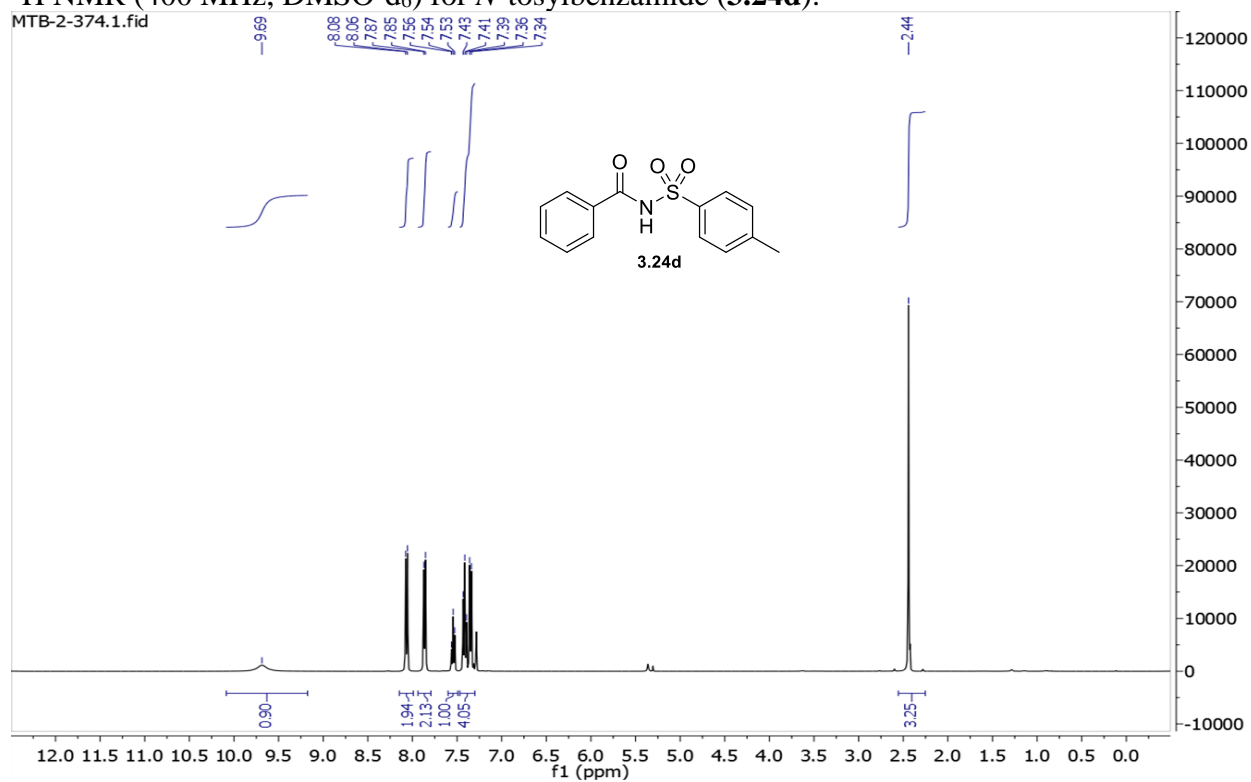
^1H NMR (400 MHz, CDCl_3) for *N*-(phenylsulfonyl)cinnamamide (**3.24c**):



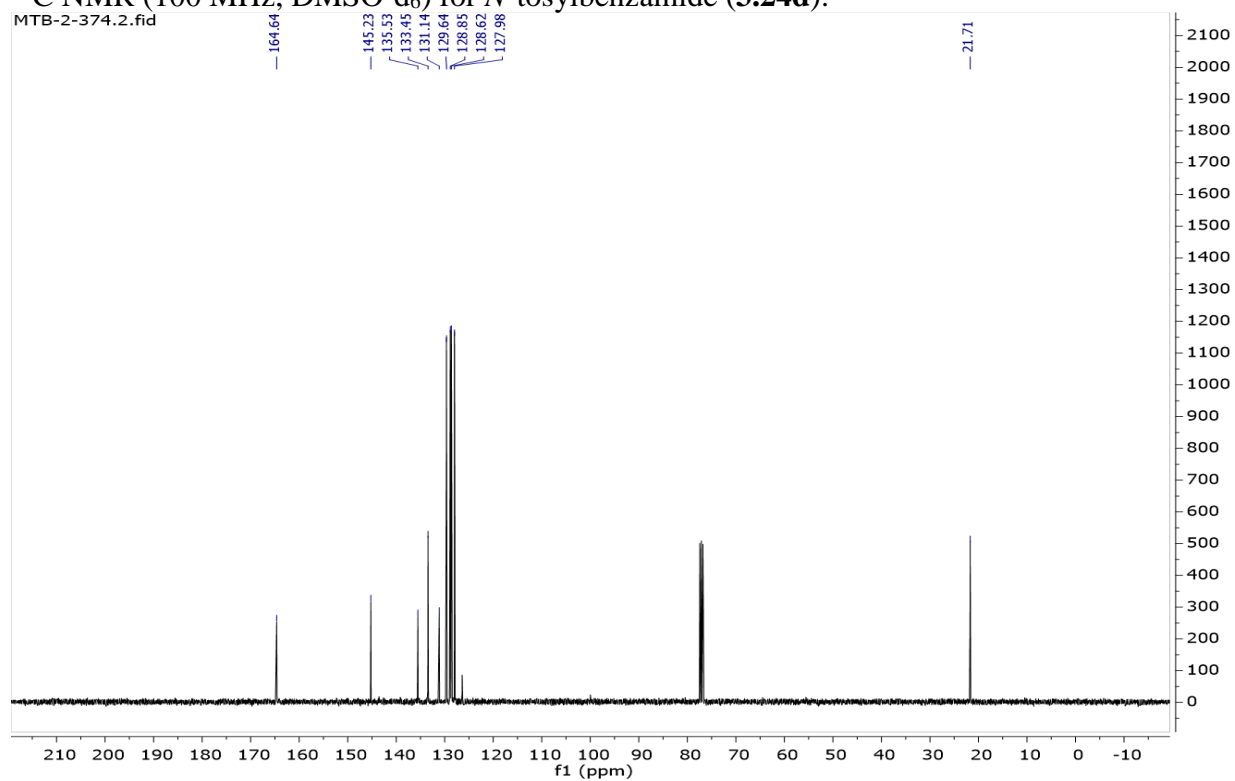
^{13}C NMR (100 MHz, CDCl_3) for *N*-(phenylsulfonyl)cinnamamide (**3.24c**):



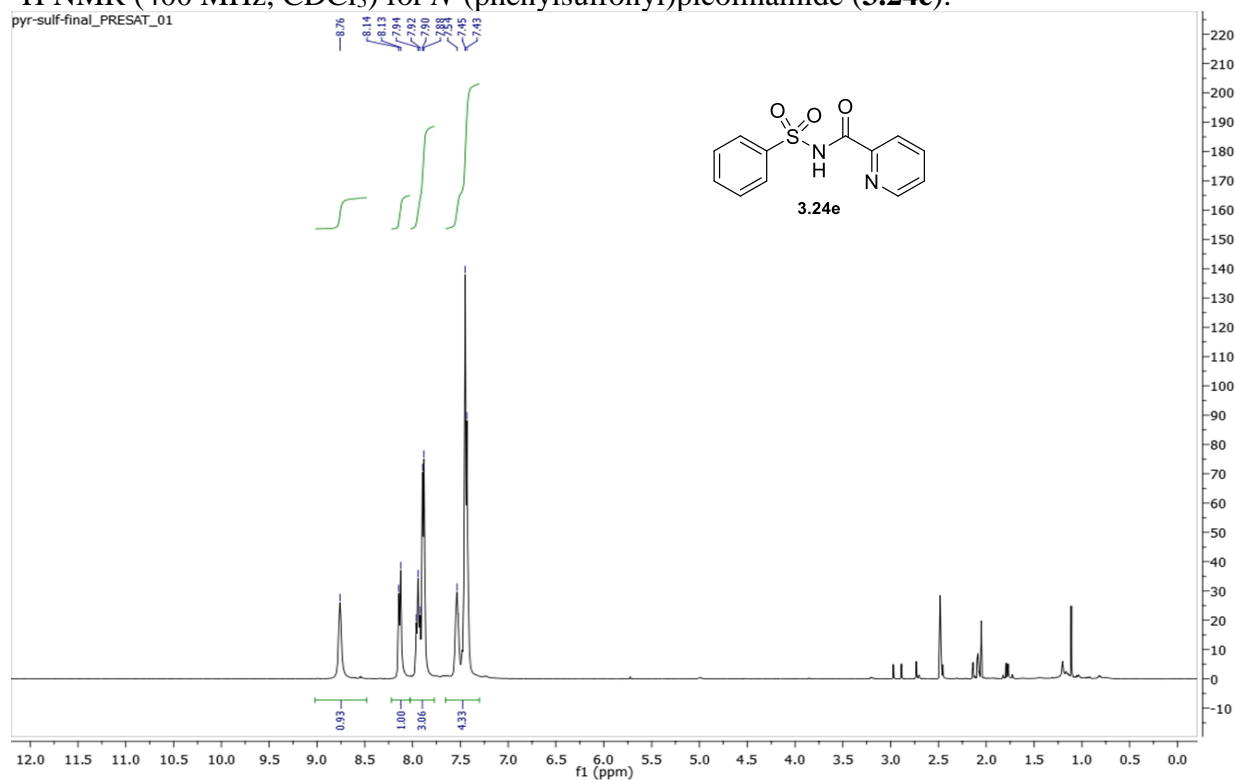
^1H NMR (400 MHz, DMSO- d_6) for *N*-tosylbenzamide (**3.24d**):



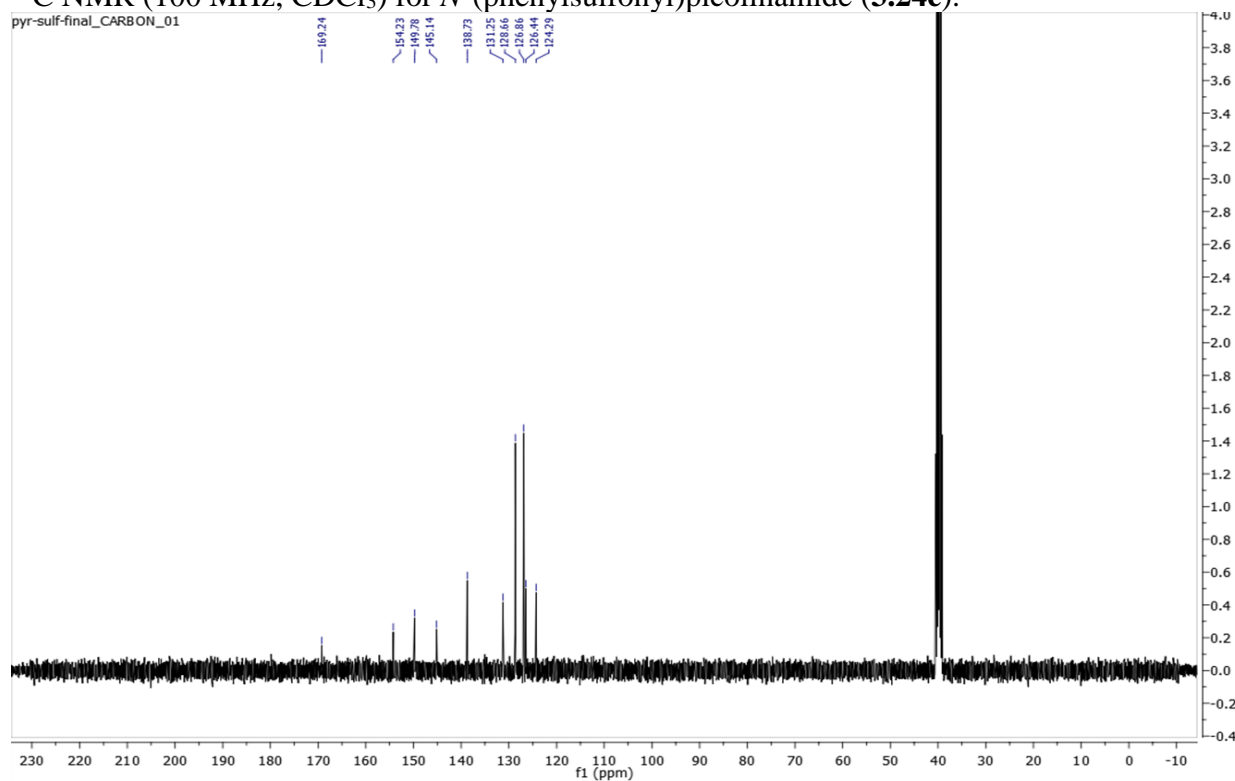
^{13}C NMR (100 MHz, DMSO- d_6) for *N*-tosylbenzamide (**3.24d**):



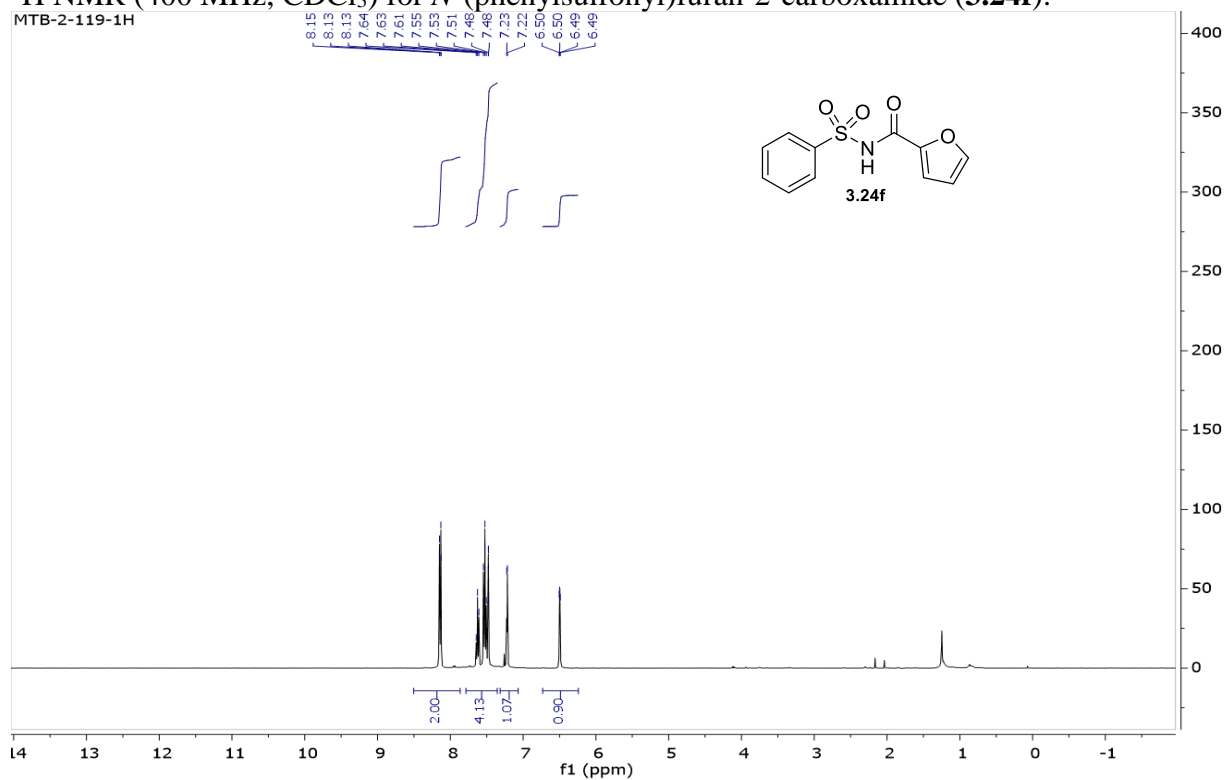
^1H NMR (400 MHz, CDCl_3) for *N*-(phenylsulfonyl)picolinamide (**3.24e**):



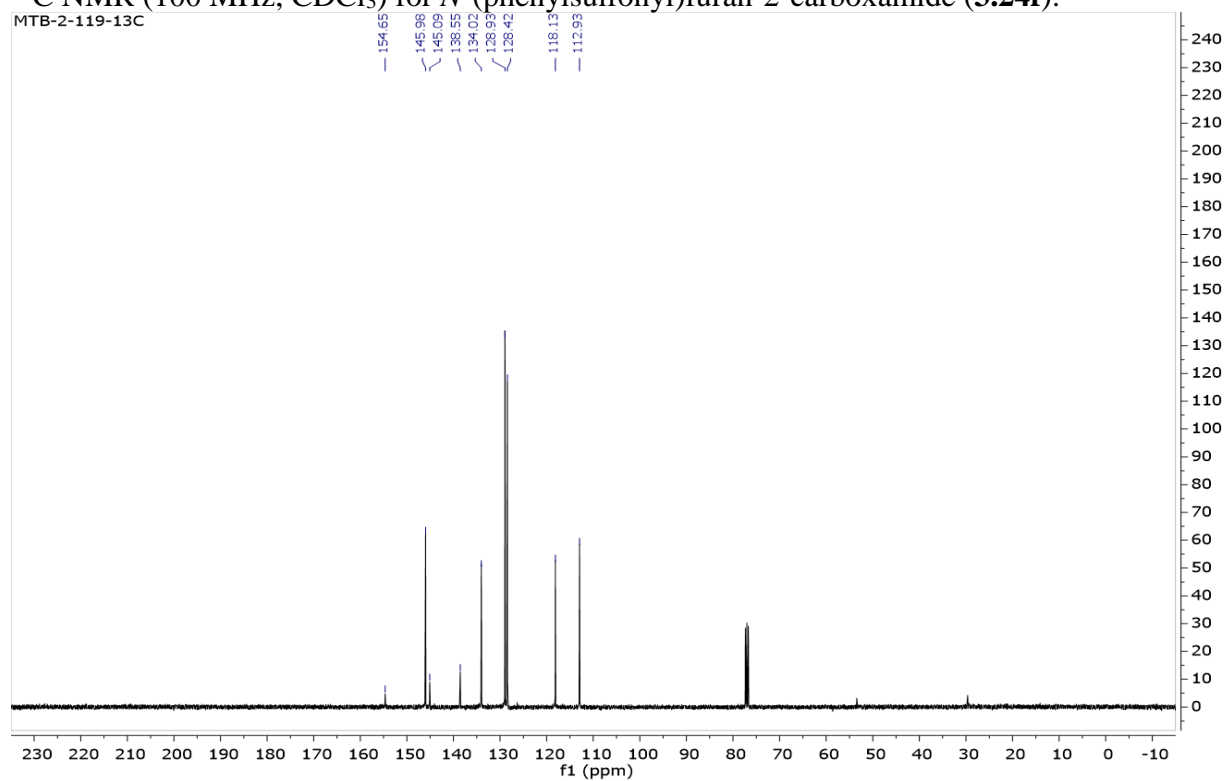
^{13}C NMR (100 MHz, CDCl_3) for *N*-(phenylsulfonyl)picolinamide (**3.24e**):



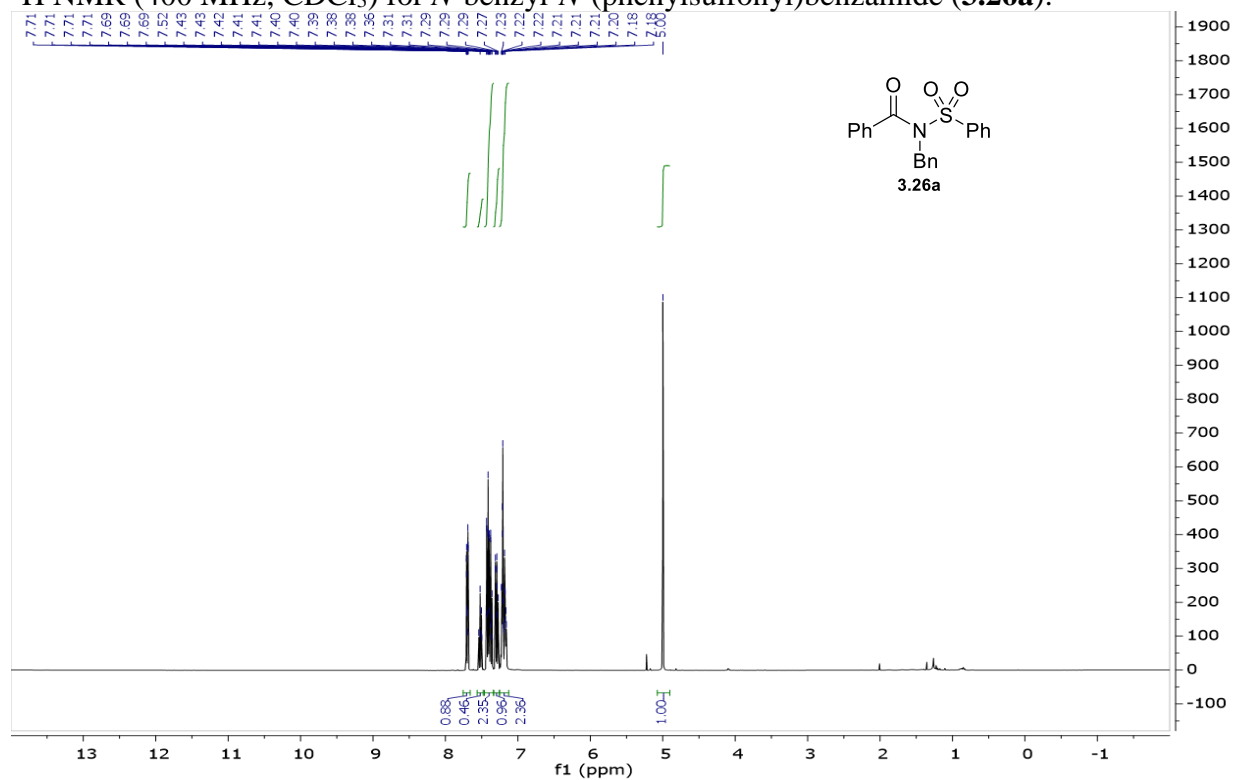
^1H NMR (400 MHz, CDCl_3) for *N*-(phenylsulfonyl)furan-2-carboxamide (**3.24f**):



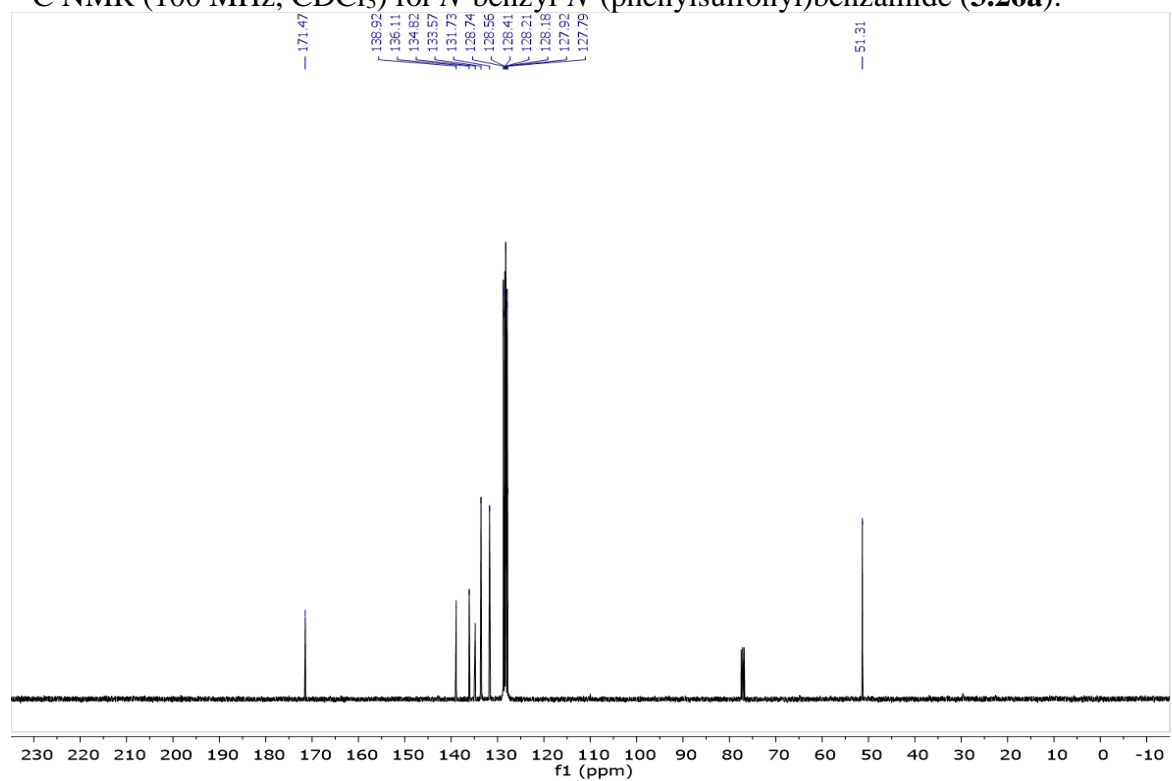
^{13}C NMR (100 MHz, CDCl_3) for *N*-(phenylsulfonyl)furan-2-carboxamide (**3.24f**):



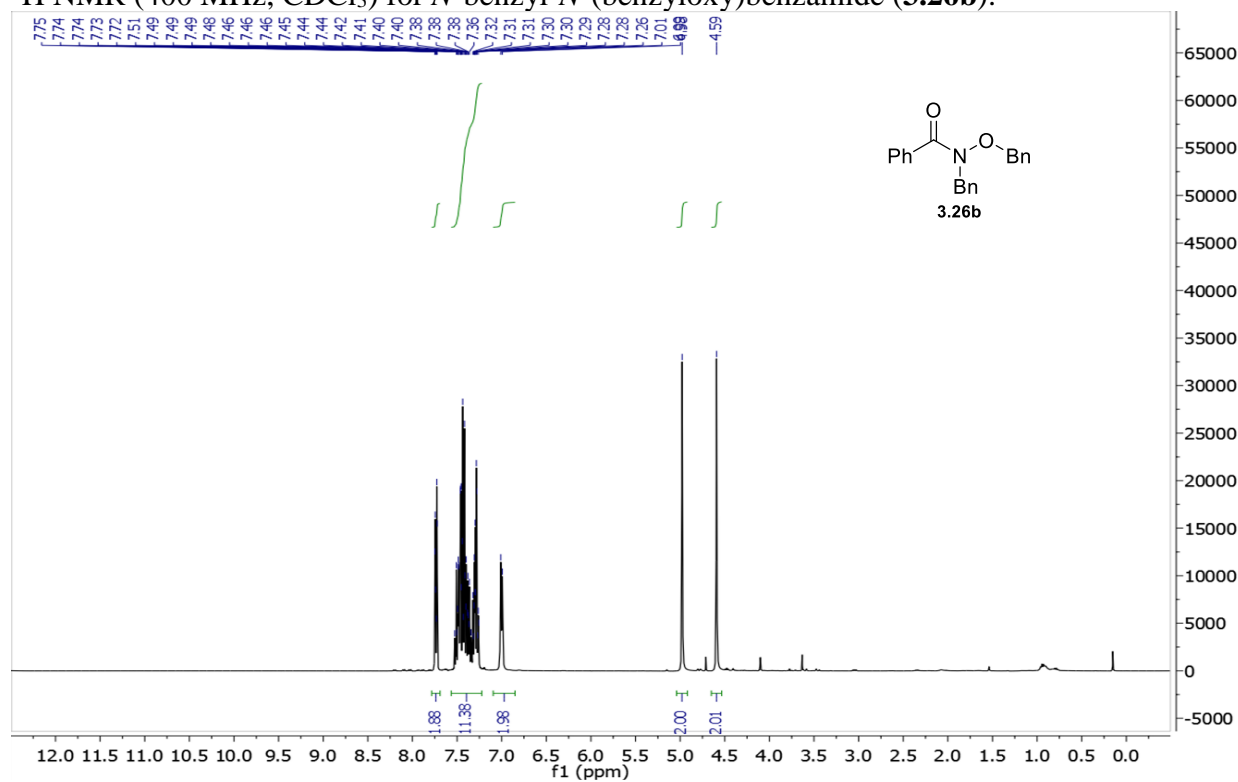
^1H NMR (400 MHz, CDCl_3) for *N*-benzyl-*N*-(phenylsulfonyl)benzamide (**3.26a**):



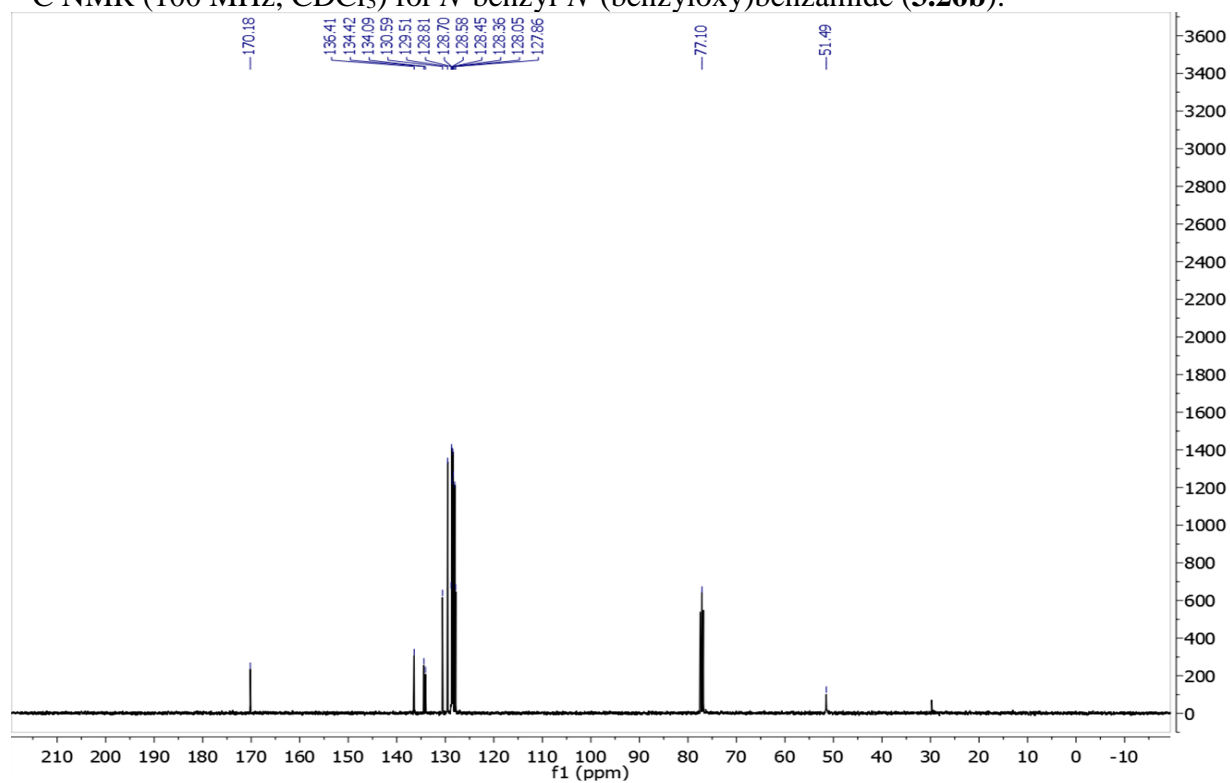
^{13}C NMR (100 MHz, CDCl_3) for *N*-benzyl-*N*-(phenylsulfonyl)benzamide (**3.26a**):



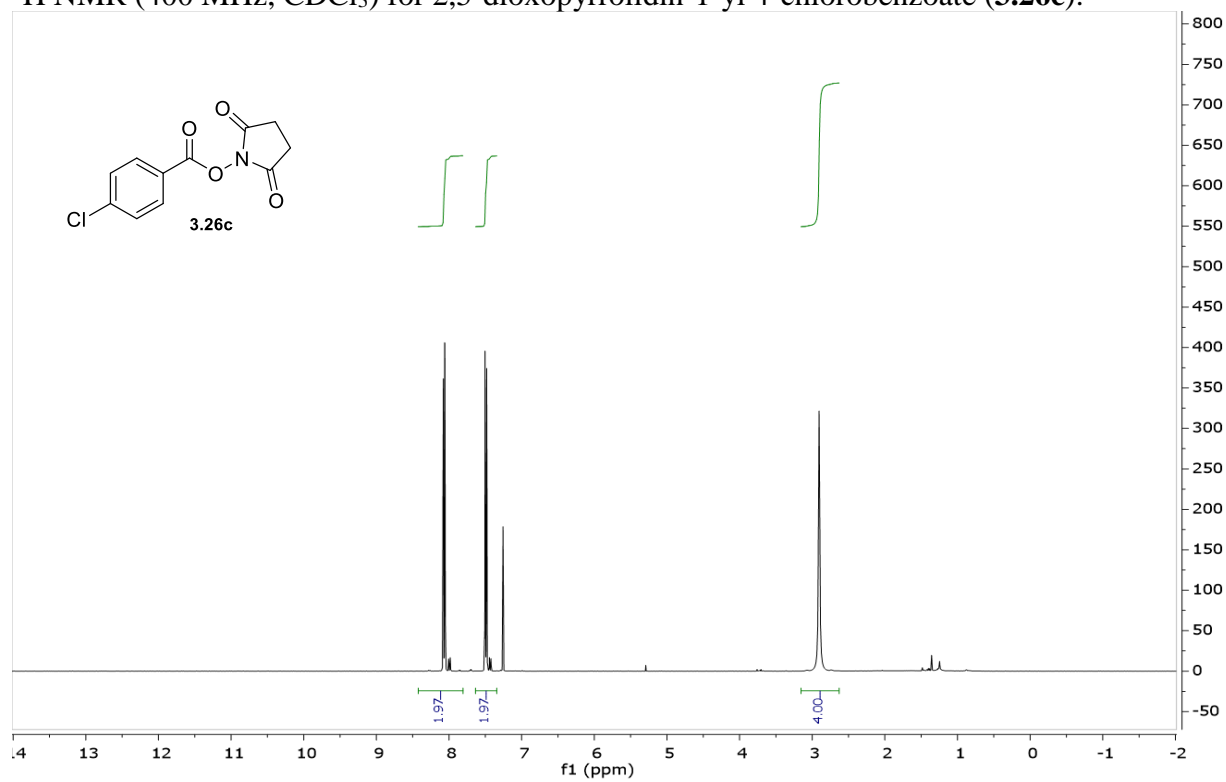
^1H NMR (400 MHz, CDCl_3) for *N*-benzyl-*N*-(benzyloxy)benzamide (**3.26b**):



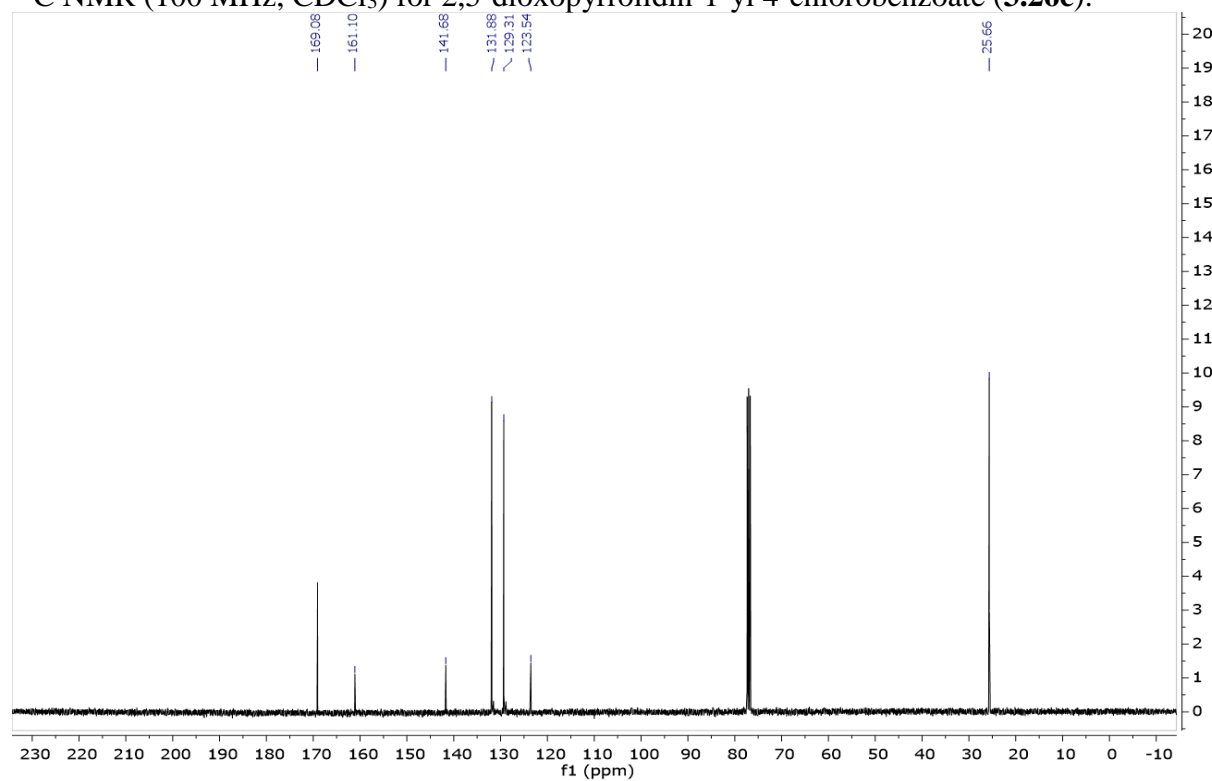
^{13}C NMR (100 MHz, CDCl_3) for *N*-benzyl-*N*-(benzyloxy)benzamide (**3.26b**):



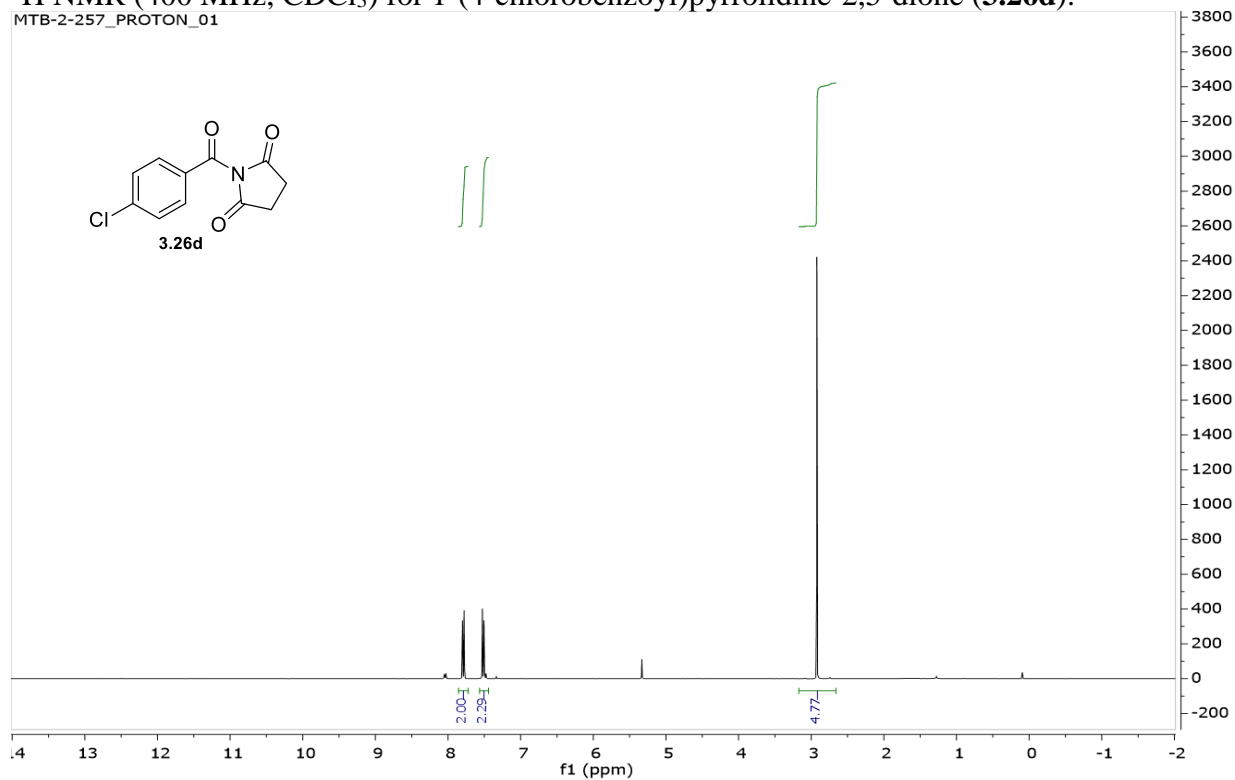
^1H NMR (400 MHz, CDCl_3) for 2,5-dioxopyrrolidin-1-yl 4-chlorobenzoate (**3.26c**):



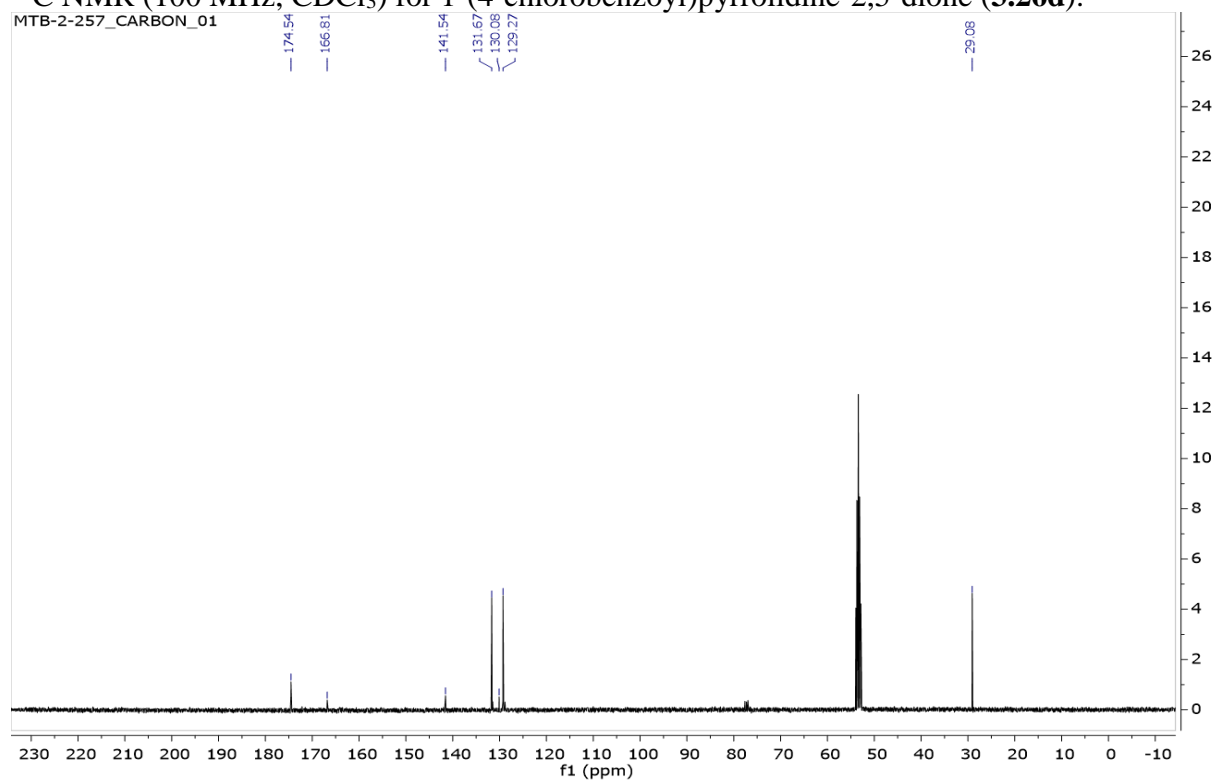
^{13}C NMR (100 MHz, CDCl_3) for 2,5-dioxopyrrolidin-1-yl 4-chlorobenzoate (**3.26c**):



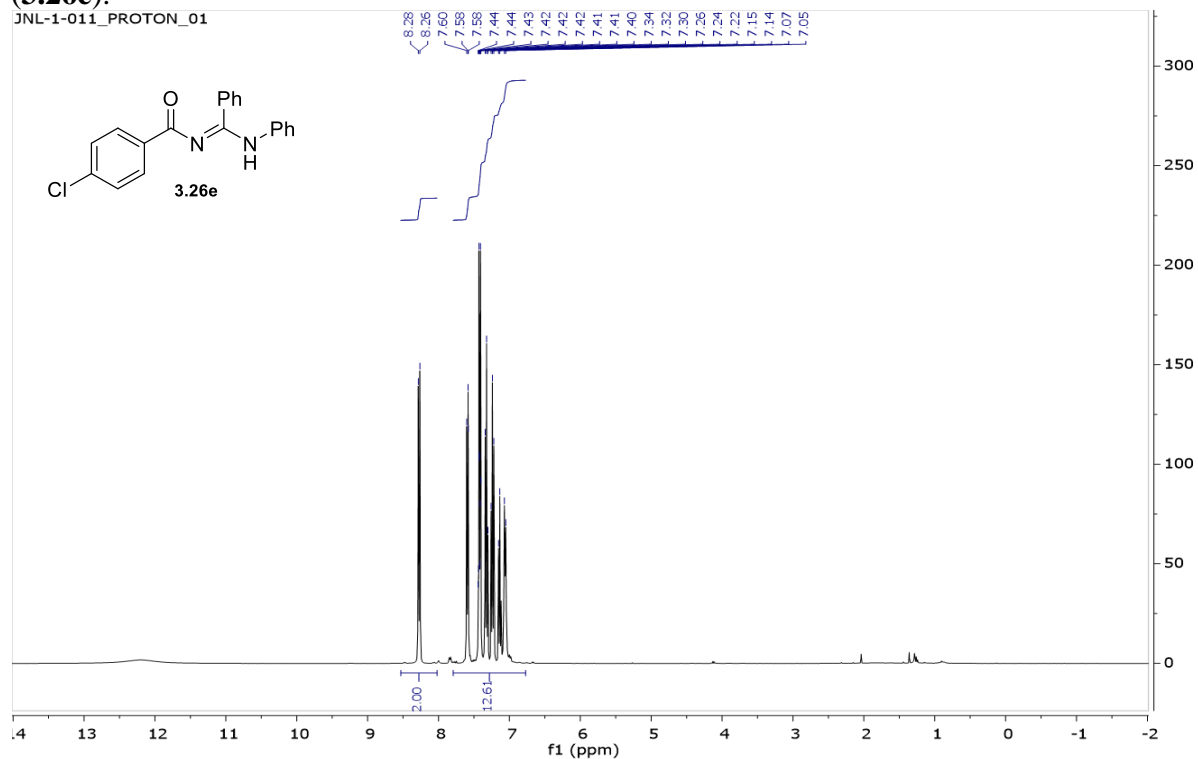
¹H NMR (400 MHz, CDCl₃) for 1-(4-chlorobenzoyl)pyrrolidine-2,5-dione (**3.26d**):



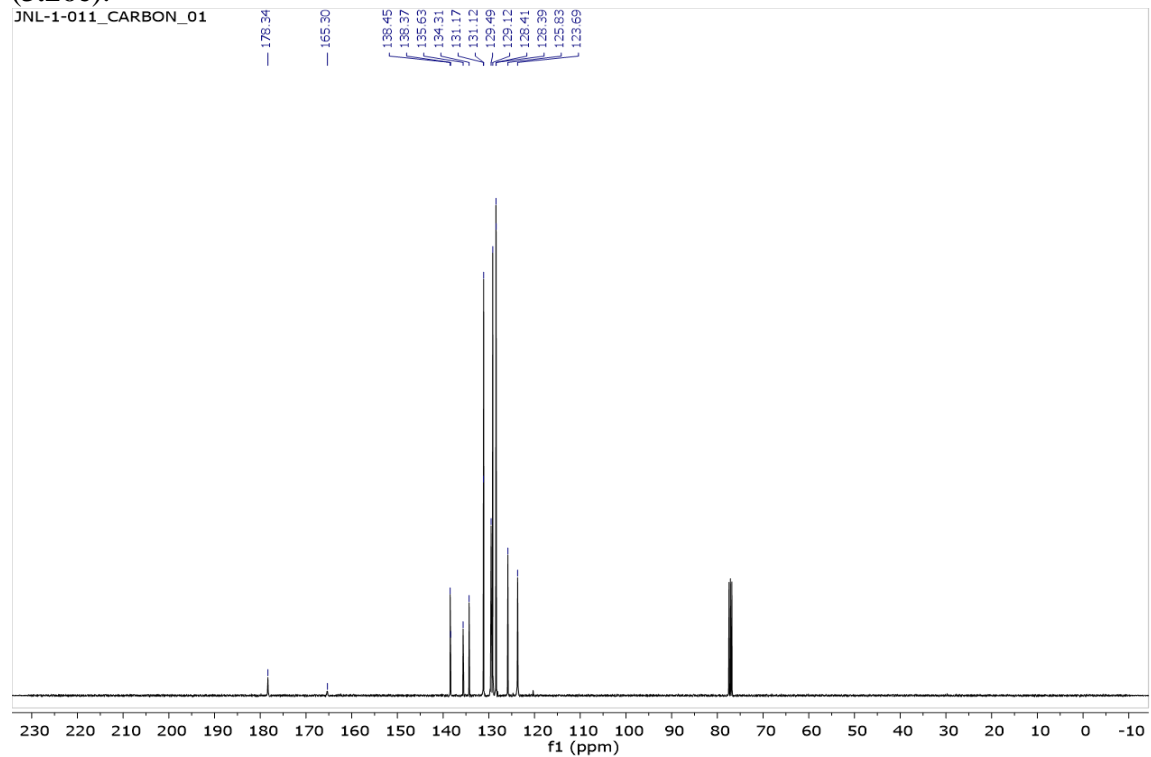
¹³C NMR (100 MHz, CDCl₃) for 1-(4-chlorobenzoyl)pyrrolidine-2,5-dione (**3.26d**):



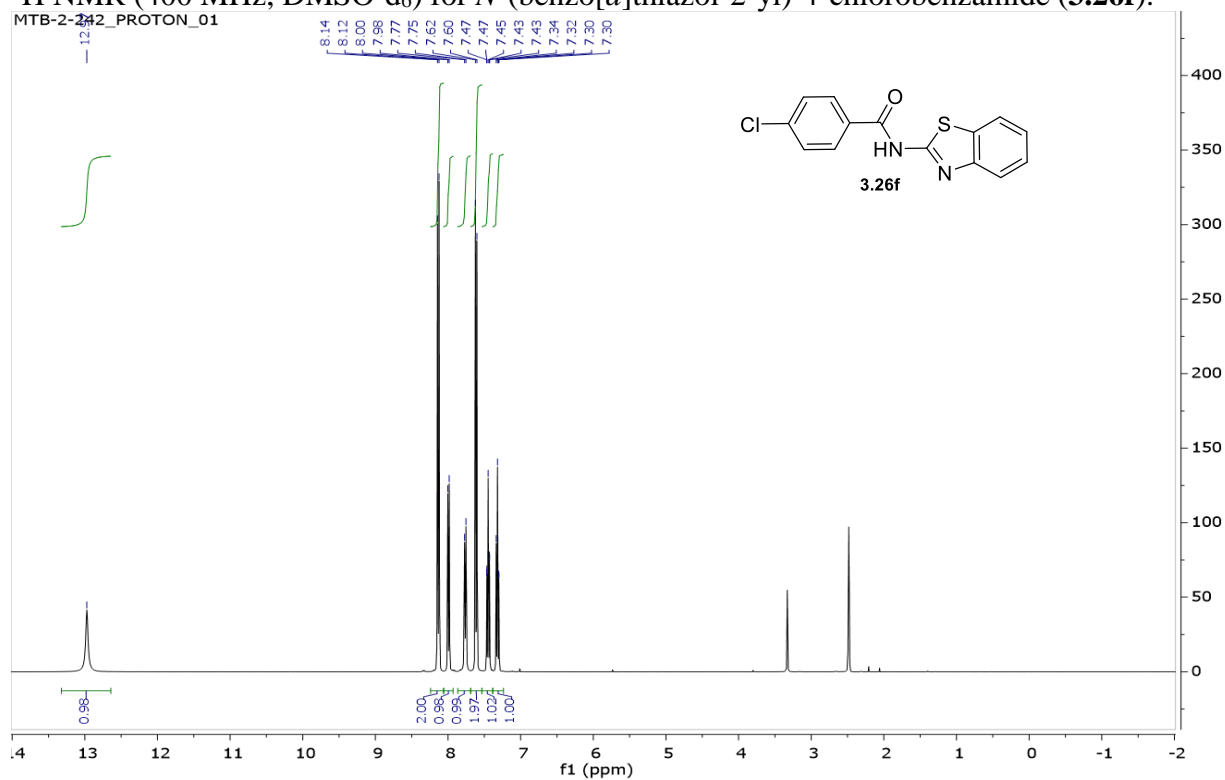
^1H NMR (400 MHz, CDCl_3) for (*E*)-4-chloro-*N*-(phenyl(phenylamino)methylene)benzamide (**3.26e**):



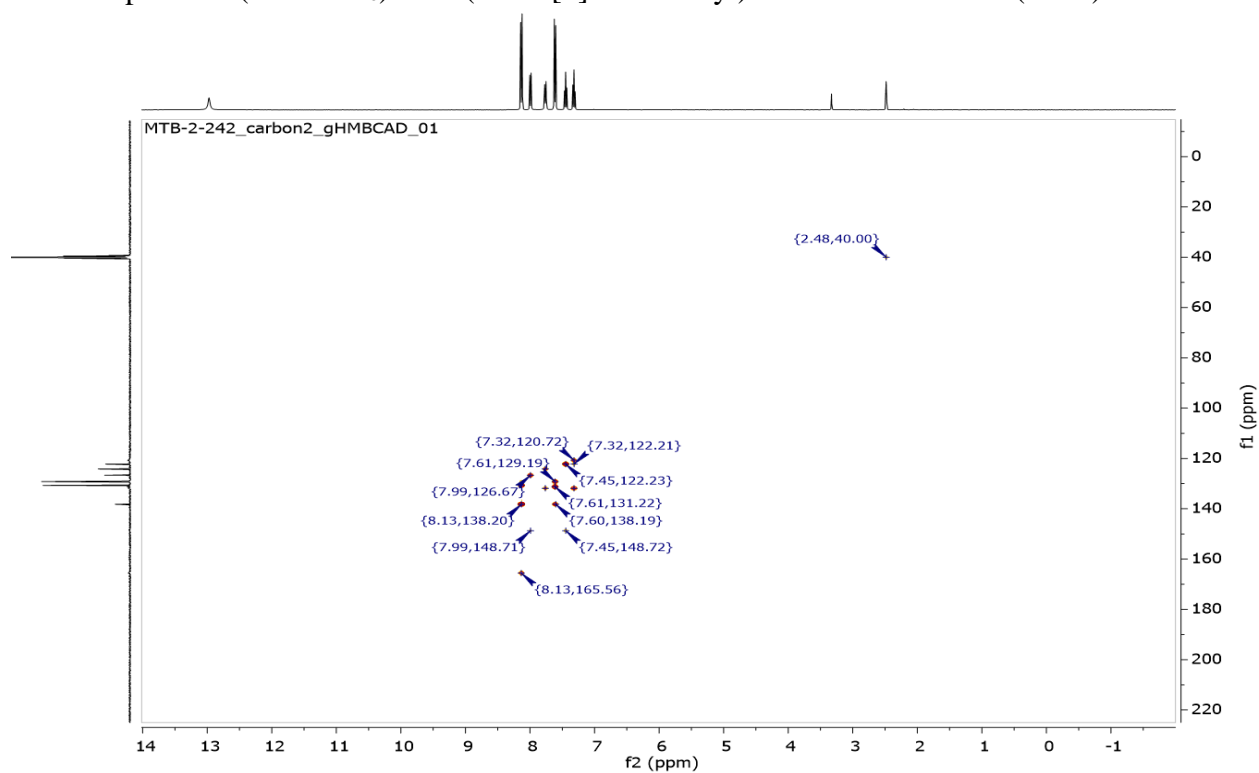
^{13}C NMR (100 MHz, CDCl_3) for (*E*)-4-chloro-*N*-(phenyl(phenylamino)methylene)benzamide (**3.26e**):



^1H NMR (400 MHz, DMSO- d_6) for *N*-(benzo[*d*]thiazol-2-yl)-4-chlorobenzamide (**3.26f**):

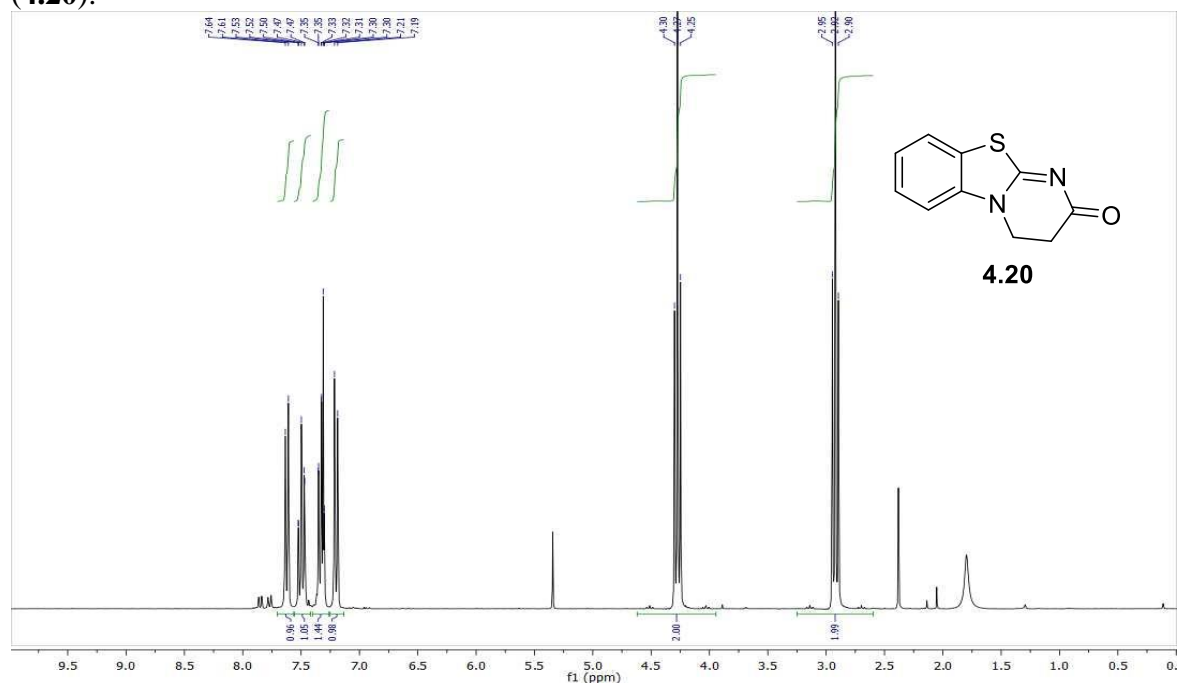


HMBC spectrum (DMSO- d_6) of *N*-(benzo[*d*]thiazol-2-yl)-4-chlorobenzamide (**3.26f**):

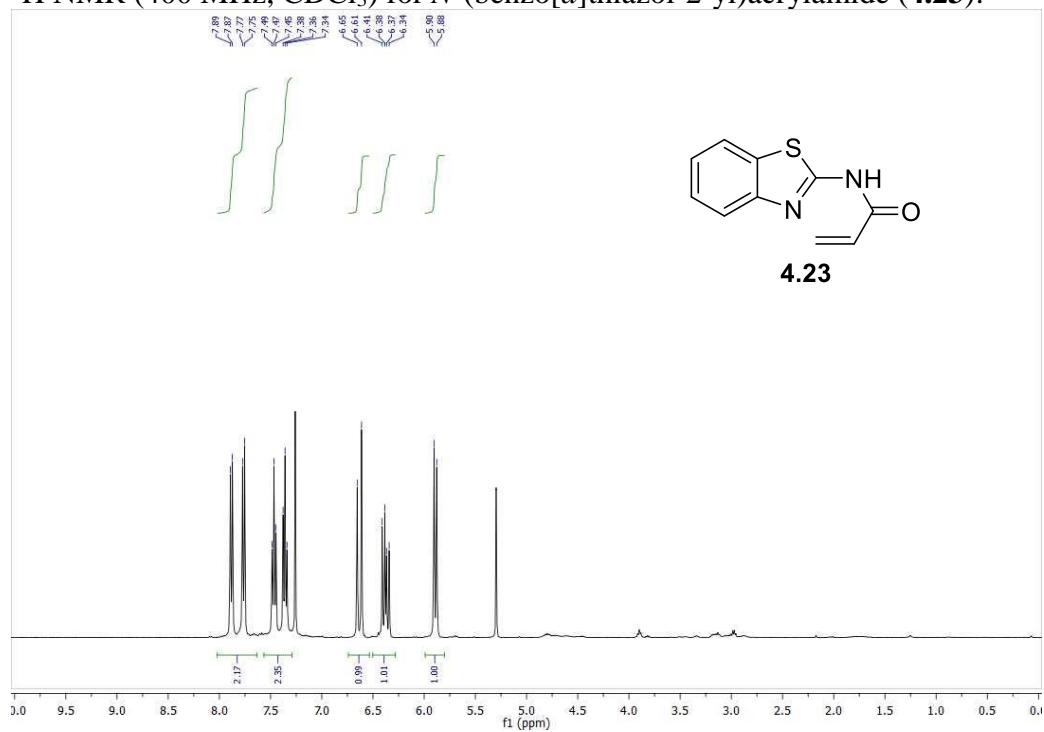


Appendix C NMR from Chapter 4

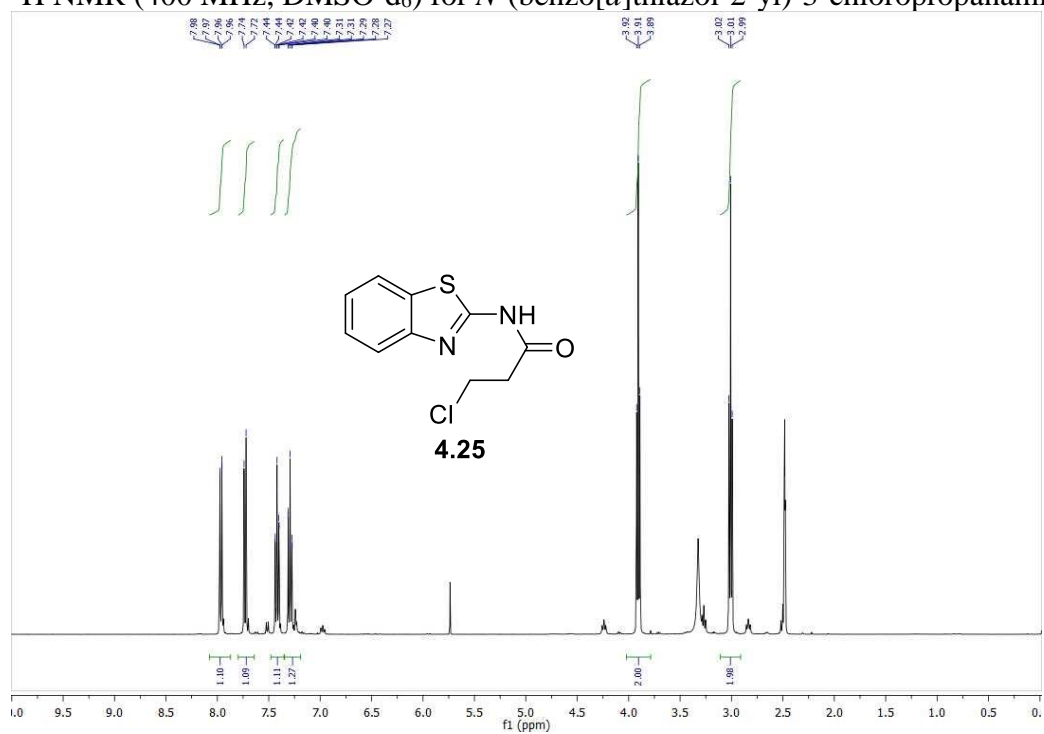
^1H NMR (300 MHz, CDCl_3) for 3,4-dihydro-2*H*-benzo[4,5]thiazolo[3,2-*a*]pyrimidin-2-one (**4.20**):



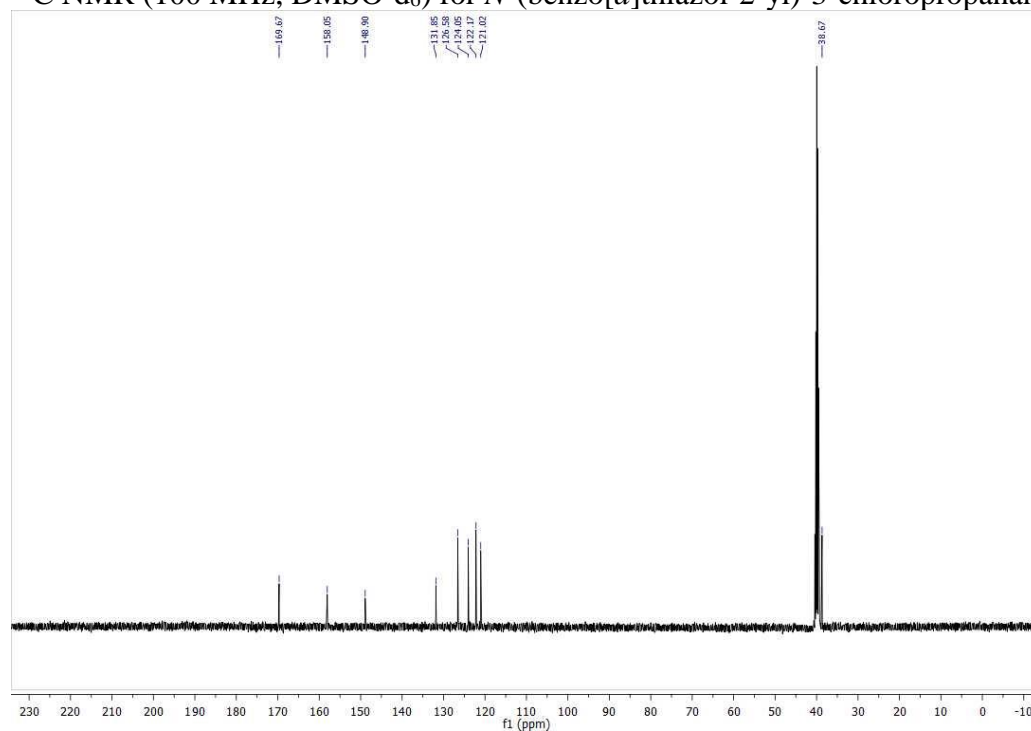
^1H NMR (400 MHz, CDCl_3) for *N*-(benzo[*d*]thiazol-2-yl)acrylamide (**4.23**):



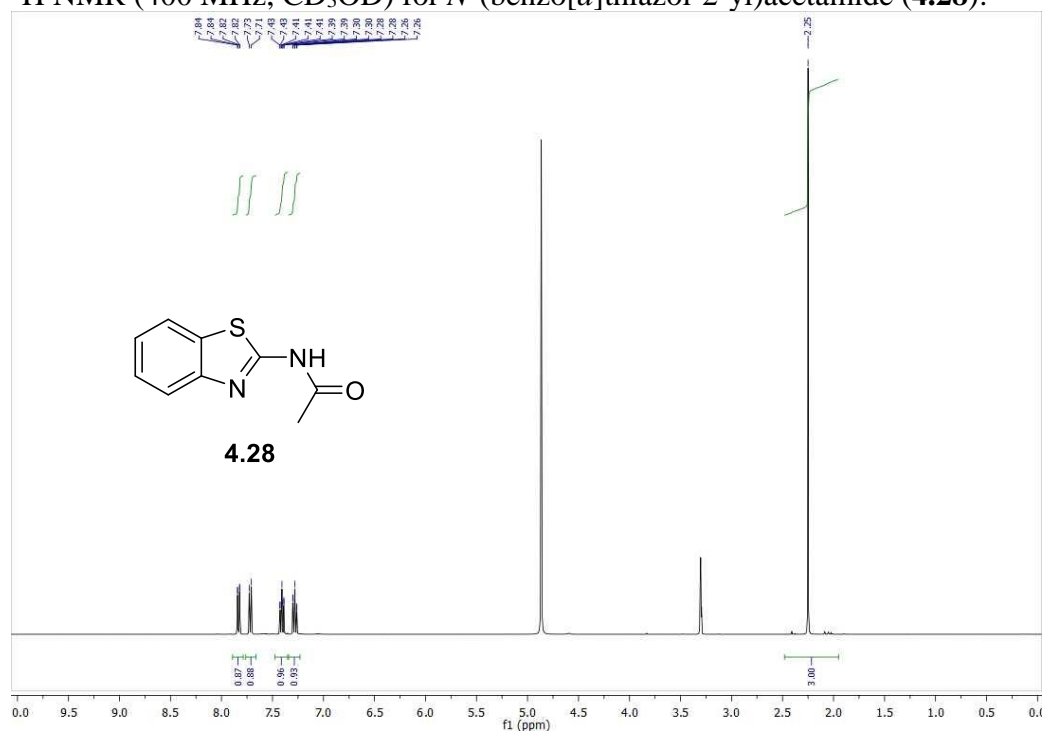
^1H NMR (400 MHz, DMSO- d_6) for *N*-(benzo[*d*]thiazol-2-yl)-3-chloropropanamide (**4.25**):



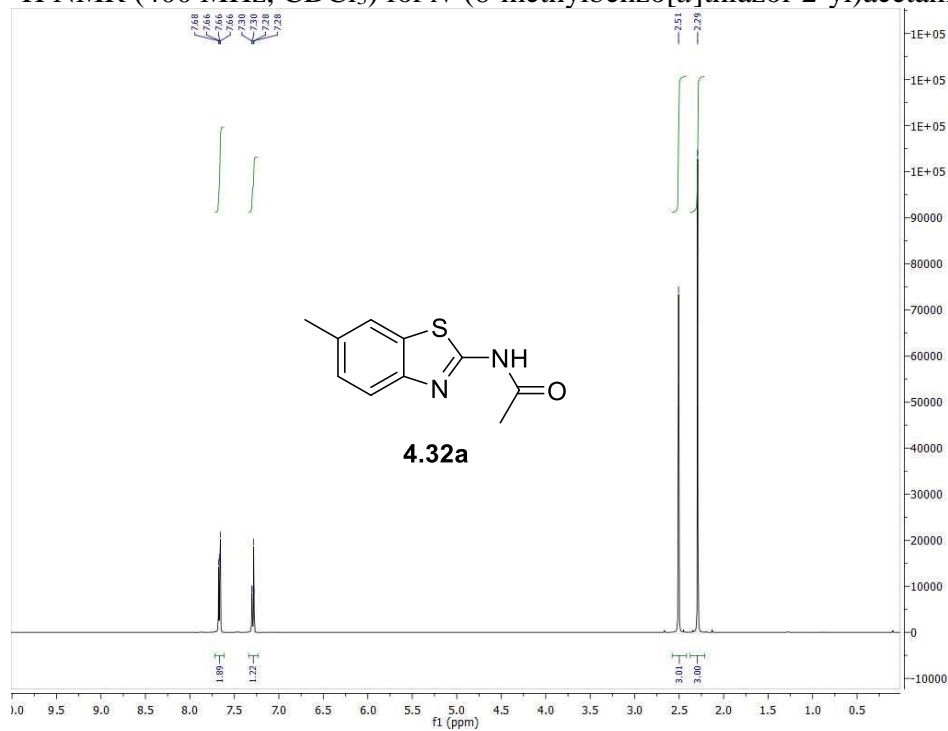
^{13}C NMR (100 MHz, DMSO- d_6) for *N*-(benzo[*d*]thiazol-2-yl)-3-chloropropanamide (**4.25**):



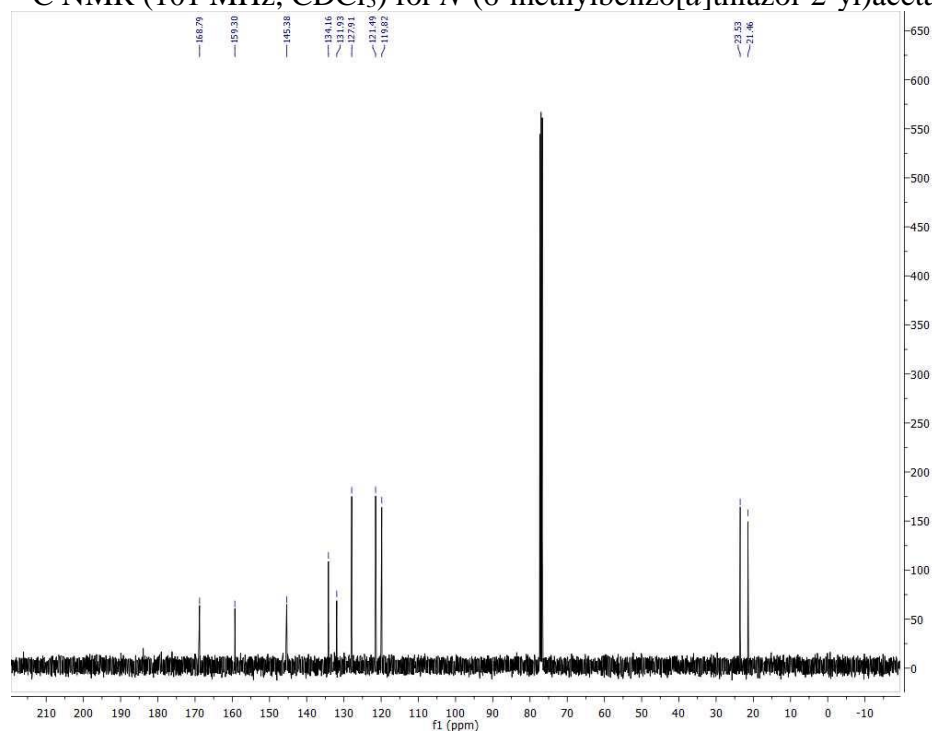
^1H NMR (400 MHz, CD_3OD) for *N*-(benzo[*d*]thiazol-2-yl)acetamide (**4.28**):



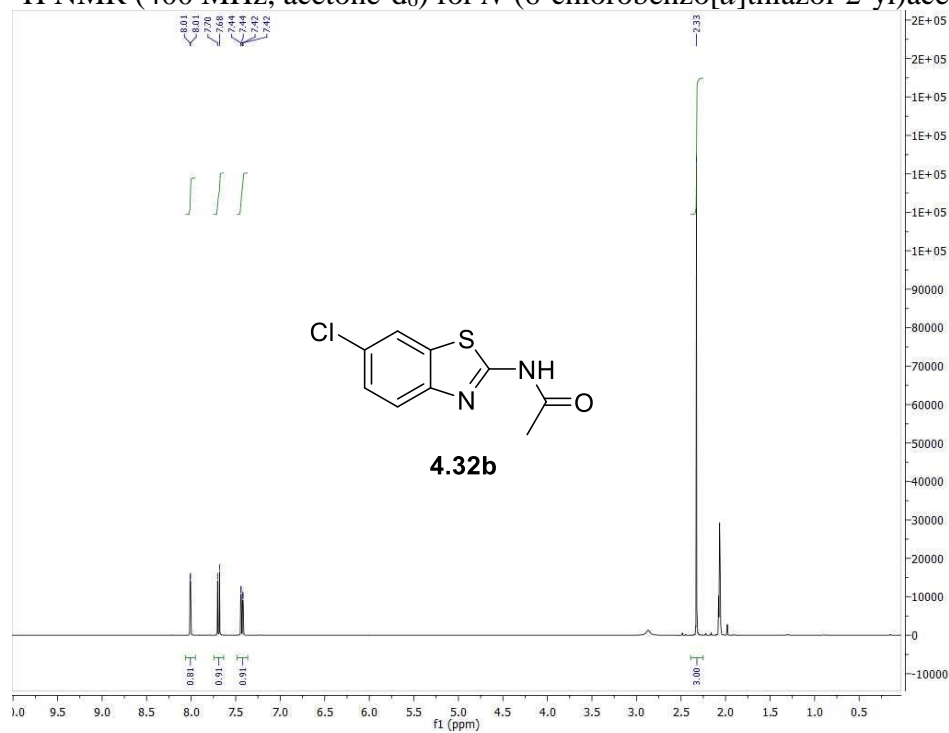
^1H NMR (400 MHz, CDCl_3) for *N*-(6-methylbenzo[*d*]thiazol-2-yl)acetamide (**4.32a**):



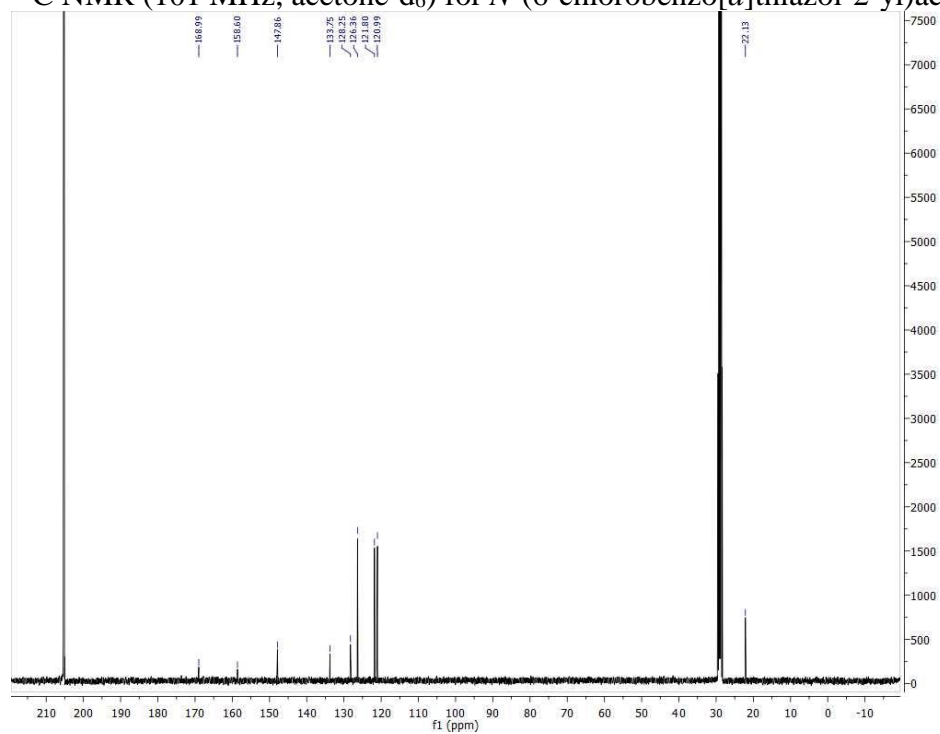
^{13}C NMR (101 MHz, CDCl_3) for *N*-(6-methylbenzo[*d*]thiazol-2-yl)acetamide (**4.32a**):



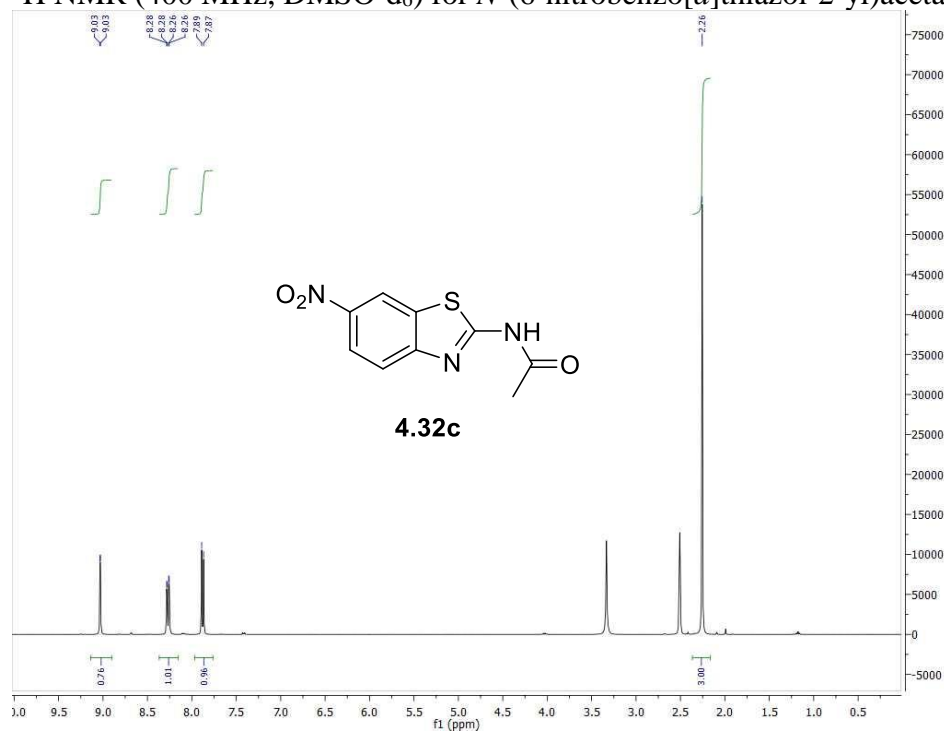
^1H NMR (400 MHz, acetone- d_6) for *N*-(6-chlorobenzo[*d*]thiazol-2-yl)acetamide (**4.32b**):



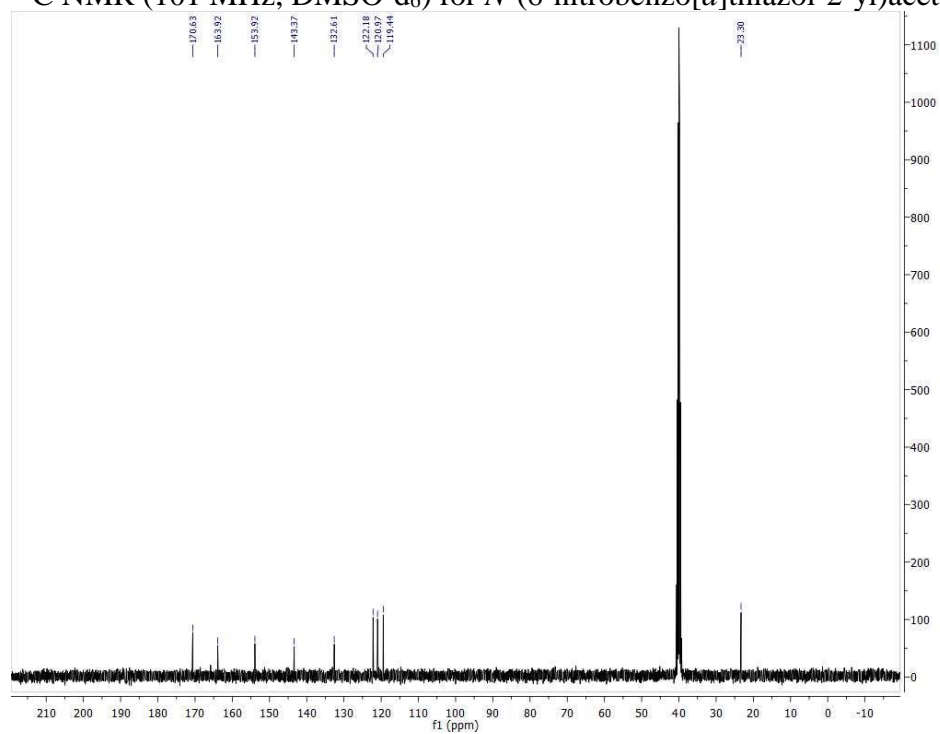
^{13}C NMR (101 MHz, acetone- d_6) for *N*-(6-chlorobenzo[*d*]thiazol-2-yl)acetamide (**4.32b**):



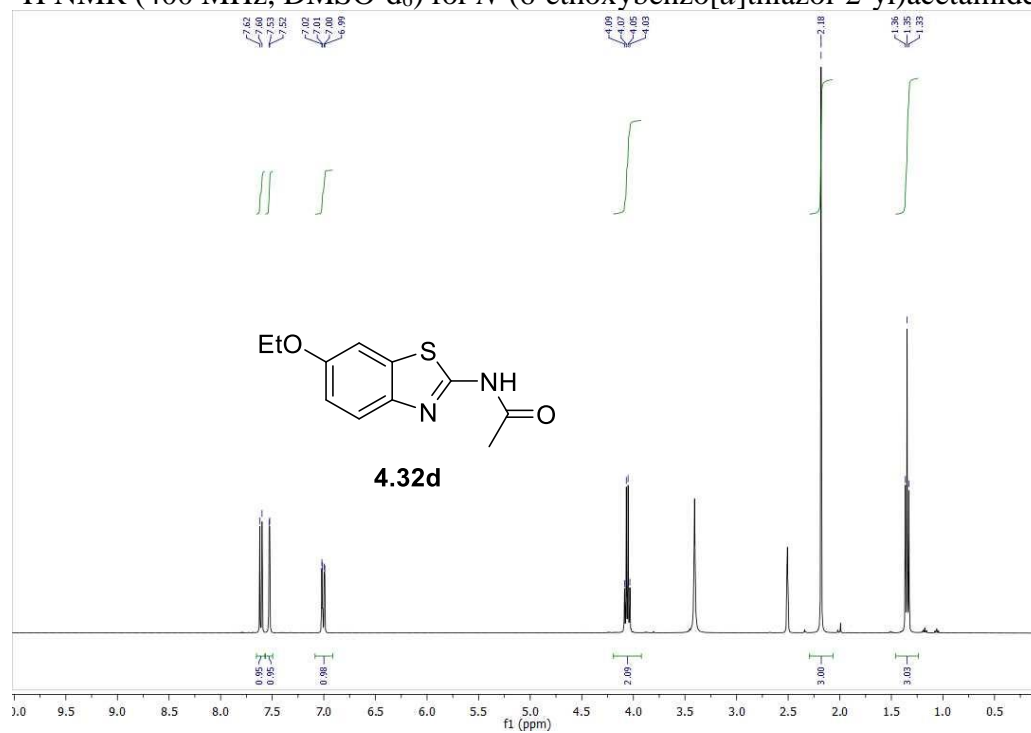
^1H NMR (400 MHz, DMSO- d_6) for *N*-(6-nitrobenzo[*d*]thiazol-2-yl)acetamide (**4.32c**):



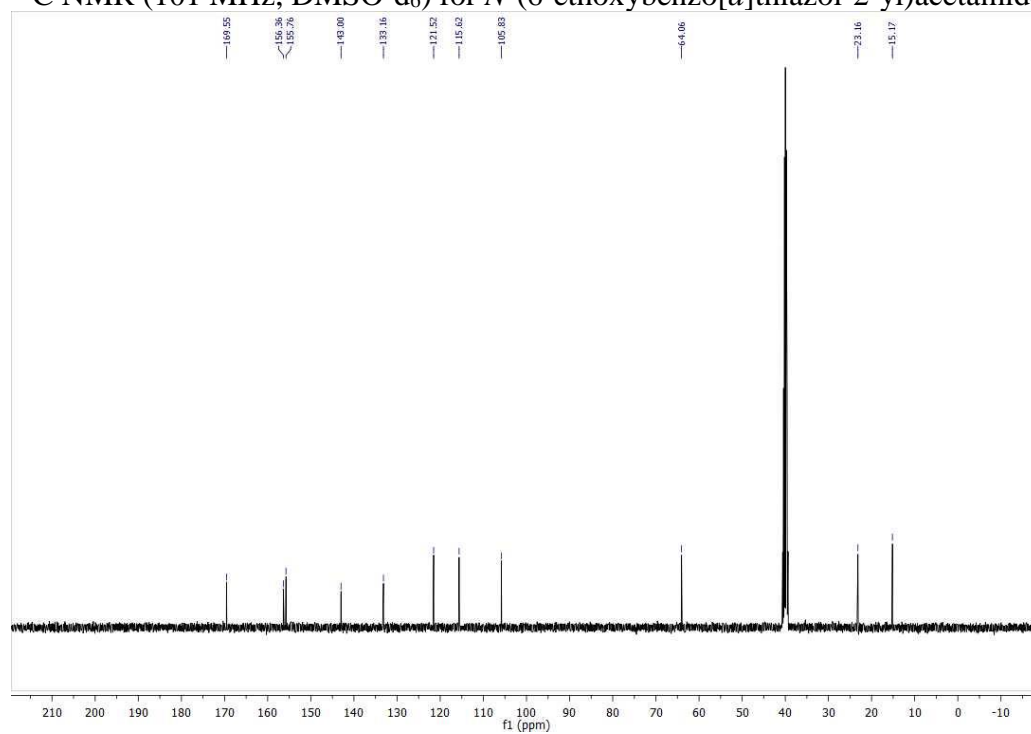
^{13}C NMR (101 MHz, DMSO- d_6) for *N*-(6-nitrobenzo[*d*]thiazol-2-yl)acetamide (**4.32c**):



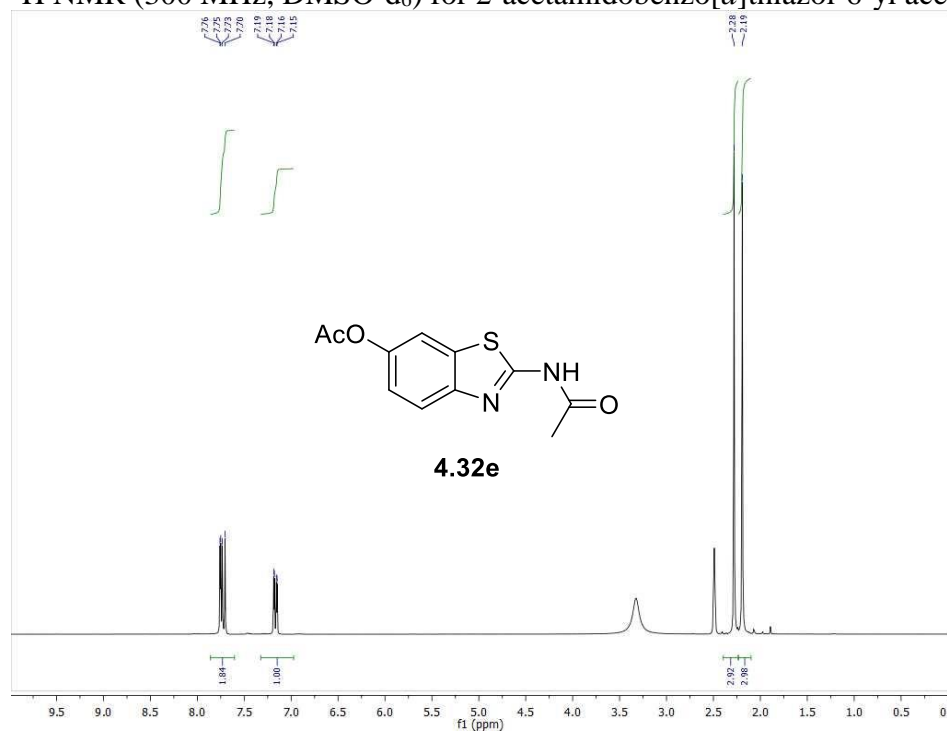
^1H NMR (400 MHz, DMSO- d_6) for *N*-(6-ethoxybenzo[*d*]thiazol-2-yl)acetamide (**4.32d**):



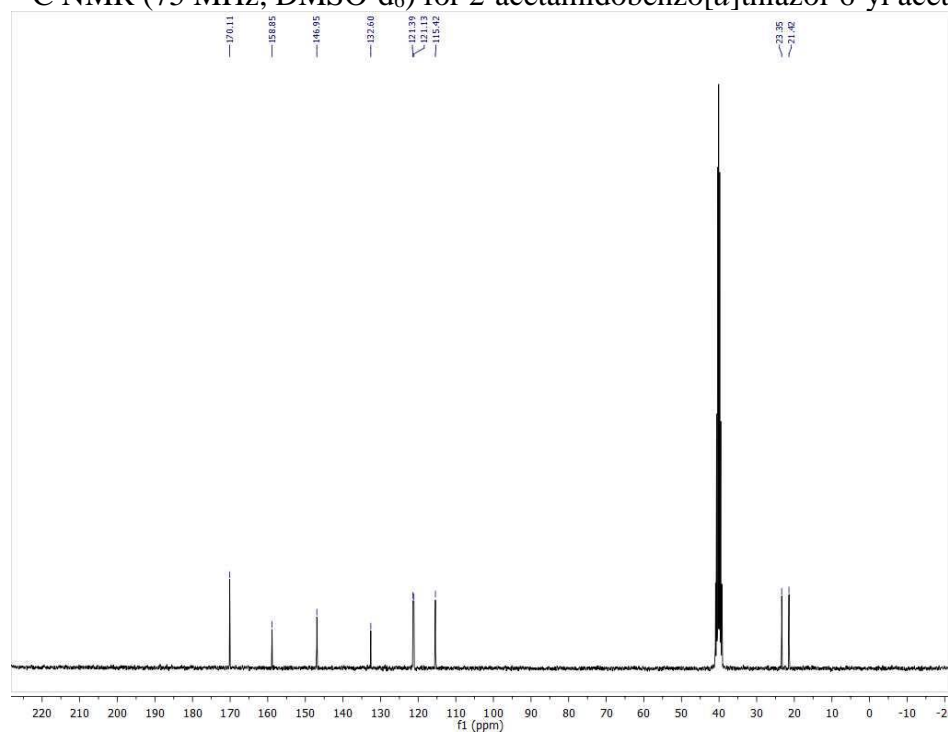
^{13}C NMR (101 MHz, DMSO-d_6) for *N*-(6-ethoxybenzo[*d*]thiazol-2-yl)acetamide (**4.32d**):



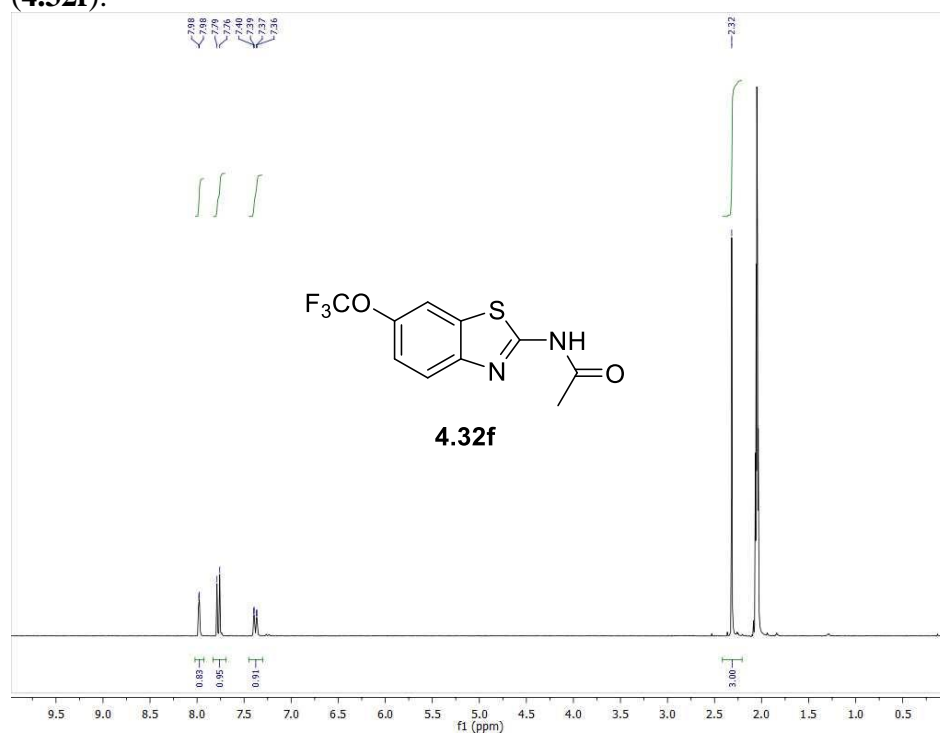
^1H NMR (300 MHz, DMSO-d_6) for 2-acetamidobenzo[*d*]thiazol-6-yl acetate (**4.32e**):



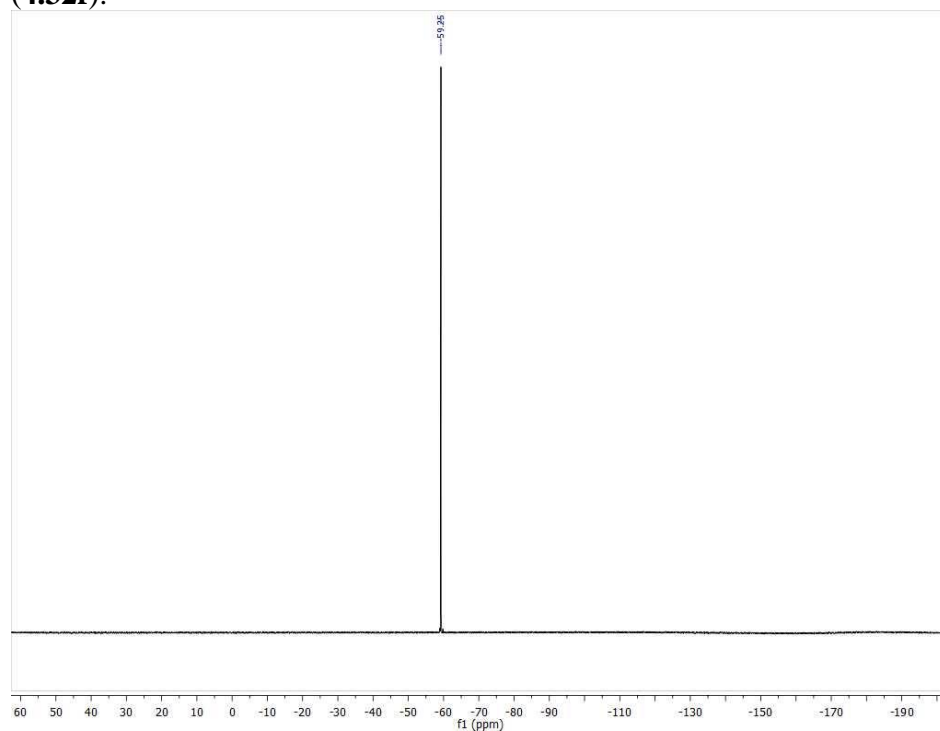
^{13}C NMR (75 MHz, DMSO-d_6) for 2-acetamidobenzo[*d*]thiazol-6-yl acetate (**4.32e**):



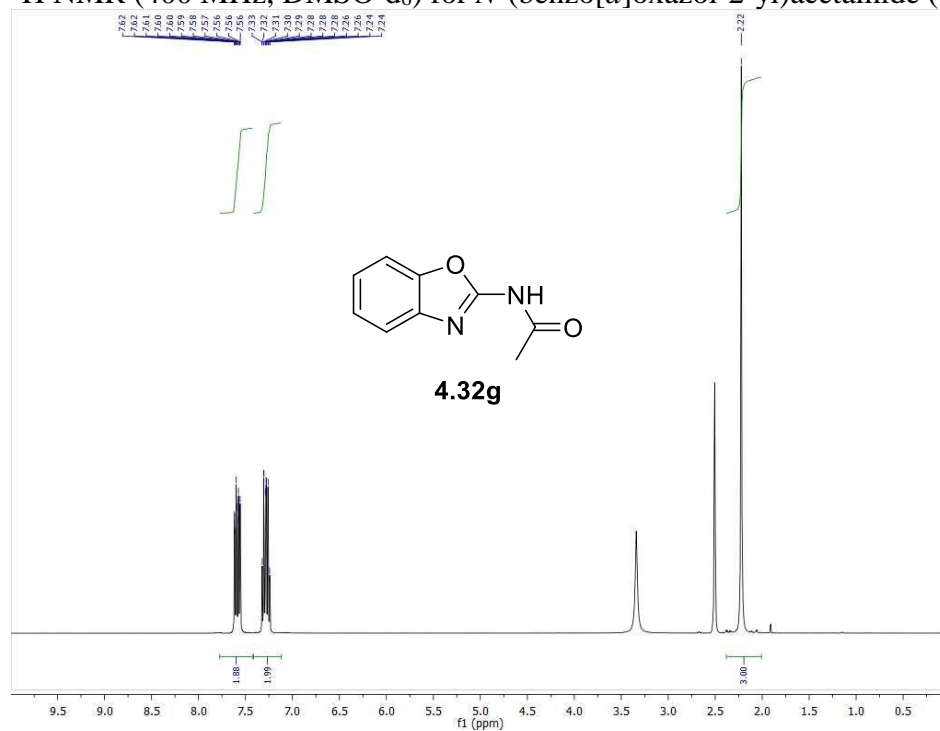
^1H NMR (300 MHz, acetone-d_6) for *N*-(6-(trifluoromethoxy)benzo[*d*]thiazol-2-yl)acetamide (**4.32f**):



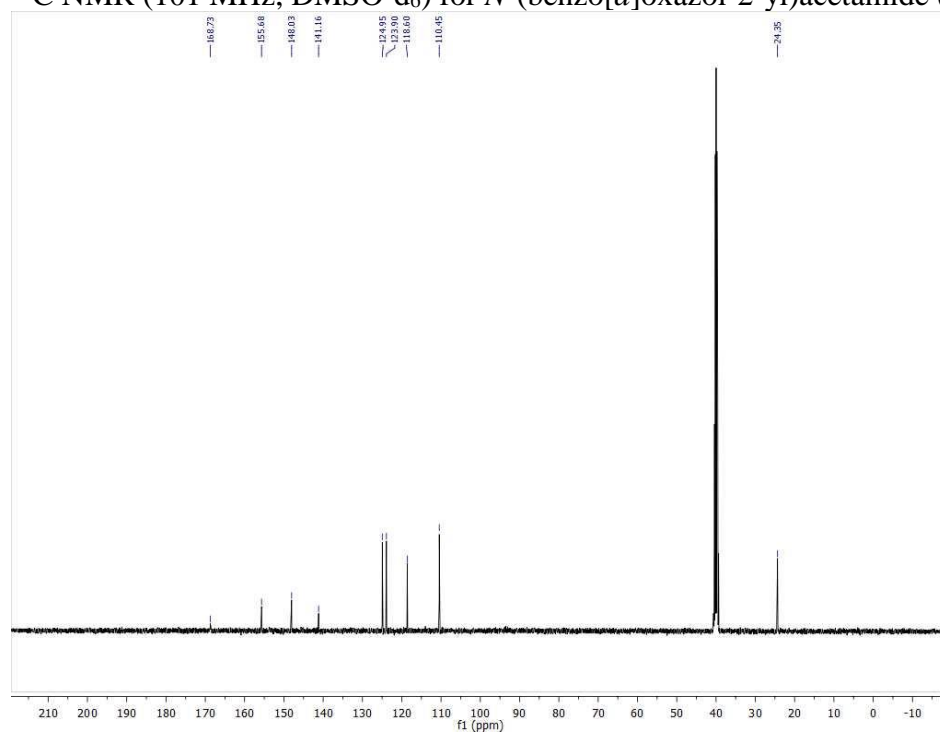
^{19}F NMR (282 MHz, acetone- d_6) for *N*-(6-(trifluoromethoxy)benzo[*d*]thiazol-2-yl)acetamide (**4.32f**):



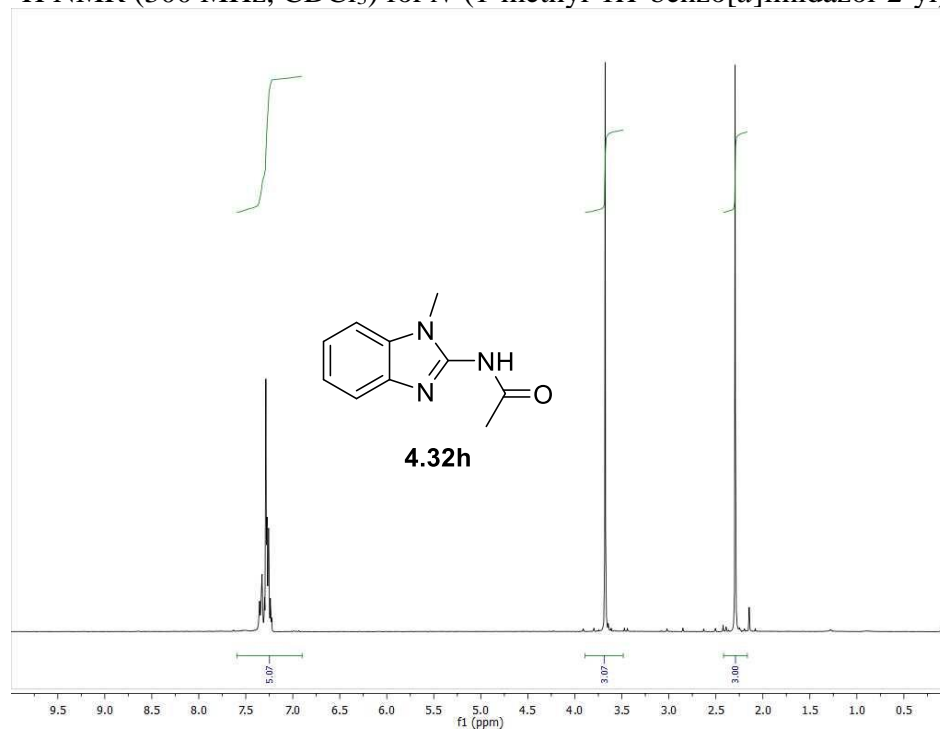
^1H NMR (400 MHz, DMSO- d_6) for *N*-(benzo[*d*]oxazol-2-yl)acetamide (**4.32g**):



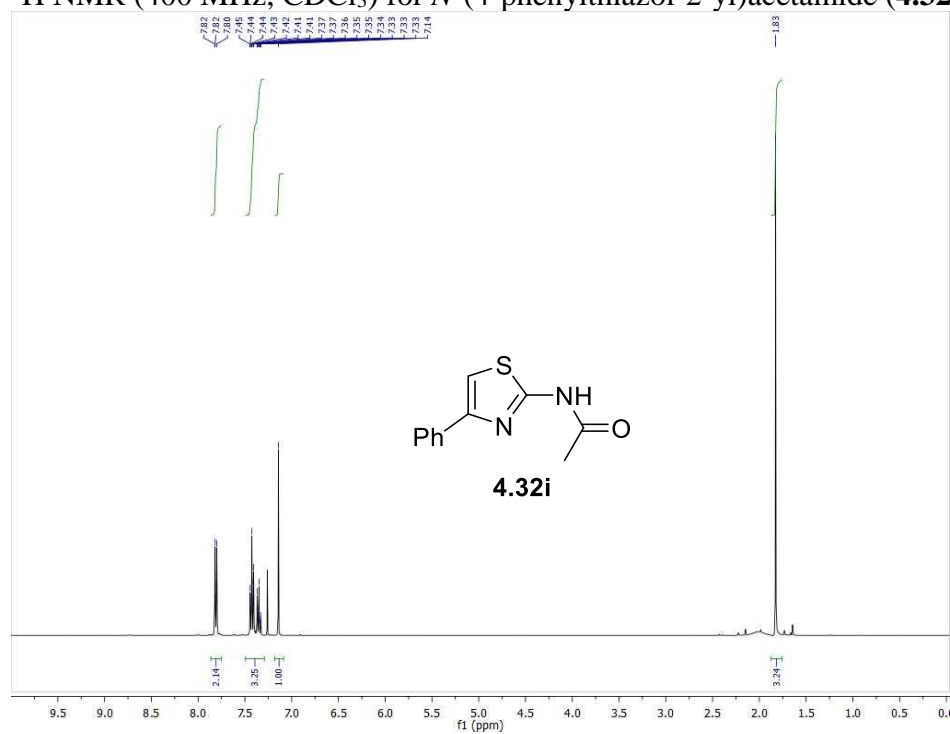
^{13}C NMR (101 MHz, DMSO-d_6) for *N*-(benzo[*d*]oxazol-2-yl)acetamide (**4.32g**):



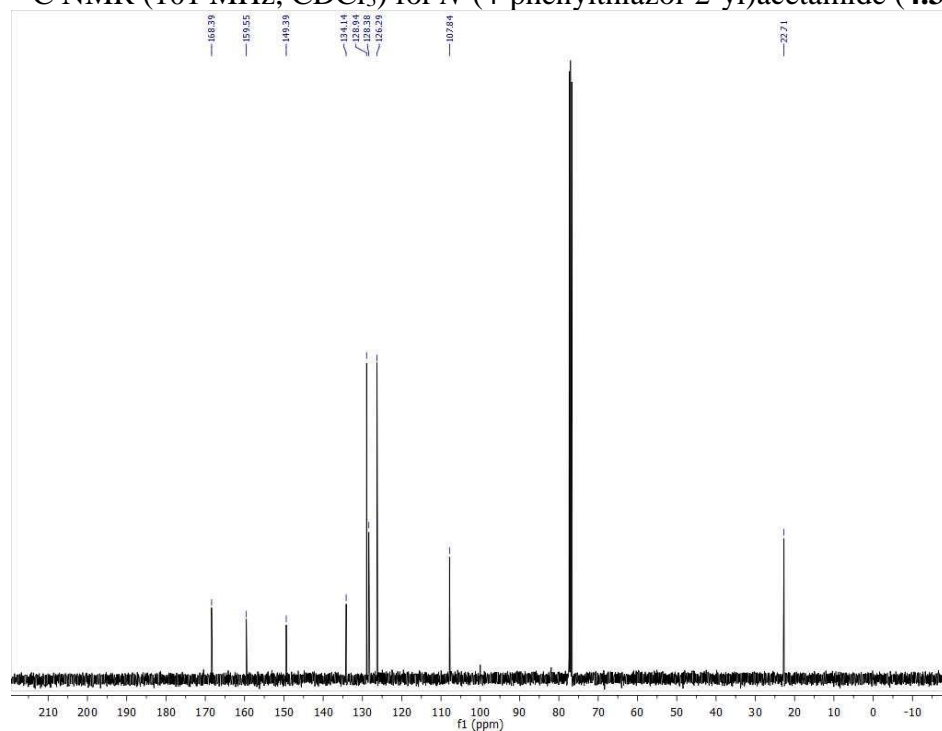
^1H NMR (300 MHz, CDCl_3) for *N*-(1-methyl-1*H*-benzo[*d*]imidazol-2-yl)acetamide (**4.32h**):



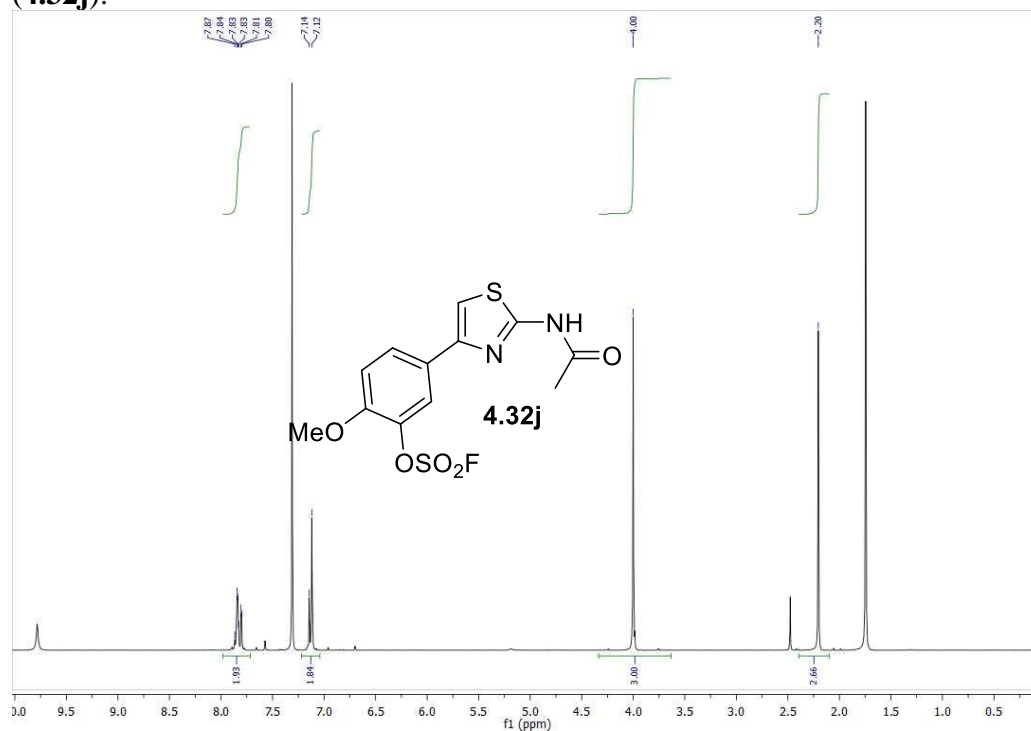
^1H NMR (400 MHz, CDCl_3) for *N*-(4-phenylthiazol-2-yl)acetamide (**4.32i**):



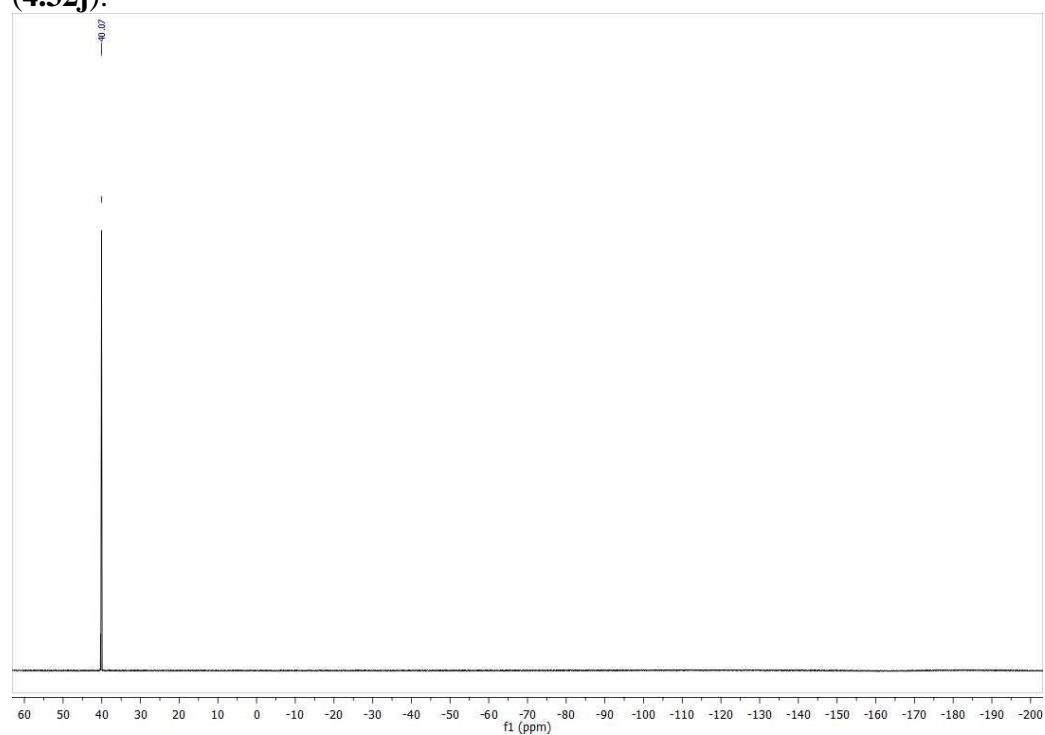
^{13}C NMR (101 MHz, CDCl_3) for *N*-(4-phenylthiazol-2-yl)acetamide (**4.32i**):



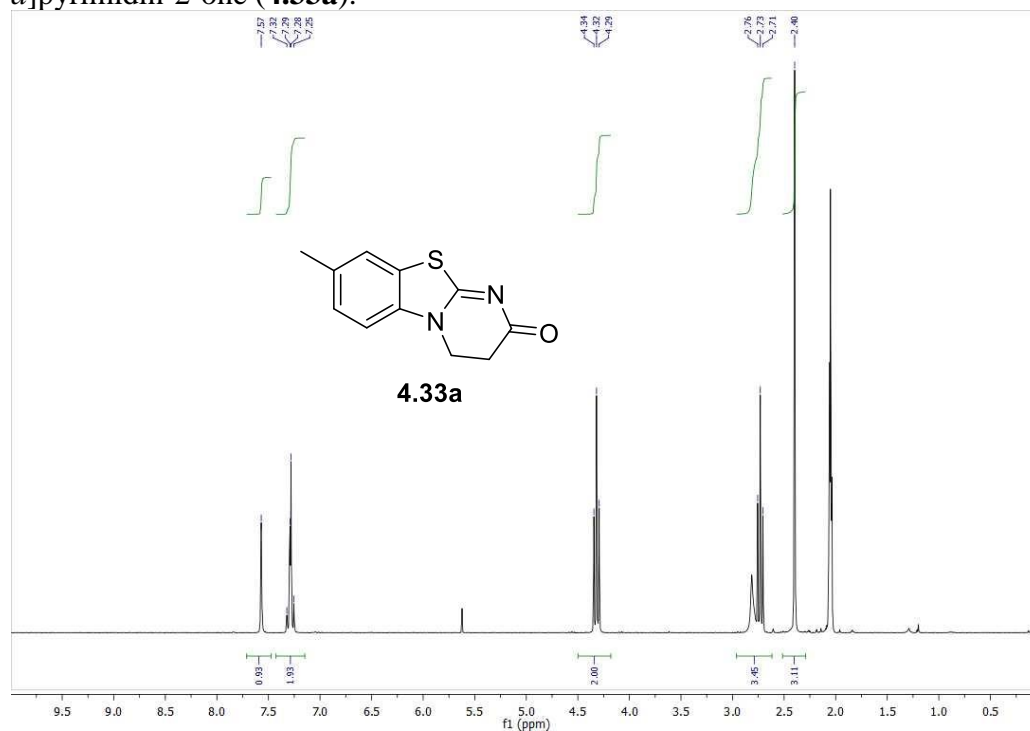
^1H NMR (300 MHz, CDCl_3) for 5-(2-acetamidothiazol-4-yl)-2-methoxyphenyl sulfurofluoridate (**4.32j**):



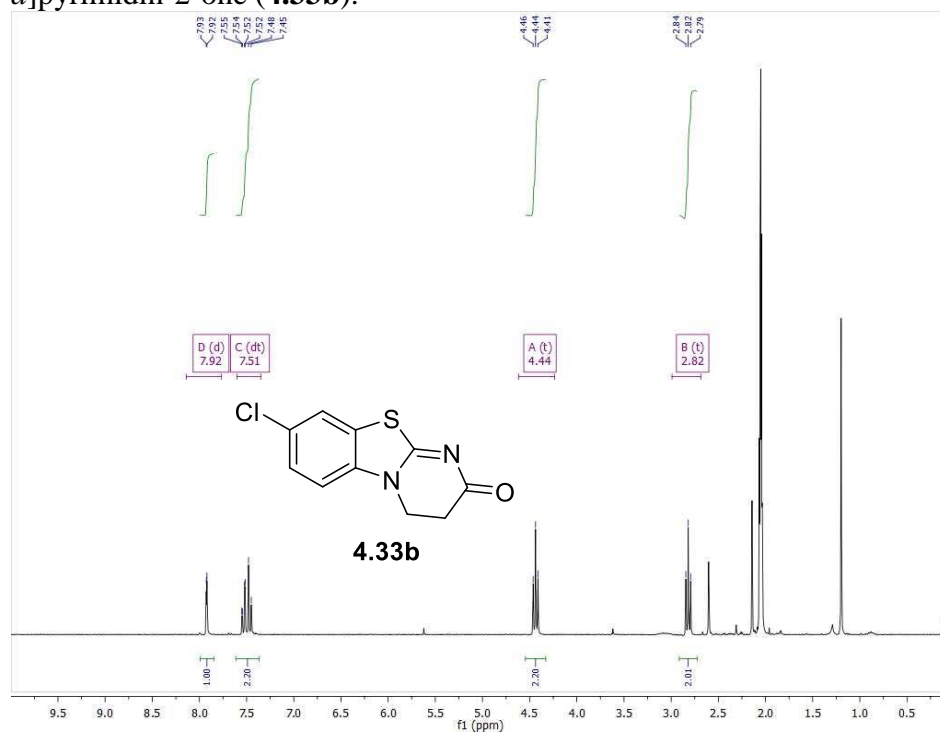
^{19}F NMR (282 MHz, CDCl_3) for 5-(2-acetamidothiazol-4-yl)-2-methoxyphenyl sulfurofluoridate (**4.32j**):



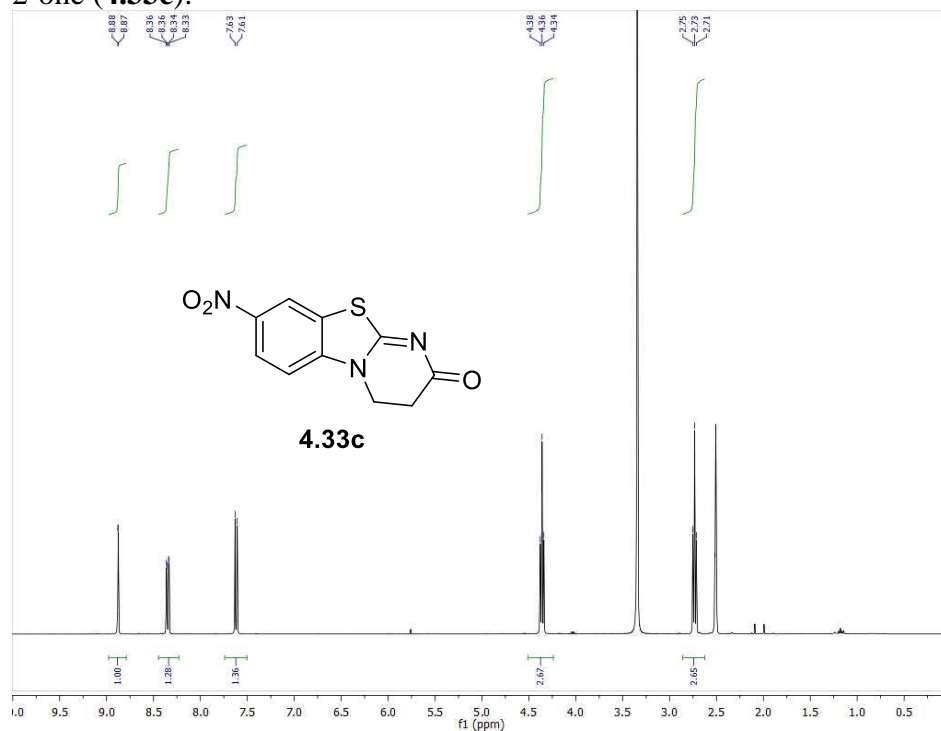
^1H NMR (300 MHz, acetone- d_6) for 8-methyl-3,4-dihydro-2*H*-benzo[4,5]thiazolo[3,2-*a*]pyrimidin-2-one (**4.33a**):



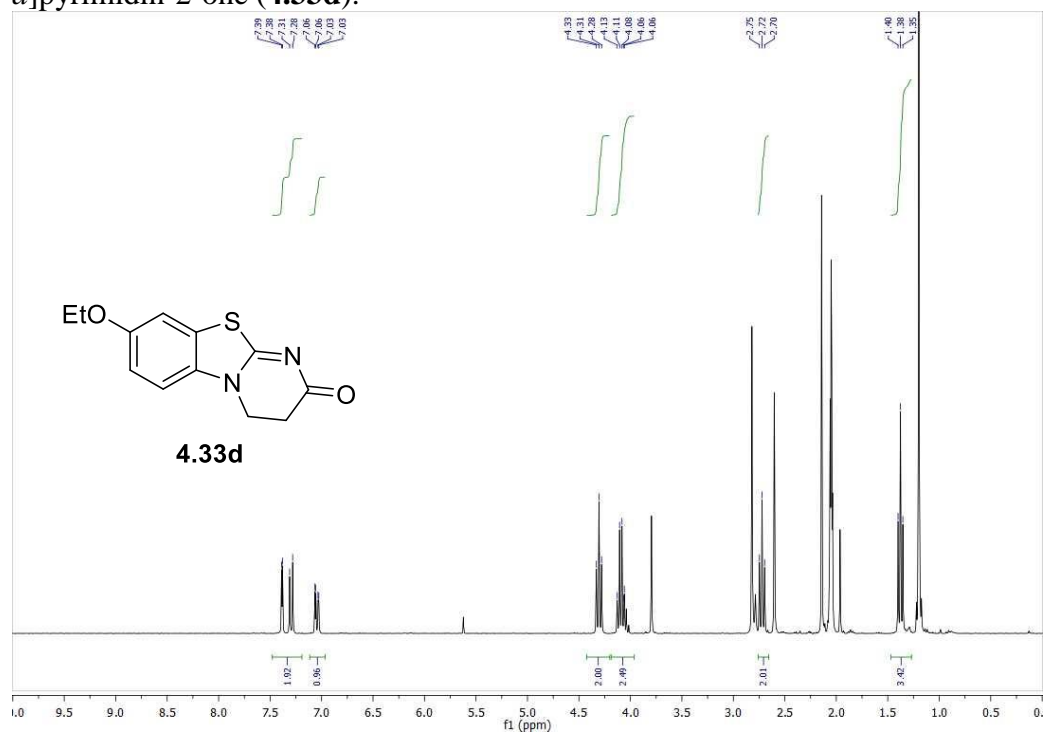
^1H NMR (300 MHz, acetone- d_6) for 8-chloro-3,4-dihydro-2*H*-benzo[4,5]thiazolo[3,2-*a*]pyrimidin-2-one (**4.33b**):



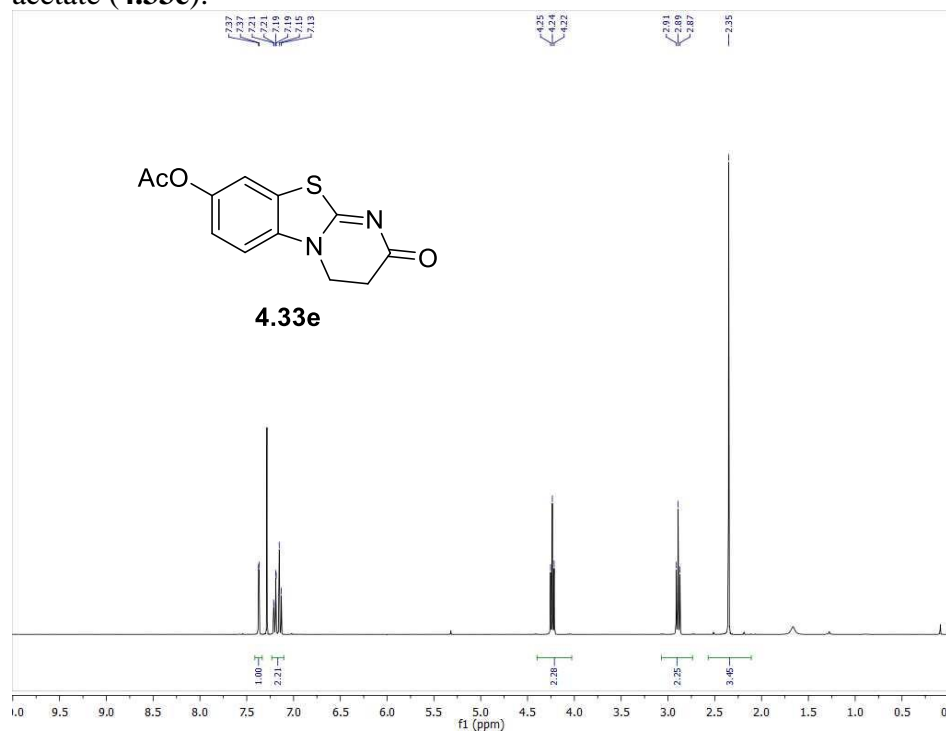
^1H NMR (400 MHz, DMSO- d_6) for 8-nitro-3,4-dihydro-2*H*-benzo[4,5]thiazolo[3,2-*a*]pyrimidin-2-one (**4.33c**):



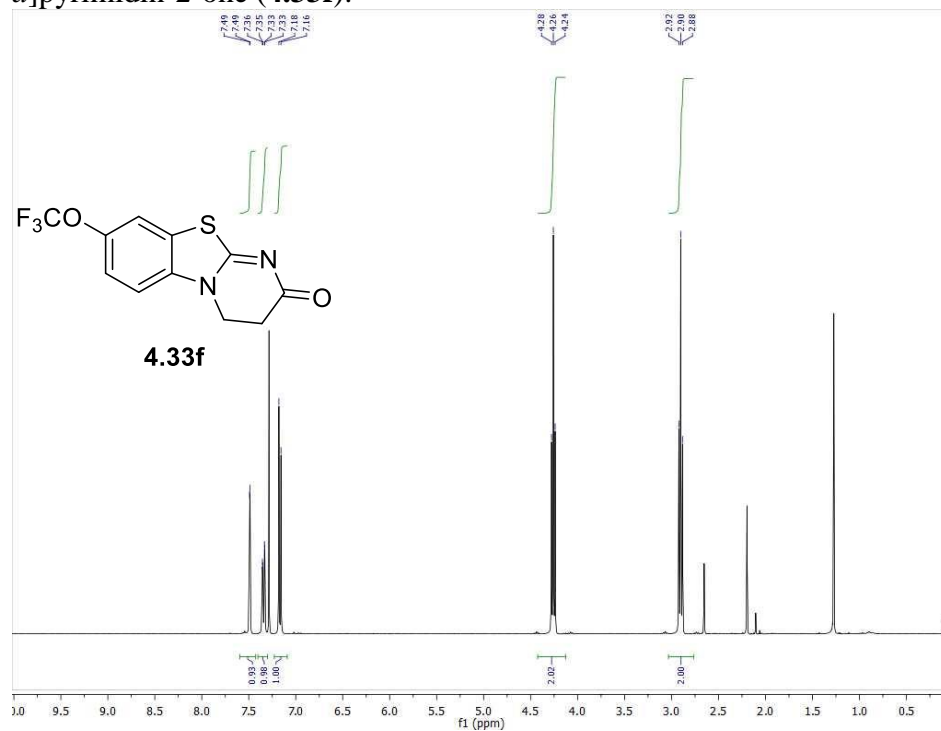
^1H NMR (300 MHz, acetone- d_6) for 8-ethoxy-3,4-dihydro-2*H*-benzo[4,5]thiazolo[3,2-*a*]pyrimidin-2-one (**4.33d**):



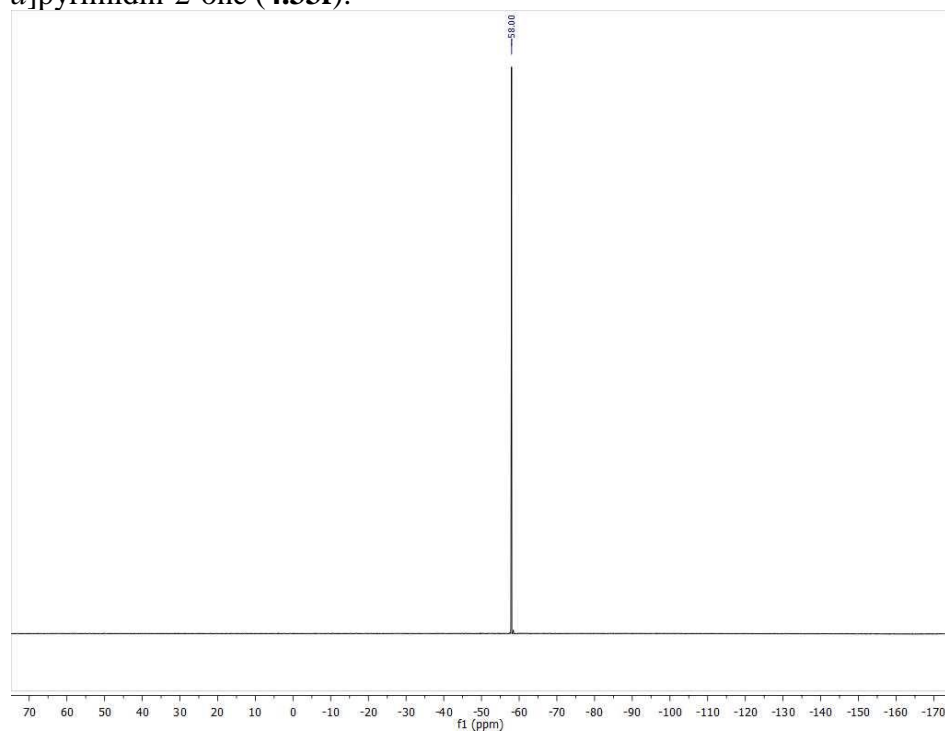
^1H NMR (400 MHz, CDCl_3) for 2-oxo-3,4-dihydro-2*H*-benzo[4,5]thiazolo[3,2-*a*]pyrimidin-8-yl acetate (**4.33e**):



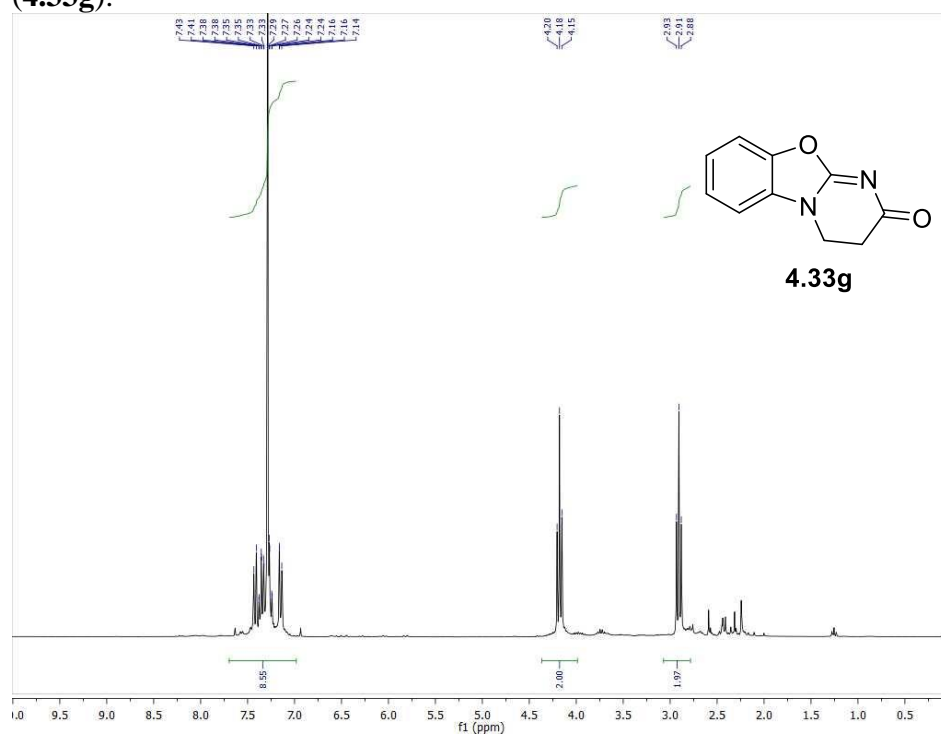
^1H NMR (400 MHz, CDCl_3) for 8-(trifluoromethoxy)-3,4-dihydro-2*H*-benzo[4,5]thiazolo[3,2-*a*]pyrimidin-2-one (**4.33f**):



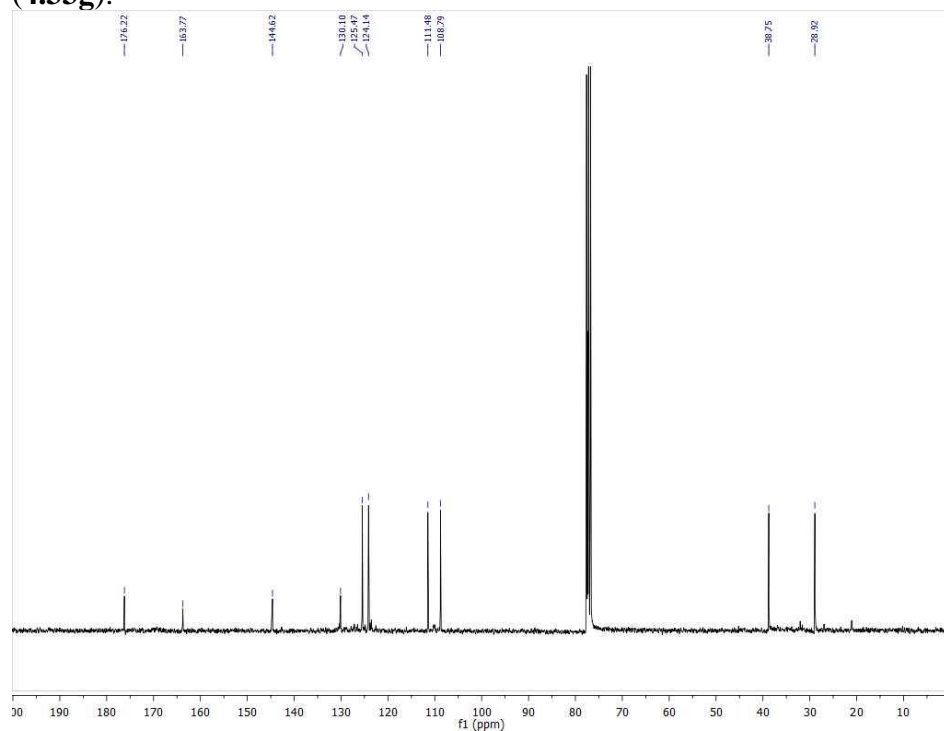
^{19}F NMR (377 MHz, CDCl_3) for 8-(trifluoromethoxy)-3,4-dihydro-2*H*-benzo[4,5]thiazolo[3,2-*a*]pyrimidin-2-one (**4.33f**):



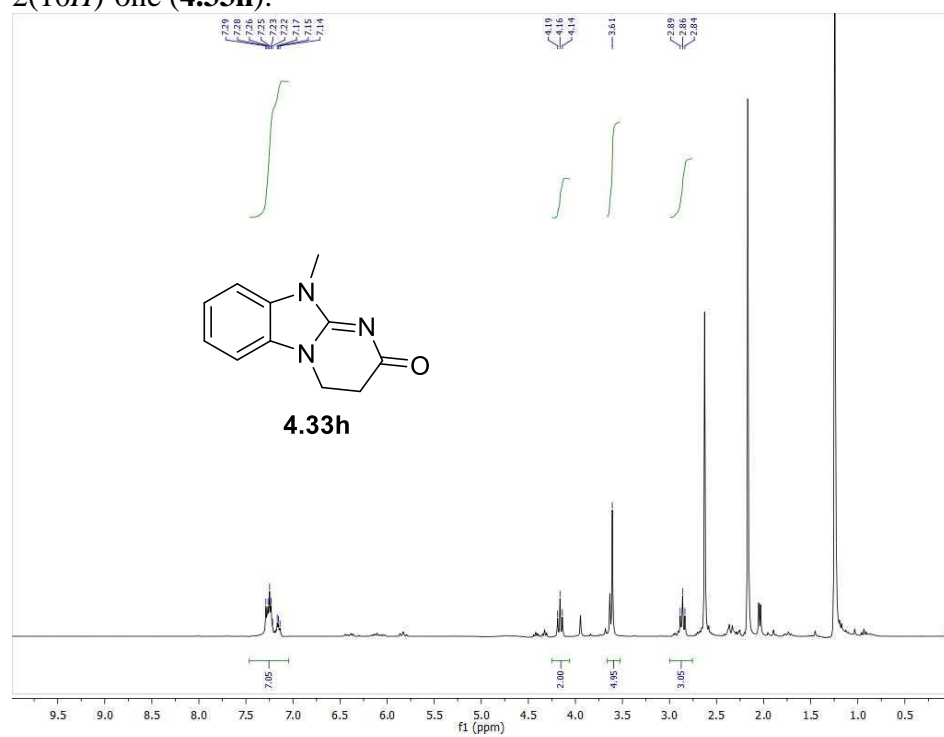
^1H NMR (300 MHz, CDCl_3) for 3,4-dihydro-2*H*-benzo[4,5]oxazolo[3,2-*a*]pyrimidin-2-one (**4.33g**):



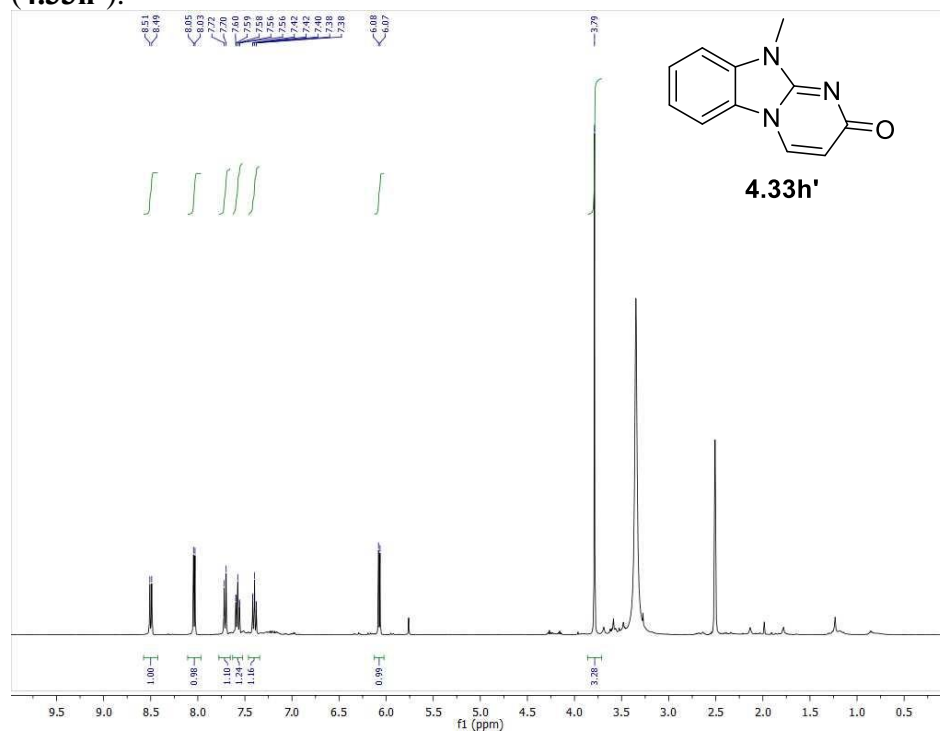
^{13}C NMR (75 MHz, CDCl_3) for 3,4-dihydro-2*H*-benzo[4,5]oxazolo[3,2-*a*]pyrimidin-2-one (**4.33g**):



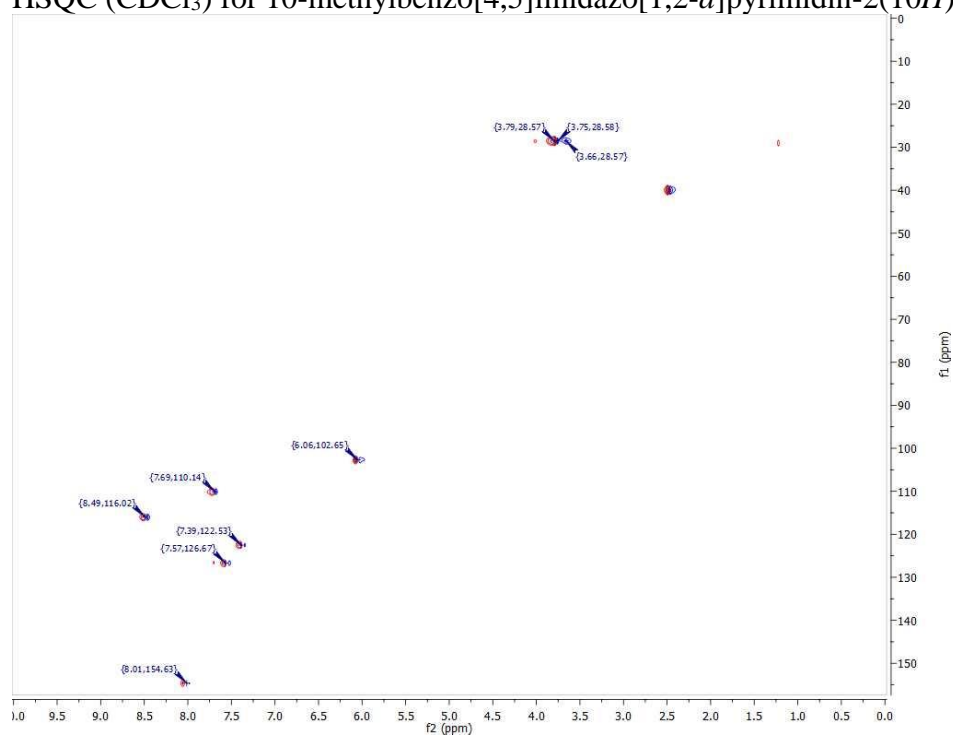
^1H NMR (300 MHz, CDCl_3) for 10-methyl-3,4-dihydrobenzo[4,5]imidazo[1,2-*a*]pyrimidin-2(10*H*)-one (**4.33h**):



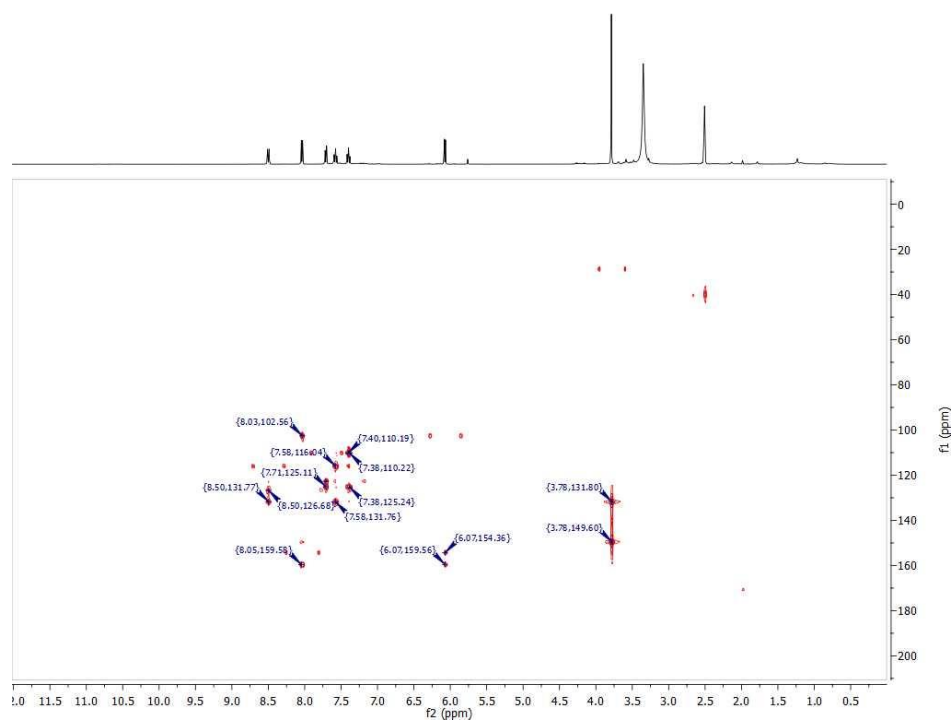
^1H NMR (300 MHz, CDCl_3) for 10-methylbenzo[4,5]imidazo[1,2-*a*]pyrimidin-2(10*H*)-one (**4.33h'**):



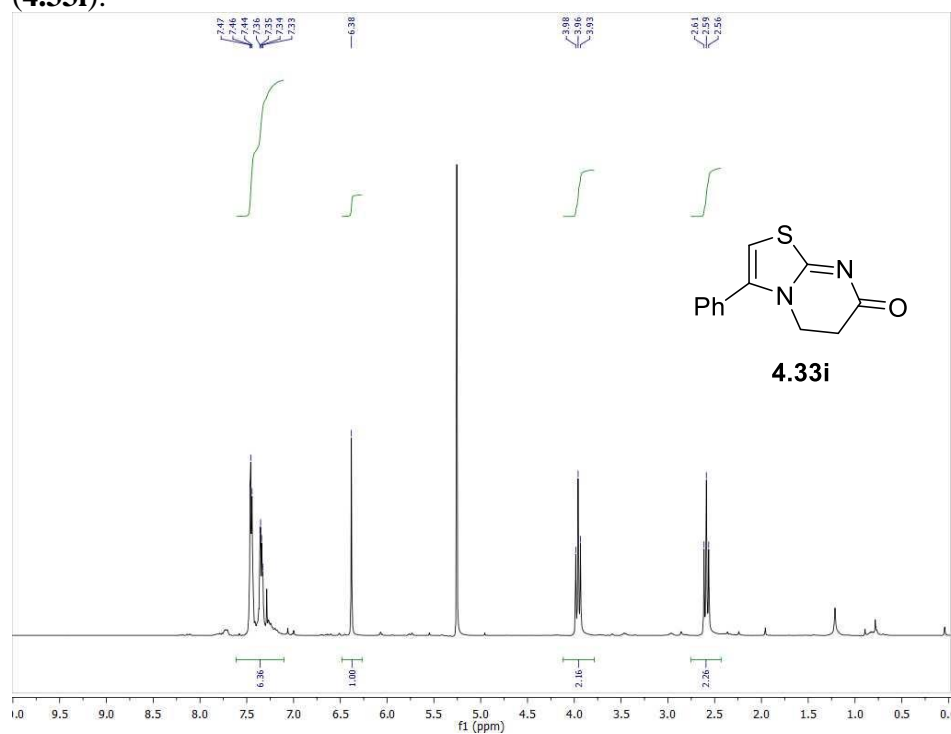
HSQC (CDCl_3) for 10-methylbenzo[4,5]imidazo[1,2-*a*]pyrimidin-2(10*H*)-one (**4.33h'**):



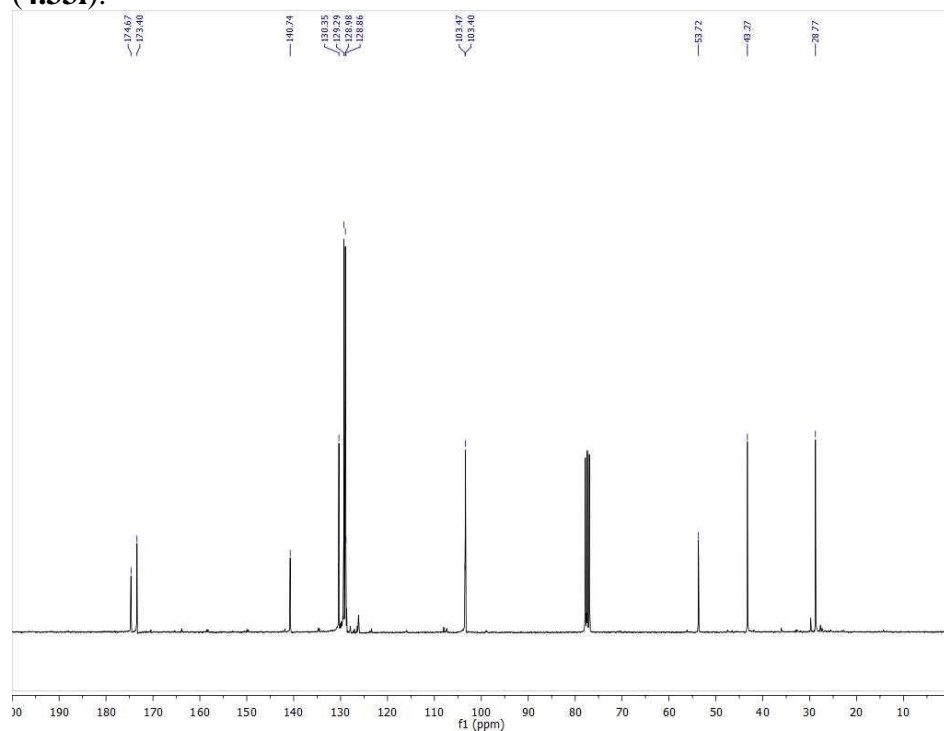
HMBC (CDCl₃) for 10-methylbenzo[4,5]imidazo[1,2-*a*]pyrimidin-2(10*H*)-one (**4.33h'**):



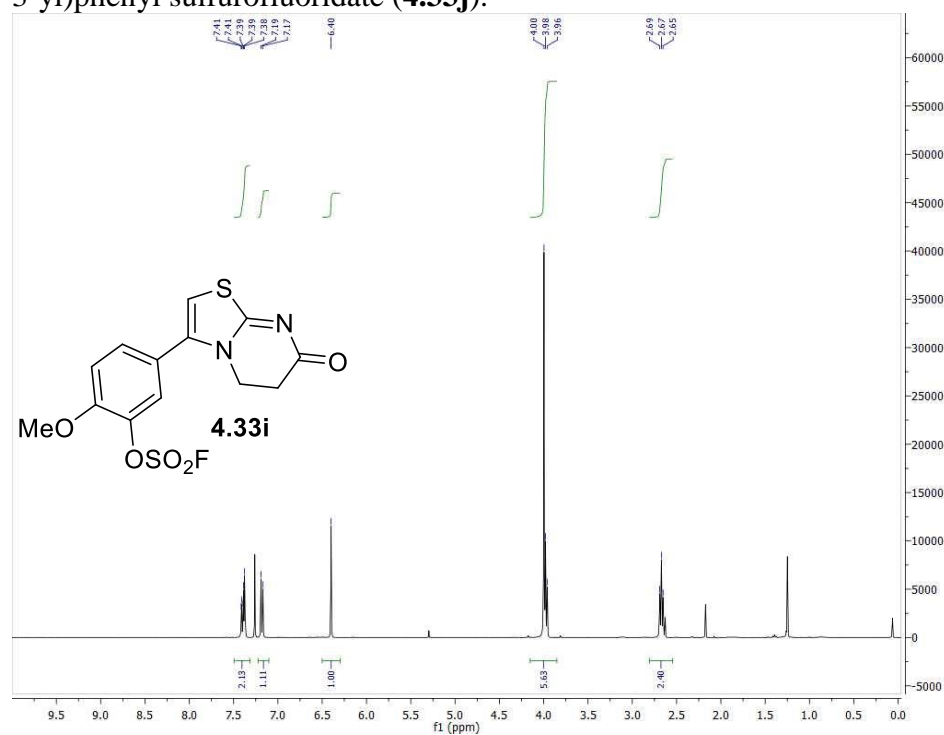
¹H NMR (300 MHz, CDCl₃) for 3-phenyl-5,6-dihydro-7*H*-thiazolo[3,2-*a*]pyrimidin-7-one (**4.33i**):



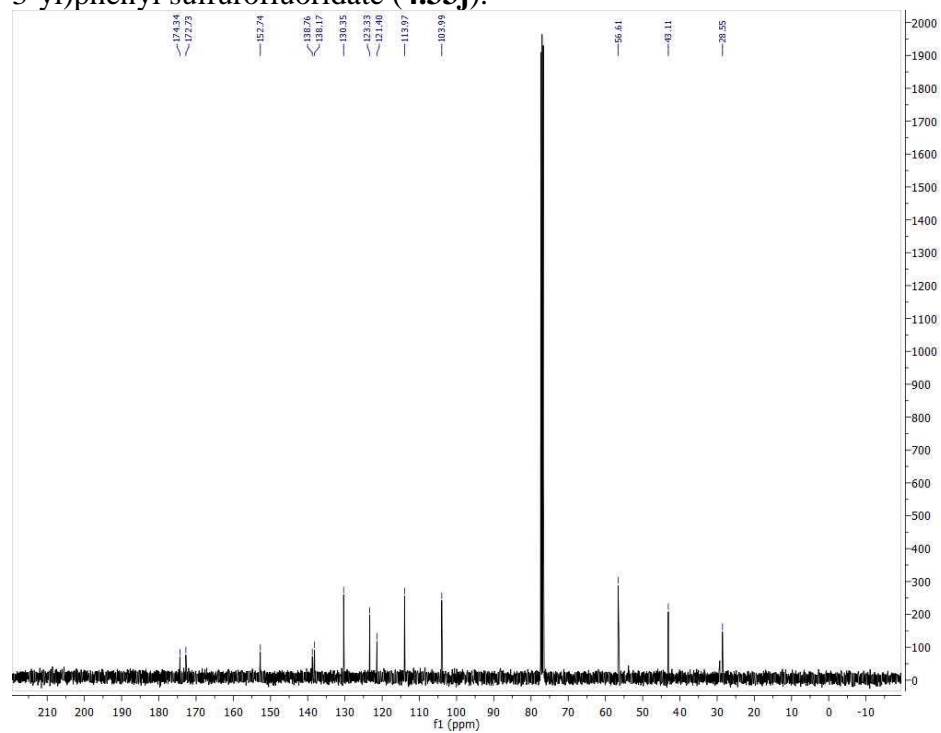
^{13}C NMR (75 MHz, CDCl_3) for 3-phenyl-5,6-dihydro-7*H*-thiazolo[3,2-*a*]pyrimidin-7-one (**4.33i**):



^1H NMR (400 MHz, CDCl_3) for 2-methoxy-5-(7-oxo-6,7-dihydro-5*H*-thiazolo[3,2-*a*]pyrimidin-3-yl)phenyl sulfurofluoridate (**4.33j**):



^{13}C NMR (101 MHz, CDCl_3) for 2-methoxy-5-(7-oxo-6,7-dihydro-5*H*-thiazolo[3,2-*a*]pyrimidin-3-yl)phenyl sulfurofluoridate (**4.33j**):



Appendix D X-ray Crystallography Data

D.1 X-ray data for compound 2.53

Experimental summary. The single crystal X-ray diffraction studies were carried out on a Bruker Kappa APEX-II CCD diffractometer equipped with Mo K α radiation ($\lambda = 0.71073$ Å). A 0.217 x 0.153 x 0.082 mm colorless block was mounted on a Cryoloop with Paratone oil. Data were collected in a nitrogen gas stream at 100(2) K using ϕ and ω scans. Crystal-to-detector distance was 35 mm and exposure time was 5 seconds per frame using a scan width of 1.0°. Data collection was 100% complete to 25.00° in θ . A total of 41773 reflections were collected covering the indices, $-10 \leq h \leq 10$, $-30 \leq k \leq 30$, $-15 \leq l \leq 15$. 5562 reflections were found to be symmetry independent, with a R_{int} of 0.0406. Indexing and unit cell refinement indicated a primitive, monoclinic lattice. The space group was found to be $P2_1/c$. The data were integrated using the Bruker SAINT software program and scaled using the SADABS software program. Solution by direct methods (SHELXT) produced a complete phasing model consistent with the proposed structure. All nonhydrogen atoms were refined anisotropically by full-matrix least-squares (SHELXL-2013). All hydrogen atoms were placed using a riding model. Their positions were constrained relative to their parent atom using the appropriate HFIX command in SHELXL-2013.

Table D.1: Crystal data and structure refinement for 2.53

Dataset ID	JCH-1-100
Empirical formula	C23 H23 Cl F6 N4 O5 S2
Molecular formula	C21 H23 Cl N3 O, C2 F6 N O4 S2

Formula weight (g/mol)	649.02
Temperature	100.0 K
Wavelength	0.71073 Å
Crystal system	Monoclinic
Space group	P 1 2 ₁ /c 1
a (Å)	8.7957(4)
b (Å)	24.5476(11)
c (Å)	12.6500(5)
α	90°
β	96.1755(16)°
γ	90°
V (Å ³)	2715.5(2)
Z	4
Density (calculated)	1.588 Mg/m ³
μ (mm ⁻¹)	0.379
F(000)	1328
Crystal size (mm ³)	0.217 x 0.153 x 0.082
θ range	1.819 to 26.408°
Reflections collected	41773
Independent reflections [R(int)]	5562 [0.0406]
Completeness to $\theta = 25.000^\circ$	100.0%
Max. and min. transmission	0.2602 and 0.2217

Data / restraints / parameters	5562 / 1 / 382
Goodness-of-fit on F^2	1.054
Final R indices [$I > 2\sigma(I)$]	$R_1 = 0.0374$, $wR_2 = 0.0847$
R indices (all data)	$R_1 = 0.0476$, $wR_2 = 0.0884$
Largest diff. peak and hole ($e/\text{\AA}^3$)	0.601 and -0.434

D.2 X-ray data for compound 3.39

Experimental summary. A colorless blade crystal of $C_{22}H_{13}N_6OF_9 \cdot CH_2Cl_2$, having approximate dimensions of 0.05 x 0.12 x 0.22 mm was mounted on a glass fiber. All measurements were made on a Bruker APEX DUO diffractometer with cross-coupled multilayer optics Cu-K α radiation. The data were collected at a temperature of -183 ± 2 °C to a maximum 2θ value of 123.5° . Data were collected in a series of ϕ and ω scans in 2° oscillations using 20.0-second exposures. The crystal-to-detector distance was 59.78 mm. Of the 14356 reflections that were collected, 3713 were unique ($R_{int} = 0.082$); equivalent reflections were merged. Data were collected and integrated using the Bruker SAINT¹⁴³ software package. The linear absorption coefficient, μ , for Cu-K α radiation is 33.23 cm^{-1} . Data were corrected for absorption effects using the multi-scan technique (SADABS¹⁴⁴), with minimum and maximum transmission coefficients of 0.683 and 0.847, respectively. The data were corrected for Lorentz and polarization effects. The structure was solved by direct methods¹⁴⁵. The material crystallizes with one molecule of solvent CH_2Cl_2 in the asymmetric unit. All non-hydrogen atoms were refined anisotropically. The hydrogen atoms on the water oxygen were placed in calculated positions. The N-H hydrogen atom was located in a difference map and refined isotropically. All C-H hydrogen atoms were

placed in calculated positions. All refinements were performed using the SHELXL-2014¹⁴⁶ via the Olex2¹⁴⁷ interface.

Table D.2: Crystal data and structure refinement for compound 3.39

Dataset ID	jh016/MTB-2-225
Empirical formula	C ₂₃ H ₁₅ N ₆ OF ₉ Cl ₂
Formula weight (g/mol)	633.31
Temperature	-183 ± 2 °
Wavelength	1.54178 Å
Crystal system	Monoclinic
Space group	<i>P</i> 2 ₁ /c (#14)
a (Å)	12.3350(4)
b (Å)	25.4444(14)
c (Å)	8.2564(7)
α	90°
β	108.771(4)°
γ	90°
V (Å ³)	2453.5(3)
Z	4
Density (calculated)	1.715 g/cm ³
μ (cm ⁻¹)	33.23
F(000)	1272.00

Crystal size (mm ³)	0.05 x 0.12 x 0.22
2θ _{max}	123.5°
Reflections collected	14356
Independent reflections [R(int)]	3713 [0.082]
Max. and min. transmission	0.847 and 0.683
Goodness-of-fit on F ²	1.06
Final R indices [I>2σ(I)]	R1 = 0.058, wR2 = 0.152
R indices (all data)	R1 = 0.083, wR2 = 0.169
Largest diff. peak and hole (e/Å ³)	0.35 and -0.78
